

PHYSICAL  
SCI. LIB.

.QE  
89  
A1  
C32  
NO.66

California. Division of Mines of  
Geology. Special Publication.

U.C.B. LIBRARY



1983  
COALINGA, CALIFORNIA  
EARTHQUAKES



SPECIAL PUBLICATION 66

UNIVERSITY OF CALIFORNIA  
DAVIS  
JUL 6 1984  
GOV'T. DOCS. - LIBRARY

CALIFORNIA DEPARTMENT OF CONSERVATION  
DIVISION OF MINES AND GEOLOGY





**STATE OF CALIFORNIA**  
GEORGE DEUKMEJIAN  
*GOVERNOR*

**THE RESOURCES AGENCY**  
GORDON K. VAN VLECK  
*SECRETARY FOR RESOURCES*

**DEPARTMENT OF CONSERVATION**  
DON L. BLUBAUGH  
*DIRECTOR*

**DIVISION OF MINES AND GEOLOGY**  
JAMES F. DAVIS  
*STATE GEOLOGIST*



# **THE 1983 COALINGA, CALIFORNIA EARTHQUAKES**

**SPECIAL PUBLICATION 66**

**1983**

---

---

*Contributions from:*

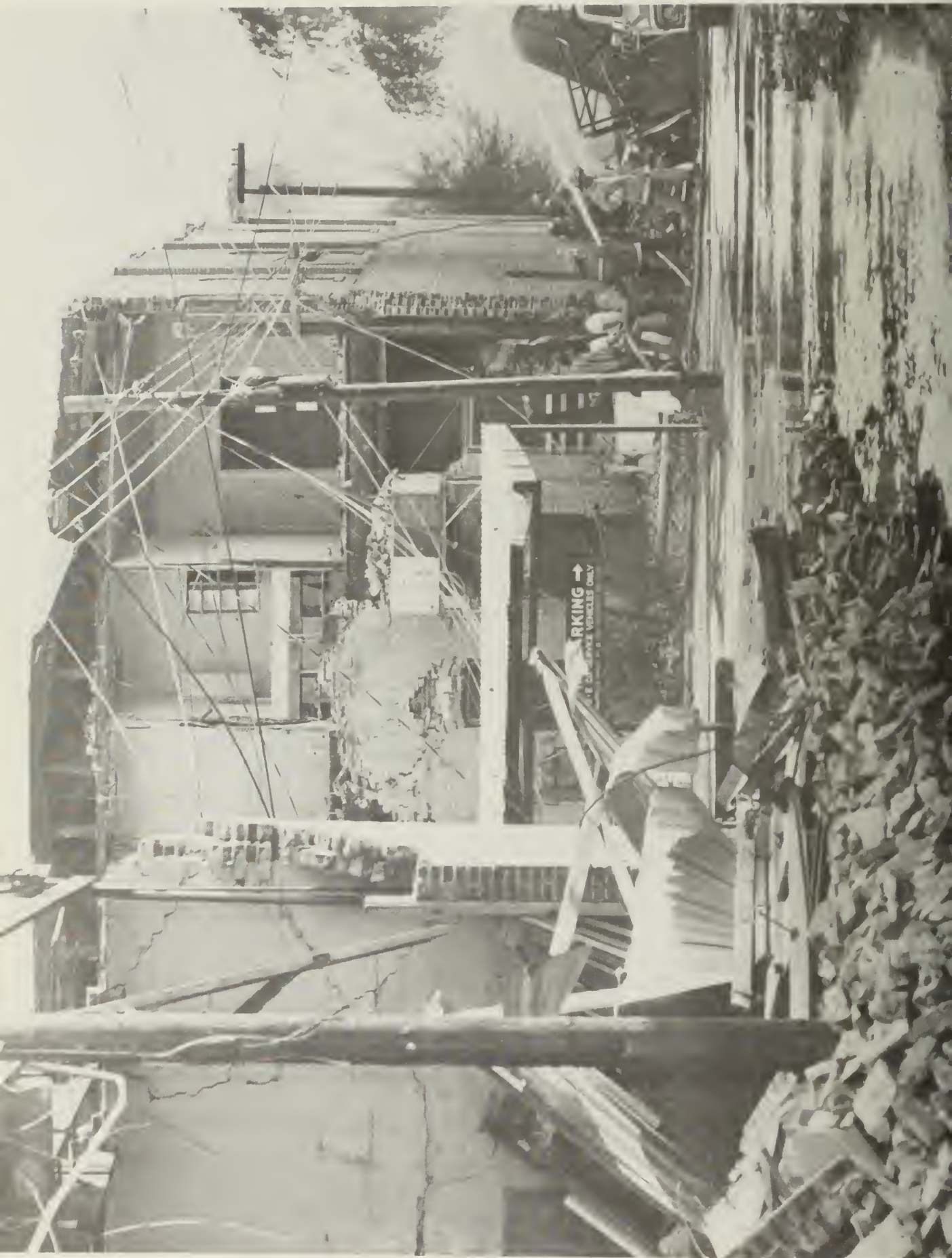
*California Institute of Technology  
Chevron U.S.A., Inc.  
Cornell University  
H.J. Degenkolb Associates, Engineers  
Pleasant Valley Water District  
San Francisco State University  
Stanford University  
State of California  
    Division of Mines and Geology  
    Department of Transportation  
    Office of the State Architect  
University of California, Berkeley  
University of California, Santa Cruz  
University of Cambridge  
U.S. Geological Survey  
Woodward-Clyde Consultants*

---

---

**John H. Bennett and Roger W. Sherburne, Editors**

**CALIFORNIA DEPARTMENT OF CONSERVATION  
DIVISION OF MINES AND GEOLOGY  
1416 Ninth Street, Rm. 1341  
Sacramento, CA 95814**



## CONTENTS

	<u>Page</u>
Preface.....	vii
Index of Contributing Authors.....	ix
<u>Section 1 - Earthquake Damage</u>	
1. Intensity Distribution and Isoseismal Map by Carl W. Stover.....	1
2. Damage Survey in Coalinga, California, for the Earthquake of May 2, 1983 by Margaret G. Hopper, Paul C. Thenhaus, Lynn M. Barnhard, and S.T. Algermissen.....	5
3. Directional Pattern of Building Displacement in the Coalinga Earthquake, May 2, 1983 by David A. Mustart, Raymond Sullivan, and Raymond Pestrong.....	9
4. Observations on the Structural Damage Caused by the Coalinga Earthquake of May 2, 1983, by Chris D. Poland, John F. Silva, and James O. Malley.....	19
5. Performance of the Public School Buildings to the 1983 Coalinga, California, Earthquakes by John F. Meehan.....	37
6. Earthquake Damage to the Coalinga Oilfields by J.P. Hughes, W. Won, and R.C. Erickson.....	55
7. Damage to Irrigation Wells and Other Facilities in the Pleasant Valley Water District Due to the May 2, 1983 Earthquake and Aftershocks by Joseph B. Summers.....	71
8. Summary of Highway Bridge Damage Coalinga Earthquake, May 2, 1983 by Eugene G. Klein, Jr.....	77
9. Clearinghouse Activities: Coalinga, California May 2, 1983 by Robert Streitz.....	87
<u>Section 2 - Geologic and Geophysical Investigations</u>	
10. Historical Seismicity and Tectonics of the Coast Ranges-Sierran Block Boundary: Implications to the 1983 Coalinga, California Earthquakes by Ivan G. Wong and Richard W. Ely.....	89
11. Regional Geology of the Coalinga, California Area by John T. Alfors.....	105



## CONTENTS (CONTD)

	<u>Page</u>
12. Evidence on the Tectonic Setting of the 1983 Coalinga Earthquakes from Deep Reflection and Refraction Profiles Across the Southeastern End of Kettleman Hills by Carl M. Wentworth, Allan W. Walter, J. Alan Bartow, and Mark D. Zoback.....	113
13. Preliminary Report on the Crustal Velocity Structure Near Coalinga, California, as Determined From Seismic Refraction Surveys in the Region by Allan W. Walter and Walter D. Mooney.....	127
14. COCORP Seismic Reflection Profiles near the 1983 Coalinga Earthquake Sequence: Deep Structures by Eric Fielding, Muawia Barazangi, Larry Brown, Jack Oliver and Sidney Kaufman.....	137
15. Reverse Slip on a Buried Fault During the 2 May 1983 Coalinga Earthquake: Evidence from Geodetic Elevation Changes by Ross S. Stein.....	151
16. Surface Folding, River Terrace Deformation Rate and Earthquake Repeat Time in a Reverse Faulting Environment: The Coalinga, California, Earthquake of May 1983 by Geoffrey King and Ross Stein.....	165
17. High-Angle Reverse Faulting, A Model for the 2 May 1983 Coalinga Earthquake by David R. Fuller and Charles R. Real.....	177
18. Gravity and Magnetic Investigation of the Coalinga Area by R.H. Chapman, G.W. Chase, and C.C. Bishop.....	185
19. Shallow Stress Changes Due to Withdrawal of Liquid from Oil Fields in the Coalinga Area, California by R.F. Yerkes, Assisted by K.M. Williams.....	195
20. Surface Faulting Northwest of Coalinga, California, June and July, 1983 by Earl W. Hart and Richard D. McJunkin.....	201

### Section 3 - The Earthquake Sequence

21. The 1983 Coalinga Earthquake Sequence: May 2 through August 1 by Robert A. Uhrhammer, Robert B. Darragh and Bruce A. Bolt....	221
22. Mechanism of the 1983 Coalinga Earthquake Determined From Long-Period Surface Waves by Hiroo Kanamori.....	233
23. Teleseismic Mechanism of the May 2, 1983 Coalinga, California, Earthquake from Long-Period P-Waves by Stephen H. Hartzell and Thomas H. Heaton.....	241

## CONTENTS (CONTD)

	<u>Page</u>
24. Waveform Modeling of Long Period P-waves From the Coalinga Earthquake of May 2, 1983 by J.A. Rial and E. Brown.....	247
25. Study of the May 2, 1983 Coalinga Earthquake and Its Aftershocks, Based on the USGS Seismic Network in Northern California by J. Eaton, R. Cockerham, and F. Lester.....	261
26. The Mainshock-Aftershock Sequence of 2 May 1983: Coalinga, California by Roger Sherburne, Karen McNally, Ethan Brown, and Arturo Aburto.....	275
27. Source Parameters of Coalinga Aftershocks From the U.C. Berkeley Portable Digital Array by Daniel R. O'Connell and Patricia E. Murtha.....	293
28. Discrepancies in Strong-Motion and Sensitive Arrival Time Data for the M6.7 Coalinga Earthquake of 2 May 1983 by Chris H. Cramer and Anthony F. Shakal.....	307
29. Strong-Motion Data From the Coalinga, California Earthquake and Aftershocks by A.F. Shakal and J.T. Ragsdale.....	321



Reduced U.S. Geological Survey Orthophoto of the Coalinga 7 1/2' Quadrangle



## PREFACE

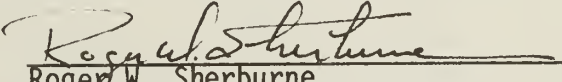
At 4:43 PDT on Monday, 2 May 1983, western Fresno County and its environs along the San Joaquin Valley margin were subjected to the sudden and violent shaking of another major California earthquake ( $M_L \sim 6.7$ ). Like other recent earthquakes (e.g. 1952 Kern County, 1971 San Fernando, and 1975 Oroville), the 1983 Coalinga earthquake was, in most respects, a surprise - a relatively large earthquake occurring in an area devoid of any recognized active faults and significant historical seismicity. The earthquake posed a number of important questions including: a) Why was there no surface rupture? b) Why was damage so severe in Coalinga while relatively light closer to the epicenter? c) Was there significance to the occurrence of the earthquake amidst producing oil fields? This special publication was undertaken to help formulate answers to these and other questions by providing a timely medium for the presentation of results and conclusions of many of the earth science and damage-related investigations.

This report presents the results of studies by individuals in federal, state, and local agencies, universities, private industry and consulting firms. It contains a total of 29 contributions arranged in three sections. Section 1 contains 9 papers describing the earthquake effects upon various structures, residential and commercial buildings, schools, bridges, oil field facilities and irrigation systems. Included in this section is a report summarizing the operation of the Earthquake Clearinghouse, operated jointly by the Division of Mines and Geology and the Earthquake Engineering Research Institute. Section 2 is comprised of 11 papers summarizing various geologic and geophysical studies of a regional nature and the particular structure and mechanism involved in this earthquake sequence. Section 3 includes 9 papers concerned with the seismological parameters of the mainshock and aftershocks.

It should be noted that the authors were required to submit camera-ready copy by August 31, 1983, just four months following the mainshock. Since significant aftershocks, some accompanied by surface rupture, continue, data and conclusions presented in some papers relevant to the seismic activity, in particular, are preliminary. In a related matter, at the time of paper submission, there was no generally accepted magnitude for the mainshock; consequently, the magnitude cited varies from 6.4 to 6.7.

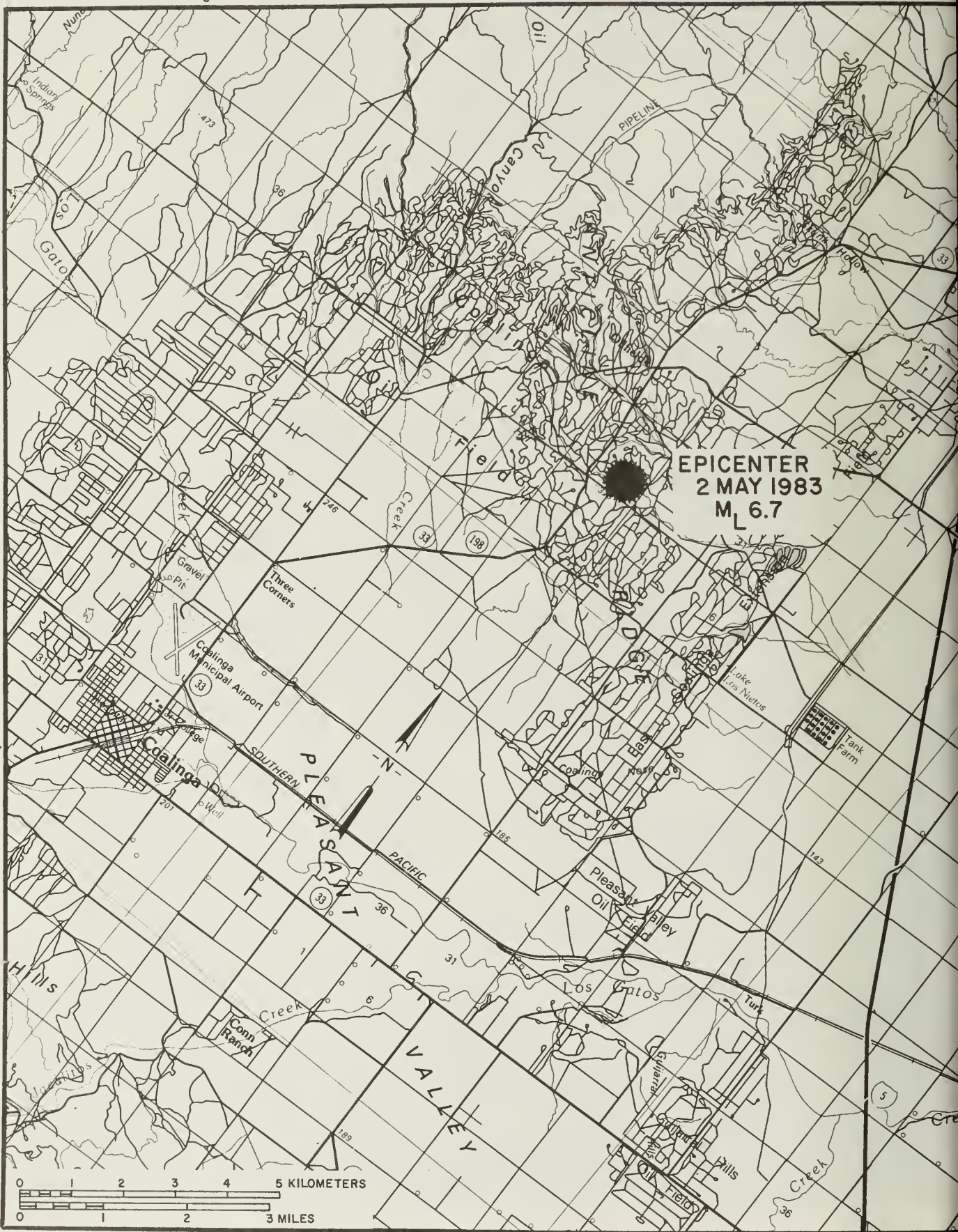
The editors, on behalf of the Division of Mines and Geology, take this opportunity to express their appreciation for the cooperation and efforts put forth by these many contributors. This compilation will provide a valuable future reference, and we are pleased that we were able to make it available. A note of appreciation is due Brian Tucker (Geophysics Officer), under whose supervision this report was prepared, and to M. Smith, J. Tambert, and E. Foster of the Geological Drafting Unit for the speed and diligence with which this publication was assembled. C. Pingree provided significant assistance with the necessary word processing.

  
John H. Bennett

  
Roger W. Sherburne

36°15'

120°22'30"



Base map is portion of U.S. Geological Survey Coalinga Quadrangle 1:100 000 scale series (planimetric)



## INDEX OF CONTRIBUTING AUTHORS

### Section 1 - Earthquake Damage

S.T. Algermissen.....	5	Raymond Pestrone.....	9
Lynn M. Barnhard.....	5	Chris D. Poland.....	19
R.C. Erickson.....	55	John F. Silva.....	19
Margaret G. Hopper.....	5	Carl W. Stover.....	1
J.P. Hughes.....	55	Robert Streitz.....	87
Eugene G. Klein, Jr.....	77	Raymond Sullivan.....	9
James O. Malley.....	19	Joseph B. Summers.....	71
John F. Meehan.....	37	Paul C. Thenhaus.....	5
David A. Mustart.....	9	W. Won.....	55

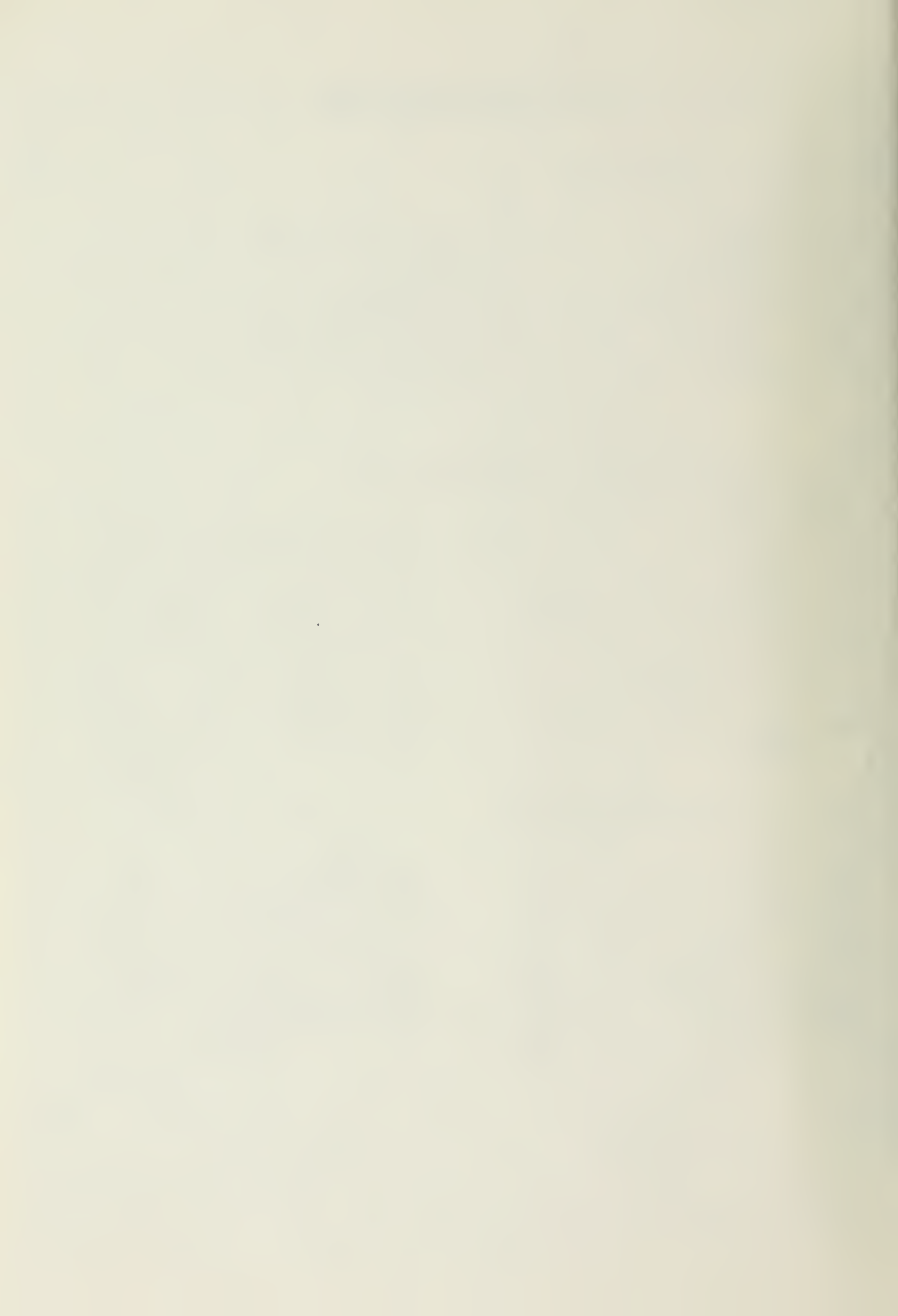
### Section 2 - Geologic and Geophysical Investigations

John T. Alfors.....	105	Geoffrey King.....	165
Muawia Barazangi.....	137	Richard D. McJunkin.....	201
J. Alan Bartow.....	113	Walter D. Mooney.....	127
C.C. Bishop.....	185	Jack Oliver.....	137
Larry Brown.....	137	Charles R. Real.....	177
R.H. Chapman.....	185	Ross S. Stein.....	151, 165
G.W. Chase.....	185	Allan W. Walter.....	113, 127
Richard W. Ely.....	89	Carl M. Wentworth.....	113
Eric Fielding.....	137	K.M. Williams.....	195
David R. Fuller.....	177	Ivan G. Wong.....	89
Earl W. Hart.....	201	R.F. Yerkes.....	195
Sidney Kaufman.....	137	Mark D. Zoback.....	113

### Section 3 - The Earthquake Sequence

Arturo Aburto.....	275	F. Lester.....	261
Bruce A. Bolt.....	221	Karen McNally.....	275
Ethan Brown.....	247, 275	Patricia E. Murtha.....	293
R. Cockerham.....	261	Daniel R. O'Connell.....	293
Chris H. Cramer.....	307	J.T. Ragsdale.....	321
Robert B. Darragh.....	221	J.A. Rial.....	247
J. Eaton.....	261	Anthony F. Shabal.....	307, 321
Stephen H. Hartzell.....	241	Roger Sherburne.....	275
Thomas H. Heaton.....	241	Robert A. Uhrhammer.....	221
Hiroo Kanamori.....	233		





## Section 1

# EARTHQUAKE DAMAGE





# INTENSITY DISTRIBUTION AND ISOSEISMAL MAP

by

Carl W. Stover<sup>1</sup>

## ABSTRACT

The Coalinga, California, earthquake of May 2, 1983, had a maximum Modified Mercalli (MM) intensity of VIII at Coalinga and Oilfields. It was felt over an area of at least 205,000 km<sup>2</sup> of the land area in California and western Nevada. In Coalinga, the only city to suffer extensive damage, damage was estimated at more than \$31 million. The severity of the damage in the epicentral area correlated with the age of the buildings and type of construction.

## INTRODUCTION

The earthquake of May 2, 1983, in the Coalinga, Calif. area was felt over an area of at least 205,000 km<sup>2</sup> of the land area in California and western Nevada (fig. 1). It was located by Eaton (1983) at lat 36° 13.99' N., long 120° 17.59' W., near the trend of the Coalinga anticline (Brown, 1983) about 10 km northeast of Coalinga.

This is a preliminary report on the intensity distribution as shown on the isoseismal map (fig. 1). The isoseismal map was compiled from data obtained from a questionnaire canvass of postmasters and police departments (within 150 km of epicenter), supplemented with information from field reports by M. G. Hopper and P. C. Thenhaus (oral commun., 1983) and numerous press reports. Intensities were rated using the Modified Mercalli Scale of 1931 (Wood and Neumann, 1931).

All of the casualties and most of the major damage occurred at Coalinga, where 1 person died from injuries, and 47 people required hospital treatment. Most of the downtown businesses and 1,936 dwelling units were damaged to some degree. The worst damage occurred in the 8-block downtown area where 141 business structures were virtually destroyed and 73 had extensive damage. An American Red Cross disaster damage assessment report (Whear, 1983) listed 309 single-family homes and 33 apartments destroyed; major damage to 558 single-family homes, 94 mobile homes, and 39 apartments; and minor damage to 811 single-family homes, 22 mobile homes, and 70 apartments. A preliminary estimate of property damage in Coalinga by the California Office of Emergency Services exceeded \$31 million.

In terms of relative size, the Coalinga earthquake is comparable to the 1971 San Fernando earthquake. The felt areas are approximately the same-- 205,000 km<sup>2</sup> for the Coalinga event and 207,000 km<sup>2</sup> for San Fernando. The

<sup>1</sup>U.S. Geological Survey, Denver

magnitudes of these events are also almost identical. Both events had computed magnitudes of 6.2 mb and 6.5 MS. The ML magnitudes were 6.5 for Coalinga and 6.4 for San Fernando. Due to much greater population density in the epicentral area, the San Fernando earthquake caused much more damage.

### INTENSITY DISTRIBUTION

Figure 1 shows the distribution of intensities associated with the earthquake. The area of maximum intensity (Modified Mercalli VIII) was concentrated in and near the town of Coalinga. The most extensive damage was to one- and two-story buildings built before 1930 in the downtown commercial area. These buildings were mostly of the unreinforced masonry type with inadequate connections between walls, floors, and roofs. The damage consisted of collapse of brick work, usually at the top of the walls, or of entire exterior brick walls and sometimes entire buildings. Many homes were damaged when they were shifted on their foundations. Residences resting on cripple-wall foundations were particularly susceptible to lateral movement and most were damaged when they fell off the foundations or the foundations collapsed. Buildings constructed of reinforced masonry or concrete in recent years suffered mostly minor damage.

Oilfields, an abandoned town located about 10 km northeast of Coalinga, was also rated at MM intensity VIII. Little remains at this site to be damaged; however, the Pacific Gas and Electric Substation No. 2, a concrete-block building, was virtually destroyed when portions of both front and back walls collapsed.

The most significant damage outside the vicinity of Coalinga occurred at Arenal (MM intensity VII), located about 30 km southeast of the epicenter. A nursery building was moved two feet off its foundation breaking sewer connections and doing considerable damage to the floor. Chimneys were reported fallen in some areas of Arenal. Plate-glass windows were shattered on Kings Street.

A comparison of the intensity distribution and associated ground factors for the Coalinga event shows that all of the intensity VI ratings correlate with alluvial valleys, principally the San Joaquin and Salinas Valleys. Most of the damage in these localities consisted of cracked plaster or brick walls; a few cracked chimneys, sidewalks, or foundations; cracked or broken windows; and broken dishes or glassware. Most of the intensity-VI-rated questionnaires reported about five percent of the buildings in the corresponding zip-code region were damaged.

The two anomalous intensity V areas located within the intensity II-IV isoseismal in the southeastern part of the felt area (fig. 1) are associated with thick alluvium near dry lake beds. The northernmost area is near Owens Lake and the other is near Searles and China Lakes.

It should be noted that Coalinga was rated at MM intensity VIII rather than IX because of the selective damage within the city. In the downtown

area, buildings built before 1930 sustained heavy damage. In contrast, structures built in later years that were designed to be more earthquake resistant had only minor-to moderate damage. Damage to private homes also depended on the type of construction. For example, homes on cripple-wall foundations were often thrown to the ground when the foundations collapsed, whereas homes with a continuous concrete or brick foundation were usually only shifted out of position.

#### REFERENCES

- Brown, R. D., 1983, Tectonic setting, in The Coalinga earthquake sequence commencing May 2, 1983: U.S. Geological Survey Open-File Report 83-511, p. 3-7.
- Eaton, J. P., 1983, Seismic setting, location and focal mechanism of the May 2, 1983, Coalinga earthquake, in The Coalinga earthquake sequence commencing May 2, 1983: U.S. Geological Survey Open-File Report 83-511, p. 20-26.
- Whear, Allen, 1983, Unpublished survey and damage assessment work sheets, American Red Cross, Western Field Office, Burlingame, California.
- Wood, H. O., and Neumann, Frank, 1931, Modified Mercalli Intensity Scale of 1931: Seismological Society of America Bulletin, v. 21, no. 4, p. 277-283.



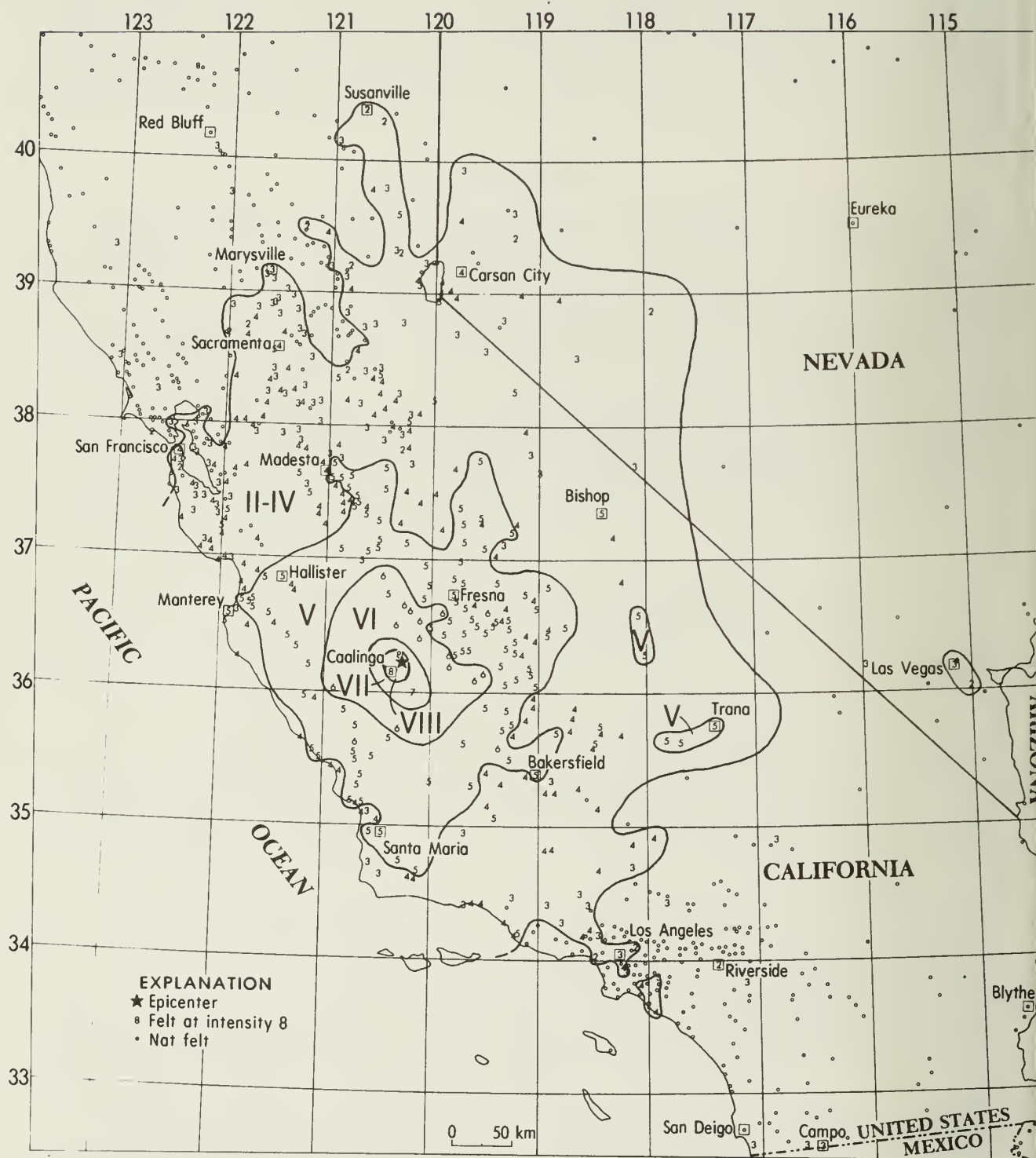


Figure 1.--Isoseismal map for the Coalinga, California, earthquake of May 2, 1983.

# DAMAGE SURVEY IN COALINGA, CALIFORNIA FOR THE EARTHQUAKE OF MAY 2, 1983

by

Margaret G. Hopper<sup>1</sup>, Paul C. Thenhaus<sup>1</sup>,  
Lynn M. Barnhard<sup>1</sup>, S.T. Algermissen<sup>1</sup>

## ABSTRACT

A damage survey of structures in Coalinga, California, immediately following the earthquake of May 2, 1983, indicated that 75 of the old, unreinforced brick structures in the downtown business district were severely damaged, and the remainder sustained moderate structural damage. Newer masonry structures in the business district had only non-structural damage. Fifteen percent of the single-family dwellings were thrown off their foundations. Many of these dwellings had been constructed on cripple walls with no lateral bracing. More than half of the chimneys were affected. Modified Mercalli intensity VIII was assigned at Coalinga. The toppling of many strong chimneys and the partial collapse of old, unreinforced masonry buildings indicate at least VIII, whereas the lack of serious damage to ordinary substantial masonry structures indicates less than IX.

## INTRODUCTION

A field party from the U.S. Geological Survey, Golden, Colorado, was dispatched on May 3, 1983, to survey structural damage in Coalinga, California. The primary objective of four days of field investigation was to systematically document damage to buildings in Coalinga. Buildings, both damaged and undamaged, were catalogued according to the Insurance Services Office classification system so that percent loss could be estimated for buildings within each structural classification. State officials' preliminary estimate of loss exceeds \$30 million.

## DOWNTOWN BUSINESS DISTRICT

Detailed damage information was obtained in a 12-block area of the downtown business district prior to May 5, when the area was restricted to all but public works personnel who were involved in the demolition of heavily damaged buildings. Fifty percent of the buildings in this 12-block area were land 2-story unreinforced brick structures in which loads were carried directly by the walls and interior partitions. Seventy-five percent of these unreinforced structures were total losses, and the remaining unreinforced buildings sustained moderate structural damage. All of these unreinforced buildings were more than 40 years old.

<sup>1</sup> U.S. Geological Survey, Denver, Colorado.

Newer unit-masonry buildings, constructed of hollow concrete blocks on a concrete slab and apparently reinforced, sustained primarily minor to moderate nonstructural damage. Many of these retail buildings were open for business within a few days following the earthquake.

Twelve percent of the buildings in the downtown area were wood or steel-framed with sheetmetal siding. This class of buildings performed quite well in the earthquake; no structural damage was noted, even in the oldest of these structures. Nonstructural damage to buildings of this type was primarily broken glass and brick veneer lost from front facades.

### SINGLE-FAMILY DWELLINGS

A systematic survey of single-family dwellings (primarily one-story, wood-frame) within the city limits of Coalinga showed that 287 of 1,938 (15%) were thrown off their foundations. Most of the homes that were damaged in this manner were more than 20 years old and were built on 18- to 24-inch-high cripple walls (upright supports between the foundation and the floor joists) with no lateral bracing. In some cases, exterior wooden-lap siding provided sufficient lateral bracing to prevent complete collapse of the cripple wall. A large majority of the houses off their foundations were thrown eastward, though some had a conspicuous southerly component. One block west of the downtown area, in one of the most severely damaged residential blocks, houses were thrown off their foundations to the west. Newer homes and wood-frame apartment buildings on the outskirts of Coalinga showed no indications of significant structural damage, although many chimneys were down, and a number of homes lost brick veneer. Of 388 chimneys counted, 206 (53%) were thrown down, and 18 chimneys were cracked but still standing.

### MODIFIED MERCALLI INTENSITY

#### Intensity at Coalinga

A preliminary assessment of the Modified Mercalli intensity at Coalinga indicates intensity VIII shaking. This intensity assignment is based on the following:

(1) Partial collapse of old, unreinforced masonry buildings in the downtown business district. All of the buildings in this category had structural damage, and most will have to be razed. This indicates an intensity of at least VIII.

(2) Nonstructural damage to somewhat newer masonry buildings. Within the area of most extreme damage were a number of substantial structures built during the last 50 years. Apparent damage to these buildings consisted mostly of minor cracking of walls and broken glass. Some of them, however, were seriously damaged by the collapse of adjacent older, unreinforced masonry buildings onto them. This indicates intensity VIII.



(3) Lack of serious damage to modern masonry buildings. In the downtown area, several buildings less than 20 years old performed very well during the earthquake. Most of these structures were laterally reinforced, steel-frame or wood-frame structures conforming to building codes in effect at the times they were constructed. It seems unlikely that they were designed specifically to resist strong horizontal shaking. This indicates intensity less than IX.

(4) Fall of many houses off foundations. Although it is unknown how many of these houses had been built on cripple walls, it could be seen that the houses characteristically landed offset from their foundations by one to two feet--the height of a normal cripple wall. It is therefore assumed that most had been on cripple walls. These houses acted as inverted pendulums, neither horizontally braced nor tied to their foundations. Many houses that were not seriously damaged were approximately as old as the damaged ones, but either had more secure horizontal bracing or were not on cripple walls at all. Common nonstructural damage was loss of brick veneer and chimneys. Shifting of houses off their foundations is usually indicative of intensity IX; however, because houses on cripple walls are inherently unstable during strong horizontal shaking, in this case it is assumed to indicate only intensity VIII.

(5) Fall of more than half of the chimneys. Chimneys were thrown down or damaged in every neighborhood in Coalinga, on every type of house from the oldest to the newest. Many of the strongest chimneys broke off at the roof line and fell in one piece. This indicates intensity VIII.

#### Maximum Intensity for the Earthquake

Intensity VIII is also assigned to the Pacific Gas and Electric substation only 4 km from the epicenter. Coalinga is about 10 km from the epicenter. Therefore, VIII is assumed to be the maximum observed intensity for the earthquake. Intensity attenuation for the Coalinga earthquake fits well with that for other Southern California earthquakes having maximum Modified Mercalli intensities of VIII.

#### CONCLUSIONS

The earthquake damage at Coalinga clearly demonstrated the marked difference in the response to strong horizontal earthquake shaking of the different types of structures prevalent in Southern California. Those that fared worst were the oldest unreinforced masonry buildings in the central business district. There are tens of thousands of such buildings in California, and they are extremely vulnerable to strong horizontal motion. Other types of structures that were seriously damaged were adobe buildings and wood-frame houses on cripple walls. In contrast, many buildings in Coalinga built during the last 50 years performed very well. These included substantial public buildings, such as the City

Hall, hospital (both built in the late 1930's), and school and college buildings. Certain types of privately owned buildings, such as reinforced masonry structures, wood-frame houses placed directly on their foundations, and metal buildings with wood or steel frames, also performed well. Many of these suffered minor or no damage.

City officials indicated that the second stories of most of the collapsed downtown buildings had been previously condemned because of fire hazards and were therefore unoccupied at the time of the earthquake. This undoubtedly was one reason why the number of injuries was so low; people escaping the second stories would have risked injury or death from crumbling walls and stairwells. Much of the economic loss to the single-family houses that fell off their foundations could have been prevented by simple bracing and bolting directly to foundations.

# DIRECTIONAL PATTERN OF BUILDING DISPLACEMENT IN THE COALINGA EARTHQUAKE, MAY 2, 1983

David A. Mustart, Raymond Sullivan & Raymond Pestrong<sup>1</sup>

## ABSTRACT

Inspection of 141 dwellings in the residential district of Coalinga following the May 2, 1983 earthquake indicated the majority (78%) of structures were displaced toward the southeast sector. This pattern showed geographic uniformity throughout the area of principal damage and suggests that ground motion was characterized by a strong northwestward pulse. The study of consistent patterns of displacement has the potential to provide useful information on ground motion, supplementing that provided by strong motion instruments.

## INTRODUCTION

Ground motion associated with the moderate earthquake of Richter magnitude  $M_L = 6.5$  centered approximately 10 km northeast of Coalinga on May 2, 1983 (Eaton 1983, Maley et al, 1983) resulted in widespread damage to older structures in the city. In the downtown area, many brick buildings were badly damaged, with a few instances of full collapse, and in the residential districts, many single family one-story wood frame dwellings were moved laterally off their foundations (See Plates 1, 2, 3). During our initial visit to the region we discovered that, with surprisingly few exceptions, damaged homes had been displaced towards the southeast. As such a pattern of building displacement might provide an independent measure of the direction of principal ground motion during the earthquake, we proceeded to collect information on more than 200 damaged dwellings in Coalinga, of which 141 were studied in detail. In previous California earthquakes, including San Francisco 1906 (Lawson, 1908 p. 160-368), Long Beach 1933 (Richter, 1958 p. 23-24) and Santa Rosa (Cloud et al, 1970, p. 52), similar patterns showing consistent directionality of building displacement have been recognized locally but not documented extensively. As a peripheral aspect of our study we recorded for each dwelling the overall construction style and foundation design in order to determine any relationships between the extent of damage and mode of construction. The strong correlation between large scale damage and lack of a securely tied foundation, provided valuable insight into the anticipated performance of wood frame structures during future earthquakes.

## CONSTRUCTION HISTORY

Establishment of the first community in the area took place in the latter part of the 19th century along a spur line of the Southern Pacific Railroad, and the town derived its name from the nearby loading site of Coaling Station A. Coalinga became the commercial center for the region when oil was discovered in 1890 in the vicinity of present day Oil City north of the town. The influx of oil workers into the valley led to the rapid growth of the

<sup>1</sup> Department of Geosciences, San Francisco State University, San Francisco, CA 94132



community and Coalinga was incorporated in 1906. The central business district, consisting primarily of two-story brick structures, emerged in the early years of the 20th century together with some of the older wooden frame residences (Fig. 1). This period is also noted for the construction of numerous small dwellings in the surrounding oil fields, many of which were later moved onto sites in town as Coalinga became further established.

In the late 1920's and early 1930's, important discoveries of oil and gas in the Kettleman Hills and other nearby areas provided further impetus to construction. Residential development took place during this period on housing tracts on the periphery of the original townsite (Fig. 1).

The most recent period of development took place following World War II with the continued expansion of the oil industry, the growth of livestock and agricultural interests (mainly associated with the construction of the Coalinga Canal) and renewal of mining activities in the New Idria area to the northwest. These post-war residences were primarily modern ranch-style dwellings. At the time of the earthquake, the Coalinga area Chamber of Commerce estimated that there were approximately 2,600 occupied dwellings within the city limit.

In general, the overall pattern of building damage can be correlated with this development history. The brick structures in the central business district of the original townsite sustained the most extensive damage, and, in some cases, suffered total collapse. In the residential areas, damage was almost wholly restricted to pre-World War II dwellings while the more modern post-war, ranch style residences sustained little or no damage.

#### FIELD PROCEDURES

During the period of mid May to late June 1983, an investigation of the nature and extent of structural damage to single family dwellings in Coalinga was carried out. For each of the 141 homes for which a sense of measureable displacement could be determined, a site report was prepared recording location and orientation of the dwelling, the nature of foundation and construction materials, and the magnitude and direction of building displacement. Displacement was measured using a brunton compass and meter stick, and most commonly taking one corner of the exposed foundation or concrete steps as a reference point in determining the compass direction and distance to the corresponding displaced corner of the dwelling (See Plate 4).

Although we attempted to collect data from as large a number of damaged homes as possible, several factors determined whether a sense of displacement could be unequivocally determined. For those houses deemed measureable, the structure was offset laterally as a unit for distances generally related to the height of support posts and reaching as much as 95 cm. However, for certain sites, measurements were not possible owing to a number of factors. In some cases, damage was so extensive that the structure had totally collapsed and no reference points could be used for measurement. Others, only moderately damaged, had in many instances been repaired and placed back on their original foundations before measurements could be taken. At a small number of sites, no unique sense of movement could be determined

since the building either had rotated or had moved in several discrete sections independently. Finally, by the time of our later visits in June, many of the homes which were severely damaged had already been levelled so that new construction could begin on the site.

### BUILDING DISPLACEMENT

As shown in the shaded portions of Figure 1, the principal areas of measureable building displacement and damage occurred in four general regions of Coalinga. These were the town center with 49 sites, west side with 36 sites, south side with 36 sites, and east side with 20 sites. Our survey of dwellings clearly showed the relationship between foundation design and severity of damage, which in turn, generally correlated with location in pre-World War II subdivisions.

Modern homes suffered only superficial damage and were liveable immediately after the earthquake. They were built utilizing concrete perimeter foundations with floor joists securely bolted to the sill and concrete base.

The older (pre-1941) homes, on the other hand, were often constructed without concrete footings although some had a perimeter of cinder blocks. The most common design was to "toe nail" the floor joists onto vertical wooden 4 inch by 4 inch posts measuring between 12 and 24 inches in length. These posts (termed cripples) typically rested directly on the ground or on wooden beams. The main purpose of the posts was to lift the dwelling above the ground to provide ventilation and crawl space. The most extensive damage to structures was found in those homes with post supports. They lacked the diagonal bracing necessary to withstand the strong lateral ground motion that occurred in the Coalinga earthquake.

The data collected on displacement of damaged dwellings is presented as a series of rose diagrams representing the residential areas of the town where damage was concentrated (See Figure 2). The information is presented in separate diagrams so as to determine if distinct areas of the city might have significantly different ground motion, and also to determine if the sense of movement might correlate in some manner with orientation of the houses. As can be seen from Figure 1, streets within the original town of Coalinga are oriented NW-SE and NE-SW, while in the surrounding subdivisions they are oriented N-S and E-W. Comparison of the four rose diagrams in Figure 2, indicates that throughout the area of damage and independent of orientation of the house, the sense of displacement is predominantly towards the southeast.

### INTERPRETATION OF DISPLACEMENT

As pointed out by Richter (1958), uniform patterns of structural displacement such as were observed at Long Beach in 1933 and at Coalinga in this study were at one time considered to give a sense of mass motion of large crustal blocks during earthquakes. Richter (1958) goes on to indicate that strong motion in one prevailing direction was later recognized as an effect of wave propagation and "probably refers to a large group of waves of relatively short duration as compared to the entire earthquake

disturbance; generally these appear to be transverse waves." Because the damaged dwellings surveyed were designed to withstand vertical loads but lacked the bracing necessary to offset strong lateral forces, the building displacement appears to reflect the horizontal component of strong ground motion experienced in the affected region. The fact that displacement was so strongly concentrated towards the southeast sector (see Figure 2) with southeast offsets observed for 78% of the houses studied in detail, suggests that damage was due to a strong pulse of ground movement to the northwest. The observation that only 3% were displaced in the opposite direction towards the northwest further suggests a predominant northwest pulse of ground motion rather than a symmetric back and forth oscillation.

### CONCLUSIONS

Our study indicated a prevailing southeast displacement of wood frame dwellings in residential areas of Coalinga, with 78% of the buildings displaced toward the southeast sector and only 3% in the opposite direction, toward the northwest. The same southeastward pattern occurred in each of the four areas of Coalinga where damage was concentrated, demonstrating geographic uniformity throughout the area investigated and suggesting a strong northwestward pulse to the ground motion. In the much larger 1906 San Francisco earthquake, local consistent directionality of building displacement was recognized, but a prevailing pattern was not maintained throughout the wide area of damage (Lawson et al, 1908). The uniformity observed in Coalinga may be due to the moderate magnitude of the quake, the relatively small area of significant damage and the uniform geological setting on Quaternary alluvium. Wherever such consistent patterns of at least local extent can be identified, the study of displacement distributions can potentially offer useful information on local ground motion, supplementing that provided by strong motion instruments.

### ACKNOWLEDGMENTS

A number of students assisted in the field portion of our study and we wish to particularly acknowledge their contribution. They are Dani Renan, Gareth Sullivan, Chris Alger, Heidi Greifeld, Christine Hannahs, Kathleen Isaacson, June Jones, and Nevin Miller. We also wish to thank Dr. Robert Nason of the United States Geological Survey for his review of the manuscript and for his numerous helpful comments. In addition, we wish to thank the following officials of the City of Coalinga who helped to facilitate our investigation: Alan Jacobsen, Director of Public Works; James Henry, Chief of Police; Gloria Sprague, Department of Recreation; and Virginia Hansen, Chamber of Commerce. Finally in preparation of the final manuscript we are most grateful for the assistance of Sally Snyder for typing, Leta Blome for drafting, and Richard Simpson for photography.

### REFERENCES

- Cloud, W. K. et al, 1970, The Santa Rosa Earthquake of October, 1969: Mineral Information Service, California Division of Mines and Geology, v. 23, no. 3, p. 43-62.



- Eaton, J., 1983, Seismic setting, location and focal mechanism: in Borchardt, R. D. (Compiler). The Coalinga Earthquake sequence commencing May 2, 1983. U.S. Geol. Survey open-file report 83-511, p. 20-26.
- Lawson, A. C. et al, 1908, The California Earthquake of April 18, 1906: Carnegie Institution of Washington, 2 volumes and atlas.
- Maley, R. et al, 1983, Analog strong-motion data and processing main event records: in Borchardt, R. D. (Compiler). The Coalinga Earthquake sequence commencing May 2, 1983. U.S. Geol. Survey open-file report 83-511, p. 38-60.
- Richter, C. F., 1958, Elementary Seismology: San Francisco and London, W. H. Freeman and Co., 768 p.

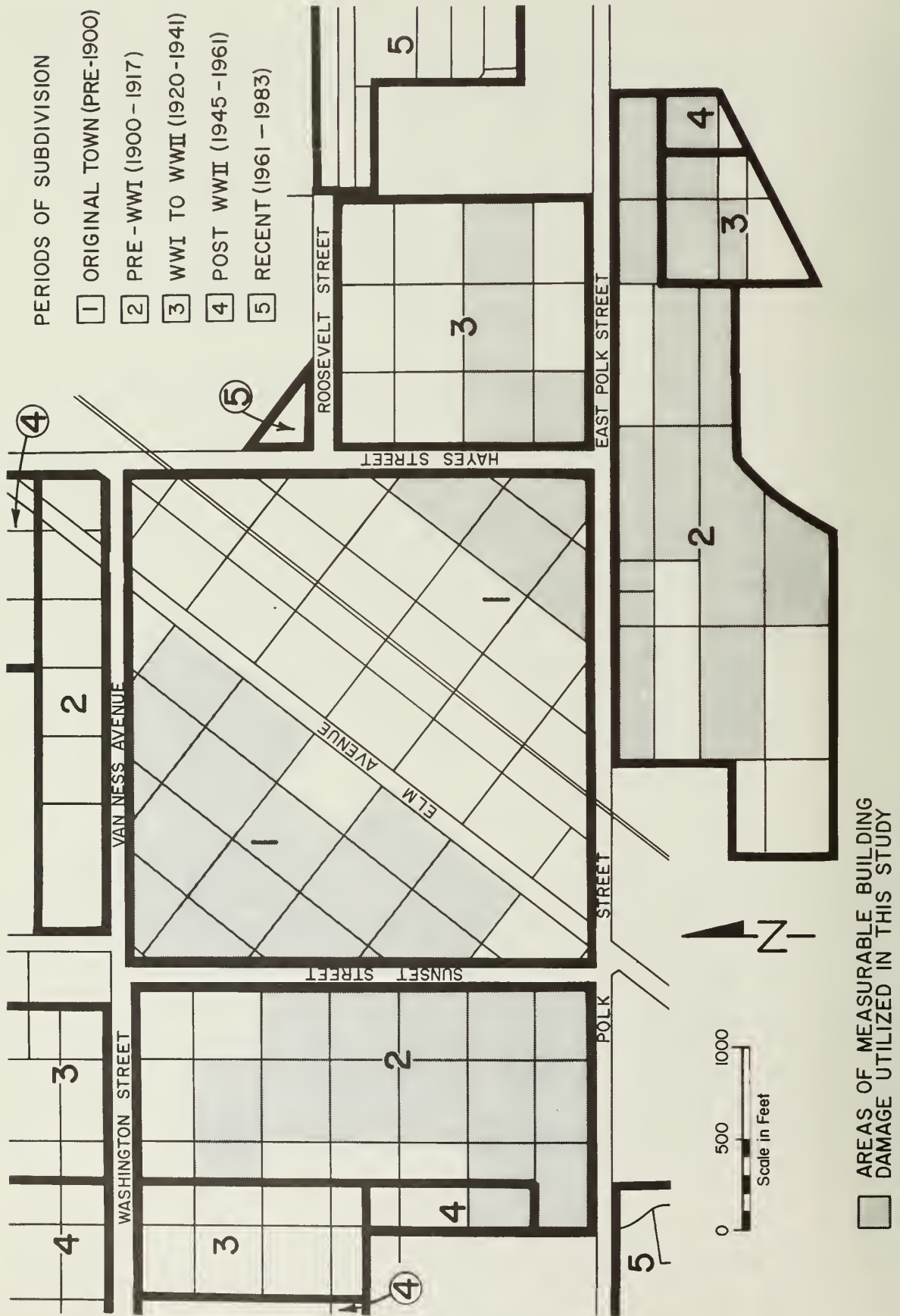


Figure 1 Map of central Coalinga showing periods of subdivision and locations of measurable building damage-

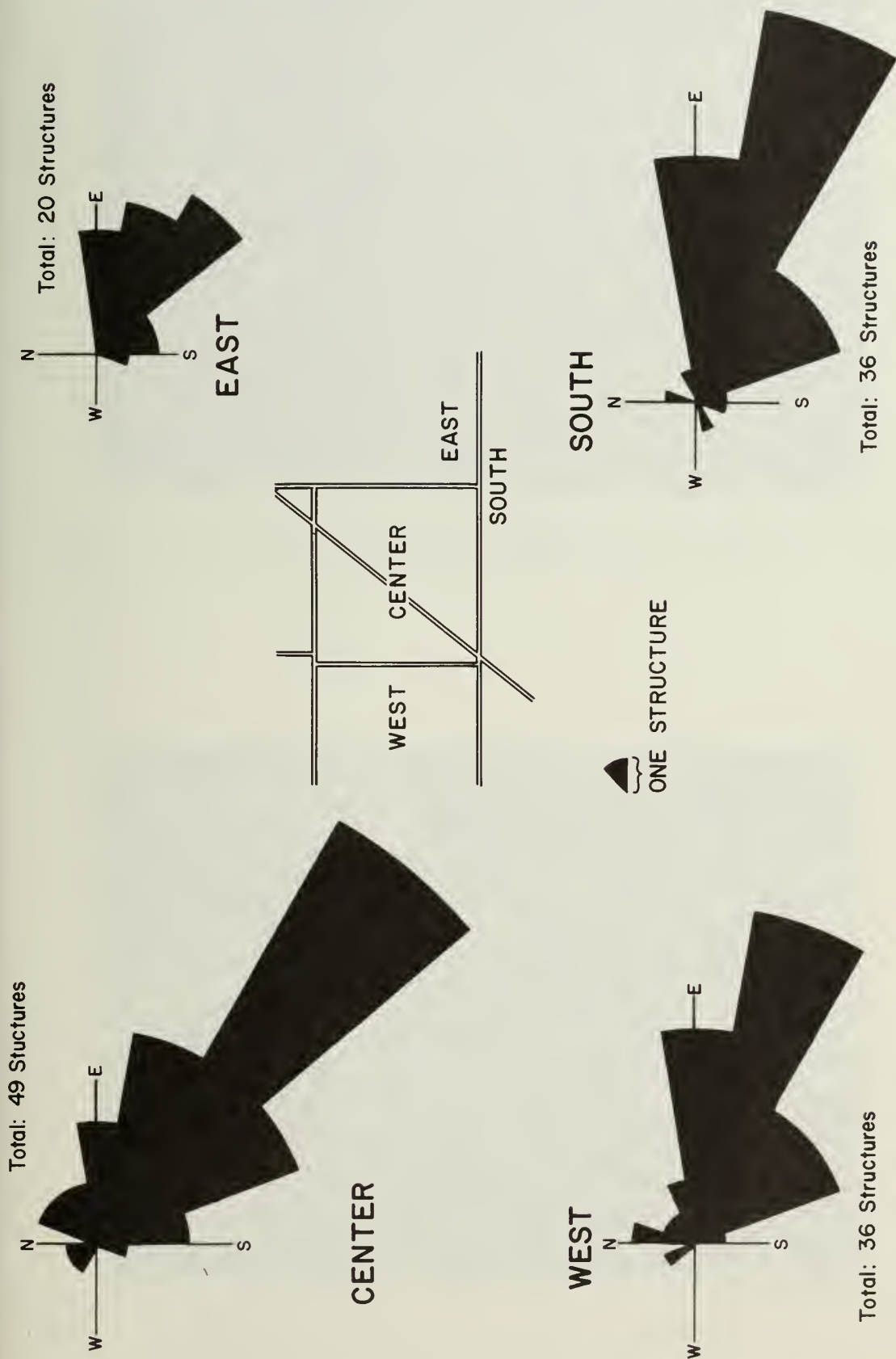


Figure 2 Outline of map of central Coalinga with rose diagrams depicting directions of building displacements for four major residential areas of the city.



Plate 1 Displacement and extensive damage occurred when wood frame structures were inadequately secured to their foundations.



Plate 2 Displacement of wood frame structure accentuated by collapse of cripple posts.

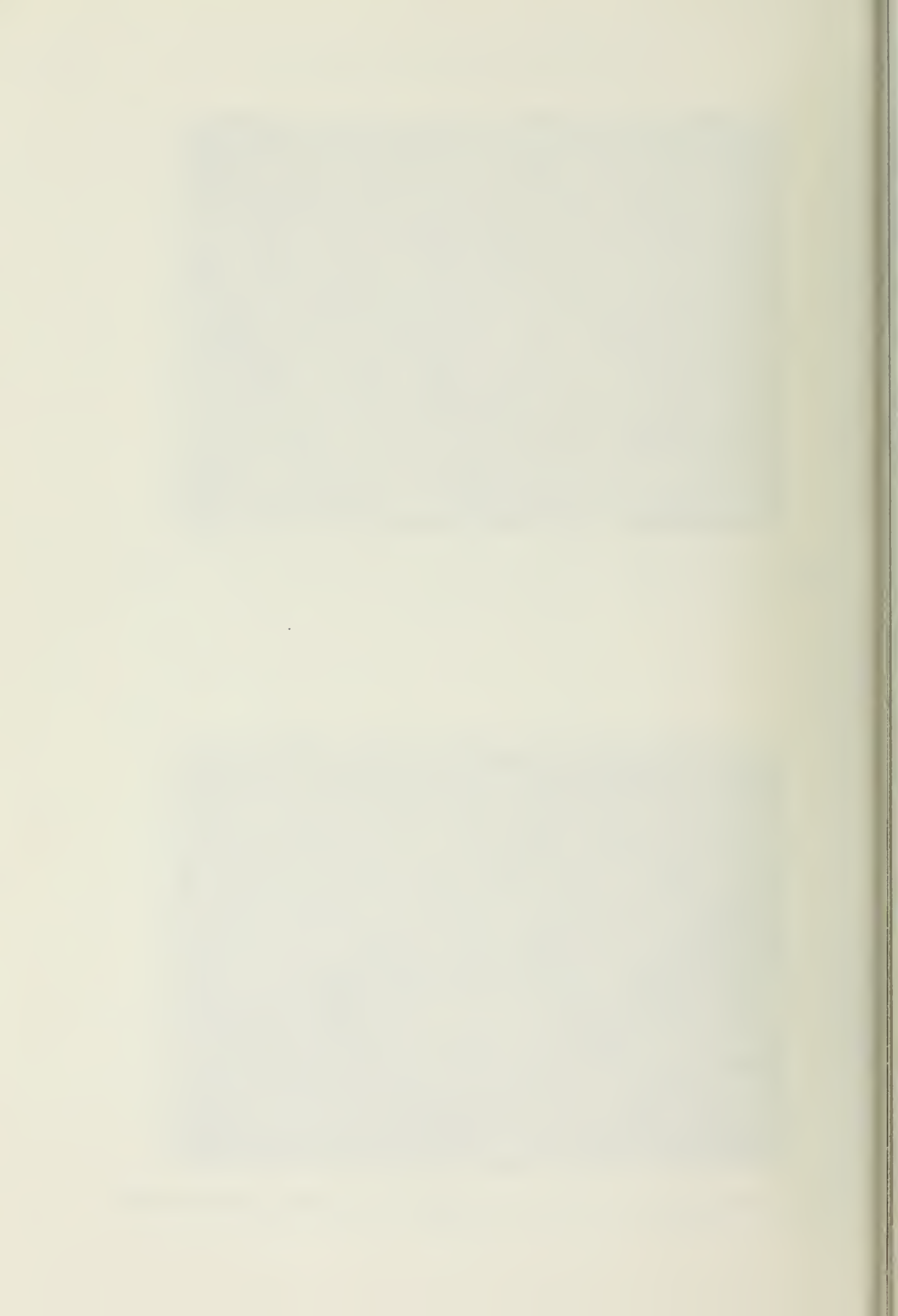




Plate 3 Lateral displacement of dwelling indicated by relative offset of structure from concrete steps.



Plate 4 Magnitude and direction of offset indicated by displacement of corresponding structural elements.



# OBSERVATIONS ON THE STRUCTURAL DAMAGE CAUSED BY THE COALINGA EARTHQUAKE OF MAY 2, 1983

by

Chris D. Poland<sup>1</sup>, John F. Silva<sup>2</sup>, and James O. Malley<sup>2</sup>

## ABSTRACT

A series of photographs of the structural damage which resulted from the Coalinga Earthquake of May 2, 1983 are presented. The performance of building types typical to this region is discussed. The damage to three sites outside the City limits are included. Conclusions concerning the expected performance of buildings with different construction methods are listed.

## INTRODUCTION

The major earthquake which shook central California on the afternoon of May 2, 1983 caused severe structural damage in the town of Coalinga. In the next ten days, H.J. Degenkolb Associates sent a total of fourteen engineers to gather information on the performance of the structures in the area. The buildings inspected included structures which suffered both minor and major damage. By inspecting the performance of all building types in the area, some general conclusions regarding their seismic resistance could be drawn. This paper includes some of the observations and photographs collected during these inspections of the damaged area. More complete documentation of these observations is given in Reference 1.

## OBSERVATIONS ON THE EXTENT OF DAMAGE

### Damage in the Town of Coalinga

Damage to buildings and structures was limited primarily to Coalinga and the surrounding vicinity. Figure 1 shows an aerial view of Coalinga. The towns of Huron and Avenal, located to the east and south of the epicentral region, respectively, showed little or no signs of earthquake damage following the main shock. The lack of damage in Huron is somewhat puzzling in light of its proximity to the epicenter. The downtown construction in Huron is similar to that in Coalinga.

<sup>1</sup>Principal, H.J. Degenkolb Associates, Engineers, San Francisco, California

<sup>2</sup>Structural Designer, H.J. Degenkolb Associates, Engineers, San Francisco, California

Figure 2 shows that the heavy damage in Coalinga was centered in the downtown district, as well as in the older residential areas to the east and north. The downtown buildings most severely affected were those of unreinforced masonry construction. Figure 3 through 7 depict some of the damage suffered by this type of construction. Houses in the residential areas suffered damage primarily as a result of inadequate bracing of timber foundation walls and/or lack of bolting of the houses to their concrete foundations, as shown in Figures 8 through 13.

Buildings of reinforced concrete and reinforced masonry construction performed well, as shown in Figures 14 and 15. Some of these structures date from the 1930s and 1940s, when most design codes did not recognize the existence of seismic forces. Their exceptional performance may in part be attributed to large member sizes which arose from the less sophisticated design procedures available at that time, resulting in inherent strengths which are not generally accounted for. It should also be recognized, however, that the earthquake of May 2, 1983 apparently did not produce the intensity of shaking which is postulated for this area. An earthquake with similar maximum acceleration but of higher intensity and longer duration could well have produced more serious damage in many of the structures examined.

Also of note is the performance of the light metal industrial buildings, such as those shown in Figures 16 and 17, which on the average behaved quite well. Some doubt has been cast, however, on the effectiveness of using rod bracing to resist longitudinal lateral forces. In some of the buildings we examined, the relatively low stiffness of these braces did not allow them to carry any load until the building sheathing had failed or fallen off. Again, shaking of greater intensity could have produced more serious results in these structures.

Only slight damage was suffered by buildings constructed since the adoption of design codes which consider seismic forces. This damage was generally limited to non-structural components such as windows and lighting fixtures, as shown in Figures 18 and 19.

#### Damage to Structures Outside of Coalinga

Although the majority of structures in the epicentral region are in the town of Coalinga, three sites in outlying regions provided some interesting information. These sites were: 1) PG&E Substation No. 2, 2) Coalinga Feed Lot, and 3) Pleasant Valley Pump Station.

PG&E Substation No. 2, located on Highway 33/198, is located about 3.2 miles west of the earthquake epicenter, and 7 miles from downtown Coalinga. The two buildings at the substation, one constructed of unreinforced block and the other of poured reinforced concrete, were erected in 1920 and 1926, respectively. The small concrete block control building was left in a state of near collapse after the main shock due to the disintegration of the end walls and the collapse of some of the interior pilasters. The original plans identify the masonry used for this structure as "interlocking cement brick". Cracking along the top of the longitudinal walls indicates that the



building attempted to resist the transverse lateral forces with frame action after the loss of the end walls. Figures 20 and 21 show these two structures, while Figure 22 depicts one of the large transformers at the substation.

The Coalinga Feed Lot is a collection of small buildings and large equipment located approximately five miles west of the epicenter. The Feed Lot's small two-story reinforced masonry office structure suffered substantial damage during the main shock, as did many of the owner-built equipment support structures. Figures 23 and 24 show some of the damage which occurred at the Feed Lot.

Figure 25 shows an aerial view of the Pleasant Valley Pumping Plant. Part of the California Aqueduct System, this station is located 4-1/2 miles north of the epicenter. It is here that strong motion instruments operated by the U.S. Bureau of Reclamation recorded peak accelerations as high as 0.54 g. The tall object in the upper center of the photo is a Surge Tower between the Pumping Station and the Aqueduct.

The pumping station is a rigid steel frame structure with brick infill walls, divided by an expansion joint at mid-length. The Plant Engineers reported that several of the ceiling lighting fixtures had collapsed and that 24 of the crane rail bolts for the 20-ton bridge crane were sheared. The crane itself had double flange wheels. No other damage was found in the structure. The expansion joint was reported to open and close with each aftershock, at times as much as 1 inch. Figure 26 shows one of the large transformers at the pumping plant.

The 100 foot Surge Tower was designed to accept pressure surges resulting from pump shut-downs. It is anchored to a concrete base with 1-1/2 inch diameter J-bolts embedded 5-1/2 feet into concrete. After the main shock, all of these bolts around the 26 foot circumference were found to have been equally stretched about 1-1/2 inches.

## CONCLUSION

The damage which resulted from the Coalinga Earthquake of May 2, 1983, reinforced Engineers' beliefs in the susceptibility of unreinforced masonry construction to seismic forces. The damage suffered by residential construction which did not provide for shear transfer below the floor level was also predictable. The good performance of reinforced masonry and reinforced concrete construction which predate seismic code provisions, such as the Coalinga High School Buildings, probably resulted from both conservative designs and the moderate intensity of shaking. The metal industrial buildings also performed well, in part due to their light mass.

The excellent behavior of new construction in Coalinga is encouraging and, hopefully, indicates that modern Building Codes are properly addressing the effects of earthquakes. However, while the level of strong ground motion experienced in Coalinga and the surrounding area may be as strong as expected, the duration of the earthquake and frequency content of the shaking were not the worst that can be expected for that area. It is expected that Coalinga, as with the rest of California, could be shaken much more intensely, most likely leading to significant damage to modern structures. Structural Engineers should design buildings with this higher intensity shaking in mind and expect that during such an earthquake, their structures will experience moderate damage to the architectural elements and finishes and minor damage to the structural elements.

#### ACKNOWLEDGMENTS

The members of H.J. Degenkolb Associates, Engineers, who investigated the structural damage resulting from the Coalinga Earthquake included Associates R. Gordon Dean, Loring A. Wyllie, Jr., and Chris D. Poland, and Engineers David R. Bonneville, Robert A. Bruce, Gail A. Cedillos, David W. Cocke, John A. Dal Pino, Richard J. Love, James O. Malley, Roy J. Moreno, Jr., Cristian M. Rodriguez, John F. Silva and Maryann T. Wagner. Dianne Quirley typed the manuscript and Wess-John Murdough aided in the preparation and presentation of the report.

#### REFERENCES

H.J. Degenkolb Associates, Engineers, "Report on Observations, Earthquake of May 2, 1983, Coalinga, California", May 1983.



Figure 1. Aerial view of Coalinga, looking southwest. From left to right, Second, Third, Fourth, Fifth, and Sixth Streets.

## COALINGA EARTHQUAKE DAMAGE MAP

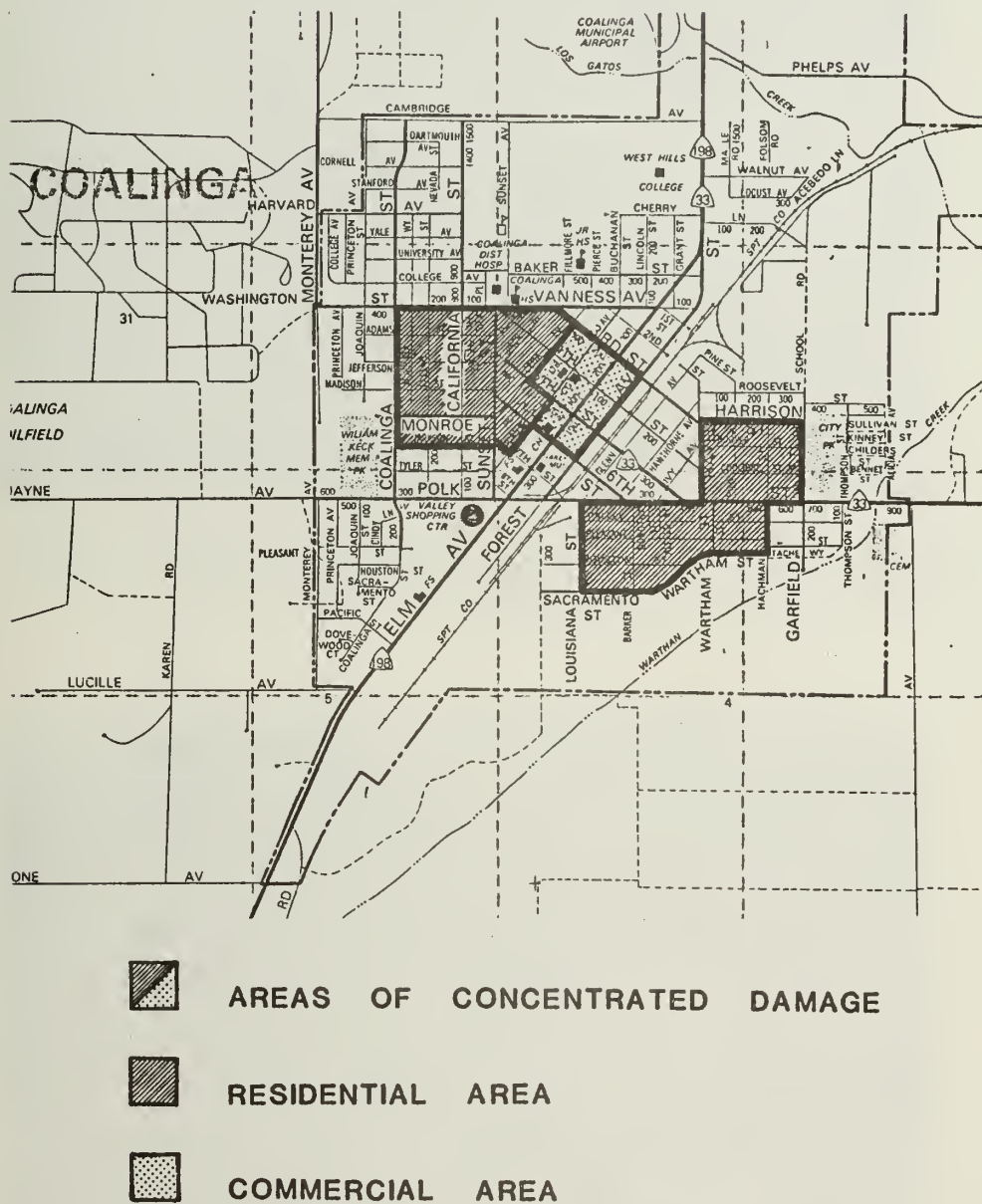


Figure 2: Map of Coalinga, California

Reproduced with permission granted by Thomas Bros Maps. This map is copyrighted by Thomas Bros Maps. It is unlawful to copy all or any part thereof, whether for personal use or resale, without permission.





Figure 3. Fifth Street. Note damaged and fallen parapets, missing lamp, collapsed structure, center left.



Figure 4. Close-up of damage on Fifth Street. Note ceiling joists at top of picture are being supported by the ceiling board.



Figure 5. Commercial structures on Forest Avenue. Inadequate tying at the roof diaphragm of masonry walls parallel to the roof trusses resulted in the collapse of the walls.



Figure 6. Forest Avenue. Note loss of masonry parapet, leaving roof joists unsupported.



Figure 7. State Theatre. This much-publicized structure of unreinforced masonry construction suffered some of the most spectacular damage in the downtown area.



Figure 8. The most common cause of severe damage to residences in Coalinga was inadequate provision for shear transfer below the floor level. Shown here is a failure of the crawl space walls, which were clad with clapboard sheathing. Many of these homes were moved to Coalinga from the oil fields during the 1950s, and at that time were set on 18" cripple stud walls which were build on, but generally not anchored to, a concrete perimeter foundation.





Figure 9. Jack post construction typical of the older wood houses in Coalinga.



Figure 10. Another home which has moved off its foundation. Damage of this kind did not occur in homes where plywood replaced or covered the clapboard sheathing.



Figure 11. This otherwise undamaged residence has moved completely off of its cripple walls, as evidenced by the position of the porch steps.



Figure 12. Collapse of wooden porch awnings demonstrates importance of proper anchorage and lateral support of such building appendages.



Figure 13. Unreinforced block masonry and poor anchorage of the walls to the diaphragms combined for disastrous results in this house on Monroe Street. A family of five escaped the wreckage unhurt.



Figure 14. Coalinga High School. Heavy cast-in-place concrete construction. This building, with a date of 1930 cast over the door, suffered virtually no damage. The success of these buildings, designed with Codes which did not recognize earthquake forces, can be attributed to the inherent strength of cast-in-place concrete shear wall buildings and the attention of the Design Engineer to proper detailing.





Figure 15. Public Library. Damage to this structure, build in 1955, was apparently limited to non-structural components - ceiling lighting fixtures dropped to the floor and books were displaced.



Figure 16. Light metal industrial building with transite panels on the south end of town. The lack of a longitudinal bracing system and the weight of the heavy transite panels resulted in substantial swaying of this structure and the subsequent loss of most of the panels on the longitudinal walls.



Figure 17. Light metal industrial building on Forest Avenue. When clad with sheathing, these structures generally performed well. This garage, however, was built against, but not anchored to a concrete wall on the left side. Several of the rod braces provided for lateral resistance along this wall were broken or buckled in the earthquake.



Figure 18. Guarantee Savings. Roughly 50% of the window glass in this building was shattered. Other damage was to ceiling panels and exterior plaster. Safe deposit boxes, stacked in the vault, overturned as well.



Figure 19. Clocktower, downtown Coalinga across from Guarantee Savings. This top-heavy structure was not adequately anchored against overturning. As a result, two of the four anchor bolts at the base broke, apparently in tension, leaving the tower free-standing on its concrete pedestal.





Figure 20. The two buildings at PG&E Substation No. 2.



Figure 21. Major damage suffered by the unreinforced block building.



Figure 22. These 70 KVA transformers at the PG&E Sugstation No. 2 each weigh 45,000 pounds. They were secured laterally by snubbers which were welded to the support skids and anchored to the concrete by means of what appeared to be 2 - 5/8" sleeve anchors. All of the welds connecting the snubbers to the skids were found to have sheared after the main shock and, in several cases, the concrete anchors were broken at the bolt, or pulled from the concrete.



Figure 23. Coalinga Feed Lot. Home-built support structures for grain bins bent predictably about weak direction of columns where the X-bracing terminates.



Figure 24. Coalinga Feed Lot. This tank showed evidence of considerable sliding on its pedestal.





Figure 25. Pleasant Valley Pumping Plant

Figure 26. The 70 KVA transformers at the Pleasant Valley Pumping Plant were anchored each with 4 - 1" diameter bolts which projected about 3 inches from the baseplate to the top flanges of the support skids. These connections failed by shearing the bolt or by loosening the baseplate, which is presumably welded to some type of concrete anchor(s).





# PERFORMANCE OF THE PUBLIC SCHOOL BUILDINGS TO THE 1983 COALINGA, CALIFORNIA EARTHQUAKE

by

John F. Meehan

## ABSTRACT

Public school buildings constructed under the provisions of the Field Act performed quite well during these earthquakes. Buildings on school sites which were not constructed under the provisions of the Field Act partially collapsed or were heavily damaged. Current code provisions are justified.

## INTRODUCTION

The 6.7 M main shock of the Coalinga earthquake swarm occurred at 4:42 p.m. PST on Monday, May 2, 1983. A team of four structural engineers from the Structural Safety Section of the Office of the State Architect (SSS/OSA) at the request of and with representatives of the Office of Emergency Services departed from Sacramento by National Guard helicopters at first light in the morning hours of the following day. In Coalinga, teams were formed with representatives of the U.S. Corps of Engineers to make rapid estimates of damage to public schools, gas, water and sewer systems, city hall, fire station, hospital and city, county and state corporation yards. These and other damage estimates were used in the determination of the state of disaster by the governor and the president.

Also during the same day, May 3, telephone contacts were made with the public schools in Kettleman City, Avenal, Huron, Stratford, Lemoore, Riverdale, Five Points and Cantua Creek who reported no damage to the school buildings (See Figure 1). Also telephone contacts were made in Fresno, San Benito and Monterey County school districts as well as those in towns along Highway 101.

In the days that followed, upon request of the local public school districts, SSS/OSA representatives visited schools to determine their performance in Coalinga, Kettleman City, Avenal, Priest Valley, King City, Greenfield, Chular and Hollister. Schools in Cantua Creek and Huron were also visited. Casual review reports were prepared for the sites visited which describe the apparent or surficial damage observed. Detailed investigations of the buildings were not performed. The casual review reports were provided to the school districts who then, if necessary, employed the services of architects and structural engineers to complete the investigation and to determine the method of repair or correction. Where the damage produced a serious or critical hazard, the school districts were so advised and recommendations given on whether the buildings should be occupied or vacated.

<sup>1</sup>Principal Structural Engineer, Research Director, Structural Safety Section, Office of the State Architect, Department of General Services

The statutes, in Sections 39140 and 81130 of the Education Code requires all reconstruction, alterations or additions to existing buildings exceeding \$20,000 in cost and all new public school building construction must conform to all of the provisions of the Field Act. That is, the Field Act requires that drawings and calculations must be prepared by an architect or structural engineer, a geologic report, fee and application must be filed for approval by the SSS/OSA. Plans are reviewed by SSS/OSA for conformance with the requirements of Title 24, California Administrative Code. The construction must be inspected and verified reports indicating that the construction met the requirements of the approved construction documents must be filed by the inspector, contractor, architect and engineers. Persons filing false reports or violates any of its provisions are guilty of a felony.

Section 39143 and 81133 of the Education Code requires that when the construction costs between \$10,000 and \$20,000 a structural engineer must examine the proposed alteration or addition project and determine if it is structural or nonstructural. If he determines that the project is a nonstructural alteration, he shall prepare a statement so indicating. If he determines that the project is structural, he shall prepare drawings and specifications for the project and shall observe the work of construction. A copy of the engineer's report stating that the work does or does not affect structural elements, or a copy of the drawings and specifications for structural work, as the case may be, shall be filed with the SSS/OSA. The Field Act is given in Sections 39140-39156 and 81146-81162, Education Code.

As of this writing, drawings for the repair or correction work are being prepared by architects or structural engineers for review by SSS/OSA. Work is also underway and some work is complete.

#### Strong Motion Acceleration Records

Others will report upon the strong motion earthquake records; however, a few points will be discussed here. The epicenter of the main 6.7 M shock is shown in Figure 1. An accelerometer located at the ground surface in the switchyard of the Pleasant Valley Pumping Station recorded a peak acceleration of 0.54g. Coalinga is located a little more than equidistant from the epicenter. Based only upon epicentral distance and not considering the influence of fault propagation, radiation pattern upon peak acceleration, nor special site conditions it could be suggested that the ground acceleration in Coalinga could have been in the range of .4g to .5g. Similarly, an accelerometer recorded a peak acceleration of 0.29g at Cantua Creek School in Cantua Creek which could suggest a ground acceleration in the range of 0.2g for Avenal and Kettleman City. No damage was found in the schools in Cantua Creek, Avenal or Kettleman City which could be attributed to the earthquake. (1 and 2) The peak acceleration recorded July 25, 1983 at the California Highway Patrol Office in Coalinga, shown in Figure 2, was 0.61 g.

#### Observed Performance of the Public School Buildings

The following highlights the performance of the public school buildings. (See Figures 1 and 2 for location of school sites.)

### Oil King School, Oilfields

This school, shown in Photo 1, is located at the intersection of Highway 33 and 198 and is the closest school site to the epicenter; the epicentral distance is about 3 miles. A number of years ago the site contained classroom buildings, kindergarten and an administration building but only the multipurpose building currently remains. The site is no longer used as a public school. Other buildings were sold and moved.

This multipurpose building has a plywood roof diaphragm supported by wood joists bearing on bent steel beams. The lateral load is resisted by plywood shear walls. There was no apparent structural damage at this site. A pier in the west exterior wall, providing architectural treatment, had some damage at the sill and a few ceramic tiles were displaced. Because of its stiffness, this wall tried to act as a shear wall but having no tie downs rotated in the plane of the wall at the bottom and thus damaged the tile. All other shear walls had tie downs at each end. Other damage consisted of a broken window and a few fallen accoustical tiles.

### Coalinga District Administration Building, Coalinga

This one story building was designed in 1958. The roof is framed with plywood over wood joists and steel beams. The lateral loads are resisted by concrete block walls. A concrete block was slightly cracked where a roof beam delivered lateral load to the top of a concrete block shear wall.

Several ceiling grid panels were displaced. The top of a non-bearing concrete block wall, added after the completion of the building, showed evidence of displacement.

### Cheney Kindergarten, Coalinga

No structural damage was observed to this building designed in 1948. There was some slight plaster cracks in the classroom ceilings. Several ceramic tiles fell off the toilet room walls and some mechanical equipment shifted.

A small concrete block toilet and storage building was constructed at this site; however, it was not constructed under the provisions of the Field Act. This building, shown in Photo No. 2, sustained considerable damage and was subsequently demolished.

It was reported that the fireplace chimneys separated about an inch from the framing at the roof and ceiling following the July 25, 1983 aftershock. The existing nominal connections will be revised to provide for the full tributary lateral load.

### Bishop Elementary, Coalinga

The buildings on this site were designed in 1958. There are three classroom buildings, an administration building and a cafeteria building. The roof is



plywood sheathing supported by wood joists supported by steel beams and reinforced concrete block walls.

There was light cracking in the concrete block walls where the roof beams, which span over openings in the exterior walls, bear on the concrete block walls. There was also some ceiling damage. It was recommended that the cracks at the ends of the reinforced concrete block wall sections be investigated to determine the extent of the damage and that the ceiling be repaired by modifying its connection. When the block wall was opened it was observed that the required hairpin reinforcing around the beam anchor bolts was not installed. It was later reported that the top horizontal reinforcing bar which functioned as the drag tie in these shear walls was not installed as shown on the plans. These conditions are being corrected.

#### Dawson Elementary School, Coalinga

This site contains eight classroom wings, an administration building, library and learning center. Four of the classroom wings, the administration building and the learning center were designed in 1940, two classroom wings were designed in 1945, and two classroom wings were designed in 1950.

The administration building and all classroom wings, except the north wings have wood truss rafters supporting diagonal sheathing, wood framed floor, and the exterior walls are concrete. The lateral loads are resisted by the exterior reinforced concrete walls which are cantilevered out of the foundation in the longitudinal direction. In the transverse direction, the reinforced concrete classroom wall, corridor floor slab and exterior corridor footing form an "L" frame which resists the lateral load. The north wings are constructed of wood frame construction. The exterior walls are wood studs with diagonal sheathing and reinforced concrete columns. The lateral loads are resisted by the diagonal wall sheathing and the reinforced concrete columns which are cantilevered from the foundations.

The learning center is framed with rod braced timber and rod trusses supporting wood joists and diagonal sheathing. The exterior walls are of reinforced concrete. The floors are wood framed. The lateral load is resisted by the roof rod bracing, diagonal sheathing and reinforced concrete walls.

The library roof consists of wood joists and diagonal sheathing supported by steel rigid frames. The exterior walls are wood studs covered with diagonal sheathing. The roof lateral load is resisted by the diagonal sheathing and rod bracing, and the diagonal sheathing and rigid frames resist the lateral loads in the vertical plane.

Damage at this site consisted of minor cracking in the plaster at the exterior and interior walls of the classroom wings and library. A few window panes were broken or cracked. Several roof mounted ventilating units were tilted, a few roof tiles were displaced and ceiling tile fell. There were some horizontal and diagonal plaster cracks in the library walls. Four rows of light fixtures fell in the library. At the west end of the north classroom wing there appears to be about 4 inches of settlement in the building but no distress to the building was observed. In the classroom number 3



a piece of ceiling plaster about 5 feet in diameter separated from the base coat and fell.

It was recommended that the above indicated repairs be made and that the settlement of the west end of the north classroom be investigated.

#### Sunset Elementary School, Coalinga

The facilities at this site consist of three classroom wings, administration office, auditorium, recreation and restrooms designed in 1938. Another classroom wing was added in 1940. The cafeteria was designed in 1949.

The classroom wings and administration office had wood roof framing with diagonal sheathing. Interior walls were non-bearing. Exterior walls were reinforced concrete cantilevered from the foundation and provided the lateral force resistance in both directions. The auditorium roof was diagonally sheathed on wood framing on steel trusses supported by reinforced concrete columns and walls. The reinforced concrete walls and columns provided the lateral force resistance in this building. The recreation building roof was laterally supported by rod braced steel rigid frames. The lateral load was resisted by the frames and by the rod bracing delivering the loads to the concrete walls. The cafeteria roof was supported by steel trusses over the main room and steel beams over the adjoining rooms supporting wood joists and diagonal sheathing. The walls were of reinforced concrete. The lateral load resistance was provided by the concrete walls and columns.

There was no structural damage at this site. A few accoustical tile fell, plaster was cracked in several locations and a few panes of window glass were broken. The water heater was not anchored and moved damaging the piping. It was recommended that these items be repaired.

The cafeteria building was used by the Red Cross after the earthquake to provide meals to the local people and visitors.

#### Coalinga Junior High School, Coalinga

The main portion of these buildings, i.e. three classroom wings, administration, cafeteria and library, were designed in 1951 and the construction was completed in 1953. Another classroom wing was added in 1956.

Library. The library roof was sheathed with diagonal sheathing supported by wood joists on steel joists. The lateral loads in the north-south direction are resisted by sheathed east and west end walls and in the east-west direction the lateral load was resisted by two steel frames cantilevered from the concrete window sill in the south wall. No lateral bracing was provided in the north wall.

Several large panes of glass, mounted in metal frames, were fractured on the north and south walls of the library as shown in Photo 3. Most of the glass fell inside the library within five to ten feet of the window. However, glass fragments were found throughout the 40 foot wide room. This building

had a considerable amount of torsion because all of the east-west horizontal force was resisted by two steel frames located on the south wall.

As indicated above, this library building was designed in 1951. At that time, Title 21, CAC, the code under which public school buildings were constructed, contained no regulations relative to drift or the installation of glass. These subjects are now covered in the current regulations which should reduce this hazard.

Classroom wings. The roof framing of the classroom wings consisted of diagonal sheathing supported by wood joists on steel joists. Lateral loads were resisted by diagonal sheathing or plywood on the roof and walls. No structural damage was observed. Glass diffusers, used in the light fixtures, fell to the floor and broke. Hot water tanks shifted and fractured some of the piping. The tanks were not anchored or braced. Several unanchored evaporative coolers on the roof were displaced.

Administration. A reinforced concrete vault was installed in the administration area. Plaster cracks occurred around this very rigid building element.

SSS/OSA recommended that the school district employ a structural engineer to review and develop a lateral force resisting system in the library capable of meeting current code requirements. This was done and he recommended adding steel rod cross bracing in the north and south walls. SSS/OSA also recommended that the glass light fixture diffusers be replaced with a fastened plastic diffuser and all equipment be anchored to current code requirements.

#### Coalinga High School, Coalinga

Auditorium. This rather large (112' x 152') auditorium building, built in 1939, includes a full stage and balcony. It has a concrete roof supported on 7' to 9' deep steel trusses bearing on reinforced concrete columns on spread footings. Walls are reinforced concrete. No structural damage was observed.

The ceiling of the auditorium is coffered, i.e. the exterior portion which is about 8 feet wide is about 6 inches lower than the main central portion of the ceiling. The main portion of the ceiling contains large air grilles and ducts. Neither the main portion of the ceiling nor the air handling equipment were braced laterally. The exterior portion of the ceiling is anchored to the exterior concrete walls. The main portion of the ceiling vibrated in its own mode, which was different from the exterior portion. This resulted in damaging and dropping to the floor portions of the decorative plaster of paris vertical closures at the junction of the higher and lower ceiling as shown in Photo 5. At the time this building was constructed there were no specific code requirements for bracing ceilings. Several panes of decorative glass in the skylights over the stairwells fell on the stairways.

SSS/OSA recommended to the school district that a lateral load resistant system of the main ceiling portion be provided and that the decorative skylight glass be replaced with a more competent material. The ceiling was braced to the lower chord of the steel trusses.

Classroom and administration complex. These buildings form a complex which is "H" shaped in plan. The west or science classroom wing and toilet rooms were built in 1934. The east classroom wing and central administration or adjoining portion were built in 1938. The boiler room was existing at the time the buildings were constructed.

The west classroom wing is three stories in height with the ground floor a partial basement. The exterior walls are reinforced concrete. The east classroom wing portion of the first and second floors are of wood frame and corridors are of reinforced concrete supported on concrete walls. The roof is wood framing supported by wood joists spanning between exterior concrete walls and also bearing on wood stud walls at the corridor. The roof has diagonal sheathing walls and square sheathing on the overhangs.

The east classroom wing is two stories. The first floor is a continuation of the 1934 portion. Exterior walls are of reinforced concrete. The first floor in the classroom is wood framing and the corridor is of reinforced concrete floor and walls. The second floor of the classrooms and corridor is of reinforced concrete supported on concrete walls. The roof is wood rafters bearing on the exterior walls and interior framing. The corridor is of reinforced concrete column and beam frames with plaster ceiling. The roof is partially sheathed with diagonal sheathing. The remaining sheathing is straight laid. Clay tile is installed on the exposed sloping portion of the roof.

Some roofing tiles were displaced. Prior to 1937 the Title 21 regulations contained no requirements for anchorage of the roof tile although tile anchorage was required in the specifications for both portions.

In the chemistry laboratory on the third floor, in the west wing, the chemicals fell to the floor and became intermixed causing considerable damage. A special work crew was employed to clean up the chemical spill.

The engineer employed by the school district recommended installing a horizontal plywood diaphragm in the second floor ceiling to stiffen the roof structure in the west wing.

Boiler room. In 1937 an examination was made by the Division of Architecture, now the SSS/OSA, of several existing buildings on the site constructed prior to the enactment of the Field Act in 1933. A portion of one of these old buildings examined was the existing boiler room. This building was reported to be unsafe. The records of the SSS/OSA do not indicate that the boiler room was retrofitted. Therefore, in accordance with Section 39227 of the Education Code, the building should not have been used. Yet it has remained in operation to serve as a boiler room for this school site. The



brick chimney of the boiler room was heavily damaged as shown in Photo 5. The chimney was later demolished and the roof damaged in the process. The boiler room will be retrofitted.

Girls gymnasium shower and locker building. The gymnasium portion was constructed in 1940, and the shower and locker additions were made in 1950 and in 1955. The gymnasium was constructed with steel rigid frames to resist lateral forces in the transverse direction and a horizontal rod bracing system in the plane of the roof beams of the frames to resist lateral forces in the longitudinal direction. Exterior longitudinal and end walls of the gymnasium are of reinforced concrete.

The two tie rods in both end bays became elongated and sagged and one end rod failed. The failure indicated that the rod was defective as evidenced by two small cracks on opposite sides within about an inch of each other. The rod failed through these cracks which contained paint and corrosion. Based on the relative rigidities of the transverse steel frames and the end concrete shear walls it is apparent that the single rods in the end bays were forced to carry the transverse lateral forces intended for the steel rigid frames. When the rods stretched or broke, the frames could then function as intended.

SSS/OSA recommended that the bracing system be investigated and corrected by the district structural engineer or architect. The engineer recommended that sufficient bracing in the end bays be provided to resist the entire transverse load.

Stadium, floodlight poles and press box. The stadium consists of earth berms supporting rows of seating on steel framing and concrete slab. It was constructed in 1950. The floodlight poles are welded square tapered steel plates and were constructed in 1965. The press box has a wood frame floor and superstructure supported on cantilever pipe columns constructed in 1972.

No structural damage was observed. Some cracking in the asphalt paving on top of berm was probably caused by shifting the concrete slab which supports the bleacher seating. Cracks were formed at the toe of the earth berm in the running track indicating that the earth berm shifted. Vertical cross tie rod bracing between the pipe columns was used to resist the longitudinal lateral forces of the press box. Several rods were loose. SSS/OSA recommended that the rods be tightened prior to the next occupancy of the press box.

Boys shower and locker building, home economics building, locker building at swimming pool, music building. There was no structural damage noted in these buildings. There was, however, some nonstructural damage such as overturned casework, some T-bar ceiling damage and the pool filters shifted breaking their pipes. SSS/OSA recommended that this damage be repaired.

Shop building. This shop building was constructed in 1940. This is of one story saw-tooth construction. Roof framing is of wood joists spanning



between steel trusses and braced with the rods. The steel roof trusses bear on reinforced concrete columns. Walls are of reinforced concrete.

In one roof bay a rod clevis was larger than the rod and the rod merely pulled out of the clevis. Exterior plaster was cracked and portions fell to the ground. The roof mounted sawdust collector was damaged and on the verge of collapse. The hook and eye anchor for the electric service came apart dropping the power lines on the roof. Some interior plaster partitions and wall tile were cracked.

Mezzanines were added by the district in the wood shop and auto shop.

SSS/OSA suggested that all tie rod clevises and turnbuckling be investigated for proper size and fit-up. Unapproved mezzanines should be investigated and strengthened as appropriate. The engineer recommended removal of the mezzanines and placement of proper size clevises and rods.

Boys gymnasium. This building was designed in 1953. The main room is about 86' by 110' containing folding bleachers and has ancillary rooms to the east and north. The gabled end walls are eleven inch thick reinforced concrete and from 18' to 26' in height. The side walls have 4' high windows under the eaves the full length of the wall except for an 8' wide pier of 6" thick concrete at each end of the building. The remaining wall below the windows between the columns is also 6" thick concrete. Composition roofing is supported by 3½" thick poured-in-place gypsum. A 24' wide roof skylight extends the full length of the room. The roofing framing consists of 8" deep steel purlins supported by steel rigid frames spaced 18'6" on centers.

The approximately 8' long wall piers, opposite the windows, were cracked in the lower corners extending in a diagonal direction away from the windows as shown in Photo 7.

SSS/OSA recommended to the district that the piers should be investigated by a structural engineer or architect. It was decided to remove the 8' wide pier and replace it with a reinforced concrete wall pier the full 18' width of each end bay.

Agricultural facility. This site, on the east side of Coalinga, contains a classroom and shop building, a portable classroom building and animal feed and shelter barns. The classroom building, shop, feed and shelter barns are steel rigid frame construction. No application or drawings were found for this portable classroom building which sits on wood mud sills.

No structural damage was noted; however, there was some nonstructural damage. Several roof vents were shaken off the roof, the ceiling grid in the hall was displaced, suspended light fixture anchorages were pulled loose and light tubes and diffusers fell to the floor, a leg on an unanchored water heater buckled, and an overhead gas line in the shop broke at a connection.

SSS/OSA recommended to the district that these items be properly anchored and braced per present code requirements.

Maintenance building (former gymnasium building). This building, constructed in 1928, was formerly the gymnasium but was converted to maintenance use after it was examined in 1937 and reported to be unsafe. In 1951 a fire occurred in the building and it was again reviewed. It was again declared unsafe, and further, it was then reported to be a collapse hazard.

Both end spans of the roof framing collapsed to the floor in the earthquake. The end walls remained standing but they were heavily cracked. These free standing, rather high end walls of concrete were in imminent danger of collapse as shown in Photo 6. The district was immediately advised by SSS/OSA to cordon off the area around this building and limit entry. The building has subsequently been demolished.

Storage building. A storage building was located adjacent to the maintenance building. During the early visits, SSS/OSA representatives were advised that the building had been abandoned and was not being used as a school building; therefore, no casual review was made. From the outside of the building it was observed that the wall was displaced with respect to the roof framing. A search of the file later disclosed that the building was originally built as a classroom building and was designed in August 1933 under the then recently enacted provisions of the Field Act. It was architecturally remodeled to a home-making building in 1953. The building was demolished simultaneously with the maintenance building.

#### West Hills College, Coalinga

Speech arts building. This building, designed in 1964, has an auditorium floor area of about 55' by 60', a stage, an orchestra pit on a hydraulic jack system and several ancillary rooms. The auditorium roof diaphragm is plywood supported by wood joists bearing on steel trusses or beams which, in turn, bear on reinforced concrete columns or walls. The building rests upon drilled piers about 15 feet below grade.

The auditorium plaster ceiling is sloped between trusses. Heavy cracking of the ceiling plaster occurred over the orchestra pit. Leaks were observed in the orchestra pit hydraulic system. Concrete was spalled off of one of the tops of the pilasters supporting the steel roof trusses and heavily cracked at two other truss bearings. The original approved drawings required four extra column ties around the bolts anchoring the truss. None were installed as shown in Photo 8.

The crucial condition of the truss and wall anchorages were immediately called to the attention of the district superintendent who cordoned off the area. Temporary wall anchorages were installed by the original contractor under the supervision of an architectural firm.

The slab on grade was cracked and the exterior slab on the east side of the building opposite the stage settled and separated about an inch.

Gymnasium. This building, designed in 1959, has a main roof with a span of 96' and is 108' long. The roof is poured gypsum deck on steel purlins bearing on tapered steel rigid frames. The exterior walls are of reinforced concrete with few openings.

The two main court basketball backstops were partially detached from their roof supports.

A wall pier in the announcer's booth exhibited diagonal cracking indicating it resisted lateral load because of its inherent stiffness. Part of this wall was subsequently separated from the main gymnasium.

This building was used immediately following the main shock as a disaster center.

Swimming pool and diving pool. These pools, designed in 1959, were poured-in-place reinforced concrete. Vertical cracks were observed in the corner of the diving pool. Deck slabs shifted and some differential shifting occurred. Piping was broken at the filters. Pool coping units became loosened.

Library. One end of a pendant light fixture fell. Books shelves added by the district were displaced. Steel book stacks anchored at the top performed well. Books generally were thrown to the floor.

In the July 25, 1983 aftershock a portion of the east wall of the reading room displaced about an inch relative to the roof framing. Toe nails on several roof joists providing the wall anchorage were omitted. Nailed sheet metal angles were installed.

Other damage. In the student center two plate glass window panes were broken in the building, designed in 1955. Kitchen equipment shifted in the cafeteria. Several tiles fell from the splined T-bar ceilings in the lecture hall. A few T-bar ceiling panels fell and shelved materials generally were thrown to the floor in the classroom buildings and a chemical spill occurred in the chemistry laboratory. The laboratory instructor neutralized the spill and cleaned it up.

SSS/OSA recommended that all light fixtures be properly anchored and ceiling tile repaired; the auditorium ceilings be properly braced and repaired and the basketball backstops be inspected and corrected. The areas under the basketball backstops were cordoned off until repairs were made.

### Lessons Learned

As evidenced by the collapse of the maintenance building and the hazardous amount of damage to the boiler room chimney on the Coalinga High School site, it is apparent that the buildings examined and determined to be unsafe were a true hazard. The owners of such buildings should be required to retrofit them or demolish them before someone is injured or killed. It is also interesting to note that the earthquake searched out the unapproved toilet



building on the Cheney Kindergarten site and the added closure wall at the District Administration Building. The maintenance building, boiler room chimney and the toilet building at Cheney Kindergarten were demolished by the school district shortly after the earthquake.

It is also apparent from the nominal amount of damage experienced by the buildings constructed under the Field Act that the current building standards for public schools are not overly conservative. One gets the impression from considering the cracks produced in the brittle finish materials as a result of the movement of the more flexible seismic resisting structural systems, that the structural systems were stressed well into the working range. Further it appeared evident that the more stringent drift requirements and other damage control criteria added to the State Building Standards after the Kern County earthquakes of 1952 and the San Fernando earthquake of 1971 were justified when one views the very hazardous window glass breakage, the suspended plaster ceilings and T-bar acoustic ceilings. This type of nonstructural damage was not only potentially hazardous to the occupants but it represented a costly property loss to the school districts.

#### Recommendation

It is recommended that further research is needed with regards to drift limitations of walls containing glass and that some means should be developed which will improve the performance of existing glass during earthquakes. This could include applying some clear or heat resistant plastic type of film which would hold the glass pane together and/or prevent it from falling or exploding out of the frames. Also needed is tighter and much more complete code and construction controls on clearance around the edges of the pane in the frame, lap of pane in the frame and strength of glass or the providing of some type of flexible gasket to hold the glass pane in the window frame which would permit considerable racking of the frame with respect to the glass. The performance of tempered glass at the instant of failure needs investigation.

It is also apparent, as it has been demonstrated in previous earthquakes, that items such as light fixtures, ventilation grilles or heaters and all items which are suspended overhead are a hazard to the occupants and must be braced, anchored and supported by safety wires or cables or otherwise connected to a part of the building structure. This condition is serious enough that existing installations which do not have this protection should be retrofitted with such safety devices.



## ACKNOWLEDGEMENTS

The many helpful suggestions, comments and the review by Mr. Donald K. ephcott, Chief Structural Engineer, SSS/OSA are gratefully acknowledged.

## REFERENCES

- 1) Shakal, A. F. and McJunkin, R. D., Summary of CDMG Strong-Motion Records, Office of Strong-Motion Studies Report 83-5.2, California Division of Mines and Geology.
- 2) Borchardt, R., et al., The Coalinga Earthquake Sequence Commencing May 2, 1983, U.S. Geological Survey Open File Report 83-511.
- 3) Kaliakin, N., (CDMG Office of Strong-Motion Studies) personal communication.

August 31, 1983

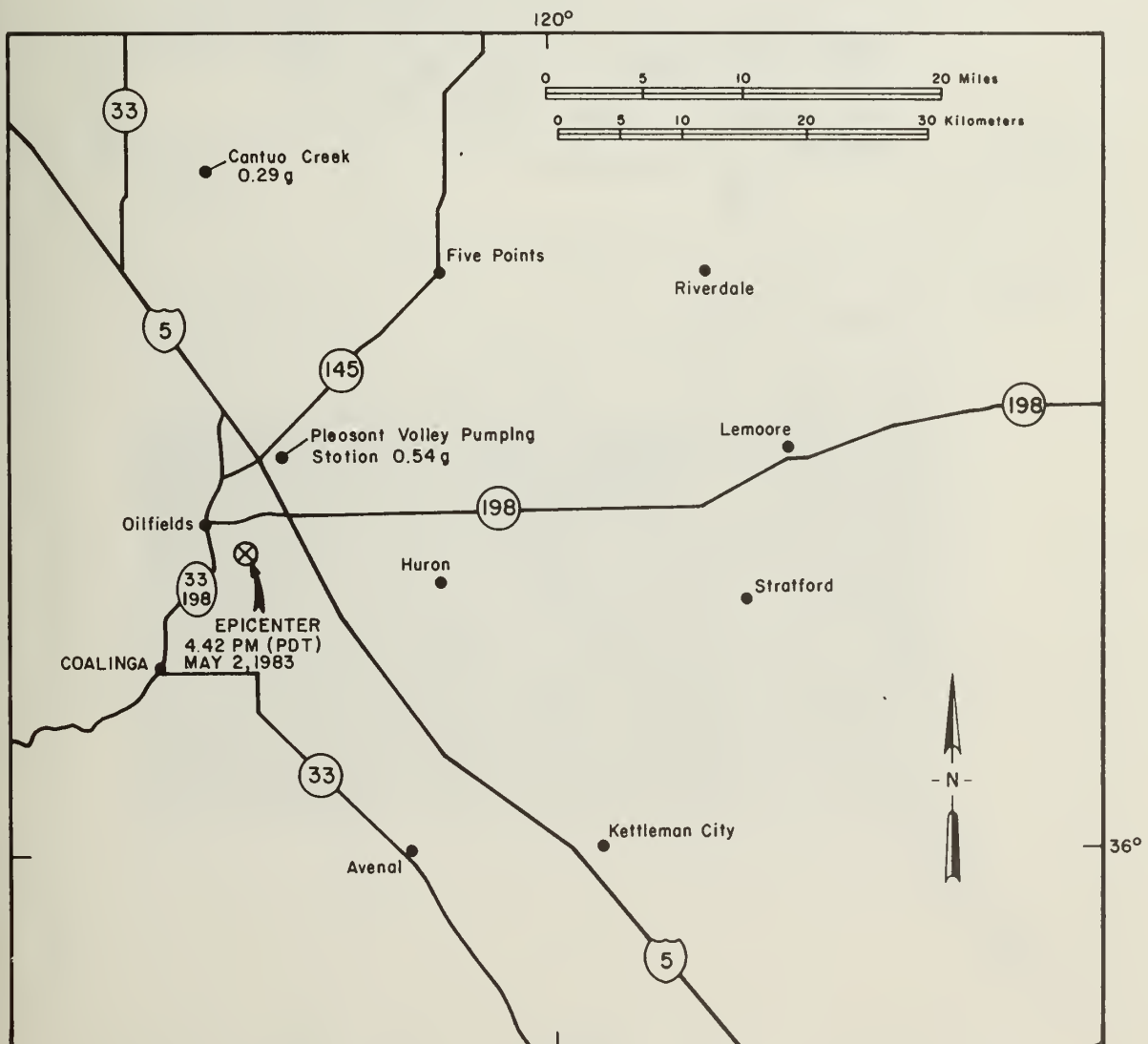


Figure 1

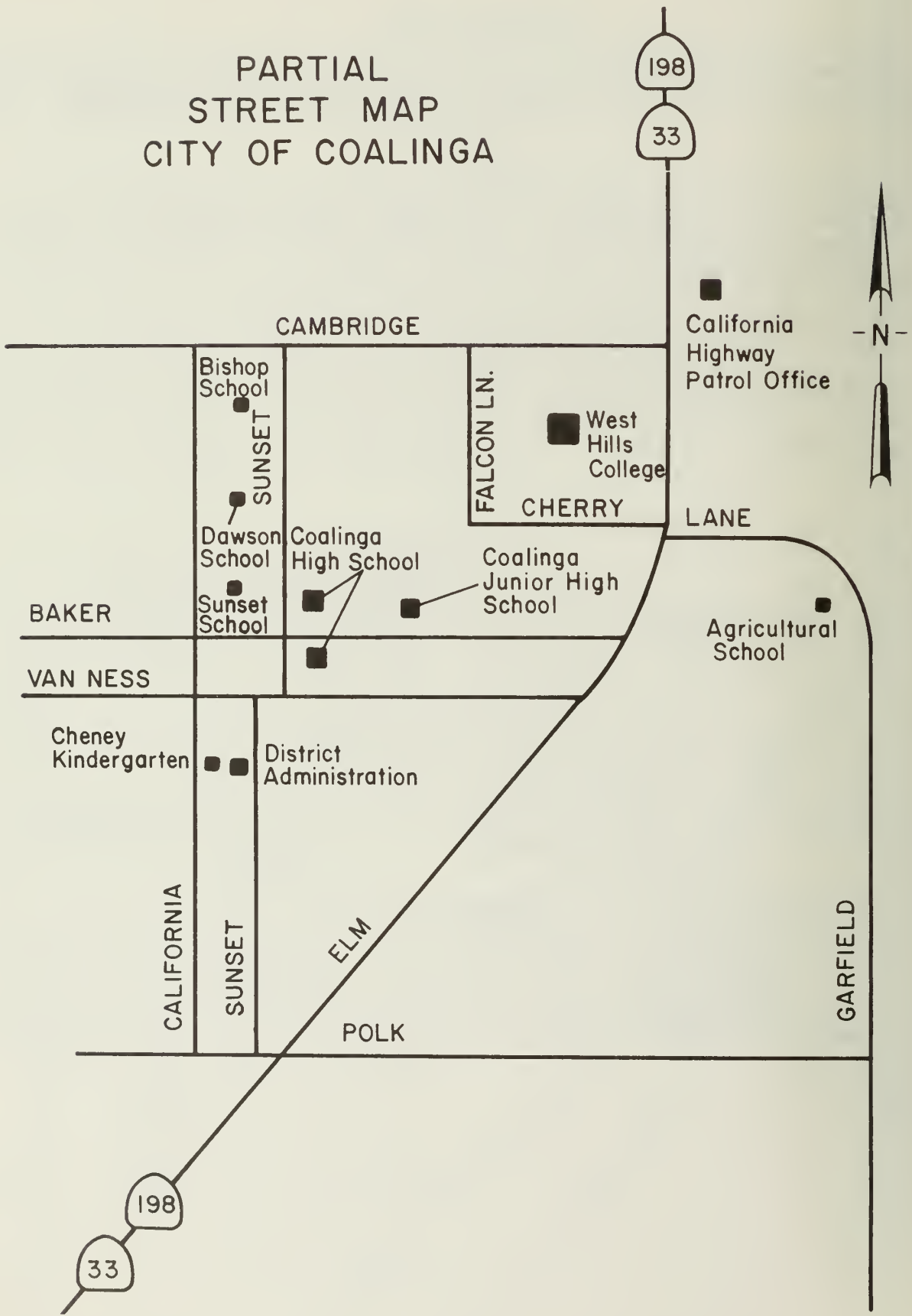


Figure 2



Photo 1. Oil King School - Intersection of Highway 33 and Highway 198



Photo 2. Cheney Kindergarten - Damaged Toilet Building





Photo 3. Coalinga Junior High School  
Library- Glass damage.  
(Photo by H. Heydt)



Photo 4. Coalinga High School Auditorium  
Ceiling damage



Photo 5. Coalinga High School Boiler Room Damage. This building was declared unsafe in 1937.



Photo 6. Coalinga High School Maintenance Building collapse. This building was declared unsafe in 1937.



Photo 7. Coalinga High School Boys Gymnasium.  
Wall piers were cracked.



Photo 8. West Hills College Speech Arts Building.  
The four horizontal ties around the steel roof  
truss anchor belts were omitted.



# EARTHQUAKE DAMAGE TO THE COALINGA OILFIELDS

by

J. P. Hughes<sup>1</sup>, W. Won<sup>2</sup>, and R. C. Erickson<sup>3</sup>

## ABSTRACT

The May 2, 1983, Coalinga earthquake caused some damage to oilfield installations and shut down all of the production for one day. By the end of July the oil fields had been returned to their former 30,000 barrels per day of production. Most of the oilfield damage occurred at the surface facilities. Very little damage occurred in the subsurface facilities. There were no surface or subsurface damage patterns that could be associated with active fault movements. Also, no pre-earthquake production changes have been noted that could be used as precursors of the earthquake.

## THE PAST

Surrounding the earthquake scarred town of Coalinga are a number of oilfields which, along with agriculture, help support the economy of this community of 7,200 people (Figure 1). The history of oil in the Coalinga area dates from the late 1800's with the first production beginning in the year 1890. All of this early production came from Cretaceous rocks in the Oil City area (Figure 1). When the statistical record of oil production began in 1896, yearly production was only 14,119 barrels (or just over 38½ barrels per day). Shortly thereafter, drilling spread to the main Coalinga oilfield (Figure 2) where production was found in the Temblor (Miocene) formation. Notwithstanding the low price of oil, which dropped down to 15 cents per barrel in 1905, the drilling increased more or less steadily until 1920 when annual production reached roughly 16,000,000 barrels. The next year an oil workers' strike started a slump in production which lasted until about World War II when an increased demand again caused drilling to pick up. By that time, drilling had spread to the East Coalinga Extension (Figure 3) and Pleasant Valley fields (Figure 1). In 1948 commercial hydrocarbons were discovered at Gujarral Hills (Figure 1). Commencing in 1953 a secondary recovery project, in the form of a pilot water flood, was started in the Coalinga field. This project proved successful and was, therefore, expanded to cover a considerable surrounding area. Other smaller water floods have also been commenced since the early 1960's. The latest secondary recovery projects, which are proving to be quite successful, involve either cyclic or continuous steam injection into the shallow Temblor oil sands. To date some 1,244 million barrels of oil have been produced from all of these Coalinga area fields. Six hundred eighty million barrels have been produced from the Coalinga field - 75% having been produced by 1960. Five hundred million barrels have been taken from East Coalinga Extension - 70% before 1960.

<sup>1</sup>Geologist, Chevron U.S.A. Inc.

<sup>2</sup>Design and Construction Engineer, Chevron U.S.A. Inc.

<sup>3</sup>Consultant, Geological Engineer, Chevron U.S.A. Inc.

The Pleasant Valley and Guijarral Hills fields have each produced 14 million barrels and 50 million barrels, respectively. Currently there are over 2,100 active producing wells in the Coalinga fields. On May 2nd the earthquake caused a shut down of production for the entire area.

### THE PRESENT

Much of the media attention has been focused on the damage sustained by the town of Coalinga. Eight city blocks - the greater part of the downtown area - collapsed. Most of these 60 year old buildings were constructed primarily of unreinforced masonry. Wood framed buildings fared much better. Most of the damage to this latter kind of structure was caused either by the frames not being anchored to the foundations, or by the collapse of unreinforced brick chimneys. Reinforced masonry structures sustained only minimal damage. In total, 165 homes were destroyed and another 398 were too badly damaged to be habitable. In all, some \$31,000,000 in damages to the city were caused by the quake.

Damage to wells and equipment in the oilfields, while minimal, was quite extensive. Since only isolated instances of oilfield related damage were mentioned in the press, the authors were asked to put together a summary of this aspect of the earthquake's effects. Toward this end, field superintendents of the major producers in the Coalinga area were interviewed during the weeks following the main shock. Since a number of the 17 current Coalinga area operators either have fairly small holdings or lacked local offices, a letter requesting a damage assessment was sent to all of the companies not interviewed.

In this summary of damage, the results have been grouped under two fairly broad categories: damage to subsurface equipment, and damage to surface equipment and facilities. These summaries are followed by a discussion of damage patterns. Some brief notes on both pre- and post-earthquake changes in oil production, etc. have been included at the end of the report.

### DAMAGE

#### Subsurface

Very little downhole wellbore damage has been reported as a result of the earthquake sequence. The following table lists earthquake damaged wells that had been reported through August 11th.

**Table 1**  
**Wells Damaged by the Earthquake Sequence**

OPERATOR	Well Location and/or Name	Nature of Damage	Depth at Which Damage Occurred
Shell	Sec. 27 - 19/15	Casing collapsed	200'
Shell	Sec. 27 - 19/15	Casing collapsed	?
Shell	Sec. 6 - 20/15	Casing collapsed/parted	30'
Shell	Sec. 6 - 20/15	Casing collapsed/parted	40'
Shell	Sec. 6 - 20/15	Casing collapsed/parted	35'
Shell	Sec. 6 - 20/15	Casing collapsed/parted	45'
Shell	Sec. 6 - 20/15	Casing collapsed/parted	30'
Shell	Sec. 6 - 20/15	Reconditioned just prior to the quake, but wouldn't take steam just after the quake (bad pipe?)	180'
Chevron	#1-5W		
"	Sec. 13 - 20/14	Packer pulled loose	709'
"	#9-10B		
"	Sec. 25 - 20/14	Parted casing	1761'
"	#3-6		
"	Sec. 11 - 19/15	Tubing stuck	1750'
"	#22		
"	Sec. 28 - 19/15	Parted casing	1545'
"	#106		
"	Sec. 35 - 19/15	Tubing stuck	2724'
"	#138		
"	Sec. 35 - 19/15	Parted casing	2350'

The Shell wells listed above were the only eight out of their 935 active wells that seem to have experienced earthquake related damage. Chevron has 785 wells in the area. It should be emphasized that except for something dramatic like parted casing, subtle wellbore or even reservoir damage might be rather hard to recognize and pinpoint.

In the Coalinga area oil fields, all of the production is lifted to the surface by either a surface pumping unit or a gas lift assembly. Following the May 2nd earthquake, all of the production facilities were shut down because of a massive electric power failure. Serious subsurface damage to the wells was, therefore, not apparent until an attempt was made to place each well back on production. Any minor deformation in a casing string or minor sanding caused by the earthquake may go undetected if it does not effect the mechanical functioning of the production system.

A post earthquake casing failure pattern is not apparent from the few damaged wells reported to date. The reported failure pattern is so randomly scattered throughout the field that it appears to be related to casing corrosion. While there are numerous shallow faults in the sedimentary section that makes up the productive zones, none of this damage appears to be associated with the mapped faults. There is also no evidence of any major reverse faulting within the productive limits of the Coalinga oilfield. This latter observation is based on the abundant oil well control.



## Surface

### Facilities:

Power. The initial shock on May 2 cut most electrical power to the oil-fields. In some cases, especially in the epicentral area, it took several days to repair downed lines and damaged transformers. In other areas power was restored quickly, but the equipment was not restarted until after a damage and safety inspection had been made. Several small fires were started by downed power lines, but these were extinguished quickly before any equipment was damaged.

Pumping Units. Although no pumping units were heavily damaged, a large number were jostled out of alignment, anywhere from 1"-4". For example, Shell reported that some 60% of their units in Sections 10, 14, 15 and 29 -T19S/RI5E had to be realigned. Chevron had 105 of their units moved around, with most of the movement occurring in sections 28 and 35 -T19S/RI5E. Texaco likewise reported about 130 pumping units that needed to be realigned. Most other operators experienced similar problems.

Tanks. Storage tanks in the Coalinga area sustained a variety of damages as a result of the earthquake ground shaking. Perhaps it should be noted first that the damage, though widespread in the area, was somewhat selective. In some cases, where there were two or more tanks in close proximity, it was not uncommon to find that one would be damaged while the others were relatively untouched. No patterns have yet been found to account for this phenomenon. Damage to tanks fell into five main categories:

1. "elephant's foot" bulges at or near the base;
2. bulges near the top (presumably due to sloshing);
3. settling of the tank into the gravel pad on which it sits;
4. leaks caused by the shearing or buckling of internal baffles; and
5. leaks caused by the shearing or buckling at connections with external pipes, valves or ladders.

A short discussion of each type of damage follows.

"Elephant's foot" bulges were fairly common in unanchored fluid storage tanks. The mechanism, which probably involved liquid slosh to one side of the tank, is illustrated in Figures 4 and 6a.

In other cases, liquid slosh was strong enough to cause bulging and occasional rupturing of one of the upper rings in partially full storage tanks. As might be expected, the damage occurred on the two opposite sides of the tanks as the contents sloshed back and forth (Figures 5 and 6b).

Shaking during the earthquake sequence caused a number of tanks to settle into their gravel pads some 1-4 inches. Occasionally this settling sheared off one or more of the lower pipe connections, causing leaks.

In some cases, tanks had internal baffles. Occasionally leaks appeared where bolts supporting these baffles were sheared off during the twisting motions imparted by the earthquakes (Figure 7).

The most common type of tank leak occurred at the point where external fittings (pipes, valves, ladders, etc.) were attached to the tanks. The problem was basically that these fittings were rigidly attached to both the tank and the ground. When differential movement took place between the tank and the ground during the shaking, the fittings either sheared off or else were pushed into the tank at the point of connection (Figure 8a). In one case, a catwalk ladder attached rigidly between two adjacent tanks caused the sides of both to be shoved in. Although there were a number of "oil spills" as a result of this kind of leak, most were contained in surrounding moats designed for that purpose.

Pipelines. Pipelines fared rather well during the earthquake sequence. Although there were quite a number of leaks, most were small in nature and easily repaired. Apparently all of the leaks were confined to coupling joints and connections. There were no reports of lines breaking other than at a connection.

Miscellaneous. Like the pumping units discussed previously, quite a number of pieces of heavy machinery slid around during the shaking and had to be realigned. Examples included "heater-treaters", steam generators, stack scrubbers, tanks on skids, water softeners, etc. Most had moved between 1/2" and 8".

A number of support buildings and offices were also damaged. As with the buildings in town, the severity of the damage seemed to depend on the type of construction.

### Ground Rupture

A fair amount of minor damage (buckling, cracking, etc.) was sustained by lease roads. Although the majority of this type of damage was found on roads in the epicentral area, some roads as far away as 10 km were also affected. A more widespread sort of ground surface damage involved slumping or sloughing on cut and fill slopes, dikes and berms. In most cases it was limited to either cracking with little or no movement, or else involved a downslope movement of only a couple of inches. There were isolated examples, however, where movement amounted to a foot or more. Once again, the slumping and sloughing was more serious in the epicentral area. A more detailed report of ground failures in the Coalinga area can be found in an article by Keefer, et al. (USGS open - File Report 83-511).

The only surface rupturing associated with an active faultline occurred along the Nunez Canyon fault following the June 10th earthquake. This nearly north-south reverse fault, located northwest of Coalinga about 10 km, caused a 15 cm displacement where it crosses the Los Gatos Creek Road.

### **SURFACE DISPLACEMENT PATTERNS**

There appears to have been a persistent pattern in terms of the preferred direction of movement of surface objects during the earthquake shaking. As a general rule, most of the movement appears to have been in either an east-west or northeast-southwest direction. The following examples illustrate this observation:

1. Many of the large pieces of heavy equipment and pumping units which slid did so in a northeast or southwest direction;
2. Pipelines running generally north-south were usually undamaged, while the majority of leaks occurred on east-west trending lines;
3. Equipment supported on stilts or short legs was often found to be leaning in either a northeast or southwest direction;
4. Many of the bulges and "elephant's feet" found near the bases of damaged tanks occurred on the northeast and/or southwest sides;
5. A pillar supporting an awning over a motorpool gas pump broke at an old weld and the upper part of the pole moved toward the east-northeast;
7. During one of the major aftershocks, several people reported that objects (books, hanging pictures, etc.) on the west walls of their homes and offices were thrown down during the initial motion. Similar items on their east side walls, however, stayed in place, indicating a possible initial movement of the building from west to east (Figure 9).
8. A large, free-standing desk in the downtown Coalinga office of the California Division of Oil and Gas slid along a newly polished floor, scratching out a trace of its path. Figure 10 is a copy of this trace, which is probably a record of the motion that the building experienced as it slid around under the desk. Note that the net movement of the desk was in an east-northeasterly direction, indicating that the building's net movement was probably toward the west-southwest.

### PRODUCTION PATTERNS

A quick review of the production records reported to the California Division of Oil and Gas (CDOG) was made to see if there were any changes that could be used as precursors of the earthquake. None were found, principally because most of the post earthquake production is not reported to the CDOG until over 30 days after the end of month. However, spot checks of records from the major producing companies in the area did not reveal any significant changes either before or after the event of May 2nd.

There are some inherent problems in the use of oil field production records for the identification of possible tectonic pressure changes within the earth's subsurface. The major problem centers on the frequency with which individual wells are gauged. According to the records from the Conservation Committee of California Oil Producers (1982), the average Coalinga Oil Field well only produces about 12 barrels of oil per day. Because of these low daily rates, it generally is standard practice for most of the operators to gauge the individual wells on a set, but periodic schedual. For example, a well producing 3 barrels per day or less may only be gauged once every 5 days. A significant short term change in production might consequently go unnoticed. Total lease production records, however, are very accurately maintained for payment of royalties.



The next problem involves reservoir pressure recordings. Unless the production is coming from a significant project this type of record is usually not obtainable. A significant project is usually one which involves a secondary recovery operation. In the case of the water floods, the injection pressures and injection intervals are periodically checked by the CDOG to make sure they are not exceeding the limits set by their initial approval of the project. These projects, as well as the cyclic steam projects, create a dynamic situation within the reservoir that will most likely mask any pressure changes due to outside tectonic forces. This is particularly evident in the cyclic steam projects where the magnitude of the production changes are quite rapid over a short period of time.

### ACKNOWLEDGEMENTS

The authors wish to express their appreciation to Chevron U.S.A., Inc. for permission to prepare and publish this paper. The following individuals generously provided information on company facilities damaged by the earthquake: Carl Bidinger (Union Oil Company of California), Cal Bottum (Santa Fe Energy Company), Dick Lewis (Shell Oil Company of California), Jim McDaniel (Chevron U.S.A. Inc.), Myles Monroe (Chevron U.S.A. Inc.), and John Young (Texaco U.S.A.). Mr. E. J. Fowkes, a geologist at West Hills College in Coalinga, Vic Van Matre of the California Division of Oil and Gas, Coalinga Office, and Tom Wright with Chevron U.S.A., also provided information useful in the preparation of this paper.

### REFERENCES

- (1) Arnold, R. and Anderson, R. (1910) "Geology and Oil Resources of the Coalinga District, California". U.S. Geological Survey, Bull. 398, p. 179-182.
- (2) California Division of Oil and Gas. (1982) California Oil and Gas Fields, Central California.
- (3) Conservation Committee of California Oil Producers. (1982) Field and Pool Production Record, November.
- (4) Kaplow, E. J. (1945) "Coalinga Oil Field". Summary of Operations, California Oil Fields. Thirty-First Annual Report of the California Department of Natural Resources, Division of Oil and Gas. Vol. 31, No. 2, p. 5-6.

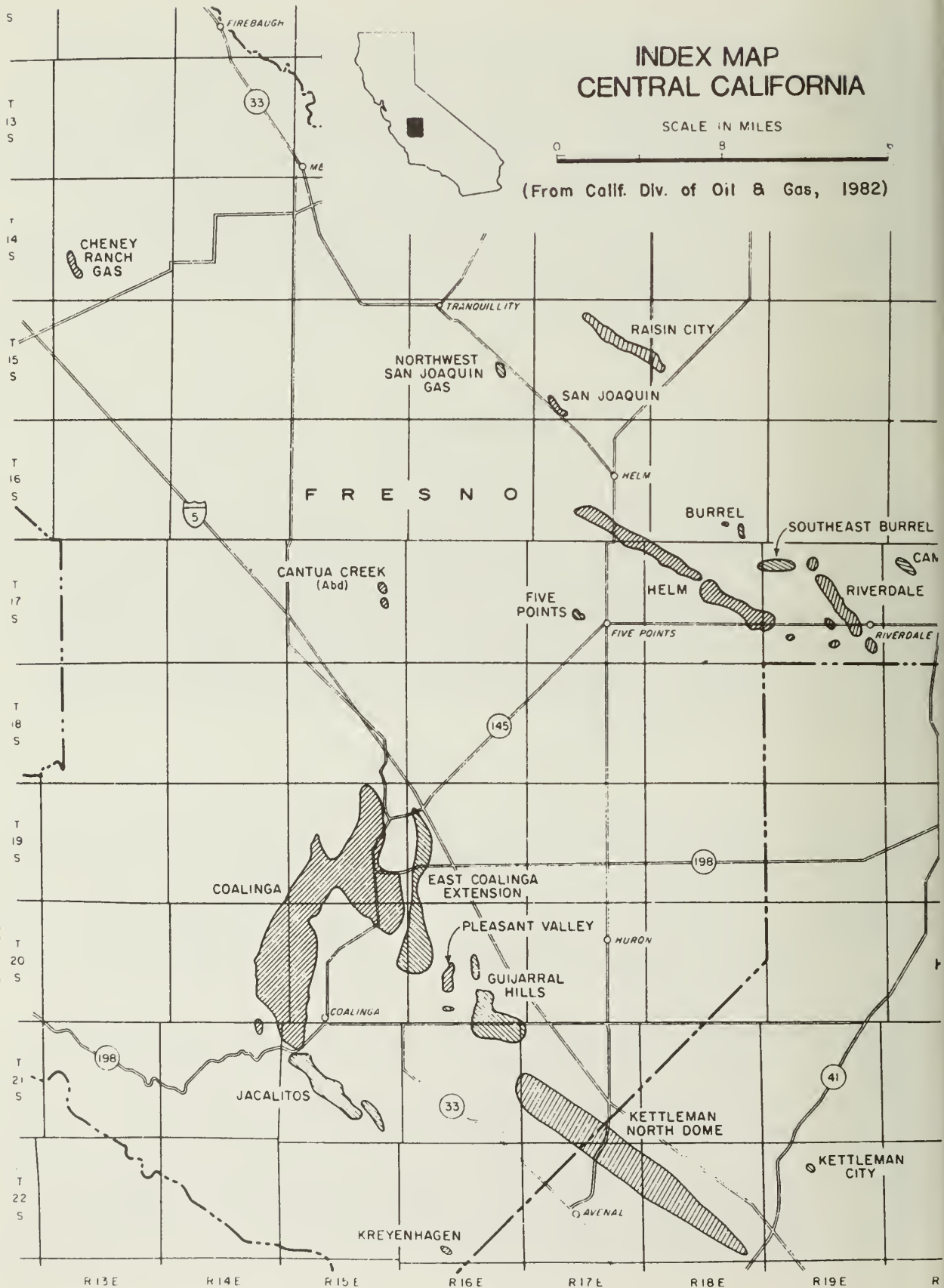
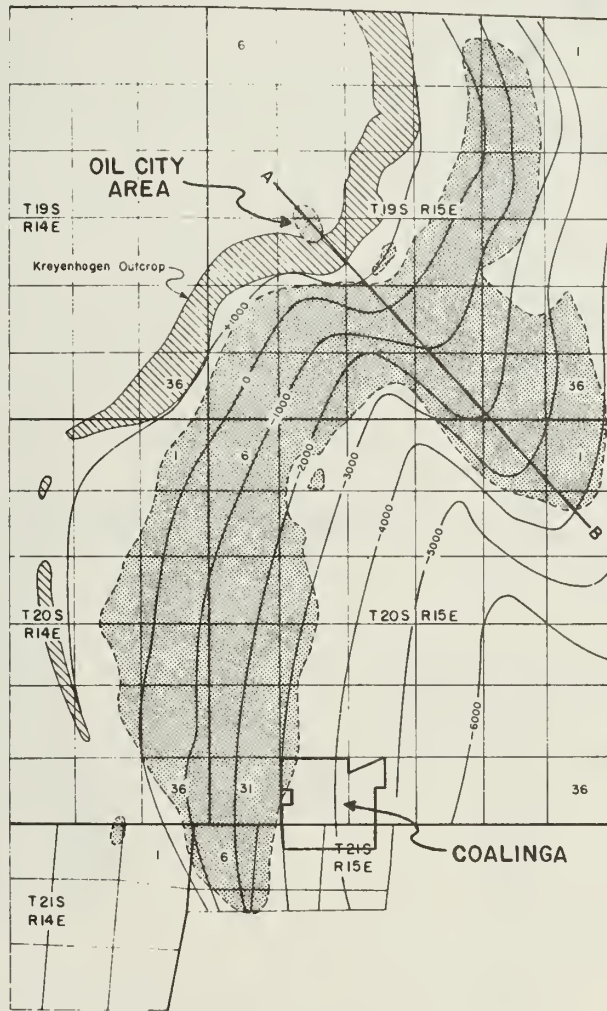
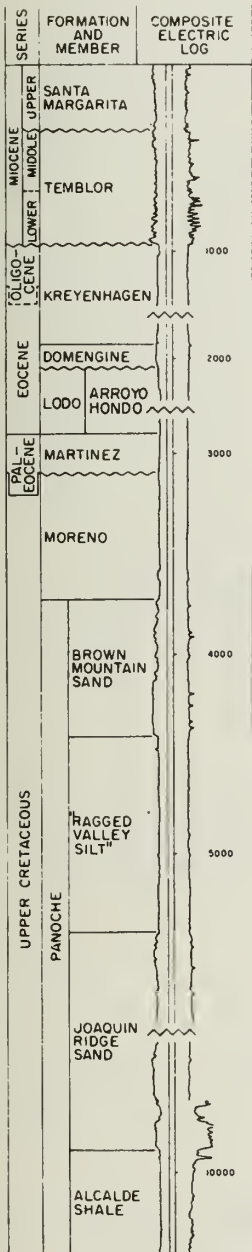
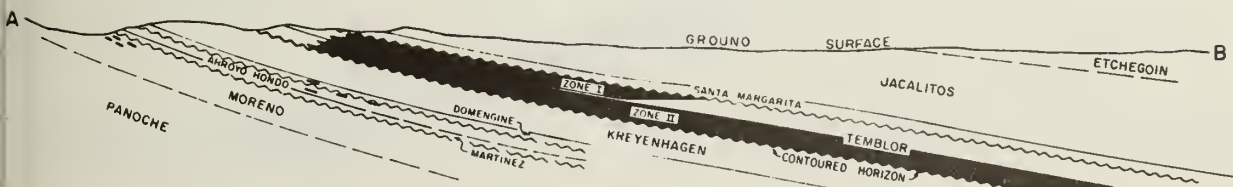


Figure 1



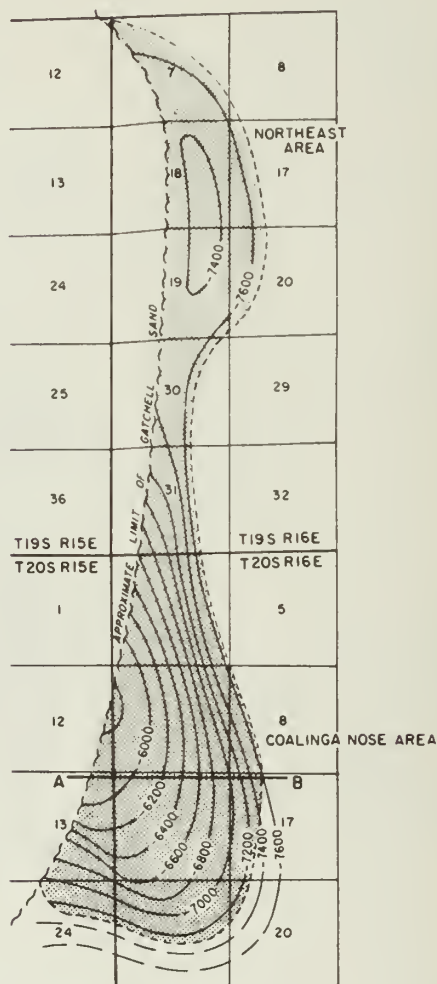
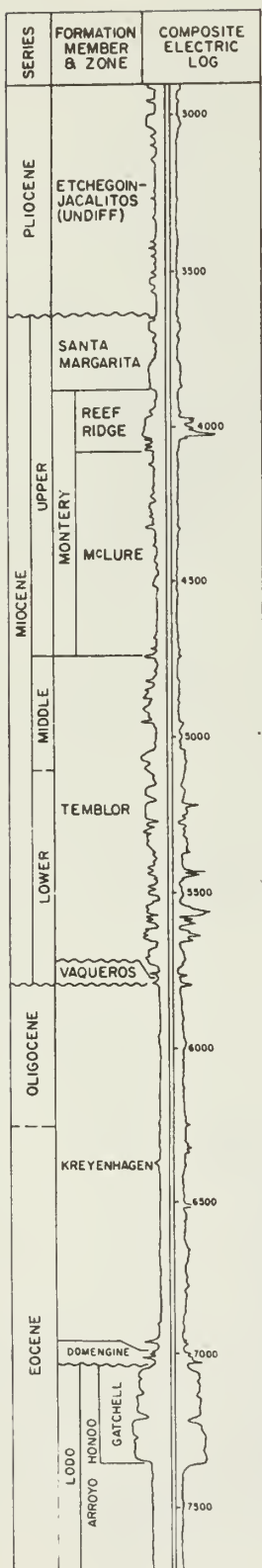
CONTOURS ON TOP OF KREYENHAGEN



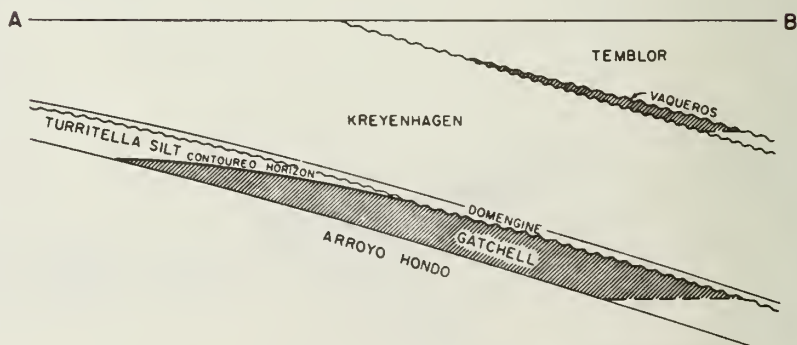
(From California Div. of Oil & Gas, 1982)

Figure 2



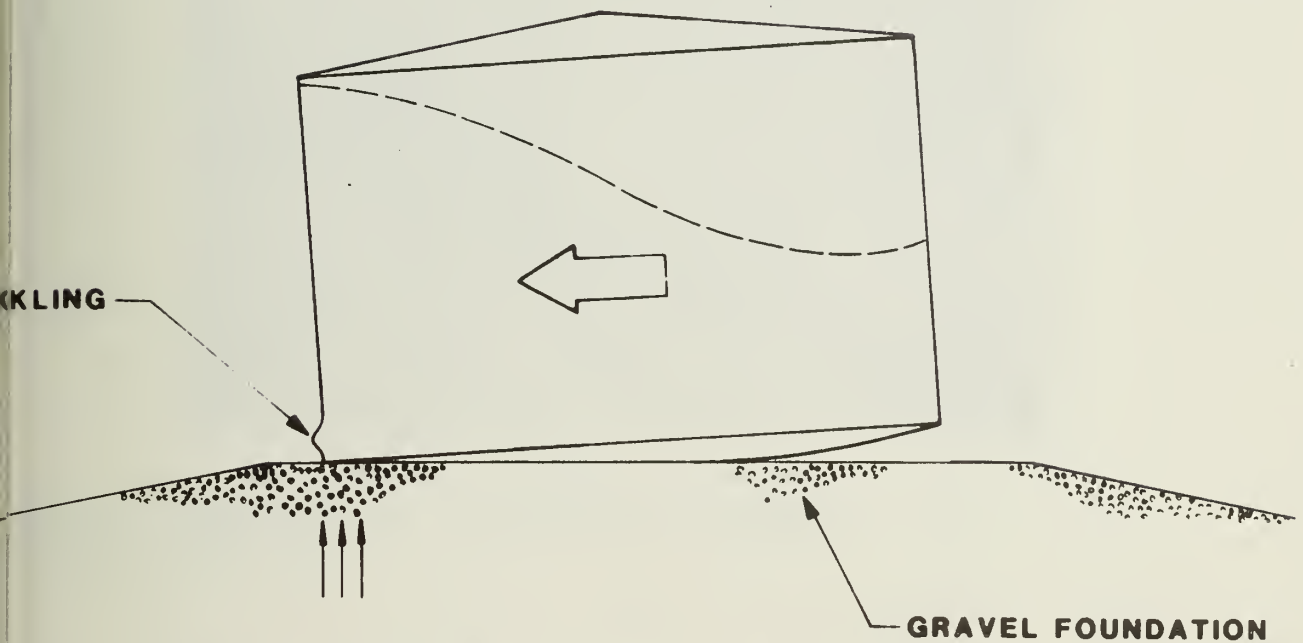


CONTOURS ON TOP OF GATCHELL SAND

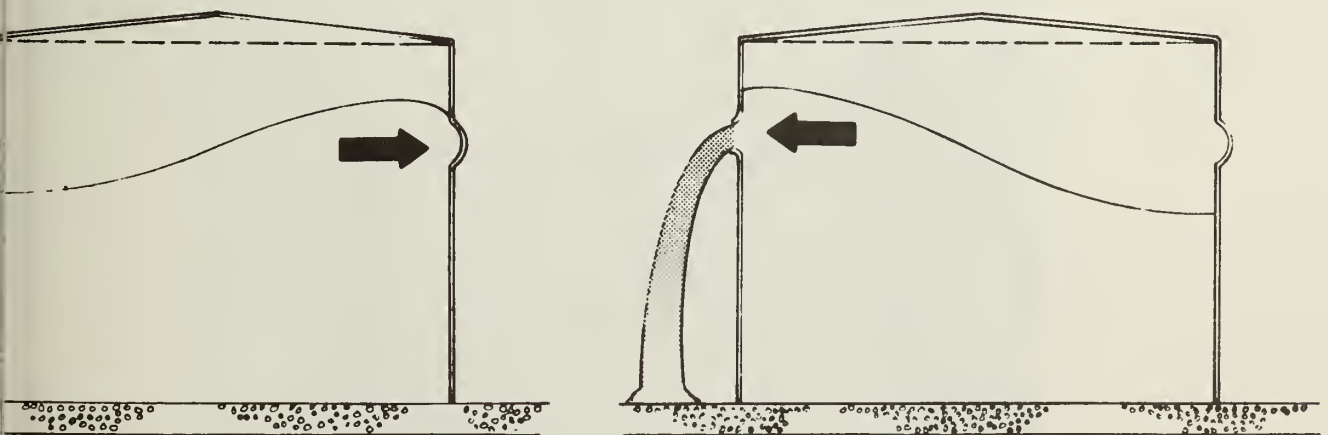


(From California Div. of Oil &amp; Gas, 1982)

Figure 3



4. Diagram showing mechanism that causes "elephant's foot" type damage at cylindrical storage tanks.



5. Diagram of probable mechanism (Liquid slosh) that caused damage sustained in the upper rings of cylindrical storage tanks.



**Fig. 6a. Elephant's Foot bulge at the base of a storage tank (Sec 13 - T20S/R14E).**



**Fig. 6b. Bulge and rupture in one of Shell's storage tanks, probably caused by liquid slosh shown in Figure 5 (Sec 26 - T19S/R16E).**



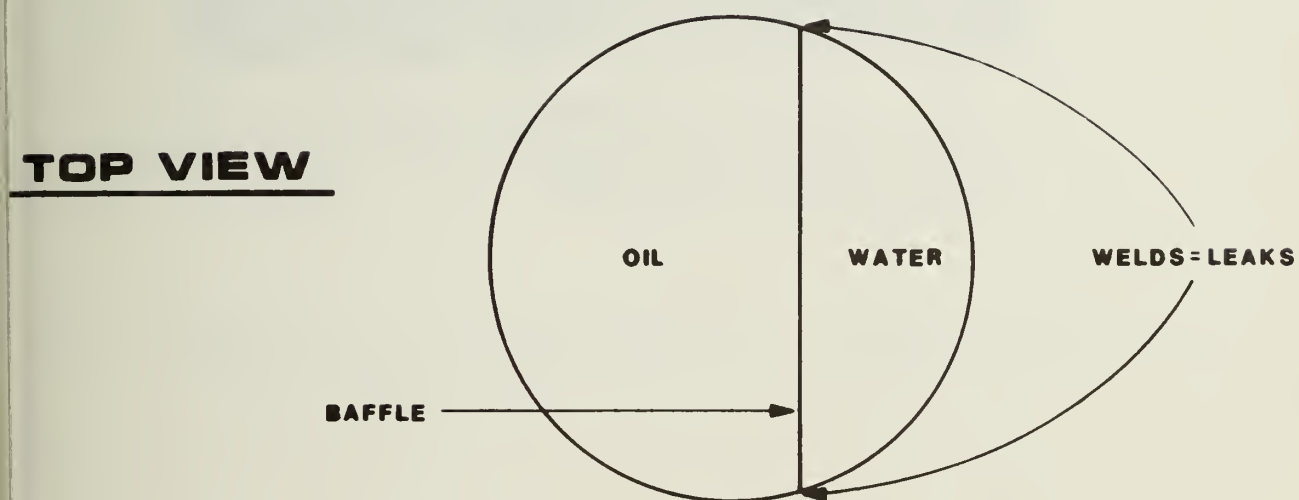


**Fig. 7. Diagram showing location of damage in the storage tanks with internal baffles.**

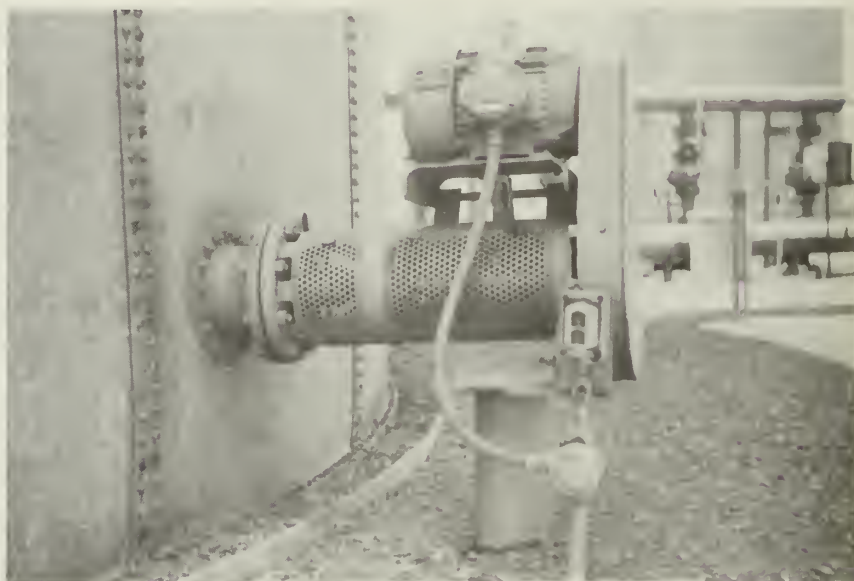


**Fig. 8a.** Indentation caused by relative movement of storage tank and mixer support column which is anchored to the grade.



**Fig. 8b.** Ripples in the top of a storage tank (Sec 13 - T20S/R14E).

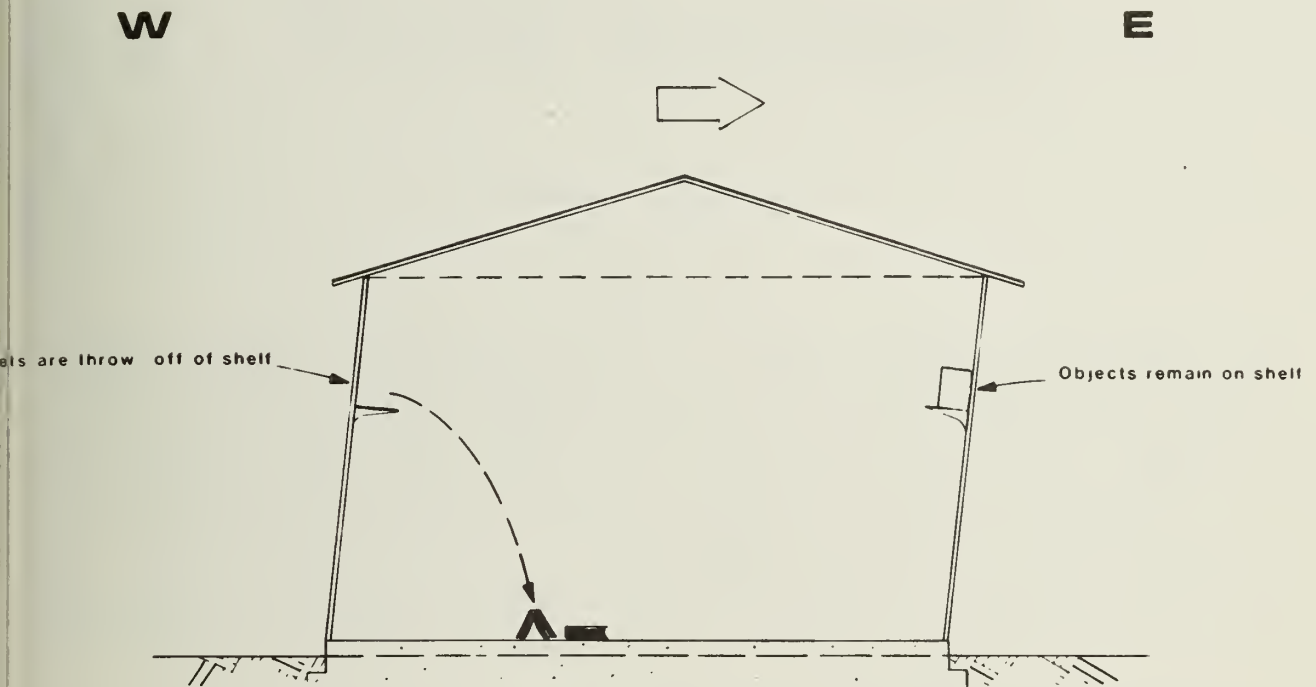
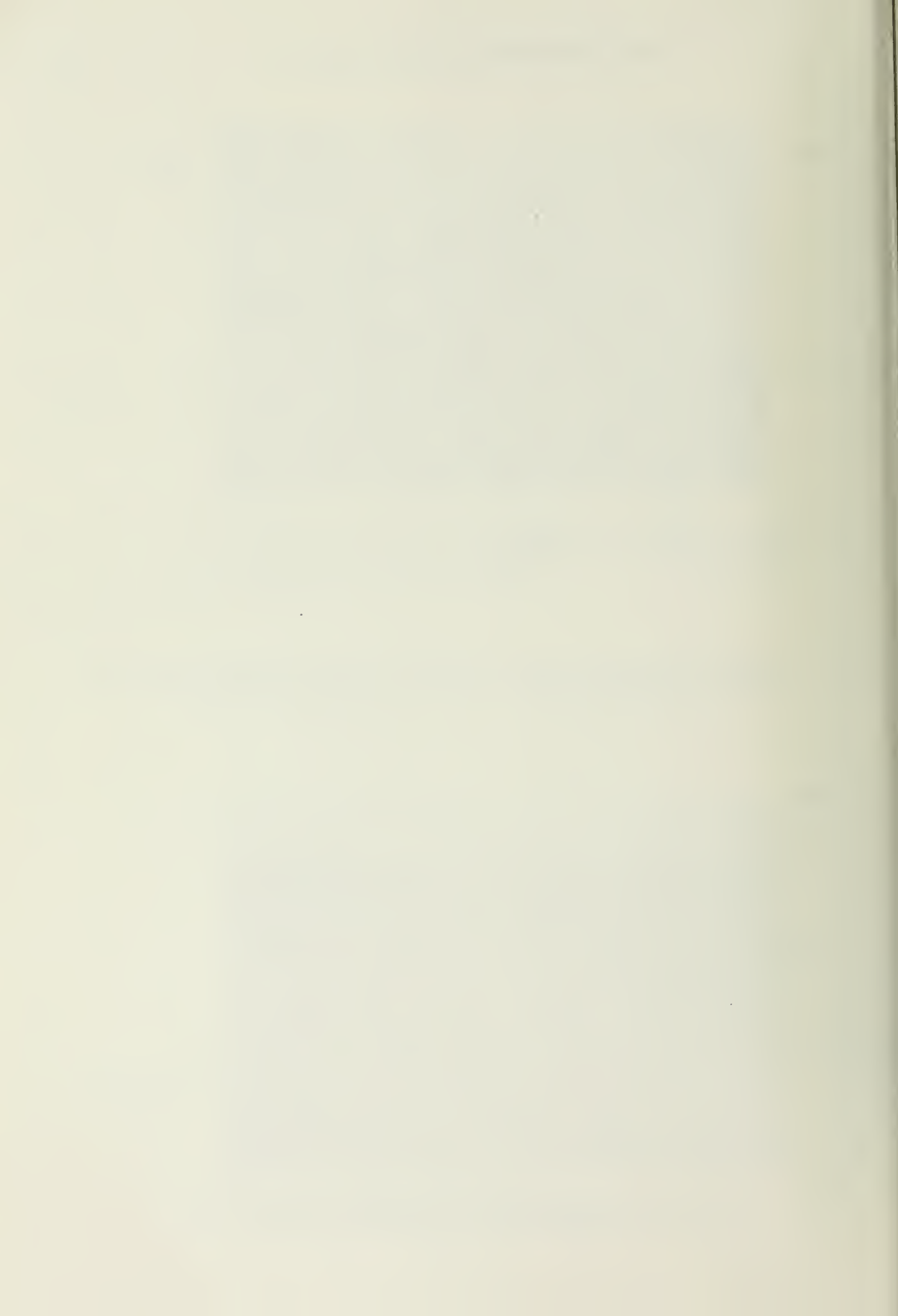


Fig. 9. Diagram showing the response of objects on shelves in oil field operations offices to the initial motion of one of the numerous aftershocks.



Fig. 10 Sketch of the relative movement of a large, free standing desk in the town of Coalinga during the May 2nd earthquake.





DAMAGE TO IRRIGATION WELLS AND OTHER FACILITIES  
IN THE PLEASANT VALLEY WATER DISTRICT DUE TO  
THE MAY 2, 1983, EARTHQUAKE AND AFTERSHOCKS

by

Joseph B. Summers <sup>1/</sup>

INTRODUCTION

The Pleasant Valley Water District is located easterly of Coalinga (see Figure 1). The District encompasses approximately 39,000 acres. Lands within the Pleasant Valley Water District are almost totally agricultural and the principal crops grown are cotton, grain, hay crops, tomatoes, miscellaneous field crops and a small acreage in orchards. The source of irrigation water for the lands within the District is from irrigation wells. The Pleasant Valley Water District does not own or operate any of the wells but was organized to develop an alternative water supply for the area. Negotiations on this alternate supply are underway and hopefully will be completed in the next few months.

Data for the information in this report was obtained from landowners, well and pump contractors who constructed the facilities and did repair work in the area, Pacific Gas and Electric Company, and discussion with officials of the Pleasant Valley Water District.

EARTHQUAKE EFFECTS

The earthquake of May 2, 1983 occurred shortly after farmers in Pleasant Valley began the summer irrigation, principally to cotton and tomatoes. The damages to irrigation facilities were principally to wells, the only source of water for the area, and distribution system pipelines. Figure 1 shows the location of the damaged facilities. A brief description of the type of damage that occurred to the wells is indicated on the tabulation. The most extensive damage was to the irrigation wells which, in some cases, required abandoning the well and in other cases resulted in reduced yield of water from the well and the pumping of sand. The photographs, Figure 2, show a damaged pump base and typical casing failure inside a well. Field observations show that in some cases the soils adjacent to the wells subsided with the pump base then positioned above the ground surface. Reports on the 1964 Alaskan earthquake and the 1966 Parkfield-Cholame earthquake indicate similar subsidence which tends to reduce the yield of wells. The earthquake also caused damage to Pacific Gas and Electric Company facilities, particularly transformers mounted on poles adjacent to pumping plants.

---

<sup>1/</sup> Consulting Engineer, Hanford, California  
District Engineer, Pleasant Valley Water District

Indicated on Figure 1 is the location of transformers that were knocked off poles and/or damaged because of the earthquake. Figure 1 also locates damaged concrete pipelines. The photographs, Figures 3 and 4, show typical damage to these facilities. The pipelines are used to convey well water to the fields for irrigation. The principal type of damage was failure of the joints and collapse of vertical structures such as pump stands, air vents, and stand pipes. Some farmers have repaired and/or replaced their damaged underground pipelines but the majority are using surface pipe or other temporary means until they can generate sufficient funds to make a permanent replacement. The aftershocks that have occurred subsequent to the May 2 earthquake have further aggravated the irrigation facilities. Repair work includes repositioning the pump heads that shift as a result of the continuing aftershocks.

At the time of the earthquake on May 2, 1983, the Ace Irrigation Company of Fresno California had a drill rig in operation with the drill bit at a depth of approximately 600 feet in Section 8, T. 20 S. R. 15 E., MDB&M. The rig did not collapse, but it was knocked off its outriggers and jacks. It is the opinion of the drill crew that if the stem had not been in the hole, the rig would have overturned. After the quake, the crew had difficulty pulling the stem from the hole. This site was abandoned and another well was drilled at a nearby site.

Following the major earthquake, Ace Irrigation Company was repairing a damaged well casing. The casing had collapsed to an out of round condition and the repair required a swedging operation which involves the reshaping of the casing by the use of a hydraulic jack which is placed inside the well forcing the casing back to a circular configuration. During this operation an aftershock occurred and it took many hours to remove the swedge which was jammed in the well. The repair of the wells has caused major concern because of the high cost of the equipment required for doing this type of work which can be damaged or lost if an aftershock should occur at the time of repair.

### CONCLUSION

The damages that have occurred have been extremely costly to the owners of the facilities within the Pleasant Valley Water District. Facilities have been repaired, sometimes more than once, and other facilities have had to be abandoned. There has also been loss to crop production because of the lack of irrigation water during the growing period. In addition there has been the cost to the utilities for replacing damaged facilities.

The damages that have been identified in this report are those that are known to have occurred. It is probable that there has been damage to other irrigation facilities not yet known or fully identified. This may include damage to well and pumping facilities, irrigation pipelines and damage to the aquifer system. These damages will not be known for a period of years depending on the continued aftershocks in the area and the long term effects to the aquifer system.

## REFERENCES

National Academy of Sciences, 1968, The Great Alaska Earthquake of 1964: Committee on the Alaska Earthquake, Publication 1603.

U.S. Department of the Interior, 1967, The Parkfield-Cholame California, Earthquakes of June-August 1966 - Surface Geologic Effects Water-Resources Aspects, and Preliminary Seismic Data: U.S. Geologic Survey Professional Paper 579.

## TABULATION OF DAMAGED IRRIGATION WELLS FROM THE MAY 2, 1983 EARTHQUAKE AND AFTERSHOCKS

Location <sup>1/</sup>	Date Drilled	Depth (feet)	Diameter <sup>3/</sup> (inches)	Yield (gpm)	Static Water Depth (ft)	Level Date	Earthquake Effects and Damages
NE 9 20/15	Feb. 1952	1000	14/12	560	618	Apr. 1981	Pump head shaken out of alinement and knocked off its foundation. Oiler broken.
NE 8 20/15	May 1983	600 <sup>2/</sup>	---	---	---	---	Drilling well at time of quake, sustained major damage. Abandoned site and relocated well.
NW 17 20/15	Jan. 1951	1000	14/12	630	465	Apr. 1981	Pump head shaken out of alinement and knocked off its foundation. Oiler broken.
NE 16 20/15	Oct. 1979	1125	16	840	489	Apr. 1980	Damaged pump and column assembly.
SW 16 20/15	June 1978	1050	16	990	621	June 1978	Pump head shaken out of alinement. Damaged pump and column assembly.
SW 14 20/15	Sep. 1973	1300	16	900	528	Feb. 1980	Damaged pump base and column assembly.
NE 20 20/15	Jan. 1951	835	16/12/10	700	---	---	Pump head shaken out of alinement and knocked off its foundation. Oiler broken.
NW 28 20/15	Mar. 1952	900	16	720	310	Fall 1982	Well damaged.
SE 30 20/16	Apr. 1958	680	18	800	279	Fall 1982	Well pumping at time of earthquake, pump seized (no rotation), damage unknown.
SE 34 20/15	June 1975	1125	16	---	307	June 1980	Pump head shaken out of alinement and knocked off its foundation. Pump bowls and casing damaged at 491'.
SW 36 20/15	Nov. 1956	1000	16/14/12	640	300	Dec. 1982	Pump damaged. Casing damaged at 340' and 460' depths.
NE 2 21/15	Oct. 1973	965	14/12	---	---	---	Pump head shaken out of alinement, knocked off its foundation and head shaft bent.
NW 2 21/15	---	600	16	590	310	Aug. 1983	Well damaged, pumping sand.
SW 4 21/15	---	---	--	---	---	---	Pump head shaken out of alinement. Power service damaged.
SE 5 21/16	Mar. 1955	825	16/14	860	330	Feb. 1980	Pump head shaken out of alinement and knocked off its foundation. Oiler broken.
SE 4 21/16	Oct. 1964	1250	16	1020	364	Apr. 1981	Well damaged, pumping sand.
NW 10 21/15	---	707	14	500	294	Apr. 1981	Well damaged, yield has declined.
NW 7 21/16	June 1958	800	16/12	1030	---	---	Well & casing collapsed, unable to repair, well abandoned.
NE 9 21/16	Sep. 1976	1000	16	1140	398	May 1980	Pump head shaken out of alinement and knocked off its foundation. Oiler broken.
SW 10 21/16	Apr. 1970	970	16	1140	351	Apr. 1981	Damaged pump and column assembly.
NW 16 21/16	Oct. 1964	1000	16	860	320	Apr. 1981	Pump damaged. Casing damaged at 295', 352', 395', and 606' depths.
NW 17 21/16	Aug. 1973	2250	16/10/8	---	---	---	Pump head shaken out of alinement and knocked off its foundation.
SE 35 21/16	---	1555	16/12	500	348	July 1983	Damaged pump bowls and column assembly.

<sup>1/</sup> Quarter, Section, Township/Range, Mount Diablo Base and Meridian

<sup>2/</sup> Approximate depth at time of earthquake

<sup>3/</sup> Multiple entries indicate reduced diameter at lower depth.



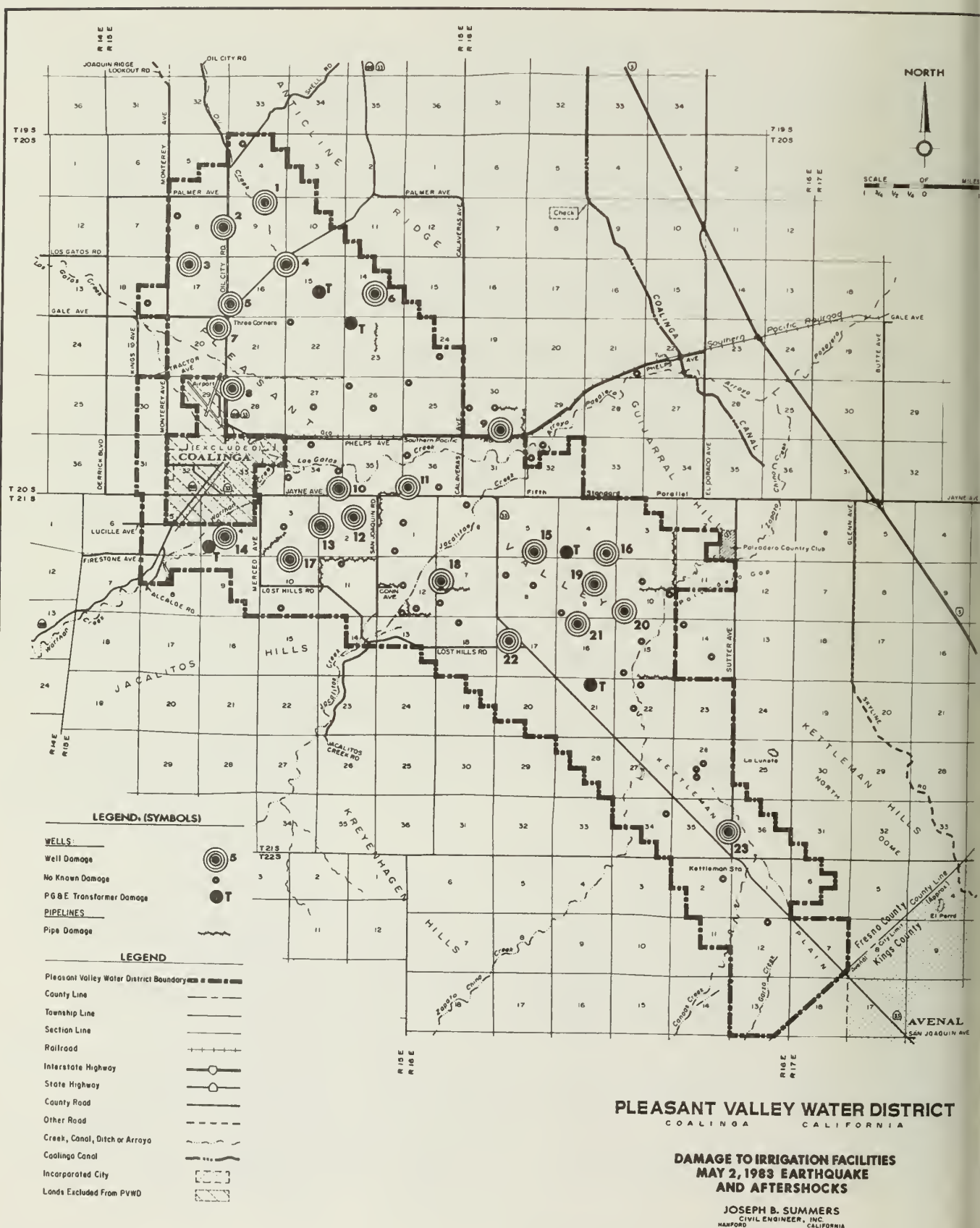


Figure 1.



Photograph of television screen looking down a typical damaged well. Spot in center is light and line at bottom is on television screen. Photograph is at 621 feet. Note collapse of casing walls.



Damaged pump base. Well no. 6.



Typical damaged standpipe.

Figure 3.



Figure 4.

Buried pipeline under operation during earthquake. Damage to top section caused by pressure surges.

SUMMARY OF HIGHWAY BRIDGE DAMAGE  
COALINGA EARTHQUAKE  
MAY 2, 1983

by

Eugene G. Klein, Jr.<sup>1</sup>

ABSTRACT

Six bridges suffered minor structural damage due to the Coalinga earthquake of May 2, 1983. Damage included hair line cracks at the tops and bottoms of columns and wingwall displacements. Ten bridges showed definite signs of movement while an additional 44 bridges surveyed showed very limited movement or none at all.

BRIDGE DAMAGE SURVEY

The Caltrans Office of Structures Design Post Earthquake Investigation Team (PEQIT) was alerted at 1800 PDT on May 2, 1983 as a result of reports of bridge damage. Team members Jim Monroe and Gene Klein prepared to move out early the next morning. The team arrived in the Coalinga area about noon on May 3, 1983. Early reports of bridge damage resulting from the earthquake proved to be unfounded. The Herndon Ave. OC had been damaged by an overheight truck which struck the north exterior girder over the southbound lanes of I-5 but no earthquake damage or movement was evident. The El Dorado Ave. OC was reported damaged but, showed no evidence of structural damage or movement.

Sixty bridge sites were included in the survey. Figure 1 shows the distribution of the bridges surveyed and the damage pattern observed. The survey was made on May 3 - 4, 1983 and included portions of the following routes.

Route 5 from Post Mile (PM) 12.36 in Kings County to PM 64.62 in Fresno County.

Route 33 from the Junction with Route 46 in Kings County to the Junction with Route 5 in Fresno County.

Route 41 in Kings County from the Kern County line to the Junction with the California Aqueduct.

<sup>1</sup>Associate Bridge Engineer, California Dept. of Transportation.



Route 145 in Fresno County from the Junction with Route 5 to the Junction with Route 269.

Route 269 in Fresno County from Kings County line to the Junction with Route 145.

Route 198 in Fresno County from the Monterey County line to the Junction with Route 33.

California Aqueduct in Fresno County from aqueduct post mile 139.35 to aqueduct post mile 144.25.

Sixteen of the bridges showed definite signs of movement caused by the earthquake. Additionally several other bridge sites showed signs of movement but not necessarily movement caused by the earthquake. Six of the 16 bridges suffered minor structural damage (Figure 2). Four of the 6 bridges are on the State Highway system and two of them belong to the Department of Water Resources.

#### BRIDGE DAMAGE

The Route 198/5 Separation, Bridge No. 42-235 located at the intersection of Route 5 and 198, is a continuous four span reinforced concrete box girder bridge approximately 336 feet long supported on two-column bents and end diaphragm abutments. The bridge is on a 30 degree skew. Considerable rotation occurred at this structure as indicated by the one to two inch gaps between the fill slopes and the wingwalls. Movements of between 1/4 and 1/2 inch are visible in the earth at the base of all the columns in this structure. The wingwalls were not damaged. The tops of all the columns in this structure have hairline cracks within about one foot of the soffit (Photo 1). The concrete has possibly separated from the reinforcing steel a small amount but none of the concrete has spalled off the columns. Very close scrutiny of these columns is required to see the damage. Cracking of the asphaltic concrete approach slabs also indicates this structure was subjected to heavy shaking. The 1/4 to 3/8 inch cracks occur at the paving notch and approximately four feet from the paving notch. The approach fills have settled about one inch.

The Jacalitos Creek, Bridge No. 42-072 is located about four miles east of Coalinga on State Route 33. The structure is a six span continuous slab bridge approximately 134 feet long with solid training walls below the flow line and pile extensions. The bridge has zero skew. All of the pile extensions have cracks within 4 inches of the soffit of the caps and one foot above the top of the solid walls (Photos 2 & 3). Some spalling of the pile extensions has occurred. Some cracks in the pile extensions of this structure were noted prior to this earthquake. These cracks have opened up more and some spalled concrete is now visible as a result of the earthquake. There was no abutment damage. The approach fill settled about 6 to 8 inches. The pavement sagged rather than dropping off abruptly at the paving notch. Maintenance forces had filled the sag before any exact measurements could be made.

The Phelps Avenue OH, Bridge No. 42-233R/L located 10 miles east of Coalinga on Route 5, consists of two parallel bridges separated by an 84 foot median. Both of these bridges are continuous four span reinforced concrete Tee-Beam structures on two-column bents and end diaphragm abutments. The total length of each structure is 180 feet with a vertical clearance of about 24 feet. The structure skew is about 23 degrees. The structure rotated in a counter-clockwise direction causing distress in the northeast wingwall and the southwest wingwall of the right and left bridge respectively. The barrier railing was offset approximately 1 inch at each location (Photo 4 ). The wingwall and parapet at both locations was severely fractured. The wingwalls were cracked with some spalling where the wingwalls joined the abutment backwall (Photo 5). There was no visible damage to the superstructure or the columns.

The Los Gatos Creek Bridge, Bridge No. 42-005 located about 1 mile northeast of Coalinga on Route 33 is a continuous four span slab bridge on solid piers and propped abutments. The structure was widened in 1959. The superstructure and piers showed no signs of damage. The bridge is approximately 82 feet long with a skew of 30 degrees. The southeast wingwall was lengthened about 24 feet since the structure was first built. The wingwall extension is a free standing retaining wall. The only connection between the extension and the original wall are two ungrouted 1 inch diameter bars about one foot long. The wall has gradually moved toward the southeast. Bridge Maintenance Engineers advised that the wall had moved about 4 inches prior to this earthquake. The wall moved an additional 5 inches and tilted toward the the stream bed as a result of this earthquake (Photo 6 & 7). The approach fill had several 1 inch cracks running parallel with the centerline of the structure.

The Jeffrey Road Bridge located at post mile 139.35 on the California Aqueduct is primarily used by the farm community. This three span precast-prestressed I Girder bridge is about 180 feet long on solid piers. This type of structure is typical of the structures over the aqueduct. The approaches to this structure are unpaved. Cracks in the top of the levee about 1 inch wide run parallel to the aqueduct. There was evidence that fill settlement had occurred at the northeast wingwall with some minor spalls at the abutments. The expansion joints over the piers showed some signs of spalling. The side slopes of the channel lining were cracked in the vicinity of the Jeffrey Road Bridge indicating that the abutments tried to move toward the channel. This structure suffered no significant structural damage despite the evidence that relatively large movements and shaking occurred. None of the bearings showed any signs of distress.

The El Dorado Bridge located over the aqueduct about 1 mile south of Route 145 is a three span precast-prestressed I Girder structure on solid piers approximately 180 feet in length. This structure is located at post mile 144.25 on the aqueduct alignment. Cracks in the approach fill were about 1/2 inch maximum width. Settlement of the fill in this area was very slight - not more than 1/2 to 1 inch. There was some spalling at the joints over the piers. At the southeast wingwall there appears to be about an 1/8 inch separation near the bottom of the abutment backwall and the wingwall. No damage to the channel lining was visible above the waterline.

### CONCLUSIONS

The typical CALTRANS overcrossings on Route I-5 are two span box girder structures on single column bents and end diaphragm abutments (Photo 8). The column transverse reinforcement was largely # 4 hoops at 12" spacing. The undercrossings for the most part are three span slab bridges on pile bents and end diaphragm abutments (Photo 9). These and several other bridges in the area showed signs of movement but no significant structural distress. These types of structures have proved to be able to withstand damaging earthquakes very satisfactorily. The earthquake damage that was evident as a result of this earthquake provided little if any additional information about bridge survival of retrofitted bridges. None of the bridges surveyed had hinges and for the most part the large architectural columns proved to be more than adequate. No bridges in the area have been identified for EQ retrofitting in the statewide program.

The swallows in the area provided a ready means of determining structure movement. Where the swallows nests remained in place and were undamaged the structure showed no evidence of movement.

Bridge damage was surveyed by Gene Klein and Jim Munro of the CALTRANS Post Earthquake Investigation Team on May 3-4, 1983

### ACKNOWLEDGMENTS

The author would like to thank Mr. James H. Gates for his guidance, encouragement, and advice. Thanks also goes to the Caltrans staff for preparation of this paper.

Special thanks goes to Ray Zelinski, and Jim Munro for reviewing the paper.



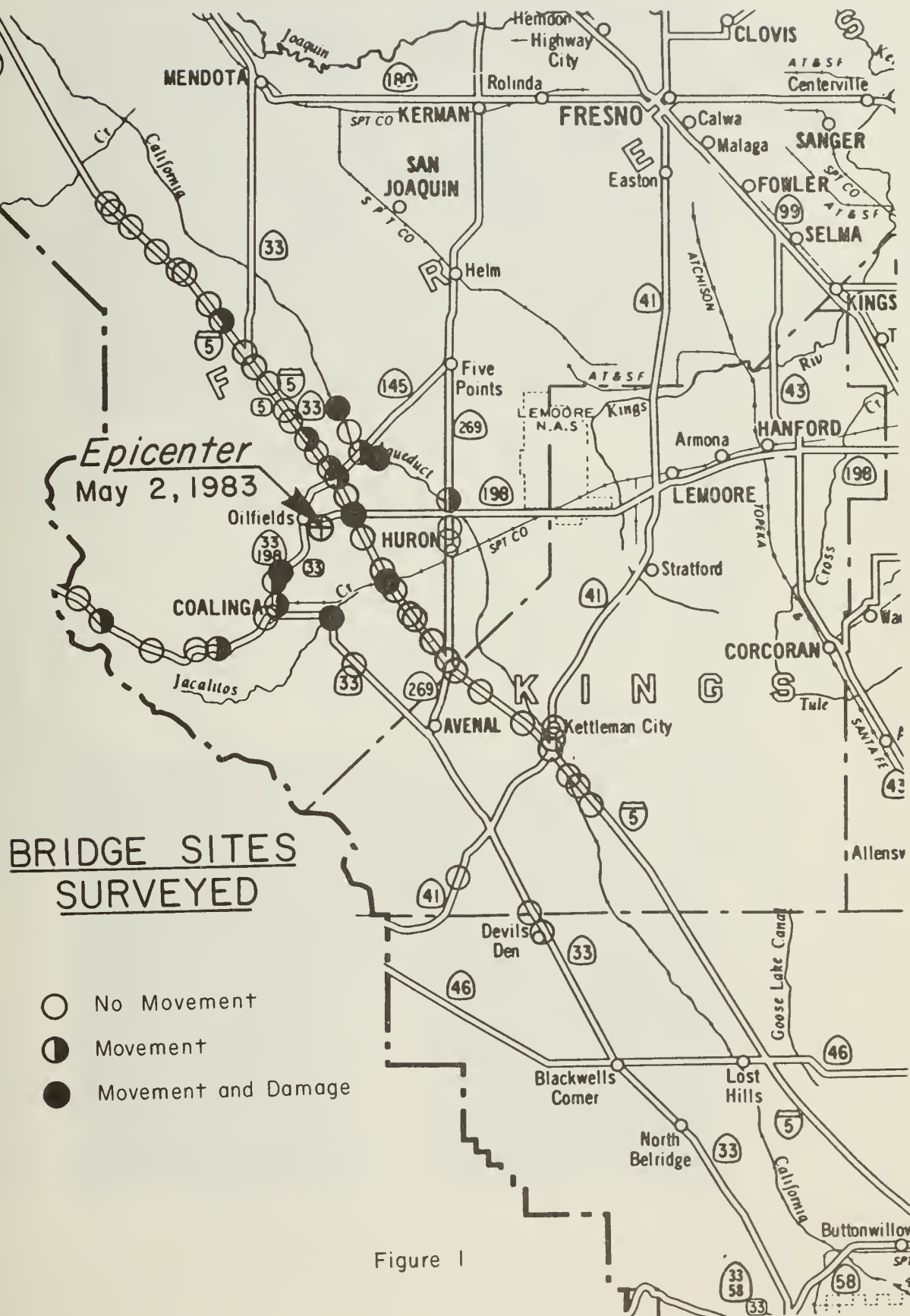








PHOTO 1 Route 198/5 Separation, Br. No. 42-235  
Bent 4 Right Column looking south.



PHOTO 2 Jacalites Creek Bridge, Br. No. 42-072  
Top of pile bent looking south.



PHOTO 3 Jacalitos Creek Bridge, Br. NO. 42-072  
Bottom of pile bent looking south.



PHOTO 4 Phelps Avenue Overhead, Br. No. 42-233 R/L  
Abut. 5 Rt. Bridge looking west.



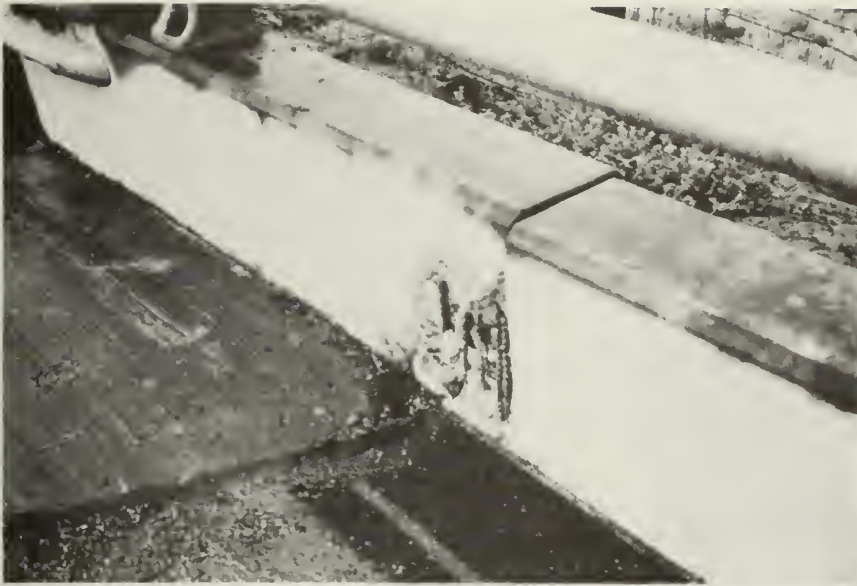


PHOTO 5 Phelps Avenue Overhead, Br. No. 42-233 R/L  
Abut. 5 Rt. Bridge looking east.



PHOTO 6 Los Gatos Creek Bridge, Br. No. 42-005  
South Abut. looking south.



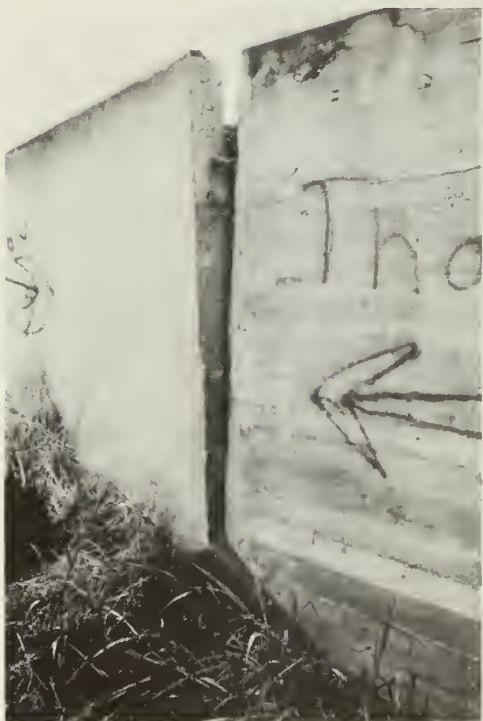


PHOTO 7 Los Gatos Creek  
Bridge, Br. No. 42-005  
South Abut. looking down.



PHOTO 8 Typical Overcrossing over I  
Two-span bridge with single colu  
bents and end diaphragm abutments.



PHOTO 9 Typical Undercrossing on I-5  
Three-span slab bridge on pile bents with end diaphragm  
abutments.

# CLEARINGHOUSE ACTIVITIES: COALINGA, CALIFORNIA EARTHQUAKE May 2, 1983

by

Robert Streitz<sup>1</sup>

## ABSTRACT

The level of response by the news media to the May 2, 1983 Coalinga, California earthquake was unexpected, and much of the clearinghouse activity involved responding to the needs of news reporters, TV camera crews, and network coordinators. This function of the clearinghouse was as important as coordinating the scientific and engineering data collection activities.

## INTRODUCTION

On Monday, May 2, 1983, an earthquake of Richter magnitude 6.7 occurred approximately 11 kilometers northeast of Coalinga, California. The Coalinga earthquake was another example of moderate (M6-7) sized California earthquakes occurring in an unexpected area. This event illustrates again the fact that most of California is earthquake country. On Tuesday, May 3, an information clearinghouse was established by the State Geologist and members of the Earthquake Engineering Research Institute to coordinate all the damage review, investigative efforts, and information collection and dissemination. The clearinghouse was housed in Everett Hall on the campus of West Hills College at the invitation of college officials and with the generous assistance of Mr. Mark Wallace, Information Officer of West Hills College.

## CLEARINGHOUSE ACTIVITIES

The goal of a clearinghouse is to coordinate all types of geologic, geophysical, and seismological investigations; collect information and engineering data to promote public safety; and disseminate information to scientific investigators, governmental agencies, local residents, and the news media.

<sup>1</sup> Geologist, Division of Mines and Geology

The clearinghouse also has the goal of orienting newly arriving scientific investigators of what has been done prior to their arrival and what at that time might prove to be the most productive additional investigative endeavors. Maps of seismograph locations, both sensitive and strong-motion instruments, are posted and kept current by clearinghouse staff as instruments are added and relocated. In this way the clearinghouse serves to funnel current scientific and engineering data to those who have need of it--the clearinghouse is an information resource center.

It was planned that the clearinghouse be staffed from 8 a.m. until 5 p.m. to receive and record data, discuss findings with scientific investigators, relay messages, and discuss findings with workers from other emergency response groups and the media. In addition, the clearinghouse was planned to be open from 7 to 11 p.m. for all investigators to discuss the day's activities, hear presentations and status reports on findings and studies, compare notes and observations, and plan the following day's work.

Two evening sessions were held. The first evening session, May 3, involved comprehensive discussion of engineering observations and structural failures presented by James Stratta and his colleagues from the Earthquake Engineering Research Institute. The second evening session, May 4, was largely devoted to a discussion of the earthquake source parameters, surficial geologic features, and seismological activities. Gary Fuis of the U.S. Geological Survey presented early findings relative to this earthquake sequence; he also assisted with staffing the clearinghouse and responding to the needs of the media and visiting scientists and engineers.

As it turned out, the Coalinga earthquake was a media event. During most of the daytime hours of clearinghouse operation, television news crews, and reporters monopolized the time of the clearinghouse coordinators to the occasional exclusion of staff coordination and message transfer. Other emergency response groups also experienced similar requests from the media for reports, commentary, opinions, pictures, and media material. The media should be responded to candidly, accurately, and courteously, and it was.

## CONCLUSION

The most important lesson learned from the Coalinga event relative to clearinghouse activities is that, in addition to coordinating the scientific investigations, a knowledgeable staff must be available to address the needs of the news media. This demand is most pressing during the hours immediately following the main shock.

Section 2

**GEOLOGIC AND  
GEOPHYSICAL INVESTIGATIONS**





HISTORICAL SEISMICITY AND TECTONICS OF  
THE COAST RANGES - SIERRAN BLOCK BOUNDARY:  
IMPLICATIONS TO THE 1983 COALINGA, CALIFORNIA EARTHQUAKES

by

Ivan G. Wong  
and  
Richard W. Ely<sup>1</sup>

ABSTRACT

Faults within the boundary zone between the Coast Ranges tectonic province and the Sierran crustal block have probably been the source of several significant earthquakes of  $M_L$  greater than 6 during historical times. Moreover, the level of moderate to large magnitude seismicity within the zone may be higher than the historical seismicity record would indicate because of probable bias in epicentral locations based upon maximum reported intensities and, to a lesser degree, the inaccuracy of instrumentally-determined locations prior to the 1960s. The boundary appears to be characterized by a change in the tectonic stress field as the direction of maximum compression rotates from approximately north-south in the Coast Ranges to northeast-southwest along the boundary and the minimum compression rotates from generally horizontal to vertical. This change is manifested primarily by shear deformation (strike-slip faulting) in the Coast Ranges, to compressional tectonics (reverse and strike-slip faulting) along the boundary zone. Based on their location, style of faulting, and the character of the tectonic stress field exhibited by fault plane solutions, the 1983 Coalinga earthquakes may be associated with the Coast Ranges-Sierran block boundary zone. Their occurrence, location, and size are not unusual in the context of the tectonics of this boundary zone.

INTRODUCTION

The historical seismicity of California, which dates back to the late 1700s, when the state was first settled, has been dominated by the San Andreas fault system and, to a lesser extent, by the Sierra Nevada-Great Basin boundary zone. Elsewhere, the level of historical seismicity has been much lower, including along the boundary zone between the Coast Ranges tectonic province and the Sierran crustal block (Figure 1). Although moderate to large earthquakes have occurred in historical times away from the two major seismic zones, the occurrence of Richter magnitude ( $M_L$ ) 6 or greater events elsewhere in California has always been somewhat surprising. Such is the case of the 2 May 1983  $M_L$  6.5 event that occurred on the western edge of the San Joaquin Valley near Coalinga, California.

---

<sup>1</sup>Senior Project Seismologist and Project Geologist, respectively; both at Woodward-Clyde Consultants, One Walnut Creek Center, 100 Pringle Avenue, Walnut Creek, CA 94596

The purpose of this paper is to evaluate the historical seismicity and tectonics of the Coast Ranges-Sierran block boundary zone, and to provide a framework within which the 1983 Coalinga earthquakes can be understood. Emphasis will be placed on the historical earthquakes within the boundary zone but outside the immediate vicinity of Coalinga. The historical seismicity in the region around Coalinga will be discussed in other papers in this report.

### TECTONIC SETTING

The 1983 Coalinga earthquakes occurred just northeast of the town and within the approximately 10-km-wide zone that marks the boundary between the Coast Ranges tectonic province on the west and the Sierran crustal block on the east (Figure 1). The Coast Ranges tectonic province is characterized by sheared, incompetent Franciscan Complex basement rocks; quasi-oceanic crust; variable heat flow; active right-slip faults; and post-early Miocene anticlinal folding and diapiric uplifts. This tectonic province locally includes the westernmost portion of the Great Valley (Ely and Packer, 1978). The Sierran crustal block is characterized by competent Paleozoic and Mesozoic igneous and metamorphic basement rocks, low subcrustal heat flow, low level seismicity (Figure 3), a generally thick continental crust, and the absence of major late Cenozoic faulting and folding. The Great Valley comprises the western half of the Sierran block (Figure 1).

The precise nature of the Sierran-Coast Ranges boundary zone in the basement is not known, because it is buried under 8 to 10 km of late Mesozoic and Cenozoic sediments (Oliver, 1977; Page and others, 1979). Evidence from deep wells and magnetic and gravity anomalies indicates that the basement beneath the Great Valley east of the boundary zone is dense magnetic rock that resembles oceanic crust (Cady, 1975). This rock is different from the sialic material characterizing the mountainous eastern portion of the Sierran block, and may be at least partially responsible for the persistent tendency of the Great Valley to subside.

The ophiolite that underlies the late Mesozoic Great Valley Sequence sediments in the Coast Ranges (Ernst, 1970) may represent the original westward extension of the Sierran block basement, or may be in tectonic contact with it (Page and others, 1979). The Coast Range thrust separates the Coast Ranges ophiolite from the underlying Franciscan Complex. This fault has been interpreted to be either a Mesozoic subduction feature (Ernst, 1970), or at least partially an early Cenozoic feature that developed after accretion of the Franciscan Complex (Page and others, 1979). The boundary zone may in part include disrupted portions of the Coast Range thrust.

The Sierran block boundary as defined in this paper is delineated by a contrast in late Cenozoic deformational style between the competent Sierran block, with its largely homoclinal sedimentary cover on the east, and the highly faulted and folded Franciscan Complex basement of the Coast Ranges on the west. The boundary at depth may be up to 10 km west of the boundary at the surface, and may consist of a zone approximately 10 km wide, in which the Sierran basement thins and becomes less competent and more faulted, and wherein the Franciscan Complex makes up an increasing proportion of the total. The near-surface expression of the western boundary of the Sierran

block is defined as the eastern limit of strong Plio-Pleistocene deformation in the Great Valley. The boundary is delineated by an abrupt, east-facing synclinal bend in Pliocene and Pleistocene deposits, which extends nearly the full length of the Great Valley. Late Cenozoic deposits west of the synclinal bend dip east at a relatively steep angle compared to those to the east, which are nearly flat lying.

The synclinal bend in the Sacramento Valley is shown on a structure contour map of the base of Pliocene Tehama and Tuscan formations (Page, 1974). The large, faulted anticlines in the Great Valley sequence to the west of the boundary lie sub-parallel to the Sierran block boundary (Jennings, 1977). Late Cenozoic structures east of the boundary consist of gently westward-dipping homoclines, broad folds, and a few minor faults (Page, 1974).

Lack of subsurface data obscures the location of the synclinal bend, if it exists, beneath the thick Quaternary deposits of the Sacramento Delta. The Sierran block boundary follows the Midland fault zone beneath the delta; this fault zone parallels the strike of the synclinal bend, and north of the delta the two features nearly coincide for 60 km (Page, 1974; Jennings, 1977).

The western Sierran block boundary in the northern half of the San Joaquin Valley is expressed as an abrupt synclinal bend in the 600,000-year-old Corcoran Clay near its western limit (Hotchkiss, 1972). The boundary in the southern San Joaquin Valley lies along the eastern flanks of the late Cenozoic anticlines (Hoots and others, 1954). Cenozoic sediments east of the boundary dip gently to the west and are affected by only a few minor faults and anticlines with small closure (Hotchkiss, 1972; Hoots and others, 1954).

The contrasting structural styles in Cenozoic sediments across the boundary zone probably reflect the underlying basement transition there. Much of the late Cenozoic compressional deformation in the Coast Ranges may be a consequence of crustal extension in the Great Basin region, which has displaced the Sierran block westward (Wright, 1976), perhaps driving the westward-tapering wedge (Oliver, 1977) of Sierran basement into or beneath the comparatively weak Franciscan Complex basement of the Coast Ranges.

### HISTORICAL SEISMICITY

The historical seismicity record for California suggests that several significant earthquakes have occurred within, but have not yet been attributed to, the Coast Ranges-Sierran block boundary zone. The historical seismicity for the region that includes the Coast Ranges-Sierran block boundary zone from Red Bluff south to Bakersfield is shown for the period 1790 through 1976 on Figures 2 and 3. A total of 9250 earthquakes of  $M_L$  greater than or equal to 2.9 or Rossi-Forel (RF) maximum intensity of II or greater<sup>2</sup> are shown. The epicentral locations of the events are based on instrumental locations or the location of the maximum reported intensity. Because population size and distribution are critical factors in reporting intensities, and because the

<sup>2</sup>If an event is reported in a published source without an assigned magnitude or maximum intensity, it has been included on these figures for completeness.



population in the 1800s and early 1900s was relatively small and unevenly distributed in this region, the accuracy of the corresponding earthquake locations may be poor. In some instances, only one felt report may exist, so an earthquake would be assigned the location of that report. Earthquake locations based on maximum intensities are shown as diamonds for relatively well defined locations (accuracy within 160 km), or as triangles if the location is ambiguous.

The historical seismicity is subdivided into two time periods: 1850 through 1929 for generally preinstrumental locations, and 1930 through 1976 for instrumental locations. The primary data sources for the preinstrumental locations are Townley and Allen (1939), Slemmons and others (1965), and Bolt and Miller (1975). Primary sources for the instrumental locations are Bolt and Miller (1975), Slemmons and others (1965), and the NOAA data file, which consists primarily of locations determined by the California Institute of Technology.

Based on their locations, the following significant earthquakes may have occurred within the Coast Ranges-Sierran block boundary zone, excluding the Coalinga area:

- 1) 12 April 1885, felt widely throughout the Great Valley and Sierran foothills, with a maximum reported Modified Mercalli (MM) intensity of VII at Las Tablas (?) somewhere on the east side of the Coast Ranges, possibly near Coalinga ( $M_L$  6.2) (Toppozada and others, 1981);
- 2) 19 May 1889, with a maximum reported MM intensity of VIII at Antioch ( $M_L$  6.0)<sup>3</sup>. The source of this earthquake is possibly the Midland fault (Figure 2);
- 3) 19 April 1892, with a maximum reported MM intensity of IX at Allendale between Vacaville and Winters ( $M_L$  6.4)<sup>3</sup>. This was one of the largest earthquakes felt in the San Francisco Bay area in historical times, followed by a  $M_L$  6.2 aftershock (Toppozada and others, 1981) (Figure 2);
- 4) 19 May 1902, with a maximum reported intensity MM VII to VIII at Elmira ( $M_L$  5.5)<sup>4</sup> (Figure 2);
- 5) 24 July 1903, with a maximum reported intensity MM VII at Willows ( $M_L$  4.5)<sup>4</sup> (Figure 2); and
- 6) 30 July 1904, with a maximum reported intensity MM VI at Woodland ( $M_L$  4.5)<sup>4</sup> (Figure 2).

#### The Patterson and 1881 Earthquakes

Until recently, detailed investigations of seismicity along the Coast Ranges-Sierran block boundary was not possible because of lack of seismograph

<sup>3</sup>Magnitudes assigned by Toppozada and others (1981).

<sup>4</sup>Magnitudes assigned by Real and others (1978).

ic coverage, especially within the Great Valley. During the period September 1977 to September 1979, Woodward-Clyde Consultants established a 22-station microearthquake network in the northern San Joaquin Valley and adjacent Sierran foothills (Wong and Savage, 1983). More recently, on 13 October 1977 at 1910 PST, an earthquake of  $M_L$  3.5 occurred 8 km northeast of the town of Patterson on the western margin of the San Joaquin Valley, probably within the Coast Ranges-Sierran block boundary zone. Seismographic coverage by this network and by the U.S. Geological Survey's central California network allowed a detailed examination of the Patterson seismicity. The mainshock was preceded by a  $M_L$  2.5 foreshock and followed by four aftershocks ( $M_L$  greater than 1.0) (Wong and Savage, 1978). The calculated focal depth of the mainshock was  $10 \text{ km} \pm 5 \text{ km}$ , although no stations were close enough to the epicenter to provide strong focal depth control. Subsequent to the October 1977 sequence, 12 additional events occurred in the Patterson area through September 1979 (Figure 4). The spatial pattern of the Patterson epicenters suggested a northwest-trending fault or system of faults parallel to the regional structural trend.

A fault plane solution of the 13 October mainshock (Figure 5) exhibits northwest-trending nodal planes, consistent with the regional structural trend and the epicentral alignment. The solution indicates either a low-angle thrust fault or a high-angle reverse fault as the source of the mainshock. The tectonic stress field indicated by the fault plane solution suggests northeast-southwest trending maximum compression and vertical minimum compressive stress. The solution is similar to the 1983 Coalinga mainshock.

The closest mapped structure to the Patterson seismicity is the Vernalis fault, a post-Eocene high-angle reverse fault located northwest of the activity (Jennings, 1977) (Figure 4). Herd (1978) postulated the existence of an 80-km long San Joaquin fault zone in the subsurface between Tracy and Los Banos. This fault zone is expressed at the surface near the base of the Diablo Range foothills and is characterized by normal faulting, east-side-down, and local reverse faults. Although no direct association can be made between the observed seismicity and either the Vernalis fault or the San Joaquin fault zone, the style of faulting exhibited by the fault plane solution is consistent with postulated complex faulting along the Great Valley-Coast Ranges boundary zone. The relatively deep focal depths of the Patterson activity (10 to 15 km) also suggest that the events occurred within the basement rock beneath the valley sediments.

Although the 1977 earthquake was only of moderate size, it had maximum intensities of MM III to IV in Modesto and was felt over a relatively large area (Figure 6). The event was felt almost exclusively north and east of the epicenter; almost no felt reports exist from the south. The isoseismal contours were elongated along the axis of the valley.

An interesting feature of the 1977 earthquake is the distance of 18 km between the epicenter (located near the margin of the valley at the edge of the felt area of the earthquake) and Modesto, where the maximum intensities of MM III to IV were reported (Figure 6). This difference between the epicentral location and the location of maximum intensity suggests that preinstrumental earthquakes previously thought to have occurred within the Great Valley based on maximum reported intensities may be biased.

A possible example is the 10 April 1881 earthquake, which is the largest historical event reported felt and supposedly located within the northern San Joaquin Valley (Figure 2). A maximum intensity of MM VI was reported in Modesto (Figure 7); its magnitude was estimated to be  $M_L$  6.0 (Toppozada and others, 1981). Two interesting features of the 1881 isoseismal map include: (1) elongation of the isoseismals along the axis of the Great Valley (a pattern observed in isoseismal maps for the Patterson earthquake and other earthquakes located near the Great Valley, probably resulting from amplification by thick unconsolidated and water-saturated sediments); and (2) the bias of higher intensities west of the Great Valley in the coastal areas, in contrast to the lower intensities in the Sierran foothills to the east. These observations suggest that, as in the case of the 1977 Patterson earthquake, the maximum reported intensities in the Great Valley interior have biased the location of the 1881 earthquake eastward (Wong and Savage, 1978). An additional factor may be that the population in the San Joaquin Valley has been concentrated in its center and is sparse on its western margin. Toppozada and others (1981) also assigned the location of the 1881 earthquake to the west of the San Joaquin Valley; however, they suggested that it was centered within the Diablo Range.

An examination of Figures 2 and 3 shows a contrast of seismicity levels within the Great Valley. Preinstrumental seismicity (pre-1930) suggests moderate to large magnitude earthquake activity throughout the Great Valley, with active sources near the towns of Willows, Sacramento, and Stockton. In contrast, the instrumental seismicity (post-1930) shows the Great Valley to exhibit a low level of seismicity, except in the vicinity of Willows and Modesto. The microearthquake monitoring in the northern San Joaquin Valley and a review of the instrumentally located events (in the portion of the valley near Modesto) suggest that the level of seismicity is very low (Wong and others, 1978). Inaccurate epicentral locations around Modesto and possibly around Willows (because of inadequate seismographic coverage and poor instrumental timing prior to 1960) provide misleading pictures of the level of seismicity in these areas. It is therefore likely that many of the historical earthquakes that have been assigned locations in the Great Valley based on maximum reported intensities, such as the 1881 earthquake, and on instrumental locations, may have actually occurred within the Coast Ranges-Sierran block boundary zone, or possibly further westward.

#### TECTONIC STRESS FIELD

A compilation of fault plane solutions for earthquakes that have occurred in the Coast Ranges province and the Sierran block in central California is shown on Figure 8. Most of the fault plane solutions in the Coast Ranges province exhibit right-lateral strike-slip faulting on nodal planes that strike northwest-southeast parallel to the San Andreas fault system and the regional structural trend. Although significant local variations exist, the tectonic stress field characterized by these fault plane solutions shows predominantly north-south maximum compression and east-west minimum compression. Eastward, however, in the vicinity of the Coast Ranges-Sierran block boundary, the limited number of fault plane solutions, including solutions for the 1977 Patterson earthquake and the 1983 Coalinga mainshock, exhibit an eastward rotation of the direction of maximum compression, which now trends northeast-



southwest perpendicular to the trend of the boundary zone, and in the cases of the Patterson and Coalinga earthquakes, a vertical minimum compressive stress. It is possible that this rotation and change in tectonic stress field characterizes the Coast Ranges-Sierran block boundary. Whereas right-lateral strike-slip faulting on northwest-southeast-trending structures (shear deformation) is characteristic of the Coast Ranges province, reverse faulting on similarly oriented northwest-southeast trending structures and right-lateral strike-slip displacement on north-south trending faults characterizes the boundary zone along the western margin of the San Joaquin Valley (e.g., Coalinga and Patterson earthquakes).

We suggest that the maximum compression perpendicular to the boundary zone is possibly caused by a westward movement of the Sierran block against the Coast Ranges province (as postulated by Wright, 1976) as a consequence of late Cenozoic crustal extension in the Great Basin region to the east. The localized eastward rotation of the regional stress field along the block boundary may be caused by the interplay of compressive forces normal to the block boundary as it is driven westward into a region characterized by shear deformation.

The two fault plane solutions located in the San Joaquin Valley in the Sierran block interior suggest a rotation of the maximum compressive stress back to a more north-south orientation (Figure 8). Zoback and Zoback (1980) considered the tectonic stress field of the Sierran block to be transitional between that of the San Andreas fault and the Great Basin. They characterized the stress field of the block as having a maximum compressive stress that is trending north-northeast nearly equal to a vertical intermediate stress, each being much greater than the west-northwest-trending least compressive stress.

Future detailed seismological investigations along the boundary zone, particularly on the western margin of the Sacramento Valley, where many of the larger historical earthquakes may have occurred, should provide valuable information on the tectonic and seismogenic characteristics of this zone.

#### SUMMARY

A review of the historical seismicity of the Coast Ranges-Sierran block boundary and the adjacent Great Valley, and a detailed examination of recent seismicity near Patterson and of fault plane solutions for the Coast Ranges province and the Sierran block yield the following observations.

- 1) Several significant historical earthquakes may be associated with faults composing the Coast Ranges-Sierran block boundary, suggesting that this zone may be capable of producing large earthquakes ( $M_L$  greater than 6).
- 2) The level of moderate to large magnitude seismicity within the boundary zone may be higher than the historical record would indicate because of the probable bias in epicentral locations based on maximum reported intensities of several historical earthquakes, and, to a lesser degree, the inaccuracy of instrumental locations prior to the 1960s.



- 3) The Coast Ranges-Sierran block boundary may be characterized by a change in the tectonic stress field such that the direction of maximum compression is rotated from north-south within the Coast Ranges province to northeast-southwest along the boundary. The minimum compressive stress also appears to rotate from horizontal to vertical, at least for the area of Coalinga and Patterson. The dominantly shear deformation (strike-slip faulting) within the Coast Ranges province changes to compressional tectonics (reverse and strike-slip faulting) along the boundary zone.
- 4) The 1983 Coalinga earthquake may be associated with the Coast Ranges-Sierran block boundary, based on its location, its style of faulting, and the tectonic stress field exhibited by its fault plane solution, which is similar to that of the 1977 Patterson earthquake. Thus the Coalinga earthquakes are probably not unusual in the context of the tectonics of the Coast Ranges-Sierran block boundary.

#### ACKNOWLEDGEMENTS

Our appreciation to the many colleagues who worked on the Pacific Gas and Electric Company's Stanislaus Nuclear Project, during which much of the data presented in this paper was derived, and for their assistance in the preparation of this paper. Our thanks in particular to the late D. Tocher, W. Savage, K. McNally, B. Munden, K. Hee, E. Grace, and V. Chernock. T. Topozada kindly provided some helpful suggestions. Special thanks to J. Eaton of the U.S. Geological Survey for his unselfish sharing of ideas and data. Critical review by K. Coppersmith and N. Biggar is appreciated.

Our gratitude to F. Conwell and the Professional Development program of Woodward-Clyde Consultants for financial assistance in the preparation of this paper.

#### REFERENCES

- Bolt, B.A., and Miller, R.D., 1975, Catalogue of earthquakes in northern California and adjoining areas (1 January 1910-31 December 1972): Seismographic Stations, University of California, Berkeley, California, 567 p.
- Bolt, B.A., Lomnitz, C., and McEvilly, T.V., 1968, Seismological evidence on the tectonics of central and northern California and the Mendocino escarpment: Seismol. Soc. of America Bull., v. 58, p. 787-812.
- Bufe, C.G., Marks, S.M., Lester, F.W., Ludwin, R.S., and Stickney, M.C., 1981, Seismicity of the Geysers-Clear Lake region: U.S. Geol. Survey Prof. Paper 1141, p. 129-137.
- Cady, J.W., 1975, Magnetic and gravity anomalies in the Great Valley and western Sierra Nevada metamorphic belt, California: Geol. Soc. America Special Paper 168, 56 p.

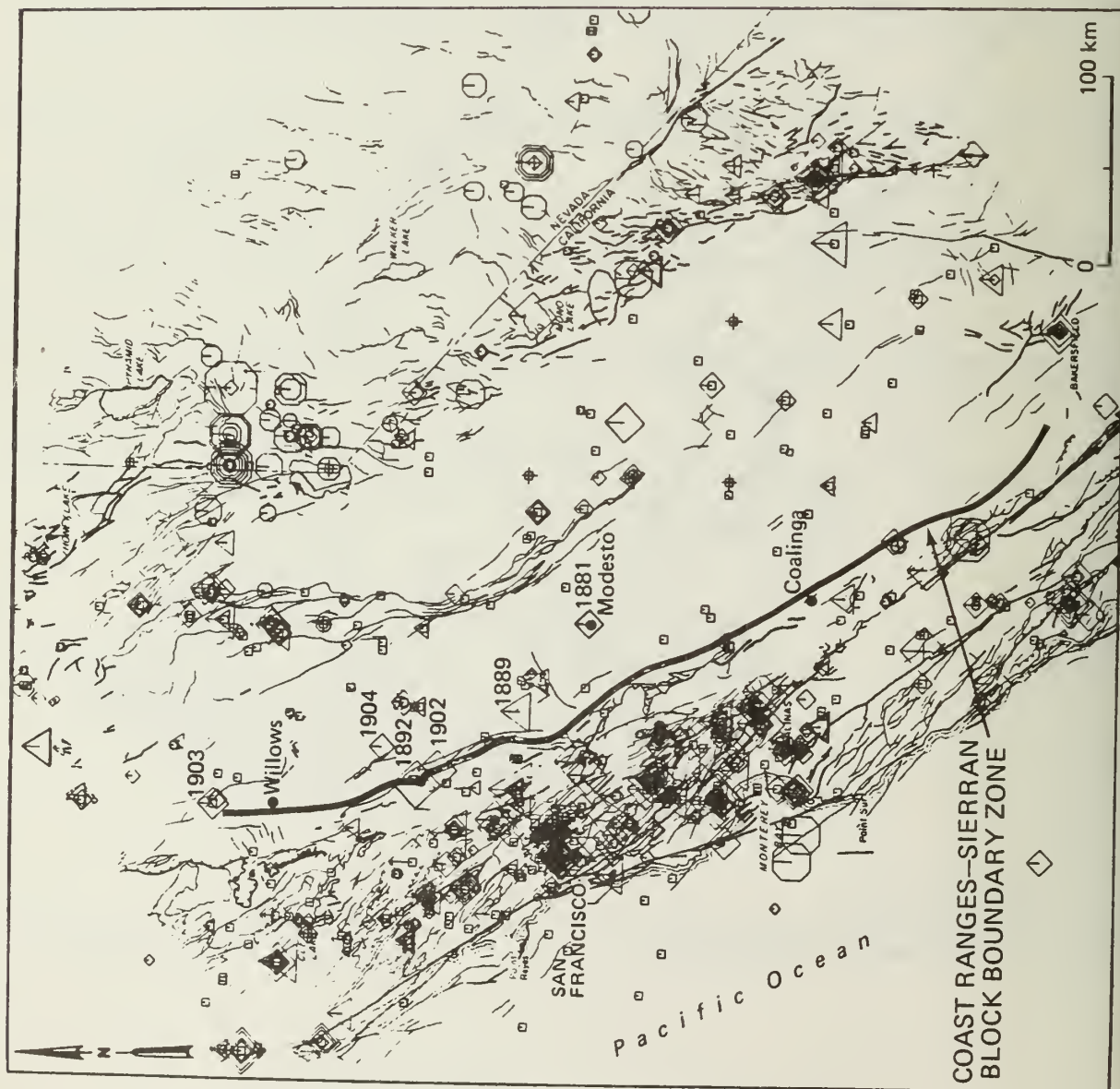
- Eaton, J.P., Cockerham, R.S., and Lester, F.W., 1983, Study of the May 2, 1983 Coalinga earthquake and its aftershocks based on the USGS seismic network in northern California: California Div. Mines and Geol. Special Publication 66.
- Ellsworth, W.L., 1975, Bear Valley, California, earthquake sequence of February-March 1982: Seismol. Soc. of America Bull., v. 65, p. 483-506.
- Ely, R.W., and Packer, D.R., 1978, The boundaries of the Sierran block, California: Earthquake Notes, v. 49, p. 85-86.
- Ernst, W.G., 1970, Tectonic contact between the Franciscan melange and the Great Valley sequence - crustal expression of a late Mesozoic Benioff zone: Journ. Geophys. Research, v. 75, p. 866-901.
- Followill, F.E., and Mills, J.M., 1982, Locations and focal mechanisms of recent microearthquakes and tectonics of Livermore Valley, California: Seismol. Soc. of America Bull., v. 72, p. 821-840.
- Herd, D.G., 1978, Neotectonic framework of Central Coastal California and its implications to microzonation of the San Francisco Bay Area: 2nd Internat. Conf. on Microzonation, San Francisco, Proc., v. I, p. 231-240.
- Hoots, H.W., Bear, T.L., and Kleinpell, W.D., 1954, Geological summary of the San Joaquin Valley, California: California Div. Mines and Geol. Bull. 170, p. 113-129.
- Hotchkiss, W.R., 1972, Generalized subsurface geology of the water-bearing deposits, northern San Joaquin Valley California: U.S. Geol. Survey Open-File Rep. 18 p.
- Jennings, C.W., 1977, Geologic map of California: California Dept. Conservation, scale 1:750,000.
- Oliver, H.W., 1977, Gravity and magnetic investigations of the Sierra Nevada batholith, California: Geol. Soc. America Bull., v. 88, p. 445-461.
- Page, B.M., Wagner, H.C., McCulloch, D.S., Silver, E.A., and Spotts, J.H., 1979, Tectonic interpretation of a geologic section of the continental margin off San Luis Obispo, the Southern Coast Ranges, and the San Joaquin Valley, California, Cross-section summary: Geol. Soc. America Bull., v. 90, p. 808-812.
- Page, R.W., 1974, Base and thickness of the post-Eocene continental deposits in the Sacramento Valley, California: U.S. Geol. Survey Water Resources Investigations 45-73, 16 p.
- Real, C.R., Toppozada, T.R., and Parke, D.L., 1978, Earthquake catalog of California, January 1, 1900 - December 31, 1974: California Div. Mines and Geol. Special Publication 52, 15 p.

- Reasenber, P., and Ellsworth, W.L., 1982, Aftershocks of the Coyote Lake, California earthquake of August 6, 1979, a detailed study: Journ. Geophys. Research, v. 86, p. 10,637-10,655.
- Slemmons, D.B., Jones, A.E., and Gimlett, J.I., 1965, Catalog of Nevada earthquakes, 1852-1960: Seismol. Soc. America Bull., v. 55, p. 537-583.
- Topozada, T.R., Real, C.R., and Parke, D.L., 1981, Preparation of isoseismal maps and summaries of reported effects for pre-1900 California earthquakes: California Div. Mines and Geol. Open-File Rep. 81-11, 78 p.
- Townley, S.D., and Allen, M.W., 1939, Descriptive catalog of earthquakes of the Pacific Coast of the United States, 1769 to 1928: Seismol. Soc. America Bull., v. 29, 294 p.
- Wong, I.G., and Savage, W.U., 1978, Epicentral location bias based on maximum intensity in the western San Joaquin Valley, California: Earthquake Notes, v. 49, p. 26-27.
- Wong, I.G., and Savage, W.U., 1983, Deep intraplate seismicity in the western Sierra Nevada, central California: Seismol. Soc. of America Bull., v. 73, p. 797-812.
- Wong, I.G., Savage, W.U., and Tocher, D., 1978, Low-level seismicity in the San Joaquin Valley, California: EOS, Trans. Am. Geophys. Union, v. 49, p. 1136.
- Wright, L., 1976, Late Cenozoic fault patterns and stress fields in the Great Basin and westward displacement of the Sierra Nevada block: Geology, v. 4, p. 489-494.
- Zoback, M.L., and Zoback, M., 1980, State of stress in the conterminus United States, Journ. Geophys. Research, v. 85, p. 6113-6156.



Figure 1. Tectonic provinces and crustal blocks of California





## REPORTED RICHTER MAGNITUDE

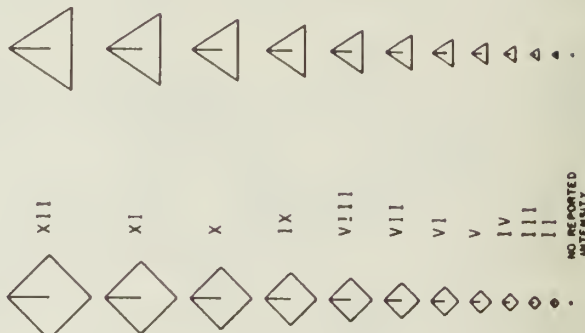
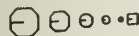
ROSSI-FOREL or MODIFIED  
MERCALLI INTENSITY

Figure 2. Historical seismicity of the Coast Ranges-Sierran block boundary zone and adjacent regions, 1850 to 1929.

REPORTED RICHTER MAGNITUDE

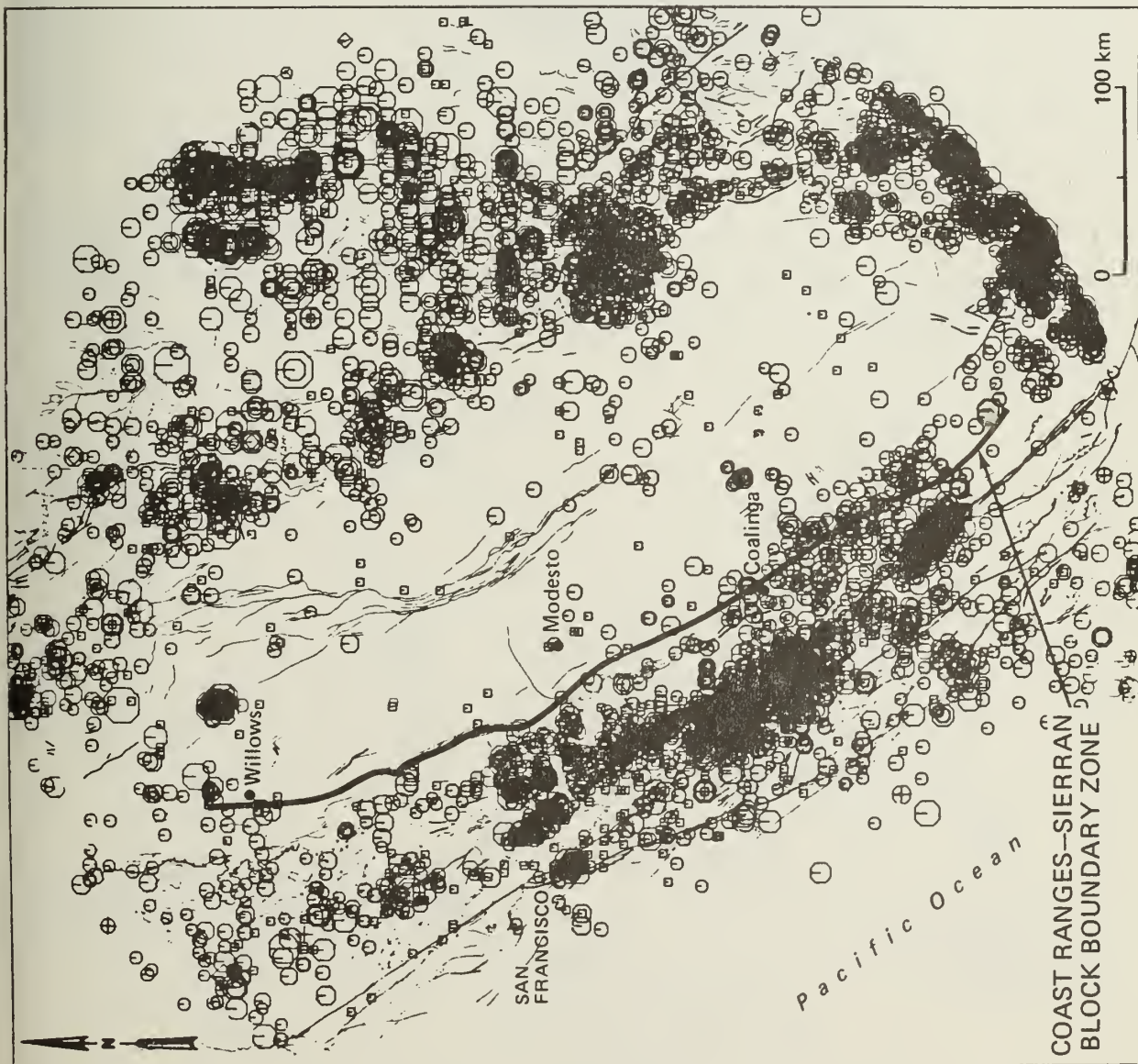
5.0  
4.0  
3.0  
2.0  
1.0  
NO REPORTED  
MAGNITUDE



8.0

7.0

6.0



COAST RANGES-SIERRAN  
BLOCK BOUNDARY ZONE

Figure 3. Historical seismicity of the Coast Ranges-Sierran block boundary zone and adjacent regions, 1930 to 1976.

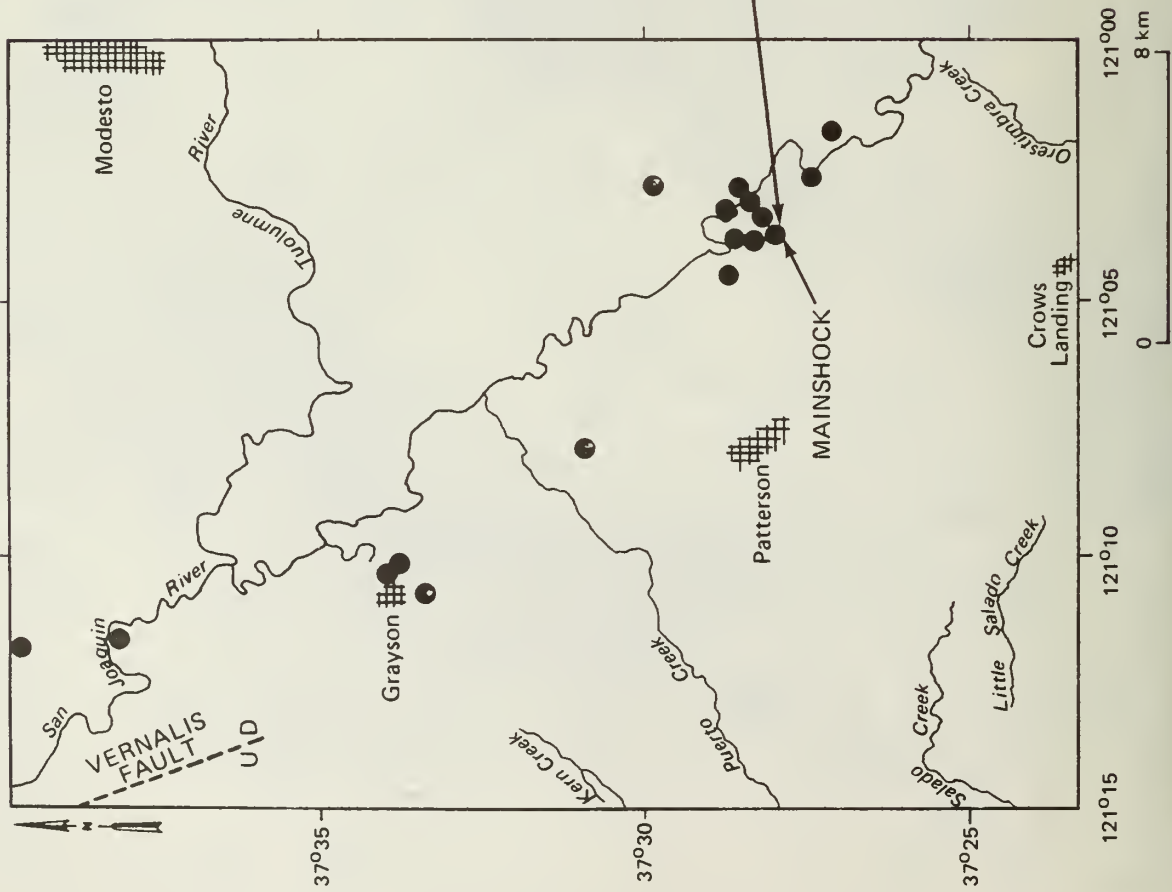


Figure 4. Seismicity near Patterson, September 1977 to September 1979

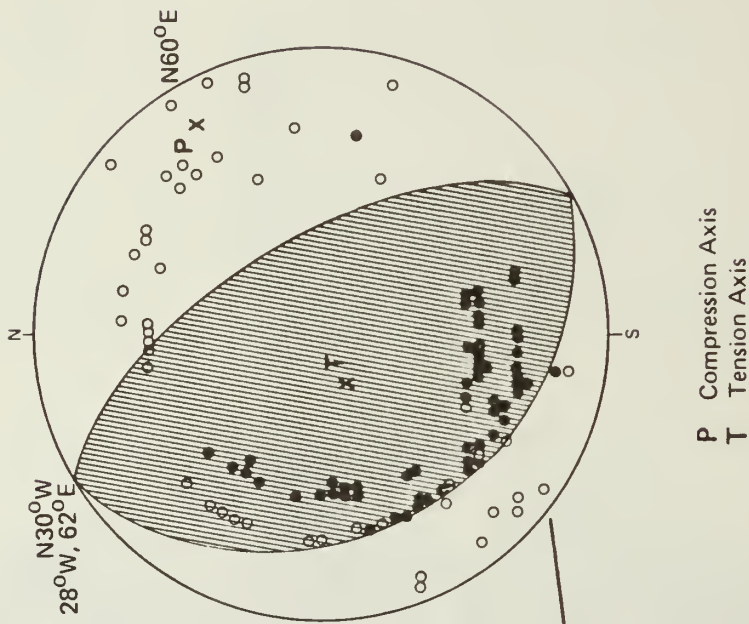


Figure 5. Fault plane solution of the 13 October 1977 ML 3.5 Patterson earthquake. Shown is a lower hemisphere projection with solid dots representing compressional first motions and open dots representing dilatations.



Figure 6. Isoseismal map of the 13 Oct 1977  $M_L$  3.5 Patterson earthquake. Note the 18 km distance between the epicenter and the maximum intensity.

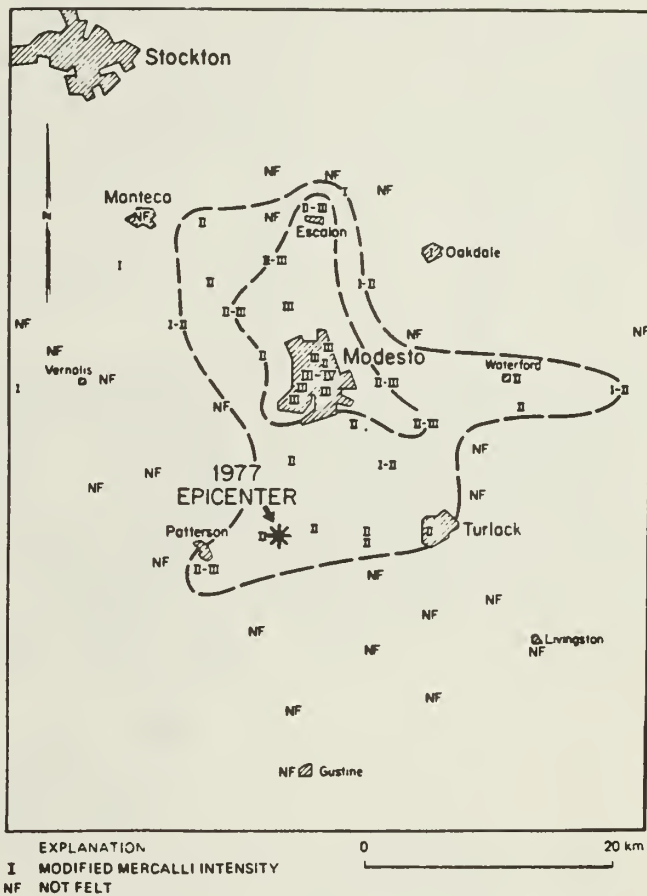
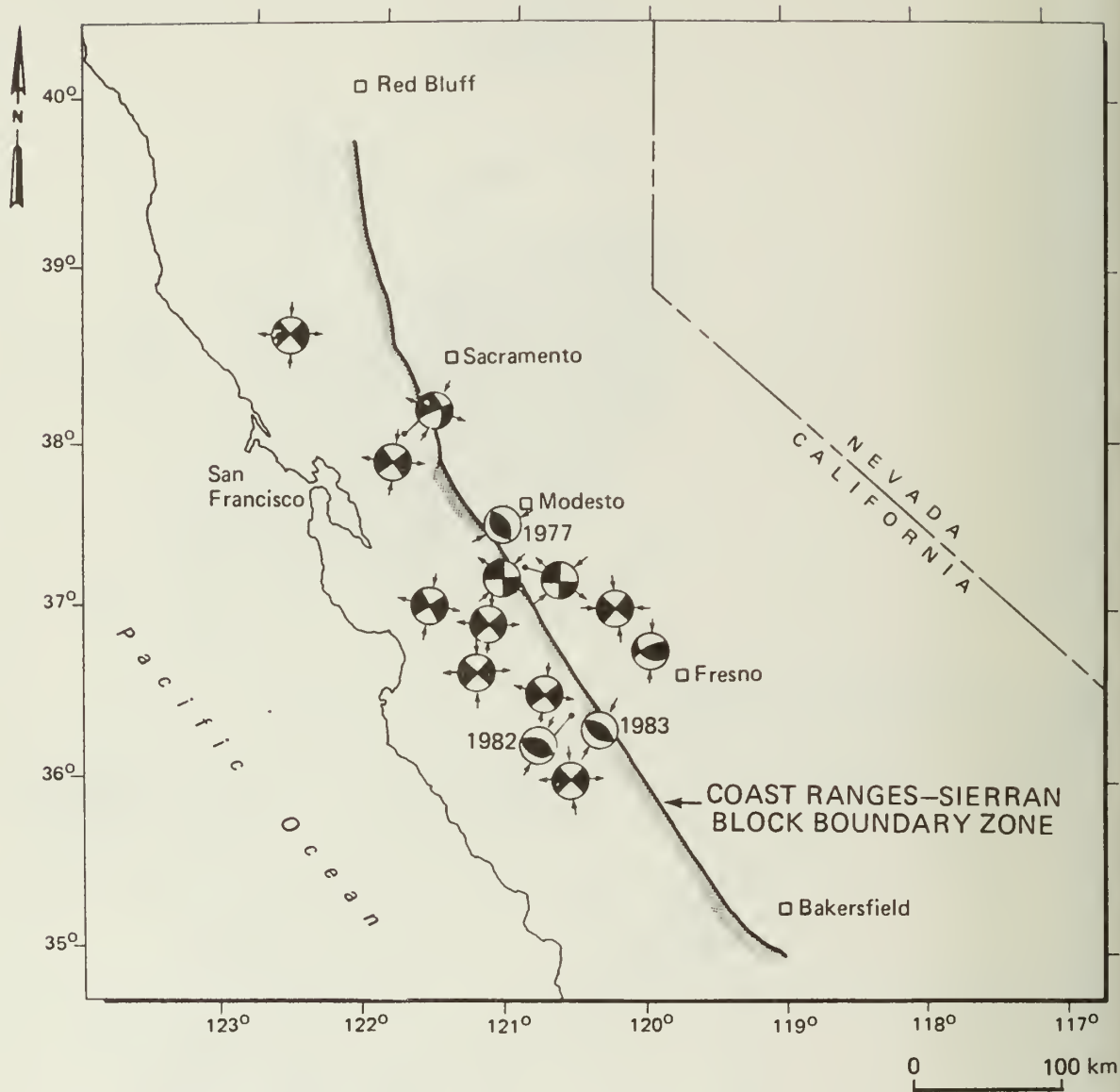


Figure 7. Isoseismal map of the 10 April 1881 Modesto earthquake. Superimposed for comparison is the felt area for the 1977 Patterson earthquake.







EXPLANATION

Strike-Slip Faulting

Reverse Faulting

Sources: Anderson and others(1982), Bolt and others(1968), Bufe and others(1981), Eaton and others(1983), Ellsworth(1975), Followill and Mills(1982), Reasenberg and Ellsworth(1982) and Wong and Savage(1983).

Figure 8. Fault plane solutions for earthquakes that have occurred in the Coast Ranges province and Sierran block, central California .

# REGIONAL GEOLOGY OF THE COALINGA, CALIFORNIA AREA

by

John T. Alfors<sup>1</sup>

## ABSTRACT

The geology of the Coalinga area has been the subject of study since early 1900. The southern Coast Ranges includes a subduction zone complex (Franciscan Complex), forearc basin sediments (Great Valley sequence), and a magmatic arc (plutonic and metamorphic rocks of the Salinian Block). From Late Jurassic time to the present, the area has been an active tectonic area. A thick sequence of Mesozoic marine sedimentary rocks were deposited in the area. During the Cenozoic, the marine depositional basin became fragmented, and during the Pleistocene, extensive uplift resulted in the area becoming the site of subareal erosion and deposition of continental sediments.

## GEOLOGIC SETTING

The Coalinga earthquake of May 2, 1983 was centered eight miles northeast of Coalinga, in southwestern Fresno County, California (see Wentworth and others, 1983, Fig. 1 this volume). The Coalinga area is located at the southern end of the Diablo Range on the eastern margin of the southern Coast Ranges. The earthquake occurred on the eastern flank of the Coalinga anticline apparently on a previously unmapped thrust fault, hence not shown on the 1:750,000 scale Geologic Map of California (Jennings, 1977). The geology of the southern Coast Ranges in the vicinity of Coalinga is complex having been involved in typical tectonic, sedimentary, and igneous processes of the Circum-Pacific orogenic belt.

---

<sup>1</sup> Supervising Geologist, California Division of Mines and Geology

## GEOLOGIC LITERATURE

The Coalinga area has been studied by many geologists. A comprehensive bibliography of the geologic literature for this area has been assembled by E.J. Fowkes (1983, p. 240-252). This bibliography covers the literature published from 1904 to 1979. Ingersoll (1983, p. 1141-1142) lists some additional references with publication dates to 1983. Much of the early geologic mapping in the area was directed at the petroleum resources of this area (Arnold and Anderson, 1910; Anderson and Pack, 1915). Professor N.L. Taliaferro and his students at the University of California, Berkeley, accomplished a large amount of field-work and interpretation (Taliaferro, 1943). T.W. Dibblee, Jr. has mapped more Coast Range geology than any other individual, and his Coalinga quadrangle was open-filed by the U.S. Geological Survey in 1971. Much of the geologic mapping by Taliaferro and Dibblee is incorporated on the Santa Cruz Sheet of the Geologic Map of California (Jennings and Strand, 1958). Professor Page (1966, 1981) of Stanford University has summarized the geology of the entire Coast Ranges of California.

The recent geologic literature dating from the mid-1960s has generally taken cognizance of plate tectonic theory. Atwater (1970) has described the Cenozoic tectonic evolution of western North America. Ingersoll (1983) has described the late Mesozoic and Paleogene history of northern and central Coast Ranges. Ernst (1979, 1981) has summarized the geotectonic development of California. A recent paper by Dickinson (1983) presents a lucid synthesis of the tectonic history of California.

## GEOLOGIC HISTORY

The geologic history of the southern Coast Ranges in the latitude of Coalinga is complex. Little is known of the area during Precambrian and Paleozoic time. Shelf facies marine deposits of Paleozoic to possible Precambrian age are present in the Salinian block along the coast west of Coalinga, but these rocks are now thought to have been deposited about 350 miles southeast of their present position (Dickinson, 1983).

The Coalinga region appears to have been an oceanic area where few or no sediments were accumulating from Precambrian to Early Jurassic time. During the Late Jurassic, a subduction zone was initiated along what is now the Coast Ranges of California. The eastward-dipping subduction zone carried the floor of the Pacific Ocean beneath the continent, where partial fusion gave rise to a magmatic arc in the area of the present Sierra Nevada (Seiders, 1983). Erosion of that arc and older parts of the continental margin supplied sediment that was spread westward off the edge of the continent and deposited in a forearc basin, which is preserved today as the Great Valley sequence. On the west, a subduction zone, now preserved as the Franciscan Complex, formed above the descending plate and tapered westward to a trench. The subduction zone grew with time, as

crustal rocks were scraped from the descending oceanic plate and added to the Franciscan Complex (Seiders, 1983). This tectonic regime continued through the Cretaceous and into the early Tertiary. During the mid-Cretaceous, left-lateral slip is inferred to have occurred on the Nacimiento fault west of Coalinga which resulted in about 350 miles of net displacement within about 10 million years (Dickinson, 1983). This displacement brought rocks of the Salinian block (for location map see Wong and Ely, 1983, Fig. 1 this volume) to the latitude of Coalinga from an area southwest of Mojave. Right-lateral strike-slip movement along the San Andreas fault in the latitude of Coalinga began as subduction at the trench ceased, caused by northwestward passage of the Mendocino triple junction (Atwater, 1970). It has been postulated that the San Andreas transform fault began about 30 million years ago near the latitude of Guaymas, Mexico and propagated northward at a rate of 6 cm/yr (Atwater, 1970). The northern end of the San Andreas fault is now at the latitude of Cape Mendocino; about 12 million years ago it was at about the latitude of Coalinga (Atwater, 1970, Fig. 5). A proto-San Andreas fault with right-lateral displacement on the order of 100 miles has been inferred with the movement occurring in latest Cretaceous to Paleocene time (Dickinson, 1983).

At the end of the Cretaceous, moderate uplift occurred in the Coalinga area that resulted in erosion of the older rocks. The Tertiary Period opened with deposition of Paleocene and early Eocene sediments (mostly sandstones and shales) into the Coast Ranges trough and its now deepening eastward extension toward the Sierra Nevada reaching the present site of Riverdale, California (Fowkes, 1982). The later Eocene sandstones were deposited in shallow seas on shelf environments while shale was deposited in a broader, deeper sea (Fowkes, 1982).

In late Eocene and Oligocene time, an uplift exposed Cretaceous rocks in the Coast Ranges basin creating an inland sea, the San Joaquin basin, between the uplifted area and the Sierra Nevada. During the Miocene, a shallow sea occupied the Coalinga area; at this time serpentinite was exposed to erosion in the uplifted area. At the close of the Miocene Epoch, an uplift exposed the Coalinga area to a brief period of erosion (Fowkes, 1982).

The San Joaquin basin resubmerged during the Pliocene Epoch with marine sediments being deposited in the southern portion and nonmarine sediments deposited in the northern portion. A major uplift of the Coast Ranges took place in the Pleistocene; fluvial and lacustrine sediments were deposited during this time (Fowkes, 1982).



## STRATIGRAPHY

The Coalinga area contains a thick sequence of sedimentary and minor volcanic rocks ranging in age from Late Jurassic to Holocene (Jennings, 1977). The geologic units are briefly described below:

Franciscan Complex: In the Coalinga area the Franciscan Complex ranges in age from Early Jurassic to Late Cretaceous and consists predominantly of graywacke with minor shale, altered mafic volcanic rock, and chert. Locally metamorphic rocks including glaucophane schist, actinolite schist, and jadeitic rocks crop out within rocks of the Franciscan Complex. Northwest of Coalinga, the large New Idria serpentinite piercement is in fault contact with Franciscan rocks. Smaller masses of serpentinite occur in other Franciscan terranes in the Coalinga area. The thickness of the Franciscan Complex in the Coalinga area is uncertain, but the thickness of the Franciscan Complex has been estimated to be more than 50,000 feet (Bailey, Irwin, and Jones, 1964).

Great Valley sequence: The Great Valley sequence near Coalinga consists of about 28,000 feet (8.5 km) of thin-bedded mudstone, sandstone, and conglomerate. The age is similar to that of the Franciscan Complex, Late Jurassic to Late Cretaceous (Mansfield, 1979). A large number of formation names have been applied to units within the Great Valley sequence. Fowkes (1982, p. 36) lists three formations: Gravelly Flat Shale, Panoche Formation, and Moreno Shale with the Panoche Formation divided into 14 members. Mansfield (1979, Fig. 2) has divided the Great Valley sequence in the Coalinga area into seven petrofacies units.

Lodo Formation: The Lodo Formation consists of about 1,150 feet of claystone of Paleocene and early Eocene age in the type area. South of the type area, sandstone units are included, and the formation has been divided into four distinct units: Cerros Sandstone, Cerros Shale, Cantua Sandstone, and Arroyo Hondo Shale. The aggregate maximum thickness of these units is 6,190 feet (Fowkes, 1982).

Yokut Sandstone: The Yokut Sandstone of middle Eocene age is a shallow-water beach sand deposit that gradationally overlies the Arroyo Hondo Shale. It attains a maximum thickness of 305 feet (Fowkes, 1982).

Domengine Sandstone: The Domengine Sandstone of middle Eocene age is a poorly-sorted arkosic sandstone with interbedded claystone and siltstone. It unconformably overlaps the Yokut Sandstone and the Lodo Formation and averages 70 feet in thickness (Fowkes, 1982).

Avenal Sandstone: The Avenal Sandstone is equivalent to the Domengine Sandstone. The Domengine Sandstone becomes the Avenal Sandstone south of Warthan Canyon, southwest of Coalinga (Fowkes, 1982).

Kreyenhagen Shale: The Kreyenhagen Shale is a diatomaceous shale that attains a maximum thickness of almost 3,000 feet. It is late Eocene to Oligocene age and conformably overlies the Domengine and Avenal Sandstones (Fowkes, 1982).

Tumey Formation: The Tumey Formation of Oligocene age was originally included with the Kreyenhagen Shale but has been separated on the basis of a sandstone member at the base of the Tumey. The arkosic sandstone member has a maximum thickness of 700 feet, and the overlying diatomaceous shale member is about 250 feet thick (Fowkes, 1982).

Temblor Formation: The Temblor Formation is early Miocene in age and consists of petroliferous sandstone, calcareous sandstone, diatomaceous and foraminiferal shale, and sandstone aggregating about 550 feet in thickness. It unconformably overlies the Kreyenhagen Shale (Fowkes, 1982).

Big Blue Serpentinous Member of Temblor Formation: Locally at the top of the Temblor Formation is a unit that contains fine to coarse serpentinite fragments. This unit attains a maximum thickness of 1,000 feet. (Fowkes, 1982).

Santa Margarita Formation: The Santa Margarita Formation is late Miocene in age and consists of fine to coarse-grained sandstone with some gravel at the base and top of the formation. It is about 700 feet thick (Fowkes, 1982).

McLure Shale: The McLure Shale is late Miocene in age and consists of about 1,000 feet of siliceous shale. It is equivalent in age to the Santa Margarita Formation (Fowkes, 1982).

Reef Ridge Shale: The Reef Ridge Shale is late Miocene in age equivalent to the Santa Margarita Formation. It is less resistant than the McLure Shale which is similar in composition (Fowkes, 1982).

Etchegoin-Jacalitos Formation: The Etchegoin-Jacalitos Formation is early Pliocene in age. It consists of relatively soft shale, gravel, and sandstone and unconformably overlies the older units (Fowkes, 1982).

San Joaquin Formation: The San Joaquin Formation is late Pliocene in age. It consists of silty sandstone, silt, and clay. Maximum thickness is over 1,800 feet (Fowkes, 1982).

Tulare Formation: The Tulare Formation is Pleistocene in age and is generally a nonmarine sandstone and conglomerate of fluvial origin and lake deposits of sandstone, clay, and limestone. The maximum thickness is 3,500 feet (Fowkes, 1982).

## GEOLOGIC STRUCTURE

The southern Coast Ranges in the latitude of Coalinga consists of three structural blocks separated by the San Andreas and Sur-Nacimiento fault zones (Seiders, 1983). The block lying northeast of the San Andreas fault is underlain by Franciscan Complex and Great Valley sequence basement rocks. The block lying between the San Andreas fault

and the Sur-Nacimiento fault zone is underlain by pre-Franciscan metamorphic rocks and Cretaceous granitic rocks. The block lying west of the Sur-Nacimiento fault zone is underlain by Franciscan Complex and Great Valley sequence basement rocks (Page, 1966; Ernst, 1979).

The following discussion will be directed to the structures within the block lying east of the San Andreas fault. A series of generally northwest-trending anticlines and synclines extend from the San Andreas fault east to the San Joaquin Valley (Fowkes, 1982, Geologic Map in pocket). The Pleasant Valley syncline is a major feature which trends northwest and lies about two miles east of Coalinga. The Coalinga anticline also trends northwest and lies about five miles east of Coalinga. The White Creek syncline lies northwest of Coalinga and extends northwest and westward for more than 20 miles. The Jacalitos dome lies a few miles south of Coalinga. North dome in the Kettleman Hills lies about 15 miles southeast of Coalinga.

A number of small faults occur within the structural block east of the San Andreas fault. One of the longest of these is the Warthan Canyon-Castle Mountain fault zone which lies about nine miles west of Coalinga. The Curry Mountain fault is a shorter (six miles long) fault that lies about six miles west of Coalinga.

The folding in the Coalinga area has been attributed to subordinate contractional effects related to movement along the San Andreas fault (Dickinson, 1981). Although the possibility of present-day folding in the southern Coast Ranges has not been vigorously tested, the presence of warped Pleistocene terraces is strongly suggestive (Page, 1981). In addition to the upturning of young peripheral strata, the fact that the Diablo Range persists as a topographic high despite the nondurable character of its rocks (for example the soft sheared serpentinite of the New Idria piercement) and the rapid rate of erosion and landsliding suggests that slow uplift may be continuing (Page, 1981). Recent geodetic surveys showing that Anticline Ridge near Oilfields has risen about 1.4 feet as a result of the Coalinga earthquake (National Geodetic Survey, 1983) provides further evidence that uplift is continuing in the southern Coast Ranges.

#### ACKNOWLEDGEMENTS

Manuscript reviewed by Richard D. McJunkin and Charles W. Jennings. Cora Pingree graciously typed the manuscript.



## REFERENCES

- Anderson, Robert, and Pack, R.W., 1915, Geology and oil resources of the west border of the San Joaquin valley north of Coalinga, California: U.S. Geological Survey Bull. 603, 220 p.
- Arnold, Ralph and Anderson, Robert, 1910, Geology and oil resources of the Coalinga district, California: U.S. Geological Survey Bull. 398, 354 p.
- Atwater, Tanya, 1970, Implications of plate tectonics for the Cenozoic tectonic evolution of western North America: Geological Society of America Bull. Vol. 81, No. 12, p. 3513-3536.
- Bailey, Edgar H., Irwin, William P., and Jones, David L., 1964, Franciscan and related rocks and their significance in the geology of western California: California Division of Mines and Geology Bull. 183, 178 p.
- Dickinson, William R., 1981, Plate tectonics and the continental margin of California p. 1-28 in Ernst, W.G., editor, 1981, The geotectonic development of California, Rubey Volume 1: Prentice-Hall, New Jersey, 706 p.
- Dickinson, William R., 1983, Cretaceous sinistral strike slip along Nacimiento fault in coastal California: American Association of Petroleum Geologists Bull. V. 67, No. 4, p. 624-645.
- Ernst, W.G., 1979, California and plate tectonics: California Geology, V. 32, No. 9, p. 187-196.
- Ernst, W.G., (editor), 1981, Geotectonic development of California: Prentice-Hall, Inc., Englewood Cliffs, New Jersey, 706 p.
- Fowkes, E.J., 1983, An educational guidebook to the geologic resources of the Coalinga District, California, West Hills College, Coalinga, California, 260 p.
- Ingersoll, Raymond V., 1983, Petrofacies and provenance of Late Mesozoic forearc basin, northern and central California, American Association of Petroleum Geologists Bulletin V. 67, No. 7, p. 1125-1142.
- Jennings, Charles W., 1977, Geologic map of California: California Division of Mines and Geology, Geologic Data Map No. 2, scale 1:750,000.
- Jennings, Charles W., and Strand, Rudolph G., 1958 (second printing 1965), Santa Cruz sheet, Geologic map of California, Olaf P. Jenkins edition: California Division of Mines and Geology, scale 1:250,000.



- Mansfield, Charles F., 1979, Upper Mesozoic subsea fan deposits in the southern Diablo Range, California: Record of the Sierra Nevada magmatic arc: Geological Society of America Bull., vol. 90, pp. 1025-1046.
- National Geodetic Survey, 1983, Results of releveled, vicinity of Coalinga, California: Earthquake studies report HGZ L24759, 15 July 1983, 3 p.
- Page, Ben M., 1966, Geology of the Coast Ranges of California, in Geology of Northern California, E.H. Bailey, (editor): California Division of Mines and Geology Bull. 190, p. 255-276.
- Page, Benjamin M., 1981, The Southern Coast Ranges, p. 327-417 in Ernst, W.G., (editor), 1981, The geotectonic development of California, Rubey Volume 1: Prentice-Hall, New Jersey, 706 p.
- Seiders, Victor M., 1983, Correlation and provenance of Upper Mesozoic chert-rich conglomerate of California: Geological Society of America Bull. v. 94, p. 875-888.
- Taliaferro, N.L., 1943, Geologic history and structure of the central Coast Ranges of California: California Division of Mines Bull. 118, p. 119-163.
- Wentworth, Carl M., Walter, Allan W., Bartow, J. Alan, and Zoback, Mark D., 1983, Evidence on the tectonic setting of the 1983 Coalinga earthquakes from deep reflection and refraction profiles across the southeastern end of Kettleman Hills: California Division of Mines and Geology Special Publication 66.
- Wong, Ivan G. and Ely, Richard W., 1983, Historical seismicity and tectonics of the Coast Ranges-Sierran block boundary: implications to the 1983 Coalinga, California earthquakes: California Division of Mines and Geology Special Publication 66.

# EVIDENCE ON THE TECTONIC SETTING OF THE 1983 COALINGA EARTHQUAKES FROM DEEP REFLECTION AND REFRACTION PROFILES ACROSS THE SOUTHEASTERN END OF KETTLEMAN HILLS

by

Carl M. Wentworth, Allan W. Walter, J. Alan Bartow, and Mark D. Zoback<sup>1</sup>

## ABSTRACT

Preliminary interpretation of seismic reflection and refraction profiles across the southeastern end of Kettleman Hills, 65 km southeast of the Coalinga epicentral area, suggests the presence of both northeast-dipping reverse faults and a southwest-dipping thrust fault beneath the Kettleman Hills anticline. Two deep reverse faults are inferred to dip steeply northeastward beneath the anticline and offset basement at a depth of about 9 km. One of these faults is aligned with a shallow northeast-dipping reverse fault in the southwest limb of the anticline that offsets upper Miocene strata about 200 m; we assume that these two faults are connected. The reverse faults have an orientation beneath the anticline approximately equivalent to that of one plane of the focal mechanism solution for the Coalinga main shock, which is the plane preferred from surface deformation studies.

The thrust fault is inferred to dip gently southwestward from 3 km beneath the northeast limb of the anticline to a depth of 10 km beneath the Diablo Range. The thrust shows about 10 km of post-late Miocene dip slip that has repeated the Tertiary and upper Mesozoic section and the underlying Franciscan assemblage. The anticline grew during the Pliocene and Quaternary at the leading edge of this thrust where the reverse faults had deformed the underlying strata.

Mafic basement unconformably underlying the Great Valley sequence beneath the San Joaquin Valley plunges southwestward at 40° to a depth of 15 km beneath the Diablo Range, rather than following the base of the Great Valley sequence up to the surface. If this is a single, continuous basement surface, an eastward-thinning wedge of Franciscan rock is defined that lies between the basement and the overlying Great Valley sequence. Farther east, however, the Great Valley sequence was deposited directly on the same mafic basement. This relation suggests that, in contrast to prevailing views about the Coast Range thrust, the Franciscan assemblage was emplaced in wedgelike fashion by northeastward thrusting beneath the Great Valley sequence but above the mafic basement.

## INTRODUCTION

The epicentral region of the 1983 Coalinga earthquakes lies about 35 km northeast of the San Andreas fault in a large field of Cenozoic folds unbroken by any exposed throughgoing faults (fig. 1). No surface-breaking Quaternary faults had been recognized in the area prior to the earthquakes. Focal mechanism solutions for the main shock and principal aftershocks show reverse or thrust faulting on planes having mainly northwest-

---

<sup>1</sup>U.S. Geological Survey, Menlo Park, California

erly strikes (Eaton, this volume). Surface deformation in the vicinity of the main shock (Stein; King and Stein, this volume) and surface faulting along the Nunez fault associated with some of the aftershocks (M. J. Rymer, oral commun., 1983; Hart and McJunkin, this volume) support those focal planes representing the northeast-dipping reverse faulting.

Occurrence of the Coalinga earthquakes near the western margin of the San Joaquin Valley provides an opportunity to apply the emerging results of a new U.S. Geological Survey project to explore deep crustal structure between the Coast Ranges and the Sierran foothills (Wentworth, Walter, Zoback and others, 1983). This project is founded on combined deep seismic reflection and refraction surveys, the first of which extends along line SJ-6 across the Diablo Range and San Joaquin Valley at the southeast end of the Kettleman Hills (fig. 1). These data suggest northeast-southwest shortening along southwest-dipping thrust and northeast-dipping reverse faults, which represent a style of deformation closely related to the folding expressed at the surface and to the Coalinga earthquakes and associated deformation.

### GEOLOGIC SETTING

The 1983 Coalinga earthquakes occur near the southeastern end of the Diablo Range (fig. 1), a narrow, northwest-trending range of mountains that is sharply bounded on the northeast by the San Joaquin Valley and on the southwest by the San Andreas and Calaveras faults (Jennings, 1977). Beneath the alluvial surface of the San Joaquin Valley a wedge of Cretaceous and Cenozoic sedimentary rocks dips gently southwestward toward the Diablo Range and thickens from a feather edge against the Sierran foothills on the northeast to as much as 9 or 10 km at the southwest side of the valley (fig. 1; Shilling, 1962). The basal unconformity dips southwestward at  $5-12^{\circ}$  across granitic and metamorphic rocks of the Sierran foothills onto presumed Mesozoic ophiolite at the southwest side of the valley. In the simplest view, the sedimentary strata turn up steeply at the southwest edge of the valley and are variously exposed on the southwest limb of an extremely asymmetric syncline along the northeast flank of the Diablo Range. The ophiolitic basement has been presumed to be folded up on the west as well, as shown, for example, by Page and others (1978).

The Diablo Range exposes a core of Mesozoic Franciscan rocks that is bounded by the coeval Mesozoic Great Valley sequence and overlying Cenozoic strata. Scattered patches of ultramafic rock are considered parts of the Coast Range ophiolite on which the marine sedimentary rocks of the Great Valley sequence were deposited. According to prevailing views, these strata and underlying ophiolitic basement were juxtaposed above the severely deformed and partially metamorphosed rocks of the Franciscan assemblage by major thrusting along the Coast Range thrust, which was subsequently obscured by Cenozoic deformation (Page, 1981).

On the southwest, the Diablo Range is obliquely truncated by the San Andreas fault, a plate transform boundary that has been active for the past 20-25 m.y. and is a principal source of earthquakes in central California. Deformation associated with San Andreas movement is undoubtedly responsible for much of the folding and local thrusting that characterize the southeastern Diablo Range and aligned Temblor Range (fig. 1).

Through most of Cenozoic time the area of the San Joaquin Valley was occupied by an elongate marine basin that was bounded on the northeast by the Sierran landmass and on the southwest by a variably emergent mobile belt in the position of the present Coast Ranges. In the Paleocene and Eocene the whole San Joaquin Valley was marine and the mobile belt consisted of a continental borderland of local basins and highs (Nilsen and



Clarke, 1975). The marine basin shrank in Oligocene time, leaving the Coalinga area partially emergent. Except for temporary enlargements in early and late Miocene time, this began the progressive retreat of the basin and final transition to continental sedimentation in late Pliocene time.

The numerous folds northeast of the San Andreas fault (fig. 1) were established and deformed at different times. In the Coalinga region, at least some of the west-northwest-trending folds were defined in the early Tertiary, presumably controlled by proto-San Andreas movement in pre-Eocene time. The Vallecitos trough was accumulating marine sediments, the New Idria high became emergent, and Coalinga nose controlled local deposition. In middle Miocene time, a local influx of serpentinite detritus along the northeast flank of Coalinga nose indicates additional deformation of the New Idria serpentinite diapir (Casey and Dickinson, 1976). This deformation may well mark the beginning of San Andreas influence in that area.

Harding (1976) suggests a regular progression of late Cenozoic folding away from the San Andreas that is best demonstrated in the southeast part of figure 1. There, the first good evidence of folding near the San Andreas appears in lower Miocene rocks, whereas the outermost folds are Quaternary.

The younger, outboard folds have predominantly northwest trends, parallel to the Diablo Range, in contrast to the more westerly-trending inboard folds. The Kettleman Hills anticline, in particular, began growing in Pliocene time; it is aligned with the northeastern margin of the Diablo Range and has folded a thick section of Pleistocene alluvial sediments (Woodring, Stewart, and Richards, 1940; Dibblee, 1973b). At Coalinga nose this trend of folding is superimposed across the more westerly trending fold that encloses the New Idria diapir (Dibblee, 1971), making distinction of the two fold generations difficult.

The Diablo Range also experienced arching and uplift during the Cenozoic, leading to exposure of its Franciscan core. Most of this uplift was accomplished by middle Miocene time, but uplift has probably continued through the Quaternary. Uplift of the Diablo Range is best recorded in the massive central part of the range northwest of figure 1, where the west-northwest-trending folds apparently did not develop. There, an inferred 3 to 9 km of vertical separation across the Tesla-Ortogonalita fault has raised the Franciscan assemblage against the steeply northeast-dipping Great Valley sequence, and, on the east flank of the range, a 600,000-year-old alluvial surface has been raised 400 m (Lettis, 1982).

#### LINE SJ-6

Seismic refraction and reflection profiles along the east-west line SJ-6 (fig. 1) provide a two-dimensional basis for examining the subsurface structure across the southeastern end of the Kettleman Hills anticlinal trend. The refraction and reflection techniques form complementary means in developing a structural cross section. Reflection profiling (here using a 67-m spacing of geophone groups and 1.8-km maximum offset) yields structural configuration in some detail. Useful seismic velocity information, needed to convert the vertical dimension from time to depth, is limited to the upper several seconds and relatively flat-lying strata. Refraction profiling yields velocities, but even with the close station spacing used here (average of 1.6 km) cannot achieve detailed structural resolution. In both techniques detail decreases with depth.



Preliminary interpretations of the seismic profiles (figs. 2 and 3) are centered on the Kettleman Hills anticline. (Note that the section is an oblique one, crossing structure at an angle of about  $40^{\circ}$ , and that figures 2 and 3 have a twofold vertical exaggeration.) Strata beneath the San Joaquin Valley dip gently toward the anticline from the east, and west of the anticline the folded strata drop into the Kettleman Plain syncline and then turn up onto the shoulder of the Diablo Range. The basement under the San Joaquin Valley does not share this upturn, however, but extends without evident interruption at steepened dip southwestward beneath the folds and deep under the Diablo Range.

### Refraction Profile

Seismic refraction profile data were collected in 1982 approximately along line SJ-6 between the Diablo Range and the Sierran foothills. Four 2000-lb shots were recorded on 100 seismographs deployed along the line between shotpoints (SP) 4 and 7 (figs. 1 and 2; SP 7 is located 41 km east of SP 6 — partial detonation produced only a weak signal). Earlier, a short refraction line trending northwest-southeast across line SJ-6 at SP 4 was collected in 1966 as part of the investigation of the 1966 Parkfield earthquake (Stewart and O'Neil, 1972). After the Coalinga earthquake in 1983, additional refraction data were collected along line SJ-6 from SP 8 and along a northwest-southeast strike line that crosses SJ-6 about 5 km east of SP 8 (Walter and Mooney, this volume).

A dipping-layer velocity model for the 1982 data was derived from the observed travel times, using data from the 1966 line to constrain the model near SP 4. This SJ-6 velocity model was then iteratively tested and improved by comparison of the observed data with arrival times calculated from the velocity model using a two-dimensional ray-tracing program. The resulting preliminary velocity model (fig. 2) will be improved by incorporation of the 1983 data in further iterative modeling. This improvement will be especially important in the complex western part of figure 2 between SP 4 and SP 5, where velocities are poorly constrained by present data.

The preliminary model shows seismic velocity in the San Joaquin Valley to increase rapidly from 1.8 km/s at the surface — a velocity indicative of water-saturated unconsolidated sediment — to 3.0 km/s near a depth of 2.5 km. Below that depth the velocity gradient decreases. To the west, uplift of previously compacted sediments has elevated the velocity-depth function. In the middle of the section beneath the western San Joaquin Valley, the presence of a low-velocity zone is indicated by a high-amplitude band of delayed secondary arrivals recorded between SP 5 and SP 6. The specific velocity and westward thickening of the zone are somewhat arbitrary, however, because a range of combinations can produce the delay time required by the seismogram.

The velocity at the top of basement between SP 5 and SP 6 is modeled at 6.5 km/s, indicating a mafic composition. The apparent velocity of arrivals recorded westward from SP 5 suggests, however, that the basement reflection at 9-km depth is from a wedge having a velocity of 5.7 km/s. Data recorded east of SP 4 require the mafic basement beneath the wedge to plunge westward to a depth of 15 km below the Kettleman Plain, although the configuration of this depth change is poorly constrained. Velocity increases slowly with depth within the mafic layer. Below that layer, wide-angle reflections observed on the shot records suggest the presence of a faster layer, here assigned a velocity of 7.2 km/s.

In the Diablo Range near SP 4, the velocity of 5.6 km/s beneath a shallow 4.5 km/s layer (from Stewart and O'Neil, 1972) agrees well with the 5.6 km/s velocity characteristic of the Franciscan assemblage farther north in the Diablo Range (Walter and

Mooney, this volume). East of SP 4 the observed traveltimes require slower velocities in the upper few kilometers and thus indicate a depression of the top of the 5.6 km/s layer, as represented by the dashed boundary at a depth of 9 km in the model. Initial calculations of apparent velocities from the 1983 refraction data indicate that this boundary may be as shallow as 6 km just west of SP 8. The velocity within this layer increases to 5.9 km/s at a depth of 15-16 km, where it overlies the 6.5-km/s basement. This depth agrees with that reported by Walter and Mooney (1982) for the base of Franciscan rocks in the Diablo Range.

### Reflection Profile

A preliminary interpretation of the part of seismic reflection line SJ-6 that crosses the area of figure 1 is shown in figure 3. SJ-6 is a 6-second VIBROSEIS profile, collected in 1981, which was purchased from Western Geophysical Company after being reprocessed to recover an additional 6 seconds of data. Velocity control for the interpretation comes from velocity-time (analogue for depth) relations developed from stacking velocity analyses east of the anticline, supplemented in the Diablo Range and beneath the folds by the modeled refraction velocities. The complex details of the present interpretation west of SP 5, where direct evidence from the reflection record is scant and refraction velocities are poorly constrained, will be tested by further work on the refraction model and reprocessing of the reflection record using velocities implied by the interpretation. The horizontal positions of features along the line in figures 2 and 3 do not quite coincide because of differences in profile alignments.

Beneath the San Joaquin Valley, clearly defined strata dip gently westward over a smooth basement surface. The stratigraphic units shown in figure 3 are principally defined by differences in interval velocity. These velocities beneath the valley, including the presence of a low-velocity zone, are similar to those in the refraction model and yield a basement depth beneath the San Joaquin trough at the west side of the valley of about 9 km. The high-velocity (2.8-4.2 km/s) interval in the middle of the section is correlated with upper Miocene siliceous rocks. The positions of three other stratigraphic horizons in the valley (top and bottom of lower Miocene strata and top of Cretaceous strata) were determined by extrapolating along reflections in the record from well control at the east side of the valley (Bartow, 1983). The base of the lower Miocene is well located, but the top could possibly be as much as 500 m higher than the position shown. For simplicity, these are shown in figure 3 only in the San Joaquin trough at the west side of the valley.

The unconformity at the probable top of Upper Cretaceous nonmarine strata on the east side of the valley (Bartow, 1983) is marked by strong reflections that carry smoothly across the valley and define a velocity boundary in the section (fig. 3). The Cretaceous and possible(?) Jurassic strata between this horizon and basement thicken gradually across the valley from 750 to 1500 m and are correlated with the late Mesozoic Great Valley sequence in the Diablo Range. The location of the marine-nonmarine transition in these strata is uncertain.

West of the San Joaquin trough, the shallow section in the reflection record turns up onto the east limb of the Kettleman Hills anticline and thins out against the fold. This relation is evident from the surface down into the upper part of the 2.2-2.8 km/s layer (lower Pliocene). Continuity at greater depths between the subhorizontal reflections west of the trough and those marking the east limb of the anticline is not evident. The position of stratigraphic horizons in the folds were identified from wells on the anticline crest (Chevron SF & FL 4-2; Sec 12, T25S, R19E; TD-3948 m) and the western limb of the



syncline (Texaco Capital Co. Two 1; Sec 19, T25S, R19E; TD-2205 m). Stratigraphic correlation across the intervening syncline was made with some difficulty because of poor definition of many reflections in the record. Complexities on the west flank of the syncline in the record are probably due to reverse faults dipping southeastward subparallel to bedding (Ritzius, 1957). This style of deformation is represented schematically on figure 3 by an arrow.

West of the syncline the Great Valley sequence is identified from its exposure in the Diablo Range. The location of its top in the section is constrained by surface exposures and the Texaco well. The unit underlying the Great Valley sequence on the west in the section is considered Franciscan assemblage, inasmuch as exposed Franciscan structurally underlies the Great Valley sequence just 5 km to the northwest (fig. 1) and the velocity is appropriate. The intervening boundary, which by prevailing views represents the position of the Coast Range thrust, is placed at the top of a band of discontinuous strong reflections in the record. Using a velocity of 4.25 km/s for the Great Valley sequence, its thickness in figure 3 is 3500 m; the exposed thickness 5 km to the north measured on Dibblee's map (1973a) is about 3000 m. Thus the Diablo Range section is about twice as thick as the equivalent 1500-m section beneath the San Joaquin Valley.

A discontinuous band of reflections is evident west of the syncline at 3.6 to 4.3 seconds in the reflection record (labelled X in fig. 3). It probably represents the 5.2/5.6-km/s boundary of the refraction model (fig. 2). Using an average velocity of 5.1 km/s between horizon X and the Great Valley sequence above retains a modest easterly dip for X in the depth section and places it in approximately the same position as the 5.2-5.6 km/s boundary in figure 2. If it is assumed that this horizon marks the base of the Great Valley sequence beneath the syncline (see below), it can be extended smoothly eastward to align with the base of the Great Valley sequence (fig. 3) and the top of the 5.7? km/s wedge (fig. 2) beneath the San Joaquin trough.

A deeper band of discontinuous reflections (labelled Y in fig. 3) is evident beneath the syncline and to the west at 6.2 to 6.5 seconds in the reflection record. This horizon slopes gently westward and is aligned with the basement reflection east of Z in the reflection record. After correction for lateral changes in the overlying velocity structure, however, this horizon shows a westward apparent dip of about  $30^{\circ}$  in the depth section. It is approximately coincident with the top of mafic basement west of SP 8 in the refraction model, rises eastward beneath the syncline, and aligns approximately with the bottom of the 5.7-km/s wedge just west of SP 5 in the refraction model. There is a 2-km mismatch beneath the syncline in the depth of horizon Y between figure 3 and the equivalent top of mafic basement in the refraction model. This discrepancy could be an indication that, despite their similarity, the reflections along horizon Y do not correlate and that a larger step in the basement surface exists at or west of Z than is shown in figure 3. The simplest interpretation, however, is to consider horizon Y to mark the top of mafic basement that dips southwestward and is continuous across the base of a westward-thickening wedge having a velocity of 5.7 km/s.

This plunge of mafic basement from the San Joaquin Valley southwestward beneath the Diablo Range contrasts with the uplift of the base of the Great Valley sequence from a depth of 9.4 km beneath the San Joaquin trough to 1 km in the Diablo Range. The contrast raises the possibility of thrust faulting, and our interpretation centers on a late Cenozoic thrust that dips southwestward and repeats the Tertiary section, the Great Valley sequence, and the underlying Franciscan assemblage. Stratigraphic identities and structural relations inherent in this interpretation imply an earlier phase of thrusting involving the Franciscan assemblage that conflicts with prevailing views concerning the nature of the Coast Range thrust.

Specific evidence for the late Cenozoic thrust is fragmentary, but yields a consistent structural picture. Reflections that define the limbs of the Kettleman Plain syncline in the seismic record appear to butt downward against underlying subhorizontal reflections at the trough of the syncline. This relation suggests a subhorizontal fault that truncates the base of the syncline at a depth of 4.8 km. The east limb of the Kettleman Hills anticline must either be nearly vertical (fig. 3) or be broken by faulting. Faulting is suggested by the lack of reflection continuity in the seismic record. Significant horizontal fault offset is suggested by contrasts in the Miocene section between the anticline and the San Joaquin trough, particularly the 500-1000 m difference in thickness of the interval between the top of lower Miocene strata and the base of the upper Miocene siliceous layer. We interpret these relations to indicate a southwest-dipping thrust fault. Its stratigraphic level beneath the northeast limb of the anticline is constrained by relations in the seismic record to lie near the top of the siliceous layer.

Such a thrust fault requires the stratigraphic section to be repeated. In the absence of evidence to the contrary, we assume the structure beneath the thrust to be simple, and reconstruction of a repeated section there produces reasonable structure and velocities (fig. 3). This reconstruction was done by first placing the upper Miocene siliceous layer beneath the truncated base of the syncline and working downward to the base of the Great Valley sequence, using velocities determined with the velocity-time relations developed in the San Joaquin Valley, and then stacking the same section above horizon X to the west using interpolated thicknesses. The shape and position of the thrust surface west of the syncline is constructed to account for fault relations with the stratigraphic units at the base of the overthrust plate. The truncated east limb of the anticline is restored to a ramp placed at P beneath the structural shoulder below SP 8, and the distance from the anticlinal core to the southwest limb of the syncline then restores the truncated base of the Great Valley sequence to a ramp at the west end of horizon X. This reconstruction identifies the 5.75 km/s wedge as Franciscan assemblage, which its velocity suggests. Accounting for the position of this wedge above the mafic basement leads to suggestion of an earlier phase of thrusting, as discussed below.

Reverse faults that dip eastward in the section are shown beneath the anticline and 10 km to the east. As discussed below, these faults probably strike northwest, parallel to the anticline, and therefore actually dip northeastward. The easternmost of these faults is clear in the reflection record; it dips about  $70^{\circ}$  northeast, offsets basement and the top of Cretaceous strata about 500 m, and warps lower Miocene strata about 150 m.

Details of the two reverse faults shown beneath the east limb of the anticline are obscured by the poor quality of the seismic record beneath the anticline. The upper fault is based on westward termination of the basement reflection and probable offset of lower Miocene reflections. A weak reflection on the downthrown side was interpreted to mark the offset basement reflection. The fault dips  $60-70^{\circ}$  northeastward and offsets basement about 900 m and lower Miocene strata about 500 m.

The lower fault is less clear; it is based on terminations of several reflections in lower Miocene strata and gaps in reflections downdip toward Z. It dips about  $55^{\circ}$  to the northeast and should offset strata below the thrust about 400 m, limited by the basement offset at Z. A separately recognized reverse fault is indicated near the surface in the west limb of the anticline by warping, termination, and offsets of reflections. This fault offsets the base of the upper Miocene siliceous section about 200 m and warps the top about 100 m. These two reverse faults are aligned across the southwest-dipping thrust. The shallow fault may be the result of folding in the anticline and the alignment with the deeper fault may only be fortuitous. With present information, however, the simplest interpretation is a single reverse fault that offsets the southwest-dipping thrust and dies



out upward in the Miocene section at a depth of about 2 km below the surface, as shown in figure 3. The passage of faults close to the base of the Chevron well required by this reconstruction is reasonable, because calcite veining and abundant fractures are reported in core taken from the bottom of the well.

### TECTONIC INTERPRETATION

The present interpretation of the SJ-6 profiles suggests that the Kettleman Hills anticline and adjacent syncline are not rooted. Instead, they seem to be underlain at a depth of about 5 km by a subhorizontal thrust fault that terminates below the east limb of the anticline where the overthrust plate overrode a latest Miocene or early Pliocene surface above the late Miocene siliceous section. Reconstruction of the thrust surface to depth westward, using stratal truncations at the base of the overthrust plate and structure within it as a guide, indicates about 15 km of separation in this section, or about 10 km perpendicular to strike (see below). The thrust probably deepens westward to a depth of about 10 km beneath the Diablo Range.

The position of the easternmost ramp on the thrust surface beneath the Kettleman Hills was probably controlled by reverse-fault deformation of the lower plate, and this ramp in turn controlled the location of Kettleman Hills anticline. This association between anticline, thrust, and reverse faults allows inference that they share a common strike, which is indicated by the axis of the fold (fig. 1).

The direction of thrust movement should be perpendicular to strike and thus should represent shortening perpendicular to the east margin of the Diablo Range. The termination of the thrust below the east flank of Kettleman Hills and alignment with the very regular east margin of the Diablo Range raises the possibility that such thrusting characterizes the whole length of the range. Certainly the range margin is an abrupt one that everywhere involves sharp upturn of the Great Valley sequence and is locally marked by folding at the margin (see, for example, Jennings, 1977, southwest of Patterson).

This type of thrusting probably continues southeastward from SJ-6 along the northeast front of the Temblor Range, where southwest-dipping thrust faults have been recognized at the surface (Dibblee, 1973a) and in the subsurface (Vedder, 1970). Such thrusting could well tie into the complex thrust systems of the San Emigdio Mountains. If so, anticlines such as Lost Hills and Elk Hills might also be controlled by underlying thrusts.

The timing of emplacement of the overthrust sheet at Kettleman Hills is indicated by the age of the stratigraphic horizon that was overridden where the thrust emerged at the surface (beneath SP 8). In figure 3 this surface is shown to be the top of the upper Miocene siliceous layer, but it could easily be as young as early Pliocene. Progressive thinning of strata against the east flank of the fold indicates that after emplacement of the overthrust sheet the anticline grew through Pliocene and Quaternary time. The progression of folding outward away from the San Andreas fault suggested by Harding (1976) could well represent outward growth of underlying thrusts, presumably driven by forces related to the San Andreas system. The change in strike from inboard to outboard folds should thus involve some change in the geometry of those thrusts, controlled either by a change in the compression direction with time or perhaps by the depth at which the thrusts are rooted and their degree of association with the San Andreas fault.

The reverse faulting beneath the anticline represents the same compression direction as the thrusting. The driving force for this thrusting is not superficial, because the faults penetrate into the basement. The reverse faults are located where the basement bends

down to the southwest to plunge beneath the Diablo Range, and this geometry may provide the fundamental control on the northeast margin of the Diablo Range. A similar deepening of basement beneath the Diablo Range is apparent in a refraction profile down Del Puerto Canyon in the northwest part of the range (W. D. Mooney and A. W. Walter unpublished data).

The difference in fault offsets above and below the thrust at the anticline in figure 3 indicates that the deeper reverse faults formed prior to local emplacement of the overthrust plate. The configuration of the upper Miocene siliceous layer beneath the thrust is arbitrary — no information is provided there by the reflection record — and it could be largely folded rather than faulted. Regardless, at least one of the reverse faults may have continued moving after arrival of the overthrust plate and penetrated upward through the west flank of the anticline to within about 2 km of the surface. Offset during that period of perhaps 5 million years was quite modest, not more than about 200 m.

The deeper structural relations inherent in this interpretation pose an enigma. The near-surface Franciscan assemblage in the Diablo Range must, according to relations in figure 3, be offset from the deep wedge of 5.75 km/s material, which then should be Franciscan as well. However, placing Franciscan rocks above the mafic basement and beneath the Great Valley sequence that unconformably overlies the same mafic basement farther east implies that the Great Valley sequence unconformably overlies the Franciscan. As the two are coeval, such an unconformable relation is not reasonable.

The only evident alternative is that the Franciscan rocks have been emplaced tectonically in wedgelike fashion along the basement contact, thus overthrusting the mafic basement and concurrently underthrusting and raising the Great Valley sequence. This thrust boundary with the overlying Great Valley sequence should represent the Coast Range thrust. In contrast to prevailing views about the Coast Range thrust, however, such wedgelike emplacement of the Franciscan would place the eastern terminus of the thrust above the mafic basement somewhere near Z in figure 3. The absence in this interpretation of oceanic basement along the base of the Great Valley sequence between the San Joaquin trough and the Diablo Range similarly challenges the accepted view of the Coast Range thrust and requires separate explanation of the ultramafic rocks typically associated with the Franciscan perimeter in the Diablo Range.

### Coalinga Earthquakes

The Coalinga earthquakes occur 65 km to the northwest along strike in a setting similar to that of line SJ-6. Coalinga nose involves Pleistocene alluvial deposits folded on a northwest-trending anticline. A reflection record that crosses the anticline along the Southern Pacific Railroad east-northeast from Coalinga shows that the west limb of the anticline there contains an easterly dipping reverse fault, and photointerpretation (R. F. Yerkes oral commun., 1983) suggests the presence of such a fault in sharply folded Pliocene and older strata exposed on the southwest flank of the nose (fig. 1). The persistence of the late Cenozoic thrust projected northwest from SJ-6 along the Kettleman Hills trend is not clear. Study of stream-terrace deformation south of Coalinga nose (King and Stein, this volume) suggests that a thrust beneath the anticline there has undergone recent movement. Thrusts have not been recognized, however, in the exposed section northwest of Coalinga nose. The end of the Kettleman Hills fold trend there (Dibblee, 1971) may represent termination of the thrust or a change in thrust configuration at depth.



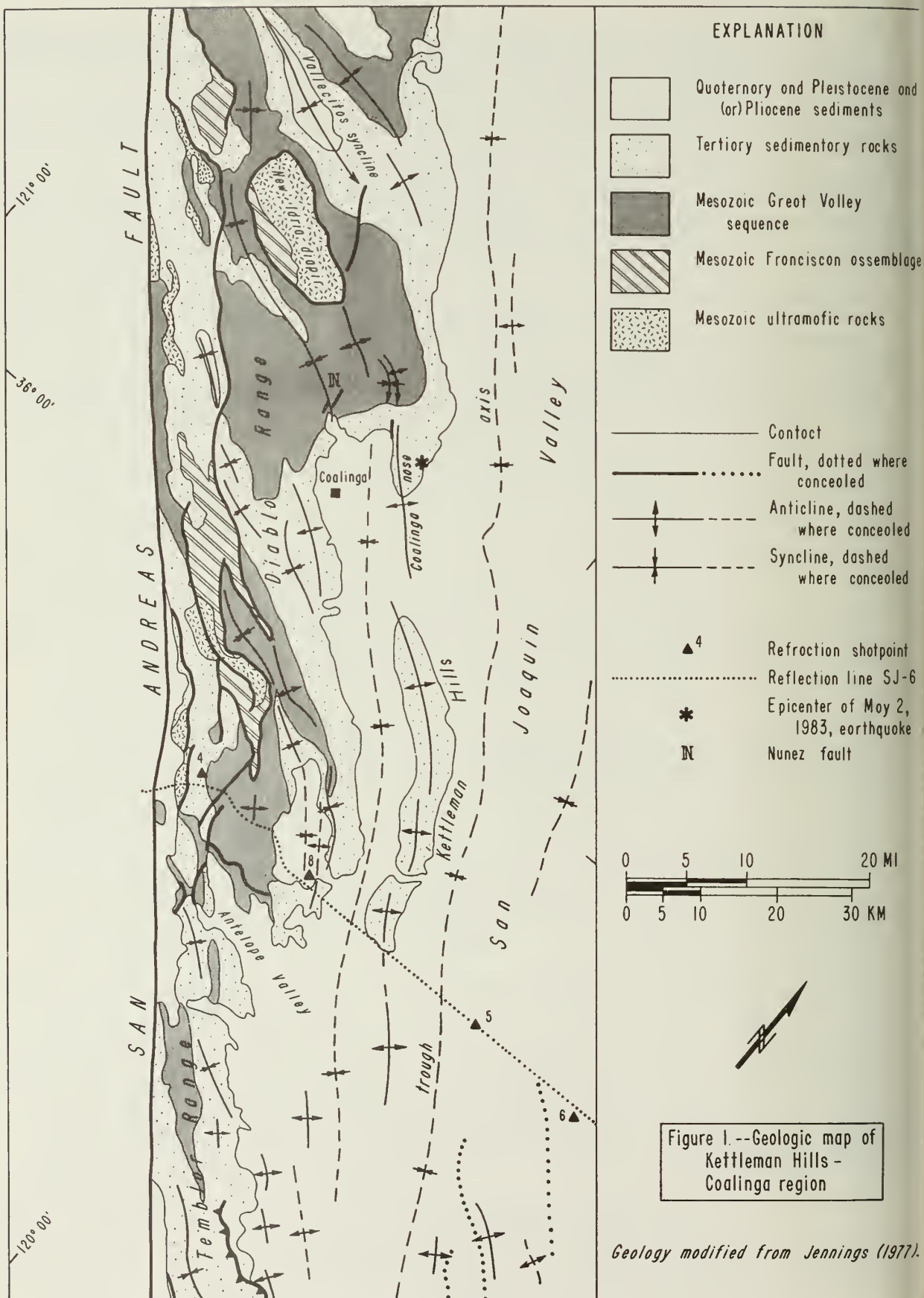
If the structure in the Coalinga area is analogous to our interpretation along SJ-6, the relation to the 1983 Coalinga earthquakes is striking. The main northeast-dipping reverse fault represents a source for the May 2 main shock, in which rupture probably occurred along a plane that dips steeply to the northeast beneath Coalinga nose and penetrated upward to within a few kilometers of the surface (Eaton; Stein; this volume). In the long term this faulting must be subordinate to uplift on the southwest, consistent with thrusting from the southwest. Compression of the syncline to the west has produced bedding-plane faulting on its west limb at the latitude of SJ-6, and the surface faulting along the east-dipping Nunez reverse fault (N in figure 1; Hart, this volume) and associated earthquakes (Eaton, this volume) shows a similar relation.

#### REFERENCES CITED

- Bartow, J. A., 1983, Geologic map and cross sections of the southeastern margin of the San Joaquin Valley, California: U.S. Geological Survey Miscellaneous Investigations Series Map I-1496, scale 1:125,000, in press.
- Casey, T. A. L., and Dickinson, W. R., 1976, Sedimentary serpentinite of the Miocene Big Blue Formation near Cantua Creek, California, in Fritsche, A. E., TerBest, Harry Jr., and Wornardt, W. W. (eds.), the Neogene symposium: Society of Economic Paleontologists and Mineralogists, Pacific Section, Annual Meeting, San Francisco, April, 1976, p. 65-74.
- Dibblee, T. W., Jr., 1971, Geologic maps of the Coalinga, Joaquin Rocks, New Idria, and Priest Valley 15 minute quadrangles, California: U.S. Geological Survey Open-File Report 71-87, Coalinga and Joaquin Rocks sheets, scale 1:62,500.
- Dibblee, T. W., Jr., 1973a, Regional geologic map of San Andreas and related faults in Carrizo Plain, Temblor, Caliente, and La Paza Ranges and vicinity, California: U.S. Geological Survey Miscellaneous Geologic Investigations Map I-757, scale 1:125,000.
- , 1973b, Stratigraphy of the southern Coast Ranges near the San Andreas fault from Cholame to Maricopo, California: U.S. Geological Survey Professional Paper 764.
- Harding, T. P., 1976, Tectonic significance and hydrocarbon trapping consequences of sequential folding synchronous with San Andreas faulting, San Joaquin Valley, California: American Association of Petroleum Geologists Bulletin, v. 60, p. 356-378.
- Jennings, C. W., 1977, Geologic map of California: California Division of Mines and Geology, Geologic Data Map No. 2, scale 1:750,000.
- Lettis, W. R., 1982, Late Cenozoic stratigraphy and structure of the western margin of the central San Joaquin Valley, California: U.S. Geological Survey Open-File Report 82-526, 203 p.
- Nilsen, T. H., and Clarke, S. H., Jr., 1975, Sedimentation and tectonics in the early Tertiary continental borderland of central California: U.S. Geological Survey Professional Paper 925, 64 p.
- Page, B. M., 1981, The southern Coast Range, in Ernst, W. G., ed., The geotectonic development of California: Prentice-Hall, Englewood Cliffs, N. J., p.329-417.
- Page, B. M., Wagner, H. C., McCulloch, D. S., Silver, E. A., and Spotts, J. H., 1979, Geologic cross section of the continental margin off San Luis Obispo, the southern Coast Ranges, and the San Joaquin Valley, California: Geological Society of America Map and Chart Series MC-28G.
- Ritzius, D. E., 1957, Alferitz area of Devils Den oil field: California Division of Oil and Gas, summary of operations—California Oil Fields, v. 43, no. 1.
- Schilling, F. A., Jr., 1962, Cretaceous geology of the Pacheco Pass area, California, in Bowen, O. E., Jr., (ed.), Geologic Guide to the Gas and Oil Fields of Northern California: California Division of Mines and Geology Bulletin 181, plate 12.



- Stewart, S. W., and O'Neil, M. E., 1972, Seismic travel times and near-surface crustal velocity structure bounding the San Andreas fault zone near Parkfield, California: U.S. Geological Survey Professional Paper 800-C, p. C117-C125.
- Wedder, J. G., 1970, Geologic map of the Wells Ranch and Elkhorn Hills quadrangles, San Luis Obispo and Kern Counties, California: U.S. Geological Survey Miscellaneous Geologic Investigations Map I-585, scale 1:24,000.
- Walter, A. W., and Mooney, W. D., 1982, Crustal structure of the Diablo and Gabilan Ranges, central California: A reinterpretation of existing data: Bulletin of the Seismological Society of America, v. 72, no. 5, p. 1567-1590.
- Ventworth, C. M., Walter, A. W., Zoback, M. D., Blake, M. C. Jr., Griscom, Andrew, Lindh, A. G., and Mooney, W. D., 1983, Deep seismic reflection profile across the southern Diablo Range and western San Joaquin Valley near Kettleman Hills, California: Evidence for possible west-over-east thrusting (abs.): American Association of Petroleum Geologists, Pacific Section; Program and Abstracts of 58th Annual Meeting, May 18-21, 1983, p. 57.
- Woodring, W. P., Stewart, R., and Richards, R. W., 1940, Geology of the Kettleman Hills Oil Field, California: U.S. Geological Survey Professional Paper 195, 170 p.



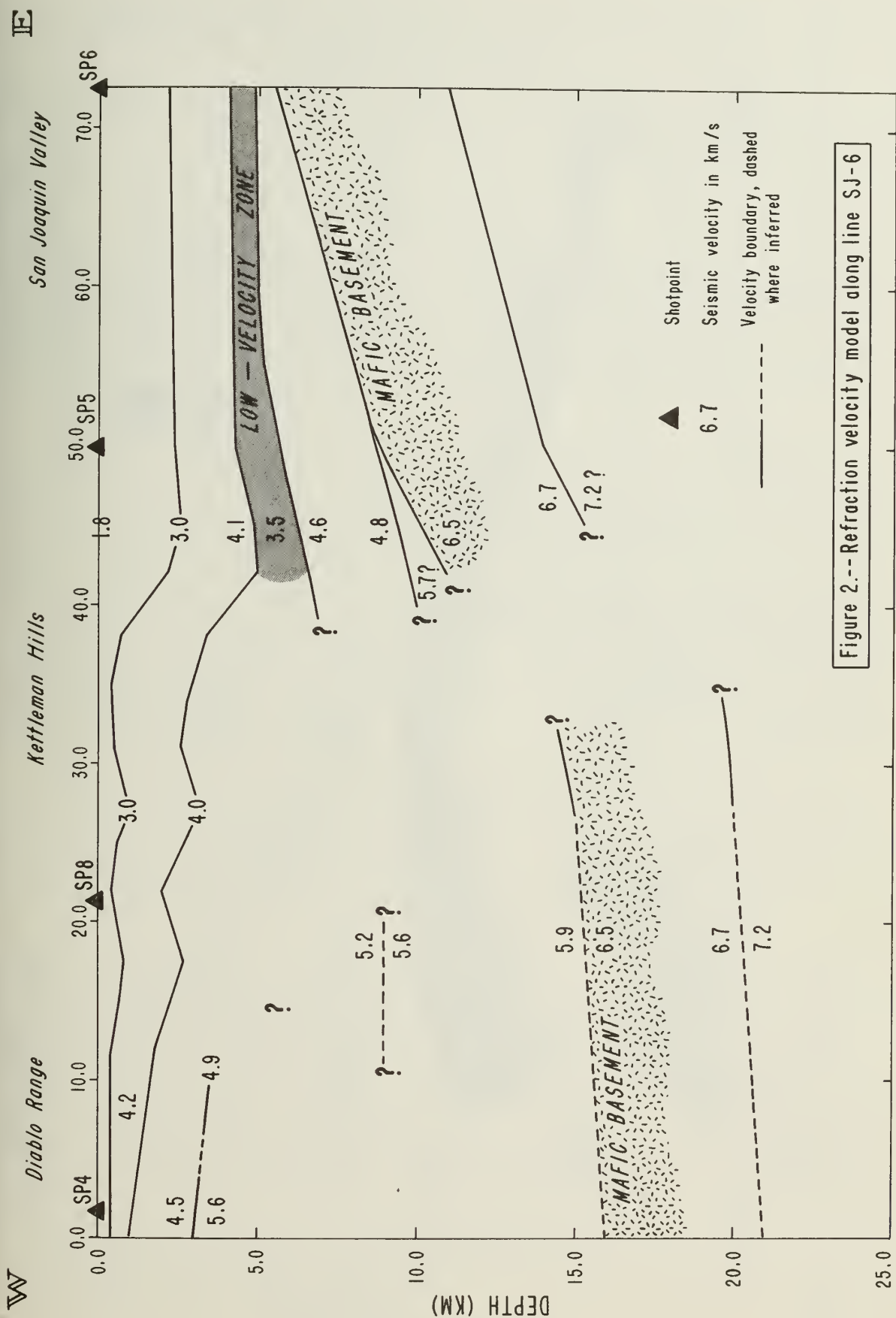
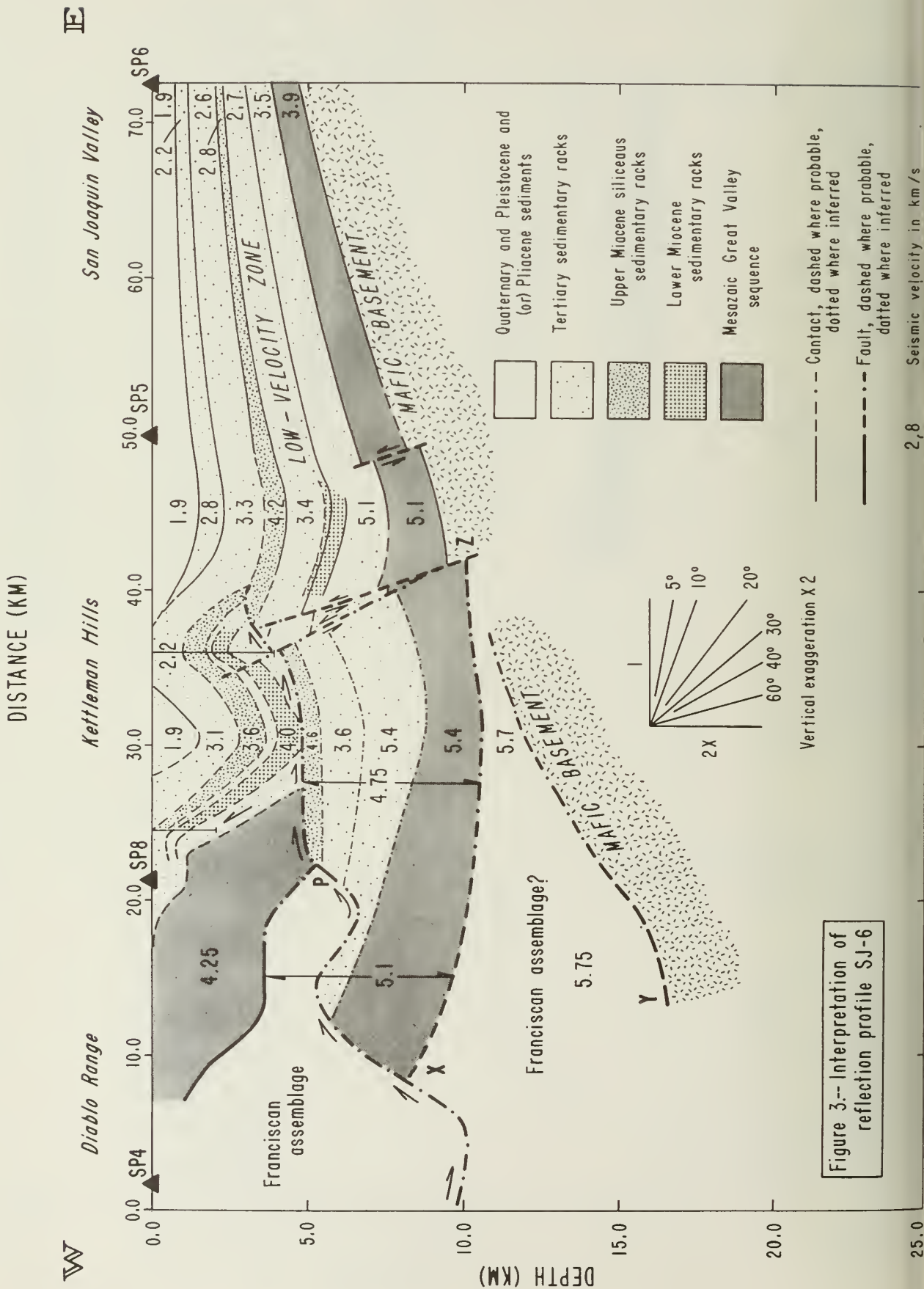


Figure 2.--Refraction velocity model along line SJ-6





PRELIMINARY REPORT ON THE CRUSTAL VELOCITY STRUCTURE NEAR  
COALINGA, CALIFORNIA AS DETERMINED FROM SEISMIC REFRACTION  
SURVEYS IN THE REGION

by

Allan W. Walter and Walter D. Mooney<sup>1</sup>

INTRODUCTION

The U.S.G.S. conducted a seismic-refraction experiment in the Coalinga area shortly after the May 2, 1983,  $M = 6.5$  earthquake in order to obtain a better knowledge of the crustal velocity structure near Coalinga. This paper presents summary of the experimental field plan, provides origin times and locations for the shot points, and gives some preliminary results. Detailed interpretation of the data will be presented elsewhere after analysis of the data is completed.

The experiment consisted of two phases of data acquisition. In the first phase, aftershocks were recorded along two profiles crossing the epicentral region of the May 2 earthquake (Figure 1). A NW-SE profile extended from the epicentral region along the syncline west of the Kettleman Hills, and an E-W profile extended from the interior of the Diablo Range across the epicentral region into the San Joaquin Valley. A total of 120 analog-tape-recording, single-vertical-component seismographs were used to record aftershocks. On the night following the main shock, the seismographs were deployed at 1-km spacing along the NW-SE profile. Two days later, the seismographs were re-deployed at .5-km spacing along the E-W profile (Figure 1). For both deployments, four 13-minute time intervals were recorded. The recording times and the number of recorded events that have magnitudes greater than 1.5 are listed in Table 1.

In May and June of 1983, the second phase of the refraction experiment used the same instruments to record nine shots along approximately the same profiles as the aftershock profiles (Figure 1). Four shots were recorded along the E-W profile and five shots along the NW-SE profile (Figure 1, Table 2). Fortunately, a  $M=2.5$  aftershock was also recorded along the NW-SE shot profile (Figure 1, Table 2).

Apparent velocities and intercept times have been calculated for all of the shots (Table 3) and for the one aftershock recorded along the NW-SE shot profile. The velocity-depth functions presented in Table 3 are for use in constructing a better velocity model for locating the Coalinga earthquakes. These functions are not corrected for the dip of the units and thus should be regarded as very rough estimates. The velocity-depth functions will be better resolved when both the shot and aftershock data are modelled by iterative two-dimensional ray-tracing. The discussion which follows summarizes the apparent velocities observed along the two profiles and compares these velocities to those determined by other nearby refraction surveys.

## E-W COALINGA PROFILE

The shotpoints along the E-W profile are numbered from east to west as SP 9 through SP 12 (Figure 1). SP 9 is located in the San Joaquin Valley about 57 km east of epicenter for the May 2 main shock, SP 10 is located about 5 km east of the axis of the San Joaquin Valley trough, SP 11 is on the anticlinal axis about 3 km southwest of the epicenter for the main shock, and SP 12 is located in the Diablo Range about 30 km northwest of Coalinga.

In the Diablo Range, the profile is parallel to the strike of the Cretaceous strata of the Great Valley Sequence that are exposed on the southern flank of the New Idria serpentinite diapir. East of the range, the profile obliquely crosses the strike of the Tertiary strata exposed in the northwest-trending folds. Across the folds the dips of the sedimentary units change continuously and some units are truncated by unconformities or faults. Along the profile in the San Joaquin Valley, the sediments dip gently to the southwest and thin as the basement rises to the northeast.

Because the thicknesses of the sedimentary units change along the profile, a unique velocity does not exist for a given unit but rather a range of velocities. Comparison between the velocity data (Table 3) for SP 9 and SP 10 with that for SP 11 and SP 12 shows a westward increase in the average velocity above a given depth horizon, consistent with the uplift of the older strata to west. Within the San Joaquin Valley the apparent velocities of the sedimentary section increase from about 1.5 km/s near the surface to about 4.4 km/s at 3.5-km depth near SP 10. Under SP 10 the flat-layer approximation is probably a good estimate of the sedimentary velocity-depth function because the apparent velocities and intercept times of the sedimentary layers are approximately the same both to the east and west. Eastward from SP 11, the velocities measured down-dip into the San Joaquin Valley increase from 2 km/s at the surface to about 4.7 km/s at 4-km depth. Westward from SP 11, the apparent velocities increase to 3.1 km/s at a depth of 0.9 km; near the Cretaceous-Tertiary contact the arrivals advance about 0.3 s and the apparent velocity becomes 4.2 km/s. If the .3 s advance is removed, the calculated depth to the 4.2 km/s layer is about 1.9 km. In the reverse direction from SP 12, no data were recorded within the first six kilometers of the shotpoint, but an apparent velocity of 4.15 km/s is observed from 8-km distance out to SP 11; the calculated depth to this horizon is less than .8 km near SP 12.

The top of the seismic basement between SP 9 and SP 10 has a down-dip apparent velocity of about 6 km/s and an up-dip apparent velocity of about 7.0 km/s. Averaging the reversing velocities gives 6.5 km/s as an estimate for true velocity. Between SP 11 and SP 12 the velocity at the top of seismic basement is between 5.6 km/s and 6.0 km/s. The record sections from SP 9, 10 and 12 show evidence for a higher velocity crustal layer below 11-km depth. Arrivals crossover to a phase with an apparent velocity of about 7.6 km/s west of both SP 9 and SP 10. This high velocity is partly due to a travel-time advance caused by the higher velocity strata in the hills west of the San Joaquin Valley. From SP 12 eastward, the basement arrivals cross over to an up-dip velocity of 8.3 km/s; it is not clear whether these arrivals are from the same layer as the 7.6 km/s arrivals.



## NW-SE COALINGA PROFILE

The shotpoints along the NW-SE profile are numbered from northwest to southeast as SP 13 through SP 17 (Figure 1). SP 13 is located near the Cretaceous-Tertiary contact on the northeast flank of the New Idria diapir (Joaquin Ridge). South of SP 13, the profile crosses the axis of Joaquin Ridge to SP 14 and follows the axis of the syncline to SP 15. From SP 15, the profile continues along the west limb of the syncline to SP 16 and SP 17. The profile is thus sub-parallel to the strike of the Tertiary folds, except where it crosses the axis of the Joaquin Ridge anticline between SP 13 and SP 14.

At the northern end of the profile over Joaquin Ridge, where the Cretaceous rocks are exposed at the surface, the shallow velocities increase from 2 km/s to 4 km/s by 1-km depth. In the syncline to the south, slower Quaternary and Tertiary sediments overlie the Cretaceous rocks and the velocity increases from about 1.6 km/s at the surface to more than 4 km/s at a depth between 2 and 3 km, which is probably the depth to the Cretaceous strata. The thickness of the slower sediments in the syncline increases southward toward SP 17.

A most remarkable feature that is observed on all of the record sections along the NW-SE profile is a decay in the amplitude of the first arrivals followed by a delayed high-amplitude reflection from the top of the seismic basement (Figure 2). This provides strong evidence for a low-velocity zone (LVZ) within the sedimentary section. The amplitude decay and delay time are different for each shot, thus the depth and velocity of the LVZ varies along the length of the NW-SE profile. The LVZ has limited E-W lateral extent because the record sections from SP 11 and SP 12 along the E-W profile do not show evidence of the amplitude decay and delayed reflection. Using the observed delay times, we have estimated the LVZ to lie between 3 and 6 km depth; the top of the LVZ is shallowest under Joaquin Ridge and deepens southward under the syncline. The velocity inversion could result from a sedimentary facies change, but the peculiar geometry and size of the LVZ suggest that it is probably due to a local thrusting of the older, higher velocity rocks over the younger, lower velocity rocks.

The apparent velocity at the top of the seismic basement varies along the length of the profile. The velocity appears to be higher under Joaquin Ridge and decreases southward under the syncline. Under the axis of Joaquin Ridge, velocities of 6.30 and 6.00 km/s are observed from SP 13 and 14. Under the axis of syncline, velocities of about 6.0 km/s are observed from SP 13, 14, and 15. Farther south in syncline, the basement under SP 16 appears to have a velocity as low as 5.3 km/s and north of SP 17 the velocity is about 5.7 km/s. At ranges over 30 km north and south of the shotpoints, reflections from within the basement crossover to velocities in the range of about 6.2 to 6.6 km/s. Delays observed in some of the long-range reflected arrivals suggest that the basement may also contain a LVZ.

At the present stage in the analysis, it is not possible to distinguish changes in velocity due to changes in dip from those due to changes in composition, such as the degree of metamorphism. Better constraints on the velocity structure of the basement will require iterative two-dimensional ray-trace modeling of the traveltimes data.

## Aftershock recorded on NW-SE profile

A  $M=2.5$  aftershock was recorded along the NW-SE shot profile. The event has a preliminary location within 1 km of the profile line (Table 2, arrow in Figure 1) and a calculated depth of 6.5 km. No clear S-wave arrivals were recorded by the vertical-component seismographs. Beyond 15-km north and south of the event, the P-wave arrivals are refracted in the basement. Velocities of 5.9, 6.25 and 6.9 km/s are observed south of the event and a velocity of 6.0 km/s is observed along the short section of profile north of the event. These apparent velocities are comparable to those observed for the shots.

## COMPARISON WITH NEARBY REFRACTION RESULTS

In July of 1982, the U.S.G.S. collected refraction data along an E-W profile that crosses the San Joaquin Valley, Kettleman Hills, and the Diablo Range at a latitude 50 km south of the Coalinga E-W profile (Figure 1). Shots were fired at the four locations labelled in Figure 1 as SP 4 to SP 7. The refraction data were modeled by two-dimensional ray-tracing techniques and the resulting velocity model was used in the interpretation of the parallel Western Geophysical reflection profile, SJ-6 (Wentworth and others, their Figure 2, this volume). We refer to this joint seismic refraction/reflection profile as the SJ-6 line.

Many of the velocity features observed along the E-W Coalinga profile are found in the velocity model derived for SJ-6. The velocities of the San Joaquin Valley sediments are similar in both profiles. The one major difference is that the SJ-6 model has a LVZ within the sedimentary section east of Kettleman Hills, whereas the data recorded on the Coalinga line do not show evidence for a LVZ in the San Joaquin Valley. The top of the seismic basement under the valley has a velocity of 6.5 km/s along both the SJ-6 and Coalinga profiles. The lower crust under the valley has a velocity of 7.2 km/s in the SJ-6 model; the existence of a higher velocity lower crust along the Coalinga profile is supported by the observations of the 7.6 km/s velocities west of SP 9 and SP 10 and the 8.3 km/s velocity east of SP 12.

In the folds west of the San Joaquin Valley, both the SJ-6 and the Coalinga data show similar increases in the shallow apparent velocities resulting from the elevation of the older sedimentary units, but the SJ-6 velocity model is too poorly constrained by the 1982 refraction data to distinguish the presence of the LVZ found along the NW-SE Coalinga profile. In May 1983, additional refraction data were recorded between SP 4 and SP 5 on SJ-6 from a shot at SP 8 (Figure 1). The refraction data from this shot show no evidence for a LVZ to the west, but to the east, the first arrivals decay in amplitude and are followed by a delayed high-amplitude basement reflection. This LVZ is consistent with the northeastward thrusting proposed by Wentworth and others (this volume) that would superimpose older, higher velocity rocks over younger, lower velocity rocks in the vicinity of the syncline west of the Kettleman Hills.

Although the velocity structure shown for the Diablo Range at the western end of the SJ-6 model is not well constrained, it is similar to the velocity structure derived from refraction data collected in the northern Diablo Range. In 1967, the USGS recorded a 200-km long refraction profile from Benicia, California down across the Livermore Valley and along the axis of the Diablo Range to Panoche Valley, 64 km northwest of Coalinga. This profile was first analysed by Stewart (1968). Walter and Mooney (1982) and Blumling and Prodehl (1983) refined the velocity model using two-dimensional ray-tracing techniques not available to Stewart. Because the Coalinga refraction profiles do not extend far enough west to provide constraints on the deeper velocity structure internal to the Diablo Range, we must rely on the velocity models derived farther north for this structure. In Walter and Mooney's velocity model the Franciscan basement consists of two layers: an upper layer about 3-km thick that has an average velocity of 5.0 km/s and a lower layer about 12-km thick that has an average velocity of 5.75 km/s. Below the Franciscan rocks is a mafic lower crust that has an average velocity of 6.9 km/s down to the Moho at about 28 km depth. This velocity model can be used to approximate the velocities in the Diablo Range west of Coalinga.

The apparent velocities observed for the seismic basement along the length of the NW-SE Coalinga profile are slightly higher from those given above for the Franciscan assemblage; these differences in velocity may in part be due to the degree of metamorphism of the meta-sediments or the presence or abundance of serpentinite. The effect of the nearby New Idria serpentinite diapir (Figure 1) on the velocity-depth function in the Diablo Range is not known; a refraction survey across the diapir would provide better constraints on the velocity-depth function northwest of Coalinga.

#### ACKNOWLEDGEMENTS

Many individuals contributed to the collection of the field data; we would like to especially thank J. M. Murphy, E. E. Criley, and G. S. Fuis for their help in organizing the experiment and G. A. Molina, L. Pace, R. M. Kaderabek, V.D. Sutton, A. Bloomfield, L. Hwang, and P.J. Meador for their support in the field. We thank C. M. Wentworth and A. G. Lindh for their review of this paper.

#### REFERENCES

- Blumling, P. and Prodehl, C., 1983, Crustal structure beneath the eastern part of the Coast Ranges (Diablo Range) of central California from explosion seismic and near earthquake data: *Physics of the Earth and Planetary Interiors*, v. 31, pp. 313-326.
- Stewart, S. W., 1968, Preliminary comparison of seismic traveltimes and inferred crustal structure adjacent to the San Andreas fault in the Diablo and Gabilan Ranges of central California: *in* Proc. Conf. Geological Problems of San Andreas Fault System, W. R. Dickinson and A. Grantz, eds., Stanford Univ. Pubs. Geol. Sci., v. 11, pp. 218-230.
- Walter, A. W., and Mooney, W. D., 1982, Crustal structure of the Diablo and Gabilan Ranges, central California: A reinterpretation of existing data: *Bulletin of the Seismological Society of America*, v. 72, no. 5, pp 1567-1590.



TABLE 1

## TIMES OF RECORDING - COALINGA AFTERSHOCK PROFILES

Profile	Date	Julian Day	Start GMT	End GMT	Events
NW-SE	May 4, 1983	124	09:00	09:13	4
			09:30	09:43	2
NW-SE	May 5, 1983	125	06:00	06:13	0
			06:30	06:43	0
E-W	May 7, 1983	127	06:00	06:13	1
			06:30	06:43	2
			09:00	09:13	0
			09:30	09:43	1

TABLE 2

## SOURCE ORIGIN TIMES AND LOCATIONS - COALINGA SHOT PROFILES

## E-W PROFILE

Shot*	Latitude	Longitude	Date-Julian Day	Shot time (GMT)
9	36 13.130'	119 41.211'	May 19, 1983 139	06:30:00.01
10	36 13.727'	120 01.769'	May 19, 1983 139	06:45:00.01
11	36 13.078'	120 18.709'	May 18, 1983 138	07:00:00.01
12	36 15.348'	120 36.866'	May 18, 1983 138	06:45:00.01

## NW-SE PROFILE

Shot	Latitude	Longitude	Date-Julian Day	Shot time (GMT)
13	36 24.086'	120 30.482'	June 30, 1983 181	07:00:00.03
14	36 15.491'	120 23.462'	June 30, 1983 181	06:30:00.01
15	36 04.203'	120 13.555'	June 30, 1983 181	07:45:00.01
16	35 47.760'	119 59.168'	June 30, 1983 181	08:00:00.01
17	35 37.851'	119 52.520'	June 30, 1983 181	06:45:00.01

## Earthquake recorded along NW-SE shot profile

Latitude	Longitude	Date-Julian Day	Time (GMT)	Z (km)	M
36 09.16'	120 16.85'	June 30, 1983 181	06:45:40.52	6.46	2.56

---

\* shots 1-8 are along profiles recorded south of the Coalinga area.

Table 3  
FLAT-LAYER VELOCITY MODELS FOR SHOTPOINTS

Va = apparent velocity (km/s); To = intercept time (s); Z, depth to top (km)

E-W PROFILE

SP 9 West			SP 10 West			SP 10 East			SP 11 West		
Va	To	Z	Va	To	Z	Va	To	Z	Va	To	Z
1.65	0.00	0.00	1.44	0.00	0.00	1.50	0.00	0.00	1.96	0.00	0.00
1.87	0.05	0.09	1.90	0.11	0.12	1.89	0.12	0.15	2.38	0.20	0.35
2.17	0.30	0.51	2.10	0.22	0.34	2.15	0.26	0.38	3.10	0.56	0.88
2.43	0.56	0.97	2.57	0.62	0.93	2.58	0.68	1.06	0.3 s advance		
2.84	0.99	1.65	3.02	1.06	1.73	2.97	1.04	1.69	4.19	0.77	1.90?
6.00	2.85	3.92	3.35	1.37	2.39	3.28	1.32	2.26	6.00	1.92	4.70?
---- delay ----			4.39	2.13	3.55	3.80	1.77	3.09			
7.66	4.83	12.90?	5.80	3.14	6.10	4.72	2.47	4.44			
			7.65	4.63	11.20	7.00	3.48	6.40			

SP 11 East			SP 12 East		
Va	To	Z	Va	To	Z
1.98	0.00	0.00	(no data, see text)		
2.99	0.56	0.74	4.15	0.24	0.7?
3.60	1.05	1.88	5.59	1.79	5.2?
4.69	2.06	4.11	---- delay ----		
---- delay ----			8.30	5.56	

NW-SE PROFILE

SP 13 South			SP 14 North			SP 14 South			SP 15 North		
Va	To	Z	Va	To	Z	Va	To	Z	Va	To	Z
2.15	0.00	0.00	1.80	0.00	0.00	1.80	0.00	0.00	1.82	0.00	0.00
2.45	0.06	0.13	2.26	0.02	0.03	2.07	0.05	0.09	2.06	0.05	0.10
3.30	0.24	0.40	2.54	0.06	0.12	2.37	0.15	0.27	2.34	0.20	0.39
3.75	0.42	0.93	3.09	0.22	0.43	3.25	0.57	0.88	2.73	0.45	0.81
4.82	0.88	1.97	4.35	0.61	1.12	4.53	1.26	2.22	3.04	0.70	1.36
5.43	1.13	2.84	---LVZ---		2.80?	---LVZ---		4.90?	4.58	1.75	2.92
---LVZ---		3.60?	6.00	1.75	4.40?	6.05	2.84	7.00?	---LVZ---		4.50?
6.30	1.90	6.20?				6.20	3.26	?	6.00	2.85	6.20?
6.65	4.36	?									

SP 15 South			SP 16 North			SP 16 South			SP 17 North		
Va	To	Z	Va	To	Z	Va	To	Z	Va	To	Z
1.56	0.00	0.00	1.60	0.00	0.00	1.60	0.00	0.00	0.80	0.00	0.00
1.94	0.05	0.07	2.43	0.07	0.07	2.31	0.07	0.08	1.89	0.15	0.07
2.25	0.20	0.33	3.01	0.36	0.65	2.88	0.36	0.54	2.18	0.28	0.31
2.62	0.45	0.77	3.91	0.84	1.55	3.77	0.93	1.47	2.55	0.47	0.61
3.00	0.70	1.21	4.43	1.28	3.03	4.27	1.28	2.91	5.18	1.91	2.45
4.26	1.58	2.61	---LVZ---		5.10?	---LVZ---		4.70?	---LVZ---		3.40?
---LVZ---		4.20?	5.29	2.58	7.40?	5.50	2.50	6.00?	5.75	2.40	4.90?
5.36	2.40	4.90?	6.13	3.46	?						
5.89	3.14	8.00?	6.40	4.15	?						

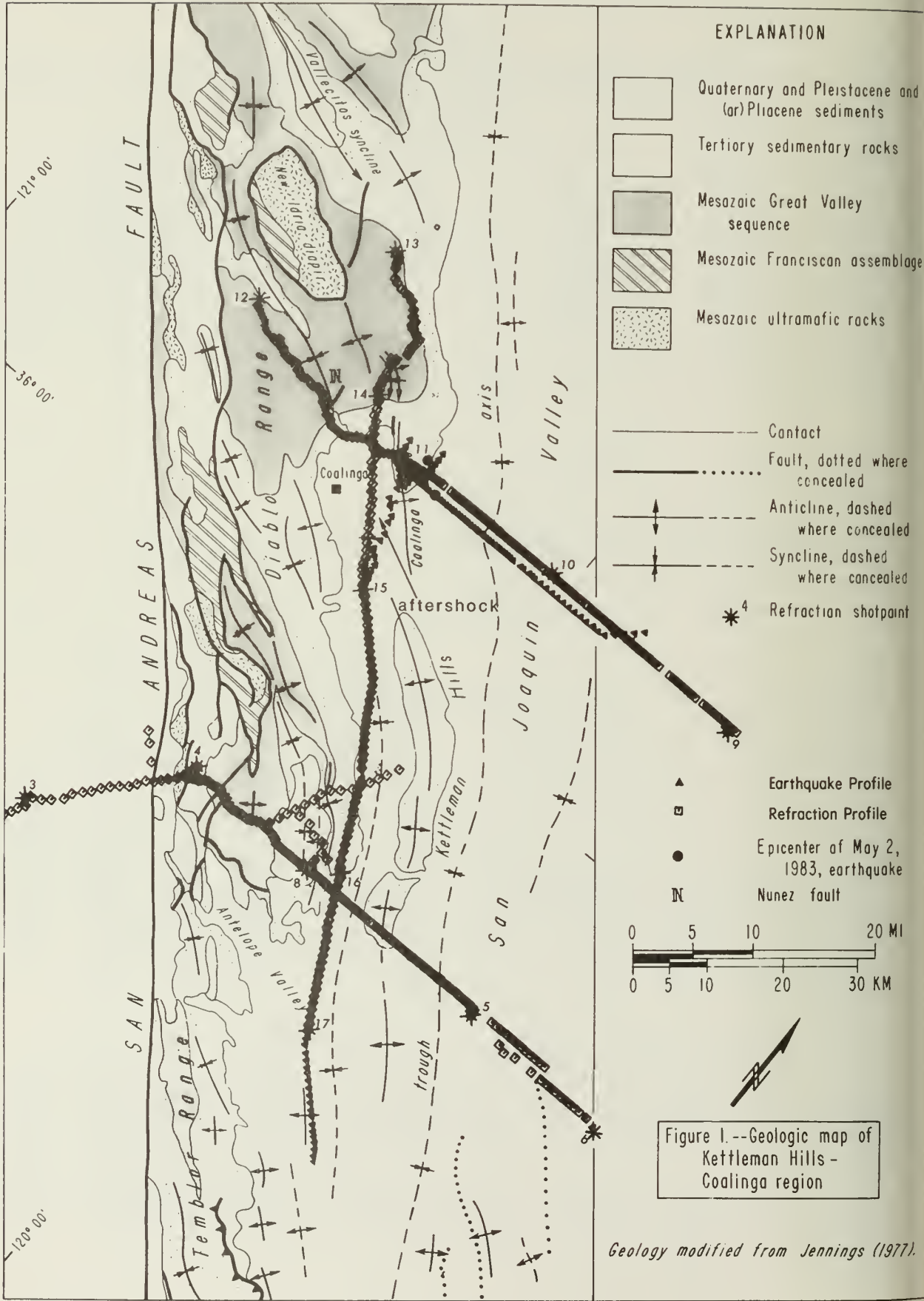


Figure 1. Geologic map of Kettleman Hills-Coalinga region.



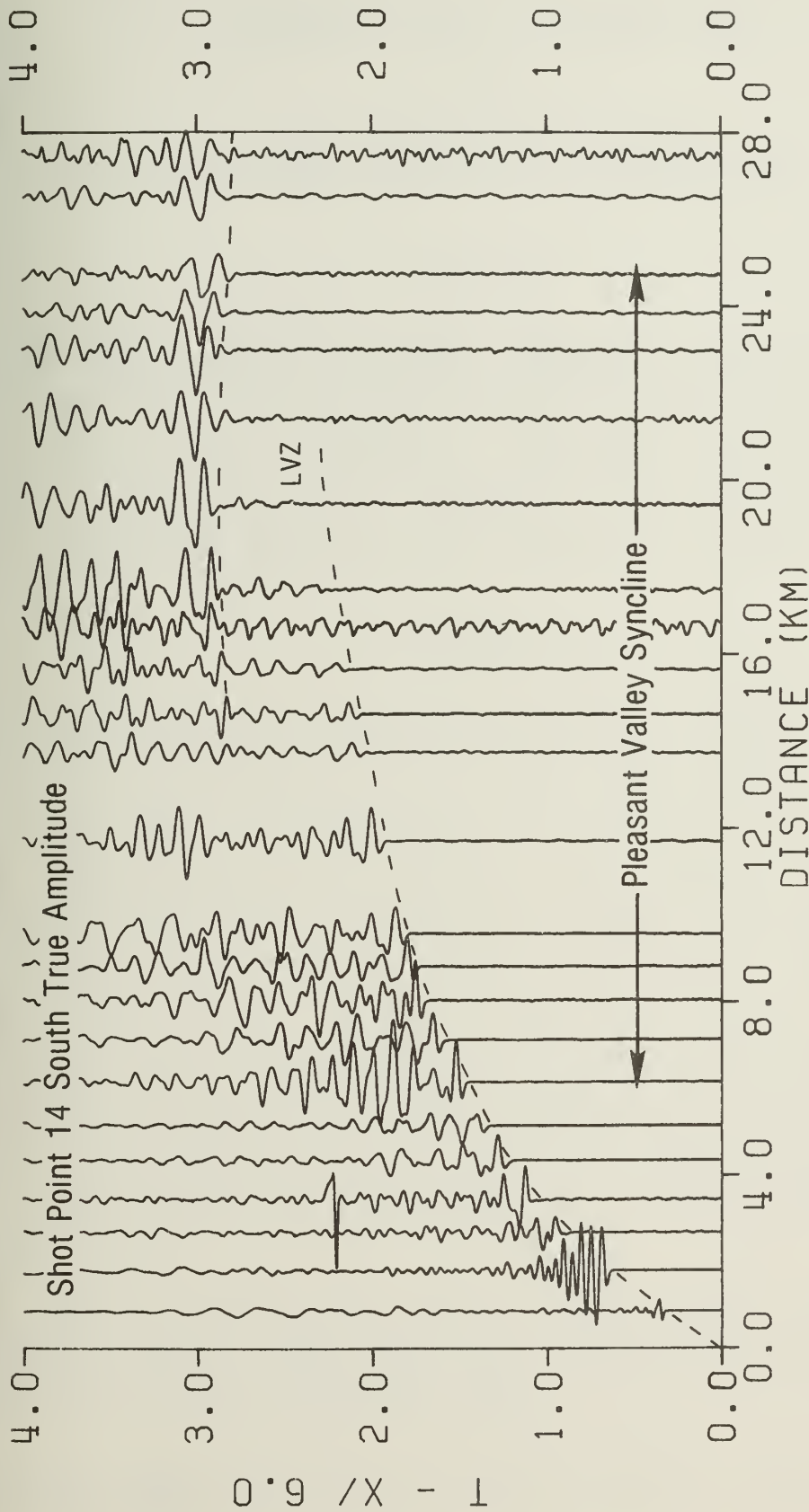
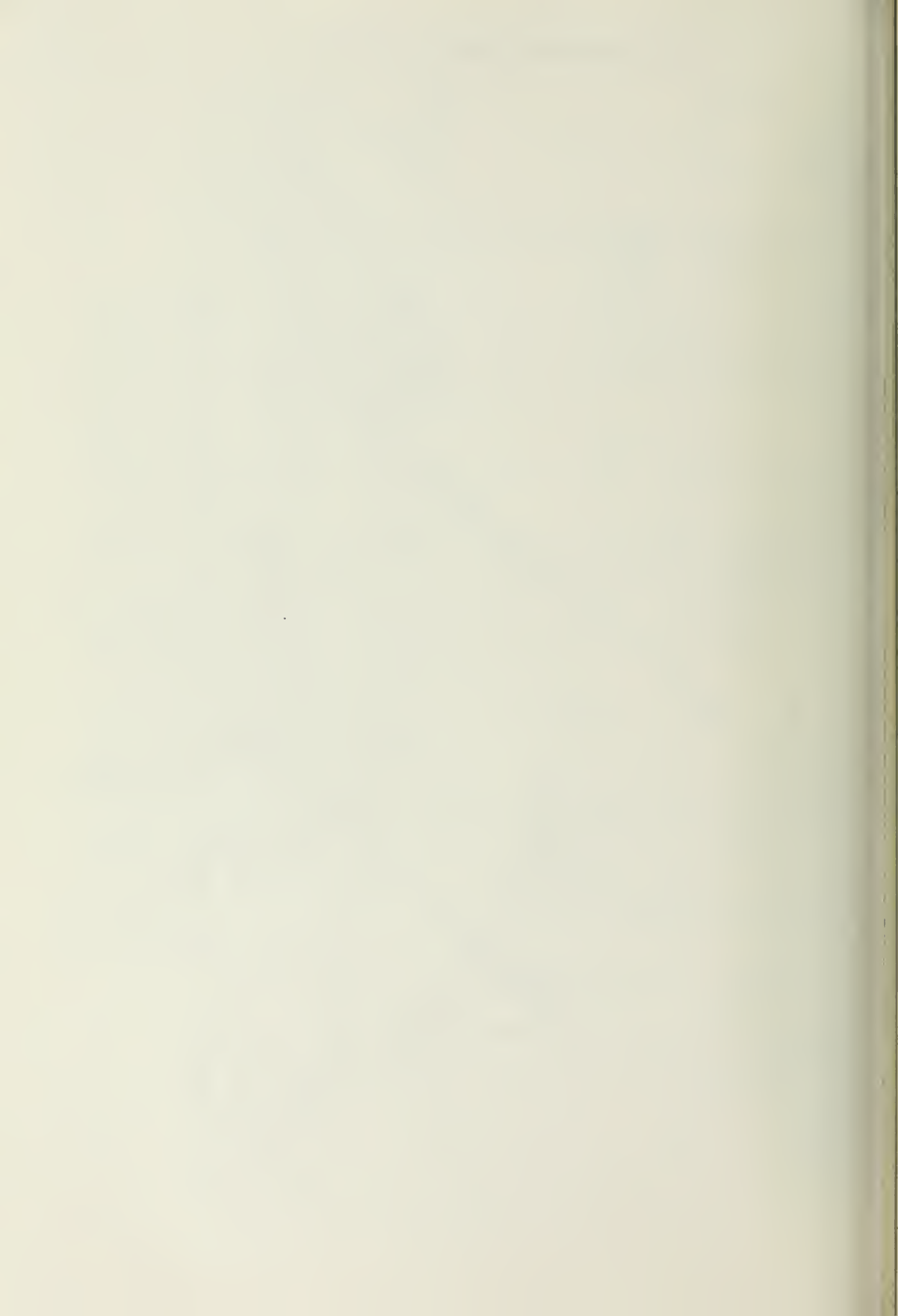


Figure 2. True-amplitude record section observed southeast of SP 14, NW-SE Profile. The time is reduced by  $(\text{distance})/6$ . The trace amplitude is scaled by  $(\text{distance})^2$ . Note the amplitude decay of the first arrivals and the delayed high-amplitude reflection from the basement. This is strong evidence for a low-velocity zone in the sedimentary section along the NW-SE Coalinga profile.



# COCORP SEISMIC REFLECTION PROFILES NEAR THE 1983 COALINGA EARTHQUAKE SEQUENCE: DEEP STRUCTURES

by

Eric Fielding, Muawia Barazangi  
Larry Brown, Jack Oliver, and Sidney Kaufman<sup>1</sup>

## ABSTRACT

COCORP seismic reflection lines shot in the Coalinga area in 1977 delineate deep Cenozoic and Mesozoic structures in the subsurface of the western San Joaquin valley beneath the 1983 earthquake sequence. The data imply several faults interpreted to be high-angle normal faults with significant movement during the Cretaceous, and provide constraints on the deep structure of the Neogene fold system under which the recent earthquakes occurred. The reverse faulting indicated by the earthquakes in the sequence may be reactivating the pre-existing, high-angle, basement faults that are inferred from the COCORP data.

## INTRODUCTION

COCORP (Consortium for Continental Reflection Profiling) collected two deep seismic reflection profiles in the area south and east of the City of Coalinga during the summer of 1977. Line 1 runs east-west just south of Coalinga for some 50 km from the base of the hills out into the San Joaquin valley, and Line 3 runs north-south for 15 km from Reef Ridge to the north end of the Kettleman Hills North Dome (KHND) (see Fig. 1). Line 1 passes about 15 km to the southeast of the May 2, 1983 epicenter. The main strand of the San Andreas fault system, which lies about 25 km to the southwest of the COCORP Coalinga lines, was crossed by COCORP's Parkfield Line 2, which was collected along with the the Coalinga lines (see Long, 1981).

These COCORP seismic reflection surveys were carried out to provide information on the deep structure of the western side of the Great Valley. The Coalinga area was chosen because of excellent stratigraphic control from exposures of the Mesozoic and Cenozoic sections in the hills west of Coalinga and from the numerous oil wells in the area. The re-entrant of the San Joaquin valley in the Coalinga area also allows seismic crews to get closer to the Coast Ranges and the San Andreas fault system, without working over high topographic relief, than is the case for other areas on the west side of the Great Valley.

The COCORP Coalinga profiles show strong reflections from Tertiary and Cretaceous strata that imply deep basement structures in the Coalinga area. Reflections from the approximately 3.5 km thick Tertiary deep and shallow marine section (AAPG, 1959; Fowlkes, 1982)

<sup>1</sup>Department of Geological Sciences, Cornell University, Ithaca,  
New York 14853



show the effects of the Neogene folding that has greatly modified the western side of the San Joaquin valley. This folding is closely associated in space and time with deformation of the southern Coast Ranges and strike-slip motion along the San Andreas fault system (Page, 1981). Reflections from the 6-8 km thick Upper Jurassic to Cretaceous Great Valley Group (GVG, previously called the Great Valley Sequence -- see Ingersoll, 1982) indicate significant faulting during the deposition of these deep marine turbidites, probably along high-angle normal faults. The recent Coalinga earthquake sequence, beginning May 2, 1983, is a manifestation of the continuing active tectonics of the area, and many of the deep reverse-fault mechanisms detected during the sequence may be reactivations of the high-angle Cretaceous faults that are inferred from the COCORP lines. A more detailed discussion of the geologic and tectonic setting of the Coalinga area can be found in Fielding and others (1983) and in other articles in this volume.

#### DATA ACQUISITION AND PROCESSING

Two Vibroseis (trademark CONOCO, Inc.) reflection profiles were collected in the Coalinga area during May and June of 1977: a 50 km east-west main line and a 15 km north-south crossline (see Fig. 1). Line 1 runs due east from the base of the hills west of Coalinga through the gap between the Gujarral Hills and the KHND and out into the San Joaquin valley. Line 3 starts at the base of Reef Ridge and runs due north across the end of the KHND to the Gujarral Hills. Common depth point (CDP) coverage on Line 3 extends only to vibration point (VP) 112, so the CDP stack for Line 3 does not cross Line 1. Data was recorded on a 48-channel recording system with 134 m station spacing, producing minimum and maximum source-to-receiver offsets of 0.6 km and 6.7 km, respectively. For Line 1, vibrator sweep (10-32 Hz) time and recording time were adjusted to produce 24 s of correlated data; the Line 3 vibrating and recording times produced 20 s of data. Vibrating every station (5 or 6 vibrators X 16 sweeps/station) resulted in nominal 24-fold CDP stacks, except at the eastern end of Line 1, where vibrating through the spread resulted in CDPs with a maximum 46-fold.

The data were originally collected by Compagnie Generale de Geophysique (CGG) under contract to COCORP and processed under contract by the Geodigit Division of CGG. The data presented here have been extensively reprocessed at Cornell using the Megaseis processing facility, starting with the demultiplexed and Vibroseis correlated VP gathers. The standard sequence followed in the reprocessing includes elevation statics corrections, CDP gathering, trace amplitude balancing, mute and velocity analyses, normal moveout (NMO) corrections, and stacking. Mutes were applied before and after NMO.

Detailed velocity analysis was performed in two stages. Velocity spectra and constant velocity stacks were used to pick an initial set of velocity functions; then variable velocity stack and moved out CDP gather panels, perturbed from the initial velocity functions by increments of 2.5 percent, were used to refine stacking (approximately equal to rms) velocities every 20-50 CDPs (about every 10-25 stations) depending on changes in structure. Velocity control is generally very good down to 4 or 5 s because of the strong reflections and the relatively long receiver array. Interval velocities calculated from the rms velocities with the Dix equation (Dobrin, 1976) have been smoothed and contoured in Fig. 2. Interval velocities are

sensitive to small changes in rms velocities, so the expected error in interval velocities is greater than 10 percent (considerably greater error expected over short intervals has been partially removed by smoothing).

More advanced processing, performed on these data, includes deconvolution, automatic residual statics, and migration. Short periodicity multiples (ringing) are very strong on both Coalinga lines, causing events close together in time to appear as one multicyclic event and also causing some low-amplitude events to be obscured by nearby reflections of high amplitude. Predictive deconvolution strongly attenuates the ringing and increases the resolution of the reflection data, but it also introduces some waveform distortion of the Vibroseis correlated pulse that appears to attenuate some genuine events. Elevation statics were not a problem owing to the lack of relief (less than 260 m) along the lines, but the continuity of the reflections was significantly improved by a surface-consistent, automatic-residual-statics program, which presumably corrected for varying near-surface delays in the Recent alluvium. The time sections displayed in Figs. 3 and 4 are not migrated, so dipping reflections on the sections have shallower dips and are displaced horizontally from their true positions in the plane of the section. However, constant velocity migrations performed on the data show the major features of the seismic sections to be only slightly changed by migration. Cultural noise was somewhat of a problem on these lines, especially where the main line passed within 2 km of the City of Coalinga and where it crossed Interstate 5 (see Fig. 1). There were also agricultural pumps operating near the lines, introducing coherent noise in some areas along the lines. The effects of this noise were sharply reduced by normalizing the amplitudes along and between the traces before stacking (trace amplitude balancing).

#### COCORP DATA INTERPRETATION

Both of the COCORP Coalinga lines show a prominent set of reflections that runs continuously through the length of the lines between about 2 and 3.5 s (Figs. 3 and 4). These reflections are by far the highest amplitude events on the two sections; other events above and below them are weaker and less continuous. In general, reflections are strongest where the layering is horizontal and where the stack fold is highest, as expected. A more detailed interpretation of the data will be published in Fielding and others (1983).

#### Stratigraphic Correlation

Stratigraphic control from wells in the Coalinga, Gujarral Hills, and Kettleman Hills oil fields is excellent (e.g. AAPG, 1959). Depths to formation tops from two nearby (about 750 m away) wells were averaged, converted to an approximate travel time (using interval velocities) and projected onto line 1 at VP 138 (see Fig. 5). The upper layers of the section, identified as Pliocene and Plio-Pleistocene to Recent in the wells, extend to about 1.5 km depth, or 1.2 s on the time section. The long COCORP receiver array is not conducive to good imaging of these less-continuously bedded upper strata, because it is optimized for deeper reflections.



The upper half of the high-amplitude continuous reflections correlates with Miocene strata, while the lower half corresponds to the rest of the Lower Tertiary section down to a depth of 3.5 km (about 2.5 s) at VP 138. Thickly interbedded sandstone and shale layers of Miocene and Eocene age probably provide numerous interfaces of high impedance contrast that produce the observed high-amplitude reflections. The 6-8 km minimum stratigraphic thickness of the Upper Jurassic-Cretaceous GVG exposed west of Coalinga, projected down-dip under Line 1 (Fig. 5), would extend to a depth of 9.5-11.5 km approximately corresponding to the deepest relatively continuous events at 5-6 s on the seismic profile. This is also near the depth at which the interval velocities reach 6 km/s (Fig. 2).

### Structures

The first-order structure seen on both Line 1 and Line 3 is the upwarping of the sedimentary section toward the Coast Ranges west and south of Coalinga. Plio-Pleistocene strata and even Quaternary terraces are involved in the upwarping, indicating ongoing deformation (Fowlkes, 1982; Fig. 5). Upwarping on the southern end of Line 3 is especially sharp, with dips measured in the Reef Ridge area up to 70°. Superimposed on this upwarping is the anticline under which the recent earthquake sequence occurred, which has an axis at about VP 145 on Line 1 and at about VP 110 on Line 3 (Figs. 1, 3, and 4). The southeast limb of the KHND appears on the north end of Line 3. The moderately complex, three-dimensional structure of this fold is shown by the structural contours derived from closely spaced oil wells (Dodd, 1931; Kaplow, 1945; Hunter, 1951; Fig. 1). The COCORP lines run through this fold on the structural saddle between the northward-plunging KHND and the southward-plunging Coalinga Nose anticline.

The asymmetric, monoclinial shape of this fold suggests that it may have been formed as a drape fold over a steep basement fault (e.g., Stearns, 1978; Reches and Johnson, 1978). The Tertiary strata reflections appear to be continuous over this fold on Line 1 at least down to 2.5 s (down to 3.5 s on migrated seismic sections). The GVG also appears largely unfaulted, though reflections from that depth are less continuous on the seismic section. The COCORP data are consistent with the interpretation of this fold as a combination of drape folding and buckling of the sedimentary section over a high-angle, eastward-dipping, reverse fault in the basement, and probably rule out a blind thrust interpretation. The displacement on the fault beneath Line 1 is probably less than that beneath the Coalinga Nose or KHND, in view of the plunge of the overlying folds. The inferred basement fault may be a reactivation of a pre-existing normal fault, as will be discussed below.

The deeper reflections of the eastern half of Line 1 show evidence of significant Cretaceous age faults that may be affecting Late Cenozoic to Recent faulting. Beneath VP 335, events A and B are offset, with the western block relatively uplifted (see Fig. 5). The orientation (especially the strike) of the fault is poorly constrained by this single seismic profile, but the preferred interpretation is that a normal fault exists at approximately 4 s and dips 50°-70° eastward in the plane of the section with about a kilometer of offset (possibly 3 km of offset with different event correlations). A reverse fault dipping to the west cannot be ruled out, but minor drape folding of the reflecting strata above event A suggest a east-dipping,



high-angle, normal fault. The overlying Tertiary reflectors are not disrupted, indicating that the fault motion probably took place during the Cretaceous. The uplifted western block is overlapped by the lowermost Tertiary layers.

West of VP 300, the reflections from the Cretaceous strata dip increasingly westward, forming a wedge-shaped sequence (see Figs. 3 and 5). Although this feature is partially masked by the traffic noise from Interstate 5, discontinuous dipping events occur as far west as event C at VP 225. Because these events are dipping fairly steeply (up to  $30^\circ$  of apparent dip in the plane of the section), their true location is updip from their location on the unmigrated section (Fig. 3). Assuming that the seismic line is close to perpendicular to the strike of these strata, the preliminary constant velocity migrations show that event C migrates to around VP 245 and dips  $30^\circ$  west. If the section is far from perpendicular to the strike of the reflectors, their true dip could be much greater.

The bottom of the wedge-shaped sequence is not unambiguously imaged on the COCORP section; the lowermost reflections are gradually lost in the background noise. The data do not well constrain the position of the bounding fault or faults, but the major structural relief occurs between VP 240 and VP 270 (Fig. 5). The fanning pattern of the reflecting strata requires significant rotation (perhaps  $30^\circ$ ) of the underlying basement during their deposition. The shape and size of this wedge-shaped sequence is similar to several sequences imaged on passive continental margins, which have been interpreted to be half-graben basins. Here also, the overlying Tertiary strata are not deformed, indicating that the probable normal faulting ended during the Cretaceous.

### Deep Reflections

Although lower crustal reflections are rare on the COCORP Coalinga lines, a particularly curious set of possible deep reflections were imaged on Line 1 at about VP 350 between 8.5 and 11.2 s. The amount of moveout across the receiver array of these events is too small for simple multiples of reflections higher in the section, but without crossline control, reflected refractions or out-of-the-plane reflections ("side-swipe") cannot be ruled out. A detailed study of the amount of attenuation within the thick sedimentary section and the effects of cultural noise presently underway may explain why lower crustal reflections were not observed elsewhere on the Coalinga lines. Refraction studies suggest that the Moho is located at about 25-km depth in this area, falling within this zone of deep reflections.

### The Coalinga Earthquake Sequence

The May 2, 1983 Coalinga earthquake ( $M_L=6.5$ ) began a sequence of thousands of aftershocks beneath the Coalinga Nose and KHND anticlines (Reasenber and others, 1983; and other papers in this volume; see Fig. 1). The aftershocks appear to define a volume that extends across COCORP Line 1 to the end of Line 3. The May 2 hypocenter has been located at a depth of 10.5 km on the axis of the Coalinga Nose anticline (Eaton, 1983; and this volume), only about 15 km northeast along the strike of the anticline from

the crossing of Line 1 (Fig. 1). However, projecting the fault plane of the May 2, 1983 main shock directly onto the COCORP reflection section is hazardous for several reasons.

The apparent complexity of the spatial distribution of the aftershock activity indicates that deformation is occurring throughout a large volume, perhaps as the thick sedimentary section accommodates probable basement faulting along one or more faults. The moderately complex, three-dimensional shape of the Coalinga Nose anticline (Fig. 1) also precludes a simplistic model of the basement fault geometry. The anticline plunges more than 2 km and flattens out considerably (from 60° dip to less than 10° dip on the southwest limb) between the hypocenter of the main shock and COCORP Line 1 (Kaplow, 1945; AAPG, 1959; Fig. 1). The anticline shape suggests that the amount of structural relief is greater under the Coalinga Nose and the KHND than under Line 1; in addition, the KHND lies about 2 km west of the projection of the Coalinga Nose, suggesting an en echelon basement fault pattern. The COCORP profiles pass through the structural saddle between the two folds at about a 45° angle to their strike. Nevertheless, there are some tentative short, but relatively high-amplitude, events and possible diffraction patterns at 5-6.5 s beneath VP 140 on Line 1 that may indicate a fault-disrupted zone at a depth of 8.5-12 km. A high-angle fault plane reflection would be located much farther east on the unmigrated seismic section in view of the nature of unmigrated sections and the angle that the profile makes with the probable strike of the fault. The interpretation of the anticline on Line 1 as a combination of drape folding and buckling over a high-angle basement fault is consistent with the interpretation of the steep NE-dipping nodal plane of the May 2 main shock being the fault plane.

### CONCLUSIONS

COCORP deep seismic reflection profiles in the Coalinga area provide some important constraints on the structure of the basement beneath the thick sedimentary section. Reflections from deformed Cretaceous strata provide evidence for significant fault movements during deposition of the GVG, most likely along an east-dipping series of high-angle normal faults. This early deformation does not affect the thick overlying Tertiary section, but the pre-existing faults could well have controlled the orientation and nature of Late Tertiary and Quaternary faulting and folding in response to Neogene tectonic stresses in the area. COCORP Line 1 shows that the Coalinga Nose anticline continues down plunge with reduced amplitude, and suggests that the fold is primarily a drape fold over a high-angle basement fault or faults. The inferred reverse fault slip may be reactivating a pre-existing normal fault. The COCORP data also indicate that the Tertiary strata involved in the Coalinga Nose folding are largely unfaulted down to at least a depth of 3.5 km, and that the uppermost Cretaceous strata are probably not significantly faulted down to about 5 km depth, which constrains the amount of displacement on the underlying fault. The complexity of the folds prevents a simple projection of the May 2 main shock onto the seismic reflection section, but the inferred high-angle basement faults are consistent with the interpretation of reverse faulting along the steep NE-dipping nodal plane of the earthquake. The possibility of earthquake recurrence on such deep basement faults beneath the thick sedimentary section of the western part of the Great Valley should be considered in any future seismic risk evaluation of the region.

## ACKNOWLEDGEMENTS

We thank R. Lillie and B. Payne of Cornell for reviewing this manuscript and discussing these data; we thank J. Eaton for kindly discussing the 1983 Coalinga earthquake sequence; and we thank C. Baxter for typing this manuscript and J. Healey for editorial assistance. The field data were collected by crew 404-48-02 of Compagnie Generale de Geophysique. The data were reprocessed on the MEGASEIS seismic data processing system at Cornell University. Supported by COCORP National Science Foundation Grants EAR 2-12445 and EAR 80-25361, Cornell contribution No. 774.

## REFERENCES

- American Assoc. of Pet. Geol., Pacific Section, 1959, Correlation section longitudinally North-South through westside San Joaquin Valley from Coalinga to Midway Sunset and across San Andreas Fault into southeast Cuyama Valley, California: AAPG correlation section, 1959 series.
- Robinson, M.B., 1976, Introduction to Geophysical Prospecting, McGraw-Hill, New York, p. 230.
- Woodward, H.V., 1931, Recent developments in the Kettleman Hills field: California Oil Fields, v. 17, no. 1, p. 5-44.
- Wyllie, J.P., 1983, Seismic setting, location, and focal mechanism of the May 2, 1983 Coalinga earthquake, in Borchardt, R.D., ed., The Coalinga Earthquake Sequence Commencing May 2, 1983: U.S. Geol. Survey Open-File Report 83-511, p. 20-26.
- Wyllie, E.J., Barazangi, M., Brown, L., Oliver, J., and Kaufman, S., 1983, COCORP seismic profiles near Coalinga, California: Subsurface structure of the western Great Valley, submitted to Geology.
- Wyllie, E.J., 1982, An Educational Guidebook to the Geologic Resources of the Coalinga District, California: Coalinga, West Hills College, pp. 260.
- Wyllie, G.W., 1951, Guajarral Hills oil field (Fresno County): California Oil Fields, v. 37, no. 1, p. 13-19.
- Wyllie, R.V., 1982, Initiation and evolution of the Great Valley forearc basin of northern and central California, U.S.A., in Leggett, J.K., ed., Trench-Forearc Geology: Geol. Soc. London, Special Pub. no. 10, p. 459-467.
- Wyllie, E.J., 1945, Coalinga oil field (Fresno County): California Oil Fields, v. 31, no. 2, p. 5-22.
- Wyllie, G.H., 1981, A COCORP Deep Seismic Reflection Profile across the San Andreas Fault, Parkfield, California: unpub. Masters thesis, Cornell University, Department of Geological Sciences.



- Page, B.M., 1981, The southern Coast Ranges, in Ernst, W.G., ed., The Geotectonic Development of California: Prentice-Hall, New Jersey, p. 329-417.
- Reasenbergs, P., Eberhart-Phillips, D., and Segall, P., 1983, Preliminary views of the aftershock distribution of the May 2, 1983, Coalinga, earthquake, in Borchardt, R.D., ed., The Coalinga Earthquake Sequence Commencing May 2, 1983: U.S. Geol. Survey Open-File Report 83-511, p. 27-37.
- Reches, Z., and Johnson, A.M., 1978, Development of monoclines: Part II. Theoretical analysis of monoclines, in Matthews, V., III, ed., Laramide Folding Associated with Basement Block Faulting in the Western United States: Geol. Soc. Amer. Memoir 151, p. 273-311.
- Stearns, D.W., 1978, Faulting and forced folding in the Rocky Mountain foreland, in Matthews, V., III, ed., Laramide Folding Associated with Basement Block Faulting in the Western United States: Geol. Soc. Amer. Memoir 151, p. 1-38.

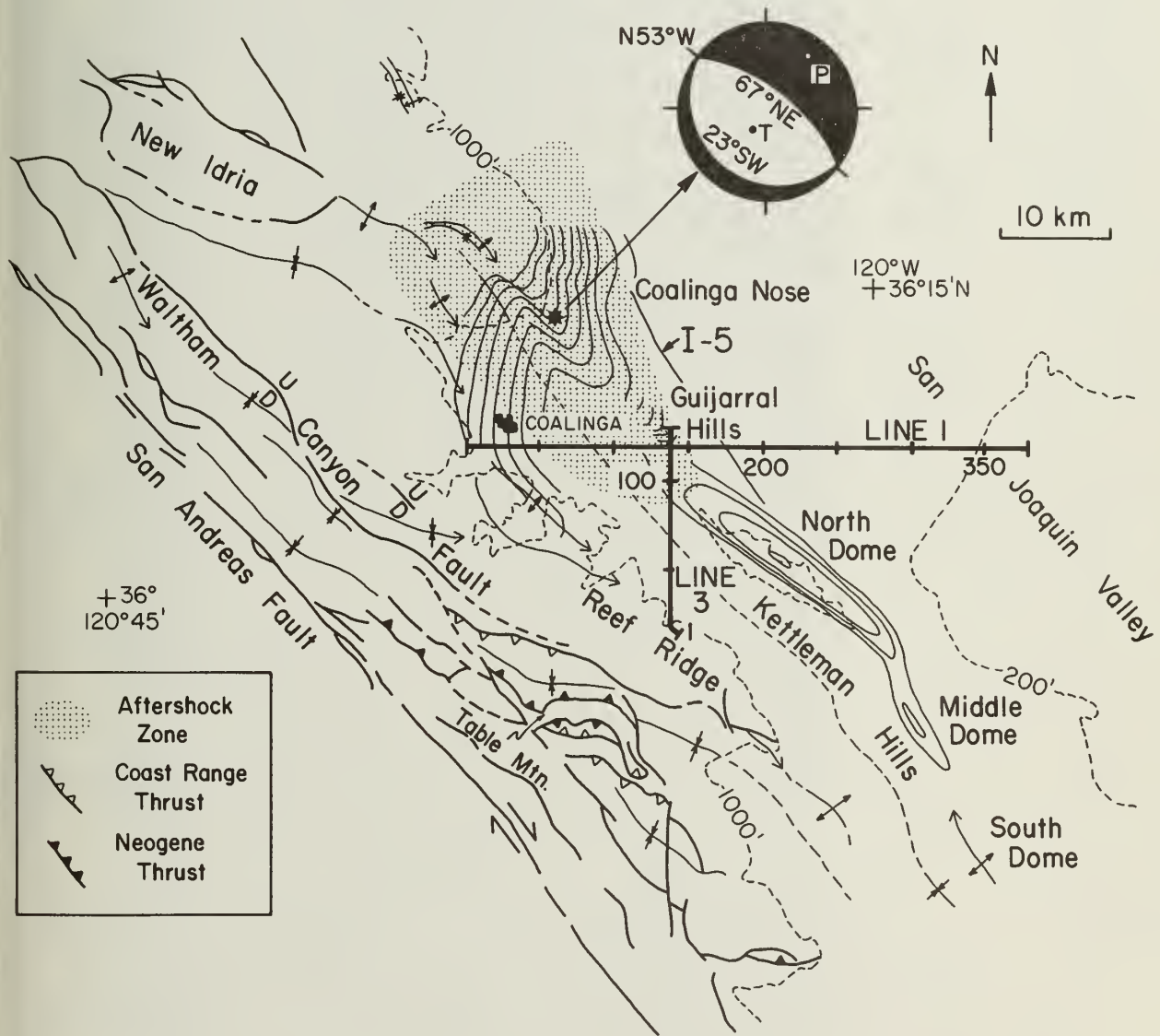


Fig. 1: Generalized tectonic map of the Coalinga area, showing location of COCORP lines, major faults and fold axes, topographic contours, 500 m structural contours on Eocene formation derived from wells in Coalinga and Kettleman Hills oil fields, location and focal mechanism of May 2, 1983 Coalinga earthquake ( $M_L=6.5$ ) and its aftershock zone through June 12, 1983.

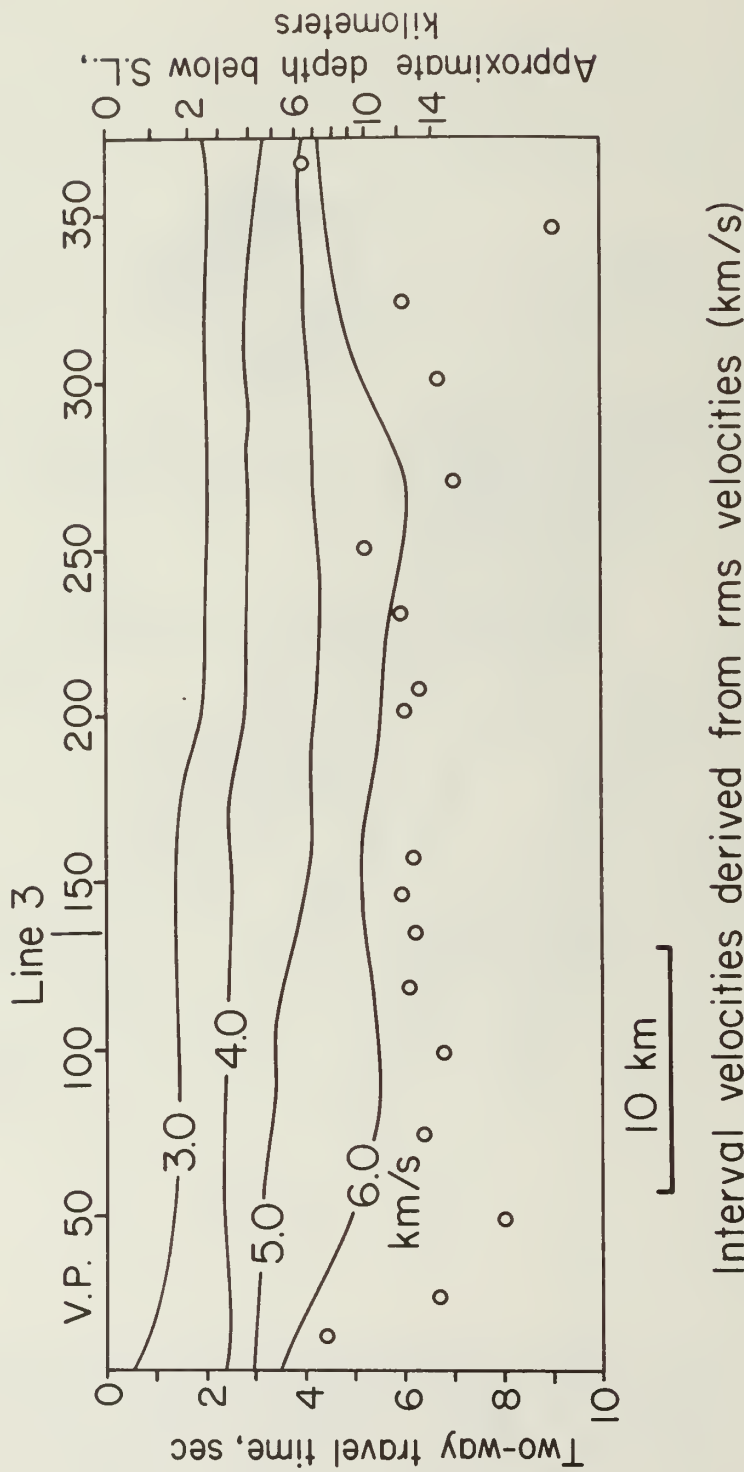


Fig. 2: Generalized contours of the interval velocities for COCORP Line 1 derived from the stacking (rms) velocities used in processing. Interval velocities are very sensitive to small changes in rms velocities, so these contours are only approximate. Crystalline basement is inferred near 6 km/s contour. Circles indicate deepest points at which a rms velocity was measured.



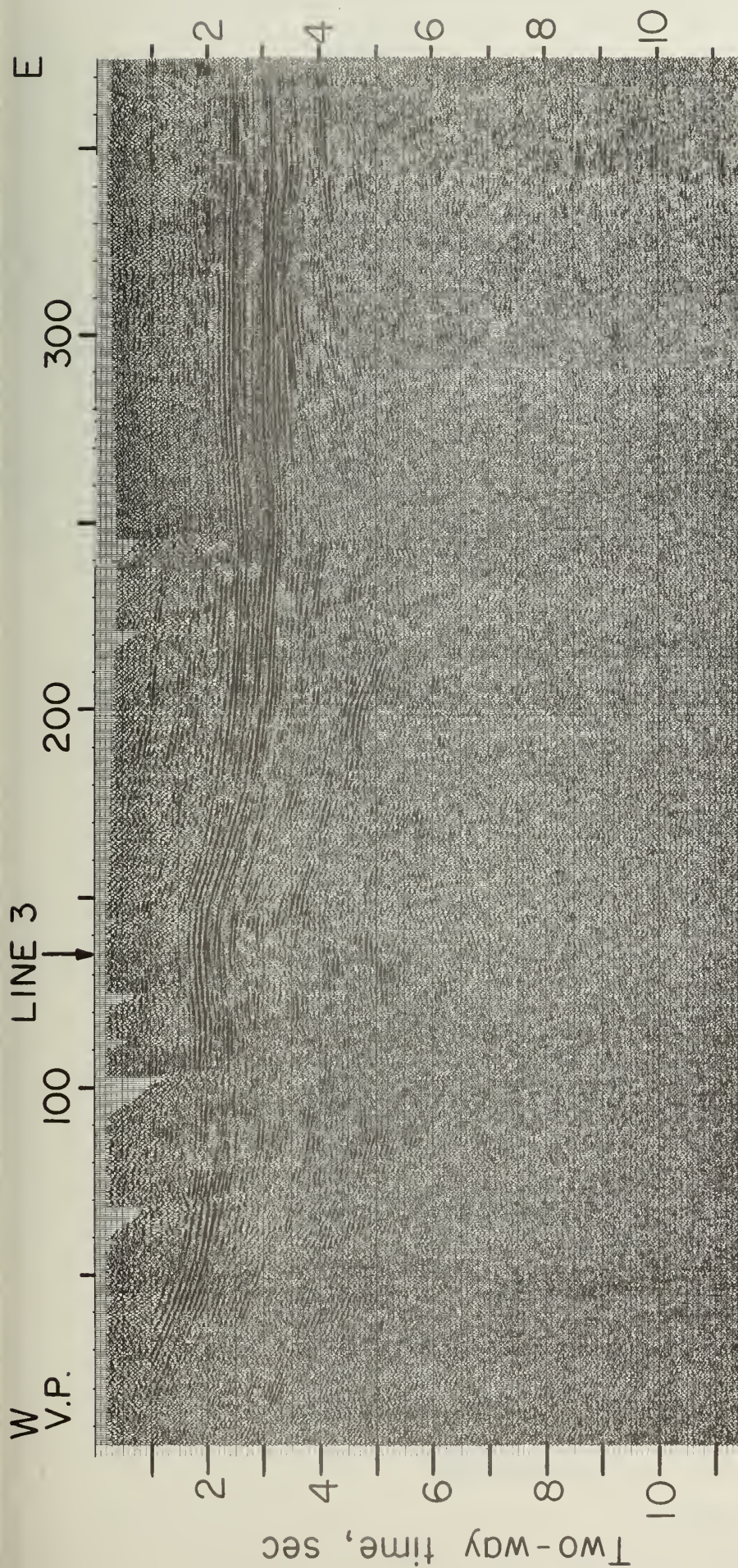


Fig. 3: COCORP Coaltinga Line 1: time section is not migrated or deconvolved. Trace amplitude balancing with a window of 0.5 s has been applied before stack. High-amplitude, continuous reflections are from Lower Tertiary section. Note structures in Cretaceous section reflectors beneath the strong Tertiary reflections.



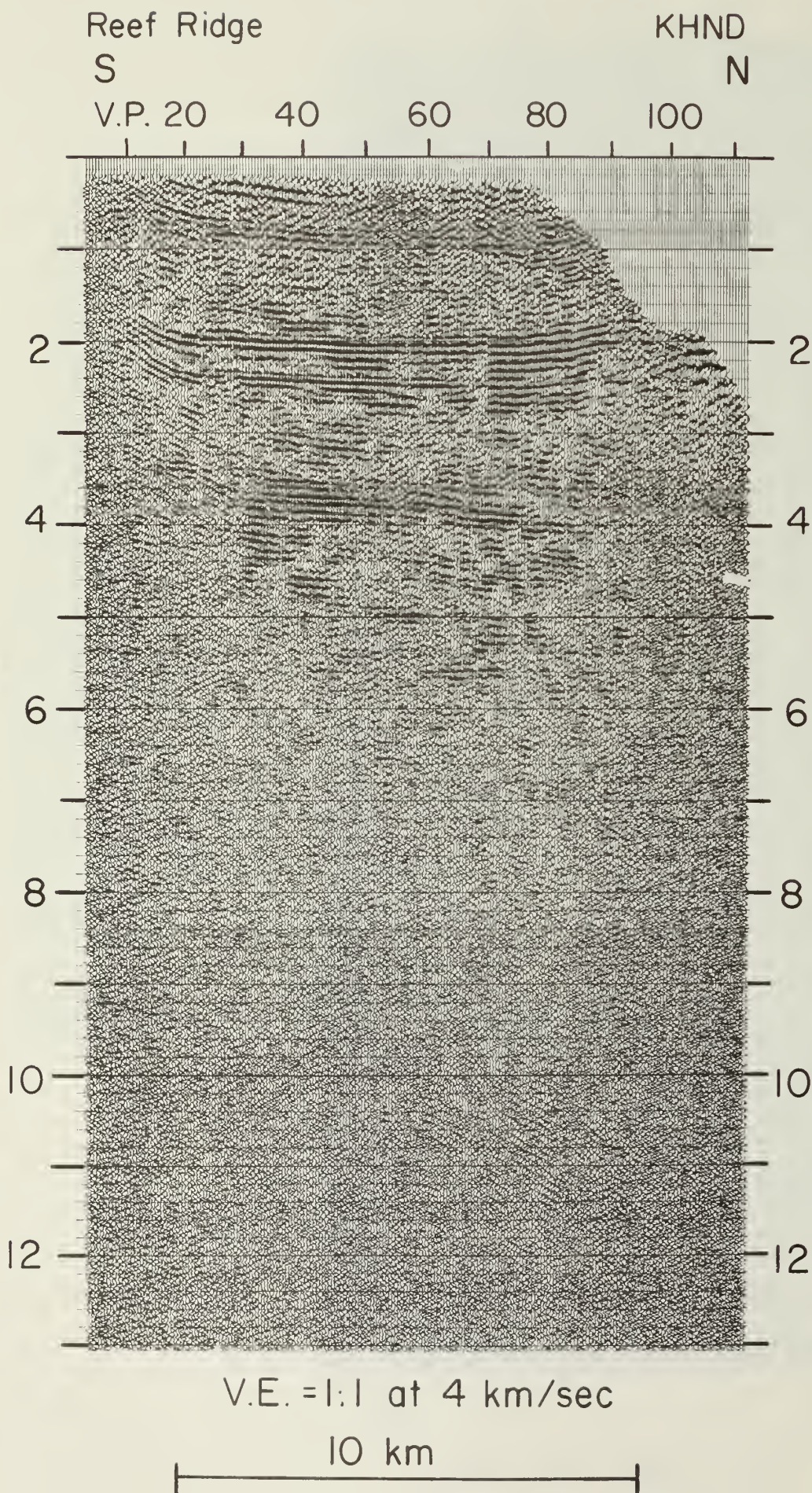


Fig. 4: COCORP C  
Line 3: time section  
migrated or decon  
Trace amplitude ba  
with a window of  
applied before stac  
sharp upwarping  
Reef Ridge on sout  
and limb of Kettler  
North Dome (KHND) o  
end. Flat part of s  
correlates with abo  
80 on Line 1.



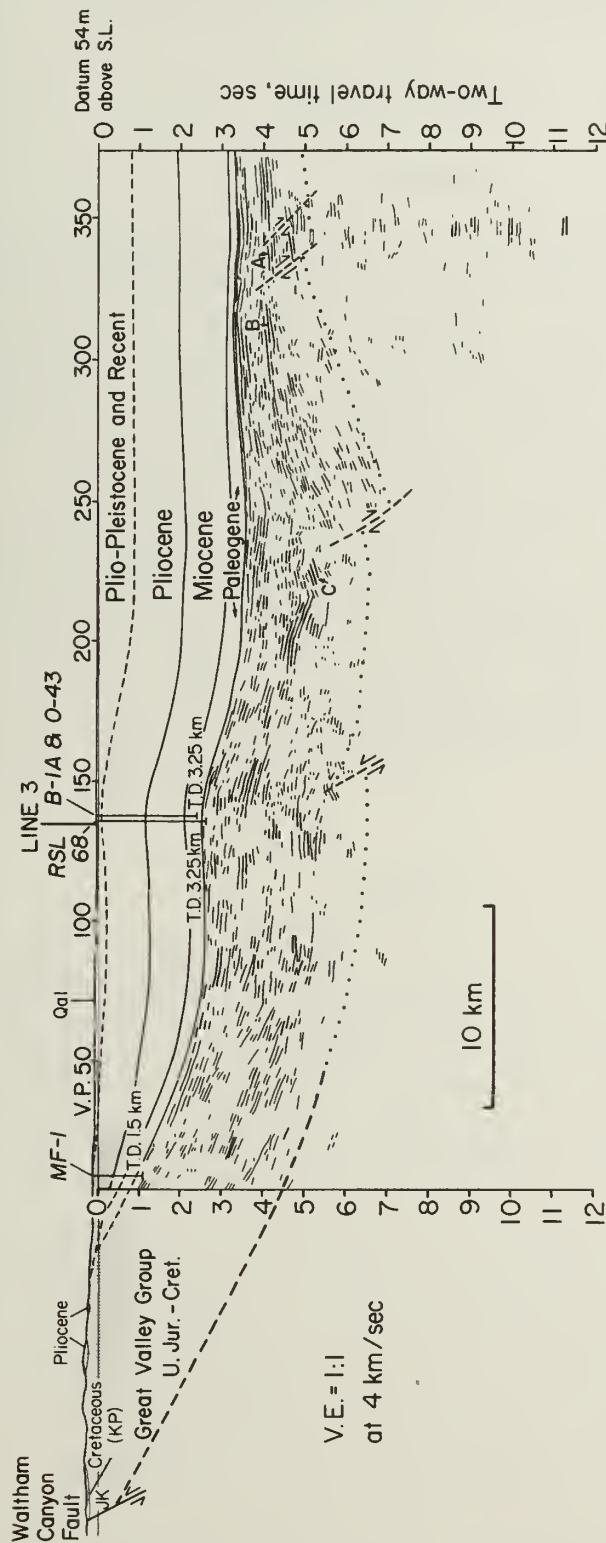


Fig. 5: Interpretation of COCORP Line 1 (unmigrated), showing surface topography and geology, stratigraphic interpretation of reflections from the Cenozoic section, line drawing abstracted from Upper Jurassic - Cretaceous section reflections, inferred basement faults and approximate location of basement. Note offset between events A and B, and the wedge-shaped package of reflectors extending to event C. Wells projected onto Section are Oils Inc. of Calif. "Magnet Fee" - 1 (MF-1), R.S. Lytle 68 (RSL 68), Chevron "Bourdieu" 1A (B-1A), and Univ. Cons. "Orr" 43 (O-43). Total depths (T.D.) in km below S.L.





# REVERSE SLIP ON A BURIED FAULT DURING THE 2 MAY 1983 COALINGA EARTHQUAKE: EVIDENCE FROM GEODETIC ELEVATION CHANGES

by

Ross S. Stein<sup>1</sup>

## ABSTRACT

The Coalinga earthquake ( $M_L=6.2-6.7$ ) uplifted Anticline Ridge one half meter, but caused no fault rupture at the ground surface, demonstrating that folding and faulting of the eastern margin of the California Coast Ranges are coincident and continuing. Elevation changes associated with the earthquake enable an estimate of the fault attitude, geometry, and slip. Small topographic relief over the route minimizes systematic leveling errors. Artificial subsidence due to fluid withdrawal is more significant, although it is still small in relation to the earthquake changes. Deep-well compaction monitors and the record of fluid pumping are used to remove the subsidence. A steeply dipping reverse fault is well fit by the geodetic and seismic data, whereas a gently dipping thrust fault is less compatible with the location and depth of the mainshock. For a  $N53^\circ W$  strike and a  $67^\circ NE$  dip, the best-fit earthquake parameters are:  $1.8 \pm 0.5$  m of dominantly reverse dip slip on a fault extending from a depth of 10-13 km to within 3-5 km from the ground;  $M_0 = 6-7 \times 10^{25}$  dyne-cm. The deformation caused by the 1983 earthquake looks strikingly like the present-day topographic form of Anticline Ridge. About 2-5 km of cumulative buried fault slip during the last million years would account for this similarity.

## INTRODUCTION

The 2 May 1983 Coalinga earthquake struck beneath Anticline Ridge, at the boundary of the San Joaquin Valley syncline to the east and the California Coast Ranges to the west. The tectonic role of the earthquake - its repeat time and the cumulative displacement on the earthquake fault - and its impact upon strain accumulation on the San Andreas fault 30 km to the west, cannot be interpreted without knowledge of the fault attitude and amount of slip. The range of fault geometries and displacements consistent with the permanent vertical deformation and earthquake mainshock are presented in this paper.

Spirit leveling measures the height of permanent bench marks (BM's) in the ground. To measure changes in elevation caused by the earthquake, the elevation of BM's surveyed largely 11 years before the earthquake is subtracted from the elevation measured one month after the 2 May 1983 earthquake. While random and systematic leveling errors prove to be negligible in comparison to the magnitude of the earthquake deformation, artificial subsidence caused by water and oil withdrawal is more substantial. Uncertainties in the proper removal of these contaminants limit the ability to model the earthquake.

The earthquake rupture is modeled with dislocations embedded in an elastic half-space. This is equivalent to making a rectangular cut within an elastic body, displacing the faces of the cut a prescribed amount, and gluing them

<sup>1</sup>U.S. Geological Survey, Menlo Park, California 94025

back together. The surface of the elastic body will be deformed, and this deformation is matched to the observed data. Dislocation models are non-unique: Here they are kept as simple as possible, limited by the constraints imposed by the mainshock fault plane solution. Because the leveling route is oriented across the geologic structure and passes near the mainshock epicenter, the pattern of surface deformation allows the fault-plane to be distinguished with fair confidence from the auxiliary plane. Subject to a poorly constrained fault length along strike, the seismic moment ( $M_0$ ) can be estimated for comparison with the moment measured from seismic waves;  $M_0$  is proportional to the slip times the fault area. The fault slip and the depths to the top and base of the fault are important to distinguish faulting from the regime above the fault where folding predominated during the earthquake.

## DATA

The 2 May 1983 Coalinga earthquake struck within a leveling network established to study compaction of unconsolidated deposits in response to ground-water withdrawal [Bull, 1975]. The 50 km-long network of leveling routes (Figure 1) was surveyed in 1960, 1966, 1969, and 1972 by the National Geodetic Survey (NGS) for the U.S. Geological Survey (USGS). The NGS releveled the net during 8-24 June 1983 at the request of the USGS. The network is ideally located to study earthquake elevation changes, but suffers from bench mark subsidence caused by ground-water withdrawal in Pleasant Valley and the San Joaquin Valley, and by oil withdrawal beneath Anticline Ridge (Figure 1). Subsidence is evident on the 1966-72 profile of elevation change before the earthquake occurred (Figure 2a).

## Leveling Errors

Sources of measurement uncertainty in leveling are dominated by slope-dependent systematic errors. These include improper calibration of the graduated leveling rods and atmospheric refraction of the line of sight between the rods and the level, a horizontal telescope. Typical errors in the length of leveling rods used during the period 1953-1979 are less than 25 ppm at the 95% level of confidence [Strange, 1980; Stein, 1981]. Because the maximum elevation difference along the leveling route is 200 m (see Figure 2d), rod errors of 5 mm are possible. Elevation changes shown in Figure 2 have been corrected for refraction error using the method of Holdahl [1981]. Most of the refraction error that accumulated along a 50 km-long test route in southern California was removed by this method, using similar procedures and under climatic conditions similar to those that prevail in Coalinga [Holdahl, 1982; unpub. data]. Residual refraction error should be less than 5 mm, assuming a 100% error in estimating the mean temperature gradient along the line of sight and a 50% error in estimating the mean distance between the level and rods for the 1972 survey. Random errors grow with the square root of the distance leveled. Because all of the leveling reported here was performed to first-order double-run standards [Federal Geodetic Control Committee, 1980], the random error should accumulate to less than 10 mm over the 35-km distance between the southwest and northeast ends of the route. Leveling errors from all sources thus sum to less than 20 mm, equal to the size of the bench mark symbols in Figure 2.



## EARTHQUAKE ELEVATION CHANGES

The 1966-72 subsidence rate is employed to remove artificial subsidence that took place after 1972, modified by the record of surficial compaction and fluid extraction during 1972-83. Bench marks in consolidated Cretaceous rocks (F1046-J944, Figure 1; BM's 1-6, Figure 2a) are assumed to have been stable during the preseismic 1966-72 period. These bench marks are also farthest from the sites of known artificial subsidence. During the 1972-83 earthquake period, this assumption is no longer tenable; no bench mark is more than 20 km from the mainshock epicenter. Therefore the position of the zero-elevation-change datum in Figures 2b and 2c (the thin horizontal line) is arbitrary.

## San Joaquin Valley Subsidence

Subsidence caused by artesian-head decline along the western margin of the San Joaquin Valley reached a peak during the mid-1950's and largely abated after construction of the California Aqueduct replaced pumping from deep aquifers [Bull, 1975]. During the period 1970-80, the aqueduct delivered 93% of the water used for irrigation [Ireland et al., 1982]. Because of the reduced rate of head decline after 1970, the rate of subsidence during 1966-72 (Figure 2a) provides an upper bound on the rate for the ensuing decade.

Poland et al. [1975] and Bull [1975] report on deep-well compaction recorders that measure the vertical strain or shortening caused by compaction of surface deposits and the heavily pumped aquifers. Compaction well 33A1, 13 m deep, is located at the northeast end of the main leveling route (marked by an X in Figure 1a). From March 1966, a year after its installation, through January 1980, the end of the published record, the well recorded 275 mm of compaction [Ireland et al., 1982]. The California Department of Water Resources leveled the route from BM Y998 USGS, adjacent to the recorder well, to BM E929 atop Anticline Ridge in February 1982 (the BM's are shown as circles in Figure 1a; BM's 27-37 in Figure 2a). Subsidence of BM Y998 USGS from March 1966 to February 1982 was 300 mm. Therefore the compaction recorder measured at least 90% of the total subsidence. The rate of compaction during the period 1972-1980 is 30% of the 1966-72 rate, suggesting that the subsidence rate also decreased by about 30%. Compaction well 23P2, 670 m deep, operated through 1974 (X at end of east spur marked by triangles in Figure 1a). During 1966-72 the well recorded 100% of the subsidence at nearby BM 888. During the succeeding two years the rate of compaction was 40% of the rate during 1966-72. Under the assumption that the aquifer continued to recharge after 1974, the projected 1972-83 subsidence rate would be about 30% of the 1966-72 rate.

The compaction history of wells with recorders therefore suggests that the elevation of bench marks surveyed during 1972 should be corrected for subsidence at a rate equal to 30% of the 1966-72 rate. Bench marks in Holocene alluvium (east of the subsidence boundary in Figure 1b) have been corrected for subsidence in Figure 2c. Probable error in the correction should be less than 50% of the estimated 1972-83 subsidence rate, or 45 mm at the end of the north spur where the 1972-83 subsidence rate is estimated to be 8 mm/yr (squares in Figure 1; BM E927), 55 mm at the end of the east spur where the rate is 10 mm/yr (triangles; BM H927), and only a few mm at the end of the main route where the 1982-83 rate of subsidence is 6 mm/yr (circles in Figure 1; BM Q1195).

### Pleasant Valley Subsidence

The rate of subsidence in Pleasant Valley during 1960-72 was about one third of the rate in the San Joaquin Valley [Propokovitch and Magleby, 1968], but subsidence in Pleasant Valley after 1972 is more uncertain because no wells record compaction there, and because no releveling was conducted there during 1972-82. Aqueduct deliveries to the Coalinga township during 1972-82 amounted to 30% of the total water consumption, whereas the aqueduct supplied only 2% of the water during 1970-71 [unpub. Bureau of Reclamation Water Delivery Records for 1983]. Estimated ground-water pumpage (for Township/Range 20S/15E) decreased by 40% from 1966-71 to 1975-77 [Mitten, 1972, 1976, 1980]. No pumping records are available for the years 1972-74 and 1978-83, but continued water-table decline increased the cost of pumping for irrigation; this probably reduced pumpage after 1977. Here it is assumed that the subsidence rate during the period 1972-83 was about 50% of the rate during 1966-72. The maximum 1972-83 subsidence rate in the Valley, at BM's 12 and 17 in Figure 2b, becomes 9 mm/yr - roughly equivalent to the rate in the San Joaquin Valley - with an uncertainty of perhaps 4 mm/yr, or 45 mm.

### Anticline Ridge Subsidence

The net liquid production rate beneath Anticline Ridge has remained unchanged since 1966, at 34 million bbl/yr [5.4 million m<sup>3</sup>/yr; Conservation Committee of California Oil Producers, 1967-1982]. This value includes the combined pumping of oil and water, minus re-injected water and steam, in the Coalinga and East Extension fields that are traversed by the leveling route. The 1966-72 subsidence rate is therefore employed to correct the earthquake elevation changes of BM's W944 - U237 and J929 - Y156 in Figure 1a (BM's 22-26 and 46-49 in Figure 2a). North of the oil fields and south of the recent alluvium, BM's Y662 - X662 showed no subsidence during 1960-72 (Figure 1; BM's 37-42, Figure 2a); therefore no corrections were made to these BM's in Figure 2c.

To summarize, subsidence corrections are generally small in comparison to the total observed elevation changes during the earthquake period; corrections nowhere exceed 110 mm. The largest corrections are made to the main leveling route in Pleasant Valley, and to the north and east spurs in the San Joaquin Valley. The portion of the main route in the San Joaquin Valley was leveled only 1.5 yrs before the earthquake, and therefore sustained little artificial subsidence.

### DISLOCATION MODELS

The earthquake elevation changes are modeled by dislocations in an elastic half-space using expressions of Mansinha and Smylie [1971] and with Poisson's ratio, the ratio of contraction of a body in one direction to the amount it is stretched in the perpendicular direction, set to 1/4. The half-space is a body with infinite depth and with a flat upper surface approximating the ground. A fault is modeled by a rectangular plane with uniform slip on its surface. Faults in the earth are not rectangular, not planar, and can not maintain uniform slip on their surfaces without producing infinite stress changes at their perimeters. However, these simplifications do not modify the vertical deformation at the ground surface enough to warrant the use of other more plausible geometries.

Testing of candidate fault models was simplified by adherence to the fault-plane solution of Eaton [1983] from first motion of P-wave polarities at 39 stations less than 100 km from the epicenter. The model fault strike was therefore fixed to be N53°W. A N37°E+20° axis of maximum compression suggests reverse dip slip. This means that up to a 20° right-lateral or left-lateral slip component is permissible. With one exception, model faults were constrained to pass within 1.5 km of the mainshock hypocenter, which is located at 36°13.99' N. lat., 120°17.59' W. long., at a depth of 10.5 km. The nodal plane dips 67°NE, and the other dips approximately 23°SW. Model faults are shown with aftershocks  $M_L \geq 3$  within the first four days of the May earthquake [Reasenberget al., 1983]. In the absence of primary ground-surface rupture [Clark et al, 1983; Hart and McJunkin, this volume], both planes were tested.

### Northeast-Dipping Reverse Fault

The general characteristics of the earthquake deformation limit the choices for the fault location and geometry. For a reverse-fault plane, the peak ground uplift occurs above the upper edge or top of the fault, and the elevation change is zero where the fault plane would intersect the ground if extended to the surface (See Figure 3a). For a fixed dip and depth to the center of the fault, the product of the slip times the fault width (the down-slip fault dimension) is shared by all acceptable models. The fault length is poorly gauged by the data, since the leveling is not extensive along strike and the aftershocks are distributed over a very large area. A fault length of 14-16 km appears consistent with the decay of elevation change at the northern and eastern ends of the leveling network (squares and triangles in Figure 1a). Thus for all successful models with pure reverse slip,  $M_0 = 6.0-6.5 \times 10^{25}$  dyne-cm ( $6.0-6.5 \times 10^{18}$  Nm), where  $M_0 = G \cdot U \cdot A$ ,  $G$  is the shear modulus, here assumed to be about  $3 \times 10^{11}$  dyne/cm<sup>2</sup> ( $3 \times 10^{10}$  N/m<sup>2</sup>),  $U$  is the slip, and  $A$  is the fault area.

For a 67°NE dip, the vertical depth to the top of the fault (the depth of burial of the fault's upper edge) is equal to about two thirds the width of the peak-to-trough elevation change. The uncertainty in the depth of burial stems from inconsistent elevation changes and uncertain artificial subsidence of BM's near Coalinga, 10 km southwest of the epicenter. To simplify the presentation of the three models shown in Figure 3a, the fit to the eastern part (triangles) is not shown. The surface projection of the fault models represented by a dotted line and by a dashed line in Figure 3a is shown in Figure 1b. The geodetic data can permit up to 20° of right-lateral or left-lateral slip on the steeply dipping reverse fault with a slight increase in  $M_0$  (Figure 3b). A left-lateral component of slip is more easily fit to the leveling data; right-lateral slip cannot be imposed unless the southeastern edge of the fault lies within a few kilometers of the mainshock epicenter.

### Southwest-Dipping Thrust Fault

The peak uplift along the leveling route occurs near the mainshock epicenter. Because the uplift must locate above the top of the fault, the upper edge of a gently dipping model fault must pass through the mainshock hypocenter. Thus the upper edge of the fault must lie at a depth of about 10 km (the dot-dash line in Figure 3c). The deeply buried fault requires more slip



to uplift the ground surface the same amount as faults at shallower depths; thus for a fault length of 14 km,  $M_0 = 9 \times 10^{25}$  dyne-cm. A mainshock at the upper edge of a fault also implies seismic rupture in the down-dip direction. The fit to the observed elevation changes is poor.

A good fit to the observations using a southwest-dipping thrust plane can be accomplished with more complex models. A thrust fault situated 6 km above Eaton's [1983] hypocentral depth with fault slip increasing down-dip provides an excellent fit to the leveling data (dotted line in figure 3c). However, the mainshock would not locate on the fault plane unless its epicenter were relocated 6.5 km to the southwest and its depth were reduced from 10.5 km to 7.5 km. In order to satisfy the condition that the model fault should pass through the mainshock, a curved fault surface or one in which the fault dip increases above the hypocenter becomes necessary (Figure 3d). The steeply dipping segment with 1 m of aseismic reverse slip brings the predicted elevation change at the northeast end of the leveling route into better agreement with the data. Some misfit remains in the region from the epicenter extending for 10 km to the southwest. The surface projection of this fault model is shown by a solid line in Figure 1b. The parameters of all the fault models shown in Figure 3 are presented in Table 1.

Table 1: Fault Models

Strike/Dip	Slip Direction <sup>1</sup>	Vertical Depth To:		Fault Width km	Moment <sup>2</sup> $M_0 \times 10^{25}$ dyne-cm	Model Fit	Fig. 3 Symbol
		Slip m	Top of Fault km				
N53°W67°NE	reverse	1.3	3.0	13.2	11.0	6.5	good a - - -
N53°W67°NE	reverse	1.8	4.0	11.2	8.0	6.0	good a ———
N53°W67°NE	reverse	2.3	5.0	10.5	6.0	6.0	good a ·····
N53°W67°NE	reverse w/ 20°rt-lat.	2.2	4.5	11.0	7.0	6.5	good b ·····
N53°W67°NE	reverse w/ 15°lft-lat.	1.8	4.0	11.5	8.0	7.0	good b ———
N53°W23°SW	thrust	2.5	10.5	13.2	10.0	9.0	poor c —·—
N53°W23°SW	thrust	1.4, top 2.0, base	4.5	7.2	9.0	5.0	good <sup>3</sup> c ·····
N53°W60°SW	reverse	1.0, top	5.0	12.0	11.0	7.5	fair d ———
N53°W23°SW	thrust	2.0, base					

Notes: <sup>1</sup>/Strike, Dip, and Slip Direction are constrained by Eaton's [1983] fault plane solution for the 2 May 1983 Mainshock. <sup>2</sup>/Fault length along strike is not well constrained; 14-16 km is used. <sup>3</sup>/Fault lies 6 km above the mainshock hypocenter.

## INTERPRETATION

## Steeply Dipping Reverse Fault or Gently Dipping Thrust?

The earthquake elevation changes are well fit by a northeast-dipping thrust fault extending from a depth of 3-5 km to 10-13 km, with 1.3-2.3 m of reverse dip slip. A southwest-dipping thrust plane can fit the data equally well if it is sufficiently shallow, and if the fault slip increases down-dip. However, the depth of seismicity argues against the likelihood that such a shallow thrust fault produced the elevation changes. Both the mainshock and the larger immediate aftershocks in the epicentral area lie beneath the 4-7 km depth of the candidate thrust fault (Figure 3c). While these hypocenters are preliminary, the presence of a seismic station 5 km northwest of the mainshock renders location and depth changes of 5 km unlikely [Reasenberget al., 1983]. The earthquake could have ruptured the curved or two-plane thrust fault shown in Figure 3d, but the fit to the leveling data is inferior to the reverse-fault models. The uncertainty of bench mark subsidence in Pleasant Valley does not permit rejection of the two-plane model. The apparent absence of seismic radiation from the steeply dipping upper portion of such a fault could be explained by seismic rupture from 10-14 km in the down-dip direction, preceded or followed by aseismic slip from a depth of 5-10 km. Barring significant relocation of the mainshock and after shocks, though, the steeply dipping reverse plane provides the most straightforward fit to the geodetic and seismic evidence. Wentworth et al. [this volume] find evidence from seismic refraction and reflection data for both a steeply dipping reverse fault and a gently dipping thrust fault beneath the southern end of the Kettleman Hills anticline, a similar structure 65 km south of Coalinga.

The seismic moment for the successful fault models was found to be in the range  $6-7 \times 10^{25}$  dyne-cm ( $6-7 \times 10^{18}$  Nm). The moment could be larger if the fault plane extended farther to the northwest or southeast along strike, but it is unlikely to be much smaller. Heaton and Hartzell [this volume] calculate  $M_0 = 3.8 \times 10^{25}$  dyne-cm from teleseismic long-period (5 s) compressional waves; Kanamori [this volume] determines  $M_0 = 5.4 \times 10^{25}$  dyne-cm from very long period (250 s) surface waves. Unless the fault length proves to be much longer than 15 km, the fair agreement between geodetic and seismic estimates of  $M_0$  implies that most slip was released seismically during the mainshock.

## Folding of Anticline Ridge

The modeling demonstrates that most of the earthquake fault slip was confined to depths greater than 3-5 km. If fault slip tapered from a depth of 5 to 3 km, the vertical deformation would look similar to that if rupture terminated at 4 km. Similarly, if slip was distributed over a fault thickness of 1 km rather than confined to a plane, the dislocation models would overestimate the upper fault depth. Thus the depth-of-burial values should be considered maximum estimates. Particularly at the ends of the fault where no deformation data exists, some slip could penetrate closer to the ground surface. It is thus striking that a number of the deepest wells in the oil fields [California Division of Oil and Gas, 1973] above the probable fault appear properly located to have sustained some primary fault rupture (Figure 1b).

Whereas elastic strains are relieved in rocks near the seismic fault at depth, the earthquake increased strains in the rocks that lie between the top of the fault and the ground surface. If earthquakes do not periodically rupture through to the surface, then the strains must be relaxed by creep. The near absence of aftershocks at depths above 4-5 km in the epicentral region, where a great thickness of unconsolidated Pleistocene sediments have folded into an anticline, suggests that these rocks are too weak to accumulate and maintain high stresses: They do not fail seismically but fold instead. This speculation finds support in the absence of a fault scarp at the base of Anticline Ridge in the Tertiary and younger rocks (Figure 1a). If numerous earthquakes with magnitudes similar to the 1983 shock occurred during the Pleistocene, such a scarp would have been produced. In contrast to the seismic behavior of the Tertiary section, very shallow aftershocks occurred in the Cretaceous section northwest of Pleasant Valley [Figure 1a; also see Reasenberget al, 1983]. On 9 May 1983, a  $M_L=5.2$  aftershock at a depth of 3.4 km produced a 4 km-long surface rupture with 0.6 m of reverse dip slip [Hart and McJunkin, this volume]. The  $M_L=7.2$  1952 Kern County earthquake - also a steeply dipping reverse fault - exhibited similar behavior. The fault ruptured the surface in Cretaceous granite, but failed to penetrate the upper 5 km of the Pliocene and Pleistocene sedimentary section of Wheeler Ridge anticline at the earthquake epicenter [Stein and Thatcher, 1981]. King and Brewer [1981] found that near-surface folding also accompanied reverse fault slip during the  $M_s=7.3$  1980 El Assam earthquake.

#### Cumulative Reverse Fault Slip During the Pleistocene

The striking similarity between the form of the earthquake deformation and the topographic profile can be seen by inspection of Figures 2c and 2d. The topographic form of the ridge also conforms to the subsurface structure (Figure 1a). Although folding of the anticline commenced in the late Eocene (40 million years ago), the rate of deformation increased during middle Pleistocene time (less than one million yrs ago): Exposed Pleistocene beds dip 20-40° on the limbs of the anticline [Harding, 1976] where the topographic slope is about 5°. The amplitude of the fold may thus be as much as four times greater than the amplitude of the topography, because erosion from highs and deposition into lows diminish the topographic gradient. In fact the topography could be created by repeated earthquakes if the fault did not often rupture to the surface. Geodetic tilt in Figure 2c is correlated with the topographic slope in Figure 2d at the 99% level of confidence; the mean slope is equal to  $800 \pm 150$  times the tilt [for the details of the correlation method, see Stein, 1981]. Because slope-dependent leveling errors cannot attain this magnitude, the correlation must reflect the growth of the fold. Since slip during the 1983 Coalinga earthquake was found to be  $1.8 \pm 0.5$  m, a cumulative displacement of 2-5 km on the fault at depths below 4 km would build the present-day topography. King and Stein [this volume] suggest an approximate repeat time for earthquakes at Coalinga of 350 yr, on the basis of uplifted and distorted river terraces formed where creeks draining the eastern Coast Ranges cut through the anticlinal axes into the San Joaquin Valley (see Figure 1a). If the fault slipped mostly during earthquakes similar in size to the 1983 event, then 2-5 km of reverse slip may have accumulated at depth during the past 350,000 - 1 million yr.



## CONCLUSION

The 2 May 1983 Coalinga earthquake most probably ruptured a fault that dips steeply to the northeast beneath Anticline Ridge. Reverse dip slip of  $1.8 \pm 0.5$  m from a depth of  $4 \pm 1$  km to the hypocenter at  $10.5 \pm 1.5$  km provides the fit most compatible with the geodetic and seismic data. A thrust fault dipping gently to the southwest is not precluded by the geodetic data, but the fit to both leveling and seismic data is less satisfactory than for the reverse fault. Folding of Anticline Ridge appears to accompany buried reverse faulting, most likely because the poorly lithified sediments are too weak to store significant elastic strain, and creep instead. This hypothesis would explain both the absence of 1983 surface breakage at the base of Anticline Ridge, and the lack of shallow aftershocks in the epicentral region. In contrast to this, both ground rupture and large shallow aftershocks are evident during the 1983 Coalinga sequence in the Cretaceous rocks northeast of Anticline Ridge. The similarity between the topographic form of Anticline Ridge and the earthquake elevation changes is compelling enough to extrapolate 2-5 km of cumulative buried fault slip during the past million years.

## ACKNOWLEDGEMENTS

The author is indebted to E. Balazs and B. Martine of the National Geodetic Survey for rapidly surveying the leveling network. Exciting discussions with A. Lindh, G. King, and C. Wentworth contributed to this effort. W. Thatcher, D. Oppenheimer, and D. Eberhart-Phillips reviewed the manuscript.

## REFERENCES

- Bull, W. B., 1975, Land subsidence due to ground-water withdrawal in the Los Banos-Kettleman City area, California. Part 2, Subsidence and compaction of deposits: U.S. Geol. Survey Prof. Paper 437-F, 90 p.
- California Division of Oil and Gas, 1973, North and east central California, Data sheets and Index maps: California Division of Oil and Gas, V.1, 22 p.
- Clark, M., Harms, K., Lienkaemper, J., Perkins, J., Rymer, M., and Sharp, R., 1983, The search for surface faulting, in Borchardt, R. D., ed., The Coalinga earthquake sequence commencing May 2, 1983: U.S. Geol. Survey open-file report 83-511, 79 p.
- Conservation Committee of California Oil Producers, 1982 and earlier, Annual review of California oil and gas production: Conservation Committee of California Oil producers, annual production statistics.
- Eaton, J., 1983, Seismic setting, location, and focal mechanism, in Borchardt, R. D., ed., The Coalinga earthquake sequence commencing May 2, 1983: U.S. Geol. Survey open-file report 83-511, 79 p.
- Federal Geodetic Control Committee, 1980, Specifications to support classification, standards of accuracy, and general specifications of geodetic control surveys: Nat. Oceanic and Atmospheric Admin., Rockville, Md, 46 p.
- Fowkes, E. J., 1982, An educational guidebook to the geologic resources of the Coalinga district, California: Shannon Publications, Coalinga, 260 p.
- Hart, E. W., and McJunkin, R. D., 1983, Surface faulting northwest of Coalinga, California, June and July 1983: This volume.

- Harding, T. P., 1976, Tectonic significance and hydrocarbon trapping consequences of sequential folding synchronous with San Andreas faulting, San Joaquin Valley, California: *American Assoc. Petrol. Geol. Bull.*, v. 60, p. 356-378.
- Hartzell, S. H., and Heaton, T. H., 1983, Teleseismic mechanism of the May 2, 1983, Coalinga, California, earthquake from long period P-waves: This vol.
- Holdahl, S. R., 1981, A model of temperature stratification for correction of leveling refraction: *Bull. Geodesique*, v. 55, p. 231-249.
- \_\_\_\_\_, 1982, Recomputation of vertical crustal motions near Palmdale, California, 1959-1975: *Jour. Geophys. Research*, v. 87, p. 9374-9388.
- Ireland, R. L., Poland, J. F., and Riley, F. S., 1982, Land subsidence in the San Joaquin Valley, California, as of 1980: U.S. Geol. Survey open-file report 82-370, 129 p.
- Kanamori, H., 1983, Mechanism of the 1983 Coalinga earthquake determined from long period surface waves: This volume.
- King, G. C. P., and Vita-Finzi, 1981, Active folding in the Algerian earthquake of 10 October 1980: *Nature*, v. 292, p. 22-26.
- King, G., and Stein, R., 1983, Surface folding, river terrace deformation rate, and earthquake repeat time in a reverse faulting environment: The Coalinga, California, earthquake of May 1983: This volume.
- Mansinha, L., and Smylie, D. E., 1971, The displacement fields on inclined faults: *Seismol. Soc. America Bull.*, v. 61, p. 1433-1440.
- Mitten, H. T., 1972, Ground-water pumpage, San Joaquin Valley, California, 1967-68: U.S. Geol. Survey open-file report [not numbered], 6 p.
- \_\_\_\_\_, 1976, Estimated ground-water pumpage in parts of the San Joaquin Valley, California, 1969-71: U.S. Geol. Survey open-file report, 7 p.
- \_\_\_\_\_, 1980, Estimated agricultural ground-water pumpage in parts of the San Joaquin Valley, California, 1975-77: U.S. Geol. Survey open-file report 80-1281, 11p.
- Poland, J. F., Lofgren, B. E., and Ireland, R. L., 1975, Land subsidence in the San Joaquin Valley, California, as of 1972: U.S. Geol. Survey Prof. Paper 437-H, 78 p.
- Prokopovitch, N. P., and Magelby, D. C., 1968, Land subsidence in Pleasant Valley: *American Water Works Assoc. Jour.*, v. 60, p. 413-424.
- Reasenbergs, P., Eberhart-Phillips, D., and Segall, P., 1983, Preliminary views of the aftershock distribution, in Borchardt, R. D., ed., The Coalinga earthquake sequence commencing May 2, 1983: U.S. Geol. Survey open-file report 83-511, 79 p.
- Stein, R. S., 1981, Discrimination of tectonic displacement from slope-dependent errors in geodetic leveling from southern California 1953-1979, in Simpson, D. W., and Richards, P. G., eds., *Earthquake Prediction, An International Review: Maurice Ewing Ser.*, v. 4, AGU, Wash., D.C., 680 p.
- Stein, R. S., and Thatcher, W., 1981, Seismic and aseismic deformation associated with the 1952 Kern County, California, earthquake and relationship to the Quaternary history of the White Wolf fault: *Jour. Geophys. Research*, v. 86, p. 4913-4928.
- Strange, W. E., 1980, The effect of systematic errors in geodynamic analysis, in Lachapelle, G., ed., 2nd Internat. Symp. on problems related to the redefinition of North American vertical geodetic network: *Canadian Inst. Surveying*, Ottawa, 978 p.
- Wentworth, C. M., Walter, A. W., Bartow, J. A., and Zoback, M. D., 1983, The tectonic setting of the 1983 Coalinga earthquakes: Evidence from deep reflection and refraction profiles across the southeastern end of the Kettleman Hills: This volume.

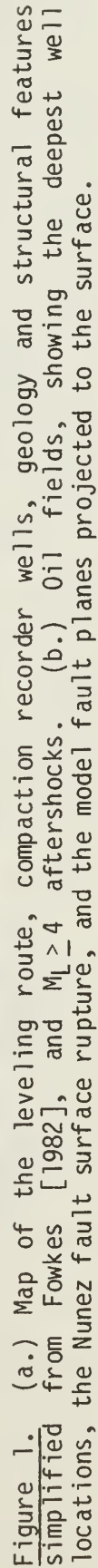


Figure 1. (a.) Map of the leveling route, compaction recorder wells, geology and structural features simplified from Fowkes [1982], and  $M_L \geq 4$  aftershocks. (b.) Oil fields, showing the deepest well locations, the Nunez fault surface rupture, and the model fault planes projected to the surface.





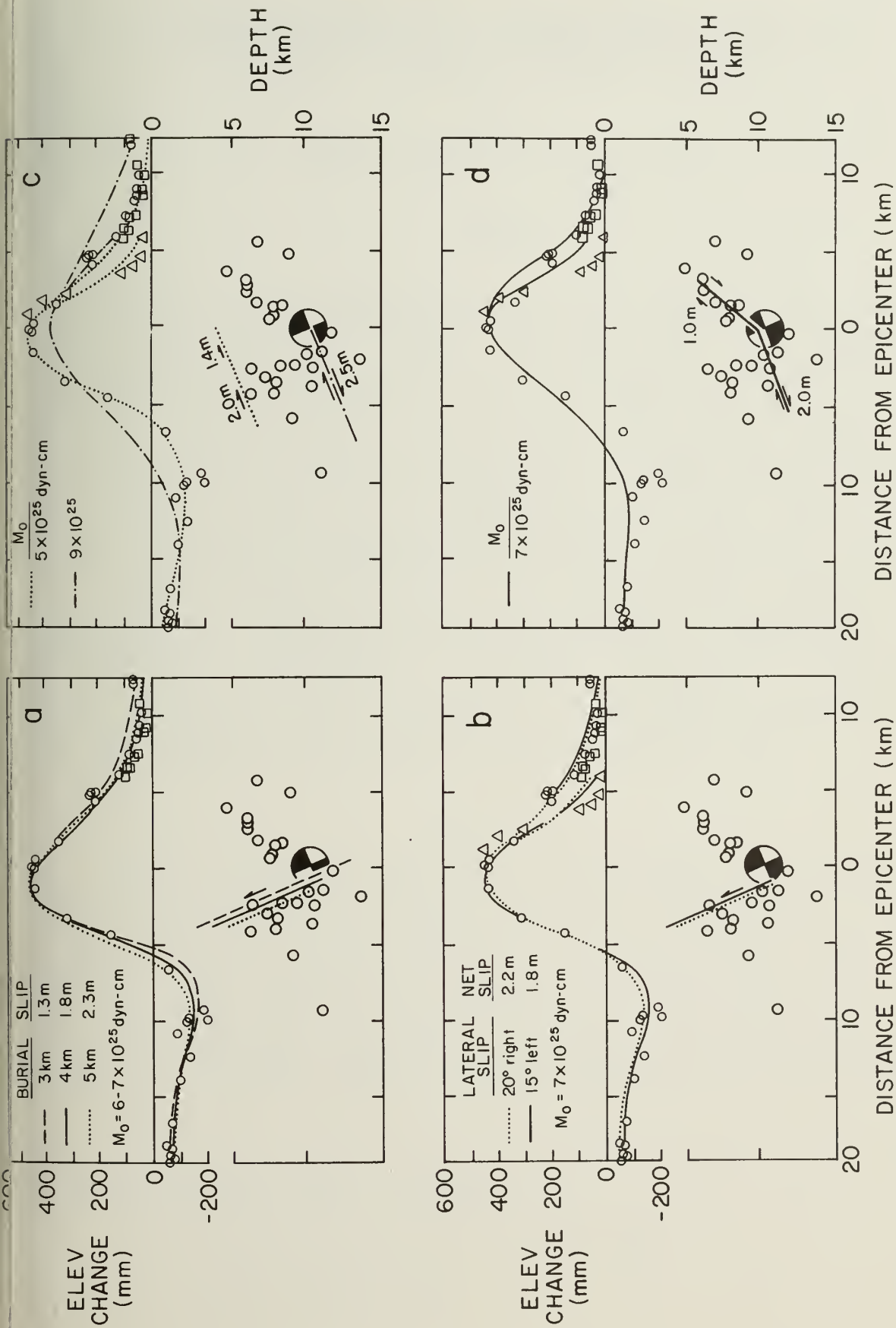


Figure 3. Earthquake elevation changes from Figure 2c compared with predicted deformation, together with a cross-section showing the model faults and the first four days of  $M_L > 3$  aftershocks, and the mainshock. (a.-b.) Reverse faults with 67°NE dips. (c.-d.) Thrust faults dipping 23°SW.





SURFACE FOLDING, RIVER TERRACE DEFORMATION RATE  
AND EARTHQUAKE REPEAT TIME IN A REVERSE FAULTING ENVIRONMENT:  
THE COALINGA, CALIFORNIA, EARTHQUAKE OF MAY 1983

by

Geoffrey King<sup>1</sup> and Ross Stein<sup>2</sup>

ABSTRACT

The May 1983 Coalinga earthquake occurred on a reverse fault at the core of an anticline (Anticline Ridge). No surface breaks were observed but leveling lines indicate a coseismic uplift of 0.5 m. This suggests that fault motion at depth is expressed as folding near the surface. The beds and terraces of two antecedent streams are uplifted where they cross the anticline. In one place a <sup>14</sup>C date indicates that an uplift of about 10 m has occurred within a period of 2,500 years. A repeat time of about 350 years for the Coalinga event can be determined from the uplifted terrace and the <sup>14</sup>C data. Much of the topography of Anticline Ridge is post-Pleistocene and this provides a second method of estimating recurrence periods. The form of the observed uplift differs in some respects from that to be expected from many repetitions of the Coalinga event suggesting that other deformation processes occur; a shallow angle, southwest dipping fault is hypothesized. The presence of such a structure is supported by the reflection data in the Kettleman Hills to the south of the epicentral area. On this basis a longer period of 1,000 years is estimated. Although the observations in this paper are restricted to the epicentral region of the Coalinga earthquake, it is apparent that the structures of the northwestern Diablo Range front have developed by earthquake-related folding.

INTRODUCTION

An intimate relationship between faults and folds has been recognized for a long time by geologists. The mechanical relation between the two, however, has been studied using either analogue materials or computer models, and it has been assumed that ductile behavior is the primary process and brittle behavior is secondary. Some recent studies (King and Vita Finzi, 1981; King and Brewer, 1983; Cisternas et al., 1982), however, have shown that, in at least some cases, the finite strains observed as folds are produced by the sum of a series of sudden elastic strain increments each of which is associated with an earthquake. Between earthquakes stress in the folds is relaxed gradually by creep. An appreciation of this connection between earthquakes

<sup>1</sup>Bullard Laboratories, Dept. of Earth Science, Univ. of Cambridge Madingley Rise, Madingley Road, Cambridge CB3 0EZ.

<sup>2</sup>U.S. Geological Survey, Menlo Park, California 94025.

[Order of authorship chosen by lot]

and fold formation provides a powerful tool for understanding both. In this paper we examine deformation in the region of the Coalinga earthquake and show that the seismic fault and recent geological structures can be related.

The Coalinga event occurred on a fault beneath an anticline structure (Anticline Ridge and Guajarral Hills). Similar structures occur along the length of the eastern edge of the Diablo Range and are known from observations of morphology and river drainage to have uplift rates of about 0.5 mm/year during the last million years (Lettis, 1983). In this paper we concentrate on the morphology of the epicentral region of the Coalinga earthquake and on the stream profiles of the Los Gatos and Zapato Chino Creeks in the same region. Although we do not extend our detailed discussion in this paper much beyond the epicentral region of the Coalinga earthquake, most of the eastern boundary of the Diablo Range can be studied in the way we describe here.

The main Coalinga event, of magnitude 6.5–6.7 Ms, apparently occurred on a plane dipping at  $67^{\circ}\text{NE}$  and striking  $\text{N}53^{\circ}\text{W}$ . This orientation is well constrained by the records from the dense array of stations to the west of Coalinga near the San Andreas fault. The plane is identified as the fault plane by the leveling data and the hypocenter of the main shock (Stein, this volume). The auxiliary plane is less well determined, particularly in strike. Consequently, the horizontal component of the slip vector can vary within  $\pm 15^{\circ}$  of  $\text{N}50^{\circ}\text{E}$ .

The seismic moment of the event is greater than  $2 \times 10^{25}$  dyne-cm and less than  $6 \times 10^{25}$  dyne-cm (Uhrhammer et al.; Kanamori, this volume). Bearing in mind that moment estimates are commonly low since they exclude later events within the main event coda and aftershocks, a nominal moment of  $6 \times 10^{25}$  dyne-cm is appropriate. This moment is provided if the fault extends from 4 km below the surface (there are no surface breaks) to 11 km (the approximate depth of the deepest aftershocks). Taking a displacement of  $1.8 \pm 0.5$  m which fits the observed uplift, the fault must be 15 km long, rather less than the length of the aftershock zone. The surface projection of a surface that fits the seismic and geodetic data is shown in Figure 1.

## OBSERVATIONS

### Morphology of the Epicentral Region and the River Systems

Some broad features of the river systems in the epicentral region can be seen in Figure 1. The Los Gatos Creek used to flow along a course nearer to Anticline Ridge but now follows a course on the west side of Pleasant Valley before it swings towards the Guajarral Hills. It becomes more sinuous and then straightens again to cross the anticline. This is consistent with a broad uplift extending into the valley. A similar broad uplift may be associated with the Kettleman Hills. The way in which the Zapato Chino Creek swings away from the northwest end of the Kettleman Range suggests broad uplift. Also, the lower Canoas Creek (lower right-hand corner of Figure 1) which apparently used to join the Zapato Chino Creek no longer does so because of uplift.

Other features are visible in the general map. Lake or marsh deposits (Levis silty clay of early Holocene age; Lettis, 1981) are shown to the south and southwest of the Guijaral Hills. The larger of these regions is associated with an abandoned river course northwest of the Guijaral Hills that appears to have drained the former lake. The similarity between these features and the temporary lake that formed as a result of anticline uplift in the El Asnam, Algeria earthquake in 1980 (King and Vita Finzi, 1981) is striking. This suggests that larger or more frequent earthquakes can temporarily dam creeks crossing the anticline.

#### River and Terrace Profiles of the Los Gatos and Zapato Chino Creeks and the Age of the Los Gatos Creek Terrace

Profiles of the elevation of the beds of the Los Gatos (a) and Zapato Chino (b) Creeks and their associated terraces or fan surfaces are shown in Figure 2. Riverbed heights, indicated by solid circles, are taken directly from the latest edition (1979) of the 7-1/2° topographic maps (surveyed 1955-56). For the Los Gatos Creek, the height of the terrace relative to the riverbed was measured in the field. The results of these measurements are shown by triangles. Measurements of terrace height were also taken from the topographic map and these are shown by open circles. The difference between the two methods of establishing terrace profile about  $\pm 0.5$  m. Consequently, the terrace level for the Zapato Chino Creek is taken from the topographic map alone.

Much of the San Joaquin Valley and Pleasant Valley have been subject to subsidence during the last 60 years as a result of the extraction of ground water by pumping (Bull, 1975). In Pleasant Valley the total movement is less than 0.5 m and may be ignored. The land downstream of our Los Gatos Creek profile (Figure 2a), however, has dropped by 6 m in this period and Munn et al. (1981) suggest that the form of the river and terrace profiles is due to this subsidence. To test their suggestion, we examined the 1937 edition of the 7-1/2° Guijaral Hills topographic map. The survey for this sheet was carried out in 1933 before appreciable subsidence had occurred, and we plotted part of the Los Gatos terrace and riverbed profile from that sheet. This covers the critical region from 10 to 20 km in Figure 2a. The results are indistinguishable from those we find using maps based on the 1955-56 survey or our 1983 measurements. We therefore conclude that the features we observe are tectonic in origin and are not the result of land subsidence due to pumping. Subsidence has not, as yet, modified the river profile.

On both profiles a solid line is drawn to indicate the form of an undisturbed river profile. It is apparent when this idealized profile is drawn that neither creek is in equilibrium. The Los Gatos Creek, however, is much closer to equilibrium than the Zapato Chino Creek. This may be explained by noting that the former has a catchment area of about five times the latter and has correspondingly greater erosional power.

To determine the amount that a terrace has been lifted, it is necessary to know its height relative to the riverbed when it was formed. Since the relevant height is determined by rare flood conditions, it is not directly observable. Bull (1964) discusses these questions for a region to the north



of our area. Here we assume that the terrace heights upstream (0-5 km) and downstream (15-20 km) of the uplifted section are representative of flood heights, and we join them with a smooth curve whose distance from the idealized riverbed varies in a monotonic fashion. This is an idealized flood terrace level and is shown by hatching to indicate that it is uncertain. It can be seen that much of the lifted terrace is well above any likely flood level (Figure 2). The lower parts may not be.

Atwater (in prep.) has determined ages for fan and terrace material at locations marked A and B (on Figures 1 and 2). Point B is in a region where the terrace or fan level is not clearly lifted above flood level and the  $^{14}\text{C}$  date of  $490 \pm 60$  years may represent a high level deposition event and not date uplift. The date of  $2,550 \pm 130$  years for detrital charcoal at Point A is more useful. The material was collected from a horizon within the terrace 4.5 m below the surface. The date indicates the time when the detrital material was deposited, and the surface of the terrace which overlies it must be younger. Hence the 2,550 years is a maximum time for the river to downcut in response to uplift.

## DISCUSSION

### Interpretation of the Form of the Terrace Profiles

The terraces are uplifted approximately along the axis of the anticline. Only the Los Gatos terrace passes near the fault that moved during the May 1983 earthquake, and the geodetic data available to compare with the terrace data is from a leveling traverse nearly 10 km to the northwest of the Los Gatos Creek. These geographical relations can be seen in Figure 1 and are indicated in sketched insets in Figure 3. The terrace profile produced by subtracting terrace height from the idealized flood level for the Los Gatos Creek (in Figure 2) is shown by a solid line (1) in Figure 3a. The vertical motion associated with the 1983 earthquake is presented in Figure 3b and the form of the topography along the same profile is shown in Figure 3c. The form of the topography and the seismic uplift are broadly similar. Despite the effects of erosion and deposition, this similarity is to be expected if Anticline Ridge has been created by many events similar to the recent earthquake.

Both the geodetic uplift (Figure 3b) and the topographic form of the anticline are broader than the zone of terrace uplift. However, in the region where the Los Gatos Creek crosses the anticline, the topographic ridge is narrower by a factor of two than it is along the geodetic profile. Although this is most clearly seen on the topographic maps, the general form can be seen in Figure 1 and the insets of Figure 3. A second dashed profile (2) is shown in Figure 3a. This is the true profile (1) stretched by a factor of two to represent the profile to be expected along section 2 (see inset Figure 3b). It may, therefore, be regarded as being created by normalizing the width of the terrace by the width of the ridge. In this way we can compare the earthquake uplift with the terrace uplift. The extrapolated terrace profile still exhibits differences in shape from the earthquake elevation changes. In particular there is terrace uplift in the zone of earthquake subsidence. This is not attributable to errors in terrace height

determination or to our interpretation of the terrace formation process since the uplift is also evident in the river channel locations referred to earlier: The current Los Gatos channel lies on the southwest side of Pleasant Valley rather than heading northwest into the region of repeated earthquake subsidence.

### Multiple Faults at Depth

The repetition of the May 1983 event may not alone be sufficient to explain the morphology in the epicentral region. The simplest alternative hypothesis is that the overall deformation results from motion on more than one fault. To find the nature of the other fault or faults we subtract the form of deformation that can be produced by repeated events of the type which occurred in May 1983 from the observed long-term deformation. The residual must result from other fault motion.

The process by which we separate the form of the terrace uplift into two contributions, one from the 1983 earthquake fault and the other from motion at depth is shown in Figure 4. Figure 4c shows the extrapolated terrace deformation from Figure 3a; Figure 4a shows the approximate form of the elevation changes caused by the earthquake from Figure 3b. The residual, a broad-domed uplift, is shown in Figure 4b. Such a deformation profile can be attributed to any shallow angle (or horizontal) slip surface at depth. We show only one of the possibilities, a shallow angle thrust fault dipping to the west.

### A Repeat Time for the Coalinga Earthquake

The existence of a relation between the uplifted terraces and repeated earthquakes is compelling and offers a method of estimating earthquake repeat time. The introduction of two faults, however, complicates the procedure.

If we ignore the broad uplift and our interpretations of multiple faults and attribute the dated part of the terrace uplift to motion on the Coalinga earthquake fault alone (i.e., 10 m in 2,500 years, an uplift rate of 4 mm/yr), then, with a surface uplift for each event of 0.5 m, we find an improbably short repeat time of about 125 years. If we conclude that the broad uplift is real and subtract it from the total uplift, then the part attributable to the 1983 earthquake fault is 3.5 m (1.4 mm/yr). This gives a longer repeat time of about 350 years and we suggest that this is more consistent with the geomorphic evidence. If the remaining uplift is attributable to a sub-horizontal fault, it is appropriate to consider whether this fault is seismically active. If it is, then in the long term, motion on the Coalinga fault will be associated with other earthquakes on the deeper fault. An examination of the geodetic data (Stein, this volume) indicates that the Coalinga earthquake fault extends to the base of the aftershock activity 10–13 km deep. A connecting low angle fault will thus most probably be beneath the seismogenic depth and therefore not be associated with earthquakes.

A much longer term estimate of the recurrence time for the Coalinga earthquake may be made from the geological information. The youngest deposits

whose distribution is not controlled by the existence of the anticline are of Eocene age (40 My). Hence some deformation may have occurred at any time since then. However, much of the deformation is considered to date from the mid-Pleistocene (Harding, 1976). This view is based on the observation that the 200 m of topographic expression conforms very closely to the shape of the subsurface structure and that Pleistocene beds with dips of 20-40° fringe the anticline. If each earthquake gives an uplift of slightly more than 0.5 m, similar to the recent event, then about 400 events have occurred since that time. The Pleistocene extends from 10,000 to 1.6 million years. Taking the mid-Pleistocene as 0.5 million years gives an earthquake repeat time of 1,250 years.

### CONCLUSIONS

Distorted river courses and profiles of uplifted river terraces indicate a history of activity on the same fault beneath Anticline Ridge that moved about 1.8 m to cause the May 1983 Coalinga earthquake. Carbon dating indicates an age of 2,500 years or less for an uplifted terrace on the Los Gatos Creek indicating a repeat time for such earthquakes of about 350 years.

A substantial proportion of Anticline Ridge has apparently formed during the last 500,000 years, and this suggests a longer repeat time of 1,250 years. Because of inaccuracies in the data available to determine these repeat times and because earthquakes do not necessarily repeat regularly but may occur in bursts followed by periods of quiescence, these repeat times must be regarded as having large uncertainties. The fact that the long-term and short-term repeat times are quite similar suggests a relatively regular temporal behavior, but the existence of the lake deposits indicates the possibility of periods of greater activity. It seems reasonable, however, that earthquakes are not less frequent than one every 2,000 years or more frequent than one every 200 years.

Anticline Ridge and the Gujarral Hills lie in a region of en echelon offset in the linear anticline structures of the Diablo Range front. The Big Blue Hills form an elongate feature to the northwest, and the Kettleman Hills form a similar feature to the southeast. Both apparently have similar uplift rates to Anticline Ridge and are presumably cored by active faults. These faults must be regarded as a seismic hazard. Because of the linearity of the fold features, their associated faults are presumably long and linear. They may, therefore, move in less frequent but larger earthquakes than the Anticline Ridge fault.

The deformation of the river terraces in the Coalinga region probably cannot be explained by repeated motion on the steeply dipping fault alone. Therefore, a shallow angle fault at a depth of 10 km or more is suggested. This fault is beneath the seismogenic zone and, therefore, moves by creep. At this depth the fault should be considered to include zones of deformation such as the ductile shear zones observed in exhumed terrains (e.g., Sibson, 1982). The geodetic data does not determine whether this structure dips to the east or to the west. However, an interpretation of the reflection profile across the Kettleman Hills (Wentworth et al., this volume) looks similar to our Figure 4c and shows both the shallow southwest dipping plane



and the high angle northeast dipping plane. A projection of the shallow plane would reach the surface immediately to the east of the Kettleman Hills.

The part of the deformation associated with the earthquake fault is readily identifiable but the evidence for motion on the shallow angle aseismic structure is less clear. However, if the average slip rate on this feature is about 5 mm/yr, then horizontal strains of about  $10^{-8}$ /year should be easily detected geodetically over time periods of 25 years or more.

#### ACKNOWLEDGMENTS

We would like to thank Bob Nason for field assistance and discussions and for reviewing this paper. We also appreciate discussions with Bill Lettis, Brian Atwater, Al Lindh, Jennifer Harden and Carl Wentworth. Ed Helley and Bob Yerkes kindly reviewed this paper at very short notice. One of us, G.K., would like to thank the United States Geological Survey, the Royal Society of London and the National Environment Research Council for financial support while in California.

#### REFERENCES

- Atwater, B. F., Adam, D. P., Bradbury, J. P., Forester, R. M., Gobalet, K. W., Lettis, W. R., Mark, R. K., and Robinson, S. W., 1983, A proxy glacial history for the Sierra Nevada: Draft article.
- Bull, W. B., 1964, Geomorphology of segmented alluvial fans in western Fresno county, California: U.S. Geol. Survey Prof. Paper 352-E.
- , 1975, Land subsidence due to ground-water withdrawal in the Los Banos-Kettleman city area, California. Part 2, Subsidence and compaction of deposits: U.S. Geol. Survey Prof. Paper 437-F, 90 p.
- Cisternas, A., Dorel, J., and Gaulon, R., 1982, Models of the complex source of the El Asnam earthquake: Bull. Seism. Soc. Am., v. 72, p. 2245-2266.
- Eaton, J., 1983, Seismic setting, location and focal mechanism, in Borchardt, R. D., ed., The Coalinga earthquake sequence commencing May 2, 1983: U.S. Geol. Survey open-file report 83-511, 79 p.
- Fowkes, E. J., 1982, An educational guidebook to the geologic resources of the Coalinga district, California: Shannon Publications, West Hills, College, Coalinga.
- Harding, T. P., 1976, Tectonic significance and hydrocarbon trapping consequences of sequential folding synchronous with San Andreas faulting, San Joaquin Valley, California: American Assoc. Petrol. Geol. Bull, v. 60, p. 356-378.
- Kanamori, H., 1983, Mechanism of the 1983 Coalinga earthquake determined from long period surface waves: this volume.

- King, G. C. P., and Brewer, J., 1983, Fault related folding near the Wind River thrust: Nature [in press].
- King, G. C. P., and Vita-Finzi, C., 1981, Active folding in the Algerian earthquake of 10 October 1980: Nature, v. 292, p. 22-26.
- Lettis, W. R., 1983, Late Cenozoic stratigraphy and structure of the western margin of the central San Joaquin Valley, California: U.S. Geol. Survey open-file report 82-526.
- Munn, T. R., Busacca, A. T., and Trott, K. E., 1981, California aqueduct sedimentation study for the Arroyo Pasajero and tributary watersheds: Calif. Dept. of Conservation Special Report, 72 p.
- Reasenbergs, P., Eberhart-Phillips, D., and Segall, P., 1983, Preliminary views on the aftershock distribution, in Borchardt, R. D., ed., The Coalinga earthquake sequence commencing May 2, 1983: U.S. Geol. Survey open-file report 83-511, 79 p.
- Sibson, R. H., 1982, Fault zone models, heat flow, and the depth distribution of earthquakes in the continental crust of the United States: Bull. Seism. Soc. Am., v. 72, p. 151-163.
- Soil Survey of the Coalinga area, California, 1952, Soil survey staff: U.S. Dept. of Agriculture Series 1944, No. 1, December.
- Stein, R. S., 1983, Reverse slip on a buried fault during the 2 May 1983 Coalinga earthquake: Evidence from geodetic elevation changes: this volume.
- Uhrhammer, R. A., Darragh, R. B., and Bolt, B. A., 1983, The 1983 Coalinga earthquake sequence: this volume.
- Wentworth, C. M., Walter, A. W., Barton, J. A., and Zoback, M. D., 1983, The tectonic setting of the 1983 Coalinga earthquakes: evidence from deep reflection and refraction profiles across the southeastern end of the Kettleman Hills: this volume.

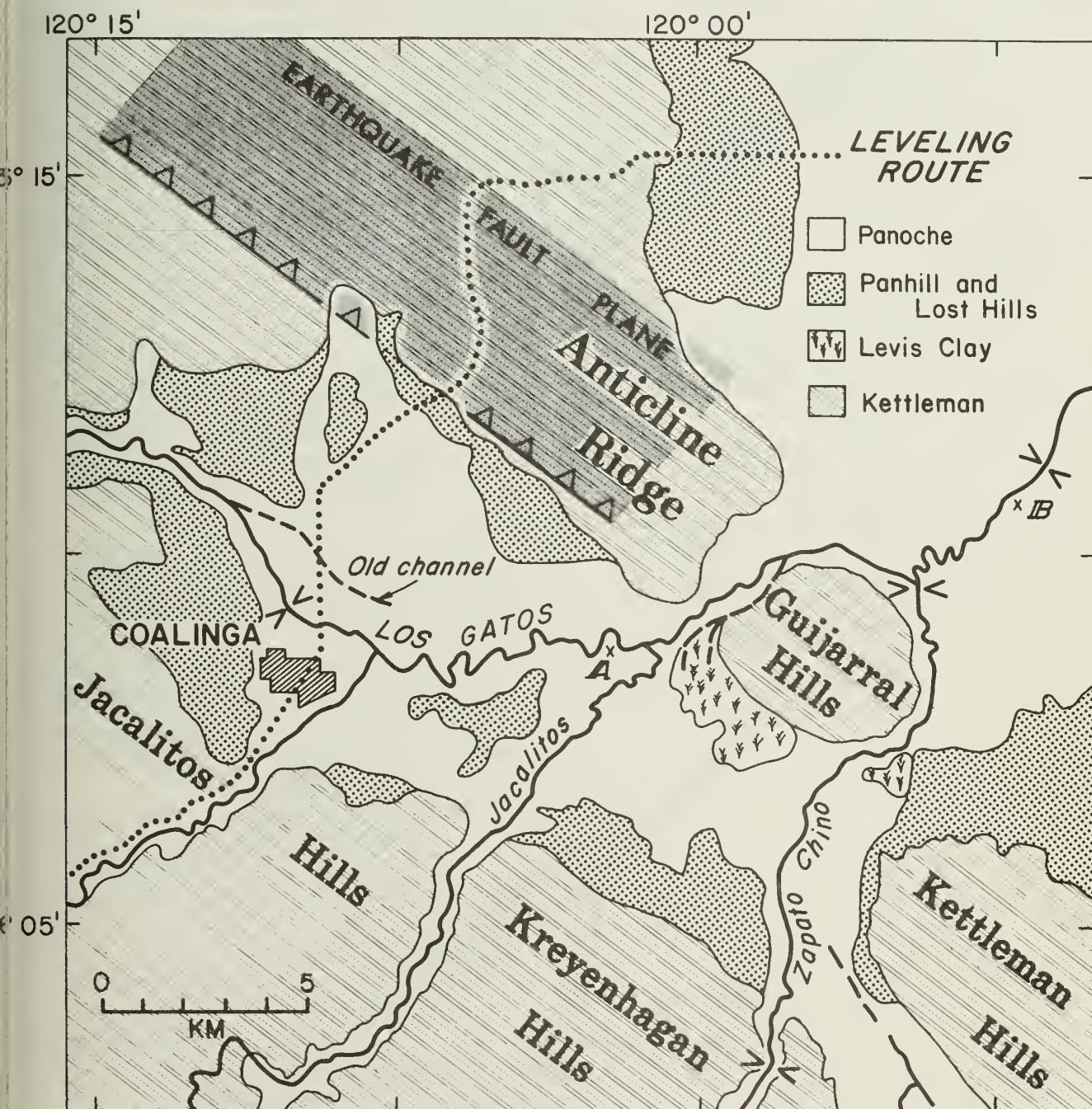


Figure 1. Simplified map of the surface deposits in the epicentral region of the May 1983 Coalinga earthquake. The approximate surface projection of a fault plane for the earthquake consistent with the seismic and geodetic data is shown. The distribution of surface deposits is taken from a detailed discussion and map in the Soil Survey of the Coalinga region (1952). The present river courses are shown by solid lines, and old river courses are shown by dashed lines. A dotted line indicates the course of the geodetic traverse. Note that the width of the structure where it is crossed by the geodetic line is about twice the width of the structure crossed by the Los Gatos Creek.



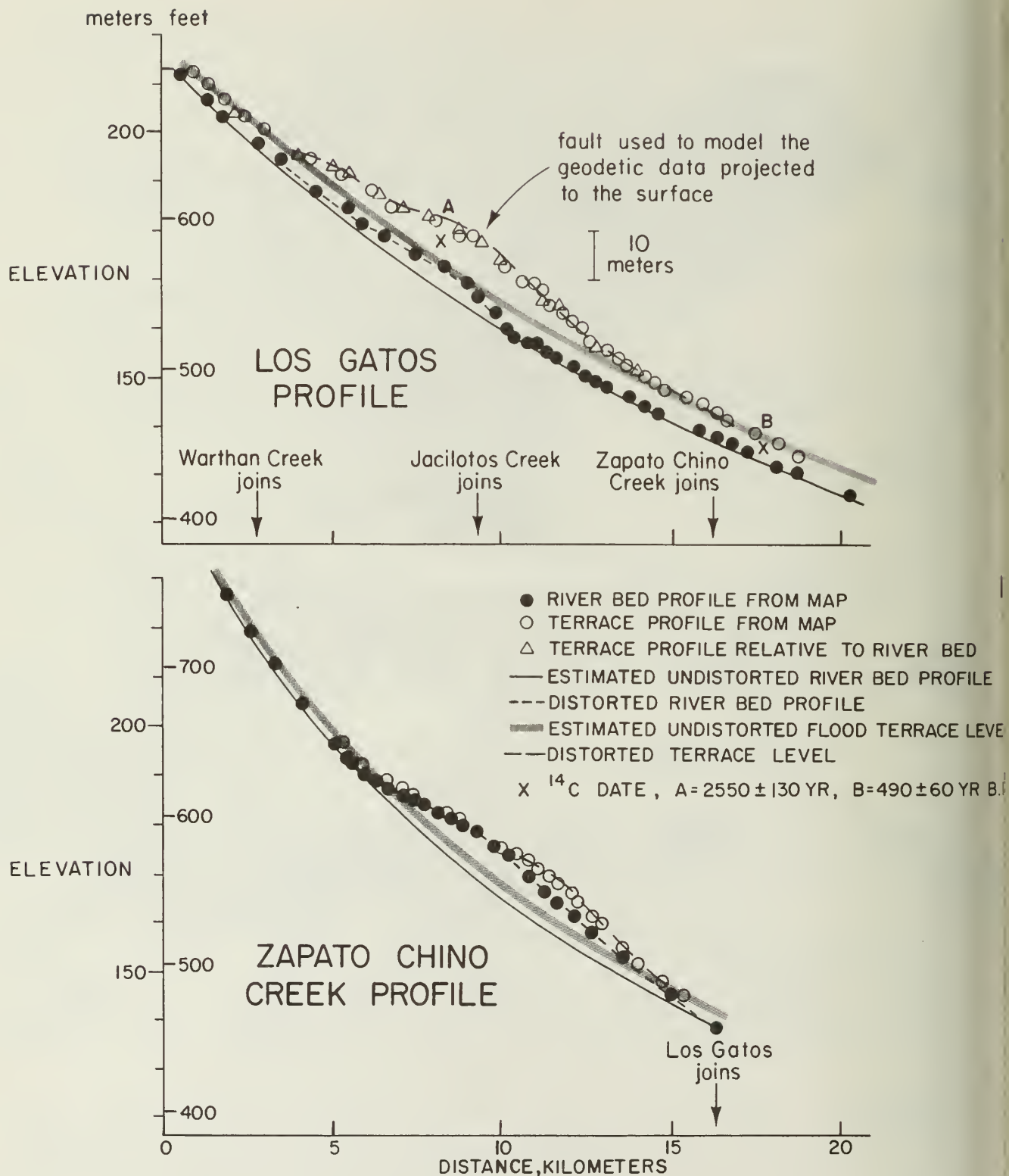


Figure 2. River terrace profiles. All of the points except those marked by triangles, which were measured in the field, are taken from the 7-1/2 topographic maps. The profiles follow the courses of the river except for some of the extreme meanders where the profile follows a direct route. The errors involved are just discernible in the profile but are less than  $\pm 0.3$  m.

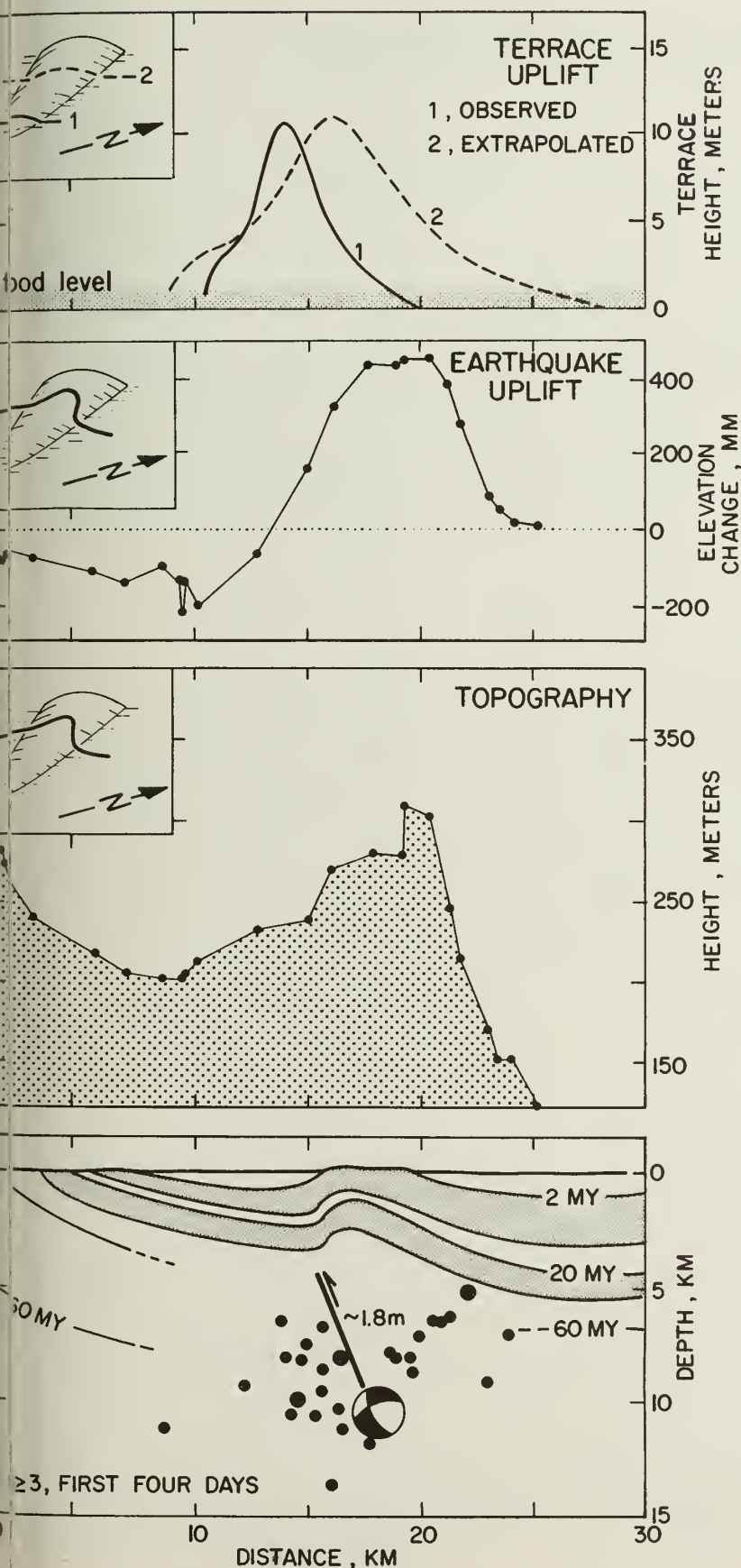


Figure 3. The terrace uplift for the Los Gatos Creek taken from Figure 2a is indicated by a solid line (1) in a). In the same figure, a profile extrapolated to the position shown in the inset sketch is shown by a dotted line (2). The 1983 earthquake uplift is shown in b) for the route shown in the accompanying sketch. The uplift is projected perpendicular to the fault strike. The topography for the same profile is shown in c). A simplified geological structure taken from Fowkes (1982) is shown in d). The location and mechanism of the main shock (Eaton, 1983) (projected on the sphere below the plane of the paper) and the location of the larger aftershocks (Reasenberget al., 1983) are also shown.

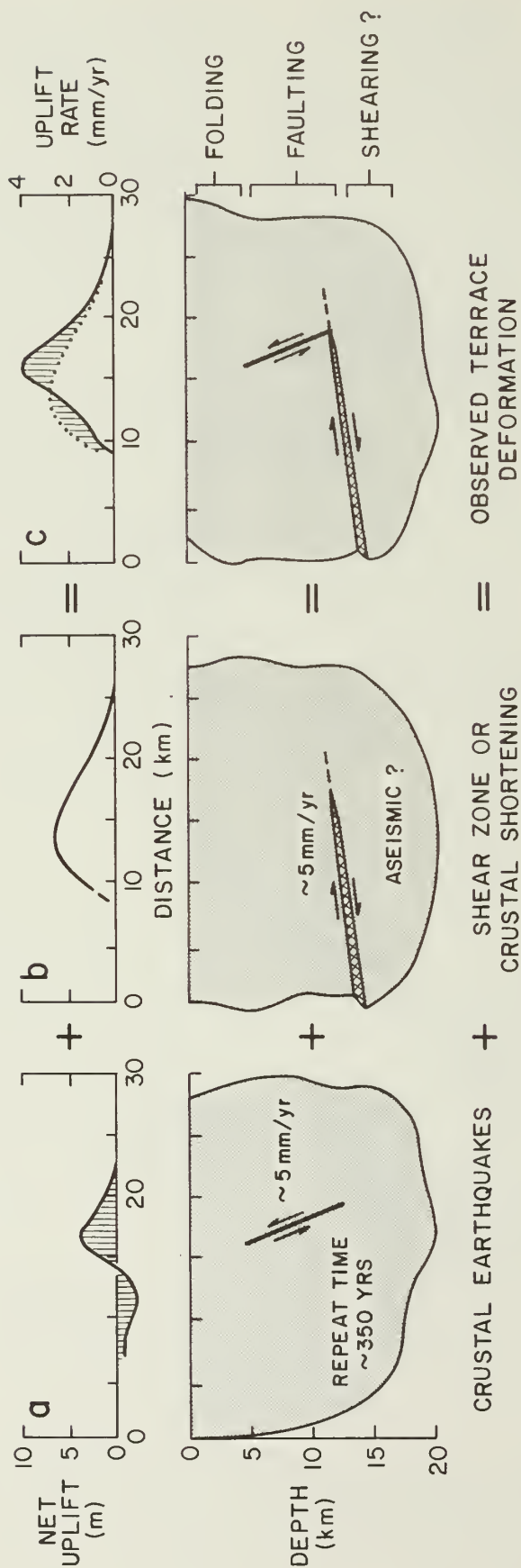


Figure 4. Interpretation of the deformation of the Los Gatos terrace. The deformation forms of diagrams a) and b) sum to provide the observed profile which is shown by a solid line in diagram c). The deformation profile in diagram a) can be produced by the earthquake fault and in diagram b) by a shallow slipping plane at depth. The data does not determine whether the plane extends to the east or to the west and does not determine the dip although it must be shallow. The westward dipping plane is chosen because it appears on reflection profiles for the Kettleman Hills (Wentworth et al., 1983).



# HIGH-ANGLE REVERSE FAULTING, A MODEL FOR THE 2 MAY 1983 COALINGA EARTHQUAKE

by

David R. Fuller<sup>1</sup> and Charles R. Rea<sup>2</sup>

## ABSTRACT

High-angle reverse faulting of the Coalinga anticline, along a northeast-dipping fault trending approximately N40W beneath Anticline Ridge, is a possible cause of the 2 May 1983,  $\sim M_L 6.5$  Coalinga earthquake. Contemporaneous folding and faulting of the anticline is in response to large-scale oblique-convergent wrenching along the San Andreas fault lithospheric plate boundary, resulting in a reduction of compressive stress across the wrench zone.

## INTRODUCTION

On 2 May 1983 at 4:43 p.m., a  $\sim M_L 6.5$  earthquake struck the small farming community of Coalinga causing widespread damage and nearly total destruction of the older buildings in the downtown district. Losses are estimated in excess of \$30 million which makes this the most destructive earthquake in California since the 1971 San Fernando earthquake. This event is significant from several other points of view as well. First, it supports the well known fact that destructive earthquakes also occur on lesser known faults that have not been active in historic time. Second, the earthquake occurred east of the San Andreas fault in a zone of deformation known for its prolific oil production. Third, the main shock was unaccompanied by any observed surface fault rupture, unexpected for an earthquake of this magnitude, leading some to speculate on a westward-dipping nearly horizontal thrust fault as a possible cause (Eaton, 1983). Fourth, in the interest of public safety, identification of the causative fault is important not only for zoning the fault for future land use decisions, but also for understanding its tectonic significance and the implications for future seismic activity in the region.

In this paper we present a model for the causative fault; a working hypothesis we believe to have two strong attributes: it is consistent with previous geological and current seismological data, and it is simple. We will speculate on the tectonic significance of this model and what it implies in terms of prospects for future seismic activity in the area.

<sup>1</sup> Geologist, California Division of Mines and Geology.

<sup>2</sup> Seismologist, California Division of Mines and Geology.

### Tectonic Setting

Regional deformational features in the Coalinga area (Figure 1) are presumed to be the result of transform and convergent motion between the North American and Pacific lithospheric plates along the San Andreas fault zone, producing the strike-slip and convergent wrench fault deformational pattern described by numerous authors (Hill and Dibblee, 1953; Moody and Hill, 1956; Crowell, 1962; Wilcox et al., 1973; Harding, 1974; and Harding, 1976).

The dominant local structure in the area is Anticline Ridge which is a long known and clearly mapped southeasterly plunging asymmetric anticline on a regional homocline (Arnold and Anderson, 1910; Kaplow, 1945; Jennings and Strand, 1958; Dibblee, 1971). This analysis is based on topographic expression, geologic mapping, and subsurface control from the many wells drilled for oil exploration and production. The structural interpretation in the early reports did not include faulting, as surface and subsurface mapping did not show any fault.

Kaplow's (1945) structural interpretation of the Coalinga oil field, as shown by a structure contour map on the top of the 1,300' thick Oligocene Kreyenhagen formation (Figure 2), has some inconsistencies:

1) a tight kinking of contour lines to fit the data, 2) a radical change in the attitude of the horizon, from N30E 11SE on Anticline Ridge (Eastside oil field) to N40W 45SW on the steep flank of the anticline and then back to N42E 16SE in the Westside oil field in a distance of about one mile, and 3) mapped faulting of the Kreyenhagen formation in outcrop northwest of Anticline Ridge. We believe these inconsistencies suggest faulting within the anticline.

### PROPOSED FAULT MODEL

We propose an alternative interpretation that fits the data on the top of the Kreyenhagen formation which includes faulting within the anticline (Figure 3), and results in smoother and simpler contouring of the structure. Furthermore, this alternate interpretation accommodates the shallow dip of the Kreyenhagen formation found in both the Eastside and Westside oil fields and the faulting of the surface outcrop of the Kreyenhagen formation as indicated by Kaplow (1945). The proposed fault has a strike of approximately N40W and is at least 12 km (8 mi.) long, where it intercepts the Kreyenhagen formation at depth. The contours indicate that the northeast side of the fault is up with respect to the southwest side, and the dip of the axial plane of the anticline would suggest that the fault dips steeply toward the NE making it a high-angle reverse fault. Oil wells in the Eastside oilfield penetrate the hanging wall an average depth of 3,100'. Records from these wells do not show penetration of a fault, which would suggest a minimum of 500-600' for the fault dip. An average dip of 64°NE (figure 4) is determined if the fault plane is constrained to pass through the reported hypocenter of the main shock (Eaton, 1983).

A preliminary focal mechanism of the main shock shows 1) a high-angle reverse fault trending N53W and dipping 67°NE, or 2) a low-angle thrust dipping about 23°SW (Eaton, 1983). One would expect rupture on a low-angle thrust fault to have a broad aftershock zone like that observed for the 1971 San Fernando earthquake (Allen *et al.*, 1971). Instead, the aftershock pattern for the Coalinga earthquake is a more narrow zone, elongated in a NW-SE direction, indicative of a steeply dipping fault. This, together with the location of the aftershock zone over Anticline Ridge (Eaton *et al.*, this volume), favors the high-angle reverse nodal plane, which is consistent with the model proposed here.

A cross-section normal to the proposed fault, through the main shock hypocenter and including attitudes of the "B" oil horizon (Arnold and Anderson, 1910) and the Kreyenhagen formation (Kaplow, 1945), suggests that the fault is along the southwestern limb and subparallel to the axial plane of the anticline (Figure 4). The sense of movement and orientation of the proposed fault is compatible with continued growth and development of the anticline. Absence of surface faulting suggests that the faulting was confined to the more tightly folded inner core of the anticline, transforming into enhanced folding of the younger, outer rock units nearer to the ground surface. Surface deformation could, consequently, be characterized by uplift and extensional fracturing without the fault reaching the ground surface.

Surface cracks from this event appear in two forms: tension cracks on the anticline and "thrust fault cracks" (discontinuous fractures with apparent reverse offsets) in the NE quarter of Section 29, T19S, R15E, with an attitude of N45W 30NE (E. Hart, personal communication 2 June 1983). The "thrust fault cracks", though not extensive enough to be considered primary faulting, occur in the northwestern portion of Anticline Ridge where the axial plane is overturned and where the proposed fault, if extended upward, would intersect the ground surface. Figure 5 shows the relationship of the surface cracks to the subsurface location of the fault, the main shock epicenter, the aftershock zone, and the topographic expression of Anticline Ridge.

#### Compatibility With Regional Wrench Faulting

The proposed faulting of the Coalinga anticline is consistent with convergent wrench faulting, which enhances compressive wrench-zone structures and can even cause reverse faulting and thrusting (Wilcox *et al.*, 1973). Modeling of convergent wrenching in the laboratory has produced upthrust blocks bounded by vertical or high-angle reverse faults (Wilcox *et al.*, 1973). Anticlinal folding on the west side of the San Joaquin Valley has occurred contemporaneously with Cenozoic movement on the San Andreas fault, with outward growth and development of structures down plunge (Harding, 1976). The older, more tightly folded portions of anticlines nearest to the San Andreas fault are commonly disrupted by more recent thrusting, interpreted to be a late-stage reaction to prolonged deformation (Harding, 1976).



Anticline Ridge exhibits these characteristics with simple anticlinal folding to the southeast, becoming more asymmetrical toward the northwest until the axial plane is overturned and the trend of the anticline is bent more toward the northwest. This is interpreted as indicating that the anticline, in this area, has been folded beyond the competence of the rock and has accommodated additional crustal shortening by reverse faulting.

### CONCLUSIONS

High-angle reverse faulting of the Coalinga anticline, beneath Anticline Ridge, is the probable cause of the 2 May 1983 Coalinga earthquake. Continued folding and contemporaneous faulting of the anticline is in response to oblique convergent wrenching along the San Andreas fault. The Coalinga earthquake can be considered a manifestation of strain accumulation related to the San Andreas fault zone which has relieved compressive stresses. Other tightly folded anticlines in the wrench zone can be expected to undergo similar development in the future, and this should be recognized in future assessments of seismic hazards along the western margin of the Great Valley.

One requirement of a viable model is its ability to stand the test of time. Two significant observations have already occurred since the inception of the model: 1) the high-angle east-dipping reverse surface displacement associated with the 11 June 1983 M5.2 aftershock, and 2) the broad uplift over Anticline Ridge determined by post-earthquake leveling surveys (Stein *et al.*, this volume). Both are compatible, and the second is predictable by the proposed model.

### ACKNOWLEDGMENTS

Acknowledgment and appreciation is given to Mason L. Hill and James E. Kahle who reviewed this paper and made helpful comments and suggestions, and to Cora Pingree for typing the manuscript.

## REFERENCES

- Allen, C.R., Engen, G.R., Hanks, T.C., Nordquist, J.M., and Thatcher, W.R., 1971, Main Shock and Larger Aftershocks of the San Fernando Earthquake, February 9 through March 1, 1971: U.S. Geological Survey Prof. Paper 733, p. 17-20.
- Arnold, R. and Anderson, R., 1910, The Geology and Oil Resources of the Coalinga District, Calif.: U.S. Geological Survey, Bulletin 398.
- Crowell, J.C., Jr., 1962, Displacement Along the San Andreas fault, California: Geol. Soc. Am. Sp. Paper No. 71, 61 p.
- Dibblee, T.W., 1971, Geologic maps of the Coalinga, Joaquin Rocks, New Idria, and Priest Valley 15' quadrangles: U.S. Geological Survey Open-File Report 71-87 (Sheets 5, 8, 10, and 15).
- Eaton, J.P., 1983, Seismic Setting, Location and Focal Mechanism of the May 2, 1983, Coalinga Earthquake: U.S. Geological Survey, Open-File Report 83-511, p. 20-26.
- Harding, T.P., 1974, Petroleum Traps Associated with Wrench Faults: American Association of Petroleum Geologists, Bulletin, v. 58, p. 1290-1304.
- Harding, T.P., 1976, Tectonic Significance and Hydrocarbon Trapping Consequences of Sequential Folding Synchronous with San Andreas Faulting, San Joaquin Valley, California: American Association of Petroleum Geologists, Bulletin, v. 60, p. 356-378.
- Hill, M.L. and Dibblee, T.W., Jr., 1953, San Andreas, Garlock, and Big Pine faults, California (a study of the character, history, and tectonic significance of their displacements): Geological Society of America, Bulletin, v. 64, p. 443-458.
- Hoots, H.W., Bear, T.L., Kleinpell, W.D., 1954, Geological Summary of the San Joaquin Valley, California: Calif. Div. Mines & Geol. Bull. 170, Chapter II, Contribution 8, Plate 5.
- Kaplow, E.J., 1945, Coalinga oil field, in Summary of operations, California oil fields; thirty-first annual report of the State Oil and Gas Supervisor: Department of Natural Resources, Division of Oil and Gas, v. 31, p. 5-22.
- Moody, J.D. and Hill, M.J., 1956, Wrench-fault tectonics: Geological Society of America, Bulletin, v. 67, p. 1207-1246.
- Wilcox, R.E., Harding, T.P., and Seely, D.R., 1973, Basic Wrench Tectonics: American Association of Petroleum Geologists, Bulletin, v. 57, p. 74-96.

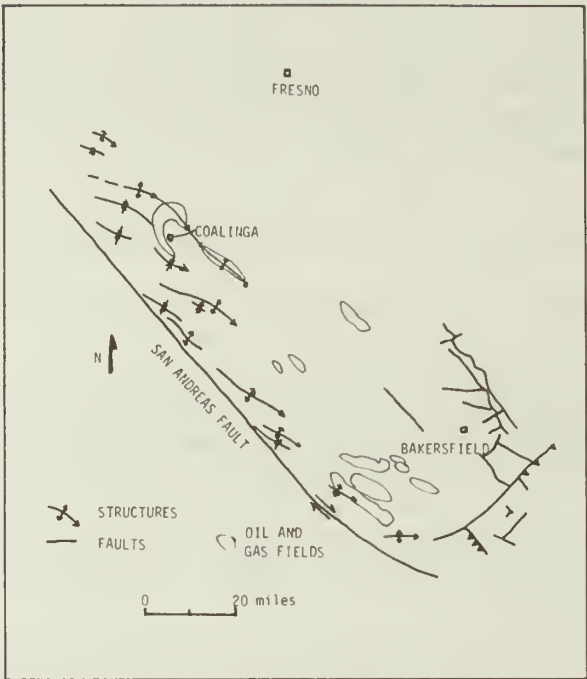


Figure 1. Region tectonic setting map for the 2 May 1983 Coalinga earthquake, after Hoots et al., (1954).

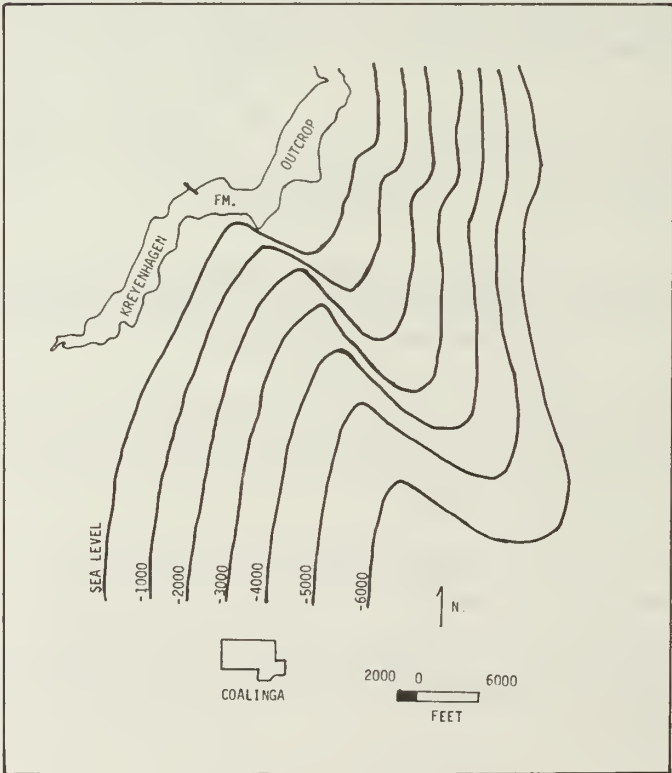


Figure 2. Structural contour map of the Coalinga Oil Field area. Contours are on the top of the Kreyenhagen formation, modified from Kaplow (1945).



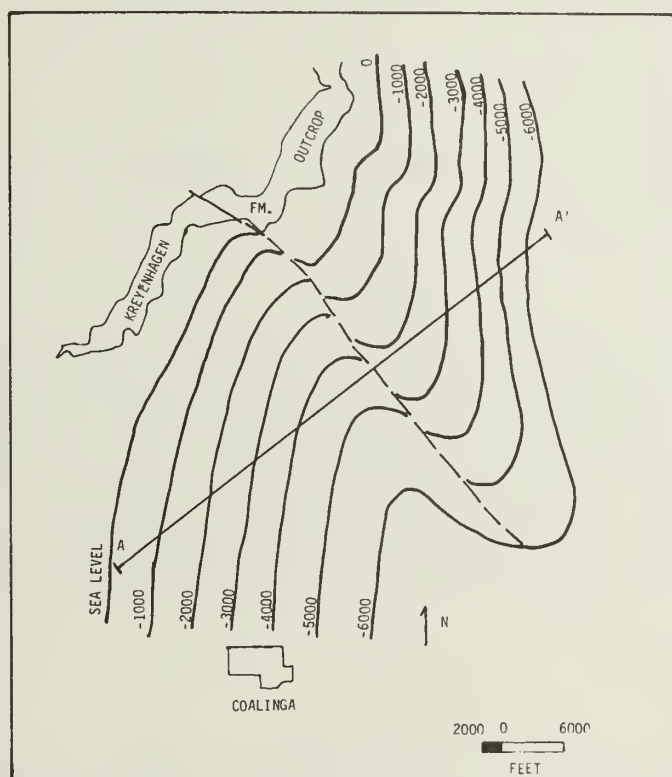


Figure 3. High angle fault interpretation. Structural contours are on the top of the Kreynhagen formation.

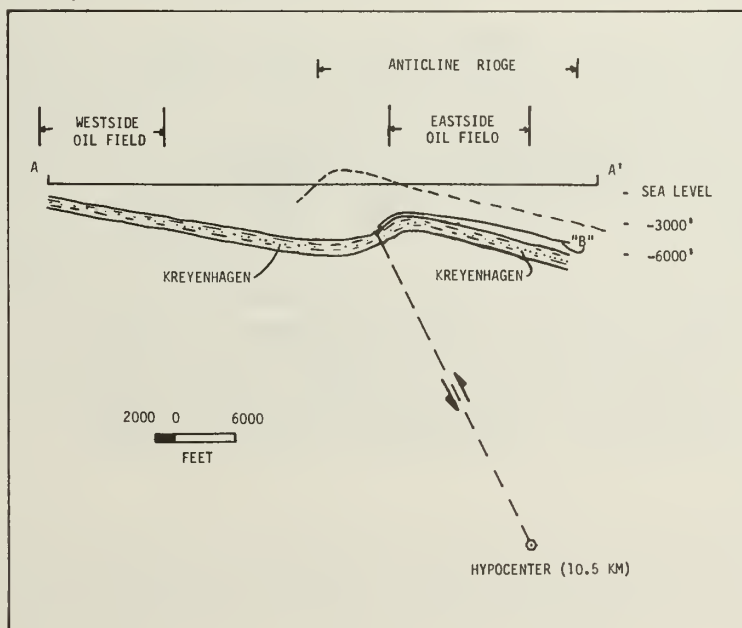


Figure 4. Cross section A - A' (Figure 3.), constructed normal to the proposed fault and through Anticline Ridge and the hypocenter.

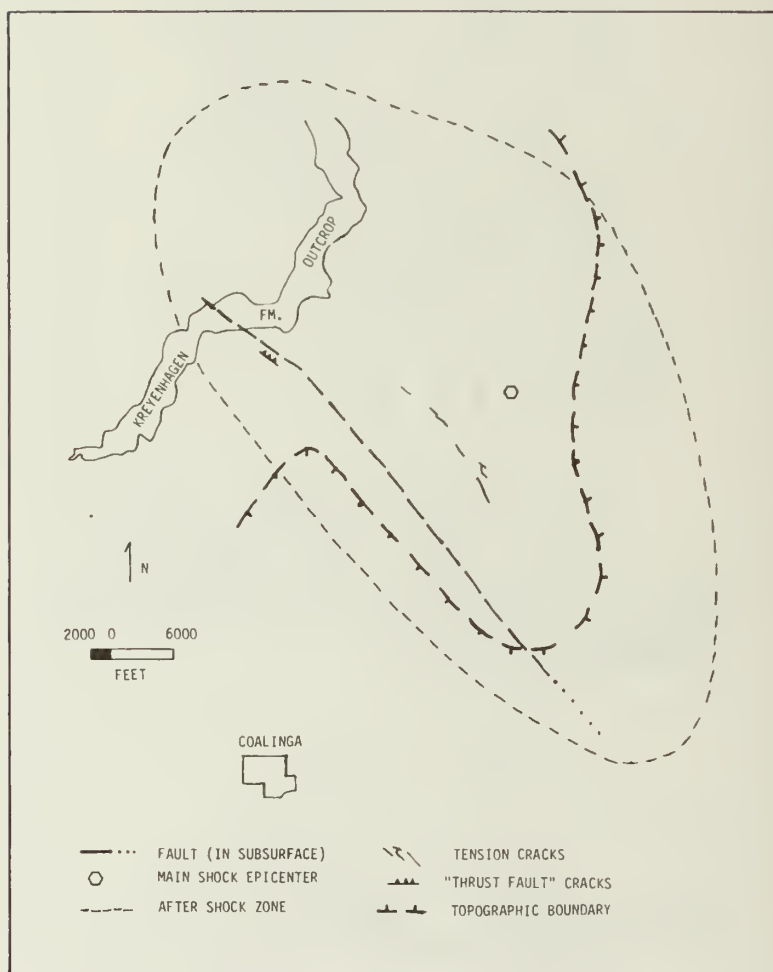


Figure 5. Map of the relationship of the surface cracks, the main shock epicenter, and the aftershock zone to the subsurface location of the fault at the Kreyenhagen horizon and the topographic expression of Anticline Ridge.

# GRAVITY AND MAGNETIC INVESTIGATION OF THE COALINGA AREA

by

R.H. Chapman<sup>1</sup>, G.W. Chase<sup>1</sup>, and C.C. Bishop<sup>2</sup>

## ABSTRACT

Gravity data in the vicinity of Coalinga reflect the principal structural features of the area including the Coalinga anticline, a syncline underlying Pleasant Valley, the Anticline Ridge fault, and other possible faults. Magnetic data also may indicate the location of the Anticline Ridge fault. Elevation changes and the location of the May 2, 1983, earthquake epicenter suggest that movement on either the Anticline Ridge fault or another fault suggested by geophysical surveys on the eastern flank of Anticline Ridge could have been the cause of the earthquake.

## INTRODUCTION

The Division of Mines and Geology conducted a brief geophysical investigation in the vicinity of Coalinga following the May 2, 1983, earthquake. The purpose of the investigation was to provide information on the geologic structure of the area and, if possible, to help locate the fault that was the cause of the earthquake.

The geophysical investigation consisted in part of a detailed east-west gravity and magnetic traverse crossing Anticline Ridge and part of Pleasant Valley north and northeast of Coalinga near the location of the earthquake epicenter. A gravity map of the area was also compiled from available data. Data on elevation changes, obtained from comparison of a post-earthquake survey by the National Geodetic Survey with an earlier 1972 survey, also were available in the vicinity of the gravity and magnetic profiles.

---

<sup>1</sup> Geophysicist, California Division of Mines and Geology, Sacramento.

<sup>2</sup> Geologist, California Division of Mines and Geology, San Francisco.



## GRAVITY AND MAGNETIC DATA

The detailed gravity and magnetic profiles completed during this study extend from Interstate 5, on the east, westward along State Highway 198 to Oilfields, and along Shell Road and Palmer Avenue to Derrick Avenue, a total road distance of about 10 miles (Figures 1 and 2). Gravity stations were occupied at intervals of 400 feet and magnetic stations at intervals of 100 feet along this traverse.

Gravity data for the detailed traverse were obtained with La Coste and Romberg geodetic gravity meter G129. Elevations were obtained by surveying. The gravity data were referenced to California Division of Mines and Geology base station 250 at Coalinga (Chapman, 1966, p. 40). Additional gravity data for the Coalinga area are from a compilation of data for the Santa Cruz (Monterey) map sheet (Chapman and Bishop, 1978) and from the Department of Defense gravity library. All gravity readings were reduced to complete Bouguer anomalies for a density of  $2.30 \text{ g/cm}^3$  and referenced to the International Ellipsoid of 1930. Terrain corrections for most stations were made manually out to a radius of 2.29 km. The remaining terrain correction for each station out to a radius of 166.7 km (100 miles) was computed by means of a U.S. Geological Survey computer program (Plouff, 1977). The choice of  $2.30 \text{ g/cm}^3$  for the reduction density was arbitrary, but it is believed to be an appropriate average density for the Tertiary sedimentary rocks exposed in the vicinity (Bishop and Chapman, 1967, p. 3).

Ground magnetic data were obtained by means of a Geometrics model 816 proton precession magnetometer. The observed magnetic data were averaged in order to remove local magnetic variations probably caused principally by pipes and culverts encountered along segments of the traverse.

Figure 1 is a complete Bouguer gravity contour map compiled from all available data, using a 2-milligal contour interval. Figure 2 includes the detailed gravity and magnetic profiles obtained during this study along line A-A' (Figure 1), a partial geologic section, and a plot of elevation changes. The gravity profile also includes data from the gravity contour map beyond the limits of the detailed profile. The detailed gravity and magnetic data shown in Figure 2 were obtained along roads, some of which are not straight. The data were projected on to straight-line segments, as indicated in Figure 1, in order to eliminate as much distortion as possible.

## INTERPRETATION OF GEOPHYSICAL DATA

### Gravity Contour Map

The area near Coalinga shown in Figure 1 includes parts of the eastern side of the Coast Ranges and the western side of the San Joaquin Valley. The gravity data show a general regional gravity slope, downward toward the east or northeast. East of the map area, the regional gravity slope culminates in a northwest-trending negative anomaly that probably

represents the approximate axis of the Great Valley syncline (Bishop and Chapman, 1967, p. 4). Gravity values increase in general toward the west where Great Valley sequence rocks of Cretaceous age are exposed. Local gravity anomalies include a north-to-northwest-trending positive anomaly associated with Anticline Ridge northeast of Coalinga and a local negative anomaly associated with Pleasant Valley.

The positive gravity anomaly associated with Anticline Ridge is represented on Figure 1 by a southeastward bowing of the contours. This feature can be traced southeastward on Figure 1 at least as far as the Gujarral Hills, but the amplitude of the anomaly decreases in this direction. This local positive anomaly probably represents rocks with relatively high densities that have been uplifted in the core of the Coalinga anticline.

Pleasant Valley is marked by a negative gravity anomaly probably caused in part by the thickness of low-density rocks in the valley, and in part by the syncline that underlies this area (Figure 2). West of Pleasant Valley, gravity values rise as the low-density rocks become thinner and outcrops of rocks of the Great Valley sequence are approached (Jennings and Strand, 1959). The steep gravity gradient west of Coalinga may represent the contact between the relatively dense Great Valley sequence rocks and the younger, less dense, Tertiary sedimentary rocks, but it could also indicate the presence of one or more faults trending north to west of north. The Nunez fault located just north of the steepest part of this gradient could be one such fault (Figure 1) (U.S. Geological Survey, 1983).

#### Profile A-A'

Figure 2 includes the detailed gravity and magnetic profiles, a topographic profile with a simplified geologic cross-section, and a plot of elevation changes derived from surveys in 1972 and 1983, of bench marks along and near the geophysical traverse (National Geodetic Survey, 1983). The gravity profile has been extended about two miles to the east and six miles to the west using gravity values from the contour map of Figure 1.

#### Gravity Data

The gravity profile shows the eastward-sloping regional gravity trend mentioned previously. Local anomalies tend to mirror the geologic structure shown in Figure 2. The Coalinga anticline is marked by a positive anomaly that has an amplitude of about 7 milligals. Relatively dense Tertiary marine sedimentary rocks of Miocene and Pliocene ages are exposed near the crest of the anticline in contact with younger, less dense, rocks on the flanks (Jennings and Strand, 1959).

The western side of the positive anomaly over the Coalinga Anticline has a relatively steep gradient which is in agreement with the apparent steep dip of the beds on this limb of the structure (Kaplow, 1945). This gradient may also mark the location of the Anticline Ridge fault which is

believed to dip at a steep angle to the east (Fuller and Real, this volume; U.S. Geological Survey, 1983). Movement on this fault may have caused the May 2, 1983 earthquake.

A negative gravity anomaly is associated with Pleasant Valley and the syncline that underlies the valley west of Anticline Ridge. Further to the west, gravity values rise toward the end of the profile over an area where relatively dense sedimentary rocks of the Great Valley sequence are exposed.

East of the anomaly over Anticline Ridge, the gravity profile has a relatively gentle gradient which corresponds to the moderate dip of the beds shown in Figure 2. About four miles west of the eastern end of the profile in Figure 2, however, there is a short section about 1,500 feet long which has a relatively steep gravity gradient. A residual gravity anomaly for this part of the profile is shown in Figure 3. The residual gravity values were obtained by subtracting a smooth gradient from the Bouguer gravity profile. The profile in Figure 3 shows a negative residual anomaly with an amplitude of about one milligal. This anomaly could have a number of different causes, but it indicates a contact near the surface between relatively high-density rocks on the west and low-density rocks on the east. The anomaly may indicate that the alluvium is thicker east of a possible fault or erosional feature, or it may indicate a change in density of the underlying Tertiary sedimentary rocks that dip at a moderate angle to the east in this area.

Figure 3 shows a model that could account for the observed anomaly if the cause is either a fault or an erosional feature. A change in thickness of about 300 feet of alluvium (offset or depth of erosion) is necessary to account for the anomaly if a density contrast of  $0.3 \text{ g/cm}^3$  between Tertiary sedimentary rocks and alluvium is assumed, as in Figure 3. This density contrast could result if the densities of Tertiary sedimentary rocks and alluvium are about  $2.3 \text{ g/cm}^3$  and  $2.0 \text{ g/cm}^3$ , respectively. There is insufficient data to determine an angle of dip for the contact, so it is assumed to be approximately vertical in Figure 3. No faults have been mapped in this area, but a fault cannot be ruled out without a more thorough geologic and/or geophysical study. The epicenters reported for the earthquake are both less than two miles west of the location of this possible fault (Figure 1). Therefore, a fault, dipping toward the west, would be consistent with the epicentral area.

#### Magnetic Data

The ground magnetic profile in Figure 2 shows an overall decrease of about 400 gammas from the east to the west end of the line. The profile also shows a local negative anomaly with an amplitude of about 200 gammas that corresponds approximately with the gravity anomaly over Anticline Ridge. This negative anomaly may indicate that the rocks exposed in the core of the anticline are less magnetic than the rocks on either side. However, the negative anomaly also corresponds approximately with the location of an oil field and the presence of many nearby wells and pipes. The cumulative effect of a number of local magnetic anomalies



could cause an apparent negative anomaly over the structure. The western end of the magnetic profile in Figure 2 also shows what may be a part of another local negative magnetic anomaly. This part of the profile is also within an oil field, and the anomaly here may have the same cause as the one over Anticline Ridge. The possible fault on the eastern part of the gravity profile has no expression on the magnetic profile. However, the Anticline Ridge fault may be indicated by a local change in the magnetic gradient.

#### Elevation Data

The plot of elevation changes (Figure 2) shows that the largest positive changes (uplift) occurred near Oilfields on Anticline Ridge. Relatively small negative elevation differences were found in the San Joaquin Valley east of profile A-A', and in Pleasant Valley south of the profile, but these are not shown in Figure 2. The Anticline Ridge fault and the possible fault east of the anticline are both within the area of uplift as shown on profile A-A'. Reverse motion at depth along the Anticline Ridge fault, accompanied by surface uplift and bending, might be the cause of the observed elevation changes. If the proposed fault east of the anticline dips to the west, however, movement on this fault might also explain the observed changes.

#### CONCLUSIONS AND RECOMMENDATIONS

Gravity data near Coalinga reflect the principal structural features of the area including the Coalinga anticline along Anticline Ridge and the syncline underlying Pleasant Valley. These data also show evidence for the Anticline Ridge fault and possible faults on the east side of the anticline and in an area west and northwest of Coalinga. The magnetic data show possible anomalies associated with Anticline Ridge and the Anticline Ridge fault. Data on elevation changes show that Anticline Ridge near Oilfields has risen about 1.4 feet since 1972, presumably as a result of coseismic deformation.

The observed elevation changes and the location of the earthquake epicenter suggest that the May 2, 1983, earthquake could have been caused by movement on the Anticline Ridge fault, the possible fault located east of Anticline Ridge, or perhaps an unidentified fault. Additional geophysical work such as a seismic refraction survey could be used to better define the location and offset of the possible fault east of Anticline Ridge. Detailed gravity data could also be used to help map the linear extent of this fault.

#### ACKNOWLEDGEMENTS

Manuscript reviewed by John Alfors and Charles Real. We would also like to thank Cora Pingree for typing the manuscript.

## REFERENCES

- Bishop, C.C., and Chapman, R.H., 1967, Bouguer gravity map of California, Santa Cruz sheet (Monterey), revised 1980: California Division of Mines and Geology, scale 1:250,000, map and 6 p. text.
- Chapman, R.H., 1966, The California Division of Mines and Geology gravity base station network: California Division of Mines and Geology Special Report 90, 49 p.
- Chapman, R.H., and Bishop, C.C., 1978, Principal facts and sources for 1743 gravity stations on the Santa Cruz 10 by 2012' quadrangle, California: California Division of Mines and Geology Open-File Report 78-14SAC, 59 p.
- Jennings, C.W. and Strand, R.G., 1959, Geologic Map of California, Olaf P. Jenkins edition, Santa Cruz sheet: California Division of Mines and Geology, scale 1:250,000.
- Kaplow, E.J., 1945, Coalinga oil field, in Summary of Operations, California Oil Fields; thirty-first annual report of the State Oil and Gas Supervisor: Department of Natural Resources, Division of Oil and Gas, v. 31, no. 2, p. 5-22.
- National Geodetic Survey, 1983, Results of releveled, vicinity of Coalinga, California: Earthquake studies report HGZ L24759, 15 July 1983, 3 p.
- Plouff, Donald, 1977, Preliminary documentation for a FORTRAN program to compute gravity terrain corrections based on topography digitized on a geographic grid: U.S. Geological Survey Open-File Report 77-535, 45 p.
- U.S. Geological Survey, 1983, Anticline Ridge fault responsible for May 2, 1983, Coalinga, California earthquake: U.S. Geological Survey press release, July 29, 1983, 2 p.

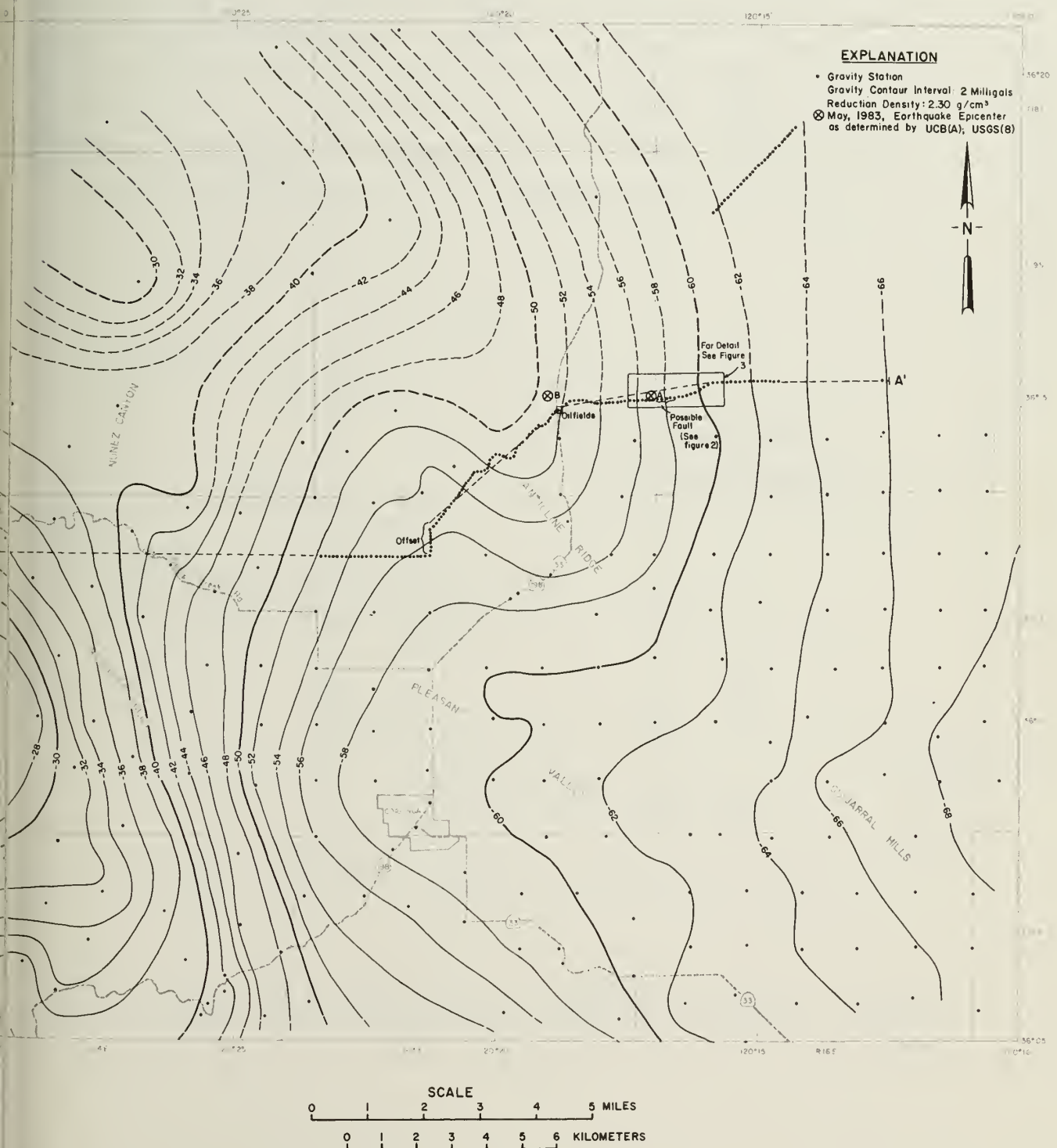


Figure 1. Bouguer Gravity Map, Coalinga area.



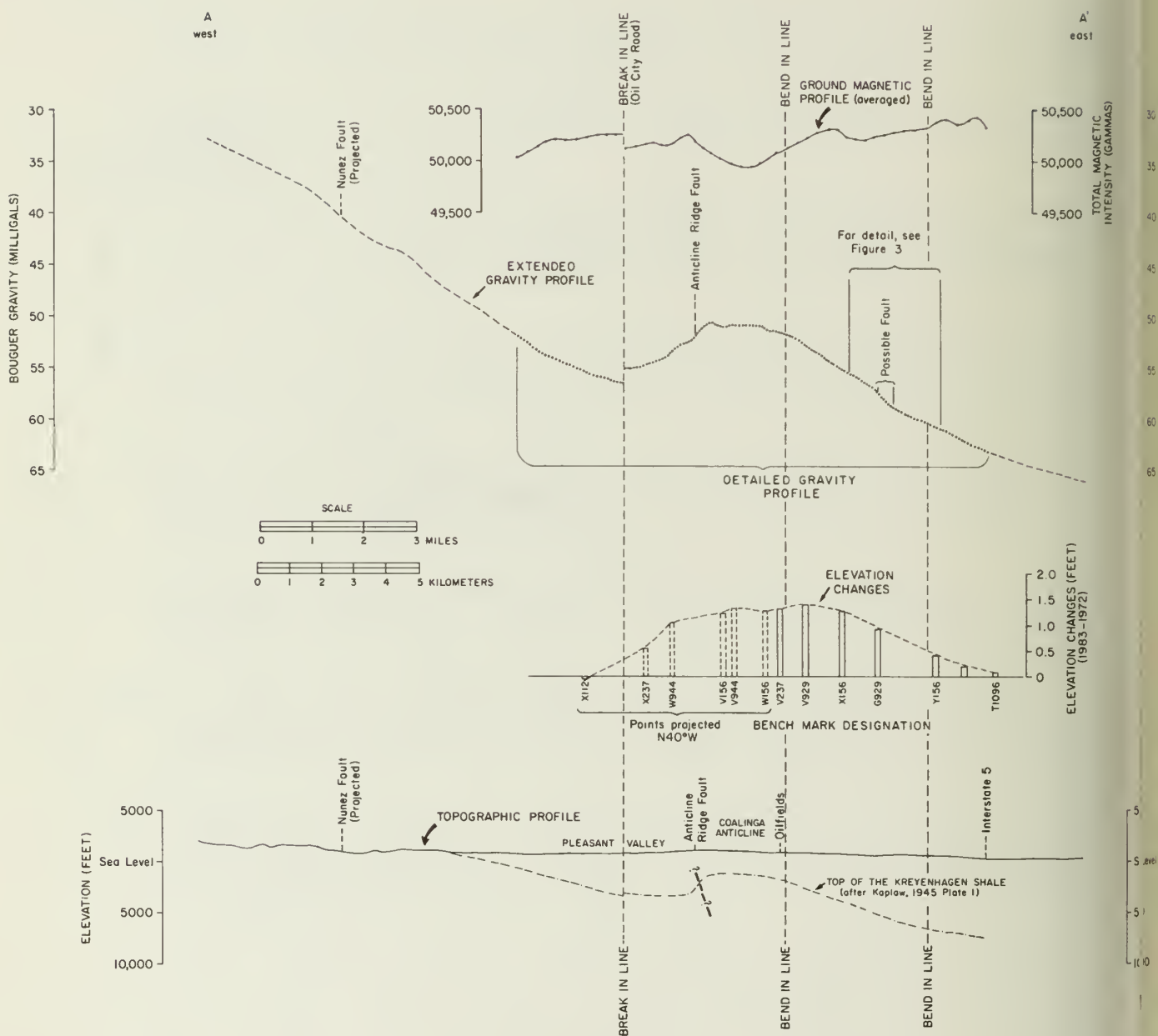


Figure 2. Line A - A' showing gravity and magnetic profiles, elevations on top of the Kreyenhagen shale, and surface elevation changes, Coalinga area.

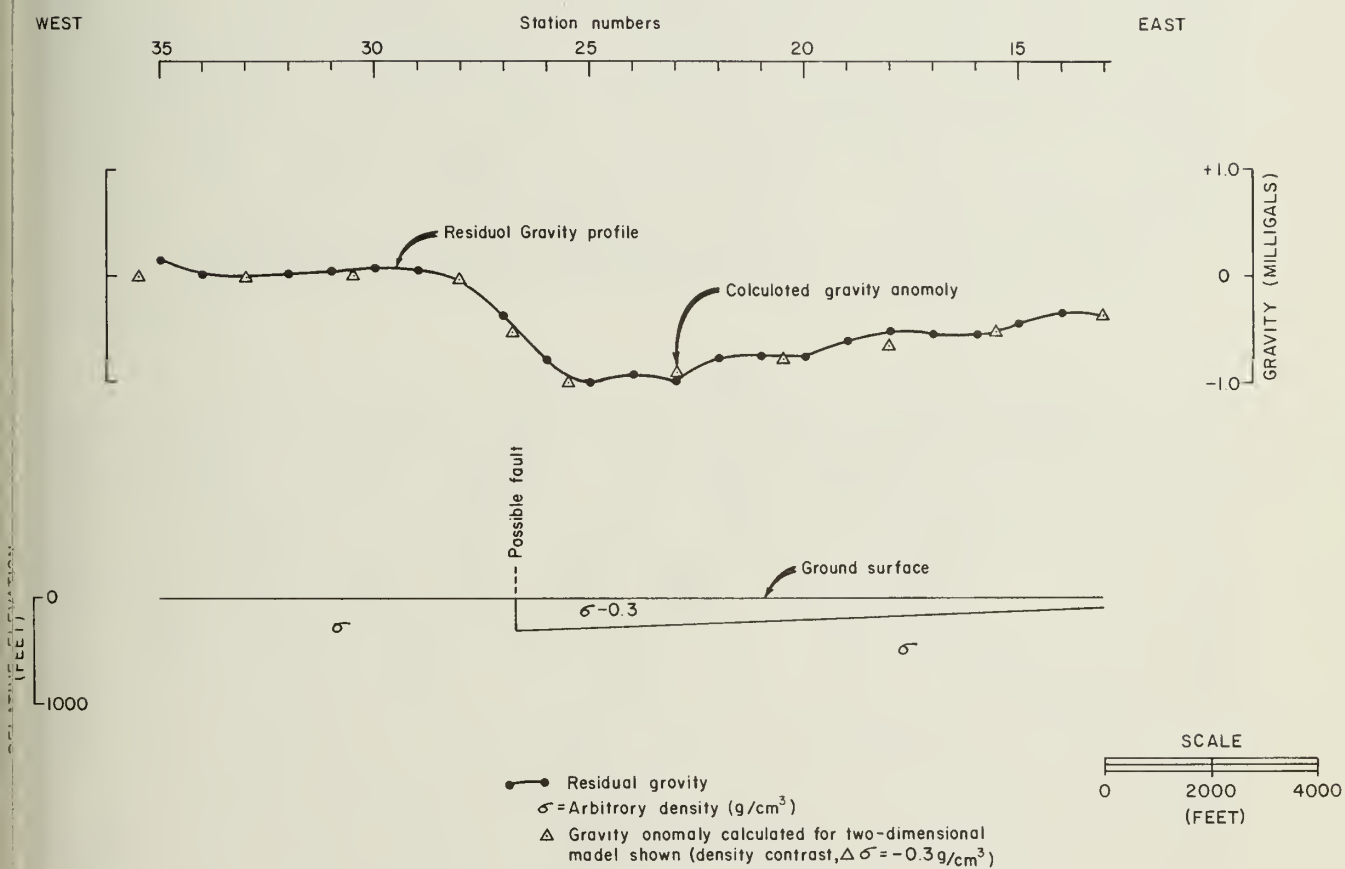


Figure 3. Residual gravity profile and interpretation, Coalinga area.





# SHALLOW STRESS CHANGES DUE TO WITHDRAWAL OF LIQUID FROM OIL FIELDS IN THE COALINGA AREA, CALIFORNIA

by

R.F. Yerkes, assisted by K.M. Williams<sup>1</sup>

The 2 May 1983 Coalinga main shock occurred in an area dominated by regional horizontal compression, where the shallow crust has been subjected to the stresses of petroleum withdrawal for more than 85 years; the area is also located along the west boundary of the world's largest basin of intense subsidence due to withdrawal of groundwater. Pre-1968 subsidence due to withdrawal of groundwater also has been identified in Pleasant Valley north of Coalinga, and both subsidence due to withdrawal of petroleum and tectonic uplift have been identified on Anticline Ridge (Bull, 1975). Stress changes due to withdrawal of fluid from the shallow crust arise from (1) reduction of mass, and (2) volumetric strain resulting from reduction of pore volume. Our purpose is to estimate the mass lost by withdrawal of petroleum liquids within 10 km of the epicenter --the approximate size of the aftershock zone--and the resulting changes in stress.

Parts or all of six oil fields are within 10 km of the epicenter: the north half of the Coalinga West field, the Coalinga East field, the Nose and Northeast areas of the East Coalinga Extension field, the Pleasant Valley field, and the northwest area of the Guijarral Hills field (fig. 1). Producing pools range in average depth from 1,800 to 10,700 feet below sea level, in average thickness from 20 to 650 feet, and the specific parts named above total about  $78 \times 10^6 \text{ m}^2$  in area (table 1). Net liquid produced (oil plus water less water returned) from pools in these specific parts totaled about  $345 \times 10^6 \text{ m}^3$  at the end of 1981 (table 2). This volume, if averaged over the area of the producing pools, is equivalent to a layer about 4.4 m thick; if averaged over the area of a circle of 10 km radius around the epicenter ( $314 \times 10^6 \text{ m}^2$ ), it is equivalent to a layer about 1.1 m thick. For a liquid of assumed average specific gravity 1.00, the removed load (decrease in vertical stress) is about 0.4 bar in the first case, and about 0.1 bar in the second case. The resulting changes in stress on a reverse or thrust fault are in the range of 0.02-0.2 bar, negative for normal stress and positive for shear stress, thus favoring movement. However, they are very small (and very slow) changes relative to the total stress field. Theoretically, the actual values of normal and shear stress (to reach failure) are functions of material shear strength, and depth, dip, and nature of the fault (Hubbert, 1951; Jaeger and Cook, 1971, p. 90, 402). To reach failure on a steep reverse fault at 10-11 km, these values presumably would exceed 2.6 kilobars, the approximate lithostatic stress at that depth.

---

<sup>1</sup> U.S. Geological Survey, 345 Middlefield Road, Menlo Park, CA 94025.

Mass loss due to withdrawal of petroleum is but one, perhaps minor, component of the stress changes man has imposed on the shallow crust in this area. First, we have not considered changes due to volumetric strain, an effect that may dominate mass loss. Second, we assume important constraints such as (a) no change in the pattern of known regional horizontal compressive strain; and (b) no inflow of fluid from outside the area. Third, we do not account for (a) changes due to known withdrawal of groundwater from the area; and (b) changes in oil-reservoir fluid pressures.

#### ACKNOWLEDGEMENTS

The comments of R.O. Castle, A.T.F. Chen, Paul Segall, and C.M. Wentworth were very helpful during preparation and review of this report.

#### REFERENCES

- Bull, W.B., 1975, Land subsidence due to ground-water withdrawal in the Los Banos-Kettleman City area, California, Part 2. Subsidence and compaction of deposits: U.S. Geological Survey Professional Paper 437-F, 90 p.
- California Division of Oil and Gas, 1973, California oil and gas fields, Volume 1, North and east central California: California Division of Oil and Gas, data sheets, maps and sections, variously paged.
- Conservation Committee of California Oil Producers, 1982 and earlier, Annual review of California oil and gas production: Conservation Committee of California Oil Producers, annual production statistics by fields and pools.
- Hubbert, M.K., 1951, Mechanical basis for certain familiar geologic structures: Geological Society of America Bulletin, v. 61, no. 4, p. 355-372.
- Jaeger, J.C., and Cook, N.G.W., 1971, Fundamentals of rock mechanics: London, Chapman and Hall Ltd., and Science Paperbacks, 515 p.
- Poland, J.F., Lofgren, B.E., Ireland, R.L., and Pugh, R.G., 1975, Land Subsidence in the San Joaquin Valley, California, as of 1972: U.S. Geological Survey Professional Paper 437-H, 78 p.
- State Oil and Gas Supervisor, 1981 and earlier, Annual Report: California Division of Oil and Gas, annual production statistics.

Table 1-Coalinga area oil fieldsDepth, average thickness, and maximum areas of producing units (From California Oil and Gas Fields, vol. 1)

FIELD Area	Temblor (Early-middle Miocene)		Vaqueros (Early Miocene)		Lodo (Eocene)		Maximum productive area	
	Average depth (ft subsea)	Average thick- ness(ft)	Average depth (ft subsea)	Average thick- ness (ft)	Average depth (ft subsea)	Average thick- ness (ft)	Acres	10 <sup>3</sup> m <sup>2</sup>
COALINGA								
East	2000	250	NP <sup>1/</sup>	--	NP	--	20216	81812
West	1850	200	NP	--	NP	--		
EAST COALINGA EXTENSION								
Nose	NP	--	6400	25	7600	625	4550	18413
Northeast	NP	--	NP	--	8000	210	3160	12788
							1390	5625
GUIJARRAL HILLS							2515	10178
Main	8000	70	-8600	350	9500	200	1790	7244
Northwest	NP	--	-8400	25	NP	--	125	506
Polvadero	8350	20	NP	--	10,700	250	560	2266
West	NP	--	-8330	30	NP	--	40	162
PLEASANT VALLEY	NP	--	NP	--	-8300	120	500	2023
1/ NP, no production						Totals	27781	112426



Table 2-Coalinga area oil fields-Cumulative net liquid production through 1981 by age of pool (From Annual Reviews, Conservation Committee California Oil Producers and Annual Reports, State Oil and Gas Supervisor)

FIELD Area	Oil ( $10^3$ barrels)			Net water ( $10^3$ bbl)	Net liquid ( $10^3$ bbl)
	Temblor	Vaqueros	Lodo		
COALINGA					
East	420,968 <sup>a/</sup>	NP <sup>1/</sup>	NP <sup>1/</sup>	532,812	1,216,973
West	263,193	NP	NP		
EAST COALINGA EXTENSION					
Nose	NP	86 <sup>b/</sup>	487,600	476,741	964,341
Northeast	NP	NP	36,054 <sup>c/</sup>	183,816	219,870
GUIJARRAL HILLS					
Main	5,448	32,831	4,399	18,351	68,001
Northwest	NP	292	NP		
Polvadero	235	NP	5,692		
West	NP	753	NP		
PLEASANT VALLEY					
	NP	NP	13,244	10,897	24,141
TOTALS	689,884	33,876	546,989	1,222,617	2,493,326 x $10^3$ bbl 396,406 x $10^3$ m <sup>3</sup>

<sup>1/</sup> NP, no production

<sup>a/</sup> May include some Lodo (Eocene) production

<sup>b/</sup> abandoned 1961

<sup>c/</sup> abandoned, 1972

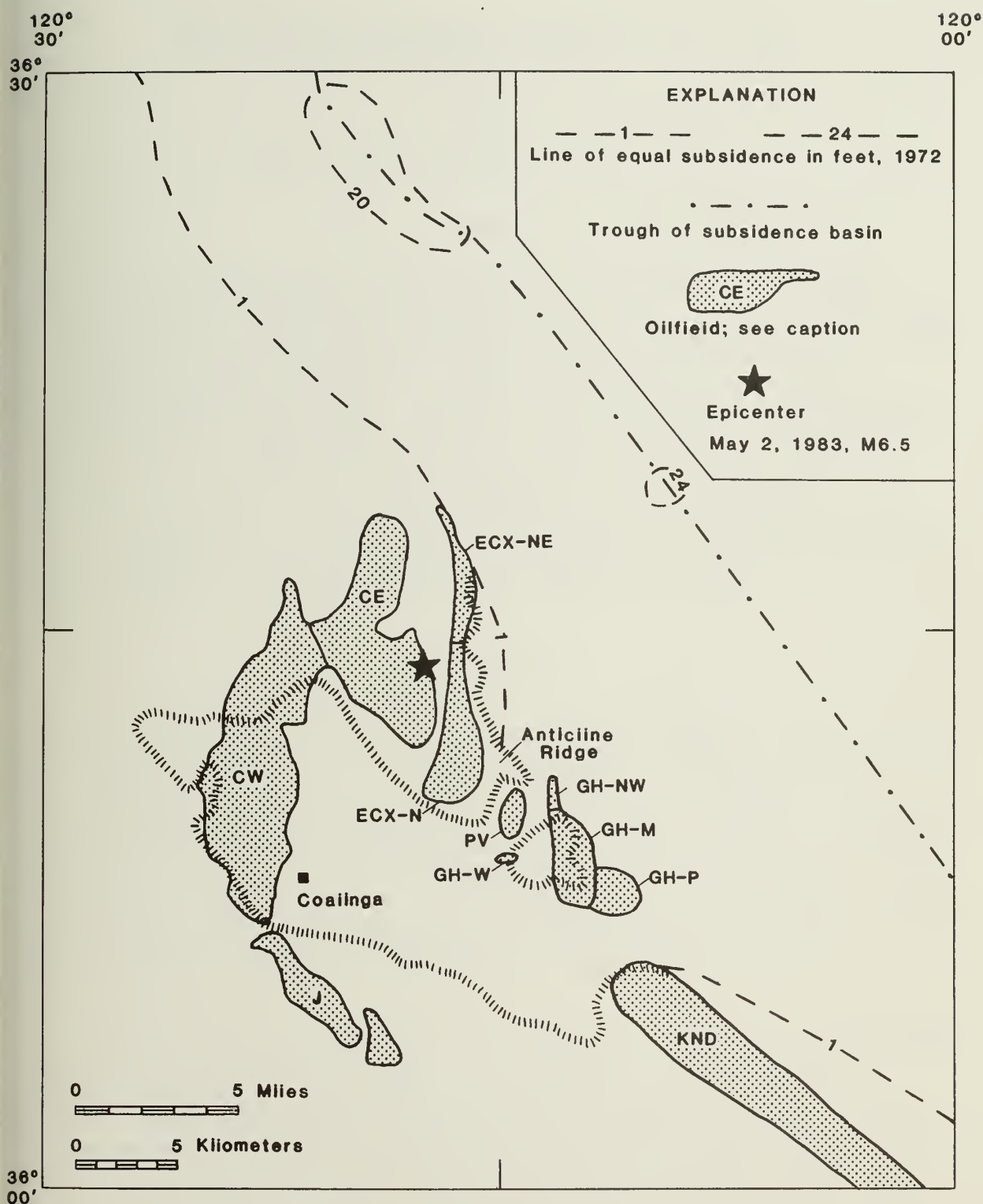


Figure 1. Map of Coalinga area showing epicenter of 2 May 1983 main shock, oil fields and areas, and west limb of northern San Joaquin Valley subsidence basin (Poland and others, 1975, fig. 17). Oil fields and areas: CE, Coalinga East; CW, Coalinga West; ECX, East Coalinga Extension: -N- Nose area, -NE- Northeast area; GH, Gujarral Hills: -M- Main area, -NW- Northwest area, -P- Polvadero area, -W- West area; J, Jacalitos; KND, Kettleman North Dome; PV, Pleasant Valley.





SURFACE FAULTING NORTHWEST OF COALINGA, CALIFORNIA  
JUNE AND JULY 1983

By

Earl W. Hart and Richard D. McJunkin<sup>1</sup>

ABSTRACT

Surface faulting occurred 12 km northwest of Coalinga, Fresno County, California, on the evening of June 10, 1983 (local time), in association with an M5.2 earthquake. Additional coseismic rupture also occurred along the same fault during the July 9, 21, and 25, 1983 earthquakes of M5.0 to M6.4. Surface rupture developed along two principal segments of a 3.3 km-long, steeply east-dipping fault zone. Reverse slip was dominant on both segments, attaining a maximum displacement of 60 cm on the northern segment and 24 cm on the southern one. A right-slip component was observed locally, attaining a maximum of 20 cm and 11 cm on the northern and southern segments, respectively. Surface rupture along the Nunez fault was a surprise, because it is a relatively minor geologic structure that was incompletely mapped and was not considered to be recently active. However, field evidence indicates that this fault had ruptured previously during Holocene time.

INTRODUCTION

On June 10, 1983, at 2010 hours (PDT) an M5.2 earthquake occurred 14 km northwest of Coalinga and was accompanied by surface faulting. This was the third of seven earthquakes that exceeded magnitude M5, beginning with the May 2 M6.7 earthquake located 14 km to the east (Figure 1). Neither of the preceding earthquakes is known to have produced surface faulting (see below for possible exception), although the vicinity of their epicenters was checked carefully by CDMG, USGS, and other geologists (Clark and others, 1983; also see Figure 1). However, each of the succeeding events--July 9, July 21 (two), and July 25--which were centered 3 to 4 km east of the June 10 rupture zone, apparently produced additional displacement along the June 10 zone of rupture. Data on these larger earthquakes are summarized in Table 1 and Figure 1.

CDMG geologists responded to the June 10 earthquake on June 13 to 15 (Hart and McJunkin), in order to document the faulting and to map location, magnitude, and sense of surface faulting as quickly as possible. Initial observations were summarized by McJunkin and Hart (1983). Field responses also were made on July 12 to 13 (McJunkin and R. Boylan) and July 22 to 23 (Hart and T. Smith), following the July 9 and 21 earthquakes, respectively, with the same purposes in mind. USGS geologists responded similarly after each event, including the July 25 earthquake. Beginning July 15, the USGS established eight monument lines, which were periodically resurveyed. Aerial photographs were flown on June 15 for the USGS investigation<sup>2</sup> and were made

---

<sup>1</sup> Geologists, California Division of Mines and Geology

<sup>2</sup> 1:7,600(approx.) scale, low-sun (morning), black and white, USGS designation GDCL

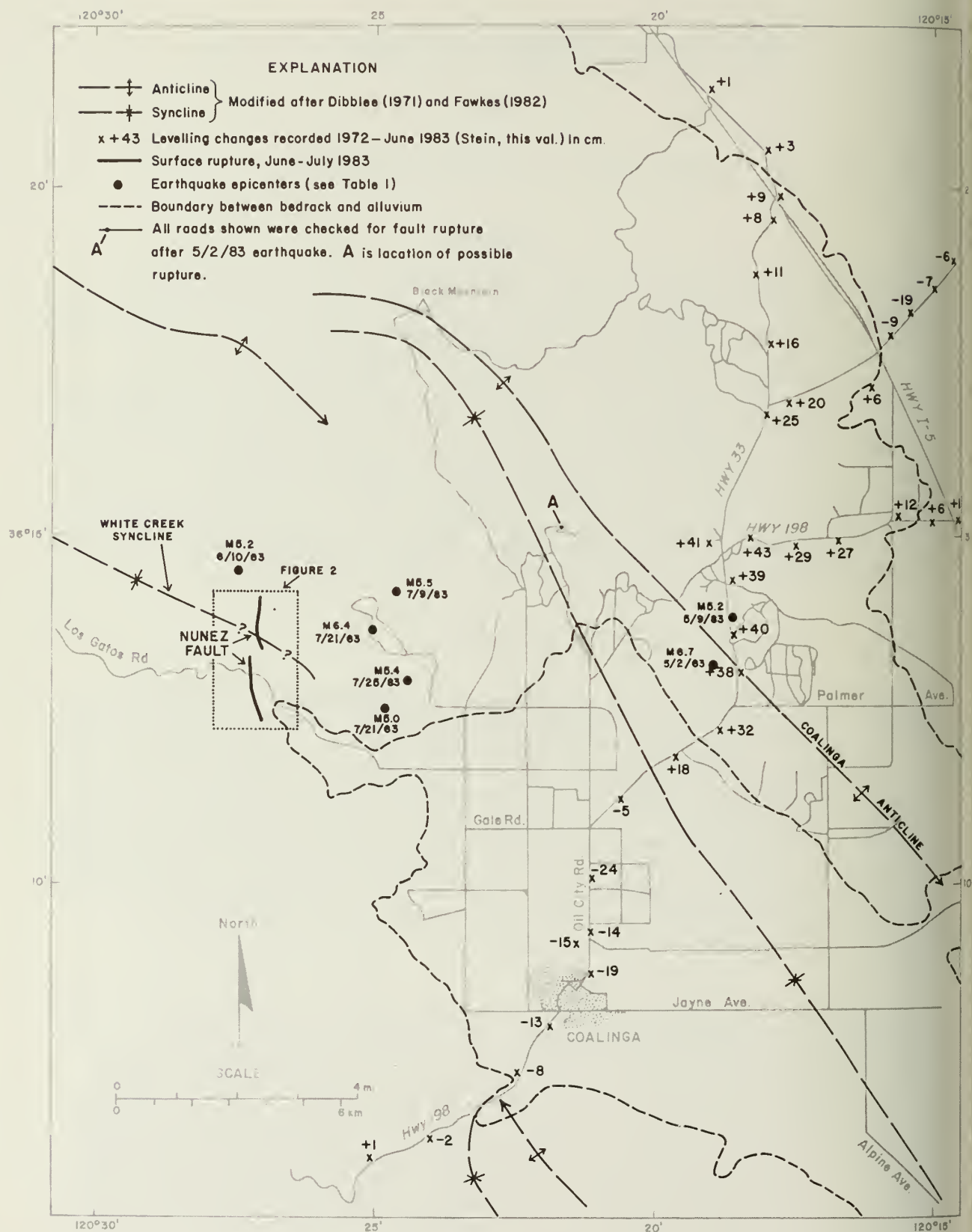


Figure 1. Map showing locations of 1983 Coalinga earthquakes, associated fault rupture, and other data.

available to CDMG. Observational data has been exchanged freely with the USGS and much of their preliminary findings (through August 9) have been kindly made available for use in this report. The observations of others, including Chevron geologists and E.J. Fowkes, also have been made available to us and are specifically cited where appropriate in this report.

The primary purpose of this report is to describe the location, sense, magnitude, and timing of the surface faulting that occurred in the Los Gatos Road area. Secondly, limited documentation is presented to suggest that new faulting coincides with pre-existing faults, and that previous recent faulting has occurred. In addition, the tectonic setting and possible causes of the faulting are briefly examined.

The surface faulting during June and July came somewhat as a surprise, inasmuch as surface fault rupture was not clearly evident following the larger May 2 earthquake. Moreover, only minor faults were known in the rupture area (Dibblee, 1971) and no Quaternary faults were known to exist. Nonetheless, considerable Quaternary tectonic deformation is evident in the Coalinga region, as shown by large-scale folding following deposition of the Tulare Formation of Pleistocene age (Dibblee, 1971; Fowkes, 1982). Evidence that crustal deformation is continuing is clearly shown by the seismicity monitored in recent years (Eaton, 1983) and by the measured uplift which has occurred across the Coalinga anticline (Figure 1).

As mentioned above, there is a possible exception to the reported absence of surface faulting associated with the May 2 earthquake. This is at locality A (Figure 1) where a 2 to 3 cm-high, 4 to 5 m-long, southwest-facing, compressional scarplet was observed May 5 in a graded road, just south of and near the crest of an east-trending ridge (NW 1/4 of NE 1/4 sec. 29, T.18S., R. 15E., Domengine Ranch 7.5-minute quadrangle). The feature which was later destroyed by grading, was characteristic of a northeast-dipping thrust and coincided with a N 30°E-dipping shear and gypsum-filled fissure in siltstone exposed in a small pit dug in the road (Photo 8). The scarp could not be followed beyond the road into the adjacent soil or fill. Although the

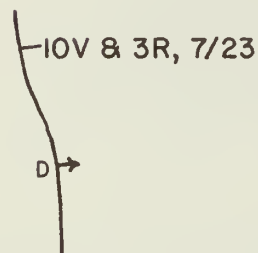
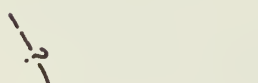
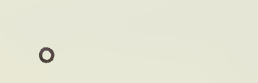
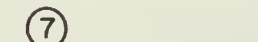
Table 1. Summary of May to July, 1983, Coalinga earthquakes larger than  $M_L$  5.0. Data from Eaton and others (this volume).

Date (PDT)	Time (hours)	Epicenter location		Magnitude ( $M_L$ )	Depth (km)
		Latitude(N)	Longitude(W)		
May 2	1643	36° 13.15'	120° 18.99'	6.7	10.2
May 9	1949	36° 13.75'	120° 18.74'	5.2	12.5
June 10	2010	36° 14.62'	120° 27.55'	5.2	4.5
July 9	0041	36° 14.20'	120° 24.54'	5.5	9.5
July 21	1940	36° 13.67'	120° 24.94'	6.4	9.2
July 21	2043	36° 12.57'	120° 24.79'	5.0	9.6
July 25	1532	36° 12.92'	120° 24.33'	5.4	9.5



Figure 2 (adjacent page). Trace of surface faulting along Nunez fault, associated with the Coalinga, California, earthquakes of June 10 and July 9, 21, and 25, 1983.

#### EXPLANATION FOR FIGURE 2

	<p>Well-defined trace of June and July 1983 fault rupture as indicated by scarps, moletracks, and cracks. Measured or estimated displacements are shown in centimeters; V is vertical offset, R is right-lateral, C is compressional. D indicates downthrown block. Date indicates month and day of observations. Arrow indicates dip of fault where observed or inferred. ( ) Parentheses indicate data from USGS.</p>
	<p>Linear zones of extensional cracks in soil suggestive of faulting, but sense and magnitude not clear. Query indicates additional uncertainty.</p>
	<p>Monument survey lines established by USGS on 7/15 (north of Los Gatos Road) and 7/23 (south of Los Gatos Road)</p>
	<p>Locality described additionally in Table 2 and text.</p>

scarplet may have been due to shaking (landslide toe), it was well developed only in bedrock, was not parallel to the slope or road, and did not appear to be associated with nearby downslope fissures that were generally oriented east-west, parallel to the road and ridgeline. Because of these facts and because it is located in steeply dipping beds on the west flank of the Coalinga anticline, we believe that the scarplet may be of tectonic origin.

Information in this report should be considered as somewhat preliminary, as the investigations of others are still in progress. Moreover, because earthquakes are continuing in the region, additional surface rupture may develop along the faults discussed here or along other faults. It is anticipated that a more complete report on surface faulting will be prepared by the USGS.

#### TECTONIC SETTING

According to Dibblee (1971) and Fowkes (1982), the fault rupture area is underlain by sandstone and shale units of the Panoche Formation (Upper Cretaceous). These bedded units dip gently to moderately and have been interpreted as being folded along the White Creek syncline and its southeasterly projection. This and other large folds of the region are shown on Figure 1. However, limited field observations and aerial photographic interpretations indicate that the strata in the fault area are more complexly warped and folded, and also are cut by a number of minor north-trending faults. These structures are only partly mapped by Dibblee and Fowkes. Elements of the Nunez fault, including some of the newly ruptured ground, can be observed on the June 15 aerial photographs. In addition, the fault can be

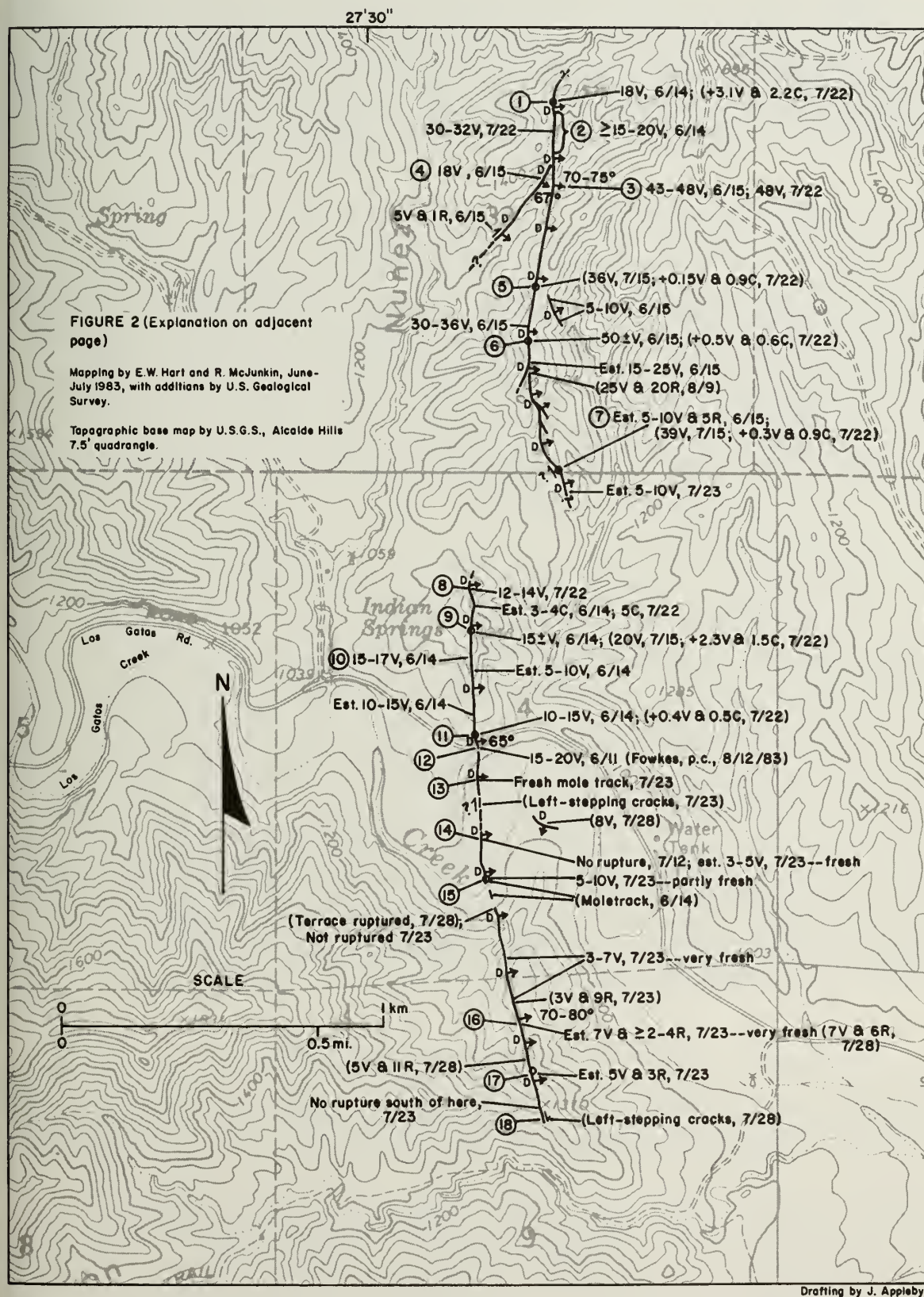


Figure 2. Nunez fault.



seen to extend south of the rupture zone into section 9 and discontinuously south of there into section 16. There is little to suggest that the Nunez fault is structurally important, either in terms of displacement or length. Other minor north-trending faults also occur to the south and west of the Nunez fault, and some of these were mapped by Dibblee and Fowkes. The orientation and close grouping of these faults suggest a common tectonic origin.

The relationship of the Nunez fault (and perhaps some of the other nearby faults) to other tectonic features in the area is not entirely clear. The fault crosses or interrupts the White Creek syncline (Figure 1) but has no obvious genetic relationship to it. The Nunez fault has a similar orientation to and lies on trend with other north- to northwest-trending faults (mostly right-lateral) in the New Idria quadrangle to the north (Dibblee, 1971) and the more distant Ortigalita fault, the latter being an important, late Quaternary right-lateral fault. Because these latter faults are coincident with a linear zone of active seismicity (Eaton, 1983, Figure 2), it is tempting to speculate that the Nunez fault is a southward extension of that zone. However, the geometry and sense of displacement of the Nunez fault do not seem to fit that right-lateral system.

Most likely, the Nunez fault is related to the compressive system of folds to the east (Figure 1) that have been active during Quaternary time (Dibblee, 1971; Jennings, 1977): The oversteepened, southwest limb of the Coalinga anticline is compatible with a northeast-dipping reverse fault at depth, which also fits the location and one of the first-motion solutions of the M6.7 earthquake of May 2, 1983 (Eaton and others, this volume). Moreover, levelling surveys show that the Coalinga anticline has been uplifted as much as 43 cm and the synclinal valley to the southwest depressed as much as 24 cm between 1972 and June 1983 (Figure 1; Stein, this volume). Although not all the facts have been examined, one might speculate that east-west crustal shortening is occurring in the Coalinga area and that the Nunez fault is genetically related to this tectonic model. Supporting this model is the presence of an east-side-up basement fault associated with the Kettleman Hills anticline (Wentworth, this volume) and east-dipping reverse and thrust faults associated with folds of the Pyramid Hills and Devils Den oil fields to the south (California Division of Oil and Gas, 1973). The association of these and other parallel folds along the west side of the San Joaquin Valley (Jennings, 1977) suggests a common tectonic cause for these features.

#### SURFACE RUPTURE OF THE NUNEZ FAULT

Surface fault rupture, about 12 km northwest of Coalinga, occurred in association with the June and July 1983 earthquakes (Figure 1). Rupture was distributed along two principal fault segments and their branches, which extend over a total distance of 3.3 km. The ruptures are systematic and characterize steeply east-dipping fault strands along which predominant reverse slip has occurred. The northern segment had a maximum of 60 cm of reverse slip with a local right-slip component as large as 20 cm. The southern segment had a maximum of 24 cm of reverse slip to the north, which diminished southward where a right-slip component (11 cm maximum) is dominant. Detailed observations of surface rupture are summarized in Figure 2 and Table 2 and are discussed below.



The ruptured segments, which presumably connect at depth, are herein referred to as the Nunez fault, after Nunez Canyon just west of the rupture zone. Only the southern end of the fault was previously identified on published maps (Dibblee, 1971; Jennings, 1977). Although the fault was shown to be part of a longer, branching fault on unpublished maps of Chevron, Inc. (R.C. Erickson, personal communication, June 1983), that fault only partly coincides with the 1983 fault ruptures. None of the previous references identified the Nunez fault as being recently active.

#### Initial Observations

Ground rupture associated with the Nunez fault was first observed around 0300 hours on June 10--about 20 minutes after the M5.2 earthquake--by a local rancher driving along Los Gatos Road (E.J. Fowkes, personal communication, August 1983). E.J. Fowkes of West Hills College verified surface offset of the road about 2100 hours and returned the following morning to measure and photograph the rupture features (Photos 1 and 2). Los Gatos Road was previously checked for faulting by CDMG, USGS, and other geologists following the larger May 2, 1983 earthquake, but none was found. Thus, it can reasonably be assumed that the Nunez fault ruptures developed concurrently with the June 10 earthquake.

#### Description of Ruptured Ground

The fault ruptures occupy narrow, rather continuous north-trending zones of compressional scarps, moletracks, and associated fissures in soil (Photos 3 and 5). The zones generally are 0.5 to 2 m wide, and are somewhat sinuous in detail. The scarps and moletracks consistently face west (with only minor exceptions) and are convex upwards, clearly demonstrating that reverse displacement has occurred on an east-dipping fault. Where sufficient slip has occurred, the dry grass and soil on the downthrown block have been overridden by soil of the hanging-wall block. These compressional features are best developed on west-facing slopes and along the crests of ridges. On east-facing slopes, the compressional features tend to form sidehill benches and, in some cases, occur along pre-existing sidehill benches (e.g. at locality 2). Because of the tall grass, the minimum scarp height detectable is about 2 to 3 cm on gentle slopes and about 3 to 5 cm on steeper slopes, except where downhill-movements of soil (from shaking) obscured the fault features.

Locally, systematic left-stepping fractures are present along the rupture zone, indicating a component of right-lateral slip. Such left-stepping cracks are well developed and dominant in section 9, but they also were observed at locality 7, southwest of locality 4, south of locality 6, and south of locality 13.

Tensional fractures, open as much as 2 to 3 cm, also are common on the downthrown block for a distance of 2 to 15 m to the east of the compressional rupture zone. In some cases, these fissures show normal dip-slip displacement. These features are most common on west-facing slopes and ridge tops. Very likely, they connect with tensional fractures in bedrock (as

indicated in the roadcut at locality 12; see Photo 2) and presumably are due to the upward flattening of dip of the reverse fault as it approaches the ground surface.

### Displacements

As described above, the surface-rupture features are indicative of reverse movement along two principal strands of an east-dipping fault and its branches. That the fault strands dip steeply eastward is indicated by the linear traces that deflect only modestly eastward across drainages and westward across ridges and spurs. A dip of about  $65^{\circ}\text{E}$  was observed in bedrock at locality 12. Dips of  $67^{\circ}$  to  $80^{\circ}$  also were measured in soil at localities 3, 4, and 16. The only exception to the easterly dips is the minor secondary fault, 300 m east of locality 14, which apparently dips to the south (M. J. Rymer, USGS, personal communication, August 1983).

An effort was made to measure or estimate the amount of apparent slip for various segments of the Nunez fault. However, dip-slip components could not be measured directly in most cases--partly because the offset surfaces were uneven or warped and because the exact dip and direction of slip could not be observed in soil. Consequently, the amount of dip-slip was approximated by measuring or estimating the height of scarps across matched surfaces. Horizontal slip components were determined by measuring extensional openings of the left-stepping cracks.

The maximum vertical displacements for the Nunez fault occurred along the northern rupture segment where 57 and 50 cm were measured at localities 3 and 6. Calculated dip-slip components for these localities are about 60 and 53 cm, respectively. About 21 cm of vertical offset was measured near the north end of this segment (locality 1) and 39 cm near the south end (locality 7), where about 5 cm of right-lateral slip was estimated. Right-lateral slip of about 20 cm along a 25 cm-high scarp also was reported 100 m south of locality 6 by Rymer. This right-slip component was not observed until August 9 and may have been overlooked during previous observations of CDMG and USGS geologists. The southern segment had less displacement with a maximum of 24 cm of dip slip being calculated at locality 9 and nearly as much at Los Gatos Road (locality 12). Dip-slip displacement diminished significantly south of Los Gatos Road. However, right slip became a prominent component in section 9, reaching a maximum of 11 cm near locality 17.

### Timing of Surface Faulting

Based on field observations following the earthquakes on June 10 and July 9, 21, and 25, 1983, and on interpretations of aerial photographs flown June 15, some general statements can be made regarding the timing of surface faulting. In general, the location, sense, and magnitude of ruptures observed (Figure 2 and Table 2) agree very well with the earthquake locations and depths (Figure 1 and Table 1).

June 10 earthquake. Most of the surface rupture mapped apparently occurred during this event. Rupture occurred on both main segments, as well as on their branches and the secondary faults north of Los Gatos Road, as the features observed were very fresh and dry grass was knocked down (the grass

was still green on May 2). South of Los Gatos Road, rupture apparently was somewhat discontinuous, although moletracks and cracked ground were reported locally by E.J. Fowkes, P. Hughes, R.C. Erickson, and M.J. Rymer in June (personal communications). Weak tonal features observed on the June 15 aerial photographs tend to support these reports. However, the inability of CDMG and USGS geologists to follow these rupture zones as continuous features in early June suggests that many of the features observed south of Los Gatos Road in July were not formed in June.

July 9 earthquake. Observations made between July 9 and 21 suggest that minor additional reverse faulting occurred along the rupture zones north of Los Gatos Road. Some of the scarps appeared somewhat higher (especially at locality 3) and the rupture zone appeared slightly better defined between localities 8 and 9. No additional ruptures were observed south of Los Gatos Road.

July 21 earthquakes. There were two earthquakes of M6.4 and M5.0 on this date, one or both of which were associated with significant additional reverse and right-slip faulting along both segments of the Nunez fault. Field mapping revealed a nearly continuous zone of apparently new ruptures south of Los Gatos Road on July 23. Some of the delicate scarps, moletracks, and cracks occurred in the river terrace (localities 13 to 15) that had been heavily grazed by cattle just prior to these events and probably would not have been preserved if they were caused by earlier events. The ruptures observed across a dirt road at locality 14 on July 23 were not seen when the road was checked July 13. South of Los Gatos Creek, the rupture zone was very continuous and easy to follow on July 23, and very likely would not have been overlooked during previous observations. Additional minor reverse faulting also occurred north of Los Gatos Road, as documented by resurveying of level lines by the USGS at localities 1,3,5,6,7,9, and 11 (J.J. Lienkaemper, personal communication, August 1983). Observations at localities 7 and 10 also suggest additional slip associated with these earthquakes.

July 25 earthquake. No additional slip was measured or reported north of Los Gatos Road along the USGS monument lines, although possible minor slip was recorded on a nail line along Los Gatos Road by the USGS (Lienkaemper). A narrow, terrace surface south of Los Gatos Creek, not observed to be ruptured on July 23 by CDMG, was reported to be faulted on July 28 (M.J. Rymer, p.c., August 1983). In addition, the southern end of the fault apparently propagated 50 to 100 m further south (Rymer) than observed by CDMG on July 23. USGS geologists also reported as much as 9 and 11 cm of right-lateral slip near localities 16 and 17 (Rymer), which is more than we estimated on July 23. It is uncertain if this represents new rupture or if we underestimated the magnitude of right slip on July 23.

#### Evidence of Previous Recent Faulting

The recent ruptures on the Nunez fault raise questions regarding the existence of an older fault along the line of rupture and whether such a fault had evidence of previous recent faulting. Although only a portion of the Nunez fault was recognized prior to the June 10 earthquake, there is evidence of truncated bedding and north-trending shears both in the field and on aerial photographs to verify the existence of this fault, as well as the existence of other minor north-trending faults nearby. Evidence of previous faulting includes: 1) the truncation of bedding at locality 12 and elsewhere, 2)



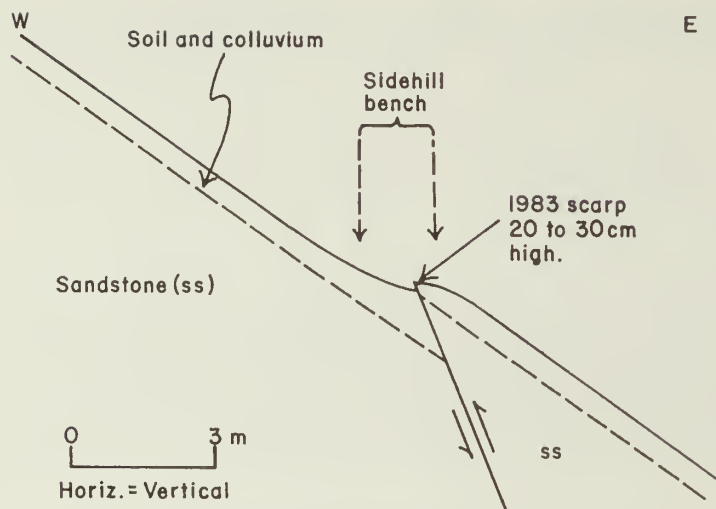


Figure 3. Idealized cross-section of sidehill bench at locality 2. Inferred subsurface relations indicate previous offset of soil-colluvial unit. Bench is not erosional.

steeply-dipping, north-trending shears and fractures in bedrock adjacent to the ruptures, 3) a groundwater barrier at locality 3, and 4) north-trending tonal features and vegetation contrasts both along and beyond the ends of the rupture zones.

Evidence for previous recent faulting was observed in several places, based largely on the coincidence of rupture with existing geomorphic features. Most prominent of these is the linear sidehill bench and sharp break in slope at locality 2. This bench is a rather continuous, though subtle, feature that is 300 m long and as much as 1 to 2 m wide (photo 4). Although the bench has not been surveyed to quantify its size and shape, it seems to be too large in places to have been produced solely by the June and July faulting. On the other hand, the bench lacks evidence of being caused by differential erosion. Because the slopes above and below it are steep (at least  $30^\circ$ ) and the downhill movements of soil and colluvium presumably are rapid, it must be concluded that the bench is an ephemeral feature of Holocene age. Its coincidence with the June and July ruptures indicate that previous, recent reverse faulting must have occurred along it. Figure 3 is a schematic section showing the possible subsurface relationships that may exist at locality 2.

Subtle west-facing scarps on west-facing slopes also suggest previous recent faulting consistent with down-to-the-west movement (e.g. near localities 7, 10, 11, 12, and 16). Subtle west-facing scarps, less than half a meter high in young (Holocene?) alluvium near localities 13 and 15 also are suggestive of previous recent faulting (although they could be erosional features), as is the abrupt, eastward thinning of soil and colluvium exposed in the roadcut at locality 12 (Photo 2). In addition, the very linear fault at Hill 1310 (mapped by Dibblee, 1971) crosses a right-laterally deflected segment of Salt Creek, which is weakly suggestive of recent right slip for this segment of the Nunez fault. These features are admittedly subtle and seemingly could have alternate explanations for their causes, if it were not for the coincidence of surface faulting that occurred in June and July.

Based on the magnitude and nature of the geomorphic features observed in the field, we conclude that previous Holocene rupture, similar in sense to the June and July rupture, probably occurred along the Nunez fault. Assuming that the previous displacements were comparable in magnitude to the June and July events, then repeated events probably occurred during Holocene time (e.g. see Figure 3). However, detailed trench evaluations and dating would be needed to verify these assumptions.

#### SUMMARY AND DISCUSSION

1. The observed surface ruptures along the Nunez fault are clearly tectonic and identify an east-dipping reverse fault with predominant dip-slip displacement and, locally, a minor right-slip component. Although two separate rupture segments were mapped, these probably connect with a common fault at depth. Observations show that most of the rupture occurred on June 10, with the largest offset being along the northern segment. Increased displacement occurred coseismically with the July 9, 21, and 25 earthquakes along the earlier zone of ruptures, and also extended the rupture zone southward.
2. The locations, depth, and general southward migration of the June and July earthquakes are compatible with the surface rupture. In addition, these events have focal mechanisms indicating reverse or thrust slip with minor right slip along an east-dipping fault zone (Eaton and others, this volume).
3. Evidence of a pre-existing fault along the Nunez rupture zone is demonstrated locally by bedrock exposures. Moreover, subtle geomorphic features (scarps, sidehill benches) indicate previous Holocene faulting. Such features are best developed north of Los Gatos Road where the 1983 dip-slip displacements were greatest. Nonetheless, the tectonic geomorphic features are subtle, suggesting a low slip-rate for the Nunez fault.
4. The Nunez fault presumably is tectonically related to folding, faulting, and general crustal shortening in the Coalinga area and elsewhere along the western margin of the San Joaquin Valley. The May 2 earthquake apparently occurred along a northeast-dipping reverse fault, at the Coalinga anticline, that also is consistent with crustal shortening.
5. The lack of clear evidence of surface faulting on May 2--indeed the lack of a significant surface fault--should be of considerable concern for geologists, seismologists, and others who determine maximum credible earthquakes for development sites in different parts of the state. In most cases, such determinations are based on the existence of recently active faults (Slemmons and Chung, 1982). However, no recently active faults were previously recognized in the Coalinga area. The only evidence of recent tectonic activity in the Coalinga anticline area, aside from recorded earthquakes, is the folding of Quaternary strata. It seems apparent that recently active folds (especially anticlines) should be considered as possible loci for future damaging earthquakes. For planning and design purposes, methods need to be devised to estimate the maximum probable or credible earthquake that can be expected for recently active folds and their associated subsurface faults.

## ACKNOWLEDGEMENTS

We wish to acknowledge the assistance of CDMG geologists R. Boylan and T.C. Smith, who assisted in the field mapping. Field mapping and observations of USGS geologists M.M. Clark, M.J. Rymer, K.K. Harms, and J.J. Lienkaemper were freely made available for this report. Their information was a significant contribution to this report and is greatly appreciated. Other observational data were provided by E.J. Fowkes of West Hills College and R.C. Erickson and P. Hughes of Chevron, Inc. We wish to express our thanks to K. Birdwell, J. Nunez, and other residents of the Los Gatos Creek area, who provided access to their properties and initial information on possible fault rupture. Technical reviews of this manuscript were performed by R.H. Sydnor, M.J. Rymer, and M.M. Clark.

## REFERENCES

- California Division of Oil and Gas, 1973, California oil and gas fields, Volume 1: north and east central California (not paginated).
- Clark, M.M., Harms, K.K., Lienkaemper, J.J., Perkins, J.A., Rymer, M.J., and Sharp, R.V., 1983, The May 2, 1983 earthquake at Coalinga, California: The search for faulting in R.D. Borchardt (compiler), The Coalinga earthquake sequence commencing May 2, 1983: U.S. Geological Survey Open-file Report 83-511, p. 8-11.
- Dibblee, T.W., 1971, Geologic maps of the Coalinga, Joaquin Rocks, New Idria, and Priest Valley 15-minute quadrangles: U.S. Geological Survey Open-file Report 71-87.
- Eaton, J.P., 1983, Seismic setting, location, and focal mechanism of the May 2, 1983, Coalinga earthquake in R.D. Borchardt (compiler), The Coalinga earthquake sequence commencing May 2, 1983: U.S. Geological Survey Open-file Report 83-511, p. 20-26.
- Fowkes, E.J., 1982, An educational guidebook to the geologic resources of the Coalinga district, California: West Hills College, Coalinga CA, 260 p. (Contains geologic map of Coalinga area and text and figures on stratigraphy, structure, references, and field trips.)
- Jennings, C.W., 1977, Geologic map of California: California Division of Mines and Geology, Geologic Data Map No. 2, 1:750,000 scale.
- McJunkin, R.D., and Hart, E.W., 1983, Ground rupture, Coalinga earthquake of 10 June 1983: California Geology, v. 36, n. 8, p. 182-184.
- Slemmons, D.B., and Chung, D.H., 1982, Maximum credible earthquake magnitudes for the Calaveras and Hayward fault zones in E.W. Hart, S.E. Hirschfeld, and S.S. Schulz (editors). Proceedings--Conference on Earthquake Hazards in the Eastern San Francisco Bay Area: California Division of Mines and Geology, Special Publication 62, p. 115-124.



Table 2. Descriptions of observed surface faulting associated with the June 10, July 9, July 21, and July 25, 1983, earthquakes. CDMG data unless otherwise indicated. Locality numbers are identified on map, Figure 2.

Locality	Observations
1.	Fresh, 18 cm-high, west-facing compressional scarp with extensional cracks on upthrown block, 6/14; aligns with other scarps and moletrack features to N and S. Scarp first seen by rancher on 6/11 or 6/12 (J. Nunez, p.c., 6/13). USGS measured 3.1 cm additional uplift and 2.2 cm shortening of monument line (established 7/15) just S of road on 7/22; no additional slip measured 7/27. Data indicate reverse movement on east-dipping fault associated with earthquakes of 6/10, 7/9(?), and 7/21.
2.	Continuous, narrow zone of ruptured ground with west-facing scarps along outer edge of pre-existing, sidehill bench on east-facing slope. Estimated vertical displacement of 15 to 20 cm or more on 6/14 along east-dipping reverse fault. Offsets appeared somewhat larger on 7/22, with maximum scarp height of 30-32 cm observed at one point.
3.	Fresh, well-developed, west-facing, compressional scarp along cattle trail in bottom of gully; estimated offset to be 43 to 48 cm on 6/15. Fissures and moletracks to N and S in moist soil adjacent to gully indicate 70° to 75° east-dipping reverse fault. Observed offset was 48 cm on 7/11. USGS observed offsets of 42 cm on 6/15 and 48 cm on 7/13. However, later USGS level surveys along the centerline of cattle trail indicate 57 cm uplift on 7/15, plus 0 to 5 cm on 7/22, and 0 cm on 7/27.
4.	Very fresh, overhanging scarp 18 cm high with fault plane exposed in soil along sidehill bench on 6/15; fault plane strikes N 50° E and dips 67° SE.
5.	Large, west-facing scarp and associated moletrack features near crest of ridge, indicate east-dipping reverse fault on 6/15. USGS monument line surveyed on 7/15 indicates 36 cm total uplift. On 7/22, USGS survey showed minor additional movement of 0.15 cm uplift and 0.9 cm compression. No movement detected 7/27.
6.	Fresh compressional scarp in soil with east-side-up vertical offset estimated to be about 50 cm on 6/15. Nearby USGS monument line indicated 50+20 cm total uplift on 7/15 with additional 0.5 cm uplift and 0.6 cm compression on 7/22. No movement detected 7/27. About 100 cm to south, USGS observed 20 cm of right-lateral slip on 8/9 along a previously observed 25 cm-high scarp. This right slip component was not previously observed, but it may have been overlooked initially (M.J. Rymer, p.c.).

7. Zone of fresh left-stepping moletracks and cracks along general southwest-facing scarp; estimated roughly 5 to 10 cm of vertical uplift on individual scarps and roughly 5 cm right slip offset at fence on 6/15, but accurate measurements not possible. Fault rupture could not be traced to south in tall grass on 6/15, but discontinuous, 3 to 4 m wide zone of low moletracks, west-facing scarps, and new(?) cracks could be followed southward an additional 150 m with difficulty on 7/23. USGS monument-line surveys indicated 39+3 cm vertical uplift across the scarp on 7/15 with an additional 0.3 cm uplift and 0.9 cm compression on 7/22. No tectonic change reported for 7/27 survey.
8. East-west wire fence along steep, east-draining gully observed to be shortened (slack wire) across the projection of the fault on 6/14. Observations on 7/22 suggest further shortening, crudely measured to be 5 cm.
9. Fresh west-facing, moletrack-like scarp estimated to be about 15 cm high on 6/14 and possibly a little higher on 7/22. USGS measurements along monument line indicated the scarp to be 20 cm high on 7/15; additional uplift of 2.3 cm and shortening of 1.5 cm were measured 7/22. No additional movement detected 7/27.
10. Two fresh(?) scarplets observed 7/22 in loose soil of recently used foot path, possibly suggesting renewed uplift along degraded, west-facing scarp initially observed 6/13. Total scarp height estimated to be 15 to 17 cm on 7/22. Continuous 5-10 cm high scarp observed 6/14 this vicinity, but specific locality not measured or estimated at that time.
11. Well-defined, 1 to 2 m wide zone of moletracks, compressional scarp, and cracks; scarp faces west and estimated to be 10 to 15 cm high on 6/13. USGS monument-line surveys indicate 0.4 cm additional uplift and 0.55 cm compression between 7/15 and 7/22. A 5 to 15 m wide zone of north-trending tension cracks open as much as 5 to 6 cm, observed 6/13 in soil immediately east of the fault, suggesting that east-dipping fault plane flattens upward.
12. Paved road offset on 6/10 and west-facing scarp observed to be 15-20 cm high on 6/11 (E.J. Fowkes, p.c., 8/12). Road was repaved 6/14 and no cracks developed thereafter through 7/27. However, surveys of recently-established USGS nail-line indicated 2 mm of east-side-up movement between 7/23 and 7/27. Pre-existing fault with fresh fractures was exposed in roadcut; dip is about 60-70°E in bedrock, but dip of fault flattens upward (to west) in soil and appears to connect with moletrack/scarp feature in soil. Tension cracks, open to 2 cm, occur in conglomerate and sandstone east of fault and align with open cracks in soil to north.

13. Narrow sinuous west-facing moletrack 7 to 10 cm high, with fresh, delicate features seen in soil of recently grazed field (young terrace) on 7/23. Moletrack indicates probable slip along reverse fault associated with 7/21 earthquakes. Possible cracks and moletrack observed nearby (?) on 6/11 (Fowkes, 6/13). Open cracks in narrow zone to south reported by USGS on 7/28 to be partly left-stepping, suggesting some right slip. Pre-existing(?), low, west-facing scarp in very young terrace surface suggests previous Holocene displacement.
14. Fresh, west-facing scarples in dirt road estimated to be 3 to 5 cm high on 7/23. No fault features or cracks observed at this locality on 7/12; indicates reverse slip along east-dipping fault associated with 7/21 earthquakes.
15. Low, sinuous moletrack and west-facing scarp about 5 to 10 cm high observed 7/23, partly very fresh and more or less continuous with newly ruptured ground to north. Some discontinuous moletracks reported in this area by E.J. Fowkes on 6/11 and M. Rymer (USGS) on 6/14. Probable rupture on 6/10 and 7/21.
16. Zone of very fresh, left-stepping cracks and west-facing scarp in cattle trail on 7/23. Estimate 7 cm uplift and at least 2 to 4 cm right slip along 70-80°E-dipping fault plane exposed in soil; fault plane is grooved, showing oblique slip (photo 7). USGS measured 7 cm vertical and 6 cm right-slip displacement on 7/28. About 100 m to south, USGS measured maximum of 11 cm right slip on 7/28, more than recognized by CDMG on 7/23. Freshness of features indicates reverse and right-lateral displacements along steeply east-dipping fault associated with 7/21 and possibly 7/25 events. No previous clear evidence of fault-rupture reported for this general locality prior to 7/23 by CDMG or USGS although "crack zone" reported in vicinity about 6/28 (P. Hughes of Chevron, Inc., p.c., 8/11).
17. Fresh, well-developed, left-stepping cracks and sharply defined moletracks in 1 to 2 m-wide zone observed 7/23. About 3 cm right-lateral slip is indicated by extensional opening of cracks. Consistent west-facing scarps indicate about 5 cm vertical offset (up on east). USGS installed monument line on 7/27; USGS observed 1.5 cm vertical and 2 cm right-lateral offset on 7/28.
18. Zone of left-stepping cracks (without scarp) observed by USGS on 7/28; indicates minor right-slip displacement. Left-stepping cracks not observed by CDMG on 7/23.





Photo 1. View to east of 15 to 20 cm-high scarp on Nunez fault where it crosses Los Gatos Road, just before road was repaired on June 11, 1983 (locality 12). (Photo courtesy West Hills College, Coalinga.)



Photo 2. Looking north at Nunez fault in Los Gatos Road cut. Reverse fault of June 10 dips about  $65^{\circ}\text{E}$ , as shown by alignment of scarp in road and cracks in cut (partly covered by debris). Dip of fault flattens upward through soil unit (arrows), emerging as scarp and moletrack features at surface (to left of photo). Fault separates conglomerate and sandstone on right from sheared material. Note that soil thins abruptly to east, suggesting previous recent faulting. Also note tension cracks in bedrock (upper right). (Photo courtesy West Hills College, Coalinga.)

Photo 3. Looking north at 18 cm-high compressional scarp in dirt road on 14 (locality 1). Feature is indicative of east-dipping reverse fault.



Photo 4. View to west of trace (arrows) of Nunez fault at locality 2. Reverse movement on fault, which dips steeply toward east, has created sidehill bench by previous displacement on east-facing slope. Scarp formed by recent faulting, ranging from 20 to 30 cm, coincides with bench.





Photo 5. Looking east at 0.5 m-high scarp on ridgecrest at locality 6 on June 15.



Photo 6. View to south of slackened wire in shortened fence caused by reverse slip on east-dipping Nunez fault, which passes between posts (locality 8).





Photo 7. Looking northeast at fresh ruptures formed along Nunez fault on July 21 (locality 16). Scarp and left-stepping cracks indicate oblique slip along steeply east-dipping fault. Fault plane in soil dips steeply east. Photo taken July 23.



Photo 8. Looking southeast along southwest-facing scarplet (arrows) in road at locality A (Figure 1). Feature indicates 3 to 4 cm of reverse slip along east-dipping fault, formed during May 2 earthquake. Thrust feature, which aligns with N30°E-dipping bedrock shears exposed in pit, may be tectonic (see text). (Photo by W.A. Bryant, 5/6/83).



## Section 3

# THE EARTHQUAKE SEQUENCE





THE 1983 COALINGA EARTHQUAKE SEQUENCE:  
MAY 2 THROUGH AUGUST 1

by

Robert A. Uhrhammer<sup>1</sup>, Robert B. Darragh<sup>2</sup> and Bruce A. Bolt<sup>3</sup>

ABSTRACT

On May 2, 1983, at 2342 UTC, a large earthquake occurred in the vicinity of Coalinga, California (epicenter  $36.23^{\circ}$  N,  $120.29^{\circ}$  W). The earthquake had a mean Richter magnitude of 6.7 and a maximum Modified Mercalli Intensity of VIII. No foreshocks were observed on U.C. seismographs for  $M_L \geq 1.5$ . By August 1, 1983, an aftershock sequence of 147 earthquakes of magnitude 3.0 or larger had occurred in the region. The two largest aftershocks of  $M_L$  5.6 and 6.0 occurred 3 min 27 sec and 80 days after the mainshock, respectively. A cumulative plot gives a b-value for the sequence of  $0.69 \pm 0.057$  for the interval of May 2 to August 1, 1983. This sequence follows Omori's relation with index 0.75.

The local rate of seismicity from historical catalogs, compiled at the University of California Seismographic Stations, yielded a value of 0.0062 earthquakes per year for  $M_L \geq 6.7$ . It follows that the average interoccurrence time for these events is 161 years and the Coalinga mainshock is not an improbable earthquake in either time or place.

A moment of  $2.3 \times 10^{25}$  dyne-cm for the mainshock was estimated from broadband displacement seismograms recorded at Jamestown ( $\Delta \approx 191$  km) and Berkeley ( $\Delta \approx 252$  km). The moment and the rupture area inferred from the aftershocks suggest a mean fault displacement of 20 cm. Seismic moments of all earthquakes with  $M_L \geq 4.0$  were estimated from Wood-Anderson seismograms recorded at Berkeley ( $\Delta \approx 252$  km). The moment for the mainshock computed from the Wood-Anderson records agrees well with the seismic moment estimated from the broadband displacement seismograms.

The focal mechanism for the mainshock is anomalous in that the tension axis trends S  $30^{\circ}$  W, because east-west extension is typically observed for earthquakes that occur in the central coast region of California.

INTRODUCTION

A damaging earthquake of Richter magnitude 6.7 occurred on May 2, 1983 (4:42 pm PDT) at the west margin of the San Joaquin Valley of California 15 km northeast of the city of Coalinga (population about 7000). The mainshock was

<sup>1</sup>Associate Research Seismologist, Seismographic Station, University of California, Berkeley.

<sup>2</sup>Research Assistant, Seismographic Station, University of California, Berkeley.

<sup>3</sup>Director, Seismographic Station, University of California, Berkeley.

followed 3 min 27 sec later by a large aftershock ( $M_L = 5.6$ ) that added to the duration of shaking and damage (see Figure 1). There were 61 aftershocks with  $M_L \geq 3.0$  and 13 aftershocks of magnitude  $M_L \geq 4.0$  in the first twenty-four hours of the sequence (see Table 1).

The failure to find fault rupture at the surface for the 6.7 mainshock was initially a surprise. Following the June 11 aftershock ( $M_L = 5.1$ ), surface rupture was observed to the west of Coalinga. The length of this rupture extended during subsequent earthquakes in July. These aftershocks are believed to lie on a different fault or faults from that of the May 2 event.

This report summarizes observations largely from the U.C. Berkeley seismographic network and is concerned with the following general seismological aspects: expectation of occurrence from historical seismicity; estimation of local magnitude ( $M_L$ ); estimation of local intensity ( $I_0$ ); estimation of seismic moment and fault mechanism; and a statistical analysis of the sequence.

### HISTORICAL SEISMICITY

Epicenters of earthquakes located in the Coalinga region from 1962 through 1982 and catalogued by the University of California (Bolt and Miller, 1975, and subsequent Seismographic Station Bulletins) are shown as full circles in Figure 2. Moderate seismicity is pervasive along the eastern front of the Coast Range from the Kettleman Hills northwest through Coalinga. In October, 1982, a sequence of four  $M_L \geq 3.0$  events, with mainshock  $M_L = 5.4$ , occurred 25 km northwest of Coalinga. A sequence in 1975, centered 40 km from Coalinga, had 14 earthquakes with  $M_L \geq 3.0$  (see Figure 2).

In all, 91 earthquakes with  $M_L \geq 3.0$  occurred in the eastern part of the central Coast Ranges from 1962 through 1982 in the area bounded by  $35.8^\circ$  N and  $37.0^\circ$  N latitude and by a line just east of the San Andreas fault. From the cumulative number of earthquakes greater than or equal to  $M_L = 3.0$ , maximum likelihood regression yielded a b-value of  $0.94 \pm 0.099$ . Removal of aftershocks from this sample decreased the number of earthquakes to 69 and gave  $b = 0.89 \pm 0.107$ .

The rate of seismicity ( $r$ ) estimated from the historical data is  $r = 10^{(2.3 - 0.67M_L)}$  earthquakes per year of magnitude  $M_L$  or larger and the corresponding variance is  $\sigma_r^2 = 5.3r^2$  ( $0.052 - 0.029 M_L + 0.0042 M_L^2$ ). The rate is normalized to a 100 km segment of the coast range. Table 2 gives the rate of seismicity, the standard error, and the 95 percent confidence intervals of the rate for the area. For magnitude 6.7 and greater events, the rate is  $0.0062 \pm 0.0030$  earthquakes per year with an average interoccurrence time of 161 years. Thus, the  $M_L$  6.7 earthquake that occurred on May 2 is not an unexpected event in either size or general location. A magnitude 6.0 earthquake could be expected in a 100 km long section of this part of the Coast Ranges (east of the San Andreas fault) about every 55 years on the average. It should be noted that reliable estimates cannot be made about the rate of occurrence for  $M_L \geq 7.0$  from the available seismicity sample, because of physical constraints on earthquake size in the region.



### MAINSHOCK CHARACTERISTICS

The mainshock occurred at 2342 UTC on 02 May 1983. The preferred Berkeley hypocentral location, based on P-readings at 15 stations of the permanent UCB, CIT, and USGS networks, is  $36^{\circ} 13.8' \text{ N}$ ,  $120^{\circ} 17.4' \text{ W}$ , at 8.4 km depth. A linear velocity gradient over a halfspace model (depth to half space is 18 km) was used to locate the mainshock. The P-wave velocity ranges from 5.2 km/sec at the surface to 7.36 km/sec above the halfspace and 7.5 km/sec in the halfspace. The velocity model parameters were estimated by calibration of readings from an aftershock ( $M_L = 3.8$  on May 7 at 00:17 UTC) adopted as a master event. This event was well-recorded by the nearby UCB Seismographic Stations and by the eleven station UCB portable digital array of three-component force-balance accelerometers deployed in the Coalinga area (Murtha and O'Connell, 1983).

The local magnitude of  $6.7 \pm 0.16$  (5 observations) for the mainshock was estimated from the maximum trace amplitude measured on the 100X torsion seismograms (see Figure 1) recorded at Berkeley (BKS:  $\Delta \approx 252 \text{ km}$ ) and from the standard Wood-Anderson torsion seismograms recorded at Mineral (MIN:  $\Delta \approx 470 \text{ km}$ ) and at Arcata (ARC:  $\Delta \approx 612 \text{ km}$ ). The seismic moment of the mainshock was estimated from the vertical broadband displacement seismogram recorded at Jamestown ( $\Delta \approx 191 \text{ km}$ ;  $Az \approx 356^{\circ}$ ) and from the three-component ultra-long-period displacement seismograms recorded at Berkeley ( $\Delta \approx 252 \text{ km}$ ;  $Az \approx 317^{\circ}$ ), using the far-field approximation:  $M_0 = 4\pi\rho V^3 r \Omega_0$  (e.g., Aki and Richards, 1980, p. 81). The  $P_g$  displacement pulse recorded at Jamestown is  $\Omega_0(P_g) = 0.60 \text{ cm-sec}$  and the  $S_g$  displacement pulse recorded at Berkeley (NE component) is  $\Omega_0(S_g) = 0.76 \text{ cm-sec}$ . The seismic moment is thus  $M_0 = (2.3 \pm 1.2) \times 10^{25} \text{ dyne-cm}$ , assuming that the effects of the free surface and of the source radiation pattern average out to unity. The corresponding  $M_W$  estimated from the moment-magnitude relation:  $M_W = 2/3 \log M_0 - 10.7$  (Hanks and Kanamori, 1979) is  $M_W = 6.21 \pm 0.15$ . The moment estimated from standard Wood-Anderson seismograms (Bolt and Herraiz, 1983) listed in Table 1 is in close agreement with the moment estimated above.

The inferred fault dimensions for the mainshock (see Figure 2 and next section) are about 15 km x 25 km. From the seismic moment and these dimensions, we infer an average fault-slip of about 20 cm in the mainshock.

Unfortunately, no accelerometers were located in the city of Coalinga at the time of the mainshock. The nearest strong-motion recording was obtained by U.S. Bureau of Reclamation/USGS accelerometers at the Pleasant Valley Pumping Plant ( $\Delta = 8.8 \text{ km}$ ). Peak ground accelerations of 0.54g horizontal and 0.37g vertical were recorded with bracketed durations above 0.10g of approximately 10-15 seconds. In Coalinga, an extensive field study by the third author on the day after the mainshock indicates a maximum Modified Mercalli Intensity of VIII as defined in the 1956 version. Damage was severe in the older city center where many unreinforced masonry structures collapsed (see Figure 5). Generally, wood frame structures were damaged in cases where the sill was not anchored to the foundation and by falling of unreinforced brick chimneys. Damage to reinforced masonry was minimal.

## SEQUENCE CHARACTERISTICS

The Coalinga earthquake sequence through August 1, 1983, consisted of 147 earthquakes with local magnitude  $M_L \geq 3.0$  and 28 earthquakes of  $M_L \geq 4.0$  (see Table 1). The local magnitude estimates ( $M_L$ ) listed in Table 1 are from the maximum trace amplitudes measured on the Wood-Anderson seismograms at Mt. Hamilton (MHC:  $\Delta \approx 173$  km), Berkeley (BKS:  $\Delta \approx 252$  km) and for the larger events at Mineral (MIN:  $\Delta \approx 470$  km) and Arcata (ARC:  $\Delta \approx 612$  km). The threshold magnitude of 3.0 corresponds to a maximum zero to peak amplitude of 0.4 mm at MHC and of 0.15 mm at BKS.

The cumulative number of earthquakes ( $M_L \geq 3.0$ ) through August 1, 1983, is plotted in Figure 3. A fit of the b-value equation yielded  $b = 0.69 \pm 0.057$ . This b-value is within the usual range for aftershock sequences following similar sized principal earthquakes in California, although it is significantly less than the long-term regional b-value given in the last section for the long-term regional seismicity.

The rate of seismicity as a function of time,  $n(t)$ , is plotted in Figure 4. Each point in the figure is estimated from 10 consecutive  $M_L \geq 3.0$  earthquakes, and the error bars represent one standard error based on the assumption that the 10 earthquakes in each of the 14 groupings have a Poisson distribution. The rate of occurrence,  $n(t)$ , may be fitted by Omori's relation:  $n(t) = A/(t+c)^p$ . The least squares solution gives  $p = 0.75 \pm 0.21$  and  $A = 8.5 \pm 2.6$ . The rate  $n(t)$  is thus about  $11 \pm 4.5$  earthquakes per hour ( $M_L \geq 3.0$ ) for the first hour of the sequence. For comparison, 11  $M_L \geq 3.0$  events per hour is  $2.2 \times 10^4$  times the background rate of  $(4.9 \pm 0.52) \times 10^{-4}$  events per hour for the previous 21 years from 1962 through 1982. If the decrease in  $n(t)$  continues to follow the trend in Figure 4, it will take  $51.2 \pm 21.1$  years to decay to the background rate for the past 21 years.

Study of the 27 largest aftershocks (see Table 1) allows some inferences to be made on the dynamics of the sequence. The master event location technique described above insures that the hypocenters of these large aftershocks are well-located relative to each other. The computed focal depths range from approximately 2 km to 15 km and, although the foci are somewhat scattered, they suggest a fault rupture for the mainshock of length about 25 km with a strike of roughly N 35° W. This result is consistent with an estimate by O'Connell and Murtha (this volume) who suggest that the fault plane strikes N 26° W and dips 13° SW based on a least-squares fit to eleven aftershock hypocenters. The hypocenter locations suggest that the low-angle thrust plane was the fault plane for the Coalinga mainshock. P-wave first motion polarities from the UCB network suggest that the auxiliary plane strikes N 38° W and dips 79° NE. The auxiliary plane is, however, not well resolved. This solution is compatible with the preferred USGS solution (Eaton, 1983) of reverse dip-slip; one allowable fault plane has a strike of N 53° W and a dip of 80° NE; the other has a strike and dip of N 53° W and 23° SW, respectively.

Generally, the strike-slip or low-angle reverse earthquakes that occur along the central coast region of California have a property in common: the least principal stress axis (extension axis) is oriented approximately east-west (Zoback and Zoback, 1980). The extension axis for the Coalinga mainshock trends S 30° W and plunges 55° SW. This axis is 60° away from the typically

observed east-west extension. Therefore it is significantly different from the regional extension axis at the 95 percent confidence level.

The seismic moments in Table 1 range from  $1.0 \times 10^{22}$  dyne-cm for a 4.0  $M_L$  earthquake to  $8.5 \times 10^{24}$  for a 6.0  $M_L$  earthquake. These values are up to 2300 times smaller than the mainshock seismic moment.

On June 11, 1983, at 0309 UTC, an  $M_L = 5.1$  aftershock occurred with focus at  $36^\circ 15.6' N$ ,  $120^\circ 27.9' W$  and a shallow depth of 1.8 km (Figure 2). This location is to the west of the previous aftershock locations. Discontinuous surface fault rupture was observed with length about 2 km after this earthquake. The surface faulting indicated 10 to 20 cm of reverse slip with east side up trending approximately north to south (McJunkin and Hart, 1983). A provisional fault plan solution (USGS, verbal communication) has one nodal plane striking  $N 24^\circ W$  and dipping  $42^\circ SW$  and the second nodal plane striking  $N 13^\circ E$  and dipping  $54^\circ SE$ . This mechanism differs significantly from the mainshock focal mechanism. Aftershocks in July, including an  $M_L = 6.0$  earthquake accompanied extension of the June 11 rupture and suggest that the fault plane for these events dips approximately  $60^\circ$  to the east. Further research is needed to explain the mechanical connections between the two fault planes.

#### ACKNOWLEDGMENTS

The authors acknowledge P.E. Murtha and D.R. O'Connell for P and S readings from the UC portable digital network established after May 2, 1983, and information of surface faulting, M.R. McKenzie for drafting the figures, and the staff of the Seismographic Stations of the University of California for assistance with this work. Financial support was from the donors to the Field Investigation Fund.

This paper was reviewed by Dr. J. Litehiser.

#### REFERENCES

- Aki, K. and P.G. Richards, 1980, Quantitative Seismology: Theory and Methods, W.H. Freeman and Co., San Francisco, California.
- Bolt, B.A. and M. Herraiz, 1983, Simplified Estimation of Seismic Moment from Seismograms, Bull. Seism. Soc. Am. 73, 735-748.
- Bolt, B.A. and R.D. Miller, 1975, Catalogue of Earthquakes in Northern California and Adjoining Areas, 1910-1972, Seismographic Stations, University of California, Berkeley.
- Eaton, J.P., 1983, Seismic setting, location and focal mechanism of the May 2, 1983, Coalinga earthquake, U.S. Geol. Survey OFR 83-511.



- Hanks, T.C. and H. Kanamori, 1979, A moment magnitude scale, J. Geophys. Res., 84, 2348-2350.
- McJunkin, R.D. and E.W. Hart, 1983, Ground rupture, Coalinga earthquake of 10 June 1983, California Geology, 8, 182-184.
- Murtha, P.E. and D.R. O'Connell, 1983, Coalinga Aftershock Parameters from UCB Strong Motion Instruments, in Scholl, R. and J. Stratta editors, The Coalinga, California Earthquake of May 2, 1983: A Reconnaissance Report.
- O'Connell, D.R. and P.E. Murtha, 1983, Source parameters of Coalinga aftershocks from the UC Berkeley portable digital array, (this volume).
- Zoback, M.L. and M. Zoback, 1980, State of stress in the coterminous United States, J. Geophys. Res., 85, 6113-6156.

TABLE 1

LISTING OF ALL EARTHQUAKES IN COALINGA  
SEQUENCE 2 MAY 1983 TO 1 AUG 1983 WITH RICHTER MAGNITUDES  
OF 4.0 OR GREATER

Date	Origin Time (UTC)	Latitude (North)	Longitude (West)	Depth (km)	Magnitude (M <sub>L</sub> )	Moment (dyne-cm)
2 May	234239.3 (±0.12)	36°13.8' (±0.8 km)	120°17.4' (±1.0 km)	8.4 (±1.1)	6.7	2.8E25
2 May	234606	36°14'	120°17'	8	5.6	
		in coda				
3 May	000924.6 (±1.27)	36°08.4' (±2.4 km)	120°17.3' (±2.1 km)	9.9 (±16.2)	4.0	2.0E22
3 May	001536.7 (±0.44)	36°09.1' (±1.7 km)	120°06.6' (±4.4 km)	7.6R	4.1	2.6E22
3 May	001801.8 (±0.48)	36°17.6' (±1.2)	120°21.4' (±4.6)	7.6R	4.4	9.4E22
3 May	003947.4 (±0.14)	36°13.1' (±0.8 km)	120°20.2' (±0.9 km)	11.2 (±1.9)	4.2	2.7E22
3 May	005023.4 (±0.55)	36°11.6' (±5.3 km)	120°13.6' (±3.1 km)	7.6R	4.0	1.4E22
3 May	005745.6 (±0.11)	36°16.3' (±0.7 km)	120°19.1' (±1.0 km)	8.6 (±0.9)	4.8	2.4E23
3 May	014146.7 (±0.36)	36°08.8' (±1.0 km)	120°10.8' (±1.3 km)	3.1 (±3.0)	4.4	5.3E22
3 May	043232.9 (±0.12)	36°17.9' (±1.6 km)	120°17.3' (±1.5 km)	7.6R	4.2	3.9E22
3 May	060446.9 (±0.51)	36°15.9' (±1.8 km)	120°22.6' (±1.4 km)	4.2 (±5.0)	4.3	3.0E22
3 May	085503.1 (±0.19)	36°08.8' (±0.7 km)	120°14.4' (±0.9 km)	7.7 (±2.0)	4.4	4.7E22
3 May	093947.7 (±0.26)	36°17.9' (±2.6 km)	120°17.8' (±2.1 km)	7.6R	4.0	1.0E22
3 May	154143.1 (±0.15)	36°15.6' (±1.4 km)	120°17.3' (±1.4 km)	7.6R	4.7	2.2E23
4 May	072840.3 (±0.14)	36°16.2' (±1.2 km)	120°19.9' (±1.4 km)	13.9 (±1.6)	4.8	1.3E23
4 May	161120.9 (±0.09)	36°17.2' (±0.7 km)	120°20.4' (±0.8 km)	10.6 (±0.9)	4.3	2.9E22
5 May	1020045.4 (±0.10)	36°17.6' (±0.8 km)	120°20.8' (±0.9 km)	11.2 (±1.1)	4.5	5.8E22
9 May	024912.8 (±0.09)	36°14.8' (±0.8 km)	120°17.4' (±0.8 km)	11.9 (±1.1)	5.1	5.1E23

TABLE 1 (continued)

09 May	032638.1 (±0.28)	36°13.4' (±1.6 km)	120°17.8' (±1.4 km)	4.9 (±3.3)	4.4	6.5E2
12 May	134108.1 (±0.10)	36°09.3' (±0.8 km)	120°15.4' (±0.9 km)	9.9 (±1.2)	4.4	4.0E2
22 May	083923.2 (±0.10)	36°08.6' (±0.8 km)	120°11.9' (±0.9 km)	8.7 (±1.4)	4.0	1.5E2
24 May	090219.0 (±0.09)	36°15.3' (±0.8 km)	120°18.3' (±0.7 km)	8.4 (±1.0)	4.6	9.5E2
11 June	030954.0 (±0.34)	36°15.6' (±2.1 km)	120°27.9' (±1.4 km)	1.8 (±3.6)	5.1	1.1E2
12 June	013129.0 (±0.09)	36°06.5' (±0.7 km)	120°18.1' (±0.9 km)	11.1 (±1.2)	4.0	1.2E2
09 July	074052.6 (±0.23)	36°15.8' (±1.4 km)	120°23.8' (±1.1 km)	6.1 (±2.7)	5.3	6.3E2
22 July	023955.3 (±0.14)	36°13.4' (±1.4 km)	120°23.7' (±1.6 km)	7.4 (±1.8)	6.0	8.5E2
22 July	034302.1 (±0.46)	36°13.3' (±2.2 km)	120°23.1' (±1.5 km)	5.9 (±4.9)	5.0	2.5E2
25 July	223140.8 (±0.11)	36° 13.2' (±1.1 km)	120°23.4' (±1.2 km)	7.9 (±1.3)	5.1	6.6E2

TABLE 2

## AVERAGE HISTORICAL RATE OF SEISMICITY IN THE COALINGA AREA

$M_L$	$\bar{r}$ (eqs/year)	$\sigma_r$ (eqs/year)	-95% CI* (eqs/year)	+95% CI* (eqs/year)
3.0	1.91	0.20	1.51	2.31
3.5	0.88	0.07	0.74	1.02
4.0	0.406	0.044	0.318	0.494
4.5	0.187	0.032	0.123	0.251
5.0	0.086	0.021	0.044	0.128
5.5	0.039	0.012	0.015	0.063
6.0	0.018	0.007	0.004	0.032
6.5	0.008	0.004	0.0006	0.0162
6.7	0.006	0.003	0.0003	0.0121
7.0	0.004	0.002	0.000	0.0008

\* CI = Confidence Interval





Photo. Damage in downtown Coalinga caused by the 2 May earthquake. Old masonry structures have collapsed or have been severely damaged. A modern single-story frame building (P.G.&E.) is not damaged and the steel water tank (only partly full at the time of the earthquake) remains standing.

BERKELEY (ESB)    Upper    Lower  
100X TORSION    E ↑    N ↑  
To=0.8 sec    W ↓    S ↓

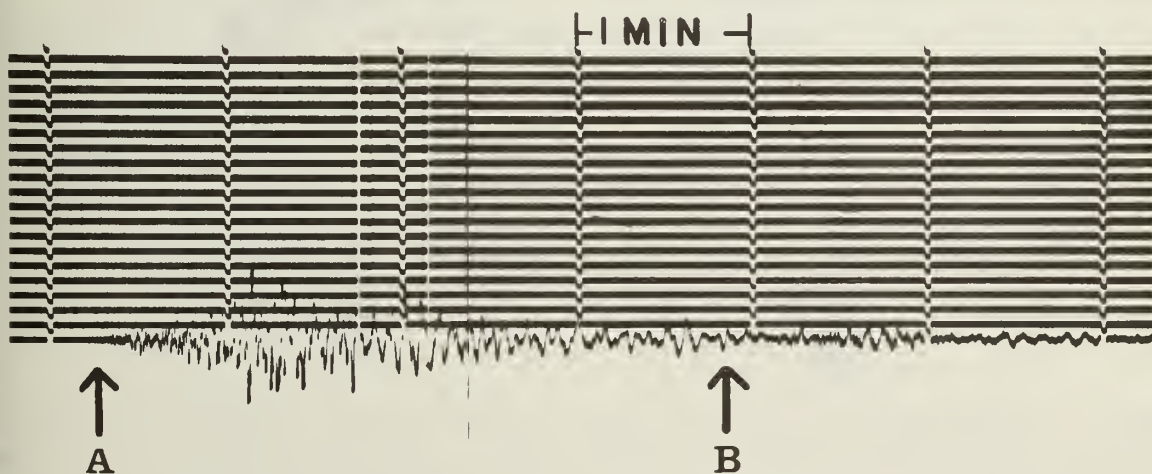


Figure 1. Seismogram recorded by a 100X torsion seismograph at Earth Sciences Building, U.C. Berkeley. The motion is in the N-S horizontal direction and offsets are one minute apart. Note the second smaller earthquake ( $M_L = 5.6$ , Point B) 3 minutes 27 seconds after the mainshock begins (Point A).

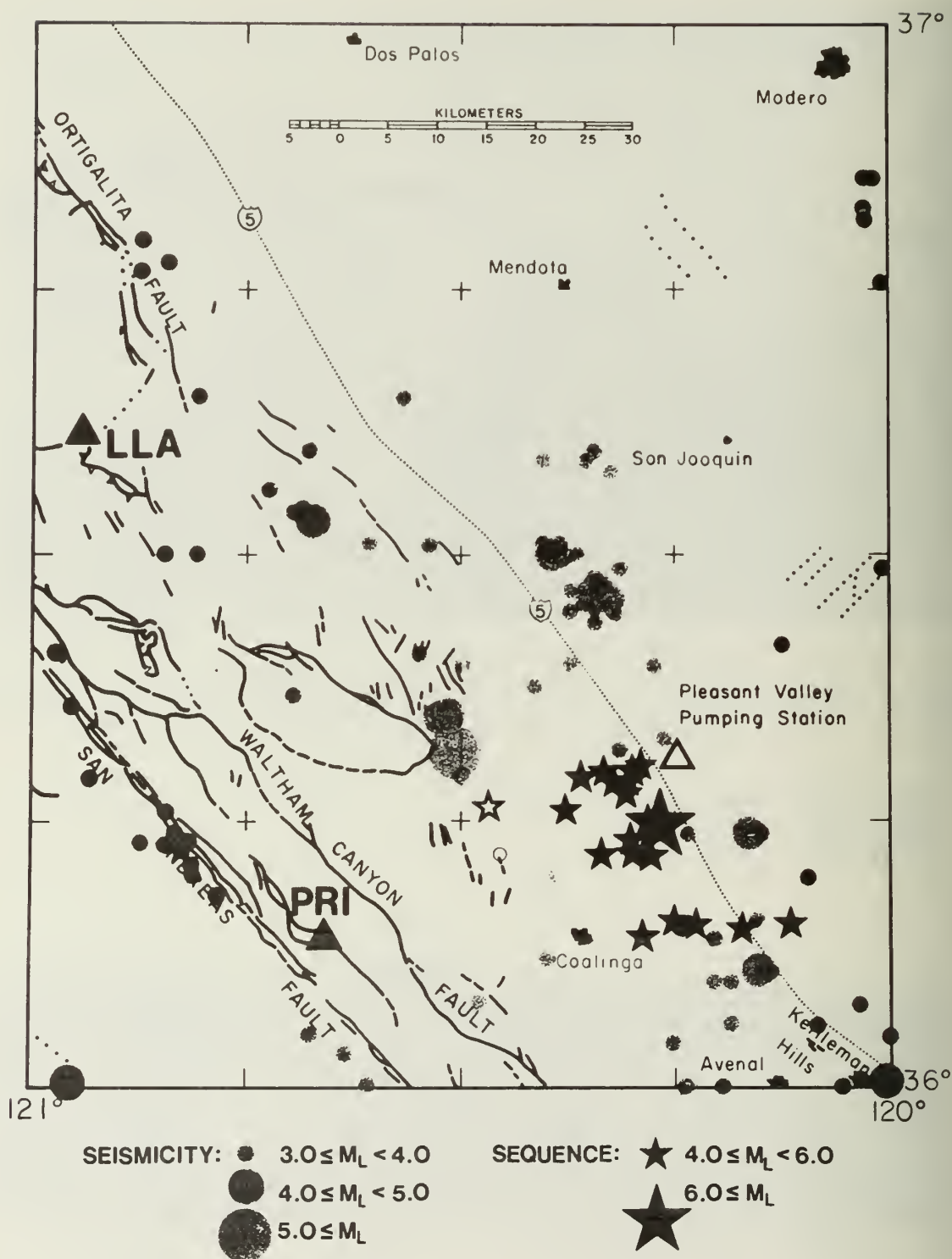


Figure 2. Epicenters of the mainshock of 2 May 1983 and principal aftershocks through 12 May 1983 are plotted as full stars. Interstate Highway 5 is shown as a fine dotted line and mapped faults in the region by full lines. The open circle is the location of surface faulting observed after the 11 June aftershock (plotted as an open star). Full circles are epicenters of earthquakes (magnitude greater than 2.5) located from 1963 to April 1983. The full triangles are permanent U.C. Seismographic Stations and the open triangle is the accelerograph site at the Pleasant Valley Pumping Station.

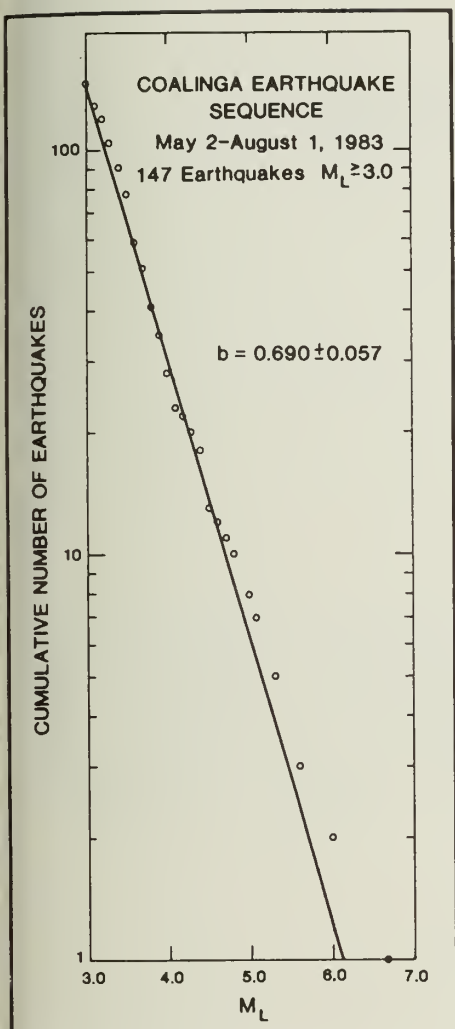


Figure 3. Cumulative number of earthquakes as a function of local magnitude for the Coalinga earthquake sequence of 2 May - 1 August 1983.

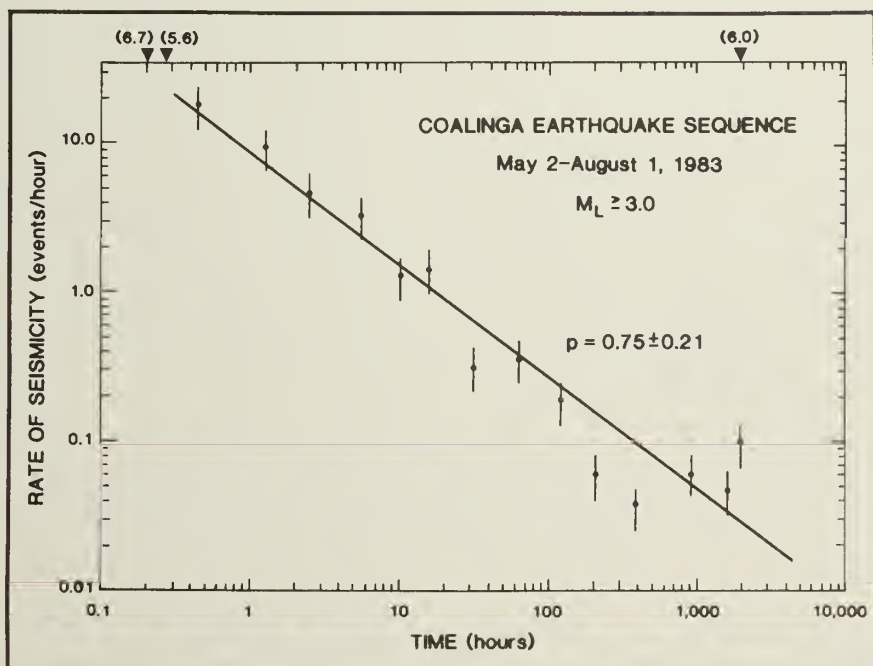


Figure 4. Rate of seismicity versus time for the Coalinga earthquake sequence of 2 May - 1 August 1983.





MECHANISM OF THE 1983 COALINGA EARTHQUAKE  
DETERMINED FROM LONG-PERIOD SURFACE WAVES

by

Hiroo Kanamori<sup>1</sup>

ABSTRACT

The mechanism of the May 2, 1983, Coalinga, California earthquake determined from long-period surface waves and first-motion data is given by dip angle =  $65^{\circ}$ , strike =  $N58^{\circ}W$ , rake =  $70^{\circ}$ , seismic moment =  $5.4 \times 10^{25}$  dyne-cm ( $M_w = 6.4$ ), and the source process time  $\approx 20$  sec. The local magnitude,  $M_L$ , is estimated to be  $6.43 \pm 0.27$ . On the  $M_L$  vs.  $M_w$  diagram, the Coalinga earthquake falls on the average trend for California earthquakes.

## INTRODUCTION

We report the source parameters of the 1983 Coalinga, California, earthquake (May 2, 23<sup>h</sup> 42<sup>m</sup> 37.8<sup>s</sup>, 36°13.99'N, 120°17.59'W, 10.5 km, Eaton, 1983) determined from long-period (256 sec) surface waves recorded by the digital stations of the IDA (International Deployment of Accelerometers) network and the Global Digital Seismographic Network (GDSN).

The mechanism solution obtained from long-period surface waves represents the overall fault geometry, and provides a reliable estimate of the seismic moment.

## ANALYSIS

The stations and the phases used are listed in Table 1. In total, 40 Rayleigh- and Love-wave phases from 19 stations are used. Using the method described by Kanamori and Given (1981), we inverted the spectral data of these surface waves at a period of 256 sec to determine the seismic moment tensor and the fault model.

Since the source depth reported by Eaton (1983) is 10.5 km, we used a point source at a depth of 9.75 km, the depth closest to 10.5 km where the excitation functions are tabulated in Kanamori and Given (1981). As is discussed by Kanamori and Given (1981), the two elements of the moment tensor,  $M_{zx}$  and  $M_{zy}$  are indeterminate for shallow events. Hence, we first set  $M_{zx} = M_{zy} = 0$  which is equivalent to restricting the solution either to a 45° dip-slip or a vertical strike-slip fault. Despite this restriction, the solutions obtained with these constraints provide useful gross estimates of fault geometry and seismic moment.

Empirical relations (Furumoto, 1979, Furumoto and Nakanishi, 1983; Dziewonski and Woodhouse, 1983) suggest a source process time,  $\tau$ , of about 10 sec for earthquakes with  $M_s \approx 6.5$ . We inverted the Rayleigh-wave data, varying  $\tau$  from 0 to 50 sec, and found that  $\tau = 20$  sec provides a best fit. Since the regional variation of Love-wave phase velocity is very large even at a period of 256 sec, we did not include Love waves for the determination of  $\tau$ . Although this value is somewhat larger than that empirically expected, the difference is probably insignificant. Nakanishi and Kanamori (1983) obtained a standard deviation of 17 sec for the measurement of the source process time from a global data set.

Using  $\tau = 20$  sec, we inverted the Rayleigh- and Love-wave spectral data together. The results are shown in Table 2, Figure 1 and Figure 2. The moment tensor can be decomposed into the major and minor double couples. The mechanism of the major double couple (constrained to be either a 45° dip-slip or a vertical strike slip) is a 45° thrust fault



with a strike of  $N36^{\circ}W$ . The seismic moment is  $4.4 \times 10^{25}$  dyne-cm. The moment of the minor double couple is only 8.9% of that of the major double couple, and is considered insignificant.

If we assume that the geometry of the source did not change during faulting, we can combine P-wave first-motion data with the surface-wave data to determine further details of the source geometry (Kanamori and Given, 1981). First-motion data were obtained from selected WWSSN (Worldwide Standardized Seismographic Network) and Canadian Network stations (Hartzell and Heaton, 1983, this volume), and RSTN (Regional Seismic Test Network) stations. These data are listed in Table 3. We computed the take-off angles using the Jeffreys-Bullen travel time curves with the velocity at the source of 6.5 km/sec. Stations ALE, VAL, WES and RSCP show a very small upward first-motion followed by a large downward motion, suggesting that these stations are located very close to the node of the P-wave radiation pattern. These stations together with other stations determine one of the nodal planes very well as shown by Figure 2. The strike of this plane is  $N58^{\circ}W$  which agrees very well with that determined by Eaton (1983) from local data ( $N53^{\circ}W$ ). The teleseismic first-motion data provide no constraint on the other nodal plane.

We then fixed the steep nodal plane and inverted the Rayleigh- and Love-wave data to determine the rake  $\lambda$  on this plane and the seismic moment. The result is shown in Table 4 and Figure 2. The RMS (root-mean-square) value of the difference between the observed and computed spectra is 0.0242 cm-sec, which is only slightly larger than that for the constrained moment tensor solution, 0.0239 cm-sec, indicating that this mechanism is a good fit to the surface-wave data. The rake on the steeply dipping plane is  $70^{\circ}$  which makes the strike of the second nodal plane almost north-south. The seismic moment for this solution is  $5.4 \times 10^{25}$  dyne-cm. Changing the depth from 9.75 to 16 km only increases the moment by 8%. This geometry is very similar to that determined by Hartzell and Heaton (1983, in this volume) from body-wave data and to that determined by inversion of GDSN waveform data (A. Dziewonski, personal communication, July 20, 1983).

Considering the relatively short source process time, the assumption that the geometry of the source for body waves is the same as that for surface waves is reasonable. Hence, we prefer this solution as the mechanism of the 1983 Coalinga earthquake.

### CONCLUSION

The mechanism of the 1983 Coalinga, California, earthquake determined from long-period surface waves and first-motion data is given in Table 3 and Figure 2. The seismic moment is  $5.4 \times 10^{25}$  dyne-cm and  $M_w = 6.4$ . The source process time is about 20 sec; no evidence for anomalously

long source process is found.

The strike of the aftershock area reported by Eaton (1983) is about  $N38^{\circ}W$  and is more parallel to the steeply dipping nodal plane than to the low-angle nodal plane of our solution, suggesting that the steep plane is the fault plane.

The local magnitudes of the Coalinga earthquake determined from six Wood-Anderson records obtained from the Southern California Network are listed in Table 5. From these data, we obtain  $M_L = 6.20 \pm 0.11$ . The local magnitude determined from the network of the University of California, Berkeley, is  $6.70 \pm 0.16$  (five observations) (B. A. Bolt, written communication, August, 1983, also this volume). The average of these two values weighted by the number of records used for each determination is  $M_L = 6.43 \pm 0.27$ . Figure 3 compares the Coalinga earthquake with other earthquakes in California (the 1976 Guatemala earthquake is included for comparison) on the  $M_L$  vs.  $M_W$  diagram which has been used to compare the high-frequency characteristics of earthquakes (Kanamori and Regan, 1982). The Coalinga earthquake falls on the average trend for California earthquakes.

#### ACKNOWLEDGMENTS

I thank Jon Berger and Jeffrey Given for their help in retrieving the RSTN data, and Bruce Bolt for providing me with the  $M_L$  data from the Berkeley network. I also thank Tom Heaton and Stephen Hartzell for useful information on their body-wave solution. The IDA and GDSN data were provided by the University of California, San Diego, and the U. S. Geological Survey respectively. This research was partially supported by U. S. Geological Survey contract No. 14-08-0001-21210. Contribution No. 3958, Division of Geological and Planetary Sciences, California Institute of Technology, Pasadena, California 91125.

#### REFERENCES

- Dziewonski, A. M., and Woodhouse, J. H., 1983, An experiment in systematic study of global seismicity: Centroid-moment tensor solutions for 201 moderate and large earthquakes of 1981, *J. Geophys. Res.*, v. 88, p. 3247-3271.
- Eaton, J. P., 1983, Seismic setting, location and focal mechanism of the May 2, 1983, Coalinga earthquake, U. S. Geological Survey, Open-File Report 83-511, p. 20-26.
- Furumoto, M., 1979, Initial phase analysis of R-waves from great earthquakes, *J. Geophys. Res.*, v. 84, p. 6867-6874.
- Furumoto, M., and Nakanishi, I., 1983, Source times and scaling relations of large earthquakes, *J. Geophys. Res.*, v. 88, p. 2191-2198.
- Kanamori, H., and Given, J. W., 1981, Use of long-period surface waves for rapid determination of earthquake-source parameters, *Phys. Earth and Planet. Int.*, v. 27, p. 8-31.

Kanamori, H., and Regan, J., 1982, Long-period surface waves, the Imperial Valley, California, earthquake of October 15, 1979, U. S. Geological Survey Professional Paper 1254, p. 55-58.

Nakanishi, I., and Kanamori, H., 1983, Source mechanisms of twenty-six large shallow earthquakes ( $M_s > 6.5$ ) during 1980 from P-wave first motion and long-period Rayleigh wave data, submitted to Seismol. Soc. Amer. Bull.

Table 1

Station	$\Delta$ (deg.)	$\phi$ (deg.)	Phases
SJG	51.0	95.7	$R_2, R_3$
KIP	36.1	256.3	$R_2, R_3$
TWO	117.8	245.7	$R_1, R_2$
CMO	32.9	338.8	$R_2, R_3$
KMY	106.6	319.9	$R_1, R_2$
ALE	50.0	8.3	$R_2, R_3$
RAR	68.4	219.8	$P_2$
ERM	71.0	308.6	$R_2$
ESK	74.0	31.9	$R_2, R_3$
HAL	43.3	60.6	$R_2, R_3$
ANTO	100.2	20.7	$R_1, R_2, G_1$
GUMO	86.0	283.9	$R_1, R_2, G_1$
NWAO	133.2	256.8	$R_1, R_2, G_1$
TATO	95.7	306.7	$R_1, R_2, G_1$
SNZO	97.5	223.7	$R_1, R_2$
CTAO	104.4	255.7	$R_1, R_2, G_1$
ZOBO	71.8	126.9	$R_2$
KONO	75.8	23.6	$R_1, R_2, G_1$
MAJO	77.3	306.1	$G_1$

Note:  $\Delta$  is the distance and  $\phi$  is the azimuth measured clockwise from the north.

Table 2

Constrained Moment Tensor

( $M_{zx} = M_{zy} = 0$ ,  $d = 9.75$  km,  $\tau = 20$  sec)

$M_{xy}$	$M_{yy} - M_{xx}$	$M_{yy} + M_{xx}$
$2.3 \pm 0.3^*$	$-1.5 \pm 0.6^*$	$-4.0 \pm 0.3^*$

Major Double Couple

Moment	dip	rake	Strike	dip	rake	strike	RMS
4.4*	45°	90°	144°	45°	90°	-36°	0.0239**

Minor Double Couple - 8.9% of the Major Double Couple

\* unit  $10^{25}$  dyne-cm

\*\* unit cm-sec



Table 3

## First-Motion Data

Station	$\Delta$ (deg.)	$\phi$ (deg.)	$i_h$ (deg.)	First Motion
AFI	69.6	234	20.1	U
AKU	62.3	27	22.6	U
ALE	50.2	8	27.2	Nodal Up
BOG	52.8	115	26.0	U
COP	80.0	24	19.3	U
ESK	74.2	31	19.2	U
KON	75.9	23	19.2	U
LPA	91.5	133	16.0	U
LPS	35.4	120	30.0	U
MAT	77.4	306	19.7	U
SHK	82.2	307	18.5	U
VAL	73.1	37	19.2	Nodal Up
WES	38.0	65	30.7	Nodal Up
FFC	22.4	28	33.8	D
PHC	15.4	342	49.7	D
RSCP	28.0	80	33.5	Nodal Up
RSNY	35.4	62	30.1	O
RSSD	14.7	52	49.8	D
RSO	24.0	44	33.3	D

Note:  $\Delta$  is the distance,  $\phi$  is the azimuth measured clockwise from the north, and  $i_h$  is the take-off angle.

Table 4

## Fault Inversion

(Depth 9.75 km, Source Process Time = 20 sec)

Seismic Moment	$(5.4 \pm 0.3) \times 10^{25}$ dyne-cm
First Nodal Plane	
{ Dip	65° (Constrained)
{ Rake	70 ± 3°
{ Strike	-58° (Constrained)
Second Nodal Plane	
{ Dip	32°
{ Rake	126°
{ Strike	163°
P axis	
{ Azimuth	47°
{ Plunge	18°
T axis	
{ Azimuth	178°
{ Plunge	64°
RMS	0.0242 cm-sec

Table 5

## Wood-Anderson Amplitude Data from Southern California Network

Station	Comp.	$\Delta$ (km)	Azimuth (Deg.)	Amp. mm	$M_L^*$
RVR	NS	364	132	53.0	6.12
RVR	EW	364	132	70.0	6.25
PLM	NS	448	135	35.2	6.15
PLM	EW	448	135	64.8	6.41
PAS	NS	301	140	99.6	6.11
PAS	EW	301	140	116.0	6.17

Av. 6.20 ± 0.11

\* Station correction, 0.1 unit is added for RVR and PAS.

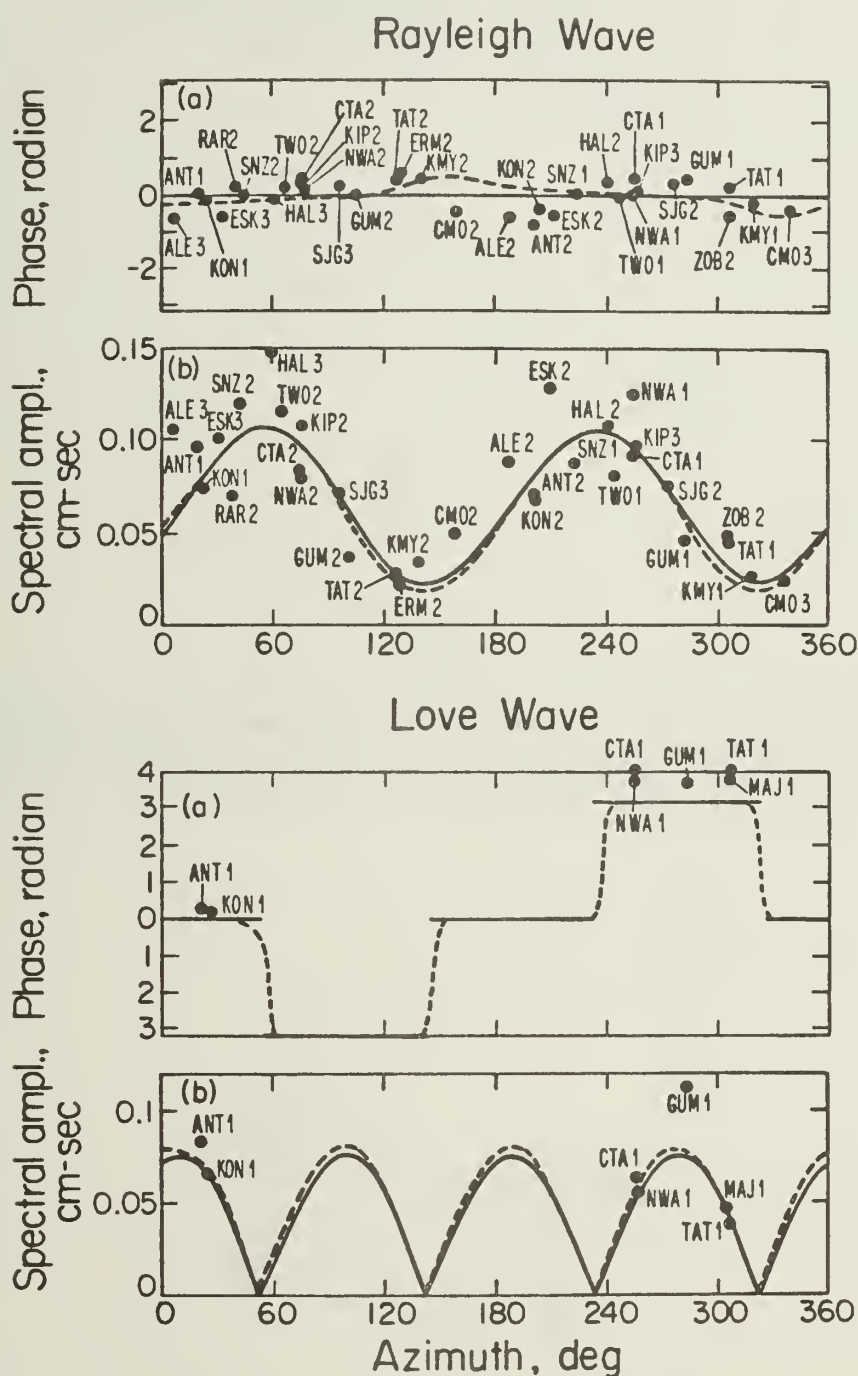


Figure 1. Phase (a) and amplitude (b) spectra of Rayleigh and Love waves at a period of 256 sec. Each data point represents the source spectrum at each station. The three-letter station code and phase number are attached to each data point. Solid and dashed curves are computed for the constrained moment tensor (Table 2) and the fault model (Table 4) respectively.

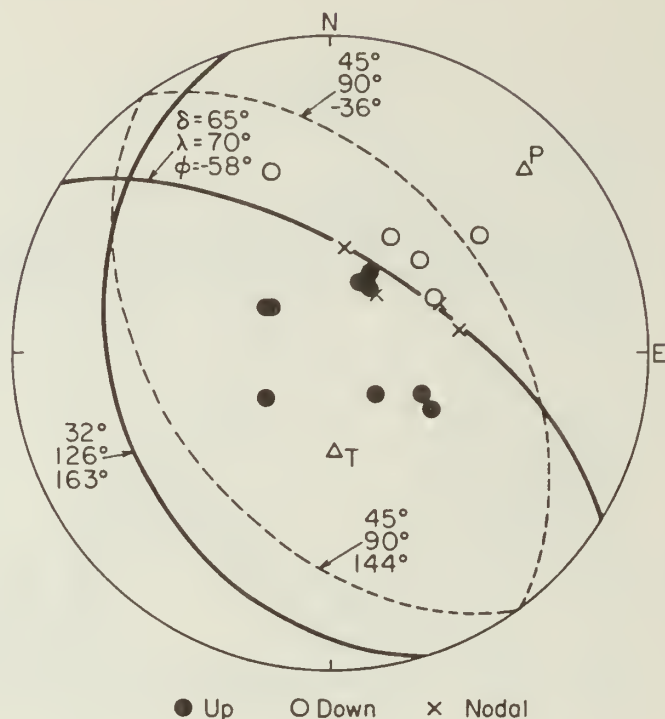


Figure 2. First-motion data and the nodal lines for the major double couple of the moment tensor solution (Table 2, dashed curve) and the fault model (Table 4, solid curve).

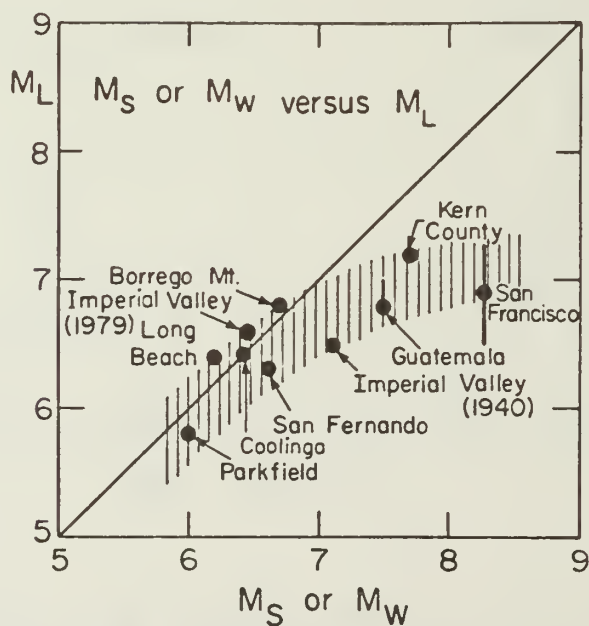


Figure 3. The relation between local magnitude,  $M_L$ , and moment magnitude,  $M_W$ , (or surface-wave magnified  $M_S$ ) for California earthquakes and the 1976 Guatemala earthquake. Diagonal line represents  $M_L = M_W$  (or  $M_S$ ), band of vertical lines defines range of  $M_L$  at a given  $M_W$  (or  $M_S$ ) for California earthquakes.



TELESEISMIC MECHANISM OF THE MAY 2, 1983  
COALINGA, CALIFORNIA, EARTHQUAKE FROM  
LONG-PERIOD P-WAVES

by

Stephen H. Hartzell<sup>1</sup>

Thomas H. Heaton<sup>2</sup>

ABSTRACT

Teleseismic, long-period P-waveforms are modeled to obtain estimates of the source parameters for the May 2, 1983 Coalinga earthquake. The best fitting focal mechanism is: strike =  $297 \pm 5^\circ$ , dip =  $64 \pm 1^\circ$ , rake =  $70 \pm 10^\circ$ . The moment is estimated to be  $3.8 \pm 1.5 \times 10^{25}$  dyne-cm with a slip duration of  $5 \pm 1$  sec. The depth is estimated at  $12 \pm 2$  km.

<sup>1</sup>Woodward-Clyde Consultants, P.O. Box 93245, Pasadena, CA 91109

<sup>2</sup>U.S. Geological Survey, California Institute of Technology,  
Pasadena, CA 91125

## ANALYSIS AND DISCUSSION

Long-period, vertical P-waves from WSSN and Canadian stations in the distance range from  $30^\circ$  to  $90^\circ$  were collected for the Coalinga earthquake. The P-waves are shown in Figure 1 (boldface traces). These waveforms are modeled using the generalized ray technique (Helmberger and Harkrider, 1978). The crustal structure used in the modeling is given in Table 1. In choosing this velocity structure, the results of refraction surveys by the U.S. Geological Survey (Walter and Mooney, 1982) were used as guidelines. Because we are using a layered crustal model, the ray expansion needed in the generalized ray method is complicated. To ensure that the ray expansion contains all significant rays, the results were checked against a Haskell matrix code. The value of  $t^*$  is assumed to be 1.0.

The strike and dip of the north-easterly-dipping nodal plane ( $297^\circ$  and  $64^\circ$ , respectively) are fairly well constrained by the downward first motion at PHC and by the nodal up first motions at ALE and WES. By fitting these key stations, the first motions at all the remaining stations are satisfied (for a thrust mechanism). Although there is some trade-off between the assumed velocity in the source region and the fault dip, reasonable perturbations in the assumed velocity structure results in variations in the dip angle of about a degree. Local first-motion data suggest a rake of near  $90^\circ$  (Eaton, 1983). However, the teleseismic P-waveforms, particularly those at MAT, SKH, and WES, appear incompatible with a rake of  $90^\circ$  or greater. These waveforms are better described by a rake of less than  $90^\circ$ . Figure 2 compares waveforms for different rakes. We have chosen a rake of  $70^\circ$  since it does not violate many of the local first motions and fits the teleseismic P-wave data well. However, the error bars are relatively large, about  $\pm 10^\circ$ . The corresponding conjugate nodal plane has a strike of  $156 \pm 15^\circ$ , a dip of  $32 \pm 5^\circ$ , and a rake of  $125 \pm 10^\circ$ . Since we approximate the source with a point source, we cannot choose between the conjugate planes based upon this analysis. A comparison of the synthetics for this mechanism with the data is shown in Figure 1. The best fitting average moment is  $3.8 \times 10^{25}$  dyne-cm. All the stations were used to obtain this value except LPA, which has an anomalously low amplitude. Amplitudes of the synthetics in Figures 1 and 2 are based on this moment. A very similar mechanism has been obtained by Kanamori (1983, this volume) from surface wave data.

The far-field source-time function used is a trapezoid (pictured in Figure 1) with a rise of 1 sec, a top of 1 sec, and a fall of 3 sec. A 5 sec total source duration is generally consistent with the duration of strong shaking recorded by the Pleasant Valley Pumping Plant Station 9.4 km from the epicenter (Maley et al., 1983). Long-period body waves are not particularly sensitive to the depth of the source. However, we can set some upper and lower bounds. Most of the P wave-forms in Figure 1 have a positive deflection about 15 sec after the first arrival. This phase is made up of crustal multiples of Moho reflections involving S to P conversions at the free surface, and gives some control on the depth.

The synthetics in Figures 1 and 2 are calculated for a depth of 12 km. The match between the synthetics and the data degrades for depths less than 10 km and greater than 14 km. There are of course trade-offs between these depths and the velocity structure.

Figure 3 shows teleseismic short-period P-waves. All the records are from WWSSN stations except ESK which is a special instrument with a response similar to WWSSN. The records are lined up on the first major upswing, which can be identified in each of the 8 seismograms. There is a fairly coherent low-amplitude arrival about two seconds ahead of this first major peak. There appears to be a two second low-amplitude initiation phase, suggesting less energetic faulting at the beginning of the rupture. This observation is consistent with initial low-level ground motions recorded on high-gain digital instruments in the Parkfield area (William Ellsworth, Menlo Park, personal communication). A similar feature in the teleseismic short-period P-waves for the 1979 Imperial Valley earthquake has been reported by Hartzell and Heaton (1983).

### CONCLUSIONS

The mechanism of the 1983 Coalinga, California earthquake determined by modeling of teleseismic long-period P-waves is found to be strike =  $297^\circ$ , dip =  $64^\circ$ , rake =  $70^\circ$ , with a moment of  $3.8 \times 10^{25}$  dyne-cm. The depth is estimated at 12 km with a source-time-function duration of 5 sec. The emergent character of the teleseismic short-period P-waves suggests that the rupture started with a 2 sec interval of less energetic faulting.

### ACKNOWLEDGMENTS

The authors are grateful to the operators of WWSSN stations who supplied records for this study. We thank Hiroo Kanamori for useful discussions and for reviewing the manuscript.



## REFERENCES

- Eaton, J. P. (1983). Seismic setting, location and focal mechanism of the May 2, 1983, Coalinga earthquake, in Coalinga earthquake sequence commencing May 2, 1983, U.S. Geological Survey Open File Report 83-511.
- Hartzell, S. H. and T. H. Heaton (1983). Inversion of strong-ground motion and teleseismic waveform data for the fault rupture history of the 1979 Imperial Valley, California earthquake, Bull Seism. Soc. Am., December.
- Helmberger, D. V. and D. Harkrider (1978). Modeling earthquakes with generalized ray theory, in Modern Problems in Elastic Wave Propagation, J. Miklowitz and J. D. Achenback, Editors, John Wiley and Sons, New York.
- Kanamori, H. (1983). Mechanism of the 1983 Coalinga earthquake determined from long-period surface waves, CDMG Special Report, The 1983 Coalinga, California, earthquake.
- Maley, R., G. Brady, E. Etheredge, D. Johnson, P. Mork, J. Switzer (1983). Analog strong motion data and processed main event records, in Coalinga earthquake sequence commencing May 2, 1983, U.S. Geological Survey Open File Report 83-511.
- Walter, A. W. and W. D. Mooney (1982). Crustal structure of the Diablo and Gabilan ranges, central California: a reinterpretation of existing data, Bull. Seism. Soc. Am., 72, 1567-1590.

Table 1

Velocity Structure

$\alpha$ (km/sec)	$\beta$ (km/sec)	$\rho$ (gm/cm <sup>3</sup> )	Th (km)
3.0	1.70	2.1	3.0
5.5	3.17	2.5	3.0
6.2	3.58	2.7	20.0
8.0	4.62	2.9	----

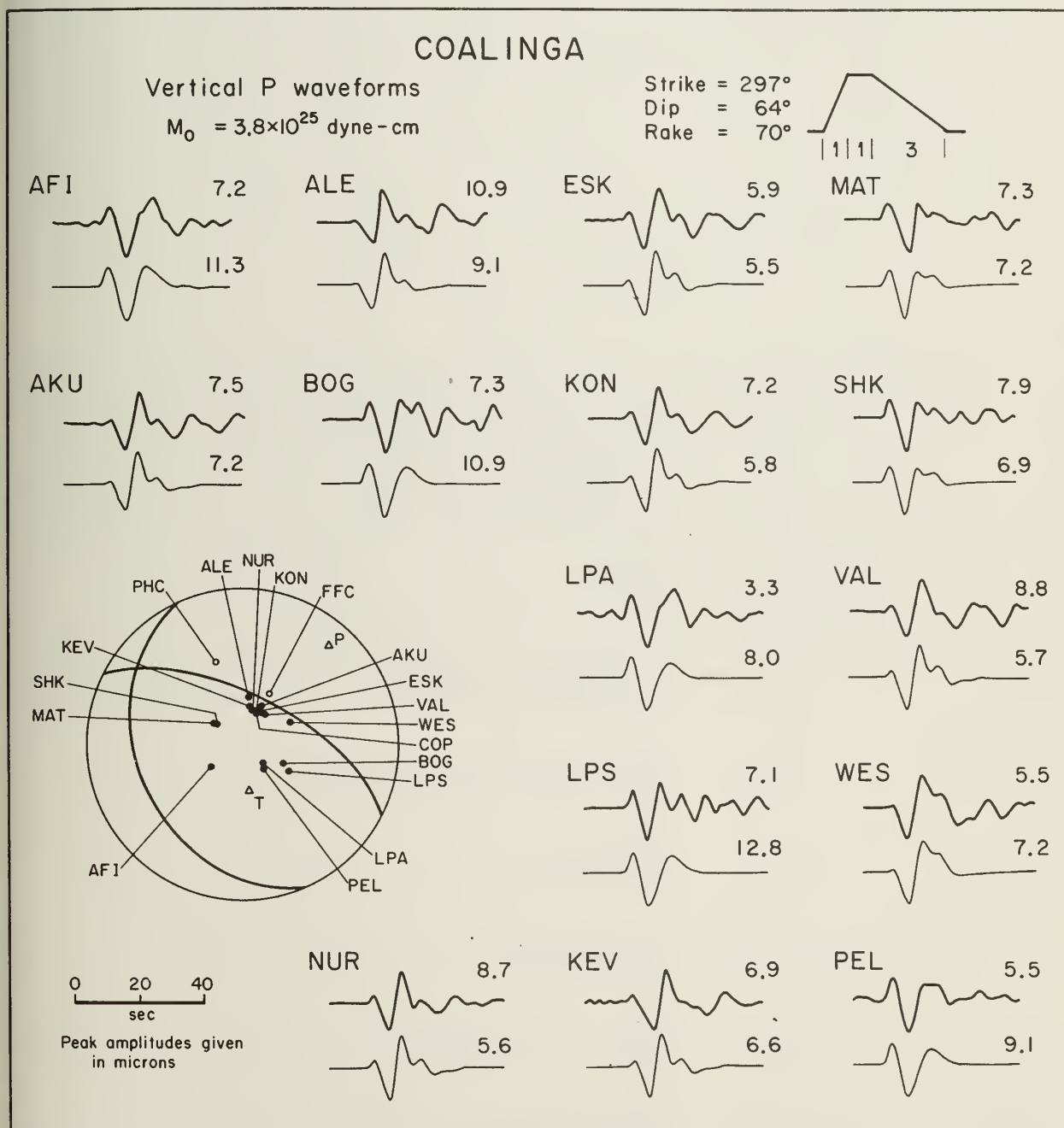


Figure 1. Comparison of observed, vertical, long-period, tele-seismic P-waveforms (boldface traces) with generalized ray synthetics for the May 2, 1983 Coalinga earthquake. The focal mechanism is an equal area projection.

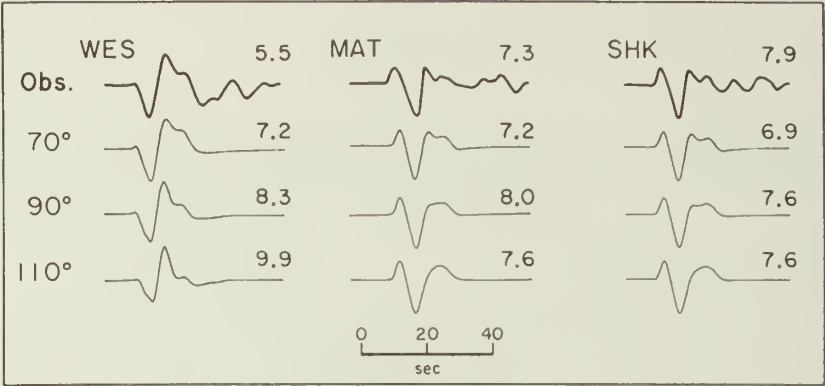


Figure 2. Comparison of P-waveforms for rakes of 70°, 90°, and 110°. Amplitudes are given in microns for a moment of  $3.8 \times 10^{25}$  dyne-cm.

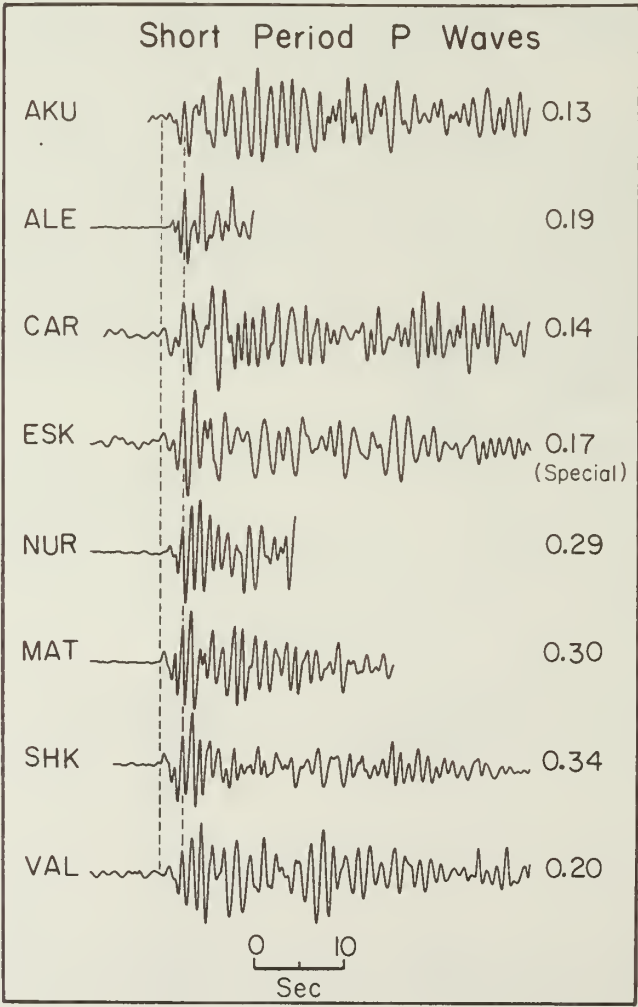


Figure 3. Short-period teleseismic P-waves. These data suggest a two second initiation phase of low-amplitude faulting. Amplitudes are given in microns.



WAVEFORM MODELING OF LONG PERIOD P-WAVES FROM THE  
COALINGA EARTHQUAKE OF MAY 2, 1983

by  
J. A. Rial and E. Brown <sup>1/</sup>

ABSTRACT

Synthetic seismograms at teleseismic distances ( $30^\circ \leq \Delta \leq 85^\circ$ ) have been computed for long-period P-waves from the Coalinga earthquake of May 2, 1983 ( $M_L=6.5$ ) as recorded at fifteen WWSSN stations. The preferred model is consistent with a thrust fault mechanism with source parameters strike= $303^\circ$ , dip= $66^\circ$ , rake= $90^\circ + 10^\circ$  (one nodal plane). The computed average P-wave moment is  $4.33 \times 10^{25}$  dyne-cm, the stress drop is 21 bars assuming a rectangular source area, and the teleseismic source time duration is 4 seconds. Complexities in the observed waveforms are interpreted as path effects caused by intracrustal low velocity layers at varying depths under some receiving stations. The existence of these velocity inversions within the crust is consistent with recently postulated models and results of deep-crust seismic reflection profiles. Their effect on long-period WWSSN synthetic seismograms is strong and easily identifiable.

<sup>1/</sup> C. F. Richter Seismological Laboratory  
University of California  
Santa Cruz, California 95064

## INTRODUCTION

Modeling teleseismic body waves by constructing synthetic seismograms has become one of the most fundamental seismological tools to determine geometric and dynamic parameters of the earthquake source. The most commonly used approach is to computer generate waveforms for either P or S long period waves at epicentral distances between  $30^{\circ}$  and  $85^{\circ}$ , and by trial and error obtain the best possible match with the observed seismograms. A model of the earthquake source is thus found that hopefully represents the physical process of rupture. When the observed waveforms are simple, the analysis is straightforward. This is rarely the case, however, since earthquake waves often interact in a complex way with the earth structure both near the source and the receiver. This interaction can occasionally result in complex waveforms that reflect not only the source processes, but also the complexity of the earth's crust.

This paper is concerned with the application of the above mentioned method to the Coalinga, California earthquake of May 2, 1983 ( $M_L=6.5$ ). We show that even though the source process itself is simple, consisting of a single rupture 4 seconds in duration along a thrust fault 10 km deep, the effects of varying crustal structure under the receiving stations add great complexity to the signal, sometimes giving the impression of source multiplicity.

The large amount of detailed local information on the Coalinga earthquakes that is available (aftershock distribution, strong ground motion records, crustal structure near the source) has provided us with important constraints on the plausible range of solutions (Sherburne et al., 1983, Borchardt, 1983). This information is enough to rule out source multiplicity, and to tightly bound possible variations in focal depth, focal mechanism and rupture area. These circumstances, plus the short duration of the rupture process (about 4 seconds), make the Coalinga earthquake an almost ideal source for the study of path-related effects. The recently emerging evidence (see for instance Oliver et al., 1983) that the crust of the earth is far more complex than long-period waveform modeling has ever considered, led us to question whether the observed complexities in the P-wave trains of the Coalinga earthquake could be related to near-receiver structure, including intracrustal low velocity layers and to investigate their effects on long period synthetic seismograms.

The results presented here are still somewhat preliminary, but we have reason to believe that synthetic seismogram studies could be improved (and interpretations of source multiplicity revised) if the effects of velocity inversion within the receiver crust are included in the computer-generated waveforms.

## Receiver crust effects

As recorded by long-period WWSSN instruments, P-waves at teleseismic distances ( $30^{\circ} \leq \Delta \leq 85^{\circ}$ ) from shallow ( $h \leq 30$  km) earthquakes are easily recognizable as being the result of the interaction of the direct

P phase and the two surface reflections pP and sP. The typical signature of this type of earthquake was described by Langston and Helmberger (1975) and since then innumerable observations have supported their description. It has also been observed that in certain instances, especially when the duration of the rupture is short (<10 secs, say), some seismograms show later arrivals either in the form of large downswings or extra phases. These have been commonly associated with near-receiver complexities. In general, these late phases are not modeled because either they do not strongly interfere with the main pulse or, if they do, the practice is not to use the record in the analysis on the grounds that the receiver structure is too complex. The importance of receiver structure in teleseismic waveform modeling has long been recognized (Burdick and Langston, 1977, Langston, 1977) but perhaps not in the light of recent models of the crust that include the "sialic low velocity layer" (Mueller, 1977), nor all the complexities that the COCORP data suggest occur at finer scales (Oliver et al., 1980, Schilt et al., 1979). We show below that incorporating velocity inversions within the crust may explain much of the apparent complexity of some seismograms from WWSSN stations for known simple earthquakes. The basic effect of these velocity inversions is the appearance of extra phases which are lagged in time with respect to the first arrival an amount proportional to the depth to top and bottom of the low velocity zone and with amplitudes proportional to the velocity/density contrast. Depending on the thickness of this zone relative to the wavelength, reverberations may occur that can easily distort the seismogram and even give the impression of source multiplicity. The late arrivals may be interpreted as a combination of multiple bounces of P and SV energy trapped between the surface and the inversion layer, P and SV multiple bounces within the inversion layer, and P to SV conversions. Similar effects can, however, be caused by dipping interfaces in a crust without velocity inversions (Langston, 1977). Nonetheless, our analysis seems to suggest (see below, figure 2) that low velocity layers in flat lying sequences are more effective in generating extra phases on the vertical component of long-period records than has been recognized before, and that dipping interfaces may in comparison, produce only second order effects.

#### Waveform modeling

Figure 1 shows the basic results of this study. Fifteen long-period vertical WWSSN records of P-waves from the May 2, 1983 Coalinga earthquake have been modeled in the time domain. Unfortunately, only very few records of near naturally rotated SH waves are available, and these correspond to stations near a maximum of the SV radiation pattern (PAL, WES). Attempts to model these signals were only partially successful because of the strong SV contamination. The list of stations used in the P-wave analysis, their distances and azimuths from the source are given in Table I.

The methodology followed has been thoroughly discussed in the seismological literature (Helmberger, 1974, Langston, 1975, Liu and Kanamori, 1980, etc.). We have used WWSSN stations in the epicentral range  $30^{\circ}$  to  $85^{\circ}$  to avoid complexities arising from the upper mantle



travel time triplications and the heterogeneities of the core-mantle boundary. The far-field seismograms are obtained by evaluating expressions of the form (Liu and Kanamori, 1980).

$$u(t) = \frac{M_0}{4\pi\rho_h a_h^3} \frac{g(\Delta, h) R_p S(t-T_0) * Q(t) * C(t) * I(t)}{r} \quad (1)$$

where  $u(t)$  = synthetic seismogram

$M_0$  = seismic moment

$h$  = source depth

$\rho_h$  = density at the source

$a_h$  = P-wave velocity at the source

$g(a, h)$  = geometrical spreading factor

$r$  = Earth's radius

$R_p$  = Radiation pattern (double couple, P-waves)

$S(t)$  = far-field source time history

$T_0$  = travel time

$Q(t)$  = attenuation operator

$C(t)$  = Receiver crust transfer function

$I(t)$  = instrument response

$*$  = convolution operator

For practical applications  $S(t)$  contains the surface-reflected phases pP and sP and any other combinations of near-source rays that may be regarded as contributing to the observed signal. For each ray,  $S(t)$  consists of a trapezoidal function (see Figure 1) that represents the rise, rupture and roll off time histories of the source rupture (see Liu and Kanamori, 1980 for a detailed explanation). By direct measurements of the seismograms a first estimate of the total duration of  $S(t)$  can be made which will be subsequently refined during the modeling process. The fault plane solution in Figure 1 was computed from the teleseismic observations and essentially is in good agreement with that obtained by the USGS local array (Eaton, 1983). The aftershock data obtained by the University of California at Santa Cruz (UCSC) and the California Division of Mines and Geology (CDMG) as well as the United States Geological Survey (USGS), arrays helped considerably in establishing realistic bounds to the rupture size and focal depth. The crustal structure at the source was adapted from the data kindly provided by Sherburne et al., 1983 (see Table II).

The attenuation operator  $Q(t)$  (Carpenter, 1966) is obtained by setting  $t_a^* = 1$ , where  $t_a^*$  is the ratio of the P-wave travel time to the average value of the quality factor  $Q$  for P-waves along the ray path. The moment  $M_0$  is held fixed at a value of  $1 \times 10^{26}$  dyne-cm and the actual P-wave moment is obtained by directly comparing the computed amplitude in the synthetic seismogram with that observed on the records. We also computed the magnitude  $M_S$  of 20 sec Rayleigh waves (vertical component) at 12 WWSSN stations mostly located in the direction of maximum SV radiation and obtained an average value of 6.75. An approximate value of  $M_0$  of  $4 \times 10^{25}$  dyne-cm was obtained (Geller, 1977), assuming that the stress drop is of the order of 50 bars. This assumption is based on the probable intraplate character of the event and the relatively short duration

of the teleseismic source time function. A focal depth of 10 km satisfies the observed data quite well and is in agreement with the results obtained by the local arrays (Sherburne et al., 1983, Eaton, 1983). The least known function in (1) is  $C(t)$ , the receiver crust transfer function. We have constructed this operator by modeling the receiver crust as a stack of layers overlying a halfspace, and using the Haskell-Thomson matrix formalism to evaluate the response at the surface.

Figure 1 reveals that the Coalinga records show strong differences in waveform from station to station. At first sight the large later arrivals at stations BOG, SCP, AAM, WES, ALE could be interpreted as a second source, similar in mechanism to the first one, with a moment 0.40 times that of the first, and occurring 15 seconds later at the same epicenter location. This model, however, produced satisfactory matches at only some of the stations in figure 1. At other stations, such as SHK, MAT, KEV, MAL, a secondary source of that size and geometry was too strong and was inconsistent with the observations. More importantly, there is no evidence in the near field accelerographic records (Borcherdt, 1983) of the occurrence of a second event of that size within the first 20 seconds after trigger time. Furthermore, the secondary arrivals at KEV, NUR, and COP are too close to the predicted arrival of PcP so that a secondary source does not appear to be necessary. In fact, at these stations the secondary arrivals were modeled as PcP by lagging the first arrival in time and correcting it for radiation pattern and reflection coefficient at the core-mantle boundary. It is a crude approximation, but it reproduces the observations quite well, making the existence of a second source still more improbable.

The structure near the source, on the other hand, could be responsible for some of the observed complexities. However, in the distance range  $30^\circ$  to  $85^\circ$  the take-off angle varies only in a very narrow range ( $25^\circ$  to  $35^\circ$  from vertical), so it appears unlikely that the structure near the source could vary azimuthally so strongly as to account for the observations. This is however an important point and we shall discuss it further below (see figure 2). We opted to assume that the source of the later arrivals was indeed related to near-receiver crustal effects, including intracrustal velocity inversions. Several models were tested, first noting their effects in all the stations and then finding station groupings that shared similar receiver crustal models. The preferred models, per station, are given in table III. An interesting observation is that by including a low velocity layer under some stations the dispersion of the computed values of  $M_0$  was reduced substantially and that better fits were obtained consistently the closer the calculated amplitudes yielded values of  $M_0$  in the neighborhood of  $4 \times 10^{25}$  dyne-cm. Thus, we analyzed each record individually, adjusting the receiver crust model so as to minimize the scatter in  $M_0$ . The final results in figure 1 show a remarkably small scatter (generally less than  $\pm 1 \times 10^{25}$ ) from the mean of  $4.33 \times 10^{25}$  dyne-cm, as well as excellent agreement between the observed and computed waveforms. Some stations did not appear to require intracrustal low velocity layers (KEV, NUR, COP, MAT, SHK, MAL, PTO). At station MAT, the crustal structure used is that reported by Asano et al. (1973) without modifications. It can be seen that the fit at MAT is excellent. As discussed before, KEV, NUR, COP and PTO later arrivals are probably PcP, so the crustal models there are obscured by

this interference. One of the most complex records is that at BOG. It appears to require a very low velocity layer at the base of the crust, a strongly dipping Moho or combination of both. In all cases where a velocity inversion in the crust seemed possible we located it at several different depths, including the surface. The best fits were obtained with low velocity layers 4 or 5 km thick, 15 to 20 km below the surface.

At this time we have not been able to do the extensive testing of results that are necessary to either refine or disprove our claims. In the interest of consistency we have, however, tested one of our proposed receiver crust models. The results of this test are shown in figure 2. The left column shows the Coalinga earthquake as recorded at SCP (bottom trace). The middle trace is the synthetic seismogram already discussed and shown in figure 1. As can be observed this is perhaps our best fit. The top trace is the synthetic seismogram obtained for SCP with the same near-receiver crustal model but excluding the 5 km thick low velocity layer. It can be appreciated that the effect of this velocity inversion is very strong. The later phase appearing about 15 seconds after the first P arrival is probably a combination of P and SV multibounces within the top layer. Their arrival time is very sensitive to the depth of the low velocity layer and their amplitude strongly depends on the velocity/density contrast at its upper boundary. It can be shown that the timing of the two strong downswings following these phases are also sensitive to the S-wave travel time within the top layer and tend to merge or disappear if the shear wave velocity contrast between the top and the low velocity layers decreases.

The column on the right in figure 2 shows a similar comparison. This time, however, the earthquake is in a totally different source area (northern Costa Rica). The recording station is, also, SCP. The epicentral distances are similar, so that the emergence angle at the base of the crust is almost identical in both cases. The back azimuths, however, differ by nearly 90 degrees. The Costa Rica event has been modeled by F. Guendel (personal communication) as a single source thrust with source parameters strike= $116^{\circ}$ , dip= $60^{\circ}$ , rake= $90^{\circ}$  (one nodal plane), a focal depth of 12 km and a teleseismic source time duration of 7 seconds. Its magnitude ( $m_b$ ) is 5.8 and occurred on February 18, 1974. It should be obvious that the only common parameters between the two synthetic seismograms shown on the middle traces of figure 2 is that both were modeled using the same near-receiver crustal structure for SCP that includes a low velocity layer. It is now possible to identify in the Costa Rica seismogram some of the features just discussed for the Coalinga earthquake in terms of the later arrivals seen, and probably caused by the inversion layer under SCP. Thus, our near-receiver crustal model for SCP is consistent with observed seismograms from different source areas. This fact strongly suggests that the local structure near the hypocenter is not responsible for the latter phases and that there is little, if any, azimuthal variation of the crust under SCP, which indicates that flat layer models are appropriate, at least in the frequency range of a long-period WWSSN instrument.

It could be argued that since the epicentral distances are barely greater than  $30^{\circ}$ , what is observed is the well known effects of travel time triplications by upper mantle structure. That this may not be the



case is clear from the record at WES,  $\Delta \approx 38^\circ$  (figure 1), which shares many of the features observed at SCP.

#### Moment, stress drop and source area

The average body wave moment determined from the synthetic seismogram is  $M_0 = 4.33 \times 10^{25}$  dyne-cm. The teleseismic source time function that best fits the data is a trapezoid with  $\delta_1=1$ ,  $\delta_2=2$ ,  $\delta_3=1$ ; where the  $\delta_1$  is the rise time,  $\delta_1+\delta_2$  the rupture time and  $\delta_3$  is the roll off time. The local array operated jointly by UCSC and CDMG gives a stable width of the aftershock zone of 10 km in cross section during the first 2 days of activity, and length of approximately 15 km along strike. The distribution of aftershocks has been represented roughly as a rectangular zone 10 km in width (W) and about 20 km in length (L) by Eaton, 1983. Reasenberget al. (1983) suggest that within a few weeks of the main event the aftershock area grew, mostly along the strike. By June 20, 1983 the total area was  $32 \times 16 \text{ km}^2$ . It does not seem that a circular fault will be a good description of the source area, so we opted for an average rupture area of  $175 \text{ km}^2$  as a first approximation. It is quite possible that the aftershock zone expanded in the first few hours of the sequence. Unfortunately, during this period the location of hypocenters was extremely difficult due to the high rate of aftershock occurrence (Reasenberget al., 1983). Thus the above area could be an overestimate of the initial rupture area. Using this value of  $175 \text{ km}^2$  in the relation  $M_0 = \mu S D$  where S is the rupture area, D the average dislocation and  $\mu$  the local rigidity ( $\approx 3.0 \times 10^{11} \text{ dyne cm}^{-2}$ ) we calculate a dislocation of 82 cm. With a fault width of 10 km we obtain from the relation (Kanamori and Anderson, 1975)

$$\Delta \sigma = 4(\mu + \lambda) \mu D / \pi(2\mu + \lambda) W \quad (2)$$

a stress drop of  $\Delta \sigma$  of 21 bar, which for intraplate earthquakes of this size appears lower than average but not unrealistic. On the other hand, had we assumed a circular fault of radius equal to 5 km the stress drop could be as high as 150 bars. Until more detailed studies of the spatial and temporal sequence of aftershocks are available, these values of stress drop can only be considered as a possible range.

If we assume  $L=2W$  the rupture area may be estimated by the relation (Geller, 1977)

$$\log S = 2/3 M_S - 2.28 \quad (3)$$

giving  $S = 166 \text{ km}^2$ , and if the stress drop is of the order of 50 bars the moment  $M_0$  can be estimated from (Geller, 1977)

$$\log M_0 = M_S + 18.89 \quad (4)$$

giving  $M_0 = 4.36 \times 10^{25}$  dyne-cm. This value is in excellent agreement with our body wave calculations. Of course scaling relations (3) and (4) must be used only to confirm whether the computed parameters are consistent with global averages or not. In our case it seems that the

Coalinga earthquake falls within the norm, assuming the stress drop was complete.

### DISCUSSION AND CONCLUSIONS

The results of the seismic waveform modeling here reported for the Coalinga earthquake are in good agreement with the fault geometry determined by local field array studies. One of the nodal planes (strike= $303^{\circ}$ , dip= $66^{\circ}$ , rake= $90^{\circ} \pm 10^{\circ}$ ) is essentially controlled by near nodal stations AAM and ALE. The fault strike can be increased to  $307^{\circ}$  as obtained from analysis of first P-wave directions from the local array stations (Eaton, 1983) without disturbing the synthetics, in that case, however, the dip should decrease by about 2 degrees. The uncertainty in the rake is as large as  $\pm 10^{\circ}$  but for stations in Japan and South America a rake of  $80^{\circ}$ - $70^{\circ}$  produces better fits than  $90^{\circ}$ . In any case the second nodal plane is not well constrained by the data. The method does not resolve which of the nodal planes is the causative fault. In the construction of synthetic seismograms it was observed that reflections of P and S waves from the bottom of the second layer in the near source crustal model (Table II) interact with the first P arrival improving the synthetics quite substantially.

The near-receiver crustal models obtained in this study, under the assumption of the existence of intracrustal low velocity layers, are by no means unique nor final. We have not included dipping layers in our crustal models, which might produce some of the effects seen, nor have we investigated the relative importance of velocity inversions and dipping layers in both the source and the receiver sides. Figure 2 seems to support our assumptions but it is obvious that more work is necessary. Perhaps the important point that emerges is that at least theoretically, the effects of intracrustal velocity inversions add visible complexities to the computed wavefields. Since new deep crustal reflection data strongly suggest the existence of low velocity layers and other large heterogeneities within the crust (Oliver et al., 1983) it appears necessary to explore up to what point these crustal models may influence the observed long period body waves from earthquakes and nuclear explosions.

### ACKNOWLEDGEMENTS

K. McNally and R. Sherburne read the manuscript and offered valuable comments. This research was supported by the USGS under contract #14-08-0001-20546. Charles F. Richter Seismological Laboratory contribution #13.

## REFERENCES

- Asano, S., H. Okada, S. Kubota, S. Suzuki, and T. Yoshii, 1973, Crustal structure in the Matsushiro earthquake area, Tectonophysics, 20, 137-145.
- Borcherdt, R.D., 1983, The Coalinga earthquake sequence commencing May 2, 1983. Compiled by R. Borcherdt, U.S.G.S. Open-File Report, 83-511, Preliminary Report, Menlo Park.
- Burdick, L. and C. Langston, 1977, Modeling crustal structures through the use of converted phases in teleseismic body-waveforms, Bull. Seism. Soc. Am., 67, 677-91.
- Carpenter, E.W., 1966, Absorption of elastic waves - An operation for a constant Q mechanism, AWRE Report 43/66, London, H.M. Stationary Office, 16 p.
- Eaton, J., 1983, Seismic setting, location and mechanism, in U.S.G.S. Open-File Report, 83-511, Compiled by R. Borcherdt, Menlo Park.
- Geller, R., 1977, Earthquake source models, magnitudes and scaling relations, Ph.D. Thesis, California Institute of Technology, Pasadena.
- Helmberger, D.V., 1974, Generalized ray theory of shear dislocations, Bull. Seism. Soc. Am., 64, 45-64.
- Kanamori, H. and D.L. Anderson, 1975, Theoretical basis of some empirical relations in seismology, Bull. Seism. Soc. Am., 65, 1073-1096.
- Langston, C., 1977, Corvallis, Oregon, crustal and upper mantle receiver structure from teleseismic P and S waves, Bull. Seism. Soc. Am., 68, 1-30.
- Langston, C. and D.V. Helmberger, 1975, A procedure for modeling shallow dislocation sources, Geophys. J., R.A.S., 42, 117-30.
- Liu, H.L. and H. Kanamori, 1980, Determination of source parameters of mid-plate earthquakes from the waveforms of body waves, Bull. Seism. Soc. Am., 70, 1989-2004.
- Mueller, S., 1977, A new model of the continental crust, in The Earth's Crust Geophysical Monograph 20, Am. Geophys. Union, 289-318.
- Oliver, J., F. Cook, and L. Brown, 1983, COCORP and the continental crust, Jour. Geophys. Res., 88, B4, 3329-47.
- Reasenbergs, P., D. Eberhart-Phillips, and P. Segall, 1983, Preliminary views of the aftershock distribution, in U.S.G.S. Open-File Report, 83-511, Compiled by R. Borcherdt, 27-37, Menlo Park.
- Sherburne, R., K. McNally, A. Arburto, and E. Brown, 1983, The



mainshock-aftershock sequence of 2 May 1983, Coalinga, California, in this volume.

Schilt, F.S., J. Ohrer, L. Brown, S. Kaufman, D. Albaugh, J. Brewer, F. Cook, L. Jensen, P. Krumhansl, G. Long, and D. Steiner, 1979, The heterogeneity of the continental crust = Results from deep seismic reflection profiling using the VIBROSEIS technique, Rev. Geophys. Space Phys., 17, 354-368.

TABLE I

LIST OF WSSN STATIONS USED IN THE ANALYSIS (P-WAVES)

<u>Station</u>	<u>Distance (°)</u>	<u>Azimuth (°)</u>	<u>Maximum Amplitude of ground motion (<math>\mu</math>)</u>
AAM	28.82	66.6	10.9
AFI	69.84	234.2	7.33
ALE	50.20	8.35	10.9
BOG	52.80	115.40	7.7
COP	79.94	25.02	10.0
KEV	71.63	11.44	7.4
MAL	86.14	46.40	12.0
MAT	77.36	306.03	7.2
NUR	79.38	16.82	8.5
PAL	36.19	68.04	5.33
PTO	80.80	45.32	8.0
RDJ	93.50*	115.8	2.8
SCP	33.24	69.04	4.7
SHK	82.16	307.20	8.0
WES	37.93	65.34	

\*Very few records were available from South America so we included this station (Rio de Janeiro) although it is out of the appropriate distance range. This is reflected in its low amplitude and relatively low computed moment  $M_0$  (see Figure I).

TABLE II

NEAR SOURCE AVERAGE CRUSTAL MODEL (ADAPTED FROM MODEL PROVIDED BY CDMG)

<u>Layer #</u>	<u>P-Wave Vel.</u> (km/s)	<u>S-Wave Vel.*</u> (km/s)	<u>Thickness</u> (km)
1	2.87	1.7	2.1
2	4.2	2.5	4.4
3	6.0	3.5	7.5

\*For a Poisson's ratio of 0.25

TABLE III  
PREFERRED MODELS OF NEAR RECEIVER CRUST

Station(s)	Layer #	Model		Density (gr/cm <sup>3</sup> )	Thickness (km)
		P-Wave Vel. (km/s)	S-Wave Vel. (km/s)		
SCP	1	6.0	3.5	2.7	20
	2	4.0	2.3	2.5	5
	3	7.0	4.3	3.0	12
	4	8.4	4.9	3.3	
PAL	1	same as SCP			
	2	4.6	2.7	2.5	7
	3	same as SCP			
	4	same as SCP			
WES	1	same as SCP			
	2	4.7	1.7	2.7	5
	3	same as SCP			
	4	same as SCP			
AAM	1	6.0	3.5	2.7	17
	2	5.0	1.6	2.5	5
	3	same as SCP			
	4	same as SCP			
KEV	1	3.4	2.0	2.7	6
	2	6.5	3.8	2.8	10
	3	7.0	4.3	3.0	20
	4	8.1	4.5	3.2	
MAT*, SHK	1	4.0	2.7	2.2	5.0
	2	6.0	3.4	3.0	30 (24 at SHK)
	3	7.7	4.2	3.3	20
ALE	1	3.4	2.0	2.3	6
	2	6.5	3.8	2.8	10
	3	5.0	3.0	2.7	7
	4	7.0	4.3	3.0	15
	5	8.1	4.5	3.3	
NUR, COP, MAL, PTO**	1	2.5	1.4	2.4	6
	2	6.5	3.4	2.7	30
	3	8.4	4.9	2.9	
AFI	1	6.3	3.5	2.6	15
	2	2.5	1.0	2.5	1.5
	3	8.1	4.5	3.0	
RDJ	1	6.2	3.0	2.7	12
	2	3.0	1.6	2.5	3
	3	7.2	4.0	3.0	15
	4	8.0	4.2	3.2	
BOG	1	4.0	2.3	2.4	7
	2	6.5	3.8	2.8	14
	3	7.0	4.0	3.0	15
	4	4.3	0.8	2.8	2
	5	8.4	4.9	3.3	-

\*From Asano et al (1973)

\*\*Least reliable structures due to PcP interference

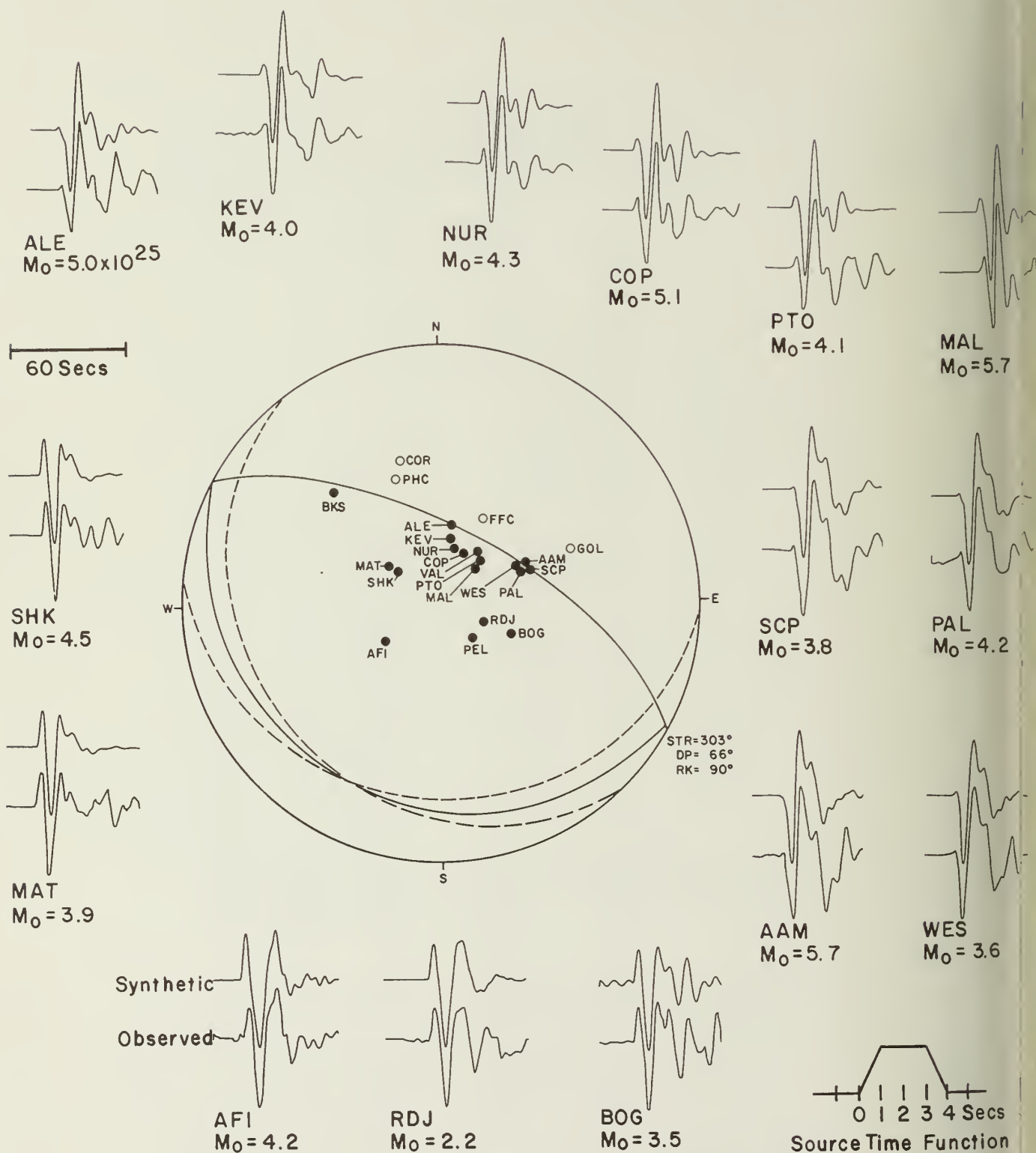


Figure 1. Comparison of synthetic and observed P-wave long period seismograms for the May 2, 1983 Coalinga earthquake. The source time function used is depicted on the lower right corner. The average computed moment,  $M_0$ , is  $4.33 \times 10^{25}$  dyne-cm.



COALINGA, 1983  
 SCP LPZ  
 $\Delta = 33.24$   
 $BA_z = 276.1$

COSTA RICA, 1974  
 SCP LPZ  
 $\Delta = 31.6$   
 $BA_z = 191.5$

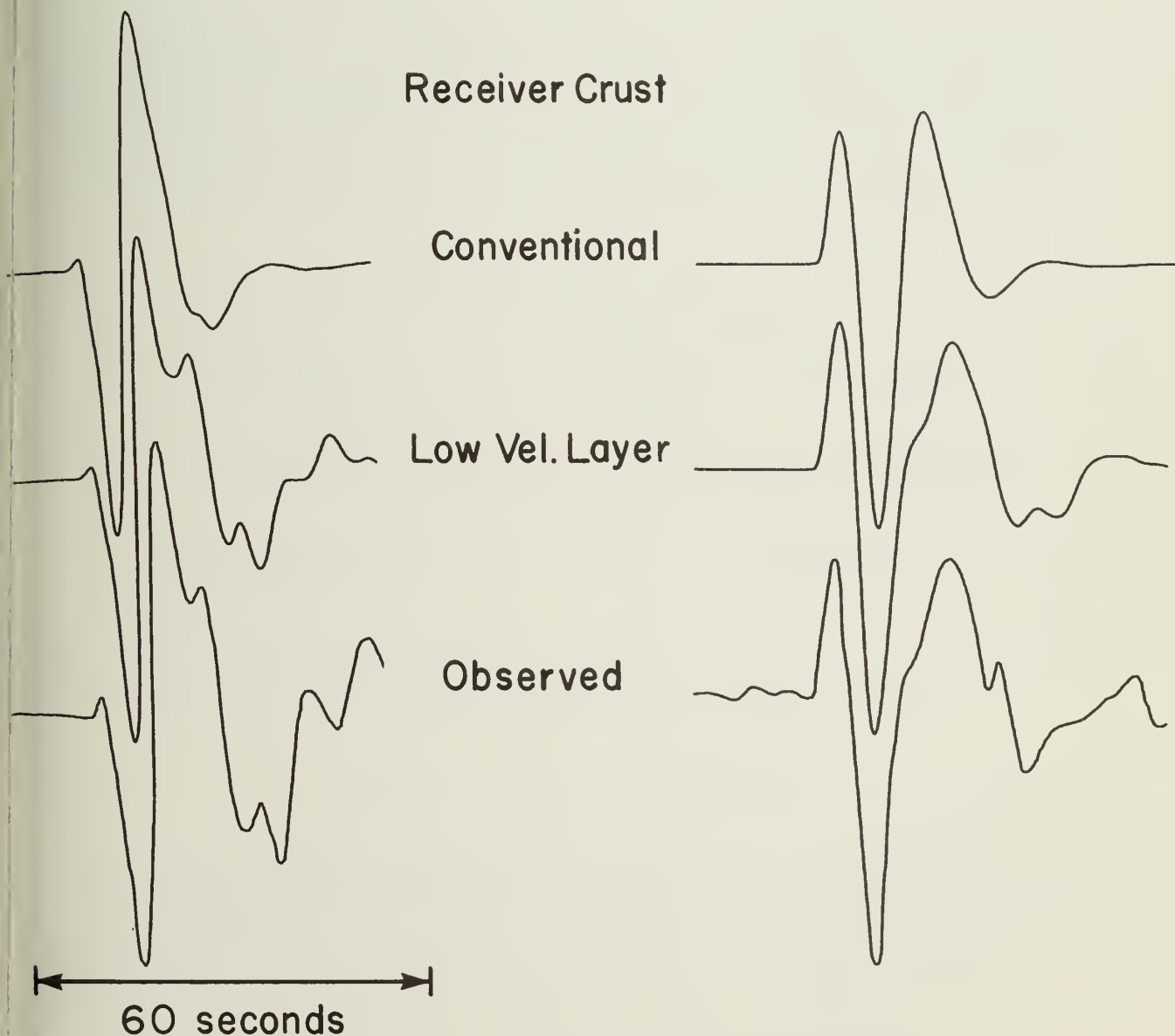


Figure 2. Effect of velocity inversion in the near-receiver crust of the SCP station (State College, Pennsylvania). The two top traces are synthetic seismograms constructed for a crustal model without (conventional) and with a low velocity layer 5 km thick 20 km below the surface. (See text for details)



# STUDY OF THE MAY 2, 1983 COALINGA EARTHQUAKE AND ITS AFTERSHOCKS, BASED ON THE USGS SEISMIC NETWORK IN NORTHERN CALIFORNIA

by

J. Eaton<sup>1</sup>, R. Cockerham<sup>1</sup>, and F. Lester<sup>1</sup>

## INTRODUCTION

The work reported in this paper is based jointly on analysis of the main Coalinga earthquake and 9 selected aftershocks from records of the entire northern California network, and on reanalysis of the raw onset times and event durations reported by the Allen/Ellis real time processor (RTP) in Menlo Park [Allen, 1982]. The reprocessing was made possible by the devoted effort of the Central California Network Processing Group, which processed the voluminous RTP data in a timely manner throughout the earthquake sequence.

The principal topics considered in this report are:

- 1) the setting of the Coalinga earthquake sequence,
- 2) the development of a crustal velocity model and associated station corrections for the Coalinga region,
- 3) the determination of fault plane solutions and the modification of the velocity model required for that purpose,
- 4) the reprocessing of the raw RTP data to improve hypocenter determinations,
- 5) the determination of magnitudes, and
- 6) the spatial distribution of hypocenters and its relation to the fault plane solutions of the larger shocks.

## SETTING OF THE COALINGA EARTHQUAKE

Background seismicity in the central Coast Ranges is dominated by a concentration of small earthquakes along the San Andreas Fault from Parkfield to San Juan Bautista. In addition, scattered small earthquakes and occasional moderate earthquakes with dense clusters of aftershocks occur throughout the region between this section of the San Andreas Fault and the Great Valley to the east.

It is difficult to discern any clear pattern in the seismicity east of the San Andreas from a single year's data. However, a clear pattern does emerge if a longer period of time is considered. Seismicity east of the

<sup>1</sup>U.S. Geological Survey, Menlo Park, California 94025



San Andreas Fault from January 1972 through April 1983 is shown in Figure 1, where the concentrated band of activity along the San Andreas Fault has been excluded. In the northwest part of the region, clusters of events are generally small, scattered events are distributed rather uniformly between the clusters, and the density of events drops off sharply northeast of a line, with an azimuth of about N 30° W, along the longitudinal axis of the region. At its northwestern end this line coincides approximately with the Ortigalita Fault. In the southeastern part of the region, clusters of epicenters from moderate earthquakes and their aftershocks are larger, and most of the activity lies northeast of the axial line described above. The year of occurrence of the more prominent clusters is shown in Figure 1.

The 1983 Coalinga aftershock region virtually fills the gap of relative quiescence between the clusters of 1976, 1980, and 1982 (Figure 1). Its large size relative to the earlier clusters corresponds to the size of the Coalinga earthquake (M6.5+) relative to the largest shocks in the other clusters (M5 to M5.5).

Other prominent gaps of seismicity in the southeast half of Figure 1 include 1) the region between the clusters of 1974, 1975, 1982, and 1983 (Coalinga) and 2) the entire region between the band of earthquakes along the San Andreas Fault and the clusters of 1982, 1983, 1976, and 1981.

#### CRUSTAL MODEL FOR THE COALINGA REGION

Coalinga is at the eastern edge of the dense seismic network in the central Coast Ranges, and the velocity model routinely used for central California earthquakes gives poor results there. Moreover, crustal structure probably varies abruptly from east to west across the Coalinga region, particularly the thickness of low velocity materials in the upper crust. Although recent refraction profiles provide better information along selected lines [Wentworth et al., 1983; Walter and Mooney, 1983], they do not yet cover a sufficiently broad region to provide an adequate model for earthquake hypocenter determinations.

We have employed 10 special study Coalinga events in an iterative process to develop a more appropriate crustal model and an associated set of station corrections. Initial station delays (delay set D0) for stations within 100 km of the main shock epicenter, which were the only ones used for hypocenter calculations, were adapted from an unpublished Pn time-term-difference study of the central California network. Starting with the standard crustal model in routine use for the central Coast Ranges (model M0), layer velocities and depths were varied systematically during a succession of relocations of the main Coalinga earthquake to minimize the rms of residuals and to permit separation of the fields of dilatations and compressions on a plot of first motion directions. The station residuals for the best-fitting model (M1) were added to the original station delays to produce station delay set D1, which elevated the main shock to the status of a master event. Next, the 10 special study quakes, including the main shock, were located using model M1 and delay set D1. The average station residuals for these 10 quakes were then added to delay set D1 to produce delay set D2.

It was our intention to use model M1 and delay set D2 to locate the rest of the aftershocks. In the course of determining fault plane solutions for the 9 aftershocks studied, however, it was necessary to further modify the crustal model to obtain first motion plots with separated fields of compressions and dilatations for the events of May 22 (model M2) and June 11 (model M3). With results from five events in hand (May 2-June 11), a composite model (M4) that satisfied all five events best was selected. Model M4 yielded good fault plane solutions for the rest of the 10 events studied in detail.

The principal differences among the models (summarized in Table 1) are between 2 and 14 km depth. For most events, the differences in location and rms of the residuals for the different models are very small. Depending on focal depth, however, the different models produce very different crossover distances between the direct wave and the first refracted wave that overtakes the direct wave. It is this last effect that is useful in separating fields of mixed dilatations and compressions in some first motion plots.

For the systematic location of all Coalinga events for maps, cross sections, and the catalog, crustal model M4 and delay set D2 were used.

Table 1

Crustal velocity models for determining focal mechanisms

Model 1		Model 2		Model 3		Model 4	
Vel. <sup>a</sup>	Depth <sup>b</sup>	Vel.	Depth	Vel.	Depth	Vel.	Depth
2.50	0.00	2.50	0.00	2.50	0.00	2.50	0.00
5.50	2.00	5.40	2.00	4.30	1.50	4.50	2.00
5.70	9.00	5.60	7.00	5.60	7.00	5.60	7.00
6.40	14.00	6.20	10.00	6.20	10.00	5.70	10.00
7.90	28.00	6.45	14.00	6.45	14.00	6.40	14.00
		7.90	27.00	7.90	27.00	7.90	28.00

<sup>a</sup> km/sec

<sup>b</sup> km

### FAULT PLANE SOLUTIONS

First motion plots and fault plane solutions for the main shock and 9 of its principal aftershocks are shown in Figure 2 and summarized in Table 2. Figure 2 also contains an index map showing the locations of these events relative to each other, to the overall aftershock zone, and to nearby stations of the seismic network. Stations PDR, PKE, PWM, and PHB were installed after the main shock. Open circles represent clear dilatational onsets, closed circles represent clear compressional onsets, and X's indicate the superposition of clear compressions and dilatations. The plots are lower hemisphere projections.

In general, the quality and quantity of the data underlying these plots are excellent. The principal variable affecting the plots was the crustal model used to determine the hypocenter (most importantly, the focal depth)

and the angles of incidence at the focus. The greatest variations in the diagrams are related to lower crust and upper mantle refractions recorded west of the epicenters.

All 10 solutions indicate thrust or high angle reverse faults. The axes of maximum pressure are generally nearly horizontal. The main shock and two nearby aftershocks (events A, B, and D) and event F at the southwest edge of the aftershock region indicate NE-SW compression of the crust. The five events west of the main shock (E, G, H, I, and J) all indicate E-W compression. Event C at the southeast edge of the aftershock region suggests N-S compression.

The main shock, which occurred before the installation of four new stations to enclose the epicentral region, has the most poorly constrained solution. Nodal plane I is well determined, but only the dip of nodal plane II is well determined. The strike of nodal plane II is constrained only to lie between N 20°W and N 80° W. Hence, the solution, drawn in Figure 2 as pure dip-slip motion, may contain a significant component of right or left lateral slip.

These fault plane solutions suggest a complex underlying structure or process. In conjunction with other data they can help in the formulation and testing of models to explain the process responsible for the Coalinga earthquake sequence.

#### RTP RECORD OF THE AFTERSHOCK SEQUENCE

Although still under development and evaluation, the Allen/Ellis real time processor (RTP) performed remarkably well throughout the heaviest part of the aftershock sequence in May and June. Hardware problems degraded its performance during July, but it continued to provide an overview of activity in the aftershock region. In addition to rapid location and magnitude determinations for tracking the progress of the aftershock sequence, the RTP provided a vast record of onset time and duration data on the individual events of the sequence. These data, reprocessed to eliminate spurious readings and relocated using an improved crustal model and station corrections, have produced a catalog of aftershocks of the Coalinga earthquake that is unparalleled in its uniformity as well as its timeliness.

Reprocessing of the RTP data was carried out in the following manner:

- 1) The daily RTP hypocenter summary list produced in routine processing was screened to select all events with 7 or more useful stations that occurred within 110 km of the Coalinga main shock epicenter. The corresponding phase data were then extracted from the daily RTP phase file.
- 2) The extracted events were relocated using crustal model M4 and station delay set D2.
- 3) The detailed hypocenter solutions (location summary plus station residuals, etc.) were examined to eliminate stations with residuals larger than three times the rms of all residuals, and a revised phase list was generated. The events were then relocated on the basis of the revised phase list.



- 4) Solutions with an rms of residuals greater than 0.25 sec. were examined by the authors. Many sub-standard solutions resulted from one or more obviously spurious readings, which were removed. Many other poor solutions resulted from mixed readings from a small preliminary event and a slightly larger later event. Most of these solutions were improved by a judicious elimination of some of the very early or very late readings.

Fewer than 1 event in 10 required this special analysis. Good solutions were ultimately obtained for almost all of the events selected for reprocessing.

### MAGNITUDES

Magnitude determinations were based chiefly on the duration times reported by the RTP. The RTP discontinues measuring durations beyond 140 seconds, corresponding to a magnitude of about 3.7, however; so other means of determining magnitudes of the larger quakes were required.

In the routine processing of central California network data, a daily list of events (scan list) is prepared from direct examination of the film (Developer) and paper (Helicorder) records. The scan list identifies each event by the station with the earliest arrival, the number of stations with timable onsets, and the average event duration on the records from which it was reported. Duration magnitudes calculated from scan list data were used instead of the RTP duration magnitudes for events larger than about M3.7.

To unravel the complicated records for the early part of the aftershock sequence, continuous strip-chart playbacks of low-gain stations at various distances from Coalinga were made. These records were used to estimate event durations for the first 3 hours of the aftershock sequence.

For the 9 large aftershocks played back from magnetic tape, magnitudes were calculated from the maximum amplitudes and associated wave periods. The recorded maximum amplitudes were reduced to the corresponding Wood-Anderson amplitudes, which were then used to determine magnitude by standard methods.

The UC Berkeley magnitudes [Uhrhammer, et al., 1983] for the main shock and its first large aftershock were adopted for this study.

### SPATIAL DISTRIBUTION OF THE HYPOCENTERS

The catalog of Coalinga events from May 2 through July 31 produced by the methods outlined above contains more than 5000 events. Of these events, 894 are of magnitude 2.5 or greater and 2258 are of magnitude 2.0 or greater.

For analysis of the spatial distribution of hypocenters a subset of 651 events that met the following requirements was selected:

- o magnitude  $\geq 2.5$
- o number of stations used in solution  $\geq 12$

- o rms of solution  $\leq 0.20$  sec.
- o distance to nearest station  $\leq 20$  km
- o estimated epicentral error  $\leq 5$  km.

Maps of these events for the first day (23:42 May 2 through 24:00 May 3) and for the entire catalog (May 2 through July 31) are shown in Figure 3. Comparison of these maps shows that the entire NW to SE length of the after-shock zone was fully involved during the first day. The broadening of the zone (SW to NE) at its northern end occurred later in the sequence, mostly during June and July. On the May 2-July 31 plot, the epicenter of the main shock lies near the center of the aftershock region just southeast of an epicenter-free band that divides the region into northern and southern parts along the line NT-NT'. The southern part is narrower and denser than the northern part. Cross sections along lines N-N' (longitudinal section) and NT-NT' (transverse section) further illustrate the differences between the two parts of the aftershock region. The longitudinal section (Figure 4A) shows that activity south of the main shock is concentrated at depths of 5 to 11 km and that large aftershocks are lacking beyond a few kilometers south of the main shock. Activity north of the main shock is concentrated between 8 and 13 km. Most of the large aftershocks occurred north of the main shock. On the transverse section (Figure 4B), the dissimilar northern and southern parts of the aftershock region are superposed, and the plot is difficult to interpret. The transverse section was divided into two parts and replotted in Figure 5.

The transverse section for the northern subregion (Figure 5A) shows zones of hypocenters in the form of a "V" with its vertex 5 km west of line N-N' (0 km) and about 12 km deep. The western limb appears to dip eastward at about  $55^\circ$  and the eastern limb appears to dip westward at  $30^\circ$  to  $35^\circ$ . The large earthquakes lie along the outer (deeper) edges of the limbs of the V. The main shock and two large aftershocks (events A, E, and H from the first motion plots) are identified on the section, and symbols showing the dip of one nodal plane, here assumed to be the fault plane, and the sense of movement on it were drawn for these events. The main shock actually lies just south of the northern region, but it was added to this section to show its relationship to the eastern limb of the V.

On the basis of the transverse cross section of hypocenters in the northern subregion, it appears that the main earthquake occurred on a westward-dipping low-angle thrust fault located at the base of the eastern limb of the V. The eastward-dipping high-angle reverse fault indicated by event E actually broke through to the earth's surface when it occurred [Hart et al., 1983]. The larger event H has a similar fault plane solution and appears to have been caused by even more extensive movement on a high-angle reverse fault located at the base of the western limb of the V.

Hypocenters are more numerous and densely packed in the southern subregion (Figure 5B) than in the north. They fill a wedge-shaped region with a western side that dips  $50^\circ$  to  $60^\circ$  toward the east and an eastern side that dips  $50^\circ$  to  $60^\circ$  toward the west. The main shock and the aftershock of May 9 both lie at or near the western side of the wedge. Fault plane solutions for both events have one plane that nearly parallels the western side of the wedge

and corresponds to high-angle reverse faulting along the western side of the region. The greatest concentration of hypocenters is in a subhorizontal band that crosses the wedge just above the level of the main shock. This band may represent the southern extension of the eastern limb of the V identified in the northern subregion. On the combined transverse section in Figure 3, it appears to fill in a sparse region in the eastern limb of the V of the northern subregion.

The apparent dip of the eastern boundary of the wedge suggests that a westward-dipping high-angle reverse fault bounds the aftershocks there also, but focal plane solutions for events along that boundary have not yet been obtained.

### CONCLUSIONS

The 1983 Coalinga earthquake and its aftershocks occurred in a section of the central Coast Ranges that has been characterized by separated moderate earthquakes with prominent aftershock clusters. The 1983 sequence filled in a large gap of relative quiet on the seismicity map for the last decade. Fault plane solutions for the main shock and 9 prominent aftershocks all indicate subhorizontal crustal compression, but the inferred orientation of the axis of maximum compression varies widely across the aftershock zone. The aftershock zone is about 30 km long in a north-northwest to south-southeast direction and is about 10 km wide at its southern end and nearly 20 km wide at its northern end. The aftershock zone expanded only slightly after the first day. The main shock occurred near the center of the aftershock zone and separates rather different patterns of hypocenter distribution to the north and south.

The seismic evidence reported here suggests that the main shock occurred on a southward-dipping low-angle thrust fault surface and that the patch on the fault that slipped during the 1983 sequence runs diagonally across the strike direction of the fault surface, lying west of a strike line through the epicenter on the north and east of that line on the south. High-angle reverse faults appear to extend toward the earth's surface from the western edge of the slipped thrust fault along the entire western margin of the aftershock zone and along the southern half of the eastern margin of the aftershock zone.



## ACKNOWLEDGEMENTS

The authors are indebted to R. Stein and D. Eberhardt-Phillips who reviewed the manuscript and made valuable suggestions for improving its clarity.

## REFERENCES

- Allen, R., 1982, Automatic phase pickers: their present use and future prospects: *Seismol. Soc. Amer. Bull.*, v. 74, p. S225-S242.
- Hart, E. W., and McJunkin, R. D., 1983, Surface faulting northwest of Coalinga, California, June and July, 1983: this volume.
- Walter, A. W., and Mooney, W. D., 1983, Preliminary report on the crustal velocity structure near Coalinga, California, as determined from seismic refraction surveys in the region: this volume.
- Wentworth, C. M., Walter, A. W., Bartow, J. A., and Zoback, M. D., 1983, The tectonic setting of the 1983 Coalinga earthquakes: Evidence from deep reflection and refraction profiles across the southeastern end of the Kettleman Hills: this volume.
- Uhrhammer, R. A., Darragh, R. B., and Bolt, B. A., 1983, The 1983 Coalinga earthquake sequence: this volume.

Table 2

Locations, magnitudes, and fault plane solutions of the main shock and selected aftershocks

Event	Date	Time	Lat. (N)	Lon. (W)	Depth (km)	Mag.	Nodal Plane I		Nodal Plane II		Pressure Axis	
							Strike	Dip	Strike	Dip	Direct.	Incl.
A	830502	234237.8	36°13.15'	120°18.99'	10.2	6.7 <sup>a</sup>	N53°W	67°NE	N53°W <sup>b</sup>	23°SW	N37°E	22°
B	830509	024911.3	36°13.75'	120°18.74'	12.5	5.2	N73°W	48°NE	N38°W	48°SW	N34°E	0°
C	830522	083921.4	36°08.28'	120°13.14'	10.3	4.3	N83°W	54°N	W	36°S	N 4°E	10°
D	830524	090217.4	36°14.27'	120°19.54'	9.9	4.7	N42°W	74°NE	N35°W	16°SW	N49°E	29°
E	830611	030952.1	36°14.62'	120°27.55'	4.5	5.2	N13°E	54°SE	N24°W	42°SW	N87°E	7°
F	830612	013127.2	36°06.85'	120°18.19'	13.5	4.0	N40°W	60°NE	N 6°W	35°SW	N69°E	14°
G	830709	074050.9	36°14.20'	120°24.54'	9.5	5.5	N24°E	41°SE	N14°W	56°SW	N88°W	8°
H	830722	023953.7	36°13.67'	120°24.94'	9.2	6.4	N20°W	34°NE	N14°W	56°SW	S70°W	11°
I	830722	034300.7	36°12.57'	120°24.79'	9.6	5.0	N40°W	34°NE	N 7°W	60°SW	S82°W	13°
J	830725	223139.2	36°12.92'	120°24.33'	9.5	5.4	N20°W	36°NE	N13°W	54°SW	S73°W	9°

<sup>a</sup> UC Berkeley magnitude

<sup>b</sup> Strike constrained only to the range N20°W to N80°W

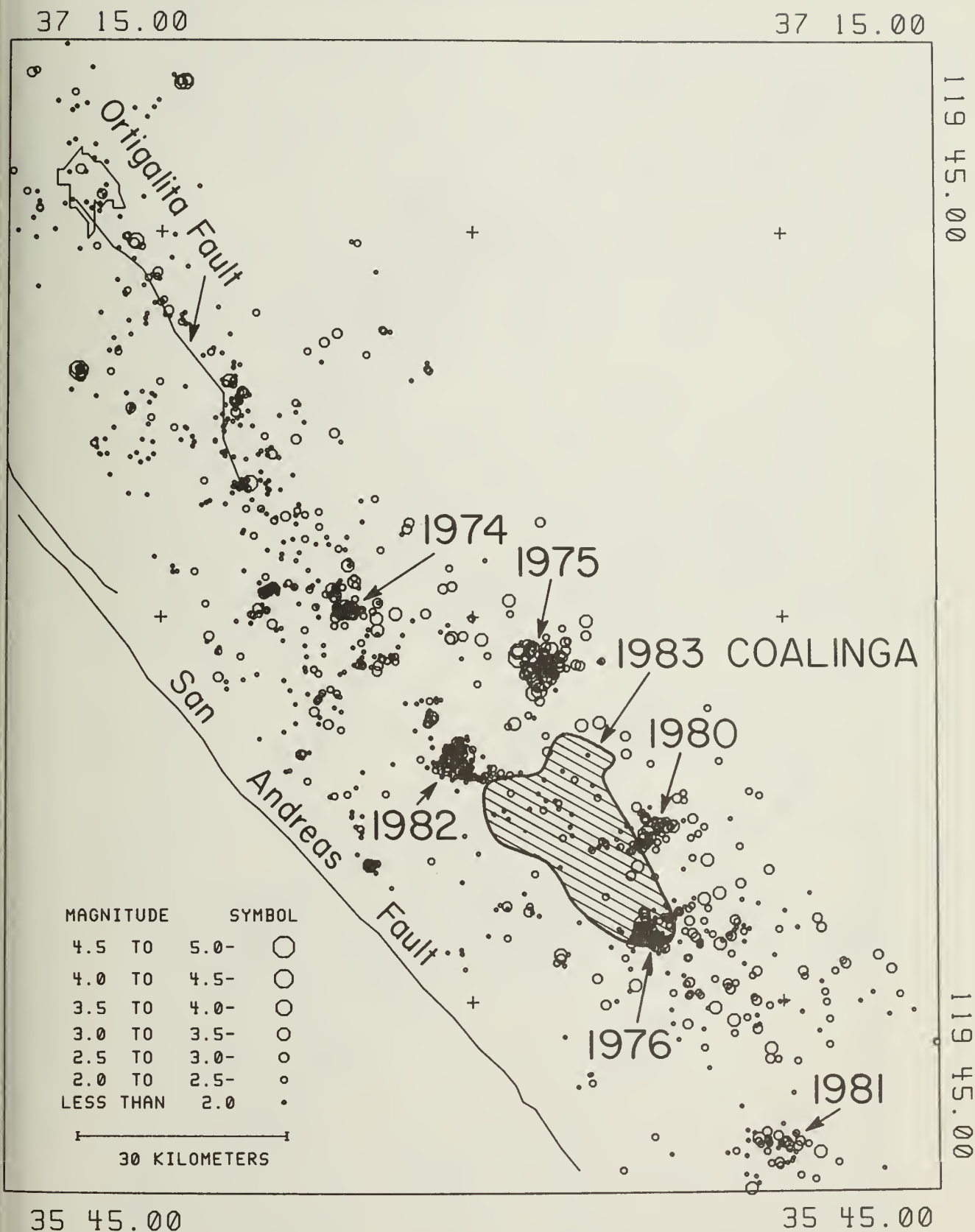


Figure 1. Map of seismicity in the central Coast Ranges east of the San Andreas Fault from January 1972 through April 1983 showing dates of occurrence of prominent aftershock clusters. San Andreas events are not shown.

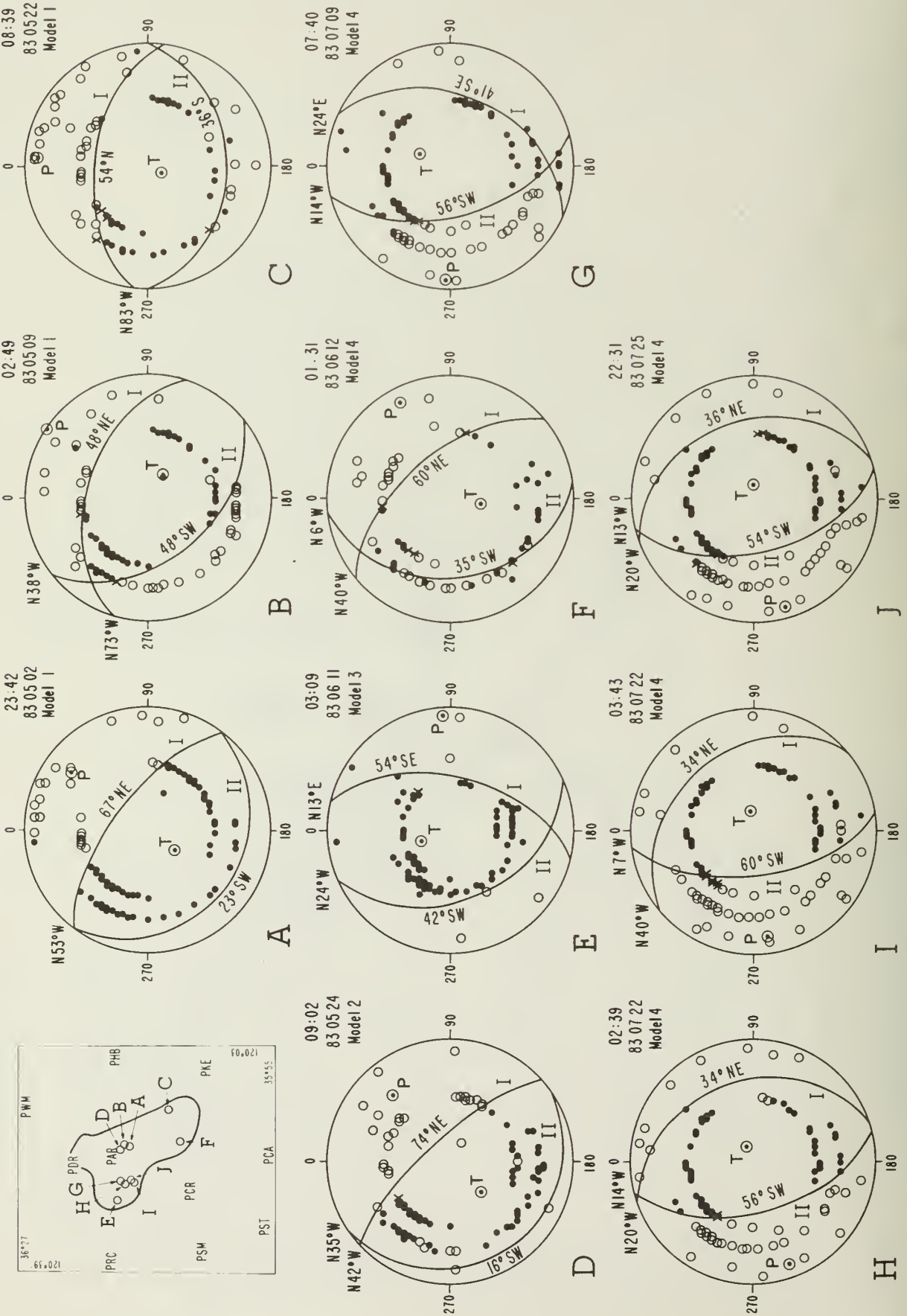


Figure 2. Index map and fault plane solutions for the Coalinga earthquake and 9 of its aftershocks. See text for explanation of symbols.



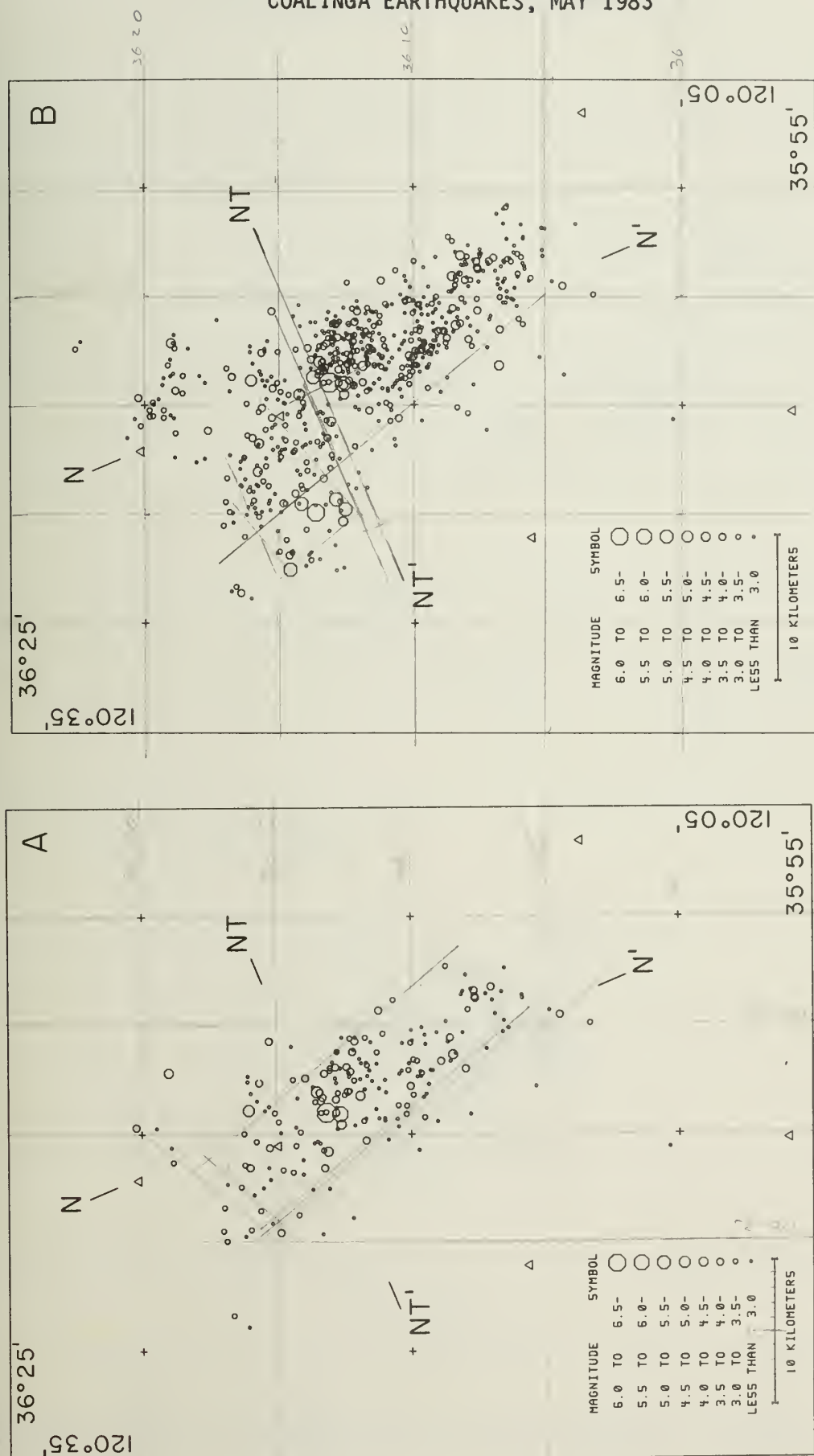
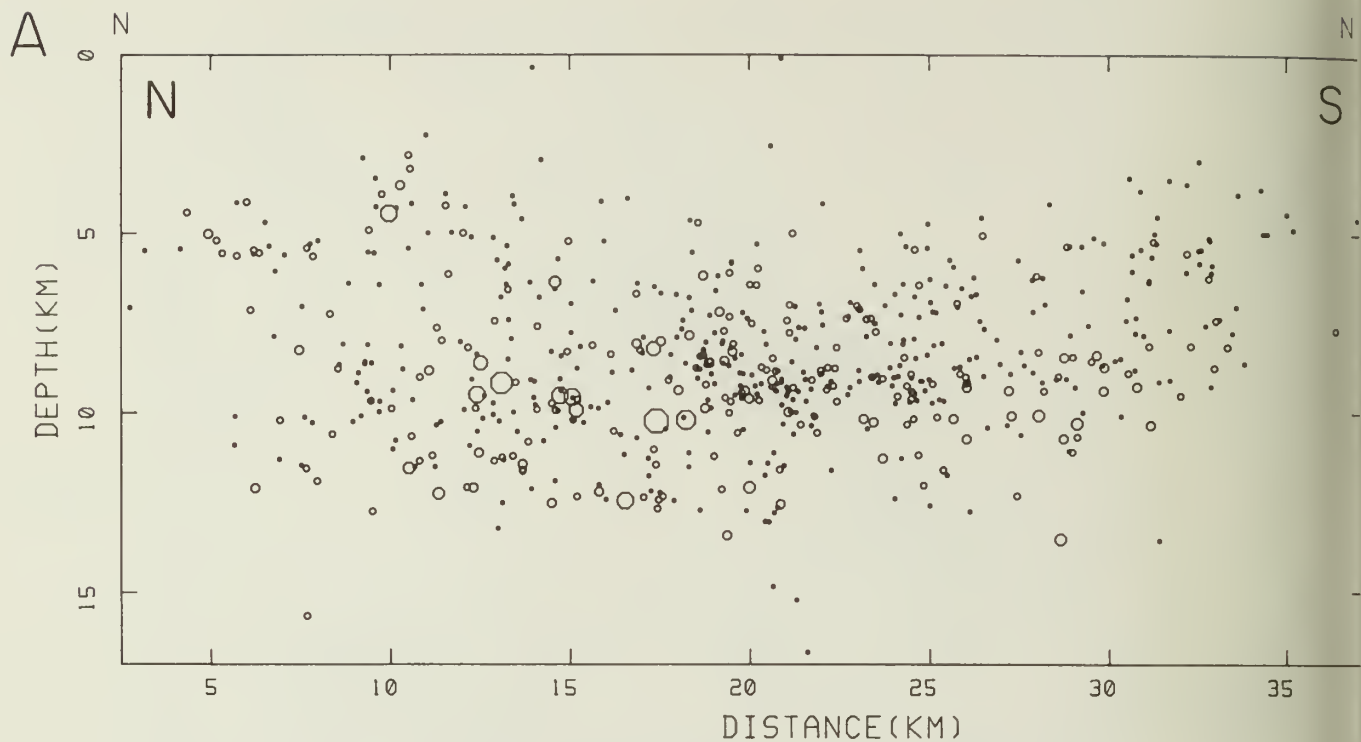
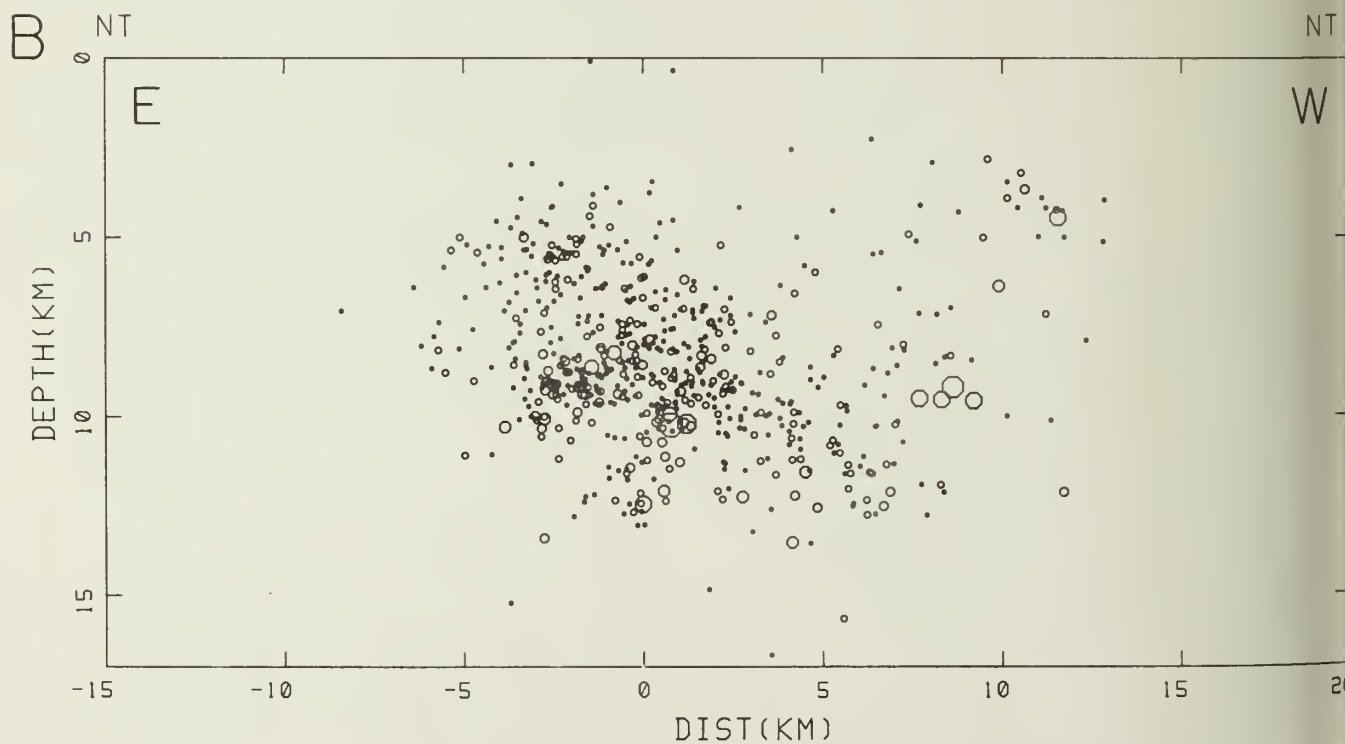


Figure 3. Epicenter plots of M2.5 and larger events of the Coalinga earthquake and its aftershocks.  
 A) 23:42 May 2 to 24:00 May 3, B) May 2 through July 31.



N=36-22.0 120-23.0 N'=36-02.0 120-12.7 May02-Jul31 M>2.5



N=36-22.0 120-23.0 N'=36-02.0 120-12.7 May02-Jul31 M>2.5

Figure 4. Longitudinal (A) and transverse (B) cross sections of the Coalinga aftershock sequence relative to the line N-N' on Figure 3B.

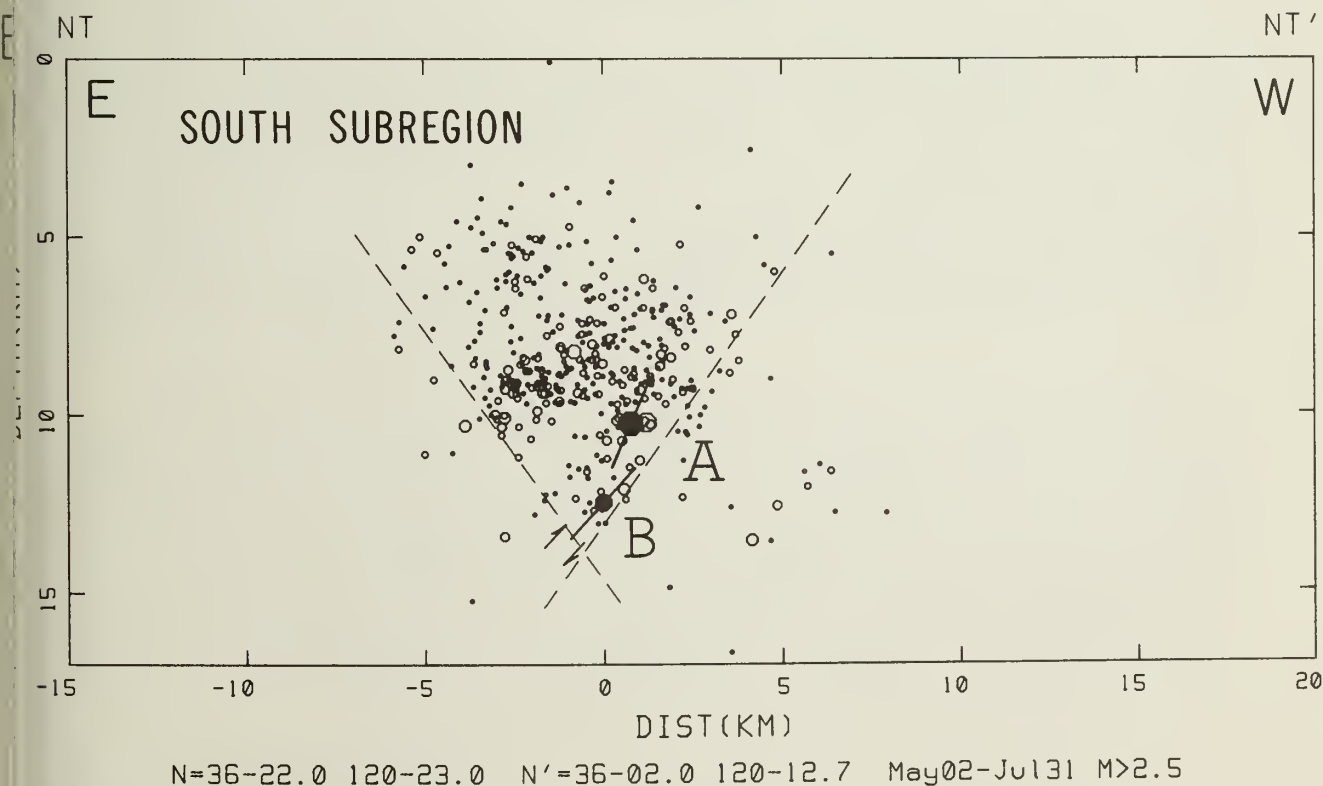
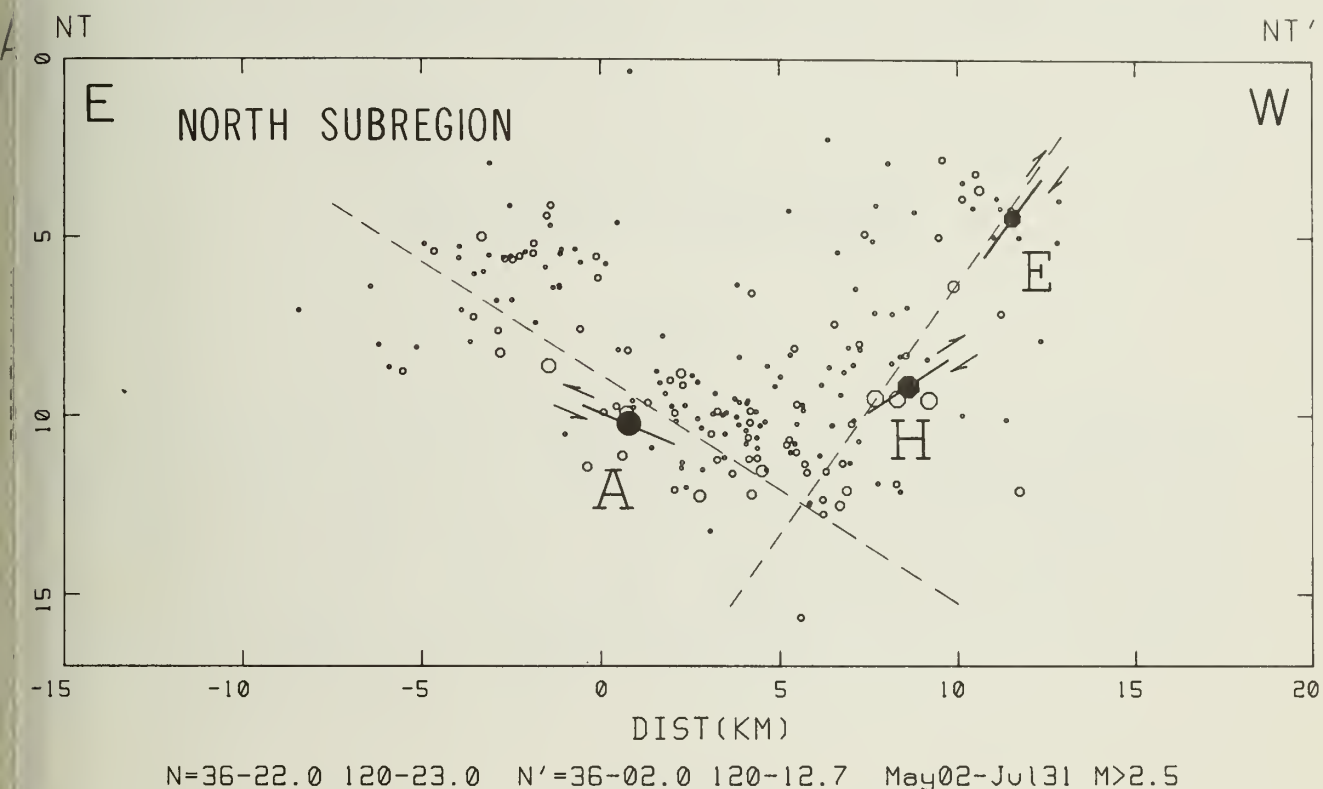


Figure 5. Separate northern subregion (A) and southern subregion (B) transverse cross sections of the Coalinga aftershock sequence relative to line N-N' on Figure 3B.





# THE MAINSHOCK-AFTERSHOCK SEQUENCE OF 2 MAY 1983: COALINGA, CALIFORNIA

by

Roger Sherburne<sup>1</sup>, Karen McNally<sup>2</sup>,  
Ethan Brown<sup>2</sup>, and Arturo Aburto<sup>3</sup>

## ABSTRACT

The University of California, Santa Cruz and California Division of Mines and Geology operated a dense local network of stations surrounding the aftershock zone of the Coalinga earthquake from May 3 to May 19. Detailed information from this study will allow precise examination of the mainshock rupture process. The mainshock has been relocated using travel time adjustments for regional stations determined by a "master event" technique. A velocity model was developed for these analyses using travel times from explosions detonated by the U.S. Geological Survey to the seismograph stations of the local network.

## INTRODUCTION

The Coalinga earthquake ( $M_L = 6.7$  [Uhrhammer et al., 1983],  $M_S = 6.75$  [Rial and Brown, 1983]) of May 2, 1983 was the largest earthquake within California since the 1980 Mammoth Lakes and Mendocino earthquakes and the largest in the San Joaquin Valley since 1952. Although earthquakes are not unknown to the Coalinga area (Beroza, Brown, and McNally, 1983), the occurrence of a  $M_L 6.7$  was a surprise to many earth scientists. The lack of surface rupture associated with the causative fault requires the application of geophysical, seismological, and geodetic methods for studying this earthquake and for determining the characteristics of the Anticline Ridge fault.

Described here are the results of the joint field work, data analysis, and seismological interpretation by the California Division of Mines and Geology (CDMG) and University of California, Santa Cruz (UCSC) related to the 1983 Coalinga earthquake. A seismograph station network of 12 stations was maintained over a 17-day time period: May 3 to May 19, 1983. Two of these stations were occupied jointly in coordination with University of California, Berkeley (UCB). Four refraction shots by the U.S. Geological Survey were also monitored for the purpose of developing a velocity model for the aftershock locations. Earthquakes were located with the computer program Hypo71 (Lee and Lahr, 1975).

---

<sup>1</sup> California Division of Mines and Geology.

<sup>2</sup> U.C. Santa Cruz, Charles F. Richter Seismological Laboratory.

<sup>3</sup> Stanford University.

Eighty-seven aftershocks have been located: Sixteen were of A-quality, fifty of B-quality, and twenty-one of C-quality.

The mainshock was relocated using adjustments to travel times at regional stations based on an "average" master event method (discussed later in text) with the following results:

Date	- May 2, 1983
Origin Time (GMT)	- 23:42 38.62
Latitude	- 36° 13.38' N
Longitude	- 120° 19.27' W
Depth (km)	- 7.43

### INSTRUMENTATION

The suite of instrumentation available to record aftershocks of this earthquake consisted of 13 Sprengnether smoke-paper recorders, eight Mark Products 1 hertz L-4C, and five Kinometrics Ranger seismometers, and a single three-component Sprengnether DR-100 seismograph system. The vertical seismograph systems at CFIR, CAVL, and C5PT were equipped with special 60dB attenuators which were necessary because of the high level of ambient noise. The goal was to deploy the instrumentation rapidly to collect data which would supplement existing networks and also be adequate for independent analysis of the aftershocks. The first station installed was near Panoche Valley, about 35 miles north of the mainshock. Within 14 hours following the mainshock four temporary stations were operating, and two of these were east and northeast of the aftershock zone (CFIR and CINT). The spatial distribution of CDMG/UCSC seismograph stations is shown in Figure 1; the approximate time of equipment installation and removal is shown in Figure 2; the specifics of site instrumentation, coordinates, elevation, and dates of operation are listed in Table 1. The network was removed May 19, 1983 following the first sequence of U.S. Geological Survey refraction shots. The sites were reoccupied on June 30, 1983 for a second series of shots by the USGS.

### REFRACTION SHOTS AND CRUSTAL VELOCITY STRUCTURE

Geologically, the aftershock zone of the Coalinga earthquakes is very complex. An area of young, thick sediments of the Great Valley have been folded and uplifted in local areas such as the Anticline Ridge and Kettleman Hills. These areas of deformation are juxtaposed with the central Coast Range and the San Andreas fault zone further to the west. The construction and use of a local velocity model were necessary for locating earthquakes within the array. The travel time data set is not extensive; however, we find that significant lateral variations in velocity exist which must be taken into consideration in the construction of a local velocity model.



Two series of crustal refraction shots were detonated by the USGS to study the geologic structure in the Coalinga area (see Wentworth, *et al.*, 1983). Described here is the data recorded by the CDMG/UCSC seismographs, and the velocity model developed for the purpose of locating aftershocks. Nine explosions were detonated in two series. The first series consisted of four shots; two detonated on May 18 and two on May 19 (GMT). The second series consisted of five shots detonated on 30 June (GMT); only two shots of this series generated usable phase data at the CDMG/UCSC seismograph stations. The shot chronology and location data are summarized in Table 2. The six explosions generated 41 values of P-phase travel times. These data are shown in Table 3 and displayed in Figure 3. The data were fit with straight line segments and then interpreted in terms of flat-lying layers.

Shots two (located near seismograph station CPAL and within the aftershock zone) and five (near station CJRG and the northern end of the aftershock zone) contributed significantly to the definition of the P-wave velocity within the first layer: 2.87 km/sec. Remaining velocities are not as well defined because of possible up and down-dip travel paths, rapid lateral variations in geologic material, and the high ambient noise level which made recording difficult at seismograph stations located in the Valley.

Scrutiny of the available data indicates that waves which have a significant portion of their travel paths in the Upper Cretaceous marine sediments (west and northwest) of Coalinga experience greater propagation velocities than would be expected of travel paths within the aftershock area. This phenomenon is demonstrated by the grouping of data points for shots one and six in Figure 3 as compared with data from shots two and five for paths through the marine sediments (CLGC, CCWR); the latter travel times suggest higher P-wave velocities than those for travel paths within the aftershock area.

A second constant velocity layer was interpreted based upon an inferred slope change in the data between 10 and 20 km. Similarly, data from shots four and five suggest the presence of an intermediate layer. Although the data is not abundant for this second layer, it was included to span the zone between 2.87 and 6.0 km/sec.

Much of the velocity information obtained from shots three and four pertain to the velocity associated with the Great Valley sediments. Shot four data clearly demonstrate the lateral velocity variability between the Quaternary Valley sediments and the older Upper Cretaceous marine sediments in the foothills west of Coalinga. Emphasis was given to data point grouping of shot four.

From the selected velocity segments, the following information may be tabulated:

<u>Layer</u>	<u>Velocity (km/sec)</u>	<u>Intercept (sec)</u>	<u>Crossover</u>
1	2.87	0.00	--
2	4.20	1.08	9.8
3	6.0	3.48	--

This information was used to calculate velocity model parameters as follows:

<u>Layer Number</u>	<u>Velocity (km/sec)</u>	<u>Depth of Layer Top (km)</u>
1	2.87	0.0
2	4.20	2.1
3	6.00	6.5
	*****	
4	6.4	14.0
5	7.9	28.0

Parameters for layers four and five were taken from Eaton, 1983, in order to complete the velocity model at depth.

#### EARTHQUAKE LOCATIONS

Earthquakes were located using the computer program Hypo71 (Lee and Lahr, 1975) and the velocity model described above. The best located events (quality A, B, and C) were used to determine the average travel time residuals at the local network stations. These residuals were then applied as station adjustments in order to compensate for local crustal heterogeneities in determining the final earthquake locations. The station adjustments used for the local network are listed in Table 4; the earthquake locations are listed in Table 5. Magnitudes have been provided by the Seismographic Station, U.C.B. Most earthquakes  $M_L > 3.0$  have been located for the time period May 4 through May 19; a few locations are not yet finalized at the time of writing.

The location of the mainshock was redetermined relative to the locations of the aftershocks and is shown in figure 1:

Date	- May 2, 1983
Origin Time (GMT)	- 23:42:38.62
Latitude	- 36° 13.38' N
Longitude	- 120° 19.27' W
Depth (km)	- 7.43

Seven aftershocks which were well located by the local network, and which were also recorded at regional stations operated by the University of California, Berkeley, the U.S. Geological Survey, and the California Institute of Technology, were used with a "master event" approach. The median values of the travel time residuals at the regional stations (relative to the locations determined independently with the local network) were selected as station adjustments, after editing for a few major travel time inconsistencies (Table 4). The statistical precision of the location is .7 km (ERH) and depth is .8 km (ERZ). The accuracy, however, may be less than the statistical precision. The accuracy was tested by relocating the seven master events using only the regional stations and the station travel time adjustments. The differences between the relocations determined from the regional stations with adjustments and the locations determined from the local network (local - regional) were:

<u>Parameter</u>	<u>Median Difference</u>	<u>Range of Difference</u>
Latitude	0.33 km south	0.77 km south to 1.52 km north
Longitude	0.27 km east	2.06 km east to 0.81 km west
Depth	0.31 km deeper	2.13 km shallower to 3.57 km deeper

These differences are expected to be realistic estimates of the relative uncertainties in the redetermined location of the mainshock. The mainshock epicenter given by Uhrhammer et al. (1983) is:

360 13.8' N  
1200 17.4' W

and by Eaton (1983) is:

360 13.99' N  
1200 17.59' W

The mainshock epicenters given by Uhrhammer et al., and Eaton are thus approximately 0.8 km north and 2.8 km east from our determination. A systematic shift of approximately 2 km north and 3 km east for the locations given by Uhrhammer et al. was also found from a comparison with our locations for 6 aftershocks. This average shift exceeds the median and range of expected uncertainty for our mainshock relocations, found from the test described above. We thus conclude that careful relocations are warranted for detailed interpretations of mainshock source rupture process when those interpretations are based on the relative locations of the mainshock and the aftershock zone determined by different array configurations.

The depth of the mainshock is probably not less than 7 km and not greater than 11 km, based on our studies to date. The statistical precision of the mainshock depth is  $7.43 \pm 0.8$  km (range 6.63 to 8.23 km, see Table 5). The accuracy estimated from the relocation tests of the master events is 5.33 to 11.03 km (see above). The larger uncertainty is probably more realistic. The waveform modeling of long period P-waves



(Rial and Brown, 1983) was performed with the same near source velocity model as used for the earthquake locations in order to provide the basis for intercomparison. The depth obtained by Rial and Brown is 10 km, with an estimated uncertainty of  $\pm 3$  km (J. Rial, personal communication). Based on these combined results, it appears that the depth of the mainshock is not less than 7 km and not greater than 11 km, relative to the near source crustal velocity model given above.

## RESULTS

The aftershocks listed in Table 5 are shown in Figure 4, and describe a roughly elliptical aftershock zone 12 km by 25 km with the long axis oriented N 35 W. There are a number of interesting spatial characteristics of the aftershock distribution in relation to the mainshock. The mainshock faulting mechanism has been determined by first motion studies and synthetic wave-form modeling (Rial and Brown, 1983; Eaton, 1983; Hartzell and Heaton, 1983) to have a strike approximately N 58 W to N 60 W (Figure 4, A - A') while the trend of the aftershock zone is more northerly at about N 35 W (Figure 4, C - C'). There also appears to be a difference between the northwest and southeast sections of the aftershock zone. Most larger aftershocks of magnitude greater than 4.0 occur in the northwest region, the area where the mainshock occurred. Aftershocks in the southeast are primarily of magnitude less than 4.0 (see Figure 4). It is also interesting to note that the prior seismicity shows the northwest half of the aftershock zone to have been devoid of earthquakes (magnitude  $> 3.0$ ) since 1930 while the southeast area showed a small swarm of activity in the early part of 1976 (Beroza, Brown, and McNally, 1983). Depths along the northwest half range from about 3 km to 12 km. In contrast, the aftershocks along the southeast half of the aftershock zone show depths ranging from about 5 km to 8 km (Figure 6, C - C'). The difference in behavior of these two areas suggests that the northwest section of the fault zone where the mainshock occurred may have different physical characteristics than the southeast section.

The distribution of earthquakes with depth suggests a complex rupture area rather than a single simple fault plane. In Figure 5 (B - B') the dip of the mainshock has been included, and one can see a fair number of events consistent with this plane; without the dip drawn, however, it would be difficult to select the rupture plane.

## ACKNOWLEDGEMENTS

We would like to thank Dr. J. Eaton and Dr. R. Lester of the U.S. Geological Survey and the personnel at the U.C. Berkeley Seismographic Station for providing data in a most helpful manner. We thank Dr. J. Rial for helpful review comments, and Haller Igel, David Parke, and Gordon Campbell for the successful operation of the field array. This study was supported by the U.S. Geological Survey under Contract 14-08-0001-20546. Charles F. Richter Seismological Laboratory contribution 14.

## REFERENCES

- Beroza, G., Brown, E., and McNally, K., 1983, Report to the Southern California Data Review Group, California Institute of Technology, Pasadena, California.
- Eaton, J., 1983, Seismic Setting, Location and Focal Mechanism of the May 2, 1983, Coalinga Earthquake, U.S. Geological Survey Open File Report 83-511, Menlo Park, Calif.
- Hartzell, S.H., and Heaton, T.H., 1983, Teleseismic Mechanism of the May 2, 1983 Coalinga, California, Earthquake From Long-Period P-Waves, this issue.
- Lee, W.H.K., and Lahr, J.C., 1975, Hypo71 (Revised): A Computer Program for Determining Hypocenter, Magnitude, and First Motion Pattern of Local Earthquakes; U.S. Geological Survey Open File Report 75-311, Menlo Park, Calif.
- Rial, J.A., and Brown, E., 1983, Waveform Modeling of Long Period P-Waves From the Coalinga Earthquake of May 2, 1983; this issue.
- Uhrhammer, R., Darragh, R., and Bolt, B., 1983, The 1983 Coalinga Earthquake Sequence, this issue.
- Wentworth, Walter, Bartow, and Zoback, 1983, Northeastward Thrusting of the Southern Diablo Range: Evidence From Deep Reflection and Refraction Profiles Across the Southeastern End of the Kettleman Hills, this issue.

Table 1. CDMG/UCSC Coalinga seismograph stations.

STN.	DATE INSTALLED		LATITUDE (°N)	LONGITUDE (°W)	ELEVATION (METERS)	SEIS.*	SM**
	ON	OFF					
CPAL	5/3/83	5/19/83	36.210	120.305	283.46	R,M	X
CFIR	5/3/83	5/19/83	36.205	120.103	112.17	R,M	X
CINT	5/3/83	5/19/83	36.282	120.305	256.34	R	X
C5PT	5/4/83	5/19/83	36.446	120.119	65.23	R	X
CAVL	5/3/83	5/19/83	35.983	120.146	244.75	R,S	
CANT	5/3/83	5/19/83	36.414	120.393	159.11	R,M	
CMER	5/4/83	5/19/83	36.108	120.343	242.32	M	
CJCN	5/4/83	5/ 6 /83	36.107	120.521	462.69	M	
CLGC	5/4/83	5/19/83	36.216	120.475	341.38	M	
CSTD	5/4/83	5/19/83	36.144	120.206	170.08	M	
CPCH	5/3/83	5/ 4 /83	36.630	120.640	158.50	M	
CJRG	5/5/83	5/19/83	36.258	120.390	466.34	M	
CCWR	5/5/83	5/19/83	36.399	120.520	434.34	R	
CDMC	5/6/83	5/19/83	36.511	120.360	100.28	M	

\* M = Marks product L-4C vertical seismometer;

R = Kinematics Ranger seismometer;

S = Sprengnether three-component DR-100.

\*\* Sites equipped with Kinematics SMA-1 strong-motion accelerometers.



Table 2. Explosion time and location data, U.S. Geological Survey refraction shots.

Reference Number	Day	Hour	Latitude (N)	Longitude (W)	Plotting Symbol
1	830518	064500.01	36°15.35'	120°36.87'	⊙
2	830518	070000.00	36°13.08'	120°18.71'	□
3	830519	063000.01	36°13.13'	119°41.21'	◇
4	830519	064500.01	36°13.73'	120°01.77'	▽
5	830630	063000.01	36°15.49'	120°23.46'	△
6	830630	070000.03	36°24.09'	120°30.48'	×

Table 3. Summary of explosion travel times\* and seismograph station distance.

Plotting Symbol	Seismograph Stations																								
	CPAL		CFIR		CINT		C5PT		CAVL		CANT		CMER		CLGC		CSTO		CJRG		CCWR		COMC		
	km	sec	km	sec	km	sec	km	sec	km	sec	km	sec	km	sec	km	sec	km	sec	km	sec	km	sec	km	sec	
1	☉	28.3	6.81			28.0	6.85							29.4	7.02	13.3	4.06	38.8	8.97	20.2	5.25	18.0	4.69	36.6	9.26
2	☐	1.0	0.53			7.1	2.70							12.5	4.22	14.7	4.12	12.6	4.42	8.3	3.10	27.4	7.02		
3	◇	55.6	11.94					46.2	10.33	49.0	11.41							47.4	10.90						
4	▽	24.8	7.57	7.1	3.41	25.4	7.61	25.3	7.26	29.3	8.84			31.3	8.64			18.5	6.20	32.6	8.85	47.9	11.25	43.1	10.75
5	△					8.2	2.84							17.2	5.29	8.9	2.77			0.1	0.05	19.4	5.15		
6	×					22.6	6.02					10.4	3.83	35.8	8.47	20.8	5.44			19.1	5.12	1.1	0.50	17.9	5.46

\* Travel times cited are for quality 0, 1, and 2 P-phase arrivals only.

Table 4

Station list with location and station delay. Regional delays were calculated using seven master events recorded by both local and regional stations (see text for details).

Local Array				Regional Network			
Stn	Lat	Long	Delay	Stn	Lat	Long	Delay
CPAL	36 12.60N	120 18.30W	.00	BMS	36 39.78N	120 47.51W	-.44
CFIR	36 12.30N	120 6.18W	.05	BRM	36 50.70N	120 49.42W	-.43
CINT	36 16.92N	120 18.30W	-.10	FRI	36 59.50N	119 42.50W	-2.28
C5PT	36 26.76N	120 7.14W	-.10	HSL	37 1.16N	121 5.13W	-1.20
CAVL	35 58.98N	120 8.76W	.10	MHD	37 7.18N	119 54.97W	-2.28
CANT	36 24.84N	120 23.58W	.20	PCR	36 5.63N	120 26.08W	-.56
CMER	36 6.48N	120 20.58W	.10	PHR	36 22.38N	120 49.10W	-.54
CJCN	36 6.42N	120 31.26W	-.50	PKE	36 3.69N	120 6.54W	-.28
CLGC	36 12.96N	120 28.50W	-.16	PPR	35 38.86N	120 42.04W	-.80
CSTD	36 8.64N	120 12.36W	-.10	PPT	36 6.50N	120 43.27W	-.37
CPCH	36 37.80N	120 38.40W	.00	PRC	36 15.37N	120 37.20W	-.35
CJRG	36 15.48N	120 23.40W	.00	PSM	36 4.18N	120 35.68W	.13
CCWR	36 23.94N	120 31.20W	-.12	WAS	35 44.29N	118 33.42W	-1.44
CDMC	36 30.66N	120 21.60W	.37	WOF	35 32.14N	118 42.75W	-1.94
				MNP	37 24.88N	119 43.68W	-1.60
				MAT	37 52.40N	119 52.00W	-.54
				WKT	35 47.64N	118 26.55W	-1.27
				PAR	36 14.95N	120 20.52W	.04

Table 5

Listing of all well located events with  $Q \geq C$  from the UCSC/CDMG aftershock study. The relocated mainshock is also included\*. Magnitudes are  $M_L$  from U.C. Berkeley. Magnitudes of events with no available Berkeley magnitude are left blank.

DATE	Hr:Mn	Sec	Lat	Long	Dpth	Mag	No	Gap	RMS	ErH	ErZ	Q	
830502	23:42	38.62	36	13.38	120	19.27	7.43	6.7	12	91	.12	.7	.8 b *
830504	7:28	39.43	36	14.89	120	21.87	8.05	4.8	6	108	.05	.9	2.2 b
830504	12: 0	26.73	36	11.88	120	18.40	8.04		6	144	.11	1.5	1.7 c
830504	12:26	9.51	36	12.09	120	17.17	6.77		8	127	.12	1.1	1.0 b
830504	13:29	15.69	36	4.72	120	14.26	4.67	3.0	9	147	.21	1.4	.9 c
830504	15:59	13.68	36	15.43	120	16.94	6.99	3.5	5	181	.09	1.6	1.7 c
830504	16:11	20.03	36	16.03	120	20.75	7.88	4.3	9	148	.20	1.6	2.1 c
830504	19:45	2.80	36	6.28	120	16.83	4.90	3.0	9	136	.22	1.1	.6 c
830504	22: 3	42.99	36	11.86	120	15.71	7.38	2.7	9	108	.17	1.2	1.7 b
830505	0:13	6.57	36	12.92	120	16.58	7.55		8	112	.07	.5	.9 b
830505	0:27	51.09	36	12.86	120	15.95	6.16	3.3	6	117	.08	.7	.5 b
830505	0:32	11.66	36	13.37	120	16.40	7.02		8	118	.14	.9	1.6 b
830505	1:56	42.54	36	12.38	120	17.17	5.75		8	121	.14	1.0	.5 b
830505	3:31	8.62	36	11.65	120	16.23	6.16		10	63	.10	.5	.2 a
830505	4:37	49.30	36	8.74	120	13.79	5.00	3.7	11	90	.32	1.5	.9 c
830505	5:54	32.29	36	12.70	120	16.39	5.00		8	65	.30	1.8	1.4 b
830505	8: 6	26.82	36	8.05	120	13.88	5.74	3.4	11	99	.14	.7	.3 b
830505	10:20	44.55	36	16.17	120	22.02	10.08	4.5	11	170	.22	1.6	2.0 c
830505	11:33	41.22	36	14.52	120	21.20	7.98	3.5	11	98	.20	1.1	1.8 b
830505	11:50	50.39	36	10.51	120	17.22	6.92	3.5	9	86	.13	.8	2.0 a
830505	12:42	16.06	36	15.14	120	23.88	9.64	3.7	8	181	.07	1.0	2.1 c
830505	14:40	8.38	36	12.70	120	16.43	5.92	3.4	11	65	.19	.9	.4 b
830505	22:46	12.62	36	16.91	120	25.35	3.50	3.4	10	157	.27	1.4	1.1 c
830506	4:57	9.75	36	11.18	120	17.96	7.55	3.3	6	99	.06	.6	1.2 b
830506	9:43	39.46	36	10.81	120	20.73	10.58	3.5	11	110	.11	.7	1.2 b
830506	11:51	44.69	36	16.03	120	22.45	5.48	3.0	6	106	.15	1.0	.7 b
830506	18:31	10.67	36	14.80	120	19.68	4.51	2.8	6	129	.13	1.3	1.0 b
830506	23:28	44.02	36	7.90	120	13.54	8.44	3.0	9	202	.11	1.1	1.5 c
830507	0:17	16.25	36	15.45	120	20.21	5.58	3.7	10	89	.16	1.0	.6 b
830507	5:43	57.82	36	12.70	120	17.37	6.53	3.3	10	62	.20	1.2	1.3 b
830508	1:20	14.97	36	11.98	120	18.40	5.69	3.0	10	117	.23	1.2	.6 b
830508	3:45	33.86	36	14.84	120	25.78	.89	2.9	9	141	.09	.4	.3 b
830508	19:18	24.91	36	15.64	120	28.60	7.14	3.4	9	202	.20	2.0	3.6 c
830508	20:25	40.18	36	12.09	120	18.71	5.00	3.4	9	81	.15	.7	.5 a
830509	2:49	11.87	36	13.65	120	18.68	11.46	5.1	11	73	.08	.4	.8 a
830509	3:19	11.67	36	13.68	120	18.40	10.13	3.4	5	139	.02	.5	.6 c
830509	3:26	37.19	36	10.32	120	20.05	11.74	4.4	7	140	.19	2.9	5.7 c
830509	11:18	23.59	36	10.69	120	19.01	5.37		10	90	.11	.6	.4 a
830509	13:24	33.96	36	11.32	120	17.06	5.00	3.1	10	94	.15	.7	.5 b
830509	20:14	35.86	36	12.34	120	17.30	4.53		9	100	.14	.7	.5 b
830510	0:28	4.99	36	11.43	120	20.21	4.26		8	131	.18	1.1	.8 b
830510	13:26	29.93	36	19.07	120	20.36	4.82	3.6	9	88	.17	.8	.6 b
830510	15:22	43.60	36	19.49	120	20.66	4.21	3.1	7	199	.15	1.4	1.0 c



(Table 5, continued)

<u>DATE</u>	<u>Hr:Mn</u>	<u>Sec</u>	<u>Lat</u>	<u>Long</u>	<u>Dpth</u>	<u>Mag</u>	<u>No</u>	<u>Gap</u>	<u>RMS</u>	<u>ErH</u>	<u>ErZ</u>	<u>Q</u>
830511	8:14	47.69	36	9.60 120 16.36	4.24	3.2	9	121	.22	1.1	1.0	b
830511	20:49	24.85	36	15.71 120 21.08	5.99	3.3	10	68	.12	.6	.3	a
830512	1:57	23.40	36	8.74 120 16.39	5.00		10	145	.22	1.5	1.0	c
830512	4: 8	17.06	36	16.21 120 24.40	6.44		9	99	.14	.8	.5	b
830512	6:42	8.20	36	14.16 120 20.50	5.95		9	79	.11	.6	.3	a
830512	7:23	59.97	36	10.61 120 18.67	5.04		9	89	.09	.4	.3	b
830512	13:41	7.25	36	9.56 120 17.49	5.95	4.4	10	117	.14	.8	.5	b
830512	19:56	7.38	36	18.25 120 18.40	6.04		8	133	.05	.4	.2	b
830512	21:30	54.22	36	11.36 120 16.81	5.95		8	96	.11	.6	.4	b
830512	22:33	56.86	36	16.19 120 25.02	10.97		9	106	.14	1.0	2.4	b
830513	6:44	5.98	36	9.34 120 17.20	5.08		12	77	.25	1.1	.7	b
830513	14:40	3.95	36	8.74 120 15.67	5.00	2.8	10	148	.25	1.7	1.1	c
830513	16:28	18.56	36	14.58 120 19.13	4.60		9	86	.16	.8	.6	b
830514	2:20	48.79	36	12.70 120 18.13	5.00		11	94	.10	.4	.3	b
830514	3: 8	48.83	36	15.58 120 25.49	1.94		12	108	.38	1.3	1.0	c
830514	5: 2	3.66	36	15.48 120 19.38	7.42	3.7	10	75	.10	.5	1.0	a
830514	5:54	45.73	36	5.59 120 12.59	6.04		8	123	.05	.3	.2	b
830514	7:16	19.16	36	9.30 120 17.19	6.37		12	78	.08	.4	.2	a
830514	13:59	19.69	36	5.81 120 14.52	5.38		10	132	.10	.6	.3	b
830514	17: 7	21.89	36	9.95 120 17.67	5.00		10	107	.16	.7	.5	b
830514	17:15	36.00	36	10.70 120 18.79	2.87	3.5	5	205	.04	.5	.5	c
830515	0:34	30.15	36	6.04 120 13.19	7.33		10	121	.10	.6	1.3	b
830515	1: 4	21.76	36	7.63 120 12.96	8.29		11	109	.09	.5	.7	b
830515	3:17	9.41	36	9.23 120 17.92	5.74		11	75	.15	.7	.4	b
830515	23:12	42.67	36	10.11 120 18.72	6.75		11	87	.09	.5	1.3	a
830516	1:31	37.97	36	7.46 120 16.01	8.82	3.4	11	110	.08	.5	.9	b
830516	12:17	43.13	36	7.01 120 12.46	6.85		10	135	.28	1.8	2.4	c
830516	14:21	48.58	36	8.74 120 16.90	6.25	3.7	10	148	.13	.7	.3	b
830516	14:52	33.62	36	8.74 120 17.73	4.73		8	204	.09	.9	.4	c
830516	18:40	16.28	36	9.77 120 18.44	6.75		10	147	.10	.7	1.8	b
830516	19: 9	37.71	36	8.75 120 18.40	7.45	3.2	7	206	.13	1.6	3.9	c
830516	19:45	38.59	36	4.69 120 13.19	5.33		9	156	.09	.7	.4	b
830517	2:34	3.08	36	11.91 120 17.51	9.64		12	72	.10	.5	.8	a
830517	7:42	11.71	36	14.79 120 22.20	7.86		12	79	.10	.5	.8	a
830517	11:40	52.47	36	10.31 120 19.01	6.31		12	91	.10	.4	.3	b
830517	18:13	6.88	36	11.50 120 16.98	6.10		11	96	.13	.6	.3	b
830517	22:22	13.34	36	12.70 120 22.08	5.19	3.3	11	104	.12	.5	.3	b
830518	2:22	27.45	36	9.82 120 17.84	5.67		12	76	.12	.5	.3	a
830518	2:46	49.40	36	11.32 120 16.05	6.30	3.4	12	63	.11	.5	.3	a
830518	3:18	51.89	36	11.38 120 15.90	6.04		12	63	.10	.5	.3	a
830518	8:13	6.45	36	4.73 120 13.18	3.96		11	138	.14	.7	.5	b
830518	9:19	.24	36	14.26 120 22.95	4.56		8	88	.18	1.0	.9	b
830518	9:39	11.81	36	10.88 120 15.60	4.29		11	68	.13	.5	.4	b
830518	20:39	32.44	36	13.91 120 21.13	5.06	3.0	10	84	.19	.8	.5	b
830519	11: 5	30.46	36	12.70 120 16.72	11.81	3.7	11	64	.06	.3	.6	a

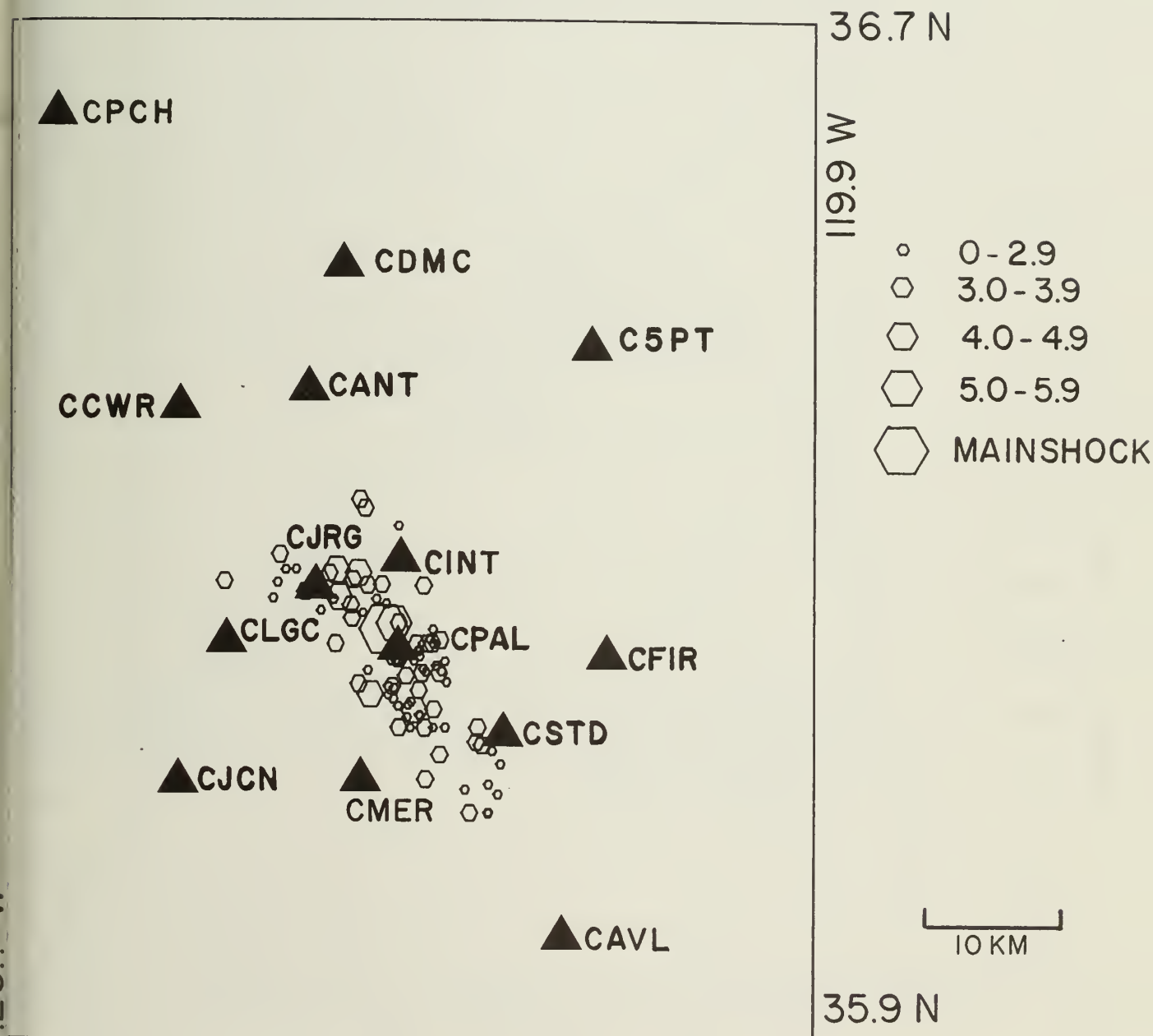


Figure 1. Well located events of quality A, B, and C over the time period of May 4 to May 19, 1983. Portable stations used in this study are shown as triangles. Earthquake symbol size is proportional to magnitude,  $M_L$ , as shown.

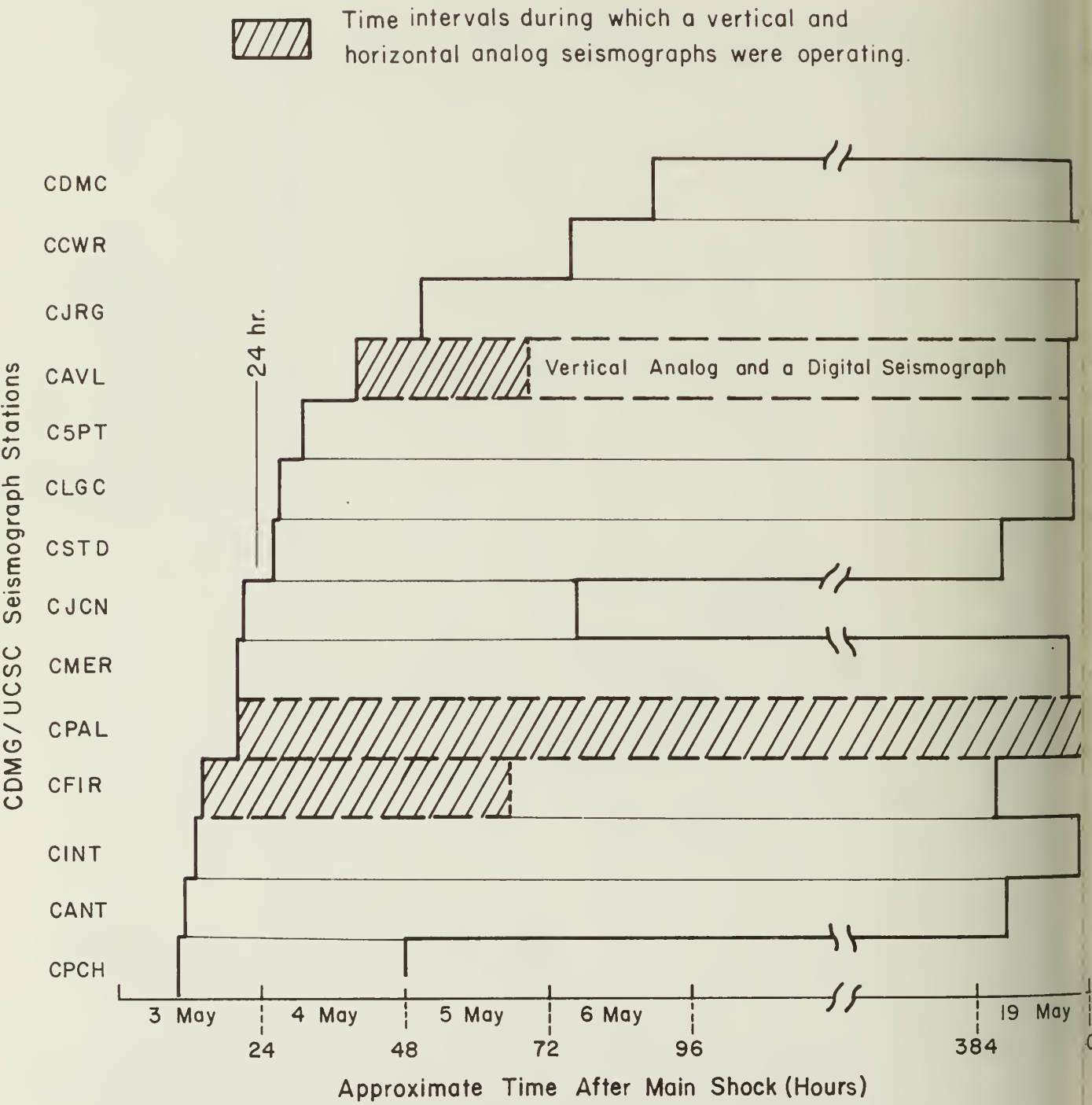


Figure 2. Histogram of times of operation of array stations.

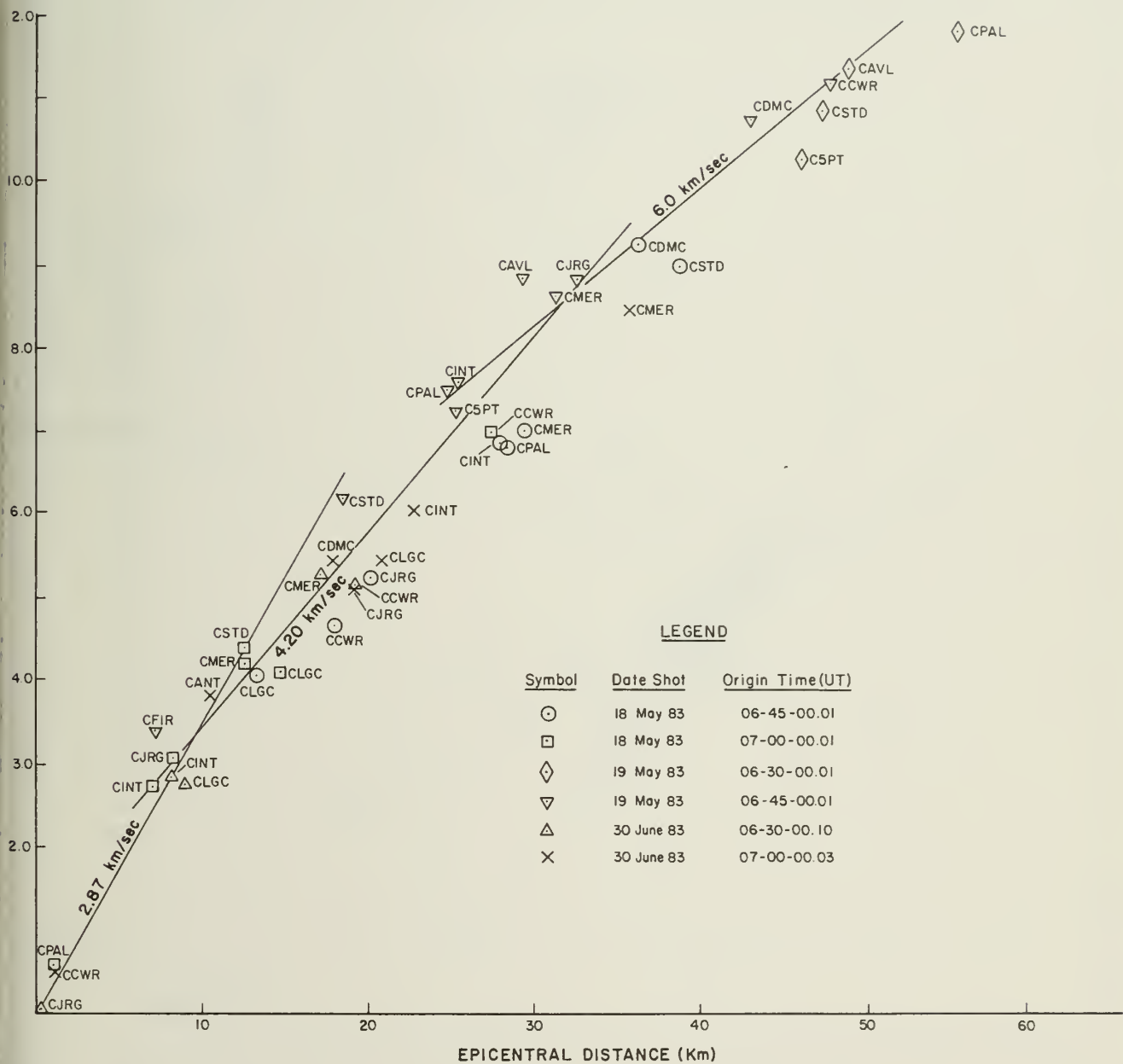


Figure 3. Velocity model used for earthquake locations as determined from U.S. Geological Survey shot data.



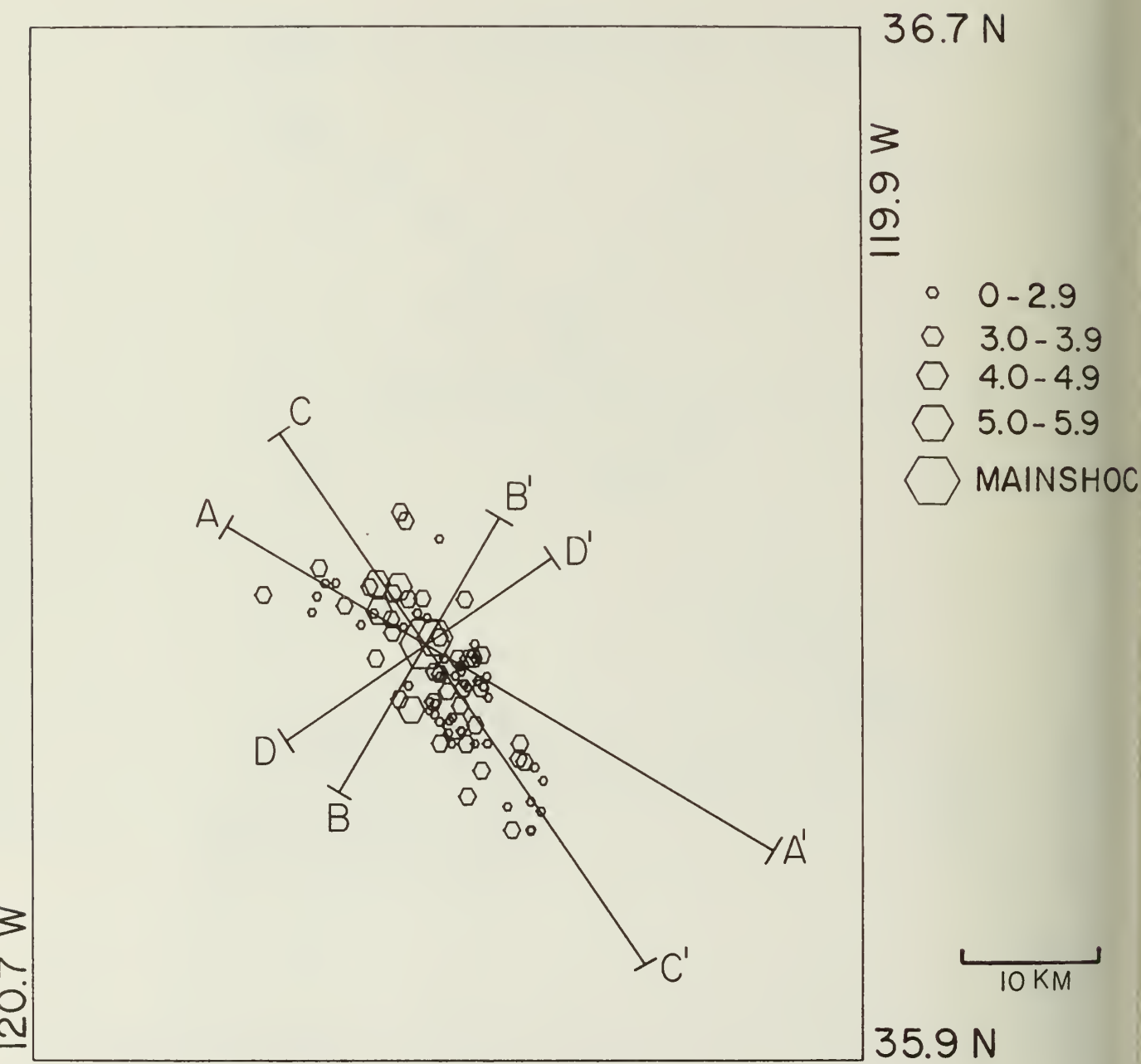


Figure 4. Well located events of quality A, B, and C with projection lines. Lines A - A', B - B' are parallel and perpendicular, respectively, to the strike of the mainshock as found by first motion studies and synthetic waveform modeling (Rial and Brown, 1983; Eaton, 1983; Hartzell and Heaton, 1983). Lines C - C', D - D' are parallel and perpendicular, respectively, to the trend of the aftershock zone (see figures 5 and 6). Earthquake symbol size is proportional to magnitude,  $M_L$ , as shown

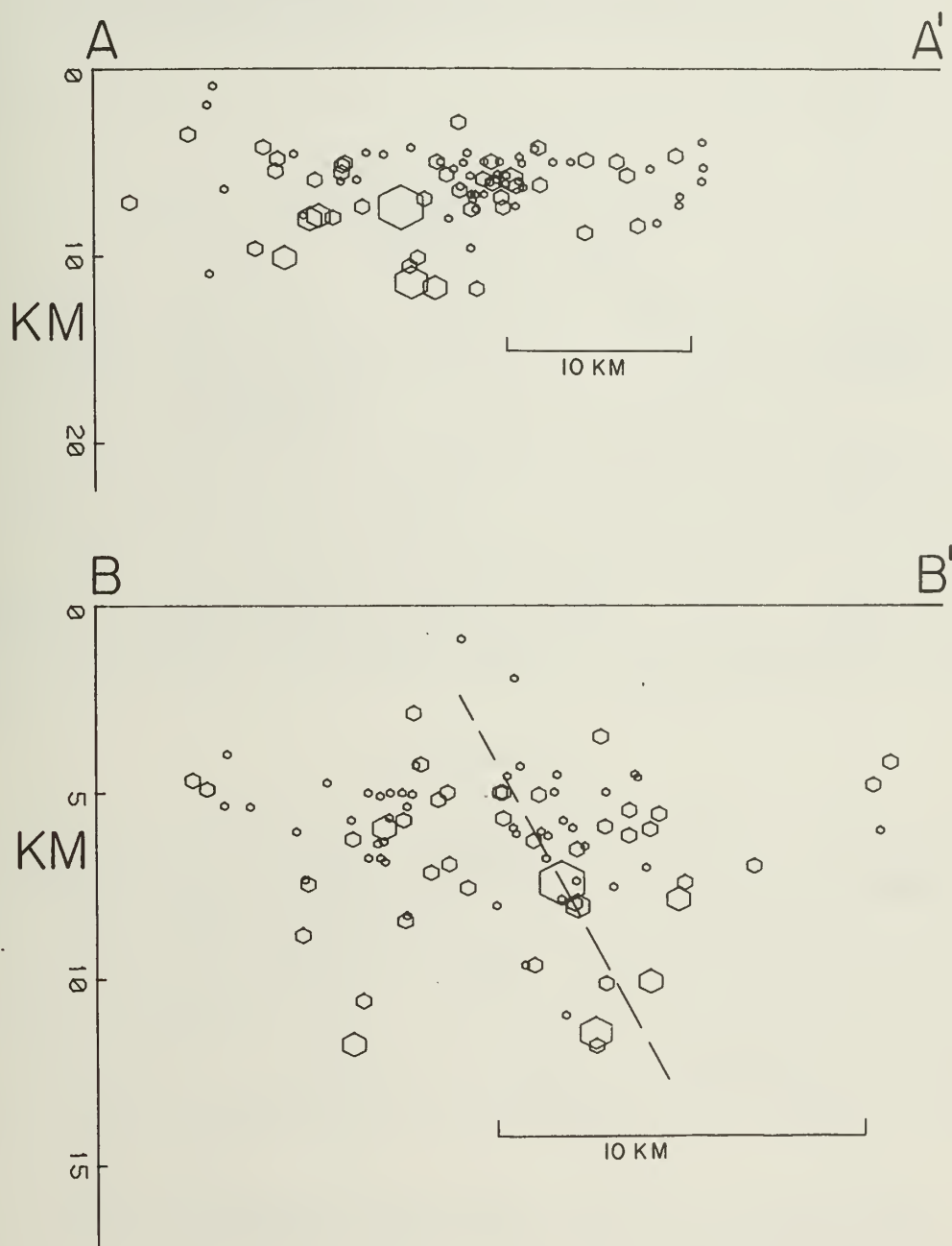


Figure 5. Depth projections parallel (A - A') and perpendicular (B - B') to the strike of the mainshock. The line through the hypocenter of the mainshock in cross section B - B' is the angle of dip found by first motion and synthetic waveform modeling studies (Rial and Brown, 1983; Eaton, 1983; Hartzell and Heaton, 1983). Scale is one to one.

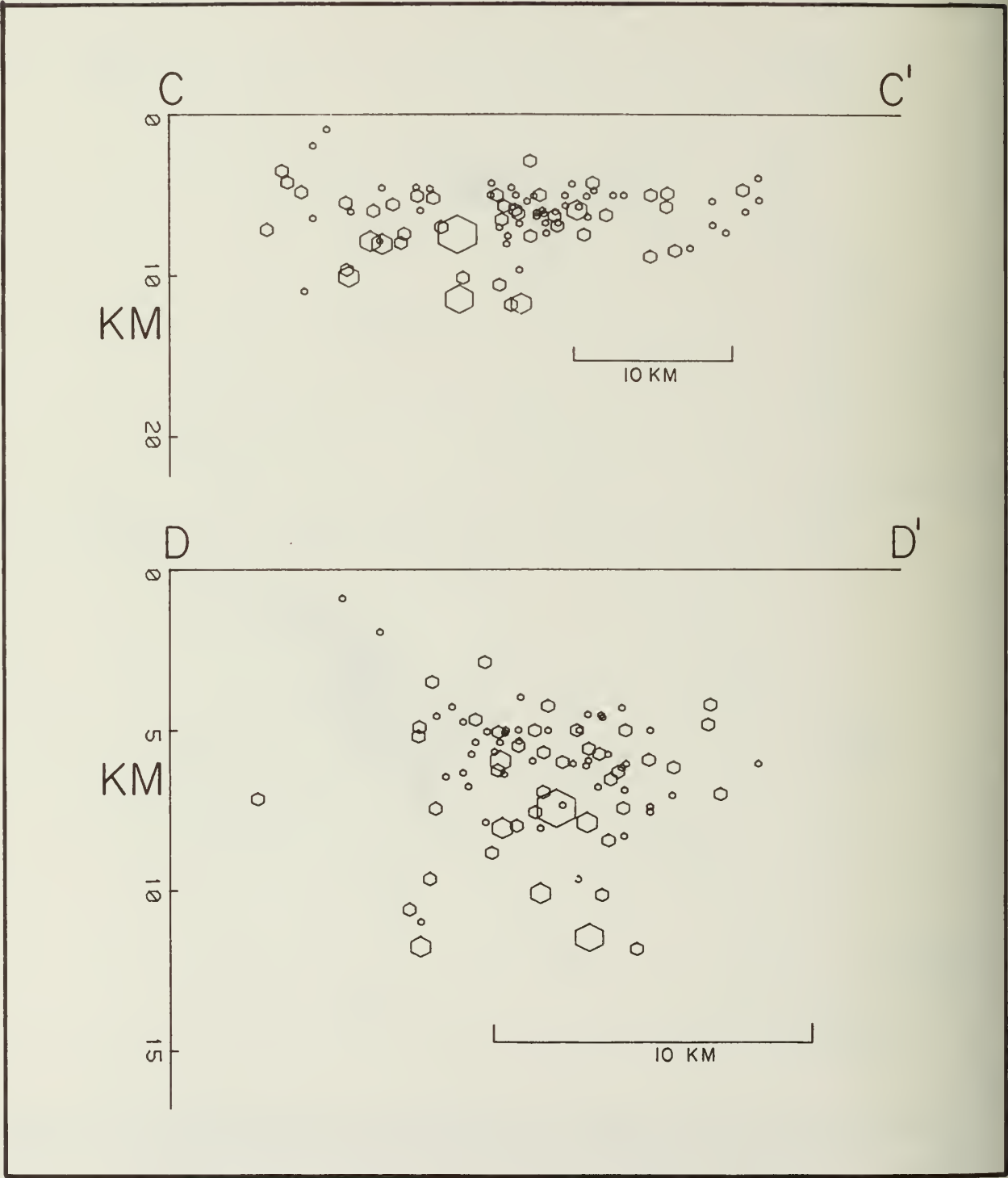


Figure 6. Depth projections parallel (C - C') and perpendicular (D - D') to the trend of the aftershock zone. Scale is one to one.

# SOURCE PARAMETERS OF COALINGA AFTERSHOCKS FROM THE UC BERKELEY PORTABLE DIGITAL ARRAY

by

Daniel R. O'Connell<sup>1</sup>  
Patricia E. Murtha<sup>2</sup>

## ABSTRACT

Eleven portable digital instruments were deployed by UC Berkeley in the near-source region of the May 2, 1983 Coalinga earthquake ( $M_L = 6.7$ ) between May 3, 1983 and May 8, 1983. The same sites were reoccupied ten days later to record four U.S.G.S. refraction explosions. Hypocenters were calculated for 43 earthquakes ( $1.0 \leq M_L \leq 4.8$ ) recorded at four or more stations during the two recording periods. Moment, stress drop, and source radius were calculated for 39 earthquakes. The moments range from a high of  $2.6 \times 10^{22}$  dyne-cm ( $M_L = 4.8$ ) to a low of  $3.1 \times 10^{17}$  dyne-cm. Stress drops range from 0.061 bars to 56 bars. The source radii range from 80 m to 979 m and SH-wave corner frequencies range from 0.86 Hz to 26 Hz. A least squares fit of a plane through the hypocenters of eleven earthquakes with  $M_L \geq 3.0$  suggests that the fault of the Coalinga mainshock is a thrust striking  $N25.5^\circ W \pm 16.6^\circ$  and dipping  $12.6^\circ \pm 4.8^\circ$  southwest.

## INTRODUCTION

The Coalinga earthquake ( $M_L = 6.7$ , UCB) of May 2, 1983 marks the beginning of a sequence of earthquakes occurring along at least two faults in the vicinity of Coalinga, California. Fault rupture associated with the June 11, 1983 earthquake ( $M_L = 5.1$ , UCB) was observed approximately 15 kilometers west of the mainshock (McJunkin and Hart, 1983). Surface expressions indicate that faulting resulted from reverse motion on a steeply east-dipping fault. No surface expression of rupture has been found for the mainshock (Clark et al., 1983). In this paper we constrain the type of faulting of the mainshock and discuss the source properties of its aftershocks. The sequence provides an excellent opportunity to study earthquake sources using nearfield strong ground motion recordings.

Eleven strong motion stations were deployed from 15 hours UTC May 3, 1983, to 05 hours UTC May 8, 1983, each consisting of a three-component force-balance accelerometer recording on a 12-bit digital event recorder. Station locations are listed in Table 1 and are shown as triangles in Figure 1. The data were recorded at 200 samples/s with a 5 pole anti-alias filter at 50 Hz. The accelerometer instrument response is flat to acceleration in the recording bandwidth (0.2 Hz to 50 Hz). The acceleration

<sup>1</sup>Research Assistant, Center for Computational Seismology, Lawrence Berkeley Laboratory.

<sup>2</sup>Research Assistant, Seismographic Station, University of California, Berkeley.



sensitivities of the recorders were set to record peak accelerations as large as 0.5 g. These acceleration sensitivities were chosen to record the larger aftershocks on scale with good bit resolution. Two stations were co-sited with the portable network deployed by CDMG-UCSC.

On May 18, 1983, the same sites were reoccupied to record four U.S.G.S. explosions along an east-west refraction line near Coalinga. Velocity transducers consisting of a three-component package of 4.5 Hz geophones were deployed instead of accelerometers to provide a better signal to noise ratio for these smaller events. Again the data were recorded on digital event recorders at 200 samples/s with a 5 pole anti-alias filter at 50 Hz. These stations operated from 06 hours UTC May 18, 1983, until 18 hours UTC May 19, 1983. Murtha and O'Connell (1983) provide a more complete summary of the recorded data.

### VELOCITY MODEL

The geologic setting of the Coalinga earthquakes suggests the presence of a layer of sediments overlying higher velocity materials, both of which have undergone folding and faulting. Lateral velocity gradients would be expected along structural features as well as distinct changes in velocity across boundaries of geologic provinces. The array straddled Anticline Ridge which is located between the Coast Range Province and the Great Valley Province. Utilization of an appropriate velocity model is limited by the inability of most earthquake location programs to handle complex velocity models.

Three shots along the U.S.G.S. east-west refraction line were well recorded by the UC Berkeley portable array: Los Gatos Creek (36.2558°N, 120.6144°W, 138°06<sup>h</sup>45<sup>m</sup>00.0<sup>s</sup>), Anticline Ridge (36.2180°N, 120.3118°W, 138°07<sup>h</sup>00<sup>m</sup>00.0<sup>s</sup>), and Huron (36.2288°N, 120.0295°W, 139°06<sup>h</sup>45<sup>m</sup>00.0<sup>s</sup>). Close-in ( $\Delta \leq 5$  km) arrival times indicate near-surface compressional velocities of 2.49 - 2.63 km/s in a layer 1.5-2.5 km thick in the vicinity of Anticline Ridge. The P-wave arrival times for the Los Gatos Creek shot are 1.35 s faster than the arrival times for the Huron shot at comparable shot-to-receiver distances ( $22 \text{ km} \leq \Delta \leq 32 \text{ km}$ ). Higher velocity metamorphic and volcanic rocks present in the Coast Ranges in contrast to the deep alluvium of the San Joaquin Valley may account for the earlier arrivals. Therefore, at these distances ( $22 \text{ km} \leq \Delta \leq 32 \text{ km}$ ), the gradient of the travel time curve and not the absolute travel time is considered to be the strongest constraint on the velocity model.

Each author independently derived a velocity model. Both velocity models, each consisting of a linear velocity gradient half-space, were derived to fit the refraction travel time data. Model 1 matches the slow, near-surface velocities and requires a steep velocity gradient to match arrival times beyond 10 km. Model 2 matches the travel time gradient beyond 20 km and averages the velocities of the slower, near-surface layers over a larger depth range by assuming a small velocity gradient. The  $V_P/V_S$  ratio derived from Wadati diagrams for 15 earthquakes is 1.9. This value is used to derive the corresponding S-wave velocity models. Both models are presented in Table 2. A more realistic velocity model that fits the refraction shot travel time data well combines a steep velocity gradient in a top layer several kilometers thick and a small

velocity gradient in an underlying half-space. As we will discuss in the next section, our earthquake locations are relatively insensitive to the differences between the two velocity models.

### EARTHQUAKE LOCATIONS

Forty three earthquakes ranging in magnitude from  $M_L \approx 1$  to  $M_L = 4.8$ , were recorded at four or more stations during the two recording periods. Eleven earthquakes recorded by accelerometers have magnitudes  $3.0 \leq M_L \leq 4.8$ . The other 32 earthquakes recorded by velocity transducers have magnitudes  $M \leq 2.0$  except for one with  $M_L = 3.7$  ( $138^{\circ}11'05''30.40^{\circ}$ ). P-wave and S-wave arrival times and first motions were read for each of the earthquakes and locations determined using both velocity models.

The Anticline Ridge shot is well located by both Model 1 and Model 2. Model 1 locates the shot at  $36.2189^{\circ}\text{N}$ ,  $120.3128^{\circ}\text{W}$ , and Model 2 locates the shot at  $36.2215^{\circ}\text{N}$ ,  $120.3117^{\circ}\text{W}$ . For comparison, the reported U.S.G.S. location is  $36.2180^{\circ}\text{N}$ ,  $120.3118^{\circ}\text{W}$ . Comparison of hypocenters between the two models indicate that the latitude and longitude are well constrained, however a trade-off between origin time and depth is evident between the models. Model 2 locates the earthquakes  $0.72 \pm 0.40$  km deeper than Model 1. The earthquakes are all located on the edge or within the array (Figure 1) and usually have both P-wave and S-wave arrival times at several stations. Thus the latitude, longitude, and depth of most earthquakes are well constrained by the array configuration regardless of which of the velocity models is used. The earthquakes are well located relative to each other for either velocity model. Earthquake locations as determined by Model 2 are shown in Figure 1 and tabulated in Table 3.

### FOCAL MECHANISMS AND FAULT PLANE SOLUTIONS

Two methods were employed to determine the constraints on the fault plane derivable from our data set. Velocity Model 2 is used in the following analysis.

The earthquakes were divided into groups based on relative spatial location. First motions were then projected onto the lower hemisphere of the focal sphere. Two groups having sufficient data to constrain at least one nodal plane are presented in Figure 2. Group A consists of 16 earthquakes located immediately northwest of the array. 70 first motions were read from these earthquakes. The preferred solution has one nodal plane striking  $\text{N}32^{\circ}\text{W}$  and dipping  $41^{\circ}$  to the southwest. The second plane strikes  $\text{N}53^{\circ}\text{W}$  and dips  $51^{\circ}$  to the northeast. Nine of the 70 first motions are inconsistent with this solution. Eight of the inconsistent readings consist of dilatations in the compressional quadrant (Figure 2). The second plane is not well constrained. 57 first motions were read from the 11 earthquakes in Group B. These earthquakes are located in the center of our array. The first motions constrain one nodal plane to strike between  $\text{N}2^{\circ}\text{W}$  and  $\text{N}12^{\circ}\text{W}$  with corresponding dips  $57^{\circ}$  NE and  $62^{\circ}$  NE. The second plane may strike from  $\text{N}29^{\circ}\text{E}$  to  $\text{N}63^{\circ}\text{W}$  due to the paucity of data in the southwest quadrant. Neither composite focal mechanism contains a shallow southwest-dipping nodal plane as obtained by Eaton (1983) for the May 2, 1983 mainshock. The steeper gradient in

velocity Model 1 produces larger take-off angles than those of Model 2, pushing the data points away from the center of the focal sphere and possibly allowing a shallower-dipping nodal plane. Reverse faulting is the predominant mechanism in both of the composite focal mechanisms.

Fitting a plane through the hypocenters allows us to estimate the strike and dip of the fault plane for the mainshock. The data were again separated into two groups: velocity data and acceleration data. The acceleration data consists of 11 earthquakes of  $M_L \geq 3.0$  recorded between May 3 and May 8, 1983. The velocity data consist of 30 earthquakes of magnitude  $M_L \leq 2.0$  recorded on May 18 and May 19, 1983. The earthquake at  $139^{\circ}15'57''40.18''$  was not used in the calculation because of its poorly determined depth. The best-fitting plane to the acceleration data strikes  $N25.5^{\circ}W \pm 16.6^{\circ}$  and dips  $12.6^{\circ} \pm 4.8^{\circ}$  to the southwest. This is consistent with the May 2, 1983, mainshock focal mechanism of Eaton (1983) and the interpretation that the faulting occurred on a southwest-dipping thrust fault. The plane through the velocity data strikes  $N58.1^{\circ}E \pm 10.6^{\circ}$  and dips  $21.6^{\circ} \pm 3.7^{\circ}$  to the southeast. The velocity data hypocenters exhibit more scatter with depth than the acceleration data hypocenters (Figure 3) and so do not clearly define a single plane. Furthermore, these earthquakes need not be along the fault plane of the May 2 earthquake. Thus, the velocity data may not be able to resolve the strike of the actual fault plane even though the shallow dip adds confidence to the interpretation of thrust faulting. The acceleration data, on the other hand, are earthquakes with  $M_L \geq 3.0$  and are more likely to be associated with rupture along the May 2 fault plane. Cross sections perpendicular to a strike of  $N25.5^{\circ}W$  are shown in Figure 3. Both cross sections show that the hypocenters are aligned in a shallow dipping-pattern.

#### SPECTRAL ANALYSIS OF SH-WAVES

SH-wave spectra were computed to determine the seismic moments,  $M_0$ , source radii,  $r$ , and stress drops,  $\Delta\sigma$ , of 39 earthquakes using the Brune (1970,1971) model. The relations are:  $M_0 = 4\pi R\rho V^3\Omega_0$ ,  $r = 2.34V/(2\pi f_0)$ , and  $\Delta\sigma = (7/16)M_0/r^3$ , where  $R$  = the distance from source to receiver,  $\rho$  = density ( $2.4 \text{ g/cm}^3 + Z*0.07 \text{ g/(km-cm}^3)$ ),  $\Omega_0$  = long period SH-wave displacement spectral level,  $f_0$  = corner frequency,  $V$  = S-wave velocity ( $2.02 \text{ km/s} + Z*0.048 \text{ /s}$ ), and  $Z$  = hypocentral depth. Spectra were corrected for the instrument response. No corrections were made for complex wave propagation effects or attenuation. The product of the free surface correction and the radiation pattern correction was assumed to be unity. Source parameters listed in Table 3 represent averages computed from two or more stations using the methods outlined in Archuleta et al. (1982). Their approach insures that that averages of the spectral source parameters will not be biased toward larger values. This approach provides a rough estimate of source parameters which allows us to do an internal comparison of these earthquakes.

The moments range from a high of  $2.6 \times 10^{22}$  dyne-cm ( $M_L = 4.8$ ) to a low of  $3.1 \times 10^{17}$  dyne-cm (c.f. also Table 1, Uhrhammer et al., this volume). UCB Richter magnitudes are not available for earthquakes smaller than  $M_L \approx 3$ . Stress drops range from 0.061



bars to 56 bars and source radii range from 80 m to 979 m. For most earthquakes, one station's estimate of the stress drop is greater than one standard error above the mean. However, there is no correlation between individual stations and high stress drop estimates. Four to nine stations are used to calculate spectral source parameters in 32 of the 39 earthquakes. Thus, estimates of average stress drops are not unduly affected by single outlying high estimates of stress drops. This data shows that single station estimates of the stress drop are not particularly reliable.

The small magnitude earthquakes ( $1 < M_L < 2$ ) have stress drops that are one to two orders of magnitude smaller than earthquakes with magnitudes greater than  $M_L = 3.0$ . Average source radii of the smaller magnitude earthquakes are only a factor of two to three smaller than the average source radius of the larger magnitude events. Corner frequencies range from 0.86 Hz to 26 Hz; corner frequencies for the smaller earthquakes range from 4 to 26 Hz. There is no clear correlation of corner frequency with hypocentral distance. Lack of correlation of corner frequency with recording stations shows that station-dependent site effects are not significant.

Since a low corner frequency would overestimate the source radius and underestimate the stress drop, there are several factors to consider before assuming that the observed decrease in stress drop with magnitude is a true source property. For example, strong attenuation of S waves may prevent us from observing the true source corner frequency. Since the spectra were not corrected for  $Q$ , a test was done to determine the minimum value of  $Q$  required to produce a significant (greater than 1.5 times) shift of the corner frequencies. Several spectra of a  $M \approx 1.8$  earthquake with corner frequencies of 5-6 Hz were corrected for whole path attenuation using successively lower values of  $Q$ . Whole path  $Q$  values of the order of 50-70 are required to produce significant shifts in the corner frequencies for all but the smallest two to six earthquakes. Such  $Q$  values seem lower than would be expected for average sedimentary rocks. Also, observed corner frequencies increase with decreasing moment within the smaller-moment earthquakes. These results indicate that the corner frequencies we observe for smaller-moment earthquakes are the true source corner frequencies although attenuation may downwardly bias the corner frequencies of some of the smallest two to six earthquakes. There is a suggestion of an  $f_{max}$  effect (Hanks, 1982) in the spectra of the smallest six earthquakes which could be a result of large near-surface attenuation. A rough estimate of  $f_{max}$  is 20 Hz, based on observed corner frequencies of the six smallest earthquakes.

Figure 4 shows that similarity (constant stress drop) holds for  $M_0 > 5.0 \times 10^{20}$  dyne-cm and nearly holds for  $M_0 < 2.0 \times 10^{19}$  dyne-cm, but not for all the earthquakes combined. Similarity breaks down between  $M_0 \approx 5.0 \times 10^{20}$  dyne-cm and  $M_0 \approx 2.0 \times 10^{19}$  dyne-cm. The nature of the transition of stress drop and source radius between these moments cannot be determined from this data set owing to the absence of any earthquakes in this moment range. Archeluta et al. (1982), Fletcher (1980), Backun et al. (1976), and Tucker and Brune (1973) have observed a breakdown of similarity for earthquakes with  $M_0 < 1.0 \times 10^{20}$  dyne-cm. As observed in these studies, there is a difference in the slope of moment versus source radius (Figure 4) between the smaller-moment earthquakes and



the larger-moment earthquakes. However, the slope difference between larger-moment earthquakes and smaller-moment earthquakes is much less pronounced in our study. At the position on Figure 4 where similarity is violated, the source radii have values of 200-250 m. In the studies mentioned above, similarity is violated where source radii have values of 100-300 m.

One explanation of the observed moment-stress drop relation is that the earthquakes with larger moments and larger stress drops may represent rupture of unbroken barriers in the rupture zone of the mainshock. The earthquakes with low moments and low stress drops may represent rupture in regions of small stress inhomogeneities created by the rupture of the mainshock. The largest earthquake in the latter recording period,  $M_L = 3.7$ , had a stress drop comparable to the stress drops of earthquakes with similar magnitudes from the earlier recording period. This result suggests that the source parameters of the large earthquakes and the small earthquakes are not changing with time.

Another explanation of the observed variations of stress drop and source radius with moment is that the assumptions implicit in the Brune-type spectral source model are not valid throughout the range of magnitudes observed in this study. For instance, corner frequencies of the smaller-magnitude earthquakes could be proportional to the source rise time and not to the source dimension. This would occur when the source rise time is much longer than the rupture time. As discussed in Archuleta et al. (1982), this might occur if the source dimension of the smaller-magnitude earthquakes were less than some critical fracture length needed for a fracture to propagate. In that case the stress drops of the smaller magnitude earthquakes could be underestimated or meaningless.

### CONCLUSIONS

Interpretation of the refraction shot travel time data gives slow surficial P-wave velocities (2.5 km/s) and suggests that P-wave velocities increase from the San Joaquin Valley in the east to the Coast Range in the west. Wadati plots of these aftershocks give a P-wave to S-wave velocity ratio of 1.90.

Locations of aftershocks are well constrained by the array configuration and the large number of close-in P-wave and S-wave arrival times. Epicentral locations are virtually independent of the the two velocity models used in the location program and hypocentral depths are only weakly dependent on the two velocity models.

Both composite focal mechanisms indicate predominant reverse faulting for most aftershocks. Results of the two composite focal mechanisms only provide a general idea of the type of faulting of these aftershocks. Determination of the focal mechanisms of some aftershocks using the complete three-component waveform data will be part of a future investigation.

A best-fitting plane through the acceleration data hypocenters is consistent with

the May 2, 1983, mainshock focal mechanism of Eaton (1983) and the interpretation that the faulting occurred on a southwest-dipping thrust fault. The best-fitting plane through velocity data hypocenters also has a shallow dip but dips to the southeast. Both results strongly suggest that thrust faulting was the focal mechanism of the May 2, 1983, mainshock.

Results of spectral analysis of SH-waves show that either there is a change in source properties between  $M > 3.0$  and  $M < 2.0$  or fundamentally different approaches to source modeling need to be used for these magnitude ranges. Attenuation does not significantly affect corner frequencies even among most smaller-moment earthquakes. Thus these aftershocks provide an opportunity to study seismic source properties in the  $1 < M < 5$  magnitude range unencumbered by strong attenuation effects. Detailed modeling of the entire three-component seismograms in the time domain and in the frequency domain to determine more about source properties and velocity structure will be a topic of future investigation.

#### ACKNOWLEDGEMENTS

We thank Charles Mueller for reviewing this paper and providing suggestions that improved its clarity and content. We are grateful to Robert Darragh, Lane Johnson and Bruce Bolt for providing helpful comments and preliminary reviews of this paper. We thank the Huron Fire Department for their help and hospitality. The California Division of Mines and Geology has been very helpful in providing information in a timely manner and in coordinating with us in the field. We wish to thank the U. S. Geological Survey for providing information about their refraction explosions. We thank the members of the UC Santa Cruz field team for their help and coordination in the field. This work was supported by the Center for Computational Seismology, Lawrence Berkeley Laboratory, University of California at Berkeley, by Contract KC04-03-03 of the Department of Energy Office of Basic Energy Research, by Contract F49620-83-C-0020 of the Advanced Research Projects Agency of the Department of Defense which is monitored by the Air Force Office of Scientific Research, and by the Field Investigation Fund of the Seismographic Station of the University of California at Berkeley.

#### REFERENCES

- Archuleta, R.J., Cranswick, E., Mueller, C., and Spudich, P.K.P., 1982, Source parameters of the 1980 Mammoth Lakes, California earthquake sequence: *J. Geophys. Res.*, v. 87, p. 4595-4607.
- Bakun, W.H., Bufe, C.G., and Stewart, R.M., 1976, Body-wave spectra of central California earthquakes: *Bull. Seism. Soc. Am.*, v. 66, p. 363-384.
- Brune, J.N., 1970, Tectonic stress and the spectra of seismic shear waves from earthquakes: *J. Geophys. Res.*, v. 75, p. 4997-5009.
- Brune, J.N., 1971, Correction: *J. Geophys. Res.*, v. 76, p. 5002.

- Clark, M.M., Harms, K.K., Lienkaemper, J.J., Perkins, J.A., Rymer, M.J., and Sharp R.V., 1983, The May 2, 1983 earthquake at Coalinga, California: The search for surface faulting: U.S. Geological Survey Open-File Report 83-5111, p. 8-19.
- Eaton, J.P., 1983, Seismic setting, location and focal mechanism of the May 2, 1983 Coalinga earthquake: U.S. Geological Survey Open-File Report 83-511, p. 20-26.
- Fletcher, J.B., 1980, Spectra from high-dynamic range digital recordings of Oroville, California aftershocks and their source parameters: Bull. Seism. Soc. Am., v. 70, p. 735-756.
- Hanks, T.C., 1982,  $f_{max}$ : Bull. Seism. Soc. Am., v.72, p. 1867-1880.
- McJunkin, R. D., and Hart, E. W., 1983, Ground rupture, Coalinga earthquake of 10 June 1983: California Geology, v. 8, p. 182-184.
- Murtha, P.E. and O'Connell, D.R., 1983, Coalinga aftershock parameters from the UCB strong motion instruments: in Scholl, R. and Stratta, J., The Coalinga, California earthquake of May 2, 1983: a reconnaissance report (in press).
- Tucker B.E. and Brune J.N., 1973, Seismograms, S-wave spectra, and source parameters for aftershocks of San Fernando earthquake: in San Fernando, California, earthquake of February 9, 1971, v. 3, Geological and geophysical studies, U.S. Government Printing Office, Washington, D.C., p. 69-121.
- Uhrhammer, R.A., Darragh, R.B., and Bolt, B.A., 1983, The 1983 Coalinga earthquake sequence: May 2 through August 1: (this volume)

Model 1
$\alpha = 2.50 \text{ km/sec} + 0.35 / \text{sec} * Z$ $\beta = 1.33 \text{ km/sec} + 0.186 / \text{sec} * Z$ $V_P/V_S = 1.9$
Model 2
$\alpha = 3.87 \text{ km/sec} + 0.09 / \text{sec} * Z$ $\beta = 2.02 \text{ km/sec} + 0.048 / \text{sec} * Z$ $V_P/V_S = 1.9$

Station Name	Station Number	Latitude	Longitude	Elevation (meters)
HU*	1	36.205° N	120.104° W	112
DR*	2	36.282° N	120.305° W	253
TR	3	36.166° N	120.382° W	224
TX	4	36.226° N	120.372° W	341
EP	5	36.211° N	120.284° W	219
SH	6	36.238° N	120.330° W	344
QP	7	36.203° N	120.210° W	138
LG	8	36.170° N	120.212° W	149
CN	9	36.178° N	120.280° W	232
CO	10	36.151° N	120.344° W	202
HT	11	36.249° N	120.272° W	201

\*Stations co-sited with CDMG-UCSC portable network.

Table 3: Source Parameters

DATE	ORIGIN TIME (hr-min-sec)	LATITUDE (°N)	LONGITUDE (°W)	DEPTH (km)	M <sub>L</sub> (Richter)	M <sub>0</sub> (dyne-cm)	r (m)	$\Delta\sigma$ (bars)	GROUP
May 3	23-46-04.78	36.1536	120.3337	10.4	3.9	4.5x10 <sup>21</sup>	355	44.	A
May 4	07-28-39.34	36.2568	120.3355	9.8	4.8	2.6x10 <sup>22</sup>	587	55.	
	15-59-13.97	36.2340	120.2740	7.6	3.7	3.6x10 <sup>21</sup>	487	14.	
	16-11-20.22	36.2805	120.3477	8.3	4.3	1.1x10 <sup>22</sup>	592	23.	A
May 5	10-20-44.53	36.2615	120.3608	10.1	4.5	2.6x10 <sup>22</sup>	979	12.	A
	11-33-41.17	36.2370	120.3484	8.5	3.6	1.1x10 <sup>21</sup>	207	56.	A
	12-42-16.30	36.2381	120.3773	9.3	3.7	2.4x10 <sup>21</sup>	271	54.	A
May 6	09-43-39.47	36.1917	120.3373	9.5	3.5	5.0x10 <sup>20</sup>	250	14.	A
	11-51-44.92	36.2598	120.3599	8.5	3.0	7.6x10 <sup>20</sup>	276	16.	
May 7	00-17-16.27	36.2588	120.3225	7.9	3.8	3.2x10 <sup>21</sup>	399	22.	
	05-43-57.56	36.2246	120.2838	7.7	3.5	1.1x10 <sup>21</sup>	315	15.	B



Table 3: Source Parameters (cont.)

DATE	ORIGIN TIME (hr-min-sec)	LATITUDE (°N)	LONGITUDE (°W)	DEPTH (km)	M <sub>L</sub> (Richter)	M <sub>0</sub> (dyne-cm)	r (m)	Δσ (bars)	GROUP
May 18	09-02-42.87	36.2158	120.2692	6.7		3.8x10 <sup>17</sup>	108	0.13	B
	09-10-25.71	36.2058	120.2526	8.1		1.5x10 <sup>18</sup>	182	0.11	B
	09-19-00.29	36.2426	120.3800	6.6		1.5x10 <sup>18</sup>	151	0.19	A
	09-30-31.87	36.1926	120.2680	8.2		2.4x10 <sup>18</sup>	219	0.099	B
	09-39-11.66	36.1817	120.2440	6.5		5.1x10 <sup>18</sup>	171	0.45	B
	09-40-48.80	36.2136	120.2818	7.4		1.6x10 <sup>18</sup>	176	0.13	
	09-49-12.70	36.2352	120.2567	7.0		3.8x10 <sup>17</sup>	80	0.32	
	10-33-37.25	36.1601	120.2607	10.6		6.1x10 <sup>18</sup>	194	0.36	
	12-13-54.38	36.1518	120.2523	10.1		1.2x10 <sup>18</sup>	122	0.28	
	12-36-50.02	36.1972	120.2476	7.8		5.6x10 <sup>17</sup>	122	0.13	B
May 19	07-38-49.33	36.2429	120.3310	8.2		5.6x10 <sup>17</sup>	117	0.15	A
	07-45-07.70	36.2541	120.3189	8.1		1.7x10 <sup>18</sup>	145	0.24	A
	08-37-29.22	36.1708	120.2882	8.4		7.5x10 <sup>17</sup>	155	0.087	
	08-38-52.21	36.2547	120.3550	8.3		1.1x10 <sup>19</sup>	161	1.2	A
	08-41-53.65	36.2485	120.2578	6.5		2.6x10 <sup>18</sup>	135	0.46	
	08-49-41.88	36.1973	120.2609	7.9		1.1x10 <sup>19</sup>	224	0.41	B
	08-51-02.62	36.2640	120.3917	6.3		5.9x10 <sup>17</sup>	117	0.16	A
	09-15-56.57	36.1853	120.2607	11.9		4.3x10 <sup>18</sup>	178	0.33	B
	09-19-26.83	36.2443	120.3343	7.2		5.0x10 <sup>18</sup>	216	0.22	A
	09-31-32.50	36.2702	120.3930	5.3		3.1x10 <sup>17</sup>	131	0.061	A
	10-05-16.03	36.2132	120.2695	6.2		1.7x10 <sup>18</sup>	212	0.080	B
	10-10-29.78	36.1681	120.2404	12.2		3.6x10 <sup>18</sup>	217	0.15	
	10-30-33.33	36.2613	120.3914	6.5		1.4x10 <sup>18</sup>	148	0.19	A
	11-05-30.40	36.2196	120.2719	11.0	3.7	8.4x10 <sup>20</sup>	364	7.7	B
	11-21-19.18	36.2187	120.2703	10.7					
	11-21-20.08	36.2145	120.2743	11.1					
	11-22-26.60	36.2197	120.2765	10.2		2.4x10 <sup>18</sup>	169	0.21	B
	12-15-46.12	36.2517	120.2298	8.8		1.5x10 <sup>18</sup>	133	0.27	
	14-50-07.97	36.2533	120.3321	8.3		4.1x10 <sup>17</sup>	102	0.17	A
	15-39-32.84	36.1577	120.1946	13.7					
	15-57-40.18	36.1236	120.2148	0.9					
	16-53-41.56	36.2498	120.2671	4.9		1.3x10 <sup>18</sup>	118	0.34	

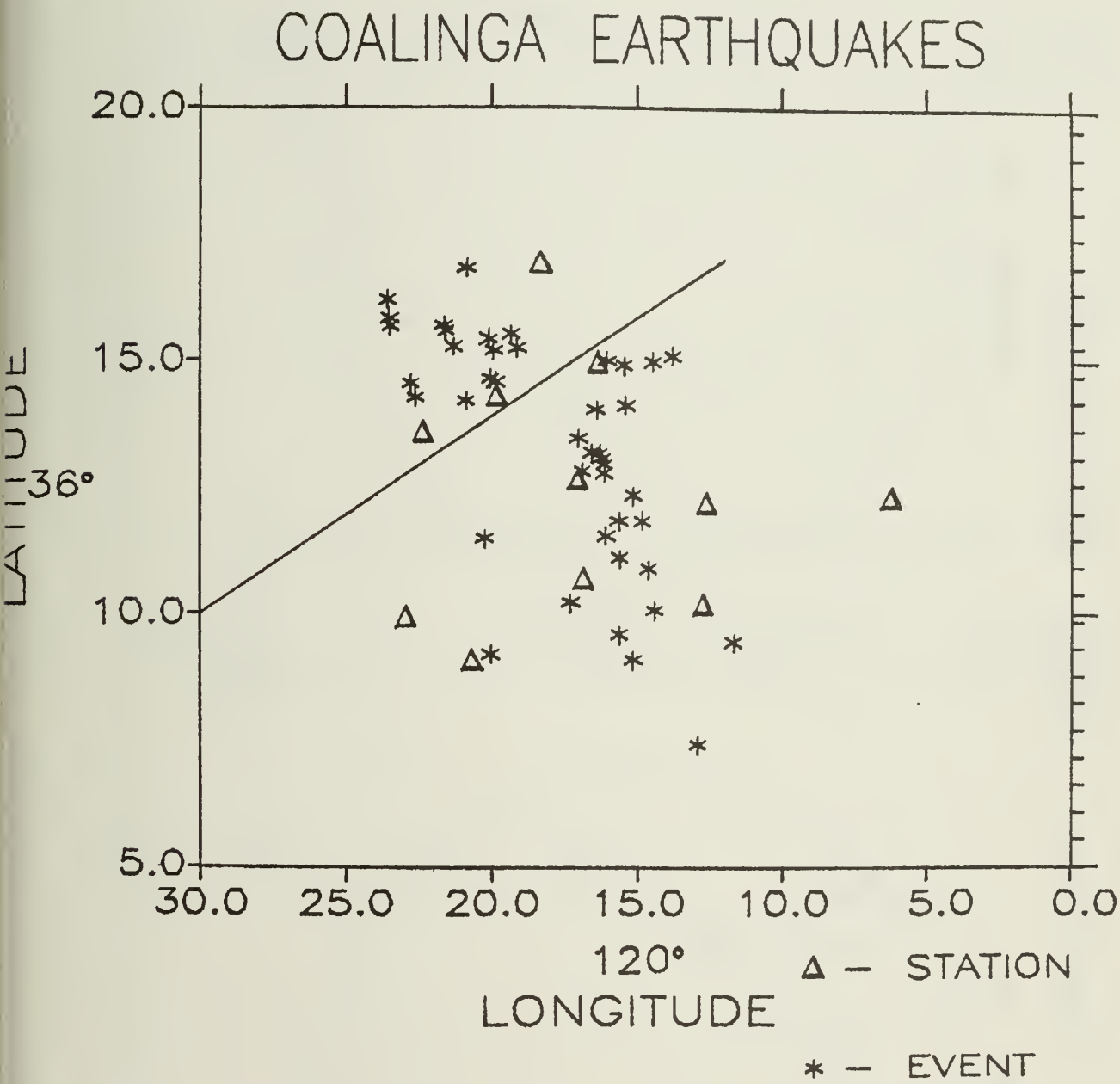


Figure 1. Epicentral plot of all the aftershocks from both the velocity data and the acceleration data, and the stations used to locate them. Latitude and longitude are shown in degrees and minutes. Note that most of the events are within the array or close to its perimeter. The location of the cross section in Figure 3 is shown as a solid line.

COMPOSITE FOCAL MECHANISMS

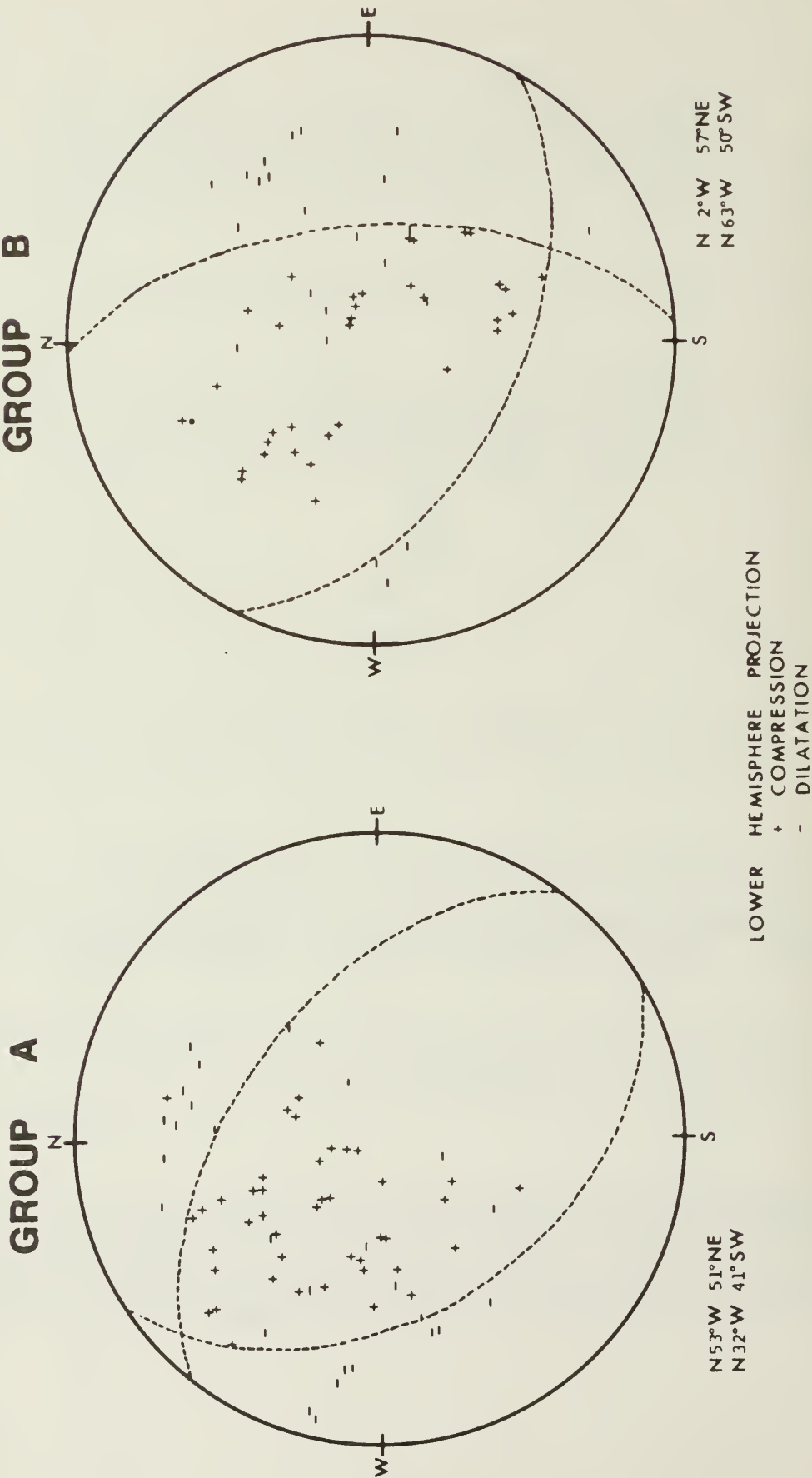


Figure 2. Composite focal mechanisms for two groups of aftershocks. Group A contains aftershocks located at the northwest corner of the array. Group B contains aftershocks located in the center of the array. Earthquakes used in the composite focal mechanisms are indicated by group type in Table 3. Refer to the text for descriptions of these solutions.

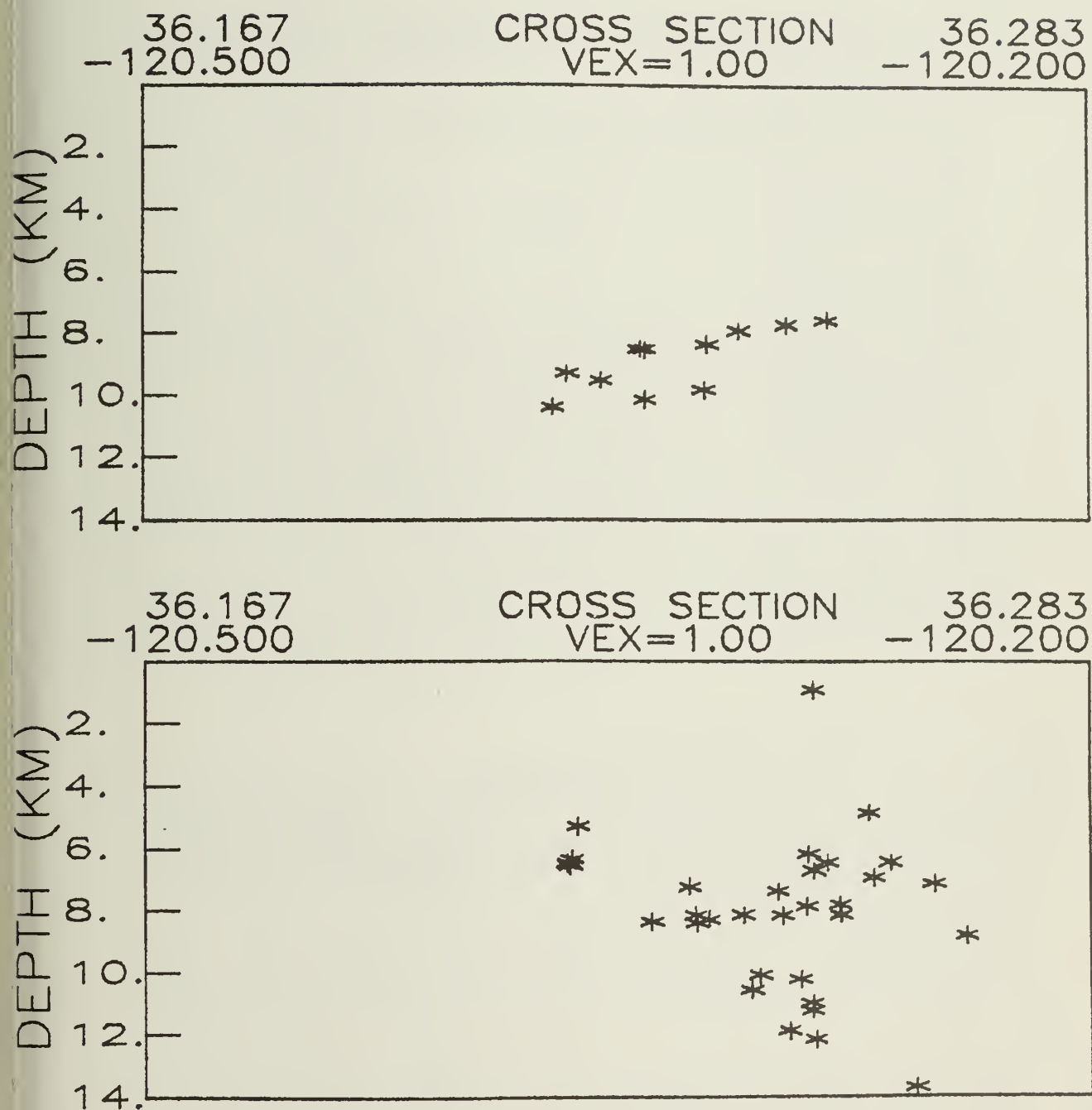


Figure 3. Two cross section plots of aftershock hypocenters. The position of the cross sections is shown on Figure 1 as a solid line. The cross sections show the southwest corner on the left edge. The top cross section contains only acceleration data hypocenters. The bottom cross section contains only velocity data hypocenters.



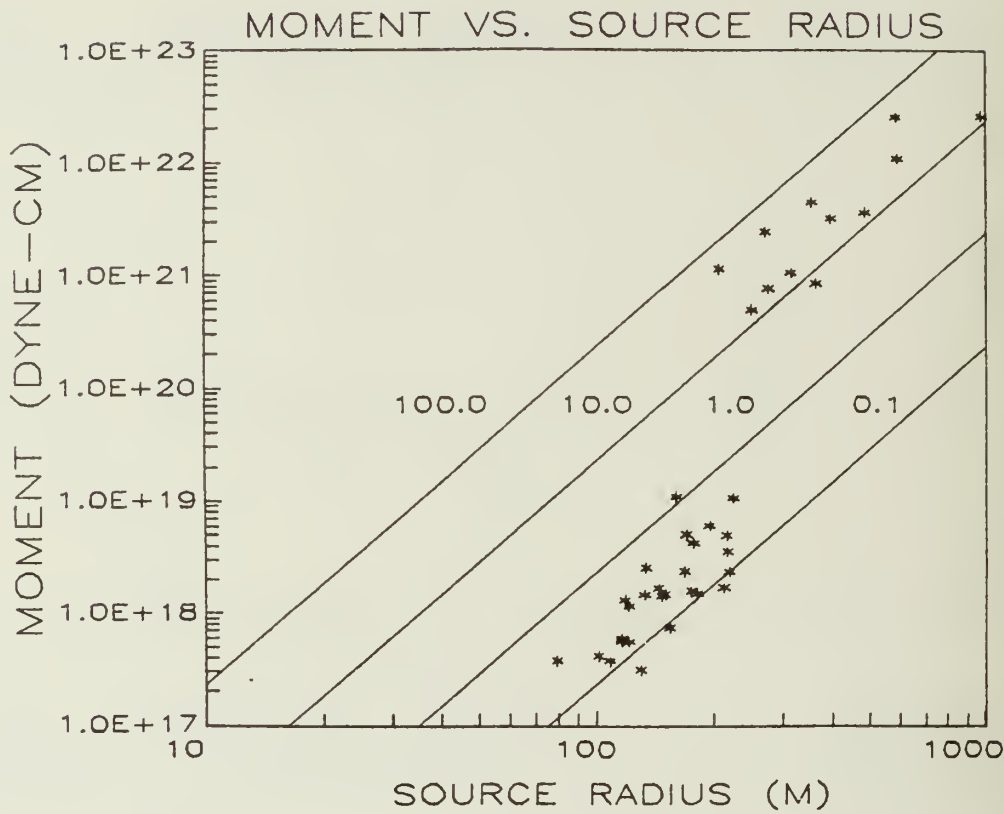


Figure 4. Log-log plot of moment vs source radius for the 39 aftershocks used in the spectra analysis. Lines of constant stress drop are shown with the associated values labeled above the lines. The source radii decrease with moment, and similarity holds within both the larger-moment and the smaller-moment groups of earthquakes.

# DISCREPANCIES IN STRONG MOTION AND SENSITIVE ARRIVAL TIME DATA FOR THE M6.7 COALINGA EARTHQUAKE OF 2 MAY 1983

by

Chris H. Cramer and Anthony F. Shakal<sup>1</sup>

## ABSTRACT

The M6.7 Coalinga Earthquake of 2 May 1983 was recorded on a large number of strong-motion recorders in the Parkfield-Coalinga, California area. A comparison of arrival times on selected strong-motion records with regional seismograph P-wave arrival times revealed discrepancies in S-P times and absolute S-wave arrival times at the strong-motion sites. S-waves arriving at the strong-motion sites appear to radiate from a different source than the P-wave energy. Possible causes for these observations have been investigated. The possibility of multiple or complex sources seems an unlikely cause. Rather, lateral variations in velocity structure and/or  $V_p/V_s$  ratios are the more likely cause. Single-station estimates of  $V_p/V_s$  ratios from digital event recorder sites indicate  $V_p/V_s$  ratios of 1.85 and higher. This high  $V_p/V_s$  ratio effectively explains observed discrepancies in S-P times. Discrepancies between the computed S-wave source location and P-wave source location may be due to variations in the  $V_p/V_s$  ratio with depth.

## INTRODUCTION

The M6.7 (BRK) Coalinga earthquake of 2 May 1983 was recorded on an extensive array of strong-motion stations in the Parkfield-Cholame area (Shakal and McJunkin, 1983; McJunkin and Shakal, 1983). The earthquake was also recorded at strong-motion sites at Slack Canyon, Cantua Creek, and Pleasant Valley Pumping Plant (Shakal and McJunkin, 1983; Maley et al., 1983). Many mainshock strong-motion records had absolute WWVB timing although reception was bad at the Cantua Creek site. The strong-motion sites are shown in figure 1.

Cursory examination of the strong-motion data indicates a large discrepancy in S-minus-trigger time at the Cantua Creek site given its distance from the main shock epicenter. The trigger to S-wave time on the Cantua record is much longer than expected. Initial attempts to locate the main event using the strong-motion data along with regional sensitive seismograph coverage indicated that the S-wave data from the strong-motion sites gave a main shock location ~7 km to the NE of the P-wave solution and an origin time about 2 sec. later.

<sup>1</sup> Seismologists, California Division of Mines and Geology

## INVESTIGATIONS

Possible causes for these discrepancies are 1) a double event or complex rupture pattern, 2) variation in  $V_p/V_s$  ratio from the usual central California value of about 1.7, and 3) inadequate modeling of the crust beneath Coalinga with a plane layered velocity model.

We reviewed the strong-motion records carefully and found no compelling evidence for a double or complex event (figure 2). (See Shakal and McJunkin, 1983, and Maley *et al.*, 1983 for copies of all the main shock strong-motion records.) There were a few later P-wave arrivals that might have been candidates for arrivals from a second main event, but attempts to use them to determine hypocenters did not improve any solutions nor remove any existing discrepancies. These arrivals are probably all secondary refracted and reflected arrivals.

### $V_p/V_s$ Study

Next, we investigated the possibility of significantly different  $V_p/V_s$  ratios in the Coalinga area. During the early aftershock sequence (5-19 May 1983), California Division of Mines and Geology (CDMG) operated a Sprengnether DR-100 digital event recorder with a Sprengnether S-6000 three-component seismometer at Avenal, southeast of Coalinga (figure 1). Also during a U.S. Geological Survey (USGS) refraction experiment at the end of June, 1983, a DR-100 with S-6000 seismometer was operated next to the strong-motion site at Cantua. (See figure 1.)

Table 1 summarizes our measurements of single-station  $V_p/V_s$  ratios. P and S-wave arrival times were measured from the DR-100 digital records (100 sps) and origin times were taken from final hypocenter solutions of Sherburne *et al.* (1983, this publication). An average  $V_p/V_s$  ratio of  $1.85 \pm 0.06$  for the Avenal site (CAVD) was determined from all 17 measurements and also from the 10 solutions with B and better qualities by all three HYP071 standards. Only one measurement was available for the Cantua Creek strong-motion site, and that value was 1.91.

Our  $V_p/V_s$  estimates suggest a higher than normal  $V_p/V_s$  ratio in the Coalinga area. Similar and higher preliminary  $V_p/V_s$  ratios were obtained from the DR-100 P and S-wave arrivals listed in Table 2 of Murtha and O'Connell (1983). Hence, a  $V_p/V_s$  ratio of 1.85 is more appropriate for the Coalinga area than the value of 1.70 originally used.

### Refraction Survey

As part of CDMG's aftershock study of this M6.7 sequence, the USGS refraction shots of 18-19 May and 30 June, 1983, were recorded on CDMG's aftershock network and were interpreted for a plane-layer P-velocity model appropriate to the Coalinga area by Sherburne *et al.* (1983, this volume). Sherburne *et al.*'s best average P-velocity model is a 2.87 k/s

layer at the surface over a 4.2 k/s layer starting at a depth of 2.1 km, over a 6.0 k/s layer starting at 6.5 km.

However, there is evidence in the shot data for lateral variations in P-velocity. The westernmost shot, well to the west of CDMG's array, gave an apparent velocity of 5.4 k/s instead of 6.0 k/s while the easternmost shot, well to the east of the array, gave an apparent velocity of 6.8 k/s. This suggests 1) a possible eastward dip on the top of the 6.0 k/s layer, 2) eastward thickening of sediments overlaying the 6.0 k/s layer, and/or 3) velocity variations across the boundary between the Coast Range and the Great Valley. This west-to-east lateral velocity variation is consistent with the known geology across the Coast Range-Great Valley boundary and with Coalinga's location close to that boundary. Thus, lateral velocity variations may have a significant effect on the main shock location.

### Mainshock Location

As a means of providing better control on the main shock location, the large M5.1 (BRK) aftershock at 0249Z on 9 May 1983 was used as a master event to calibrate the regional stations. The upper crustal P-velocity model of Sherburne, et al. (1983) was blended with the lower crustal part of the USGS central California velocity model (Eaton, 1983) (6.4 k/s layer starting at 14.0 km and a 7.9 k/s half-space starting at 28.0 km) for travel time calculations to the regional stations. The local CDMG array and the velocity model with station corrections (Sherburne et al.) provided the master event location shown in Table 2 and the Appendix. Station corrections to selected regional stations within 250 km of the Coalinga sequence were taken from travel-time residuals to those stations for the master event (See Appendix).

Table 2 lists our best locations for the main shock using P-wave data only, the strong-motion S-wave data, and both data sets combined. The P-wave only solution provides the best quality solution. A  $V_p/V_s$  ratio of 1.85 was used to also incorporate the S-P time from the Cantua Creek strong-motion record. The 1.85  $V_p/V_s$  ratio, based on our measurements, provides a much better fit for the S-P time at Cantua Creek (residual of 0.3 sec. instead of over one second when the 1.7  $V_p/V_s$  ratio was used - see Appendix).

The S-wave arrivals from the strong-motion data still tend to pull the main shock location to the northeast as indicated in both the S only solution and the combined data solution in Table 2. The poorer solution qualities for these two solutions is due to the effect of the S-wave data (see Appendix). Examining the S-wave residuals from the P-wave only solution shows discrepancies of  $\pm 1.5$  sec. for S-wave arrivals between epicentral distances of 29 and 40 km. This suggests that the S-wave discrepancy might be due to variations in  $V_p/V_s$  ratio with depth rather than actual hypocentral differences in P and S-wave sources during the main shock.



## CONCLUSIONS

Our investigation into discrepancies between strong-motion S-wave arrival times and seismographic P-wave arrival times for the main event at Coalinga indicates that  $V_p/V_s$  ratios in the Coalinga area are higher than normal for Central California. We measured average single-station  $V_p/V_s$  ratios of  $1.85 \pm 0.06$  for one digital seismograph site (Avenal, CA). A single measurement of 1.91 was obtained from a digital seismograph at the strong-motion site at Cantua Creek, CA. A  $V_p/V_s$  ratio of 1.85 greatly reduces S-P time discrepancies for the main event, particularly for the Cantua Creek strong-motion site. High  $V_p/V_s$  ratios have also been measured in other parts of Central California (i.e., McEvilly and Johnson, 1974). High  $V_p/V_s$  ratios suggest greater water saturation in crustal rocks and, in the case of the Coalinga area, may be associated with a region of higher pore pressure or pore fluid content associated with the Great Valley sequence trapping metamorphic fluids in the underlying Franciscan formation (Erwin and Barnes, 1975).

There remains a discrepancy in the strong-motion S-wave arrival times that tends to pull the main shock location to the northeast. Although the cause of this difference in hypocenter location has not been fully resolved, it seems more likely that the discrepancy is due to lateral variations in velocity structure and probably variations in  $V_p/V_s$  ratio with depth than it is due to complex or multiple sources of P and S-wave energy during the M6.5 main shock. Further work is required to resolve possible velocity variations.  $V_p/V_s$  ratios should be measured at the other strong-motion sites in addition to the Cantua Creek site in order to calibrate those sites and look for systematic variations in  $V_p/V_s$ .

## ACKNOWLEDGEMENTS

We wish to thank Dr. Paul Morrison for allowing us access to the Department of Water Resources regional seismograph records for the main event and the M5.1 aftershock used as a master event for the regional coverage. We also would like to thank Mr. John Meeker of the University of California, Berkeley Seismographic Stations for providing P-wave arrival times at stations LLA and PRS for both the main shock and master aftershock, and Dr. Kate Hutton of the California Institute of Technology Seismological Laboratory for providing a P-wave arrival time at ISA for the master aftershock. We are grateful to Dr. Roger Borchardt for providing us advanced copies of their Pleasant Valley Pumping Plant strong-motion record for the main event.

The manuscript was reviewed by Tousson Topozada, Roger Sherburne, and Charles Real. Their comments were very helpful and greatly appreciated.

## REFERENCES

- Eaton, J.P., 1983, Seismic setting, location and focal mechanism of the May 2, 1983, Coalinga earthquake: in Borchardt, R., editor, The Coalinga earthquake sequence commencing May 2, 1983: U.S. Geological Survey, Open-File Report 83-511, p. 20-26.
- Irwin, W.P., and Barnes, I., 1975, Effects of geologic structure and metamorphic fluids on seismic behavior of the San Andreas fault system in central and northern California: *Geology*, vol. 3, p. 713-716.
- Lahr, J.C., 1983, HYPOELLIPSE/VAX: A computer program for determining local earthquake hypocentral parameters, magnitude, and first-motion patterns: U.S. Geological Survey, Open-File Report 80-59 (revised 1983), 67 p.
- Lee, W.H.K., and J.C. Lahr, 1972, HYP071: A computer program for determining hypocenter, magnitude, and first-motion patterns of local earthquakes: U.S. Geological Survey, Open-File Report, 100 p.
- Maley, R., Brady, G., Etheridge, E., Johnson, D., Mork, P., and Switzer, J., 1983, Analog strong-motion data and processed main event records: in Borchardt, R., editor, The Coalinga earthquake sequence commencing May 2, 1983: U.S. Geological Survey, Open-File Report 83-511, p. 38-60.
- McEvelly, T.V., and Johnson, L.R., 1974, Stability of P and S velocities from central California quarry blasts: *Bulletin of the Seismological Society of America*, vol. 64, p. 343-354.
- McJunkin, R.D., and Shakal, A.F., 1983, The Parkfield strong-motion array: *California Geology*, v. 36, p. 27-34.
- Murtha, P.E., and O'Connell, D.R., 1983, Coalinga aftershock parameters from UCB strong motion instruments: Preprint of paper for EERI publication on the Coalinga earthquake, 11 pp.
- Shakal, A.F., and McJunkin, R.D., 1983, Preliminary summary of CDMG strong-motion records from the 2 May 1983 Coalinga, California, earthquake: California Division of Mines and Geology, report OSMS 83-5.2, 49 pp.
- Sherburne, R., McNailey, K., Roburto, A., and Brown, E.D., 1983, Mainshock-aftershock sequence of the 2 May 1983 Coalinga, California, earthquake: California Division of Mines and Geology, Special Publication 66 (this volume).

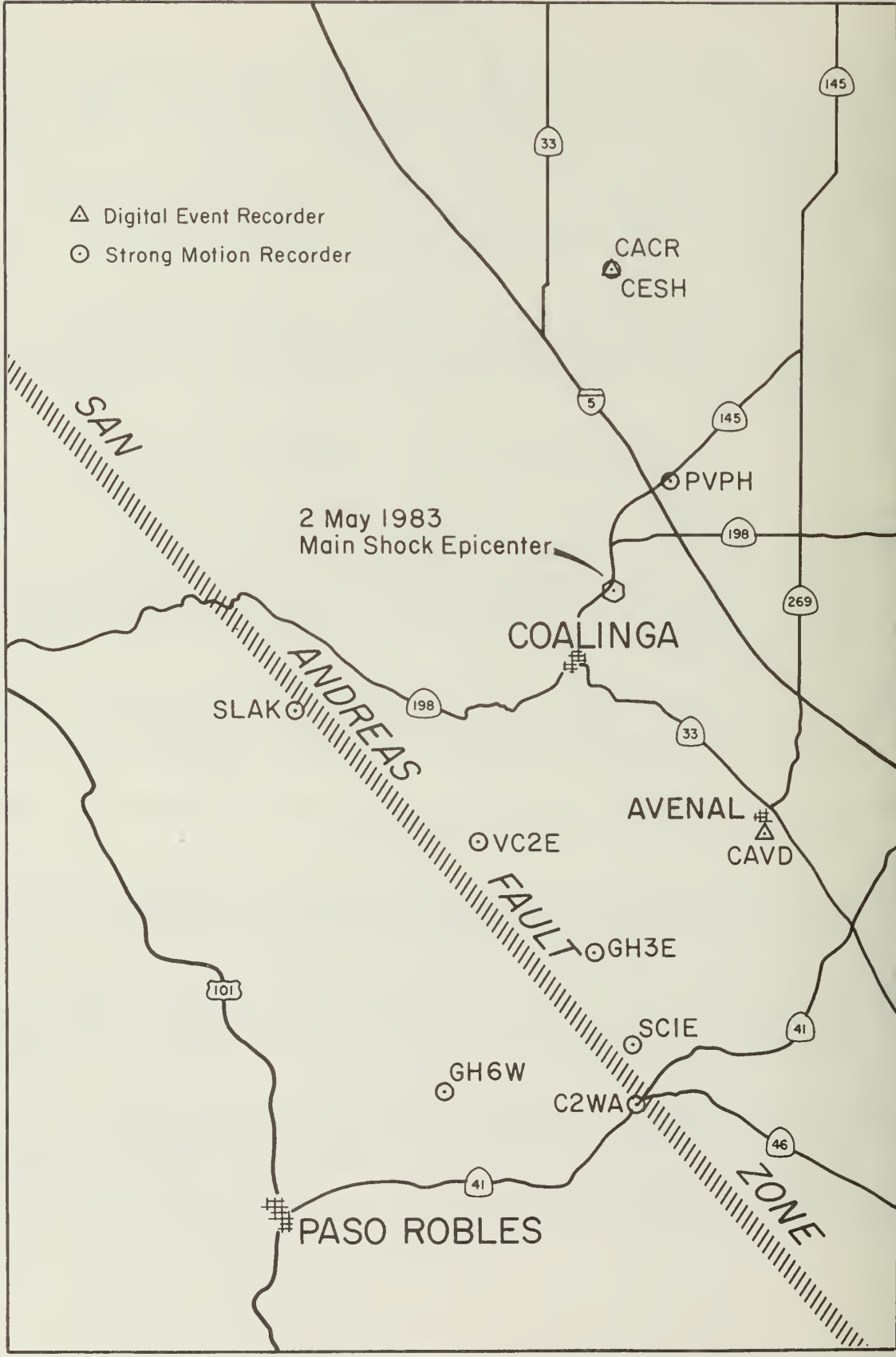


Figure 1. Map of Coalinga, California. Area showing strong motion sites and digital event recorder sites used in this study. Our best main shock location is also shown.

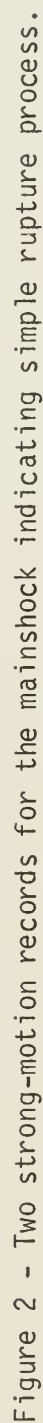


Figure 2 - Two strong-motion records for the mainshock indicating simple rupture process.



TABLE 1

Summary of Measurements of Vp/Vs ratios at COMG digital event recorder sites CAVD and CESH.

Stn.	Date	Origin	Time	Q*	tp*	ts	Vp/Vs (Ts/Tp)
CAVO	830507	0543	57.77	BCA	EP3 64.070	ES3 69.57	1.87
	830507	1242	30.83	CCB	EP3 39.180	ES4 45.34	1.74
	830508	0738	11.57	BAB	IP1 19.26A	ES3 25.18	1.77
	830514	0220	48.73	BBB	IP0 55.36A	ES2 61.58	1.94
	830514	0502	03.66	BBA	EP3 10.810	ES2 16.79	1.84
					IP0 10.75A		[1.85]
	830514	0554	45.72	CCB	IP1 49.650	ES2 53.27	1.92
					IP0 49.60A		[1.95]
	830514	1359	19.70	CCB	EP2 23.850	ES3 27.53	1.89
					IP0 23.86A		[1.88]
	830515	0034	30.21	BBB	EP1 34.090	IS2 37.45	1.87
					IP0 34.08A		[1.87]
	830515	0104	21.84	BBB	IP1 26.170	ES2 29.79	1.84
					IP0 26.15A		[1.84]
	830516	1840	16.26	CBC	IP0 21.85A	ES3 26.47	1.83
	830516	1909	37.77	CCC	EP2 43.33A	ES3 47.91	1.82
	830516	1945	38.63	CBC	IP1 42.330	IS2 45.71	1.91
					IP0 42.33A		[1.91]
	830517	1813	06.86	BBB	IP0 12.83A	ES3 17.44	1.77
	830517	2222	13.33	BBB	EP2 20.32A	ES2 26.72	1.92
	830518	0222	27.43	BBA	EP3 33.120	ES3 37.70	1.80
					IP0 33.06A		[1.82]
	830518	0246	49.41	BBA	EP2 55.28D	ES2 60.56	1.90
					IP0 55.25A		[1.91]
	830519	1105	30.38	BBA	IP1 36.78D	ES3 42.08	1.83
					IP0 36.81A		[1.82]
CESH	830630	0204	11.96	BBB	IP1 18.140	ES2 23.89	1.93

\* Q - HYP071 (Lee and Lahr, 1972) Location Qualities; 1st-overall; 2nd-solution; 3rd-station distribution.

\* P-wave times: 0-from digital record; A-from analog smoke-drum record. All S-wave times from digital records.

CAVO mean Vp/Vs ratio:  $1.85 \pm 0.06$  (17 events) - all events listed  
 $1.85 \pm 0.06$  (10 events) - B and better for all qualities.

TABLE 2

Mainshock and master-event aftershock locations and HYP071 qualities.

(See Appendix for complete solution print out.)

					Depth	ERH	ERZ		
	Date	Origin	Time	N.Lat.	W.Long.	(km)	(km)	(km)	Q*
Main:	830502	2342							
P only:			38.60	36°12.59'	120°18.85'	9.49	0.8	1.4	8AC
S only*:			37.62	36°15.08'	120°15.86'	20.92	7.5	13.9	OCD
All data:			38.95	36°13.43'	120°18.32'	13.04	1.4	1.6	CCB
Master:	830509	0249	11.95	36°13.78'	120°18.55'	10.70	0.8	1.8	BBA

All hypocenters determined by using the HYPOELLIPSE computer program (Lahr, 1983).

\* As in Table 1, HYP071 location qualities: 1st-Overall; 2nd-Solution; 3rd-Station Distribution.

\* Strong-motion data.

## APPENDIX

Solution listings for hypocenter determination listed in Table 2.

Station abbreviations for strong-motion sites used in solutions:

CACR - Cantua Creek site (CDMG)

C2WA - Cholame 2WA site (CDMG)

GH3E - Gold Hill 3E site (CDMG)

GH6W - Gold Hill 6W site (CDMG)

PVPH - Pleasant Valley Pumping Plant site (USGS)

SC1E - Stone Corral 1E site (CDMG)

SLAK - Slack Canyon site (CDMG)

VC2E - Vineyard Canyon site (CDMG)

A) P-ONLY SOLUTION:

HORIZONTAL  
SE = 0.58  
AZ = -76.  
VERTICAL  
SE = 1.36  
QUALITY = A

DATE ORIGIN LAT LONG DEPTH MAG NO D3 GAP M RMS ERH ERZ Q SOD ADJ IN NR AVR AAR NM AVXM SDXM NF AVFM SDFM  
830502 2342 38.60 36N12.59 120W18.85 9.49 16 72 107 1 0.09 0.8 1.4 B A C 0.10 10 44 0.01 0.06 0 0.0 0.0 0 0.0 0.0  
SE OF ORIG = 0.072 5 ITERATIONS TOTAL

(- STATION DATA -) (----- P-WAVE TRAVEL-TIME DATA AND DELAYS -----) VARI (---- S-WAVE TRAVEL-TIME DATA --) (--- MAGNITUDE DATA ---																				
STN	DIST	AZM	AIN	PSEC	PRMK+TCOR-O=TTTB-TTCAL-DELAY-EDLY=	P-RES	P-WT	THIC	SSEC	KRMS	TTOB	TTCAL	S-RES	S-WT	AMX	PR	XMAG	R	FMP	FMA
PVPH	12.5:	27	111	42.04ET	3	3.44	3.57	-0.14	0.099	45.44	S	4	6.84	6.61	0.23	0.0				
VC2E	29.7:	208	97	46.40ET	4	7.80	6.36	1.43	0.0	52.00	S	4	13.40	11.77	1.62	0.0				
SLAK	31.6:	232	97	46.85ET	4	8.25	6.68	1.57	0.0	52.50	S	4	13.90	12.36	1.54	0.0				
PRI	32.5:	257	96	45.45IPDO		6.85	6.82	0.02	1.580											
CACR	32.5:	358	96	45.00ET	9	6.40	6.84	0.29	0.395	51.10ES	2	6.10	5.81	0.29	SMP					
GH3E	37.8:	183	95	48.80ET	4	10.20	7.70	2.50	0.0	54.50	S	4	15.90	14.25	1.65	0.0				
SC1E	46.8:	178	94	49.60ET	4	11.00	9.21	1.79	0.0	56.40	S	4	17.80	17.03	0.76	0.0				
C2WA	53.0:	178	94	50.60ET	4	12.00	10.22	1.77	0.0	58.00	S	4	19.40	18.91	0.49	0.0				
GH6W	55.1:	198	93	52.15ET	4	13.55	10.57	2.98	0.0	58.55	S	4	19.95	19.56	0.39	0.0				
LLA	72.3:	309	70	51.00IP	1	12.40	13.43	-1.06	0.02	0.889										
PRS	95.8:	278	70	54.80IP	1	16.20	17.11	-0.82	-0.10	0.889										
FRI	102.3:	32	70	54.50IPDO		15.90	18.12	-2.22	-0.01	1.580										
SFO	118.6:	302	49	57.90IPUO		19.30	20.45	-1.22	0.07	1.580										
SLD	125.6:	320	49	58.50IPUO		19.90	21.34	-1.38	-0.06	1.580										
MON	150.2:	287	49	61.80IPUO		23.20	24.45	-1.34	0.08	1.580										
MHC	172.7:	317	49	64.75IPU1		26.15	27.29	-1.24	0.09	0.889										
ISA	176.8:	110	49	65.55IPDO		26.95	27.82	-0.89	0.02	1.580										
SYP	189.2:	171	49	67.65IPD4		29.05	29.39	-0.34	0.0											
JAS	193.1:	357	49	67.90IPDO		29.30	29.87	-0.56	-0.02	1.580										
FTC	196.4:	139	49	66.80EPD2		28.20	30.30	-2.14	0.04	0.395										
ECF	223.9:	150	49	11.40EPD2		32.80	33.78	-0.91	-0.07	0.395										
PYR	231.5:	141	49	71.90EP+3		33.30	34.74	-1.83	0.39	0.099										
PCC	233.8:	309	49	11.90IPU1		33.30	35.03	-1.51	-0.22	0.889										
SBB	282.0:	126	49	18.30IPU1		39.70	41.14	-1.44	-1.44	0.0										
GSC	333.0:	107	49	25.40EPD3		46.80	47.58	-0.87	0.08	0.0										
NMH	341.6:	324	49	25.50EP-2		46.90	48.68	-1.70	-0.08	0.0										
SDW	343.7:	120	49	25.85EPD2		47.25	48.94	-1.84	0.15	0.0										
VPD	353.3:	138	49	27.30EP+3		48.70	50.16	-1.46	0.0											
AOH	361.0:	347	49	29.80EPD2		51.20	51.13	-0.24	0.30	0.0										
ORV	385.7:	345	49	92.55EPD2		53.95	54.26	-0.02	-0.30	0.0										
OCH	426.4:	343	49	37.50EPD2		58.90	59.41	-0.58	0.07	0.0										
PLM	447.4:	134	49	38.85EPD2		60.25	62.07	-1.83	0.0											
MIN	472.7:	347	49	44.50EPD3		65.90	65.27	-0.62	0.62	0.0										
WDC	522.6:	339	49	48.45EPD3		69.85	71.59	-1.74	0.0											
IKP	552.6:	134	49	52.15EPD3		73.55	75.38	-1.83	0.0											
FHC	601.9:	329	49	60.70EPD3		82.10	81.62	-0.48	0.48	0.0										
GLA	612.9:	123	49	58.40EPD3		79.80	83.02	-2.64	-0.58	0.0										

QUALITY EVALUATION

DIAGONALS IN ORDER OF STRENGTH Z SW N NW NE SE E  
AVE. OF END POINTS 0.26 0.51 0.64 0.64 0.66 0.69 0.86

NUMBER RMS MIN DRMS AVE DRMS QUALITY  
16 0.09 0.35 0.64 A

B) S-ONLY SOLUTION: SE = 3.15 SE = 7.49 SE = 13.90 QUALITY = D  
AZ = -85. AZ = 5. AZ = 0.0

HORIZONTAL VERTICAL

DATE ORIGIN LAT LONG DEPTH MAG NO D3 GAP M RMS ERH ERZ Q SQD ADJ IN NR AVR AAR NM AVXM SDXM NF AVFM SDFM  
830502 2342 37.62 36N15.08 120W15.86 20.92 8 36 338 1 0.22 7.5 13.9 D C D 0.06 10 13 0.03 0.17 0 0.0 0.0 0.0 0.0  
SE OF ORIG = 1.566 11 ITERATIONS TOTAL

(- STATION DATA -) (----- P-WAVE TRAVEL-TIME DATA AND DELAYS -----) VARI (----- S-WAVE TRAVEL-TIME DATA -----) (--- MAGNITUDE DATA ---)  
STN DIST AZM AIN PSEC PRMK+TCOR-O=TTOT-TTCAL-DELAY-EDLY= P-RES P-WT THIC SSEC KRMS TTOB TTCL S-RES S-WT AMX PR XMAG R FMP FMA  
PVPH 6.6: 11 159 42.54EPU3 4.92 4.30 0.62 0.136 45.44 S 1 7.82 7.95 -0.13 1.220  
CACR 28.5:349 118 45.00ET 9 7.38 6.66 0.44 0.542 51.10ES 2 6.10 5.66 0.44 SMP  
VC2E 35.9:211 111 46.40ET 4 8.78 7.72 1.07 0.0 52.00 S 1 14.38 14.27 0.11 1.220  
SLAK 38.0:231 110 47.15EP 4 9.53 8.02 1.51 0.0 52.50 S 1 14.88 14.83 0.05 1.220  
SC1E 51.5:183 103 49.60ET 4 11.98 10.05 1.93 0.0 56.40 S 1 18.78 18.60 0.18 1.220  
C2WA 57.6:182 101 50.60ET 4 12.98 10.98 2.00 0.0 58.00 S 1 20.38 20.32 0.06 1.220  
GH6W 60.9:201 100 52.15ET 4 14.53 11.50 3.03 0.0 58.55 S 1 20.93 21.27 -0.34 1.220

QUALITY EVALUATION

DIAGONALS IN ORDER OF STRENGTH NW NE E Z SE N SW  
AVE. OF END POINTS 0.34 0.52 0.60 0.70 0.92 1.13 1.16

NUMBER RMS MIN DRMS AVE DRMS QUALITY  
8 0.22 0.19 0.77 B



C) ALL DATA SOLUTION:

HORIZONTAL  
SE = 0.88  
AZ = 9.  
VERTICAL  
SE = 1.40  
AZ = -81.  
QUALITY = A

DATE	ORIGIN	LAT	LONG	DEPTH	MAG	NO	D3	GAP	M	RMS	ERH	ERZ	Q	SQD	ADJ	IN	NR	AVR	AAR	NM	AVXM	SDXM	NF	AVFM	SDFM			
830502	2342	38.95	36N13.43	120W18.32	13.04	23	31	104	1	0.30	1.4	1.6	C	C	B	0.06	10	44	0.01	0.24	0	0.0	0.0	0	0.0	0.0		
SE OF ORIG = 0.097					5 ITERATIONS TOTAL																							
(- STATION DATA -) (----- P-WAVE TRAVEL-TIME DATA AND DELAYS -----) VARI (---- S-WAVE TRAVEL-TIME DATA ----) (--- MAGNITUDE DATA ---)																												
STN	DIST	AZM	AIN	PSEC	PRMK+TCOR-O=	TTOB-TTCAL-DELAY-EDLY=	P-RES	P-WT	THIC	SSEC	KRMS	TTOB	TTCAL	S-RES	S-WT	AMX	PR	XMAG	R	FMP	FMA							
PVPH	10.8:	28	132	42.04ET	3	3.09	3.64	-0.56	0.105	45.44	S	1	6.49	6.74	-0.25	0.941												
CACR	31.0:	357	104	45.00ET	9	6.05	6.69	0.41	0.418	51.10ES	2	6.10	5.69	0.41	SMP													
VC2E	31.4:	208	104	46.40ET	4	7.45	6.75	0.69	0.0	52.00	S	1	13.05	12.50	0.55	0.941												
SLAK	33.2:	231	103	46.85ET	4	7.90	7.04	0.86	0.0	52.50	S	1	13.55	13.02	0.53	0.941												
PRI	33.6:	254	103	45.45IPD0		6.50	7.11	-0.61	1.673																			
GH3E	39.4:	184	101	48.80ET	4	9.85	8.04	1.81	0.0	54.50	S	2	15.55	14.87	0.67	0.418												
SC1E	48.4:	179	70	49.60ET	4	10.65	9.49	1.15	0.0	56.40	S	1	17.45	17.56	-0.12	0.941												
C2WA	54.5:	179	70	50.60ET	4	11.65	10.45	1.20	0.0	58.00	S	1	19.05	19.33	-0.28	0.941												
GH6W	56.8:	199	70	52.15ET	4	13.20	10.81	2.39	0.0	58.55	S	1	19.60	20.00	-0.40	0.941												
LLA	71.9:	307	70	51.00IP	1	12.05	13.17	-1.06	0.941																			
PRS	96.4:	277	70	54.80IP	1	15.85	17.00	-0.82	0.941																			
FRI	100.6:	32	70	54.50IPD0		15.55	17.65	-2.22																				
SAO	118.4:	301	49	57.90IPD0		18.95	20.04	-1.22																				
SLD	124.9:	319	49	58.50IPD0		19.55	20.87	-1.38																				
MON	150.5:	287	49	61.80IPD0		22.85	24.10	-1.34																				
MHC	172.1:	317	49	64.75IPD1		25.80	26.83	-1.24																				
ISA	176.6:	110	49	65.55IPD0		26.60	27.41	-0.89																				
SYP	190.6:	171	49	67.65IPD4		28.70	29.18																					
JAS	191.6:	357	49	67.90IPD0		28.95	29.30	-0.56																				
FTC	197.1:	139	49	66.80EPD2		27.85	30.00	-2.14																				
ECF	224.9:	150	49	11.40EPD2		32.45	33.52	-0.91																				
PYR	232.2:	142	49	71.90EP+3		32.95	34.45	-1.83																				
PCC	233.4:	308	49	11.90IPD1		32.95	34.60	-1.51																				
SBB	282.3:	126	49	18.30IPD1		39.35	40.79																					
GSC	332.7:	107	49	25.40EPD3		46.45	47.16	-0.87																				
NMH	340.8:	324	49	25.50EP-2		46.55	48.19	-1.70																				
SDW	343.8:	120	49	25.85EPD2		46.90	48.57	-1.84																				
VPD	353.9:	138	49	27.30EP+3		48.35	49.85																					
AOH	359.7:	347	49	29.80EPD2		50.85	50.58	-0.24																				
ORV	384.4:	344	49	92.55EPD2		53.60	53.71	-0.02																				
OCH	425.1:	343	49	37.50EPD2		58.55	58.87	-0.58																				
PLM	447.9:	134	49	38.85EPD2		59.90	61.75																					
MIN	471.4:	346	49	44.50EPD3		65.55	64.72																					
WDC	521.5:	339	49	48.45EPD3		69.50	71.06																					
IKP	553.1:	135	49	52.15EPD3		73.20	75.06																					
FHC	600.9:	329	49	60.70EPD3		81.75	81.12																					
GLA	613.1:	123	49	58.40EPD3		79.45	82.66	-2.64																				

QUALITY EVALUATION

DIAGONALS IN ORDER OF STRENGTH	Z	SE	E	SW	NW	NE	N
AVE. OF END POINTS	0.42	0.70	0.72	0.80	0.89	1.02	1.23
NUMBER	RMS	MIN	DRMS	AVE	DRMS	QUALITY	B
23	0.30	0.64	0.87				





# STRONG-MOTION DATA FROM THE COALINGA, CALIFORNIA EARTHQUAKE AND AFTERSHOCKS

by

A.F. Shakal<sup>1</sup> and J.T. Ragsdale<sup>2</sup>

## ABSTRACT

Strong-motion records from the Coalinga aftershocks indicate that accelerations in the city of Coalinga are commonly three times higher than at a rock site 3 km west of the city. The high levels of damage in Coalinga during the mainshock are probably due in part to this effect. The alluvium underlying the Coalinga valley appears to be the reason for the increased accelerations relative to the rock site at the valley edge, observed in all but one of the six large (5 - 6 ML) aftershocks. No strong-motion records were obtained in Coalinga during the mainshock but accelerations as high as 70% in the aftershocks imply that equivalent or larger accelerations probably occurred during the mainshock.

The set of free-field strong-motion records obtained during the Coalinga earthquake is the largest ever obtained from a single event. The data set is important for studies of ground motion attenuation and local variations of ground motion. Proximate stations in the Parkfield strong-motion array recorded significantly different acceleration levels though sited on the same geologic formation.

Significant records were also obtained from the Coalinga aftershocks. The 5.1 ML event of 9 May was very well recorded, with some 26 strong-motion records obtained in the epicentral area by various agencies. Deployment of co-located analog and digital accelerographs for instrument-evaluation purposes yielded several accelerogram pairs and triplets with peak accelerations of 10 - 70%g.

## INTRODUCTION

The 6.7 ML (BRK) Coalinga earthquake of 2 May 1983 and its aftershocks generated a large set of important strong-motion data. The first part of this paper is an overview of the mainshock strong-motion data. The second part considers in greater detail the strong-motion records from the aftershocks. These records were recovered from instruments deployed in the immediate epicentral area as well as in the city of Coalinga. Accelerations of over 70%g were recorded in Coalinga.

<sup>1</sup> Seismologist, California Division of Mines and Geology

<sup>2</sup> Structural Engineer, California Division of Mines and Geology



## COALINGA MAINSHOCK STRONG-MOTION DATA

The Coalinga earthquake generated the largest set of strong-motion records since the San Fernando earthquake of 1971. Nearly 100 records were recovered from the earthquake, mostly from stations in the 25-60 km distance range. Sixty records were recovered by stations of the California Strong-Motion Instrumentation Program (CSMIP). A report on these records by Shakal and McJunkin (1983) gives the station locations, accelerations, and reproductions of the records. The largest accelerations recorded at CSMIP stations were about 30%g, at about 30 km from the epicenter. Most of the CSMIP records were obtained at stations of the recently completed Parkfield strong-motion array described by McJunkin and Shakal (1983).

In addition to the 60 CSMIP records, 37 records were recovered from stations maintained by the USGS. One of these stations, at the Pleasant Valley Pumping Plant, was only about 10 km from the epicenter. The records obtained at this station are described by Maley et al. (1983). The remaining USGS data are from distant (> 75 km) stations.

In many ways, the strong-motion data set from the Coalinga earthquake is similar to that from the San Fernando earthquake of 1971. The earthquakes had similar magnitudes and both were of thrust mechanism. For both earthquakes, the predominance of data was recorded at stations on the down-thrown block, at epicentral distances of 30-80 km. The Coalinga data set will moderate the influence of the San Fernando data on ground motion attenuation relationships. A significant feature of the Coalinga data set is that most records were obtained in small instrument shelters (described in McJunkin and Shakal, 1983). Much of the San Fernando data were recorded in moderate to large structures which can significantly affect the recorded strong motion (e.g., Boore et al., 1980).

## Peak Acceleration versus Distance

Study of the attenuation of strong shaking with distance is often complicated by the need to define source-to-station distance (e.g., Shakal and Bernreuter, 1981). However, epicentral distance is adequate for initial comparison of the data from the Coalinga and San Fernando earthquakes because of their similar source mechanisms and earthquake-station geometries.

The Coalinga peak-acceleration data are plotted against epicentral distance in Fig. 1. The San Fernando data, from Maley and Cloud (1973), are also plotted (open symbols). The similarity of the data sets is apparent, with much of the data for both earthquakes being recovered from distances between 30 and 80 km. There appears to be some evidence for higher accelerations from the Coalinga earthquake than the San Fernando event at a given epicentral distance but more detailed studies will be necessary to investigate the differences between the two data sets. Boore et al. (1983) have begun detailed analyses incorporating the distance to a postulated surface of fault rupture.

### Differences in Ground Motion at Nearby Stations

The CSMIP Parkfield strong-motion array (Fig. 2) recorded the Coalinga mainshock at 46 stations within a 20 km by 30 km area. The records obtained at some nearby stations show marked differences, both in frequency and amplitude. For example, the accelerograms from three nearby stations are compared in Fig. 3. These stations, Fault-Zone stations 9, 14 and 15, are all on the west side of the San Andreas fault, and are underlain by materials of the Pliocene-Pleistocene Paso Robles Formation (McJunkin and Shakal, 1983). They are also very close to one another relative to their epicentral distance (approx. 40 km). Yet, as shown in Fig. 3, the station 14 record is significantly higher in amplitude and shows a predominance of long period energy compared to either the station 9 or 15 record. The amplification at station 14 may be due to low-velocity materials at depth, not indicated by the surficial geology. That would be consistent with the arrival times indicated in Fig. 3. The S(?) signal arrives at station 14 over 1/2 sec later than at station 15, although station 14 is only 1/2 km more distant from the epicenter.

The response spectra computed from the records after digitization are shown in Fig. 4. The spectrum from station 14 is three times as high as the station 9 or 15 spectra near 1 Hz. At higher frequencies, the station 9 spectrum is quite low compared to the station 14 and 15 spectra. Full understanding of these differences will require increased knowledge of the geologic materials underlying the sites as well as analyses of possible topographic effects.

Records from other neighboring stations in the Parkfield array also show significant differences. However, these generally appear explainable in terms of the site geology. For example, station Cholame 1E, at the southeast end of Cholame Valley, shows amplitudes more than double those at Cholame 2E (formerly Temblor II), approximately 1.5 km away. This is consistent with the contrasting geology at the two sites, however. Cholame 2E is on sandstone while Cholame 1E is in the middle of the valley, underlain by recent alluvium. In fact, the long period nature of the Cholame 1E record is shared by nearly all the stations located in Cholame Valley. Further analyses of these data will improve our understanding of site effects on velocity and displacement as well as acceleration.

### STRONG-MOTION DATA FROM COALINGA AFTERSHOCKS

The 2 May 1983 Coalinga earthquake occurred in an area with few existing strong-motion instruments. Within a few days following the earthquake, however, various agencies had deployed a total of over 30 strong-motion recorders in the epicentral area. Significant results from these deployments are outlined here, in addition to the presentation of the principal results of CDMG/SMIP deployments.

## Coalinga Aftershock of 9 May, 02:49 UTC

During the days following the Coalinga mainshock on 2 May there were many aftershocks, but none were large enough to trigger many of the strong-motion recorders deployed in the area. However, a 5.1 ML (BRK) aftershock at 02:49 UTC on 9 May, located near the mainshock epicenter, triggered nearly all of the recorders in place at that time. CDMG personnel, in a joint effort with personnel of U.C. Santa Cruz, had nine accelerographs deployed during this aftershock. The station locations are shown on Fig. 5 and are listed in Table 1. Accelerograms were recovered at five stations from this aftershock. The accelerograms are shown in Fig. 6. A peak acceleration of 35%g was obtained at the Skunk Hollow station; 28%g was recorded at the Palmer Ave. station; 13%g was recorded in the city of Coalinga (CHP station).

In addition to the records shown in Fig. 6, records were obtained by other agencies during the 9 May aftershock. Caltech recovered accelerograms from 5 stations in the area, recording a peak acceleration of 30%g near the Palmer Ave. station shown in Fig. 5 and 16%g in a residence in the city of Coalinga (Jennings, 1983). Records were recovered at six temporary USGS accelerograph stations (Maley et al., 1983) as well as at the permanent Pleasant Valley Pumping Plant which recorded the main shock. Maley et al. (1983) report a peak acceleration of over 50%g at a station about 4 km NW of the Palmer Ave. station in Fig. 5. Accelerograms were also recovered from 9 additional USGS temporary stations at which digital accelerographs had been deployed (Borcherdt et al., 1983). This total set of 26 accelerograms is an unprecedented suite of strong-motion data from the epicentral area of a moderate earthquake and will allow important studies of the earthquake source and radiation.

## Increased Shaking Levels in Coalinga

During the week after the earthquake, CDMG deployed an accelerograph in the city of Coalinga, which overlies an alluvial valley, and one on Pliocene rock at the western edge of the valley. The Coalinga station (CHP) is at the California Highway Patrol building, which suffered significant damage during the mainshock. The valley-edge station (Baths) is at an abandoned mineral baths facility. Fig. 5 shows the relative locations of the stations and the local geology. These two instruments were left in place after other temporaries were withdrawn. Pairs of records were obtained from the six  $M > 5$  aftershocks which occurred during the following three months, including the magnitude 5.9 ML (BRK) event on 22 July, 02:40 UTC. Comparisons of the four largest record pairs are shown in Fig. 7. These records indicate a significantly higher intensity of shaking in downtown Coalinga than at the rock site to the west. The highest acceleration obtained was 71%g during the 5.1 ML earthquake of 25 July; the corresponding acceleration at the valley-edge station was only 19%g. It is interesting that this event was recorded with higher acceleration than the 53%g of the largest aftershock (5.9 ML), though it had nearly the same epicenter. The media quoted Coalinga residents as stating that the 25 July event produced the strongest shaking since the mainshock; the records of Fig. 7 confirm that fact, at least in terms of ground acceleration. In addition, the implication is that the mainshock itself had an acceleration level of at least 71%g in Coalinga.



The four accelerogram pairs in Fig. 7 (events 4 through 7 in Fig. 5 and Table 2) all show amplitudes approximately three times larger at station CHP than at the valley-edge station. All six of the  $M > 5$  aftershocks showed the higher accelerations at CHP (event 2 is shown in Fig. 6) except for event 3, which was recorded with very small amplitudes (near 5%g) at both stations. It is of interest that event 3 is also the only shallow event, and the only event of the entire sequence for which surface rupture was observed (Hart and McJunkin, 1983). Analyses of these data is just beginning and will require digitization and spectral analysis of the records. The CHP records, for example, seem to indicate a predominance of 6–8 Hz energy in the Coalinga ground shaking. The spectral analysis will allow the clarification of this response and study of its stability from earthquake to earthquake.

#### Comparison Between Analog and Digital Accelerographs

The ongoing Coalinga aftershocks provide the opportunity for field evaluation of new types of strong-motion instruments. The most popular analog accelerograph is the SMA-1 (Kinometrics), which produces a record of the acceleration time-history on a 70-mm photographic film. During the last few years several digital recorders designed for deployment as strong-motion accelerographs have been introduced. Following the Coalinga earthquake, two types of digital accelerographs were co-located with analog recorders. The 25 July aftershock, which was recorded at CHP with a peak acceleration of 71%g, was actually recorded by three adjacent accelerographs: the analog SMA-1, a digital DSA-1 (Kinometrics), and a digital DCA-333 (Terra Technology). The analog record and the strip-chart playbacks of the digital records are shown in Fig. 8.

Other comparative recordings were also obtained, but with lower amplitudes or fewer recorders. For example, the 22 July events of 02:40 and 03:43 UTC (events 5 and 6) were recorded by both the SMA-1 and DSA-1 at CHP (peak accelerations of 53 and 21%g). An additional deployment (in cooperation with Lawrence Livermore Laboratory) of a DSA-1 near the SMA-1 at Cantua Creek also yielded a pair of records, of about 30%g. Jennings (1983) reports on a co-location which resulted in a SMA-1/PDR-1 (Kinometrics) record pair, of about 12%g. Digitization of these various analog records in conjunction with processing of the digital records will provide invaluable checks on instrument performance as well as certification of digitization procedures.

#### ACKNOWLEDGEMENTS

The CSMIP technical staff installed and maintained the stations of the Parkfield array and is responsible for the high level of accelerograph performance. Gene Guyer maintained the digital accelerographs deployed for evaluation and assisted in the instrument comparison effort. K. McNally of UC Santa Cruz worked with R. McJunkin and other CDMG personnel in the deployment of accelerographs at the temporary CDMG/UC Santa Cruz sensitive seismographic stations. J. Scheimer of Lawrence Livermore National Laboratory cooperated in the analog/digital accelerograph co-location experiment at the CDMG Cantua Creek station. B. Tucker reviewed the manuscript and made suggestions materially improving its structure.



## REFERENCES

- Boore, D.M., W.B. Joyner, A.A. Oliver and R.A. Page, 1980, Peak acceleration, velocity and displacement from strong-motion records: Bull. Seism. Soc. Amer., v. 70, 305-321.
- Boore, D.M., B.E. Tucker, A.G. Lindh, A.F. Shakal and R.D. McJunkin, 1983, Some studies concerning site response: Part 1. Preliminary analysis of Parkfield array recordings of the Coalinga earthquake; Part 2. Stability of empirical estimates of site response: Proceedings of NRC/USGS Conference on Site Effects, Santa Fe, NM, July 1983, in press.
- Hart, E.W. and R.D. McJunkin, 1983, Surface faulting northwest of Coalinga, California, June and July 1983: this volume.
- Jennings, P.C., 1983, Strong motion aftershock studies, California Institute of Technology: in Earthq. Eng. Res. Inst. Reconnaissance Report on the Coalinga earthquake, R. Scholl, ed., in press.
- Jennings, C.W. and R.G. Strand, 1958, Geologic map of California, Santa Cruz sheet: Calif. Div. Mines and Geology, Sacramento, CA.
- Maley, R.P. and W.K. Cloud, 1973, Strong-motion accelerograph results, p. 325-348 in San Fernando, California, Earthquake of February 9, 1971, Vol. III, U.S. Dept. Commerce.
- Maley, R.P., G. Brady, E. Etheridge, D. Johnson, P. Mork, and J. Switzer, 1983, Analog strong motion data and processed main event records obtained by U.S. Geological Survey near Coalinga, California: p38-60 in The Coalinga Earthquake Sequence Commencing May 2, 1983, compiled by R.D. Borchardt, U.S.G.S Open-File Report 83-511.
- McJunkin, R.D. and A.F. Shakal, 1983, The Parkfield strong-motion array: Calif. Geology, v. 36, p. 27-34.
- Shakal, A.F. and D.L. Bernreuter, 1981, Empirical analysis of near-source ground motion: Lawrence Livermore National Laboratory Report, NUREG/CR-2095, 65p.
- Shakal, A.F. and R.D. McJunkin, 1983, Preliminary summary of CDMG strong-motion records from the 2 May 1983 Coalinga, California, earthquake: CDMG Office of Strong Motion Studies, Report OSMS 83-5.2, 50p.
- Sherburne, R.W., K. McNally, E. Brown and A. Aburto, 1983, The mainshock-aftershock sequence of 2 May 1983: Coalinga, California: this volume.

TABLE 1

## Coalinga Temporary Accelerograph Stations

Station No.	Name	N.Lat. W.Long.	Dates of Occupancy	Instr. Ser.No.	
36T01	Avenal	35.983 120.146	5/3 - 5/19	5036*	CAVL
46T01	Huron - CDF Garage	36.205 120.103	5/3 - 5/6	2522	
46T02	Huron - CDF Grounds	36.205 120.103	5/3 - 5/19	5065*	CFIR
46T03	Coalinga - Sulphur Baths	36.121 120.397	5/6 - N.A.	2592	
46T04	Coalinga - CHP	36.151 120.353	5/6 - N.A.	4813	
46T05	Anticline Ridge - Palmer Ave.	36.210 120.305	5/3 - 5/19	1860	CPAL
46T06	Oilfields - Skunk Hollow	36.282 120.305	5/3 - 5/19	1700	CINT
45T07	Harris Ranch Hdqtrs	36.343 120.216	5/6 - 5/19	2522	
46T08	Five Points - Airway Farms	36.446 120.119	5/3 - 5/19	4571*	C5PT
46T09	Cantua - Gravel Quarry	36.414 120.393	5/3 - 5/19	4574*	CANT

\* Instruments deployed in cooperation with UC Santa Cruz. Four-letter code is the name of the sensitive station co-located with the accelerograph, as described in Sherburne et al. (1983).

TABLE 2

## Coalinga Mainshock and Aftershock Parameters#

Event	Date	Time(UTC)	N.Lat.	W.Long.	Depth (km)	Magnitude ML (BRK)
1	2 May	23:42:38	36.233	120.293	10.5	6.7
2	9 May	02:49:12	36.231	120.312	12.5	5.1
3	11 June	03:09:52	36.242	120.457	3.4	5.0
4	9 July	07:40:51	36.237	120.409	9.5	5.2
5	22 July	02:39:54	36.228	120.416	9.2	5.9
6	22 July	03:43:01	36.209	120.413	9.5	5.0
7	25 July	22:31:39	36.216	120.406	9.5	5.1

# Hypocenter and origin times as determined by the USGS network (Cockerham, personal communication, 1983).



Figure 1. Peak acceleration data from the 2 May 1983 Coalinga earthquake with data from the 1971 San Fernando earthquake included for reference. This plot is preliminary and does not include the Coalinga data from the distant ( $> 75$  km) stations mentioned by Maley et al. (1983)

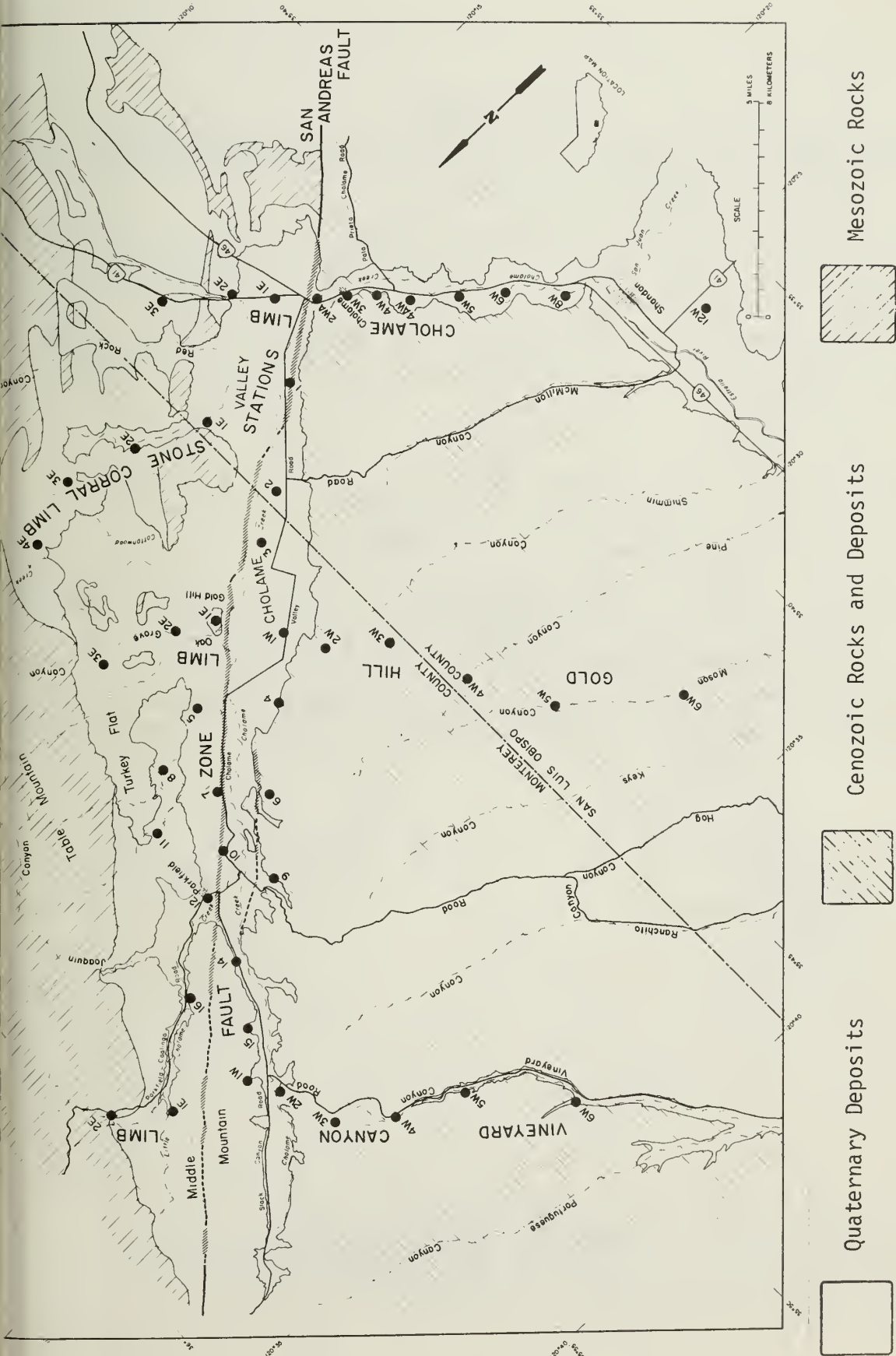


Figure 2. CDMG Parkfield strong-motion array and generalized geology. The array configuration forms four limbs (Cholame, Stone Corral, Gold Hill, Vineyard Canyon) oriented perpendicular to the San Andreas and a central zone of stations paralleling the fault. Fault trace (diagrammatically shown) is of ground rupture in the 1966 Parkfield earthquake. (From McJunkin and Shakal, 1983).



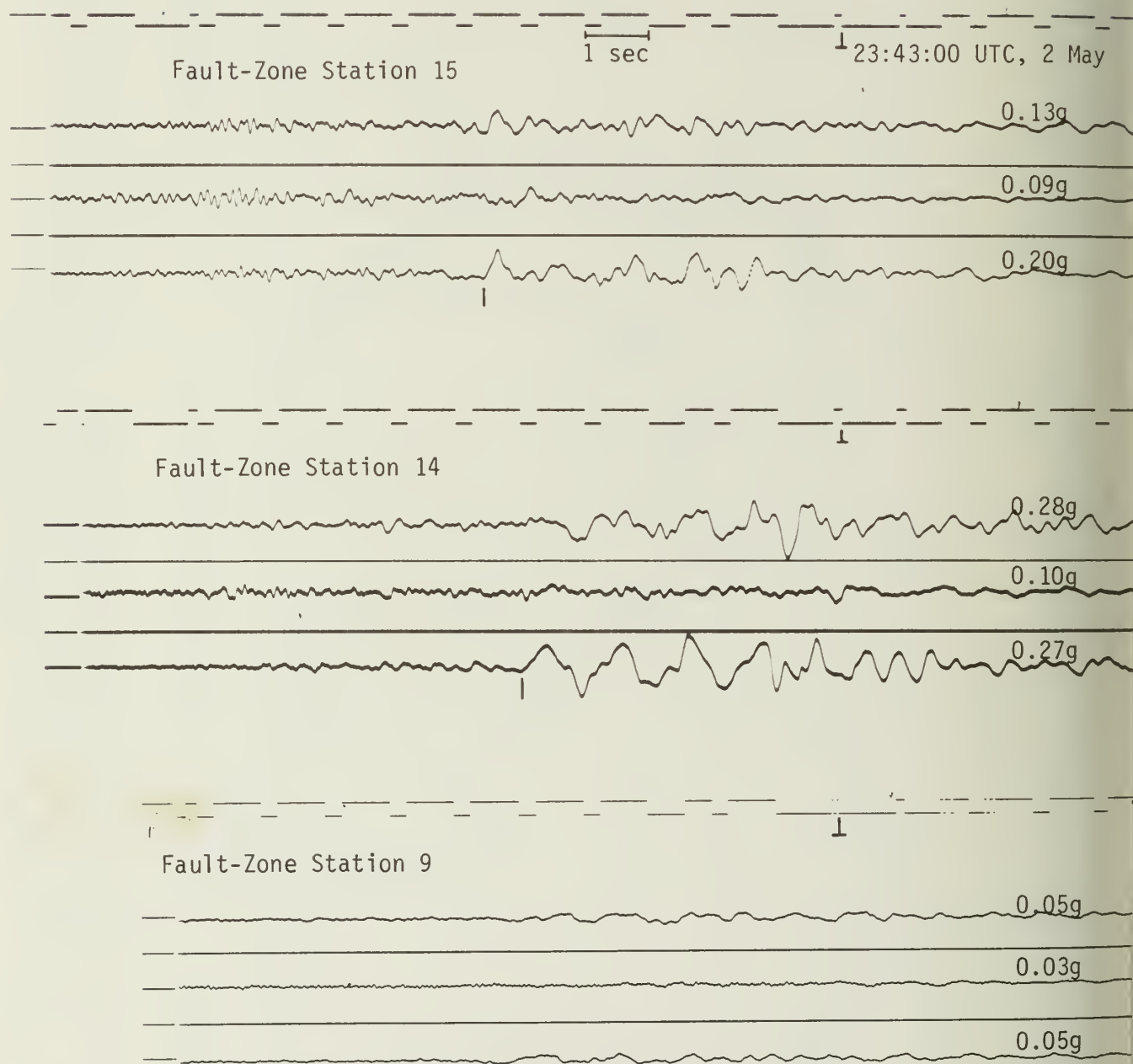


Figure 3. Accelerograms recorded at three neighboring stations in the Parkfield array during the 2 May 1983 Coalinga earthquake. The accelerograms are aligned relative to the WWVB time code on the records. The components are East, Up, and North, respectively.

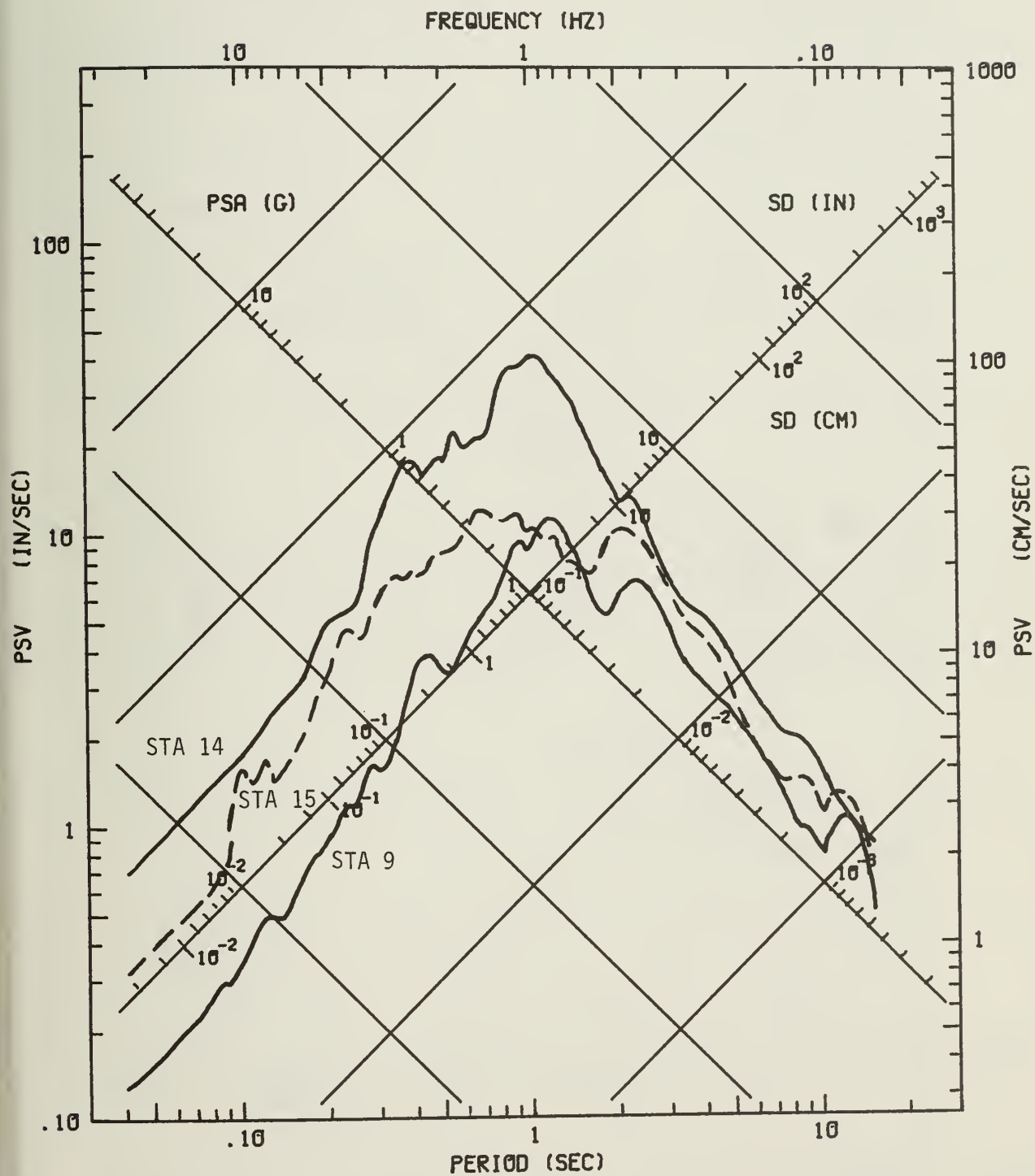


Figure 4. Response spectra (5% damping) for the accelerograms of Fig. 3, East component (chan 1).

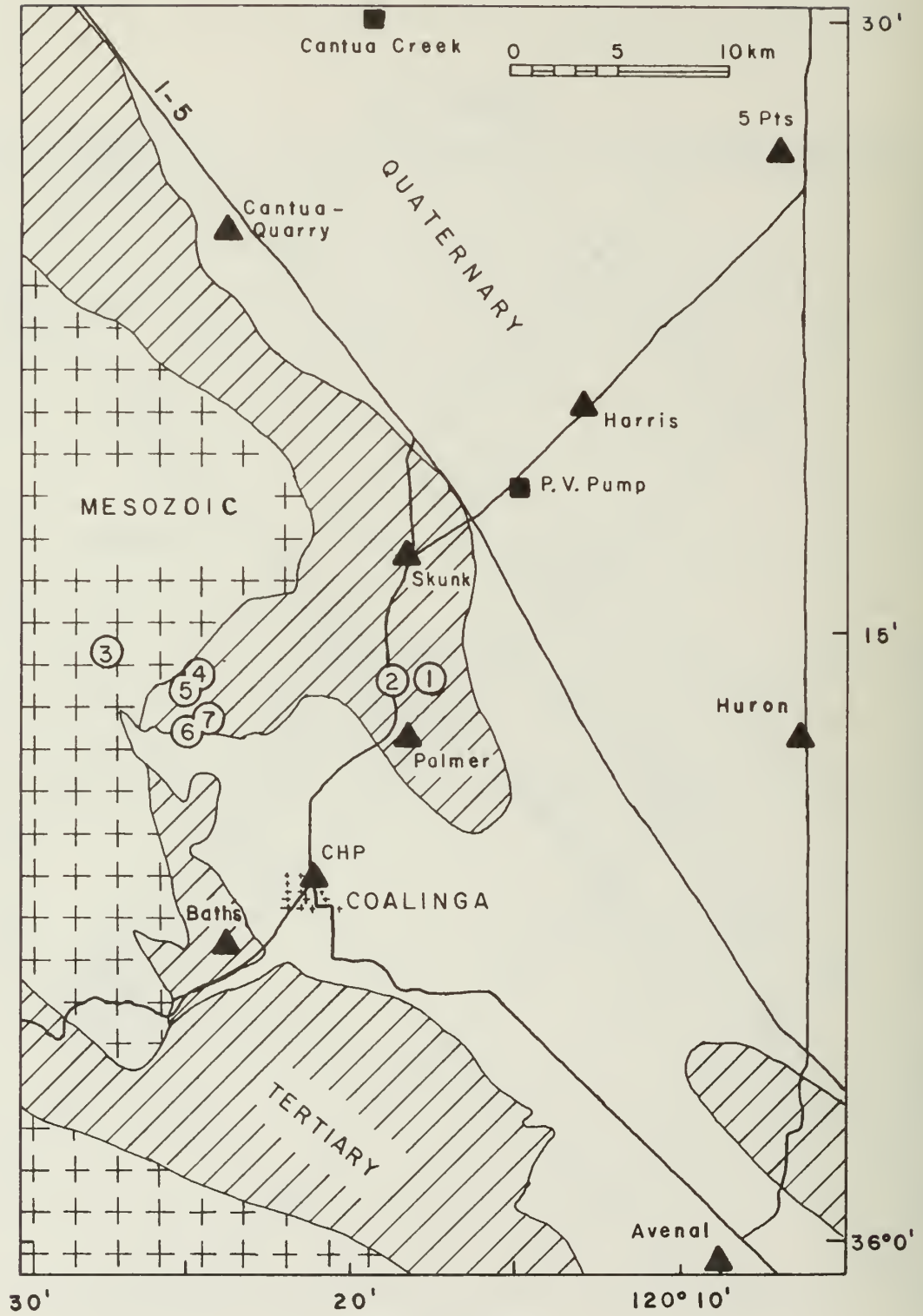


Figure 5. Accelerograph stations, epicenter locations, and local geology in the vicinity of Coalinga (geology simplified from Jennings and Strand, 1958). Temporary accelerograph stations (triangles) were deployed to augment the two permanent stations (squares) at Cantua Creek (CDMG) and Pleasant Valley pump station (USGS) which recorded the mainshock. The epicenters (circles) are numbered from 1 (mainshock) through 7, and are identified in Table 2.

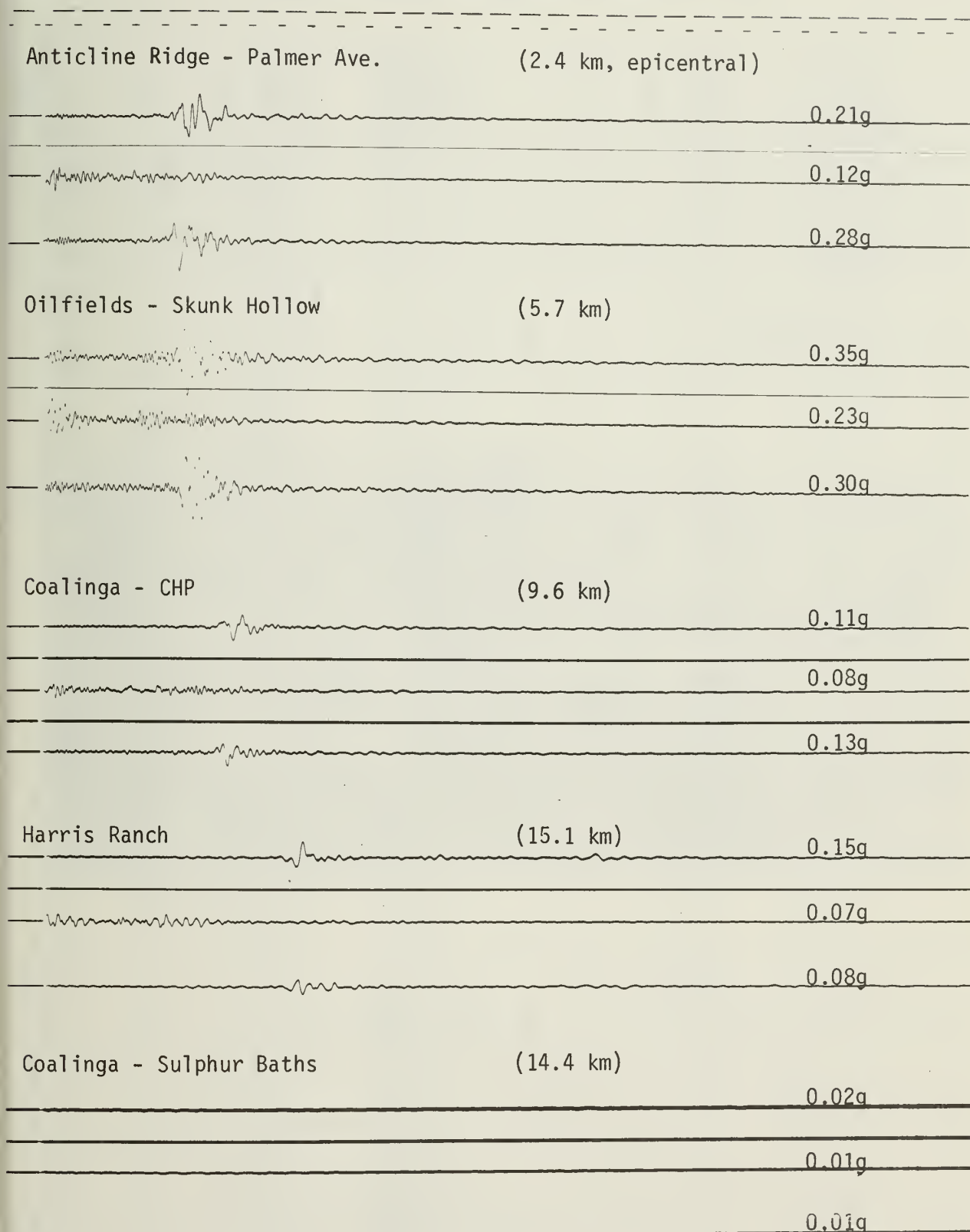


Figure 6. Accelerograms recovered from the 9 May 5.1  $M_L$  aftershock (event 2 of Fig. 5 and Table 2). Components are East, Up and North, respectively.



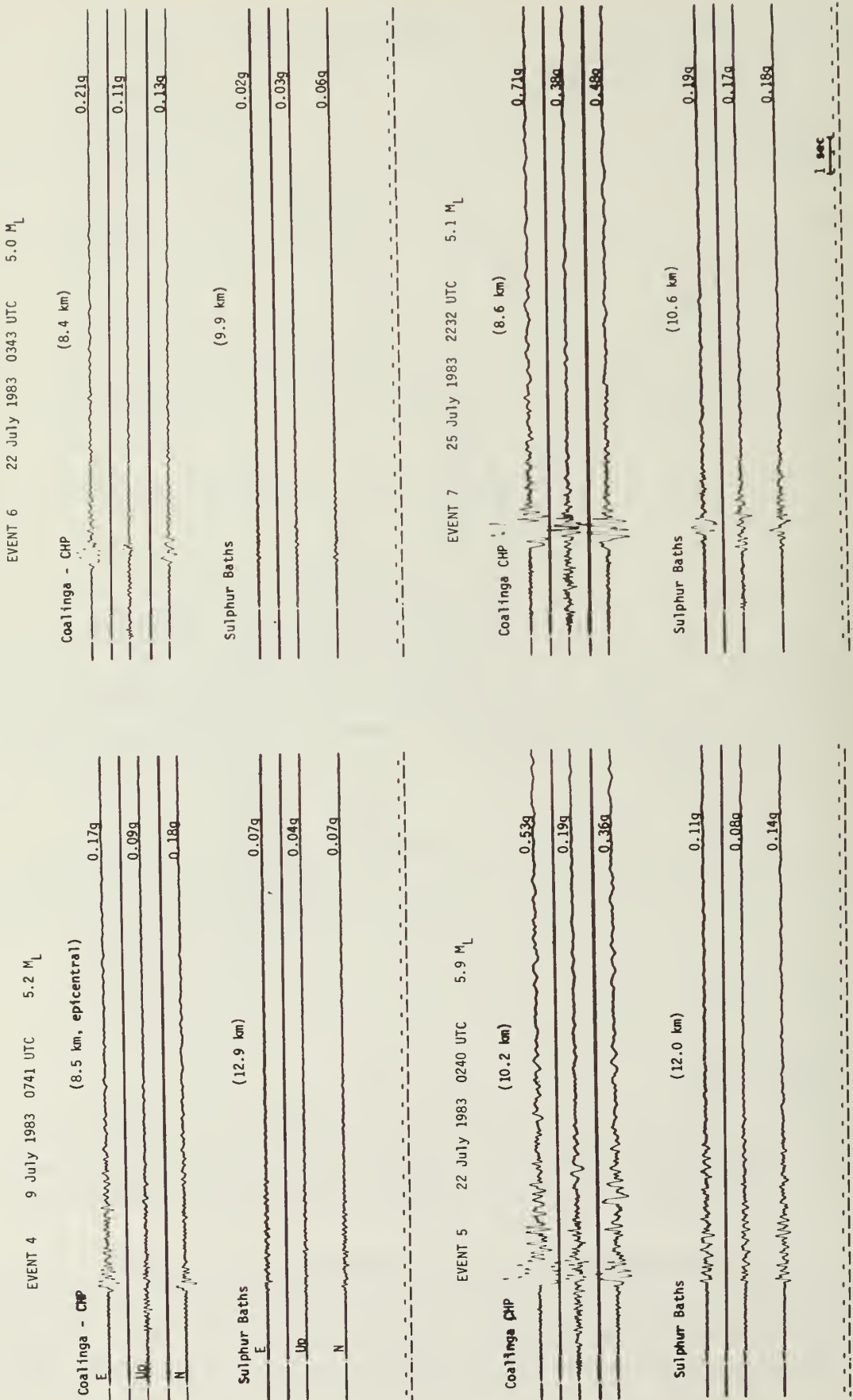


Figure 7. Coalinga aftershock accelerograms recorded at a station in Coalinga (CHP) and at a station on Pliocene rock at the edge of the valley (Sulphur Baths).

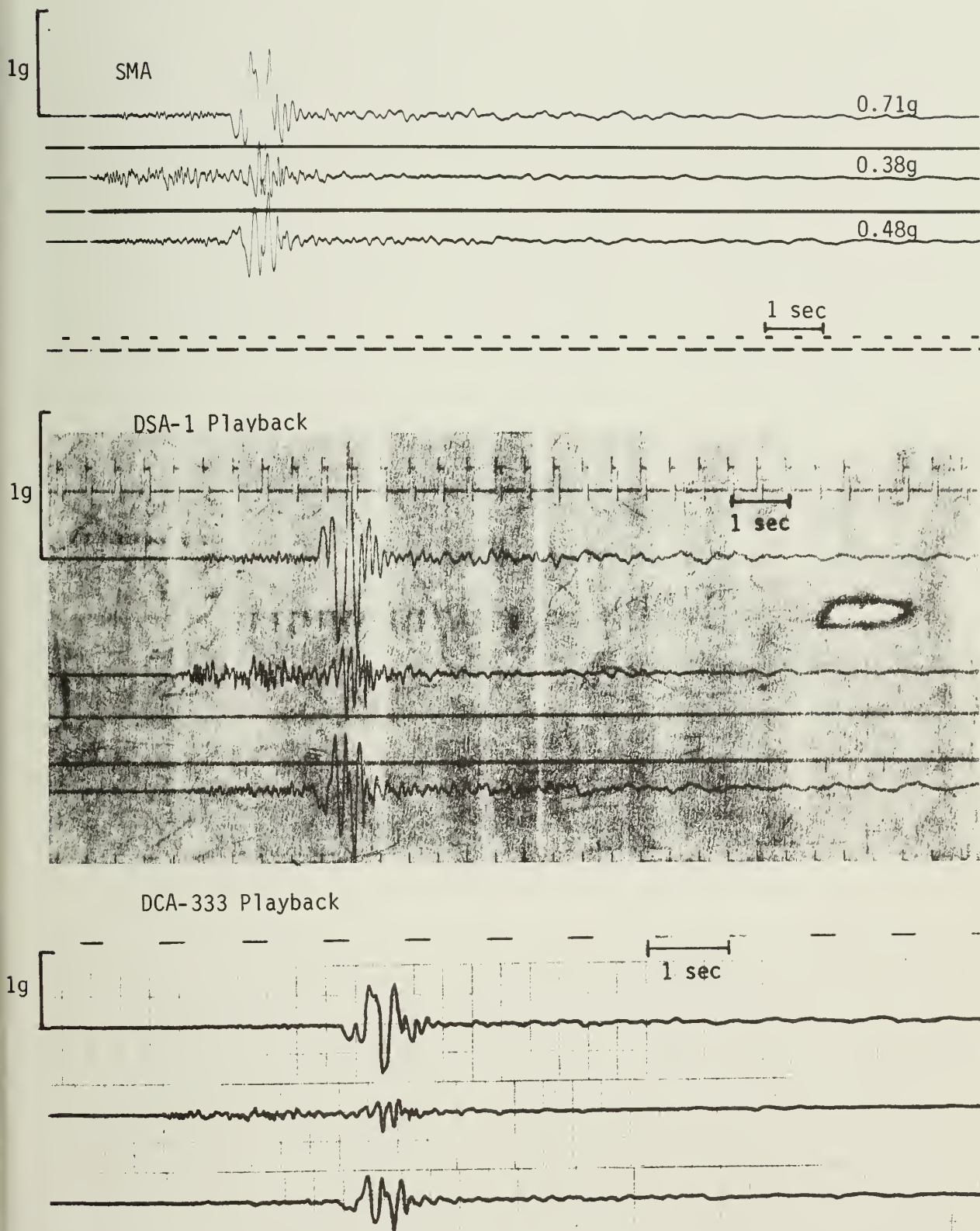
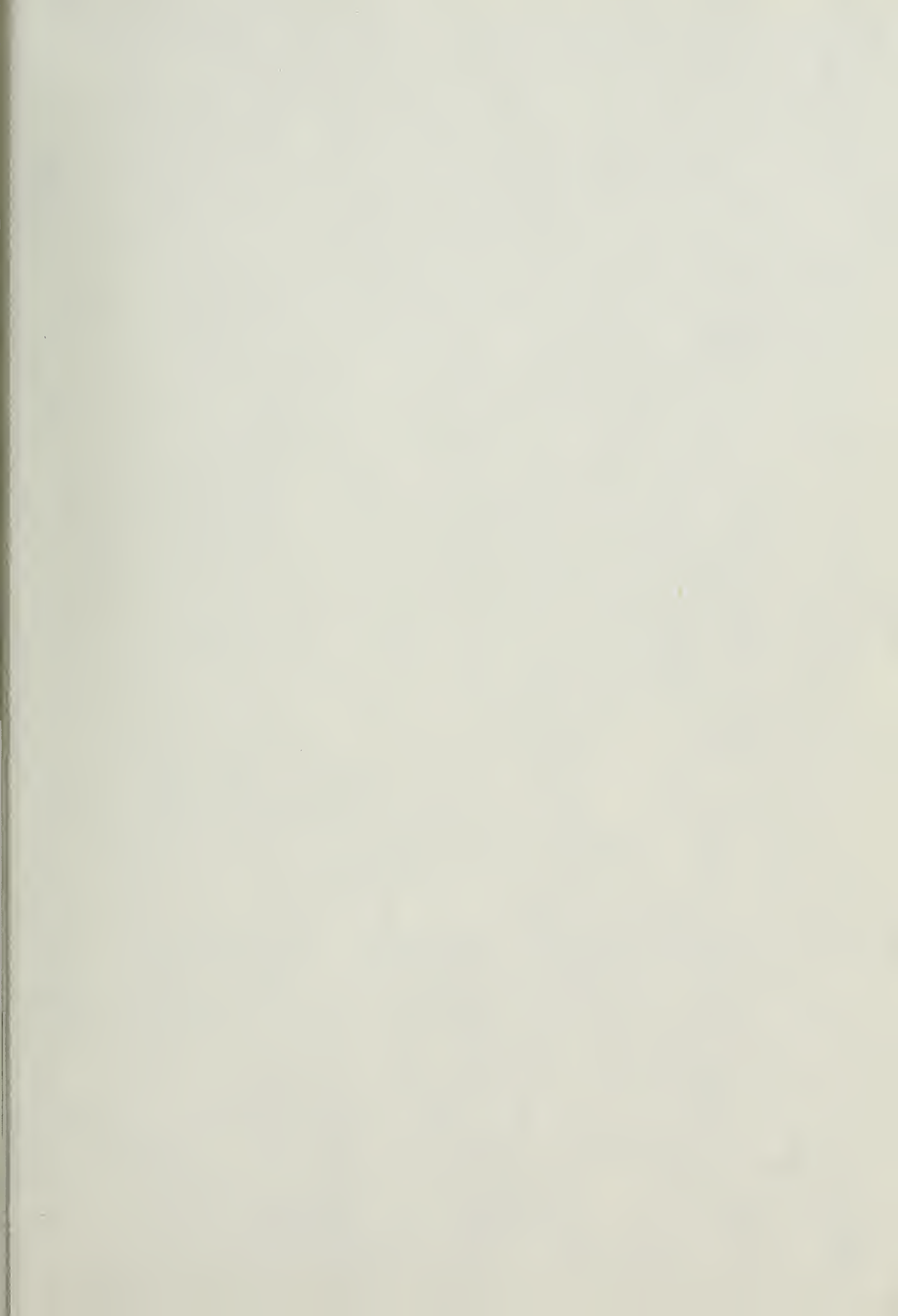


Figure 8. Accelerograms from analog (SMA) and digital (DSA-1, DCA-333) accelerographs co-located at Coalinga-CHP during the 25 July 1983 aftershock. Channel polarities and scaling on the digital playbacks differ from the SMA.











THIS BOOK IS DUE ON THE LAST DATE  
STAMPED BELOW

BOOKS REQUESTED BY ANOTHER BORROWER  
ARE SUBJECT TO IMMEDIATE RECALL

PHYSICAL SCS. LIBRARY

MAR 27 2000  
1995 - 8 17

RECEIVED

RECEIVED

MAR 14 2000

Physical Sciences Library

DEC 15 1995

RECEIVED

JAN 4 - 1000

PHYSICAL SCS. LIBRARY

MAR 27 1996

RECEIVED

MAR 15 1996

PHYSICAL SCS. LIBRARY

LIBRARY, UNIVERSITY OF CALIFORNIA, DAVIS

D4613 (7/92)M



3 1175 00935 0292



